TRANSACTIONS
OF THE ASME
Series E

Journal of APPLIED MECHANICS

September 1959

DYNAMICS • VIBRATIONS • ELASTICITY • LUBRICATION AND WEAR
RHEOLOGY • FRACTURES • STRUCTURES • HYDRAULICS • AERODYNAMICS
INTERNAL FLOW • MECHANICAL PROPERTIES OF METALS • THERMODYNAMICS
TURBULENCE • HEAT TRANSFER • COMPUTING DEVICES AND METHODS
BOUNDARY LAYERS • AEROELASTICITY • EXPERIMENTAL STRESS ANALYSIS

Published Quarterly by
THE AMERICAN SOCIETY OF MECHANICAL ENGINEERS

TRANSACTIONS
OF THE ASME
Series E

EDITORIAL DEPARTMENT

Editor, J. J. JAKLITSCH, JR.
Consulting Editor, LEO SLOGGETT
Art Editor, HENRY BALFOUR
Production, HILDA K. WILGUS

APPLIED MECHANICS DIVISION

Chairman, W. FRASER
Secretary, E. D. BATDORF
Technical Editor, D. C. DRUCKER
Technical Editor, J. KESTIN
Acting Technical Editor, P. P. MAEDER
Honorary Editor, JOHN M. LESSELLS

OFFICERS OF THE ASME

President, S. S. WARNER
Secretary, O. B. SCHIER, II
Treasurer, E. J. KATES
Assistant Treasurer, H. J. BAUER

PUBLICATIONS COMMITTEE

Chairman, JOHN de S. COUTINHO
B. G. A. SKROTZKI
HEWBLEY H. BLACKBURN
R. D. MINDLIN
MARTIN GOLAND
Junior Representatives
A. T. WUSKA
A. S. GOLDSTEIN

REGIONAL ADVISORY BOARD

Region I, ROY L. PARSELL
Region II, GLENN R. FRYLING
Region III, F. J. HEINZE
Region IV, FRANCIS C. SMITH
Region V, H. M. GATHER
Region VI, C. B. EARLE
Region VII, M. POPOVICH
Region VIII, LINN HELANDER

Published quarterly by The American Society of Mechanical Engineers. Publication office at 20th and Northampton Streets, Easton, Pa. The editorial department is located at the headquarters of the Society, 29 West Thirty-Ninth Street, New York 18, N. Y. Cable address, "Mechanize," New York. Price $5.00 a copy, $10.00 annually; to members, $1.50 a copy, $6.00 annually. Add 50 cents for postage to all countries outside the United States and Canada. Changes of address must be received at Society headquarters seven weeks before they are to be effective on the mailing list. Please send old as well as new address. . . . By-Laws: The Society shall not be responsible for statements or opinions advanced in papers or . . . printed in its publications (B13, Par. 4). . . . Second-class mail privileges authorized at Easton, Penna. This publication is authorized to be mailed at the special rates of postage prescribed by Section 132.122 . . . © Copyrighted, 1959, by The American Society of Mechanical Engineers. Reprints from this publication may be made on condition that full credit be given the TRANSACTIONS of the ASME, Series E—Journal of Applied Mechanics, and the author, and that date of publication be stated.

TRANSACTIONS OF THE ASME
is indexed by the Engineering Index, Inc.

Journal of APPLIED MECHANICS

VOLUME 26 • SERIES E • NUMBER 3
September 1959

CONTENTS

TECHNICAL PAPERS

319 **On Supersonic Wind Tunnels With Low Free-Stream Disturbances**
M. V. Morkovin

325 **Velocity and Temperature Fluctuation Measurements in a Turbulent Boundary Layer**
D. S. Johnson

337 **Density Variation Effects in Stepped-Thrust Bearings**
C. F. Kettleborough

341 **Response of a Nonlinear String to Random Loading**
T. K. Caughey

345 **Response of Van Der Pol's Oscillator to Random Excitation**
T. K. Caughey

349 **A Perturbation Solution of the Equations of Motion of a Gyroscope**
Robert Goodstein

353 **Vibration of Beam-Mass Systems With Time-Dependent Boundary Conditions**
T. C. Yen and S. Kao

357 **Dynamic Loading Tests of an Aircraft-Type Beam**
E. A. Ripperger and W. R. Barton

367 **Viscous Damping in Flexural Vibrations of Bars**
M. K. Newman

377 **Natural Modes and Their Stability in Two-Degree-of-Freedom Systems**
R. M. Rosenberg and C. P. Atkinson

386 **On Finite Bending of Pressurized Tubes**
Eric Reissner

393 **Instability and Folding Deformation of a Viscoelastic Medium in Compression**
M. A. Biot

401 **Stress Distribution in Semi-Infinite Strip Subjected to Concentrated Load**
P. S. Theocaris

407 **Postbuckling Behavior of Rectangular Plates With Small Initial Curvature**
Noboru Yamaki

415 **New Theory of Elastic Sandwich Plates—One-Dimensional Case**
Yi-Yuan Yu

422 **On Invariant Perforation in an Infinite Strip**
Chih-Bing Ling

432 **Thermal Stresses in Moderately Thick Elastic Plates**
B. E. Gatewood

437 **Analysis of Plane Stress in Polar Co-ordinates**
H. D. Conway

440 **The Stress Function of a Radial Strain**
F. Goded

442 **Determination of Safe Loads of Beams Subjected to Twisting and Bending Moments**
P. G. Hodge, Jr., and R. Sankaranarayanan

CONTENTS

DESIGN DATA AND METHODS

448 Factors of Stress Concentration Due to Elliptical Fillets, *M. M. Frocht and D. Landsberg*

BRIEF NOTES

451 Creep of Elastic Belt on a Pulley, *G. V. Tordion*

452 Modification of Rayleigh's Principle for Calculating Beam Frequencies, *F. M. Lewis*

454 Yield Point Load of an Annular Plate, *P. G. Hodge, Jr.*

455 Analysis of Indeterminate Structures by Displacement Method, *P. H. Denke and C. K. Wang*

456 Internal Damping of Thermal Origin in Thin Wires, *P. Srinivasan*

457 Lateral Buckling of Tapered Narrow Beam, *L. H. N. Lee*

458 Stresses in Infinite Wedges Tapered in Width and Thickness, *H. D. Conway*

460 Minimization of Spring Torque, *T. Vreeland, Jr.*

461 Steady-State Response of Linear Vibration Systems, *M. E. Gurtin*

462 Further Understanding of Shakedown Theorems, *Melvin Zaid*

463 Series Solution for Ellipsoidal Shells, *Robert Schmidt*

DISCUSSION

465 Discussion of previously published papers by *E. L. Reiss; G. N. Hatsopoulos and J. H. Keenan; F. A. McClintock; F. M. White, B. F. Barfield, and M. J. Goglia; M. M. Abbassi; Eli Sternberg and W. T. Koiter; M. J. Schilhansl*

BOOK REVIEWS

475 Study of Mechanical Vibration, 476 Automation, Computation, and Control

475 Mathematics of Physics, 476 Engineering Vibrations

TRANSACTIONS OF THE ASME Series A

Journal of ENGINEERING FOR POWER

Volume 81 • Series A • Number 3

CONTENTS FOR JULY, 1959

1958 Gas Turbine Progress Report

215 Introduction, by R. T. Sawyer. (58—A-46 A)
219 Materials, by A. W. Herbenar and G. R. Heckman. (58—A-46 B)
226 Turbine Cooling, by J. B. Esgar. (58—A-46 C)
234 Fuels, by A. D. Foster. (58—A-46 D)
244 Cycle Components, by P. F. Martinuzzi. (58—A-46 E)
259 Compound Piston-and-Turbine Engines, by A. L. London. (58—A-46 F)
265 Aviation, by O. E. Lancaster. (58—A-46 G)
280 Rocket Turbines, by O. E. Lancaster and C. J. Bates. (58—A-46 H)
290 Automotive, by F. L. Schwartz. (58—A-46 I)
298 Railroad, by P. R. Broadley, W. M. Meyer, D. S. Neuhart, E. L. Barlow, R. C. Bond, D. S. D. Williams, and B. W. C. Cooke. (58—A-46 J)
311 Marine, by J. W. Sawyer and H. M. Simpson. (58—A-46 K)
344 Industrial and Central Station, by B. G. A. Skrotzki. (58—A-46 L)
352 Nuclear, by R. P. Godwin and E. S. Dennison. (58—A-46 M)

TRANSACTIONS OF THE ASME Series B

Journal of ENGINEERING FOR INDUSTRY

Volume 81 • Series B • Number 3

CONTENTS FOR AUGUST, 1959

187 Factors Influencing the Performance of Grinding Wheels, by E. J. Krabacher. (58—SA-40)
201 Vibrations of Flexible Precision Grinding Spindles, by R. S. Hahn. (58—A-97)
207 The Effect of Process Variables on Extrusion Pressures of Lead, by J. Frisch and E. G. Thomsen. (58—A-109)
217 Approximate Solutions to a Problem of Press Forging, by S. Kobayashi and E. G. Thomsen. (58—A-140)
228 Theory and Experiment of Press Forging Axisymmetric Parts of Aluminum and Lead, by S. Kobayashi, R. Herzog, J. T. Lapsley, Jr., and E. G. Thomsen. (58—A-154)
239 A Three-Dimensional, Tool-Life Equation—Machining Economics, by B. N. Colding. (58—A-123)
251 Some Observations on the Shearing Process in Metal Cutting, by S. Kobayashi and E. G. Thomsen. (58—A-139)
263 Observations on the Angle Relationships in Metal Cutting, by D. M. Eggleston, R. Herzog, and E. G. Thomsen. (58—A-138)

TRANSACTIONS
Series C

Journal of
HEAT TRANSFER
Vol. 81 • Series C • No. 3

CONTENTS FOR AUGUST, 1959

175 Heat Transfer Between Concentric Rotating Cylinders, by I. S. Bjorklund and W. M. Kays. (58—A-99)

187 Full-Scale Human-Body-Model Thermal Exchange Compared With Equational Condensations of Human Calorimetric Data, by L. P. Herrington. (58—A-181)

195 The Emissivity and Absorptivity of Parachute Fabrics, by J. P. Hartnett, E. R. G. Eckert, and R. Birkebak. (58—A-125)

202 An Experimental and Analytical Study of Vortex-Flow Temperature Separation by Superposition of Spiral and Axial Flows—Part I, by J. E. Lay. (58—SA-71)

213 An Experimental and Analytical Study of Vortex-Flow Temperature Separation by Superposition of Spiral and Axial Flows—Part II, by J. E. Lay. (58—A-90)

223 Analysis of the Aerodynamic Heating for a Re-Entrant Space Vehicle, by M. J. Brunner. (59—Av-5)

230 A Photographic Study of Boiling in the Absence of Gravity, by R. Siegel and C. Usiskin. (59—Av-37)

237 Some Radiator Design Criteria for Space Vehicles, by J. P. Callinan and W. P. Berggren. (59—Av-29)

245 Optimization of a Conventional-Fuel-Fired Thermoelectric Generator, by B. W. Swanson and E. V. Somers. (59—SA-14)

Technical Briefs

249 Heat Transfer From a Rotating Disk to Fluids of Any Prandtl Number, by E. M. Sparrow and J. L. Gregg.

251 An Approximate Treatment of Unsteady Heat Conduction in Semi-Infinite Solids With Variable Thermal Properties, by K.-T. Yang and Albin Szewczyk.

TRANSACTIONS
Series D

Journal of
BASIC ENGINEERING
Vol. 81 • Series D • No. 3

CONTENTS FOR SEPTEMBER, 1959

275 Static and Dynamic Control Characteristics of Flapper-Nozzle Valves, by T.-Y. Feng. (58—A-160)

285 Some Measurements of Boundary-Layer Growth in a Two-Dimensional Diffuser, by J. F. Norbury. (58—A-196)

297 The Skewed Boundary Layer, by E. S. Taylor. (58—A-113)

305 On the Nature of Stall, by S. J. Kline. (58—A-170)

321 Optimum Design of Straight-Walled Diffusers, by S. J. Kline, D. E. Abbott, and R. W. Fox. (58—A-137)

332 Labyrinth-Seal Leakage Analysis, by W. Zabriskie and B. Sternlicht. (58—A-118)

341 Centrifugal Manometer, by J. F. Kemp. (58—A-111)

349 The Aerodynamic Design of Two-Dimensional Turbine Cascades for Incompressible Flow With a High-Speed Computer, by H. N. Cantrell and J. E. Fowler. (58—A-141)

362 An Analysis of Axial Compressor Cascade Aerodynamics, Part I, by G. L. Mellor. (58—A-83)

379 An Analysis of Axial Compressor Cascade Aerodynamics, Part II, by G. L. Mellor. (58—A-84)

387 Loss and Stall Analysis of Compressor Cascades, by Seymour Lieblein. (58—A-91)

401 Stall Prediction in Gas-Turbine Engines, by R. J. Lubick and L. E. Wallner. (58—A-133)

409 A Survey of Stall Propagation—Experiment and Theory, by H. W. Emmons, R. E. Kronauer, and J. A. Rockett. (58—A-150)

417 Modulation Phenomena in Stall Propagation, by J. A. Rockett. (58—A-152)

426 Studies of Jet Compression—I, Apparatus and Methods. Results With Air at Room Temperature, by H. J. Hoge, S. S. Eichacker, and D. L. Fiske. (58—SA-13)

On Supersonic Wind Tunnels With Low Free-Stream Disturbances[1]

M. V. MORKOVIN

Lecturer, Department of Aeronautics,
The Johns Hopkins University,
Baltimore, Md.
Mem. ASME[2]

Measurements in supersonic wind tunnels have become almost routine in the last decade and yet little is known about the free-stream disturbances, which are present, and about the means of minimizing them. The present note outlines the problems of minimizing the mean as well as the unsteady variations of velocity and temperature and gives guidance where the trends are clear. It is found that in many wind tunnels the free-stream fluctuations are likely to be dominated by aerodynamic sound in the sense of Lighthill and by shivering Mach waves. Only conjectures can be offered on the means of minimizing the resulting sound intensity at the present time.

DISTURBANCES in the free stream of supersonic sections can be classified as (*a*) nonuniformities in the mean flow, observable by d-c instruments, and (*b*) unsteady disturbances. The tolerable level of these disturbances obviously depends upon the objectives of the experimental programs in the tunnel. The task of keeping the disturbances extra small, which is often expensive and time-consuming, may not always be warranted while for some experiments such as those on instability and transition of shear flows, an all-out effort is indicated. Certain principles for minimizing the disturbances, however, appear to be generally valid.

Mean-Flow Nonuniformities

The cause of mean-flow nonuniformities (*a*) observed in supersonic tunnels has been almost invariably traced to imperfections in nozzle and wall contours. There exists a large literature on the subject of prevention of and corrections for such nonuniformities (see, for instance, bibliographies in Kenney and Webb [1],[3] Meyer [2], MacDermott [3], and so on). It is generally agreed that, in order to make nonuniformities small, contours should be curved gently, and continuously; that very close attention must be paid to joints in the walls or to eliminate them if possible; and that the development of the boundary layer on the walls best be taken into account. A number of good tunnels have been built along those principles.

The author is not familiar with any references where mean-velocity nonuniformities in the supersonic sections have been traced to nonuniformities of the subsonic mean flow upstream of the nozzle (except for a case of a mild axial swirl and obvious cases of local separation). There is some experimental evidence that constant-pressure mean temperature nonuniformities (stratifications) tend to persist in the flow. The extremely rapid passage through the nozzle must be essentially isentropic so that the deviations ΔT of the static absolute temperatures T from the mean decrease only in proportion to the absolute temperatures (see Corrsin [11], Equation 7):

$$\frac{\Delta T_2}{T_2} = \frac{\Delta T_1}{T_1} \tag{1}$$

The corresponding influence on the Mach-number nonuniformity in the supersonic section, however, appears to be small and on the same order as the influence of the velocity nonuniformities. This can be concluded from the remainder of the compressible perturbation equations of Corrsin [11], corrected and modified:

$$\frac{\Delta M_2}{M_2} = \left(\frac{M_1^2}{M_2^2}\right)\left(\frac{1 + \frac{\gamma - 1}{2} M_2^2}{1 + \frac{\gamma - 1}{2} M_1^2}\right)\left(\frac{\Delta M_1}{M_1}\right), \tag{2}$$

[1] Most of the investigations, which form the background for the note, have been sponsored by the Office of Scientific Research, U. S. Air Force, and by the Office of Naval Research, U. S. Navy, and were conducted in The Johns Hopkins Supersonic Wind Tunnel. Many of the ideas were evolved in discussions with L. S. G. Kovasznay, F. H. Clauser, S. Corrsin, L. T. Miller, R. E. Phinney, and J. Sternberg. The original report was issued as an Air Force OSR Technical Note 56-540 in November, 1956.

[2] Also, Chief, Aerophysics Research Staff, Flight Vehicle Design Department, The Martin Company.

Presented at the Summer Conference of the Applied Mechanics Division, Troy, N. Y., June 18–20, 1959, of THE AMERICAN SOCIETY OF MECHANICAL ENGINEERS.

Discussion of this paper should be addressed to the Secretary, ASME, 29 West 39th Street, New York, N. Y., and will be accepted until October 10, 1959, for publication at a later date. Discussion received after the closing date will be returned.

NOTE: Statements and opinions advanced in papers are to be understood as individual expressions of their authors and not those of the Society. Manuscript received by ASME Applied Mechanics Division, February 27, 1958. Paper No. 59—APM-10.

[3] Numbers in brackets designate References at end of paper.

Nomenclature

$\mathcal{L}$ = effective nozzle length
L = size of integral scale of fluctuations
M = local Mach number
t = time in sec
T = absolute static temperature
T_t = absolute stagnation or total temperature
U = velocity
U_τ = "friction" velocity, $\left(\frac{\tau}{\rho}\right)^{1/2}$, at wall
u = horizontal component of velocity perturbation
γ = ratio of specific heats
$\Delta(\ )$ = perturbation in the quantity $(\ )$
δ = boundary-layer thickness
ρ = density
τ = viscous shear

Subscripts

1 = conditions is settling chamber
2 = conditions in supersonic test section

Superscript

prime = rms value

$$\frac{\Delta M}{M} = \frac{\Delta U}{U} - \frac{1}{2}\frac{\Delta T}{T} = \left(1 + \frac{\gamma - 1}{2} M^2\right)\left[\frac{\Delta U}{U} - \frac{1}{2}\frac{\Delta T_t}{T_t}\right], \quad (3)$$

where T_t is the mean stagnation temperature:

$$T_t = T_1\left(1 + \frac{\gamma - 1}{2} M_1^2\right) = T_2\left(1 + \frac{\gamma - 1}{2} M_2^2\right) \quad (4)$$

Large contraction ratios to the sonic throat make M_1^2 small in Equation (2) and minimize these nonuniformities, $\Delta M_2/M_2$.

One other nonuniformity of the mean stream is known to exist in two-dimensional nozzles (from scattered, unpublished experimental data) but has not apparently been explored carefully. There is a lateral flow in the boundary layer, tending to accumulate a ridge of low-speed air on the axis of symmetry of the sidewalls. The corresponding variations of displacement thickness induce a pressure field, often not insignificant, which is difficult to trace during tunnel calibration because of its three-dimensional nature.

Unsteady Disturbances

Turning to unsteady disturbances [category (*b*)], criteria for judging the unsteady disturbance level in a supersonic tunnel and for designing for one of low-disturbance level have been essentially nonexistent. One reason for this gap was the poor understanding of just what these unsteady disturbances were, what were their sources, and how they could be measured. Partial answers to these questions were recently given by Kovasznay [4] and Morkovin [5] and [6]. In particular from the discussion of free-stream disturbances in [6], the following concept emerges, Fig. 1. Free-stream disturbances in supersonic tunnels generally consist of comparable contributions from vorticity-mode fluctuations (turbulence), entropy-mode fluctuations (temperature spottiness), and sound-mode fluctuations. Here "comparable" means that the unsteady velocity fluctuations corresponding to the vorticity mode and to the sound mode are of the same order, and the unsteady temperature fluctuations corresponding to the entropy mode and sound mode are comparable. As a consequence, an electrical signal from a hot-wire anemometer corresponds to all three modes (except near $M = 1$, where the low sound sensitivity suppresses the sound contribution; Morkovin [5]). However, the signal from a single hot wire cannot be generally decomposed into the contributions from the three modes. This follows from the fact that at supersonic speeds the relationship between the hot-wire sensitivities is such that the information content consists of three numbers only.[4] Generally, one needs four to ten constants to describe the three modes and their interrelationship in the free stream.[5] With systematic assumptions of the missing information one can bracket the intensities of the fluctuation modes as was done in [6] for the measurements in the Johns Hopkins Supersonic Wind Tunnel. Comparison of these inferences with simplified theories of the contraction effect, Ribner and Tucker [7], Moore [8], and corresponding low-speed measurements of Uberoi [9], together with additional subsonic to supersonic measurements, leads to the following observations and working precepts.

Suppression of Vorticity Fluctuations

It is relatively easy to minimize the vorticity fluctuations (turbulence) by simply designing for a large speed ratio across the nozzle, U_2/U_1; i.e., by choosing a large ratio of settling-chamber cross-sectional area to sonic throat area. The charts of Ribner-Tucker [7] appear to give a satisfactory guide for the upper bound on the vorticity expected in the supersonic section for a given settling-chamber turbulence. Since both the axial and lateral fluctuation velocities u' and v' decrease very rapidly as the speed ratio U_2/U_1 increases, it is not necessary to use excessive effort to reduce the settling-chamber turbulence to very low levels unless there is a constraint on the usable settling-chamber area.

When the level of turbulence in the supersonic test section of a tunnel already completed turns out to be undesirably high, the remedy lies in the low-speed techniques of minimization of settling-chamber turbulence by several screens of decreasing meshes. Because of the foregoing suppression of turbulence associated with large values of U_2/U_1, a relatively high turbulence level of 0.5 per cent or less in the settling chamber should prove satisfactory even for measurements of transition in the supersonic section.

If one wishes to measure the disturbances in the supersonic test section one should place an effective fine filter (cloth or paper) in the settling chamber so that dust and dirt particles flying at high speeds do not cause breakage or pitting of the sensitive elements of the meter. Larger settling-chamber areas and correspondingly smaller settling-chamber velocities facilitate the installation of the filter. A larger settling chamber also allows ready accessibility (if planned for). Accessibility to the regions of potential sources of disturbances, such as the settling chamber and the nozzle region, is very helpful when one needs to identify and eliminate existing disturbances. In particular, one can locate and eliminate sources of irregular low-frequency oscillations sometimes observed in supersonic tunnels (e.g., Lukasiewicz [10], unpublished JHU findings, and others). Many of these fluctuations have been traced to locally separated regions at the wall of the settling chamber; e.g., at beginning of nozzle contraction; immediately downstream from a high-density screen or filter; in diffuser of settling chamber, and so on.

Entropy or Temperature Fluctuations

The sources of entropy fluctuations (temperature spottiness) are traceable to the settling chamber and farther upstream, Fig. 1, especially to where dried air is introduced into the main flow circuit, and to the cooling stations. Entropy-temperature fluctuations are, of course, evened out by heat conduction as they are convected downstream. Townsend[6] considers a sinusoidal temperature distribution of wave length L in a direction x, $\Delta T = \Delta T_0 \cos(2\pi x/L)$, and shows that, after a time t, the amplitude ΔT will be diminished by the exponential factor

$$\mathfrak{F} = e^{-kt(2\pi/L)^2} \quad (5)$$

For laminar flow, the expression (5) is exact and k stands for the molecular heat conductivity of the medium. For turbulent flow the expression (5) is only approximate and k represents an average turbulent diffusion coefficient, which is essentially proportional to the square of the turbulent fluctuations and which is usually much larger than its molecular counterpart.

When the temperature is also stratified sinusoidally in the y-direction, the decay factor becomes $\mathfrak{F}^2$. For sinusoidal cellular structure of equal scales L in three directions, the decay of the spots is accelerated further by an additional power of the factor $\mathfrak{F}$. Although realistic temperature distributions are not regular and usually represent a mixture of all sizes, it is clear that one can suppress the temperature variations substantially faster by increasing their three-dimensional character. One can even speak of an effective scale L (Townsend[6]).

[4] Morkovin [5], p. 15.

[5] Ibid., equation (3.4) enlarged for different sources of sound.

[6] Reference [12], pp. 58–62.

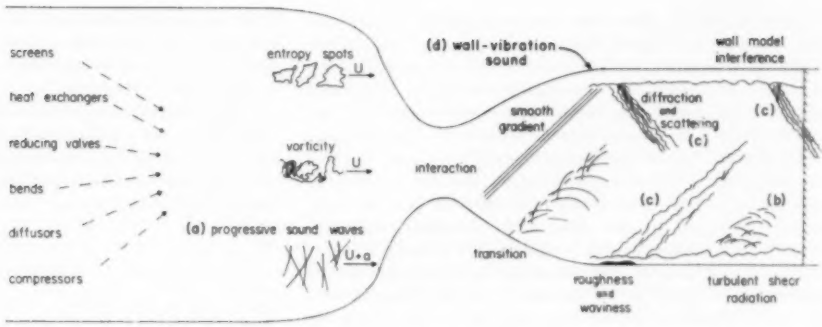

Fig. 1 Free-stream disturbances in supersonic wind tunnels

Mixing, due to turbulence in the ducts and due to the effect of the screens, accelerates the decay primarily through the terms k and L in Equation (5). These factors vary from tunnel to tunnel but the rms temperature fluctuations in the settling chambers of four different supersonic tunnels were found to be inconsequential or were made so by relatively simple precautions. In particular, it is well to provide separate temperature controls on any channels running in parallel so that at least the mean temperatures can be matched at each junction. Large-scale temperature stratifications should be avoided since they appear to decay slowly as would be expected from Equation (5). Maximum passage time should be provided between the junctures of parallel channels, in which there is energy exchange, and the supersonic section. The velocity in ducts being usually on the order 50–150 fps the passage times through the ducting tend to be rather short. A large settling chamber with screens of decreasing size can double or triple the passage time in question and also bring about faster decay by increasing the effective k and by "filamenting" the temperature spots, thus rendering the effective L smaller.

The high acceleration through the nozzle makes the transit time small (approximately $\mathfrak{L}/U_2 \log_e(U_2/U_1)$ where $\mathfrak{L}$ is the nozzle length) so that the corresponding decay is probably negligible. In the test section the temperature fluctuations due to the entropy mode (or their upper bounds) would then be related isentropically to those in the settling chamber; i.e., they would be smaller in proportion to the absolute static temperature ratio, similarly to the steady mean-flow variations of Equation (1).

The high acceleration of the associated density spots could generate sound waves and vorticity fluctuations (Fig. 1, labeled "interaction") which would make the analysis in the test section much more complicated. Quasi-one-dimensional treatment of Moore [8] leads to insignificant sound intensities propagating into the supersonic section, largely because of the choking effect of the sonic throat which is probably exaggerated by the one-dimensionality. Otherwise, little appears to be known about these interactions in the nozzle, theoretically or experimentally. In one exploratory attempt to create large but pure entropy fluctuations in the Johns Hopkins Supersonic Tunnel, a makeshift heater made of six $^3/_8$-in. U-shaped rods (net length 30 in. per rod) was placed in the cone diffuser to the settling chamber (upstream of most of the screens, where local speed U_1 was approximately 10 fps) and heat was discharged into the tunnel at the rate of 0.8 kw per rod. The signals of the hot-wire anemometer in the supersonic section (a little over a second downstream of the heater) disclosed stratifications as expected, with the entropy fluctuations indeed dominant over the vorticity and sound signals. The maximum rms value measured corresponded to 0.56 deg where the static mean temperature T was 186 deg K. The vorticity measured was almost perfectly anticorrelated, as is reasonable,[7] with the entropy signal and corresponded to mere 0.3 fps in u' (with free-stream speed $U_2 \sim 1500$ fps and $M_2 = 1.76$). The smallness of the vorticity testifies not only to the effectiveness of the screens and contraction in suppressing the velocity wake from the heater rods but indicates that there could not have been appreciable generation of new vorticity during the acceleration through the nozzle. If this conclusion is general, then the significant entropy and vorticity fluctuations found in the supersonic test section are generally traceable to the settling chamber and farther upstream and can therefore be minimized by the various precautions already discussed.

Intensity of Classical Aerodynamic Sound

The same cannot be said for sound fluctuations. The sound levels in the supersonic test sections cannot be measured with precision with a single hot wire, but the decibel level may reach 120 to 130 and higher, Morkovin [6], at moderate supersonic Mach numbers. As explained in [6], the generators of such intense sound are to be found in the turbulent boundary layer on the walls (or models) of the supersonic section, Fig. 1, rather than in the settling chamber.

The general concepts of aerodynamic generation of sound of Lighthill [13], [14], and [15], in free stream, and of Curle [16] in presence of solid boundaries, do provide partial appreciation for the sound sources in the supersonic test section, but in words of reference [13]: "As a final restriction, the theory is effectively confined in its application to completely subsonic flows. . . . ." Information from shadowgraphs of bullets in free flight, from hot-wire anemometers [5, 6], and from intuitive arguments[8] agrees that the sound energy in supersonic streams is predominantly radiated in the general direction of the free-stream Mach waves, even though individual wave fronts may be inclined at different (variable) angles if the effective "sources" are moving with respect to the free stream and the solid boundary.

The truly aerodynamic sound in the sense of Lighthill, category (*b*) of Fig. 1, and of Morkovin [6], is radiated from a distribution of quadrupoles over the volume where the turbulence is large, i.e., over the volume within the boundary layer, and from a surface distribution of (turbulent-pressure) dipoles, Equation (2.18) of Curle [16]. Dimensional considerations indicate that the dipoles may be dominated by the quadrupoles at high speeds but similar dimensional reasoning had apparently oversimplified the picture in the case of high-speed jets[9] when compared with experiment. At any rate, no other estimates for the dipole radiation are available at this time.

As for the quadrupole radiation, it should depend (as at subsonic speeds) upon the intensity of turbulence, scale or frequency of intermediate-size eddies (Lighthill [14]), and effective convection velocities. Furthermore, it is strongly amplified by mean shear, while mean temperature gradients have little effect. This

[7] The fluid lumps which received the most heat from the heater were those that were slowed down the most.

[8] Lighthill [14], pp. 29–30, for example.

[9] Ibid., p. 1.

information, however, does little to answer practical questions such as whether, for a given Mach number, one can reduce the radiation by thickening the boundary layer. In so doing, one probably would reduce the turbulent intensity and the mean shear, but would increase the volume over which the quadrupoles are distributed so that the net effect is not certain. Similarly, for a given Reynolds number per inch in the supply section, the rate of increase of the radiation intensity with increasing Mach number of the test section is obscured by the rate of thickening of the boundary layer and by the drop-off of the skin-friction coefficient.[10] Furthermore, there is evidence (Morkovin [17] and Kistler [24]) that the turbulent velocities, even when nondimensionalized with respect to the significant Prandtl shear velocity U_τ [$(\tau/\rho)^{1/2}$, where τ is the viscous shear at the wall and ρ the corresponding density] are considerably lower at supersonic speeds than at low speeds.[11] These intensities are likely to drop farther with increase in Mach number.

The foregoing considerations have a particular bearing on the sound generation in the boundary layer of the nozzle, where the favorable pressure gradient tends to develop a thin layer of high mean shear near the wall. Exploratory traverses with a hot wire in the nozzle of the JHU tunnel disclosed the presence of a distinct high-intensity thin turbulent layer within a much thicker turbulent boundary layer. Since turbulence in a boundary layer is produced largely near the wall[12] and is then "diffused" outward, one can interpret the thin layer of vigorous activity as a "diffusion front" associated with the higher shear. (The effect is probably similar to that documented in Morkovin [17] when a sudden rapid expansion wave distorts a supersonic boundary layer.) The sound from the throat area then radiates into the test section proper. If the high-intensity turbulence and the amplifying high mean shear should have more effect on sound generation than the total quadrupole volume within the boundary layer, this nozzle region could contribute heavily to the total sound level in the tunnel. Increasing the length of the nozzle expansion would tend to decrease the shear and the local turbulence level while the boundary-layer thickness would grow. There is probably an optimum nozzle length in which the advantages of slower expansion are balanced by the additional contributions from the lengthened layer.

Shivering Mach Waves

Another type of sound, the unsteady Mach waves, Fig. 1, category (*c*) of Morkovin [6], however, needs to be considered in any criteria for optimum geometry. The incremental contributions to sound intensity (above the more or less homogeneous background) due to a steady pressure gradient, which is diffracted, scattered, or reflected by a shear layer, can be measured quite well if the gradient is sufficiently sharp, Morkovin [5]. The small positive-negative mean pressure gradients generated by the imperfections of the nozzle contour, window joints, and so on, are often "sufficiently sharp" at supersonic speeds. There is in fact little doubt that this type of sound dominates in many wind tunnels where its intensity often reaches above 130 decibels, at least locally, Morkovin [6].

A fixed observer senses this sound because the wrinkled Mach-wave fronts are displaced back and forth with respect to him. For a linear steady pressure gradient, $\partial p/\partial x$, the nondimensionalized rms acoustic condensation, $\Delta\rho'/\rho$, outside the shear layer should vary approximately as follows:

$$\frac{\Delta\rho'}{\rho} = \frac{\Delta p'}{\gamma p} \sim \frac{C(\mathbf{M})}{p}\,\frac{\partial p}{\partial x}\,\delta\Delta\mathbf{M}' \qquad (6)$$

Here $C(\mathbf{M})$ is a factor characterizing the wave-front geometry and $\Delta\mathbf{M}'$ a fluctuation in Mach number, representative of the layer (which is due to both vorticity and entropy fluctuations). The x-displacement of the fronts is accounted for by the term δ, the boundary-layer thickness in (6). Actually this term puts emphasis on the large-size eddies; i.e., on lower frequency fluctuations. (When the velocity of a perturbed wave front is integrated to obtain the displacement, the frequency f appears in the denominator, thus indeed favoring lower frequencies. Similar trends can be seen in the experimental Fig. 4 of Morkovin [6].) The mean pressure gradient in Equation (6) is approximately that which would exist in an inviscid flow for the same wall geometry (with imperfections) except for the softening effects due to the boundary layer, of the type discussed by Lighthill in connection with "upstream influence," [19]. When positive and negative pressure gradients follow each other, such as those caused by bumps and waviness on the wall, the softening effects appear stronger and may cause the net mean Δp to be some 30 per cent less than the inviscid Δp (Morkovin [20]).

Clearly, much of this type of sound is suppressed when the mean-flow nonuniformities due to contour imperfections are decreased. The efforts in keeping the wall smooth and continuously curving pay then double dividends. In some tunnels such measures would constitute the single major improvement of unsteady disturbances in the stream.

The continuous design-pressure gradient in the nozzle, however, will always remain and will therefore contribute to sound in accordance with Equation (6). It would appear promising to lengthen the expansion nozzle since $\partial p/\partial x$ would decrease proportionately, while the increase in δ would probably be compensated by a decrease in $\Delta\mathbf{M}'$. However, the mean Mach line through a fixed point in the test section would now pass through the boundary layer more times between the throat and the point in question. The sound generated by diffraction of a given mean pressure gradient at two successive passages through the boundary layer would be largely uncorrelated so that the rms amplitude would rise by a factor of $\sqrt{2}$ rather than 2. If, furthermore, the intensity of the unsteady plus-minus pressure waves were damped upon each reflection from the wall, there could actually be an advantage in lengthening the nozzle. Since it also is easier to avoid or to polish away the offending waves and bumps for contours which are more gradual, a longer nozzle could well be helpful in decreasing the sound from "shivering Mach waves."

Hot-wire traverses in the JHU tunnel at $\mathbf{M}_2$ of 1.76 have not disclosed any isolated shivering Mach waves associated with contour nonuniformities (other than those produced on purpose). This fortunate circumstance probably stems from several construction features. Perhaps it is well to conclude the discussion with description of these features from an unavailable 1950 report by L. T. Miller:

[10] Recent unpublished hot-wire measurements by J. Laufer and T. Vrebalovich in the 18 × 20-in. and 12 × 12-in. tunnels of the Jet Propulsion Laboratory of the California Institute of Technology indicate that the radiated sound intensity decreases [!] as the Reynolds number per inch increases at constant Mach number. Furthermore, for a given Reynolds number per inch, the measured sound intensity increases as the square of the Mach number and tends to dominate other free-stream disturbances.

[11] Lighthill suspects a similar decrease in jets [14]. It would explain the disagreement of experiments with the dimensional predictions, which assume u_2' in a fixed proportion to U_2 as U_2 varies.

[12] Schubauer [18], p. 18.

"The nozzle contour is formed by two 1/4-in. brass plates which were warped to the approximate basic contour and then filed and lapped to compensate for secondary bending. Each plate is positioned by an end block and 84 jack screws arranged in groups of three across the nozzle width. . . . The jack screws have a differential adjustment of 0.0035 in./rev through the use of an 8-36 and 10-32 thread. Coarse adjustment is provided by the 10-32 screw. The jack screws are attached to the contour plate by threading into a tapped hole 1/8 inch deep. Tests of this attachment method showed that the combination of tapped hole and attaching stud avoided the production of local flats[13] on the contour surface since it maintained the local stiffness of the plate approximately at its original value."

Removable windows extend from upstream of the throat to the end of the test section without joints. They also provide ready accessibility to the nozzle region. In particular, the final adjustment of the jack screws was carried out optically; reflections of a line light source from the nozzle contour were viewed and the screws adjusted until no distortion of the deflections due to waviness was observable.

Sound From Wall Vibrations

Most supersonic tunnels have a construction at least as rugged as the one just described, as required by the criterion of very small deflections under load. One would then expect that the sound radiated into the tunnel by unsteady lateral deflections of the walls would be considerably smaller than the sound radiated into fuselages of high-speed aircraft. Assessments of this sound, (category (*d*) of Fig. 1, and of Morkovin [6]) along the lines of Ribner [21] and Corcos and Liepmann [22], confirm these expectations and indicate a level of 70–95 db for the JHU tunnel from this source depending on particular assumptions.[14] The main factors which limit inward radiation from the walls are (*a*) relatively large thickness of the wall, (*b*) the very low air density near the wall, (*c*) the relatively high density of the wall material, and (*d*) the relative thinness of the boundary layer which governs the scale of the pressure fluctuations.

One observes also that the same wall undulations must give rise to pressure fluctuations outside the tunnel, which in the immediate vicinity of the walls are not radically smaller than their counterparts inside the tunnel. Since pressure fluctuation levels from all sources just next to the wall or windows of tunnels seldom exceed 90 db, the sound of category (*d*) inside should not be expected to reach 110 db. Unless it were concentrated in a critical frequency band, its effect can be neglected in comparison with the boundary-layer sound in the sense of Lighthill and with the shivering Mach waves.

Conclusions

Mean-flow nonuniformities in supersonic tunnels apparently can be made sufficiently small by standard techniques. A large ratio of the settling-chamber area to the area of the sonic throat decreases effectively those mean Mach-number nonuniformities which come from upstream of the throat. Great care in keeping nozzle contours continuously curving without bumps or waviness minimizes not only the mean-disturbance wave pattern seen in many schlieren photographs, but also the unsteady, often dominating, sound level from shivering Mach waves.

Supersonic turbulence (vorticity fluctuation) is effectively suppressed by a large contraction ratio.

Entropy (temperature) fluctuations can be reduced by matching mean temperatures at any duct junctures and by providing "long passage time" from such junctures to the test section. In particular, a low-velocity settling chamber with graduated screens to decrease the effective scale of the temperature nonuniformities is thought effective.

In considering the effects of free-stream disturbances, their spectral distribution may be relevant, for instance, in connection with the excitation of Tollmien-Schlichting waves. Vorticity and entropy fluctuations will not be important in the frequency range above 8 kc, Morkovin [6], because they are generated in low-speed passages and because the high-frequency components decay very rapidly. The sound generated in the supersonic section, however, will have frequencies characteristic of thin high-speed layers; i.e., up to 60 kc and higher.

The offending sound in the supersonic section is generated in the wall boundary layer: by surface dipole and volume-quadrupole distributions and by unsteady displacement of mean pressure gradients causing the shivering Mach waves. This sound is very difficult to measure experimentally or to predict theoretically. Furthermore, it appears that little can be done to reduce its level appreciably (except in tunnels with contour nonuniformities). One could (*a*) attempt to change the boundary-layer thickness without changing nozzle geometry, (*b*) seek an optimum nozzle length. In either case there appear to be compensating trends.

It is important to keep in mind, however, that the residual sound level, as large as it may be, may not affect the experimental objectives in the tunnels. It is probably irrelevant except in transition studies.

[13] Which plague most flexible-wall tunnels.

[14] Note that experience of JHU as well as calculations, based on Mair's estimates [23], indicate that Mach waves just observable by sensitive schlieren apparatus have an a-c component, which corresponds to a sound intensity of 120 to 130 db.

References

1 J. T. Kenney and L. M. Webb, "A Summary of the Techniques of Variable Mach Number Supersonic Wind Tunnel Nozzle Design," AGARDograph No. 3, NATO, October, 1954.

2 R. E. Meyer, "Perturbations of Supersonic Nozzle Flows," *Aeronautical Quarterly*, vol. 7, February, 1956 pp. 71–84.

3 W. N. MacDermott, "The Correction of Flexible Plate Supersonic Nozzle Contours by Influence Methods," *Journal of the Aeronautical Sciences*, vol. 22, May, 1955, pp. 289–296.

4 L. S. G. Kovasznay, "Turbulence in Supersonic Flow," *Journal of the Aeronautical Sciences*, vol. 20, October, 1953, pp. 657–674.

5 M. V. Morkovin, "Fluctuations and Hot-Wire Anemometry in Compressible Flows," AGARDograph No. 24, NATO, Nov., 1956, 102 pp.

6 M. V. Morkovin, "On Transition Experiments at Moderate Supersonic Speeds," *Journal of the Aeronautical Sciences*, vol. 24, July, 1957, pp. 480–486.

7 H. S. Ribner and M. Tucker, "Spectrum of Turbulence in a Contracting Stream," NACA Technical Report No. 1113, originally Technical Note No. 2606, 1952.

8 F. K. Moore, "Passage of Flow Disturbances Through a Duct Containing Screens, Shocks, or Contractions," Proceedings of Third Midwestern Conference on Fluid Mechanics, University of Minnesota, March, 1953.

9 M. S. Uberoi, "Effect of Wind-Tunnel Contraction on Free-Stream Turbulence," *Journal of the Aeronautical Sciences*, vol. 23, August, 1956, pp. 754–764.

10 J. Lukasiewicz, "Elimination of Flow Instability in Two High-Speed Wind Tunnels by Means of High-Drag Screens," National Aeronautical Establishment, Canada, Laboratory Report No. LR-83, November, 1953.

11 S. Corrsin, "Effect of Wind-Tunnel Nozzle on Steady-Flow Nonuniformities," *Journal of the Aeronautical Sciences*, vol. 19, February, 1952.

12 A. A. Townsend, "The Structure of Turbulent Shear Flow," Cambridge University Press, 1956.

13 M. J. Lighthill, "On Sound Generated Aerodynamically, Part I: General Theory," *Proceedings of the Royal Society*, series A, vol. 211, 1952, pp. 564–587.

14 M. J. Lighthill, "Part II: Turbulence as a Source of Sound," *Proceedings of the Royal Society*, series A, vol. 222, 1954, pp. 1–32.

15 M. J. Lighthill, "On the Energy Scattered From the Interaction of Turbulence With Sound or Shock Waves," *Proceedings of the Cambridge Philosophical Society*, vol. 49, part 3, 1953, pp. 531–551.

16 N. Curle, "The Influence of Solid Boundaries Upon Aerodynamic Sound," *Proceedings of the Royal Society*, series A, vol. 231, 1955, pp. 505–514.

17 M. V. Morkovin, "Effects of High Acceleration on a Turbulent Supersonic Shear Layer," Proceedings, Heat Transfer and Fluid Mechanics Institute, University of California, Los Angeles, Calif., June, 1955.

18 G. B. Schubauer, "Turbulence Processes as Observed in Boundary Layer and Pipe," *Journal of Applied Physics*, vol. 25, 1954, pp. 188–196.

19 M. J. Lighthill, "On Boundary Layers and Upstream Influence in Supersonic Flows Without Separation, "*Proceedings of the Royal Society*, series A, vol. 217, 1953, p. 478.

20 M. V. Morkovin, Critical Review No. 1223 of reference [3] in *Applied Mechanics Reviews*, vol. 9, April, 1956.

21 H. S. Ribner, "Boundary-Layer-Induced Noise in the Interior of Aircraft," Report No. 37, University of Toronto, Institute of Aerophysics, April, 1956.

22 G. M. Corcos and H. W. Liepmann, "On the Contribution of Turbulent Boundary Layers to the Noise Inside a Fuselage," NACA Technical Memorandum No. 1420, December, 1956.

23 W. A. Mair, "The Sensitivity and Range Required in a Toepler Schlieren Apparatus for Photography of High-Speed Air Flow," *Aeronautical Quarterly*, vol. 4, August, 1952, pp. 19–54.

24 A. Kistler, "Turbulent Boundary Layer Fluctuations at Supersonic Velocities," Ball. Res. Lab Report 1052, 1958, Aberdeen Proving Grounds, Md.

Velocity and Temperature Fluctuation Measurements in a Turbulent Boundary Layer Downstream of a Stepwise Discontinuity in Wall Temperature[1]

D. S. JOHNSON

Research Assistant,
Department of Aeronautics,
The Johns Hopkins University,
Baltimore, Md.
Currently, Member of
Technical Staff,
Bell Telephone Laboratories, Inc.,
Whippany, N. J.

Results are presented of an experimental investigation of the coexisting thermal and velocity fluctuation fields in a turbulent boundary layer downstream of a small stepwise discontinuity in wall temperature. The statistical behaviors of several relevant fluctuating quantities have been obtained at a typical cross section of the boundary layer in the region where the thermal boundary layer has not yet reached the free stream. The instantaneous surface of demarcation between heated and unheated fluid was found to be sharp and distinct at all points, resulting in intermittent temperature fluctuation signals well within the fully turbulent region of the momentum boundary layer. From the measurements at one section, the balances of turbulent kinetic energy and of turbulent temperature fluctuations across the boundary layer have been evaluated. In addition, the distribution of the local turbulent Prandtl number (ratio of the turbulent diffusivities of momentum and heat) through the boundary layer has been obtained; it is not constant and varies between limits of 0.8 and 1.2.

Introduction

CONVECTIVE heat transfer through a turbulent boundary layer is a specific case of the general phenomenon of turbulence and turbulent fluid flows. No theoretical solution has been obtained for such flows, but their occurrence in nature and technology is so frequent that it has been necessary to learn as much as possible about them. This has led to a great number of experimental studies, some of which have resulted in technically useful empirical or semiempirical analyses. The concept of isotropic turbulence and the concomitant accent upon the statistical nature of turbulent motion, together with the introduction of the hot-wire anemometer as an experimental tool, considerably increased the depth of such studies.

The results presented here were obtained in the course of an experimental study of the velocity and thermal fields in a turbulent boundary layer immediately downstream of a stepwise discontinuity in wall temperature. As an aid in the interpretation of results, the number of controlling factors was reduced by imposing simple, reproducible boundary conditions and by restricting flow velocities to values low enough to permit neglecting the effects of compressibility. In particular, it was desired that the dynamically significant properties of the working fluid be unaffected, within the limits of experimental accuracy, by the addition of heat.[2] Such a restriction has the advantage of simplifying the problem to one involving an existing "known" flow with the transfer process simply superimposed. Furthermore, since

[1] Based on part of a dissertation submitted to The Johns Hopkins University in August, 1955, in conformity with the requirements for the degree of Doctor of Engineering. The work was supported by the Office of Scientific Research, Air Research and Development Command, under Contract AF 18 (600)-671.

Contributed by the Applied Mechanics Division and presented at the Annual Meeting, November 30–December 5, 1958, New York, N. Y., of THE AMERICAN SOCIETY OF MECHANICAL ENGINEERS.

Discussion of this paper should be addressed to the Secretary, ASME, 29 West 39th Street, New York, N. Y., and will be accepted until October 10, 1959, for publication at a later date. Discussion received after the closing date will be returned.

NOTE: Statements and opinions advanced in papers are to be understood as individual expressions of their authors and not those of the Society. Manuscript received by ASME Applied Mechanics Division, May 9, 1958. Paper No. 58—A-81.

[2] This implies a relatively small value of a parameter such as $(T_M - T_0)/T_0$, where T_M is the maximum mean temperature encountered and T_0 is a reference temperature such as that of the ambient or free stream.

Nomenclature

c_p = specific heat at constant pressure

$F_\xi \equiv \overline{\xi^4}/(\overline{\xi^2})^2$, flattening factor of fluctuating quantity ξ

$f(Y)$, $g(Y)$ = two-point turbulent velocity correlation coefficients—see equations (14) and (15)

k = thermal conductivity

L, L_f = integral scales of turbulent velocity field—see equations (14) and (15)

l = microscale of turbulent temperature field

$m(Y)$ = two-point turbulent temperature correlation coefficient—see equation (17)

P = instantaneous value of static pressure

Pe = Péclet number

p = instantaneous value of static pressure fluctuation

Q = heat flux per unit area

$q^2 \equiv \overline{u^2} + \overline{v^2} + \overline{w^2}$

R_a = Reynolds number formed using length a

$R_{ab} \equiv \overline{ab}/a'b'$, coefficient of correlation between fluctuating quantities a and b

$R_{ab^2} \equiv \overline{ab^2}/a'\overline{b^2}$, triple correlation coefficient

$S_\xi \equiv \overline{\xi^3}/(\overline{\xi^2})^{3/2}$, skewness of fluctuating quantity

Sc = Schmidt number

$Sc_T \equiv \epsilon_M/\epsilon_W$, turbulent Schmidt number

(*Continued on next page*)

the "contaminant" (heat) does not affect the turbulent motion which transports it, measurements of appropriate properties of the contaminant through the flow give further information about the undisturbed turbulent motion itself.

Previous measurements of heat transfer in a turbulent boundary layer were usually made to obtain heat-transfer data and hence have not included detailed information on the fluctuation fields. However, certain of these have reported some results which are comparable with a portion of the results reported here; detailed comparisons are made later in connection with the particular quantities involved. The only other known turbulent-boundary-layer measurements generally similar to those of the present investigation are those of Nicholl which are described briefly by Batchelor [1].[2] The object of these, however, was to study the effect on the turbulent motion of rather strong heating or cooling of the wall, a condition avoided as far as possible in the present work.

The paper presents results of an experimental investigation of the velocity and temperature fluctuation fields occurring when the temperature of the wall on which a turbulent boundary layer has formed is given a stepwise increase. The physical situation studied is sketched in Fig. 1. With the experimental configuration used, the heated wall was not long enough for the thermal boundary layer to grow out to the momentum-free stream. Results of measurements of the distribution of mean properties and heat-transfer coefficients for this same set of conditions have been reported elsewhere [2].

[2] Numbers in brackets designate References at end of paper.

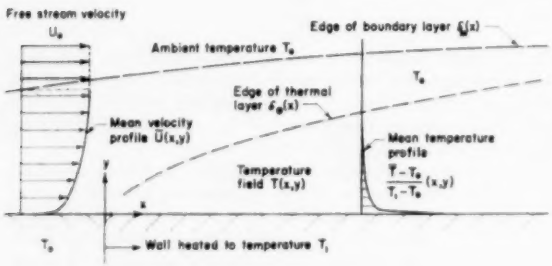

Fig. 1 Sketch of velocity and temperature fields

Pertinent Analytical Relations

Turbulent-Energy Equation. In Cartesian co-ordinates, the turbulent-energy equation can be expressed as

$$\frac{\partial \overline{q^2}}{\partial t} + \bar{U}_k \frac{\partial \overline{q^2}}{\partial x_k} = -2\overline{u_i u_j}\frac{\partial \bar{U}_i}{\partial x_j} - \frac{\partial}{\partial x_m}(\overline{u_m q^2}) - \frac{2}{\rho}\frac{\partial}{\partial x_k}(\overline{pu_k}) + \nu \frac{\partial^2 \overline{q^2}}{\partial x_i \partial x_k} - 2\nu \overline{\left(\frac{\partial u_i}{\partial x_j}\right)\left(\frac{\partial u_i}{\partial x_j}\right)} \quad (1)$$

where $q^2 = u_k u_k$ and the Reynolds restriction,

$$U_i(t) = \bar{U}_i + u_i(t);\ P(t) = \bar{P} + p(t);\ \bar{u}_i = \bar{p} \equiv 0 \quad (2)$$

has been applied.[4] Equation (1) is a relation governing mean turbulent kinetic energy and represents the balance existing at a point among the processes of production, transfer, and dissipation. For a two-dimensional, steady boundary layer with $\partial \bar{P}/\partial x = 0$ and axes oriented as in Fig. 1, equation (1) reduces to

$$\bar{U}\frac{\partial \overline{q^2}}{\partial x} + \bar{V}\frac{\partial \overline{q^2}}{\partial y} = -2\overline{uv}\frac{\partial \bar{U}}{\partial y} - \frac{\partial}{\partial y}(\overline{vq^2}) - \frac{2}{\rho}\frac{\partial}{\partial y}(\overline{pv}) + \nu \frac{\partial^2 \overline{q^2}}{\partial y^2} - 2\nu \overline{\left(\frac{\partial u_i}{\partial x_j}\right)\left(\frac{\partial u_i}{\partial x_j}\right)} \quad (3)$$

The terms on the left side of this equation represent convection of mean turbulent kinetic energy by the mean flow and those on the right side are, in order, production of turbulent energy from the mean motion, transport by the turbulent motion (sometimes called turbulent convection or diffusion), pressure work done in turbulent transport (alternatively denoted "pressure diffusion"), and (the last two terms together) energy changes due to viscous transport and dissipation [3].

In the case of isotropic turbulence, the viscous effect is only dissipative and can be written in Taylor's form

$$-10\nu \frac{\overline{q^2}}{\lambda^2} \quad (4)$$

[4] A repeated index indicates summation.

Nomenclature

T = absolute temperature
$T^* \equiv Q_1/\rho c_p U_*$, friction temperature
t = time
U, V, W = instantaneous value of velocity components in direction of x, y, z-axes, respectively
$U_* \equiv (\tau_1/\rho)^{1/2}$, friction velocity
u, v, w = instantaneous values of turbulent velocity fluctuations in direction of x, y, z, respectively
x, y, z = co-ordinate axes
x = distance downstream of leading edge of heated plate
y = distance from wall
z = distance from tunnel center line
Y = distance between two points used to define f, g, and m
$\alpha \equiv k/\rho c_p$, thermal diffusivity
γ = intermittency factor for u velocity fluctuations
γ_θ = intermittency factor for temperature fluctuations
$\delta_c \equiv \int_0^\infty \frac{\bar{U}}{U_0}\left(\frac{\bar{T}-T_0}{T_1-T_0}\right)dy$, convection thickness of thermal layer
δ_θ = geometric thickness of thermal layer
δ_m = geometric thickness of momentum boundary layer
$\delta^{**} \equiv \int_0^\infty \frac{\bar{U}}{U_0}\left(1-\frac{\bar{U}}{U_0}\right)dy$, momentum thickness of momentum boundary layer
$\epsilon_M, \epsilon_H, \epsilon_W$ = turbulent diffusivity for momentum, heat and mass, respectively
ϑ = instantaneous value of temperature fluctuation
Λ = integral scale of temperature fluctuation field—see equation (16)
λ = microscale of turbulent velocity field based on $g(Y)$
λ_f = microscale of turbulent velocity field based on $f(Y)$
μ = dynamic viscosity
$\nu \equiv \mu/\rho$, kinematic viscosity
ρ = density
$\sigma \equiv \mu c_p/k$, Prandtl number
$\sigma_T \equiv \epsilon_M/\epsilon_H$, turbulent Prandtl number
τ = shearing stress

Notation

$(\,)_i$, refers to ith co-ordinate axis (Cartesian tensor notation)
$(\,)_0$, free-stream condition
$(\,)_1$, condition at wall
$(\,)' \equiv [\overline{(\,)^2}]^{1/2}$, root-mean-square value
$\overline{(\,)}$, time (or ensemble) average; i.e., mean value

where λ is the "microscale" defined by Taylor [4] and is a length characterizing the dissipative eddies in isotropic turbulence. Kolmogoroff's theory of "local isotropy" [5] states that, for sufficiently large Reynolds number of the turbulence (e.g., $R_\lambda \equiv u'\lambda/\nu$), the small-eddy structure of a shear flow may be isotropic. Since large-Reynolds-number dissipation occurs chiefly in the small eddies, it is often assumed that at very high R_λ the dissipation rate in shear flow is approximated by expression (4). For fixed R_λ, this estimate may be expected to be worse in regions of higher shear; e.g., near the wall in the boundary layer. Also, it may not apply in the intermittent outer region of the layer. Some of these matters have been examined by Klebanoff [6] and Uberoi [7].

Turbulent-Temperature-Fluctuation Equation. The temperature fluctuation equation is derived from the mean heat-transfer equation by a procedure analogous to that leading to the turbulent-energy equation from the Navier-Stokes equations. In Cartesian co-ordinates, it is written as [8, 9]

$$\frac{\partial \overline{\vartheta^2}}{\partial t} + U_k \frac{\partial \overline{\vartheta^2}}{\partial x_k} = -2\overline{u_m \vartheta} \frac{\partial T}{\partial x_m} - \frac{\partial}{\partial x_i}(\overline{u_i \vartheta^2}) + \alpha \nabla^2 \overline{\vartheta^2} - 2\alpha \overline{\left(\frac{\partial \vartheta}{\partial x_i}\right)\left(\frac{\partial \vartheta}{\partial x_i}\right)} \quad (5)$$

where a Reynolds restriction has been assumed for the temperature as well as the velocity:

$$T(t) = \bar{T} + \vartheta(t);\ U_i(t) = \bar{U}_i + u_i(t);\ \bar{\vartheta} = \bar{u}_i \equiv 0 \quad (6$$

Although this equation resembles (3), there is no term corresponding to the pressure-velocity correlation. In the turbulent boundary layer with steady two-dimensional mean flow, equation (5) reduces to

$$U \frac{\partial \overline{\vartheta^2}}{\partial x} + V \frac{\partial \overline{\vartheta^2}}{\partial y} = -2\overline{v\vartheta} \frac{\partial T}{\partial y} - \frac{\partial}{\partial y}(\overline{v\vartheta^2}) + \alpha \frac{\partial^2 \overline{\vartheta^2}}{\partial y^2} - 2\alpha \overline{\left(\frac{\partial \vartheta}{\partial x_i}\right)\left(\frac{\partial \vartheta}{\partial x_i}\right)} \quad (7)$$

Like the turbulent-energy equation, this expresses the balance at a point among convection, production, and molecular effects on the mean-squared value of the turbulent temperature fluctuations. The terms on the left side of the equation represent mean flow convection; the first two on the right side correspond to the production of $\overline{\vartheta^2}$ from the mean temperature field and the turbulent convection of $\overline{\vartheta^2}$, respectively. The last two terms together represent the combined effects of molecular transport and molecular "smearing" (analogous to the dissipation of turbulent kinetic energy to heat).

When the velocity and temperature fluctuations are isotropic, it is convenient to introduce a temperature microscale l defined in a manner similar to the velocity microscale λ. For the isotropic case, the conductive terms in equation (7) reduce to [10]

$$-12\alpha \frac{\overline{\vartheta^2}}{l^2} \quad (8)$$

Hence if an assumption of locally isotropic conductive smearing of the temperature field is made [9], this expression can be used to approximate the final term of equation (7). A requirement for this substitution is the existence of a sufficiently large turbulence Péclet number, $u'l/\alpha$.

Turbulent Prandtl Number. In the study of turbulent shear flow, it has sometimes been assumed that the momentum transport (shear stress) due to the turbulent motion can be expressed in the same mathematical form as that in laminar flow; this led to the introduction of a "turbulent (or eddy) viscosity" ϵ_M which, for two-dimensional boundary-layer-type flow, is defined by

$$-\overline{uv} \equiv \epsilon_M \frac{\partial U}{\partial y} \quad (9)[5]$$

The same idea has been applied to scalar transport processes; thus the turbulent diffusivity (or "exchange coefficient") for heat transfer in the boundary layer is given by

$$-\overline{v\vartheta} \equiv \epsilon_H \frac{\partial T}{\partial y} \quad (10)$$

The turbulent diffusivities ϵ_M and ϵ_H should not be expected to be independent of position in the flow.

Just as the molecular (fluid) Prandtl number is a measure of the relative magnitudes of momentum and heat diffusivity in laminar flow, an analogous "turbulent Prandtl number" has been formed as

$$\sigma_T \equiv \epsilon_M/\epsilon_H \quad (11)[6]$$

to express the relative magnitudes of the local turbulent diffusivities. Its magnitude can be considered as a characteristic of a given turbulent transfer configuration; comparison of values from different experiments or configurations is of interest. Using equations (9) and (10), the local turbulent Prandtl number in the boundary layer is given by

$$\sigma_T = \frac{\overline{uv}}{\overline{v\vartheta}} \frac{\left(\frac{\partial T}{\partial y}\right)}{\left(\frac{\partial U}{\partial y}\right)} \quad (12)$$

For a turbulent mass-transfer process, where the Schmidt number Sc serves the same function as the Prandtl number in heat transfer, a "turbulent Schmidt number" corresponding to σ_T would be

$$\mathrm{Sc}_T \equiv \epsilon_M/\epsilon_W \quad (13)$$

where ϵ_M is the turbulent diffusivity of momentum and ϵ_W that of mass. Since the heat-transfer and mass-transfer equations have the same form for very small contaminant levels (such that physical properties are constant), it is to be expected that under analogous boundary conditions the two transport phenomena will be analogous. In fact, for such "dilute" cases, equality of fluid Prandtl and Schmidt numbers should lead to identical turbulent transport problems for heat and mass.

In jets, the turbulent transport rates of these scalar contaminants have been found experimentally to be equal and, in addition, quite independent of molecular properties, at least for fluid Prandtl number about 0.7 and Schmidt number between 0.6 and 800 [13, 14].

Additional Quantities of Interest: (a) Intermittency. Intermittency is a measurement phenomenon associated with the boundary region between turbulent and nonturbulent fluid, such as at the outer edge of a turbulent boundary layer. In such a region, the flow recorded by an instrument at a fixed point alternates between turbulent and nonturbulent as the sharp but irregularly shaped boundary between the two types of flow is convected past. Corrsin and Kistler [15] have analyzed the properties associated with the turbulence intermittency at the edge of the boundary layer, jet, and wake. A convenient measure of intermittency at a point is the "intermittency factor" γ, which is the fraction of time during which the passing flow is turbulent.[7]

Since the turbulent velocity field is the chief agent in the turbu-

[5] Originally suggested by Boussinesq [11].

[6] The definition (11) is arbitrary; Reichardt [12] has defined a "generalized Prandtl number" which is σ/σ_T.

[7] This definition of γ is due to Townsend [16].

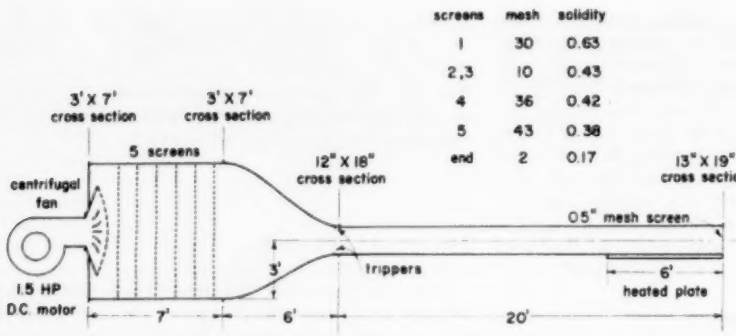

Fig. 2 Sketch of wind tunnel

lent transfer of a scalar property such as temperature or mass (away from the boundary, and with σ or Sc not $\ll 1$), it is plausible to expect that there will be intermittent regions associated with the fluctuation fields of these quantities as well. In particular, one would anticipate finding a region of temperature intermittency occurring at about the same location as that for the velocity in the case of fully developed heat transfer through a turbulent boundary layer. Such a phenomenon was noted for a warm jet in reference [15]. Similarities and differences between the two would be of interest.

Here we are concerned with the possible intermittent character of the temperature signal when the thermal boundary layer is still appreciably thinner than the momentum boundary layer.

(b) Integral Scales. In the statistical theory of isotropic turbulence, Taylor [4] defined lengths which are characteristic of the larger scale (low wave number) portion of the turbulent motion. For steady mean motion, these integral scales may be defined in terms of the two-point velocity correlations. For "transverse correlation," $g(Y)$, the parallel velocity components are normal to the line segment Y connecting the observation points:

$$g(Y) \equiv \frac{\overline{u_1 u_2}}{u_1' u_2'} \quad \text{and} \quad L \equiv \int_0^\infty g(Y)dY \tag{14}$$

For "longitudinal correlation," $f(Y)$, the velocity components are aligned with the vector $\bar{Y}$:

$$f(Y) \equiv \frac{\overline{v_1 v_2}}{v_1' v_2'} \quad \text{and} \quad L_f \equiv \int_0^\infty f(Y)dY \tag{15}$$

Corrsin [10] has defined the analogous thermal integral scale for the case of steady isotropic temperature fluctuations as

$$\Lambda \equiv \int_0^\infty m(Y)dy \tag{16}$$

where

$$m(Y) \equiv \frac{\overline{\vartheta_1 \vartheta_2}}{\vartheta_1' \vartheta_2'} \tag{17}$$

Here ϑ_1 and ϑ_2 are the simultaneous temperature fluctuations at two points separated by a distance Y.

Although integral scales are simply meaningful only in homogeneous fields, their association with large-scale structure (they may also be interpreted as an "average eddy size") makes them useful for order-of-magnitude comparisons among various flows and fields.

(c) Other Statistical Properties of Fluctuation Fields. Just as the integral scale and microscale are quantities characteristic of a given turbulent field, so other statistical properties can be informative even though they may not be specifically involved in the simplest governing equations of the field. Among these might be mentioned the skewness and the flattening factor of a fluctuation quantity; these are defined, respectively, as

$$S_\xi \equiv \frac{\overline{\xi^3}}{(\overline{\xi^2})^{3/2}} \tag{18}$$

and

$$F_\xi \equiv \frac{\overline{\xi^4}}{(\overline{\xi^2})^2} \tag{19}$$

where ξ is the fluctuating quantity. The former is particularly indicative of the probabilistic unsymmetry of ξ and hence is pertinent in any nonlinear stochastic phenomenon. The flattening factor is a measure of symmetrical peakedness of the probability, hence varying with intermittency.

Equipment and Measurement Procedures

The measurements reported here were made in the simple open-return, blowing-type wind tunnel sketched in Fig. 2. The walls and roof were adjusted to give a constant static pressure through the test section and all measurements were made at a free-stream air speed of 25 fps, at which condition the free-stream longitudinal turbulence level u'/U_0 is 0.07 per cent at the entrance to the test section.

Data were taken in the boundary layer along the last 6 ft of floor of the test section, where the boundary layer is between 4 and 5 in. thick. This portion of floor is "satin-finished" aluminum-alloy plate whose temperature can be raised as much as 35 deg C above ambient by means of electrical resistance coils directly beneath. The temperature distribution over the area of the plate is given by 25 copper-constantan thermocouple junctions whose voltages are measured with reference to a junction in the free stream ahead of the plate. The junctions in the plate are soft-soldered into brass plugs pressed into holes in the aluminum; after finishing, each junction is flush with the plate surface. Measurements were made with the plate heated 15 deg C above free-stream temperature; this gives a value of 0.05 for the parameter $(T_1 - T_0)/T_0$ and was chosen after comparing mean-velocity and longitudinal turbulence-level profiles at several overheats with those over the unheated plate. Some measurements were also made with the plate unheated, as noted later. At the plate temperature and flow velocity used, the thermal boundary layer did not grow at a rate sufficient to reach the free stream before the downstream end of the plate was reached.

Probes are positioned normal to the plate surface by a device similar to a vernier height gage; the zero reading for any traverse (made with the tunnel running) is obtained by measuring the distance between the probe and its reflection in the plate through a telescope having a reticle scale. The estimated accuracy of location is ± 0.0015 in. in the first inch of travel and ± 0.004 in. beyond the first inch.

The hot-wire anemometry equipment used is a duplicate of that described by Kovasznay [17] except for some physical rearrangements and minor circuit changes. The distributions of velocity

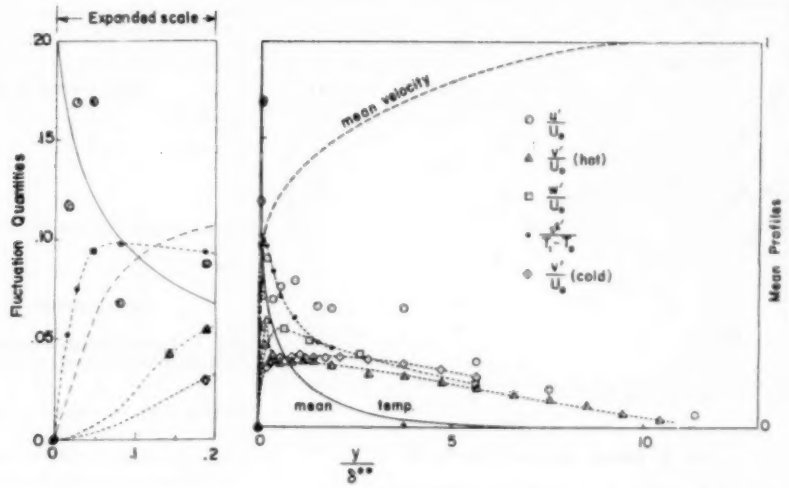

Fig. 3 Fluctuation levels

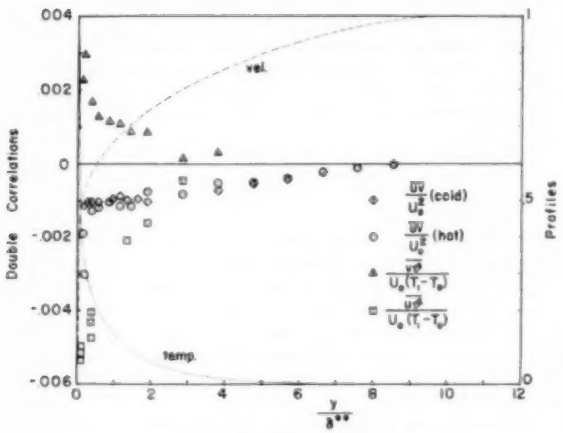

Fig. 4 Double correlations

and temperature fluctuation levels, pertinent correlations, and so on, were measured on the center line 47 in. from the leading edge of the heated plate. Where gradients in the direction of flow were required, additional data were obtained at 59 in.

All measurements were made with hot-wire anemometers; no length or wall-proximity corrections have been applied but results have been corrected for temperature loading according to the method given by Ruetenik.[8] Depending upon the quantity to be measured, a single-wire or two-wire ("X-meter") probe was used; the former were made with 0.0001 and 0.00005 in. nominal diameter platinum wires and the latter with 0.00015 in. nominal diameter tungsten wires. Wire lengths varied from 0.8 to 3 mm.

Details of the measurement procedures and of the special equipment and techniques utilized will not be given here; a full description is contained in reference [18]. It may be mentioned, however, that the distributions of some of the quantities involving the transverse velocity fluctuation component v were measured in both the "hot" and "cold" boundary layer (not including, of course, those quantities also containing the temperature fluctuation ϑ). Quantities containing both v and ϑ., i.e., $\overline{v\vartheta}$ and $\overline{v\vartheta^2}$, were measured with two separate probes—an X-meter for v and a single high-resistance wire for ϑ—spaced about 0.015 in. apart laterally. The intermittency factor γ was measured for both u-velocity and temperature fluctuations with the aid of an electronic circuit which passed pulses when the hot-wire probe indicated turbulent conditions. The total number of pulses passed in a given time interval is thus a measure of the intermittency factor.

Results of Measurements[9]

Fluctuation Levels and Double Correlations. The distributions of u'/U_0, v'/U_0, w'/U_0, and $\vartheta'/(T_1 - T_0)$ through the boundary layer at $x = 47$ in. are plotted in dimensionless form in Fig. 3; values of v'/U_0 from measurements in both the "hot" "and cold" boundary layer are included. Fig. 4 shows the variation of the double correlations $\overline{uv}/U_0^2$, $\overline{v\vartheta}/U_0(T_1 - T_0)$, and $\overline{u\vartheta}/U_0(T_1 - T_0)$ at the same location, and the corresponding correlation coefficients are plotted in Fig. 5. The extreme scatter in $R_{v\vartheta}$ for $y/\delta^{**} > 2$ is doubtless a result of the very low thermal signal-to-noise ratio. Two sets of values for $\overline{uv}/U_0^2$ and R_{uv} are given as in the case of v'/U_0. The values of $\overline{u\vartheta}/U_0(T_1 - T_0)$ and $R_{u\vartheta}$ represent the best mean among results of measurements by a single hot wire at several overheats and of estimating values from correlation diagrams obtained as time-exposure photographs of oscilloscope patterns.[10]

The quantities v'/U_0 and $\overline{uv}/U_0^2$ measured in the boundary layer over the unheated plate differ by more than normal experimental scatter from those obtained with the plate heated. This discrepancy is particularly apparent near the wall where there is an unusually sharp rise in the latter. The reason for the difference is not readily ascertained, but is probably due to experi-

[8] J. R. Ruetenik, "Investigation of Equilibrium Flow in a Slightly Divergent Channel," Report I-19, Department of Mechanical Engineering, The Johns Hopkins University, August, 1954, pp. 23–24, and Appendix III.

[9] The data have been plotted in dimensionless form, using U_0 and $(T_1 - T_0)$ to normalize the velocity and temperature fluctuations, respectively. It may be more appropriate to utilize the "friction velocity" $U_* \equiv (\tau_1/\rho)^{1/2}$ and "friction temperature" $T_* \equiv Q_1/\rho c_p U_*$ instead. These are analogous quantities and it has been found in studies of the distributions of mean properties in isothermal boundary layers that normalization with U_* eliminates certain effects of wall roughness and Reynolds number variation. (See, for example, F. H. Clauser, "Turbulent Boundary Layers in Adverse Pressure Gradients," *Journal of the Aeronautical Sciences*, vol. 21, 1954, pp. 91–108.) The values of U_*/U_0 and $T_*/(T_1 - T_0)$ applying to the data presented here are 0.037 and 0.076, respectively.

[10] S. Goldstein, editor, "Modern Developments in Fluid Dynamics," Oxford University Press, England, 1938, vol. I, pp. 269–270.

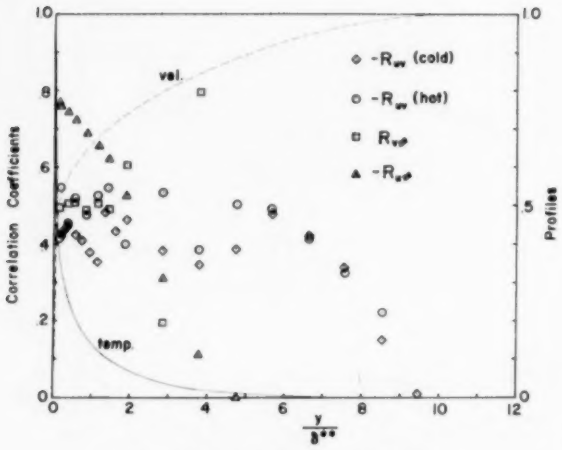

Fig. 5 Double correlation coefficients

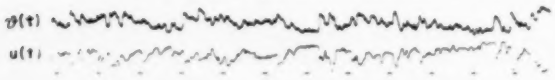

y = 0.075", Very high negative correlation, $R_{u\vartheta} = -0.8$

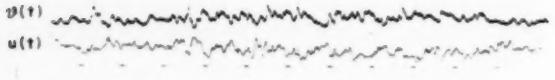

y = 0.8", $R_{u\vartheta} = -0.6$

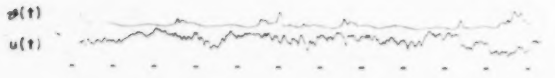

y = 2.2", Thermal intermittency in absense of velocity intermittency. ($\vartheta(t)$ signal uncompensated here)

Fig. 6 Simultaneous temperature and velocity fluctuations at three positions in boundary layer. Timing pulse = $^1/_{60}$ sec, instrument sensitivities such that approximate match in amplitudes; δ_m = 5 in., δ_ϑ = 3 in.

mental error. Some portion may perhaps be ascribed to the greater complexity of the measurements in the heated boundary layer as compared with the simple X-meter technique utilized in a flow without thermal effects. Furthermore, the values obtained in the cold layer are as consistent with the results of Klebanoff [6] as are the measurements of u'/U_0 in the heated layer. Consequently, the measurements of v'/U_0 and $\overline{uv}/U_0$ in the unheated boundary layer have been accepted as the more reliable ones.

Typical oscillograms of the simultaneous temperature and longitudinal velocity fluctuations at three distances from the wall are presented in Fig. 6. The high negative correlation between these two variables is quite evident at the point closest to the wall and it appears to decrease with distance from the wall, as indicated by the numerical data in Fig. 5.

A second fact revealed by the oscillograms is that the temperature fluctuations become intermittent as the edge of the thermal boundary layer is approached, even though the velocity field there is still fully turbulent.[11] This same occurrence was

[11] This phenomenon has been discovered independently by Nicholl; see Batchelor [1].

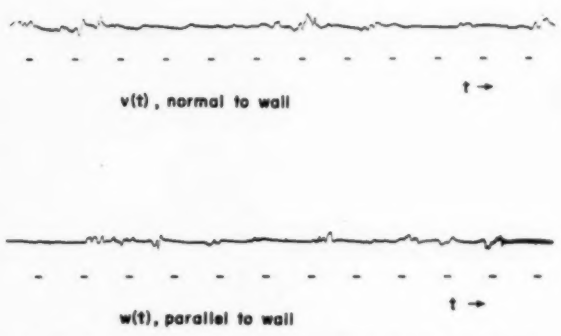

Fig. 7 Typical (nonsimultaneous) intermittent signals from lateral velocity fluctuations at y = 4.0 in. (δ_m = 5 in.)

observed over the entire length of the plate and, in all cases, the fluctuations in any turbulent "burst" were distinctly one-sided, i.e., positive with respect to the nonturbulent "base line."

Oscillograms showing the character of the v and w fluctuations in the intermittent region of the boundary layer also were obtained; these are given in Fig. 7.

Triple Correlations and Mean Cubes. The distributions of $\overline{vu^2}/U_0^3$, $\overline{v^3}/U_0^3$, and $\overline{vw^2}/U_0^3$ through the boundary layer are presented in Fig. 8 and those of $\overline{v\vartheta^2}/U_0(T_1 - T_0)^2$ and $\overline{\vartheta^3}/(T_1 - T_0)^3$, together with the skewness of ϑ, in Fig. 9. The corresponding correlation coefficients

$$R_{vu^2} \equiv \frac{\overline{vu^2}}{v'\overline{u^2}}, \quad R_{vw^2} \equiv \frac{\overline{vw^2}}{v'\overline{w^2}}, \quad R_{v\vartheta^2} \equiv \frac{\overline{v\vartheta^2}}{v'\overline{\vartheta^2}}$$

and the skewness of v are plotted in Fig. 10. The accuracy of determination of these quantities becomes less in the outer portion of the boundary layer where the fluctuation levels decrease. This fact is generally true in the measurement of fluctuating quantities, of course, but its effect is probably more pronounced in the case of a triple correlation where the end value involves relatively small differences between quantities independently subject to random error.

Microscales and Integral Scales. The longitudinal velocity and temperature microscales at x = 47 in. are plotted in Fig. 11. Results of measurements of the transverse correlations were too scattered to permit any reliable estimates of the transverse microscales to be made and hence no values are presented for these. Also indicated in Fig. 11 are the values obtained by Townsend [19] and Klebanoff [6] as estimated from their plots of results. These have been corrected for the differences between the Reynolds numbers of their flows and that of the present investigation (the latter is approximately 64,000 based on geometric thickness of the boundary layer).

For the case of isotropic temperature fluctuations in an isotropic velocity field, Corrsin [10] has given the value $\sqrt{1/\sigma}$ as an estimate for the ratio of microscales at a point. For air, with a value of 0.72 for σ, this ratio is 1.2. The ratio of measured microscales in the present case is of the order of 1.4 in the region where the temperature field is fully turbulent.

Longitudinal velocity integral scales through the boundary layer are shown in Fig. 12; single values for the transverse temperature and velocity integral scales at y = 0.5 in. are also plotted.

In the fluctuation fields studied here, the turbulent Reynolds number $R_{\lambda_f} \equiv u'\lambda_f/\nu$ and the turbulent Péclet number $u'l/\alpha$ are of the order of 160 and 90, respectively.

Intermittency Factors. The intermittency factors for both temperature and longitudinal velocity fluctuations as measured at x = 47 in. are plotted in Fig. 13(a); the occurrence of the zone of temperature intermittency within the fully turbulent velocity

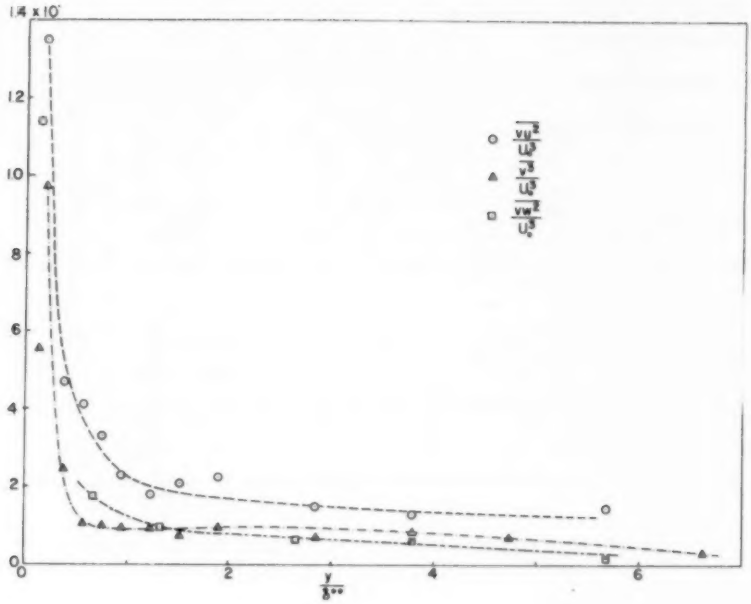

Fig. 8 Triple correlations and mean cubed velocity terms

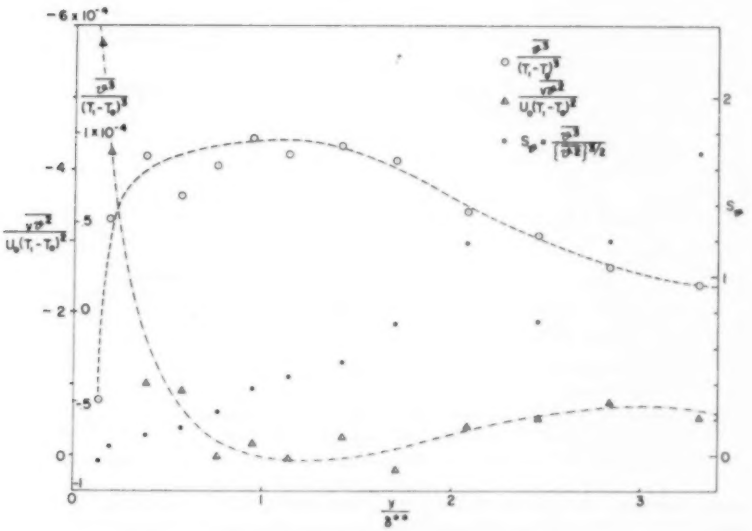

Fig. 9 Triple correlations and mean cubed thermal term, skewness of ϑ

field is quite evident. A comparison of the form of the two distributions of intermittency factor is provided by Fig. 13(*b*) where each has been plotted in terms of its appropriate dimensionless distance from the wall and zero shift has been applied to one scale to make the curves cross at about $\gamma = 0.5$. No similarity is evident in this case where the thermal boundary layer is not fully developed.

Corrsin and Kistler [15] found that the distribution of intermittency factor as a function of distance was Gaussian over most of the intermittent region in a boundary layer, jet, and wake. For the boundary layer, this was verified by Klebanoff [6]. Fig. 14 is a plot on Gaussian scale of γ and γ_ϑ as measured in the heated boundary layer; it is seen that the velocity intermittency is Gaussian within experimental accuracy, agreeing with the earlier findings. The temperature intermittency, however, is clearly non-Gaussian for the case studied.

Discussion of Results

Turbulent Shearing Stress and Turbulent Heat Transfer. It is pointed out in reference [2] that the distributions of turbulent shearing stress $\overline{uv}(y)$ and turbulent heat transfer $\overline{v\vartheta}(y)$ through the boundary layer can be calculated from measured distributions of mean velocity $\bar{U}(x, y)$ and mean temperature $\bar{T}(x, y)$. These calculations have been carried out and the results are compared with the directly measured quantities in Figs. 15 and 16. The agreement is much better for $\overline{v\vartheta}/U_0(T_1 - T_0)$ than for $\overline{uv}/U_0^2$, although there is a region of some disparity near the wall in the case of the former. The disagreement between measured and calculated values of $\overline{uv}/U_0^2$ is not immediately explainable. There is, however, some evidence that a slight deviation from two-dimensionality existed in the mean flow; this was felt to be a principal reason why the skin-friction coefficient at $x = 47$ in. did not have

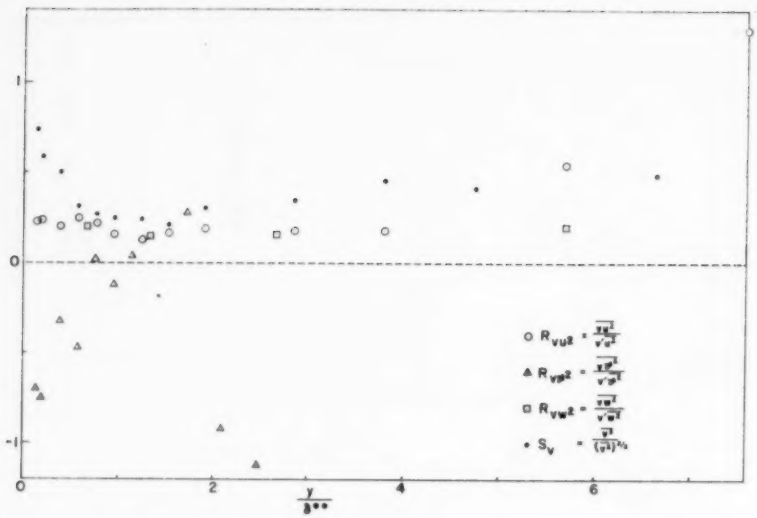

Fig. 10 Triple correlation coefficients, skewness of transverse velocity v

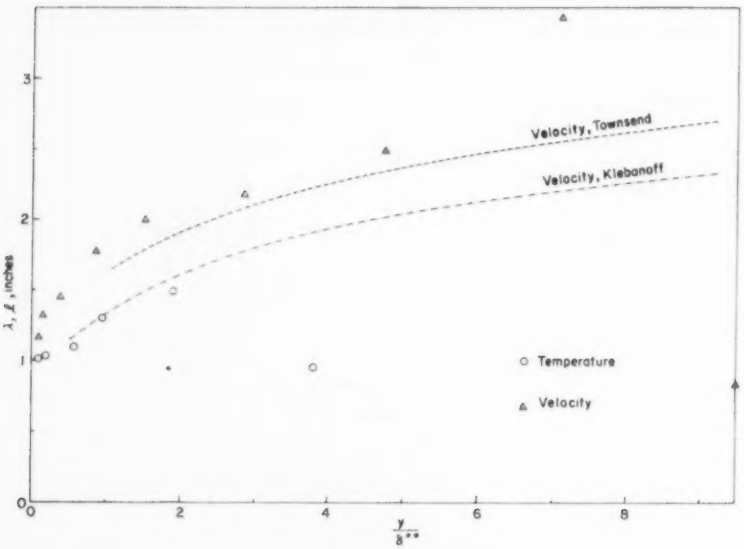

Fig. 11 Longitudinal microscales

about the same numerical value when determined by several independent methods. It is possible that the same condition which led to a rather wide variation in apparent skin-friction coefficient values also resulted in the difference between directly measured and calculated values of $\overline{uv}/U_0^2$. The same measured mean velocity distributions are involved in both determinations. It is also possible, of course, that experimental errors (measurement techniques, etc.) account for a portion of the disagreement in $\overline{uv}/U_0^2$.

Turbulent-Energy Balance. All the terms in the turbulent-energy equation (3) with the exception of that containing the pressure-velocity correlation can be evaluated from the experimental data if the isotropic form (4) is assumed for the dissipation. This has been done and the results are plotted in Fig. 17, where the net unbalance has been assigned to the pressure-diffusion term.

It should be noted that the substitution of the isotropic expression for the dissipation term was made knowing that this operation is not fully justified in the light of experimental investigations of various flows. Among these might be mentioned the results obtained by Klebanoff [6], Sandborn and Braun [20], and Uberoi [7] in the boundary layer, and by Laufer [21] in fully developed pipe flow. The isotropic expression for the dissipation term was used in the present work to obtain an estimate which would permit evaluation of the turbulent-energy equation without requiring the more extensive measurements necessary for more exact determination of the dissipation. These, while desirable, were not felt to be of primary importance in this initial investigation of the coexisting turbulent velocity and temperature fields.

Keeping in mind the approximation just noted, a comparison of Fig. 17 with the corresponding results of Townsend [19] and Klebanoff shows that there is agreement among the three sets of measurements as to the general behavior of the various terms in the turbulent-energy equation through the boundary layer. There are, however, differences in relative magnitude which are not readily explained. It is possible that Reynolds number effects could account for some of this, although the range of $R_{\delta^{**}}$ in the three cases is from about 50,000 (Townsend) to 74,000 (Kle-

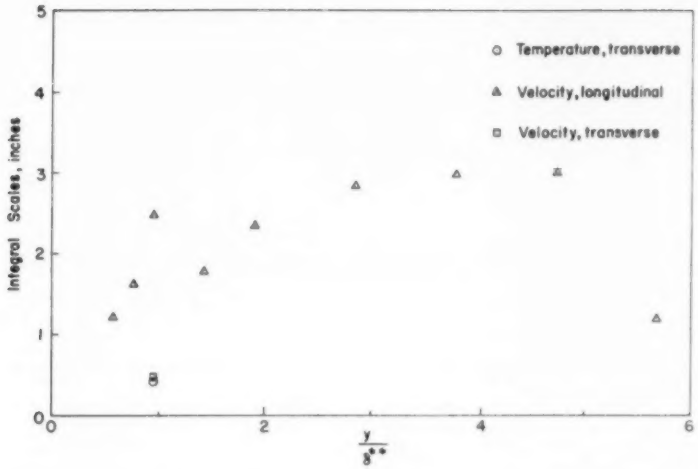

Fig. 12 Integral scales

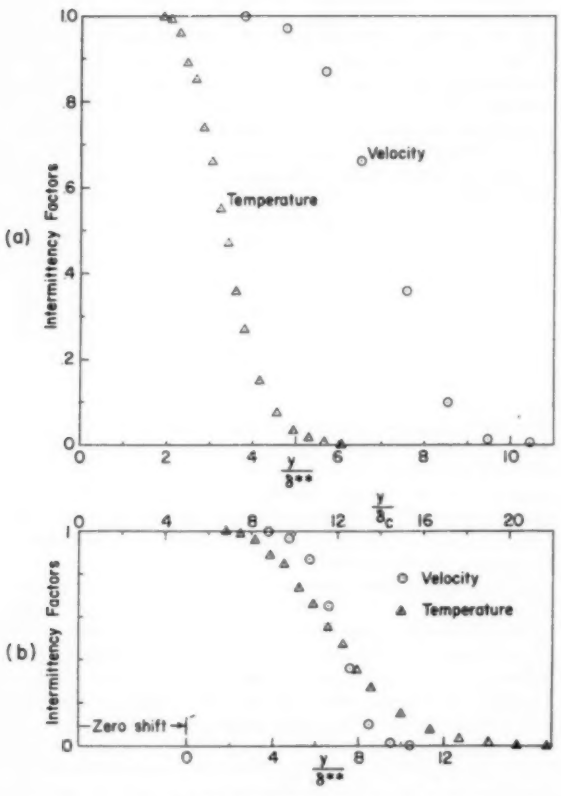

Fig. 13 Intermittency factors

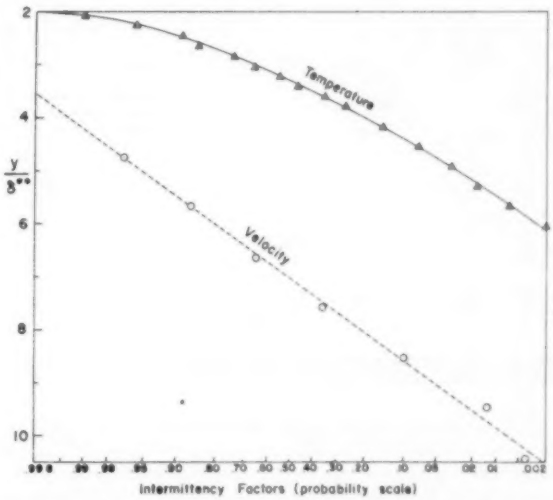

Fig. 14 Intermittency factors plotted on Gaussian probability scale

banoff) with the present measurements at some 64,000—certainly not an order-of-magnitude range. In this connection, it may be mentioned that Laufer's measurements in pipe flows at Reynolds numbers of 50,000 and 500,000, reference [21], did indicate some small increase in the magnitude of the turbulent convection term relative to production over that range. It is to be expected, however, that variations in experimental methods and accuracy will account for much of the discrepancy noted.

A more intensive investigation of the region immediately neighboring the wall, such as was done for pipe flow by Laufer and in part for the boundary layer by Klebanoff, would be of interest; this is especially so in view of the former's findings that the turbulent-convection and pressure diffusion terms reverse sign in that region.

Temperature-Fluctuation Balance. Results of measurements at $x = 47$ in. enable a complete evaluation of the turbulent temperature fluctuation equation (7) to be carried out across the thermal boundary layer at that point. The results are shown in Fig. 18, where the net unbalance has been indicated. Because the isotropic approximation of equation (8) was assumed for the computation of the "dissipation," it is not surprising that there should be an appreciable unbalance near the wall where there is least likelihood of the fluctuations being isotropic. An indication of the departure from isotropy in the simultaneous temperature and velocity fields is given by the value of the microscale ratio, l/λ_f, cited in the preceding (Results) section; this is of the order of 1.2 for isotropic conditions while the measured ratio is about 1.4. Through the middle of the thermal layer, however, the unbalance is of the order of the smallest term (the mean flow convection); only where all terms are of the same order of magnitude does it become larger than any. Since the accuracy of determination of the terms themselves is lowest in this region, such a result is not too surprising.

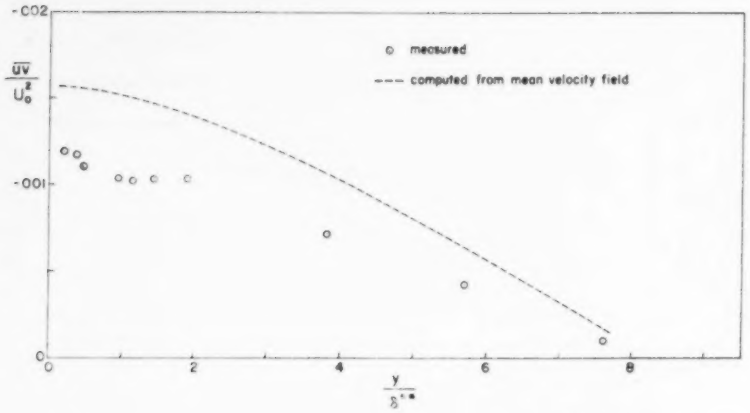

Fig. 15 Turbulent shearing stress as measured and as computed from mean velocity field

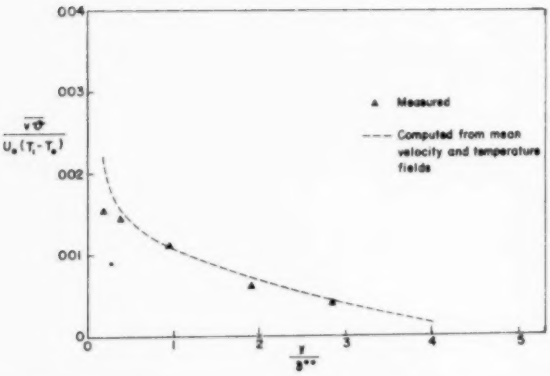

Fig. 16 Turbulent heat transfer as measured and as computed from mean velocity and temperature fields

The shapes and relative magnitudes of the various terms in the temperature-fluctuation equation, as plotted in Fig. 18, correspond fairly well with the analogous terms in the turbulent-energy equation, Fig. 17, with one exception: the turbulent convections in the two cases are of opposite sign. One would at first thought expect them to have the same "polarity," at least when the thermal layer is fully developed, but it is possible that the absence of term corresponding to the pressure-velocity correlation is an indication of a fundamental difference in the two fluctuation fields. Corrsin [8] has pointed out that it may therefore be more appropriate to compare the temperature fluctuation equation (more likely, the temperature-gradient fluctuation) with the equation which represents the balance of fluctuating vorticity. The sign difference also may be merely an indirect result of opposite local curvatures in the curves of $\overline{q^2}(y)$ and $\overline{\vartheta^2}(y)$; for a simple gradient transfer process, the sign of net influx by transport depends upon the sign of the second derivative of the contaminant distributions. Of course these convective terms cannot be regarded quantitatively as simple gradient transfer, but may be useful as a qualitative guide. Unfortunately, the experimental scatters in $\overline{q^2}(y)$ and $\overline{\vartheta^2}(y)$ are too great to confirm or deny this interpretation.

Turbulent Prandtl Number. The local turbulent Prandtl number, computed from the measured data according to equation (12), is plotted in Fig. 19. Although the flow studied was not fully developed as far as the thermal field is concerned, it may be that the distribution of σ_T in the region nearer the wall will be comparable with the results of similar measurements in other flows.

The most directly comparable data are those of Schwarz and Hoelscher [22] from measurements of the evaporation of water from the inner wall into a fully developed pipe flow at a Reynolds number, based on diameter, of 25,000. The boundary conditions in this flow were quite similar to those in the present investigation, viz., a fully developed shear flow with a stepwise discontinuity in wall conditions—dry to wet in their case. From measurements of the distribution of mean velocity and mean humidity, the turbulent Schmidt number Sc_T was computed according to equation (13) (using cylindrical co-ordinates). Assuming similarity of mass and temperature transfer processes, as discussed previously, their results should be comparable with the present work, at least in the region away from the center of the pipe where the flow is roughly similar to that in the boundary layer. In this portion of the flow, they obtained values of Sc_T between 1 and 2, as compared with limits of roughly 0.8 and 1.1 in the present case.

The data available on the measurements of Elias [23] in a turbulent boundary layer over a heated plate are not in a form permitting a reliable estimate of σ_T. Reichardt [24] estimates $1 > \sigma_T > 0.5$ through the boundary layer, based on this work, with the highest value reached at the wall and the lowest at the outer edge. He also concludes that an over-all mean value of σ_T (defined by an integral through the boundary layer) of 0.77 applies to heat transfer in both the boundary layer and fully developed pipe flow. Using a similarity solution of the heat-transfer equation, Davies [25] finds that Elias' measurements are best fitted by $\sigma_T = 1$, where σ_T is assumed beforehand to be constant through the boundary layer.

Spengos and Cermak [26] have reported measurements in a turbulent boundary layer over a heated plate; these covered a range of Reynolds numbers, based on geometric thickness, from about 23,000 to 65,000 (estimated from plotted results). The wall temperatures listed were 28 and 50 deg C above ambient. They find their results agree best with the solution obtained by Davies when a value of 1 is assumed for σ_T through the boundary layer. They note, however, that σ_T does not appear to be constant through the layer and estimate a variation from 0.1 near the wall to 0.2 at $1/3\ \delta_m$ and increasing beyond. It may be remarked that relatively high wall temperatures were used for these measurements and it is quite possible that buoyancy effects were relatively large, thus altering the velocity fluctuation field in the hot boundary layer compared to that in the "cold." The authors note that the magnitude of ϵ_M, as calculated from measurements of $\overline{uv}$ and $\partial\bar{U}/\partial y$, increased by a factor of 3 from the isothermal to the heated boundary layer even though the mean velocity profiles in the two cases were apparently the same.

A final comparison can be made with the results of measurements in fully developed pipe flow with the wall heated to a constant temperature as obtained by Seban and Shimazki [27]. They estimate the turbulent Prandtl number to be nonconstant

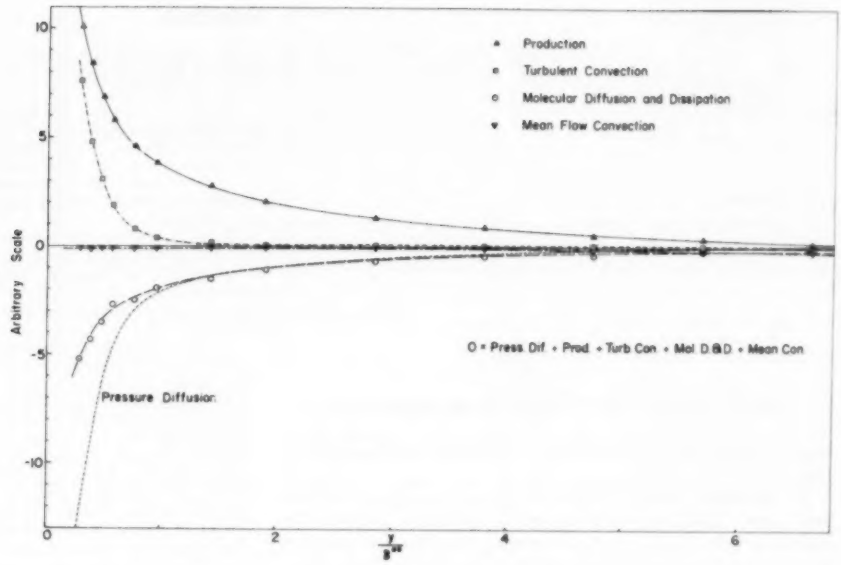

Fig. 17(a) Turbulent energy balance across boundary layer

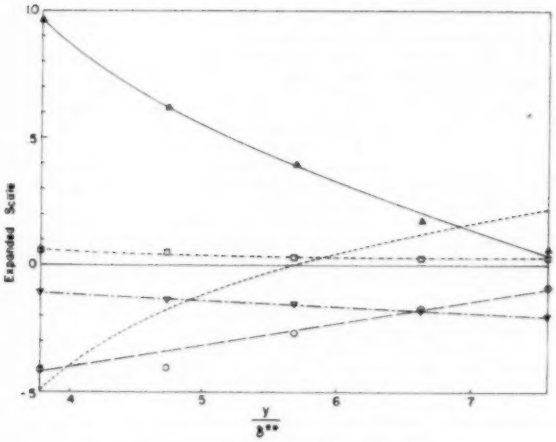

Fig. 17(b) Outer portion of boundary layer

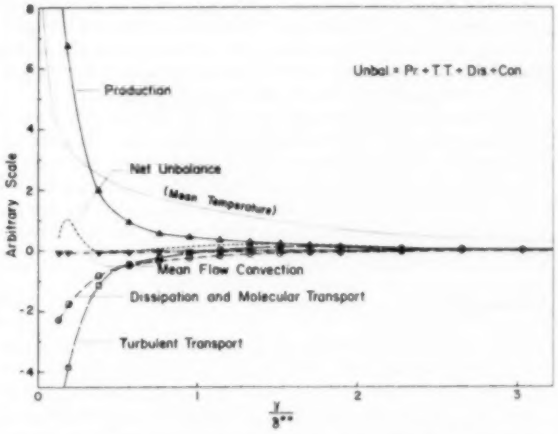

Fig. 18 Turbulent temperature-fluctuation balance through thermal layer

across the turbulent region and to have a maximum value of 1.20.

It would appear from the foregoing that the turbulent Prandtl number is not constant across the boundary layer and that the value will probably lie between 0.8 and 1.2.

Intermittency and Skewness of Fluctuating Quantities. The observed intermittency of temperature fluctuations within the fully turbulent region of velocity fluctuations, Figs. 6 and 13, is perhaps the most novel result of this investigation. Although a discussion of the wider implications of this phenomenon is not within the scope of this paper, it may be remarked that (*a*) the sharpness of the thermal front indicates that molecular conduction is in a sense overshadowed by turbulent transport and fluid surface stretching, and (*b*) relatively large-scale v-velocity fluctuations (composed of unheated air) are present well into the boundary layer toward the wall, as evidenced by thermal intermittency observed at relatively small values of y near the leading edge of the heated plate where the mean thermal layer is still thin. Very close to the plate, of course, this could not occur owing to the decrease in turbulent-velocity fluctuations; furthermore, molecular conduction would be the controlling process in this case since the mean temperature gradient probably would be quite large.

Measurements of the skewness of the temperature fluctuations, Fig. 9, also are of interest in connection with the foregoing. At any point in the boundary layer, the instantaneous temperature can be no greater than the wall temperature T_1 nor less than the free stream temperature T_0. The character of the temperature fluctuations through the thermal layer might then be described crudely by saying that, near the wall, the instantaneous value is near T_1 most of the time (this would be more nearly true for an insulated wall) with occasional decreases to T_0, while toward the outer edge in the intermittent region, the opposite is true. A simple binary behavior such as this would predict the skewness of ϑ to be negative near the wall and positive at the outer edge, increasing monotonically between; such is indeed the case as is evidenced in Fig. 9. The actual fluctuations are not of this nature, of course, since the instantaneous temperature may have any value between the two bounds just stated. Also, it is doubtful that the instantaneous temperature ever reaches the value T_1 near the outer edge. The binary form of temperature fluctuations is approached more closely near the edge of the thermal

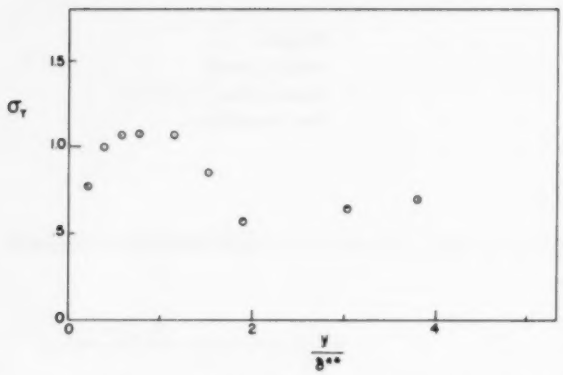

Fig. 19 Turbulent Prandtl number through thermal layer

wake close behind a heated wire in a flowing isotropic turbulence [28].

As discussed in reference [15], the average velocity in a turbulent "burst" is less than the average nonturbulent velocity in the case of u-velocity component intermittency. Such a behavior gives u a decided negative skewness in the outer portion of the boundary layer. In contrast with this, the measurements of v-skewness, Fig. 10, showed it to be positive in the same region. Although not so evident as with u, the oscillograms confirm this, Fig. 7. This behavior is to be expected because the turbulent "hills" must grow by means of positive v fluctuations.

The skewness of w should presumably be zero and, so far as can be inferred from the oscillograms, such is the case. No measurements were made of the skewness of either u or w, however, so numerical comparisons cannot be made. The oscillograms of all three velocity components were made primarily for illustration and comparison of their general character in the intermittent zone.

Conclusions

The experimental investigation of the velocity and temperature fluctuation fields in a turbulent boundary layer downstream of a stepwise discontinuity in wall temperature has provided information on the details of this configuration of turbulent heat transfer. The following general results may be stated for the region where the thermal boundary layer has not become fully developed, i.e., of the same order of thickness as the existing momentum boundary layer.

(a) Temperature fluctuation signals are intermittent near the edge of the thermal layer even though the velocity field at the same point may be fully turbulent; hence the boundary between heated and unheated air remains relatively sharp.

(b) The local turbulent Prandtl number (ratio of turbulent diffusivities of momentum and heat) is not constant across the thermal layer and varies between limits of the order of 0.8 and 1.2. The same orders of magnitude have been reported for fully developed heat transfer in turbulent pipe flow and in the analogous case of mass transfer in pipe flow.

Acknowledgment

The investigation reported here was aided by many members of the Department of Aeronautics of The Johns Hopkins University. Especial thanks are due Prof. Stanley Corrsin (now in the Mechanical Engineering Department), under whose guidance and direction the work was conducted, and Mr. Werner Furth, who carried out most of the reduction of data.

References

1 G. K. Batchelor, "Heat Convection and Buoyancy Effects in Fluids," *Quarterly Journal of the Royal Meteorological Society*, vol. 80, 1954, pp. 339–358.

2 D. S. Johnson, "Velocity, Temperature, and Heat-Transfer Measurements in a Turbulent Boundary Layer Downstream of a Stepwise Discontinuity in Wall Temperature," JOURNAL OF APPLIED MECHANICS, vol. 24, TRANS. ASME, vol. 79, 1957, pp. 2–8.

3 S. Corrsin, "Interpretation of Viscous Terms in the Turbulent Energy Equation," *Journal of the Aeronautical Sciences*, vol. 20, 1953, pp. 853–854.

4 G. I. Taylor, "Statistical Theory of Turbulence," *Proceedings of the Royal Society*, series A, vol. 151, 1935, pp. 421–478.

5 A. N. Kolmogoroff, "The Local Structure of Turbulence in Incompressible Viscous Fluid for Very Large Reynolds Numbers," *Compt. Rendu, Academy of Science*, URSS (Doklady), vol. 30, 1941, p. 301.

6 P. S. Klebanoff, "Characteristics of Turbulence in a Boundary Layer With Zero Pressure Gradient," NACA Technical Note 3178, July, 1954.

7 Mahinder S. Uberoi, "Equipartition of Energy and Local Isotropy in Turbulent Flows," *Journal of Applied Physics*, vol. 28, 1957, pp. 1165–1170.

8 S. Corrsin, "Remarks on Turbulent Heat Transfer," Proceedings of the First Iowa Symposium on Thermodynamics, State University of Iowa, April, 1953.

9 S. Corrsin, "Heat Transfer in Isotropic Turbulence," *Journal of Applied Physics*, vol. 23, 1952, pp. 113–118.

10 S. Corrsin, "The Decay of Isotropic Temperature Fluctuations in an Isotropic Turbulence," *Journal of the Aeronautical Sciences*, vol. 18, 1951, pp. 417–423.

11 J. Boussinesq, "Théorie de l'Ecoulement Tourbillonnant et Tumultueux des Liquides," Paris, 1897.

12 H. Reichardt, "Heat Transfer Through Turbulent Friction Layers," NACA Technical Mem. 1047, September, 1943.

13 W. Forstall, Jr., and A. H. Shapiro, "Momentum and Mass Transfer in Coaxial Gas Jets," JOURNAL OF APPLIED MECHANICS, vol. 17, TRANS. ASME, vol. 72, 1950, pp. 399–408.

14 J. O. Hinze and B. G. Van Der Hegge Zijnen, "Heat and Mass Transfer in the Turbulent Mixing Zone of an Axially Symmetrical Jet," Proceedings of the Seventh International Congress for Applied Mechanics, London, England, 1948.

15 S. Corrsin and A. L. Kistler, "The Free-Stream Boundaries of Turbulent Flows," NACA Technical Note 3133, January, 1954.

16 A. A. Townsend, "Local Isotropy in the Turbulent Wake of a Cylinder," *Australian Journal of Scientific Research*, series A, vol. 1, June, 1948.

17 L. S. G. Kovasznay, "Development of Turbulence-Measuring Equipment," NACA Technical Report 1209, 1955.

18 Donald S. Johnson, "Turbulent Heat Transfer in a Boundary Layer With Discontinuous Wall Temperature," Department of Aeronautics, The Johns Hopkins University, Baltimore, Md., Publication No. 55, August, 1955 (OSR Technical Note 55-289, Office of Scientific Research, Air Research and Development Command, USAF).

19 A. A. Townsend, "The Structure of the Turbulent Boundary Layer," *Proceedings of the Cambridge Philosophical Society*, vol. 47, part 2, April, 1951, pp. 375–395.

20 V. A. Sandborn and W. H. Braun, "Turbulent Shear Spectra and Local Isotropy in the Low-Speed Boundary Layer," NACA Technical Note 3761, September, 1956.

21 J. Laufer, "The Structure of Turbulence in Fully Developed Pipe Flow," NACA Technical Note 2954, June, 1953.

22 W. H. Schwarz and H. E. Hoelscher, "Mass Transfer in a Wetted-Wall Column: Turbulent Flow," *Journal of the American Institute of Chemical Engineers*, vol. 2, March, 1956, pp. 101–106.

23 F. Elias, "The Transference of Heat From a Hot Plate to an Air Stream," NACA Technical Mem. 614, April, 1931.

24 H. Reichardt, "The Principles of Turbulent Heat Transfer," NACA Technical Memorandum 1408, September, 1957.

25 D. R. Davies, "Heat Transfer From a Flat Plate Through a Turbulent Boundary Layer," *Quarterly Journal of Mechanics and Applied Mathematics*, vol. 8, 1955, pp. 326–337.

26 A. C. Spengos and J. B. Cermak, "Heat Transfer by Forced Convection From a Horizontal Flat Plate Into a Turbulent Boundary Layer," Preprints 1956 Heat Transfer and Fluid Mechanics Institute, Stanford University Press, Stanford, Calif., pp. 89–104.

27 R. A. Seban and T. T. Shimazki, "Temperature Distribution of Air Flowing Turbulently in a Smooth Heated Pipe," General Discussion on Heat Transfer, The Institution of Mechanical Engineers—The American Society of Mechanical Engineers, September 11–13, 1951, pp. 122–126.

28 M. S. Uberoi and S. Corrsin, "Diffusion of Heat From a Line Source in Isotropic Turbulence," NACA Tech. Note 2710, June, 1952.

C. F. KETTLEBOROUGH
Professor and Head,
Department of Mechanical Engineering,
University of Auckland,
Auckland, New Zealand

Density Variation Effects in Stepped-Thrust Bearings

The problem of the stepped-thrust bearing is considered but, whereas normally volumetric continuity is assumed, the equations are solved assuming mass continuity; i.e., the variation of density is also considered as well as the effect of the stepped discontinuity on the load-carrying capacity and the coefficient of friction. Computed theoretical curves illustrate the importance of the density on the operation of this bearing and, in part, explain results already published.

THE science of lubrication dates from 1886 when Osborne Reynolds applied the Navier-Stokes' equations to this problem and produced his well-known classical paper [1].[1] This work has been the subsequent starting point of all future theoretical work. A comprehensive theoretical survey was given by Lord Rayleigh [2], who also investigated the optimum film shape for maximum load capacity. Using the calculus of variation and with side leakage neglected he showed that a stepped-shaped film as shown in Fig. 1 was capable of supporting 29 per cent more load, for the same value of the minimum film thickness, than the simple wedged-shaped film as used by Michell [3] in the solution of the thrust-bearing problem. The solution of the stepped-bearing with side leakage considered was given by Archibald [4] for the straight step perpendicular to the direction of motion.

Further theoretical predictions and experimental results for thrust bearings with straight or curved steps have been presented in references [5, 6, and 7]. In the last mentioned reference experimental results were frankly presented but without a satisfactory explanation. During the course of an experimental investigation the results shown in Fig. 2 were obtained. When the minimum film thickness h_1 was plotted against the operating parameter $\eta N/p$, a change in slope of the graph occurred at the lower values of the operating parameter. Theoretically it was

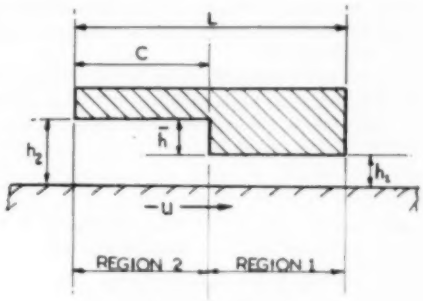

Fig. 1 Stepped-film thrust bearing

[1] Numbers in brackets designate References at end of paper.

Presented at the Summer Conference of the Applied Mechanics Division, Troy N. Y., June 18–20, 1959, of THE AMERICAN SOCIETY OF MECHANICAL ENGINEERS.

Discussion of this paper should be addressed to the Secretary, ASME, 29 West 39th Street, New York, N. Y., and will be accepted until October 10, 1959, for publication at a later date. Discussion received after the closing date will be returned.

NOTE: Statements and opinions advanced in papers are to be understood as individual expressions of their authors and not those of the Society. Manuscript received by ASME Applied Mechanics Division, January 24, 1958. Paper No. 59—APM-19.

Nomenclature

b = relative density-change ratio, region 1
B = relative density-change ratio, region 2
C = fraction of pad length from inlet edge to step
f = friction force
F = total friction force
F_1 = nondimensional friction force region 1
F_2 = nondimensional friction force region 2
h = film thickness
$\bar{h}$ = step height
j = specific heat of lubricant; assumed constant at 0.4 Btu/lb/deg F
J = mechanical equivalent of heat; 9336 in-lb per Btu
k = film ratio
K_1, K_2, K_3, K_4 = constants of integration
L = length of pad in direction of motion
N = rpm
p = pressure
P' = load, psi
P = nondimensional pressure parameter
P_c = value of P at step
q = oil flow between bearing surfaces per unit width
Q = nondimensional flow parameter
t = temperature rise
u = velocity of oil within oil film
U = velocity of moving member
w = average value of density used for determining temperature rise; assumed to be 0.03 lb/in.[3]
W = total load per unit width
W_1 = nondimensional load parameter; region 1
W_2 = nondimensional load parameter; region 2
x = co-ordinate in direction of motion
X = nondimensional co-ordinate in x-direction
y = co-ordinate in direction of oil-film thickness
α = density function; region 1
β = density function; region 2
η = viscosity
μ = coefficient of friction
ρ = density
ρ_0 = density at step
ρ_1 = density at outlet edge
ρ_2 = density at inlet edge
$\eta N/p$ = duty parameter; in this combination η is in poise; N is in rpm, and p is in psi

Subscripts 1 and 2 refer to outlet and inlet regions, respectively, unless otherwise noted in foregoing.

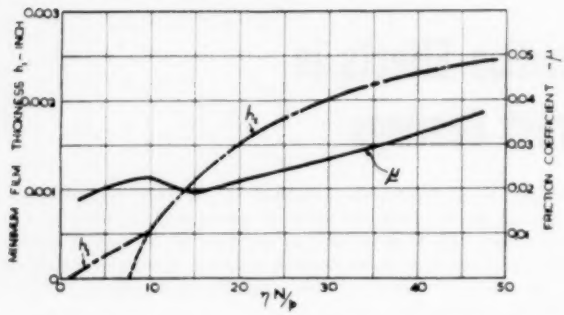

Fig. 2 Experimental friction and film-thickness curves as reported in reference [7]

expected that the curve should continue as shown dotted and eventually cut the abscissa as indicated. At the same time the coefficient-of-friction curve behaved in a strange manner as also shown in Fig. 2.

Osborne Reynolds' work was based on a volume continuity equation. It was not until 1946 when Fogg [8] and later Shaw [9] discussed the "thermal-wedge" effect as applied to parallel surface bearings in which there is no geometrical restriction to the flow of oil, which normally causes hydrodynamic pressures to be generated. The thermal wedge is the effect which results from density changes caused by a rise in temperature of the oil as it flows through the bearing clearance, this temperature rise being due to viscous friction.

When Reynolds' equation is solved for the stepped bearing, but using the mass continuity equation instead of the volume-continuity equation, it will be shown that theoretical curves are similar to those shown in Fig. 2.

Theory

Reynolds' equation for the pressure distribution in a hydrodynamically lubricated bearing of infinite width is

$$\frac{\partial}{\partial x}\left(\frac{\rho h^3}{6\eta}\frac{\partial p}{\partial x}\right) = hU\frac{\partial \rho}{\partial x} \qquad (1)^2$$

Assuming the viscosity remains constant at some average value

$$\frac{\partial}{\partial x}\left(\rho\frac{\partial p}{\partial x}\right) = \frac{6\eta U}{h^2}\frac{\partial \rho}{\partial x} \qquad (2)$$

This equation will be solved separately for regions 1 and 2, as defined in Fig. 1.

Region 1

$$\frac{\partial}{\partial x}\left(\rho\frac{\partial p}{\partial x}\right) = \frac{6\eta U}{h_1^2}\frac{\partial \rho}{\partial x} \qquad (3)$$

Equation (3) is made nondimensional by the following substitutions:

$$x = LX \qquad (4a)$$

$$p = \frac{6\eta UL}{h_1^2}P \qquad (4b)$$

$$\rho = \rho_0\alpha \qquad (4c)$$

$$\frac{\partial}{\partial X}\left(\alpha\frac{\partial P}{\partial X}\right) = \frac{\partial \alpha}{\partial X} \qquad (5)$$

The solution of this equation is

$$P_1 = X + K_1\int\frac{dX}{\alpha} + K_2 \qquad (6)$$

α is a function of the density change and the integral can readily be solved graphically for any given variation of α with X.

However, assuming that the density varies linearly as the oil passes through the bearing,[3] the function α can be written as

$$\alpha = \rho/\rho_0 = [1 + b(X - C)] \qquad (7)$$

When $X = 1$, i.e., at the outlet edge of the bearing $\rho = \rho_1$ and therefore

$$b = \left(\frac{\rho_1}{\rho_0} - 1\right)\Big/(1 - C) \qquad (8)$$

Substituting (7) into (6)

$$P_1 = X + K_1\frac{\log_e\{1 + b(X - C)\}}{b} + K_2 \qquad (9)$$

Region 2

$$\frac{\partial}{\partial x}\left(\rho\frac{\partial p}{\partial x}\right) = \frac{6\eta U}{h_2^2}\frac{\partial \rho}{\partial x} \qquad (10)$$

Substituting from (4*a*) and (4*b*) and expressing the density change by

$$\rho = \rho_0\beta \qquad (11)$$

the solution of (10) is

$$P_2 = \frac{X}{k^3} + K_3\int\frac{dX}{\beta} + K_4 \qquad (12)$$

Expressing β as a linear density change as for region 1

$$\beta = \frac{\rho}{\rho_0} = [1 + B(C - X)] \qquad (13)$$

when $X = 0$, i.e., at the inlet edge, $\rho = \rho_2$ and

$$B = \left(\frac{\rho_2}{\rho_0} - 1\right)\Big/C \qquad (14)$$

$$P_2 = X/k^3 - K_3\log_e[1 + B(C - X)]/B + K_4 \qquad (15)$$

The constants of integration are determined from the following boundary conditions:

(*i*), (*ii*) Zero pressure (relative to atmosphere) around the periphery of the pad yield

$$P_1 = 0 \quad \text{when} \quad X = 1$$

$$P_2 = 0 \quad \text{when} \quad X = 0$$

(*iii*) The pressure intensity at the step must be the same for both regions, i.e.,

$$(P_1 \text{ when } X = C) = (P_2 \text{ when } X = C)$$

(*iv*) Continuity demands that the oil crossing the step leaving region 2 must be identical with the amount of oil entering region 1; i.e.,

$$\left[\frac{Uh_2}{2} - \frac{h_2^3}{12\eta}\left(\frac{\partial p}{\partial x}\right)_2\right] = \left[\frac{Uh_1}{2} - \frac{h_1^3}{12\eta}\left(\frac{\partial p}{\partial x}\right)_1\right]$$

Rearranging in nondimensional terms

$$\left[k^3\left(\frac{\partial P}{\partial X}\right)_2 - \left(\frac{\partial P}{\partial X}\right)_1\right] = (k - 1)$$

[2] Reference [10], p. 303.

[3] Discussed in reference [10], p. 305.

$(\partial P/\partial X)_1$ is the slope of the pressure field for region 1 at the step; i.e., when $X = C$. Similarly, $(\partial P/\partial X)_2$ refers to region 2 when $X = C$. These functions are obtained from equations (9) and (15), respectively.

These four boundary conditions yield the following equations from which the constants can be determined:

$$K_2 + K_1 \frac{\log_e \{1 + b(1 - C)\}}{b} + 1 = 0 \tag{16}$$

$$K_4 - K_3 \frac{\log_e \{1 + BC\}}{B} = 0 \tag{17}$$

$$K_2 - K_4 = C\left[\frac{1}{k^3} - 1\right] \tag{18}$$

$$k^3K_3 - K_1 = (k - 1) \tag{19}$$

Total Load. The load carried by the bearing per unit width is

$$W = \int_0^x p dx = \frac{6\eta UL^2}{h_1^2} \int_0^1 P dX \tag{20}$$

$$= \frac{6\eta UL^2}{h_1^2}\left[\int_c^1 P_1 dX + \int_0^c P_2 dX\right]$$

$$= \frac{6\eta UL^2}{h_1^2}[W_1 + W_2] \tag{21}$$

where

$$W_1 = \left[\frac{1 - C^2}{2}\right] + \frac{K_1}{b^2}\{[1 + b(1 - C)]\log_e[1 + b(1 - C)]$$

$$- b(1 - C)\} + K_2(1 - C) \tag{22}$$

$$W_2 = \frac{c^2}{2k^3} - \frac{K_3}{B^2}\{1 + (1 + BC)[\log_e(1 + BC) - 1]\}$$

$$+ K_4C \tag{23}$$

Substituting $h_1 = \bar{h}/(k - 1)$ into (21) and rearranging

$$\left(\frac{\eta U}{W}\right)\left(\frac{L^2}{\bar{h}^2}\right) = 1/6(k - 1)^2[W_1 + W_2] \tag{24}$$

Friction Force. The friction force per unit width acting on the moving member is found from

$$F = \int \eta \left(\frac{du}{dy}\right)_{y=0} dx = f_1 + f_2 \tag{25}$$

The velocity distribution across the oil film is given by

$$u = \frac{1}{2\eta}\frac{\partial p}{\partial x}(y - h)y + \left(\frac{h - y}{h}\right)U \tag{26}$$

therefore

$$f_1 = -\int_C^1 \left[\frac{h_1}{2}\frac{\partial p}{\partial x} + \frac{\eta U}{h_1}\right] dx$$

$$= -\frac{\eta UL}{h_1}[3(-P_C) + (1 - C)] \tag{27}$$

Substituting from (9); when $X = C, P_C = C + K_2$

$$f_1 = -\frac{\eta UL}{h_1}[1 - 4C - 3K_2] = -\frac{\eta UL}{h_1}[F_1] \tag{28}$$

Similarly

$$f_2 = -\frac{\eta UL}{h_1}\left[\frac{3C}{k^2} + 3kK_4 + \frac{C}{k}\right] = -\frac{\eta UL}{h_1}[F_2] \tag{29}$$

A measure of efficiency of the bearing as far as power loss is concerned is given by the ratio of friction force to the total load carried.

$$\mu = \frac{F}{W} = \frac{h_1}{6L}\frac{(F_1 + F_2)}{(W_1 + W_2)} \tag{30}$$

$$\frac{\mu L}{\bar{h}} = \frac{1}{6(k - 1)}\frac{(F_1 + F_2)}{(W_1 + W_2)} \tag{31}$$

Temperature Rise Through Bearing. This is determined by equating the power loss due to friction in terms of heat units to the heat gained by the oil.

$$FU/J = q\omega j\delta t \tag{32}$$

The temperature rise was determined for each region separately. As a first approximation the temperature rise calculations were carried out using the simplified equations assuming the oil density remained constant. The oil-flow rate q is required.

$$q = \int_0^{h_2} u dy = \int_0^{h_1} u dy = \frac{Uh_2}{2} - \frac{h_2^3}{12\eta}\frac{dp}{dx}$$

substituting for dp/dx from (9) and assuming constant density (i.e., $b = 0$)

$$q = \frac{Uh_1}{2}\left[1 - \frac{(k - 1)C}{k^3(C - 1) - C}\right] = \frac{Uh_1}{2}Q \tag{33}$$

therefore

$$\delta t_1 = f_1U/q\omega jJ \quad \text{and} \quad \delta t_2 = f_2U/q\omega jJ \tag{34}$$

Substituting for f_1 and f_2 from equations (28) and (29), respectively, and for q from equation (33) and eliminating h_1 by substituting from equation (21) the equation for the temperature rise becomes in degrees F

$$\delta t_1 = 0.02380\, P'\left\{\frac{F_1}{QW_1}\right\}$$

$$\delta t_2 = 0.02380\, P'\left\{\frac{F_2}{QW_2}\right\} \tag{35}$$

The nondimensional functions are functions of the film ratio k only and when the density is constant are given simply by

$$W_1 = \frac{(k - 1)C(1 - C)^2}{2\{k^3(1 - C) + C\}} \tag{36}$$

$$W_2 = \frac{(k - 1)C^2(1 - C)}{2\{k^3(1 - C) + C\}} \tag{37}$$

$$F_1 = (1 - C) + \frac{3C(1 - C)(k - 1)}{k^3(C - 1) - C} \tag{38}$$

$$F_2 = \frac{C}{k} + \frac{3kC(C - 1)(k - 1)}{k^3(C - 1) - C} \tag{39}$$

$$Q = 1 - \frac{(k - 1)C}{k^3(C - 1) - C} \tag{40}$$

Computations

In order to calculate operating characteristics the following procedure is necessary:

(a) Assume a definite value for the bearing load in pounds per square inch.

(b) Calculate the temperature rises δt_1 and δt_2 from equation (35) using equations (36) through (40).

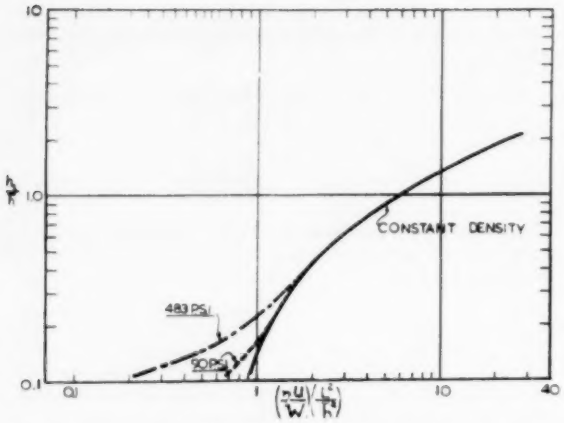

Fig. 3 Load criterion $(\eta U/W)(L^2/\bar{h}^2)$ plotted against film-thickness function $h_1/\bar{h}$

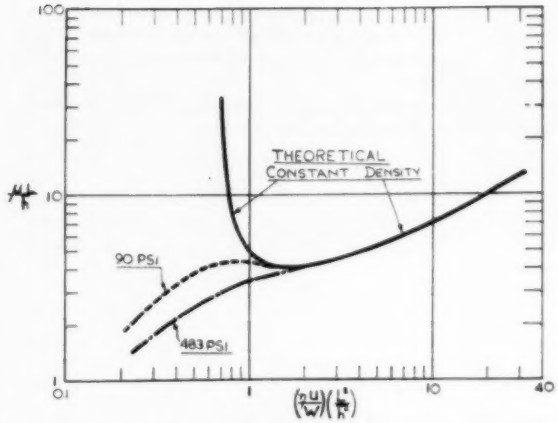

Fig. 4 Friction criterion $(\mu L/\bar{h})$ plotted against load criterion $(\eta U/W)(L^2/\bar{h}^2)$

(*c*) Determine the density ratios using information given in reference [10][8] from which

$$b = -0.0004\,\delta t_1/(1 - C)$$

$$B = \left(\frac{0.0004\,\delta t_2}{1 - 0.0004\,\delta t_2}\right)\Big/C$$

(*d*) Compute the load criterion

$$\left(\frac{\eta U}{W}\right)\left(\frac{L^2}{\bar{h}^2}\right)$$

given in equation (24) and the friction criterion $\mu L/\bar{h}$ given by equation (31).

Steps (*b*) through (*d*) were computed for film ratios from 1.50 to 50.

Results

Fig. 3 shows the load criterion

$$\left(\frac{\eta U}{W}\right)\left(\frac{L^2}{\bar{h}^2}\right)$$

plotted against the film thickness function

$$h_1/\bar{h} = 1/(k - 1)$$

for a bearing with a central step; i.e., $C = 1/2$. The full line is the theoretical curve when the density is assumed constant.

Assuming a load intensity of 483 psi there is no significant variation from the constant-density case for values of $h_1/\bar{h} > 0.4$; i.e., for conditions of thick oil films. As the film thickness decreases, the friction increases while the oil flow decreases, thus causing an increased temperature rise and an increased density-variation effect. This is shown by the departure of the curve from the constant-density curve.

The theoretical friction-criterion curve based on constant density is shown in Fig. 4. At a load intensity of 483 psi the graph obtained which allows for density changes entirely suppresses the negative-slope part of the previous curve.

Curves also have been computed for a load intensity of 90 psi and are also shown in Figs. 3 and 4. As the temperature rise and therefore density variations are directly proportional to the load intensity, the density variations are less than for the 483-psi loading. Hence the deviation from the constant-density curves occur later; i.e., at smaller values of the

$$\left(\frac{\eta U}{W}\right)\left(\frac{L^2}{\bar{h}^2}\right)$$

parameter and at smaller values of the film thickness.

Fig. 4 shows that, for a load of 90 psi, the purely hydrodynamic component predominates until beyond the minimum value of $\mu L/\bar{h}$. Then the density-variation effect becomes sufficiently large and takes control.

The friction curve for a load of 90 psi, as shown in Fig. 4, is similar in form to that obtained experimentally in Fig. 2.

As the loading is decreased the friction curve will follow the constant-density curve farther up that portion having a negative slope before breaking away. However, a different curve is obtained for each distinct value of the applied load except when hydrodynamic conditions predominate at higher values of the film thickness. These distinct curves have not been reproduced in experiments.

It should be noted that the co-ordinates of Figs. 3 and 4 are identical with those of Fig. 2, except for a scale effect, as $\bar{h}$ and L are constants.

References

1 O. Reynolds, "On the Theory of Lubrication and its Application to Mr. Beauchamp Tower's Experiments, Including an Experimental Determination of the Viscosity of Olive Oil," *Transactions of the Royal Society*, London, vol. 177, part 1, 1886, p. 157.

2 Lord Rayleigh, "Notes on the Theory of Lubrication," *Philosophical Magazine*, vol. 35, 1918, p. 1.

3 A. G. M. Michell, "The Lubrication of Plane Surfaces," *Zeitschrift für Mathematik und Physik*, vol. 52, 1905, p. 123.

4 F. R. Archibald, "A Simple Hydrodynamic Thrust Bearing," TRANS. ASME, vol. 72, 1950, p. 393.

5 C. F. Kettleborough, "An Electrolytic Tank Investigation Into Stepped-Thrust Bearings," *Proceedings of The Institution of Mechanical Engineers*, vol. 169, 1955, p. 679.

6 R. C. R. Johnston and C. F. Kettleborough, "An Experimental Investigation Into Stepped-Thrust Bearings," *Proceedings of The Institution of Mechanical Engineers*, vol. 170, 1956, p. 511.

7 C. F. Kettleborough, "Further Experiments on Stepped-Thrust Bearings; the Effect of Step Height," *Proceedings of The Institution of Mechanical Engineers*, International Lubrication Conference, London, October, 1957.

8 A. Fogg, "Film Lubrication of Parallel Thrust Surfaces," *Proceedings of The Institution of Mechanical Engineers*, vol. 155, 1946, p. 49.

9 M. C. Shaw, "An Analysis of the Parallel Surface Thrust Bearing," TRANS. ASME, vol. 69, 1947, p. 381.

10 M. C. Shaw and E. F. Macks, "Analysis and Lubrication of Bearings," McGraw-Hill Book Company, New York, N. Y., 1949.

Response of a Nonlinear String to Random Loading

T. K. CAUGHEY
Assistant Professor of Applied Mechanics,
Division of Engineering,
California Institute of Technology,
Pasadena, Calif.

This paper considers the response of a nonlinear string to random excitation. It is shown that, owing to the additional stress induced by the stretching of the string, the mean squared deflection at every point is smaller than that for the equivalent linear string.

THE RESPONSE of a nonlinear string to deterministic loading has been analyzed by several authors.[1–4] G. F. Carrier[1,2] has analyzed the free oscillations of a nonlinear string, while Lee[3] and the author[4] have analyzed the response of a nonlinear string to deterministic loading. This paper is devoted to the study of a nonlinear string subjected to a random excitation. It is shown that, as in the case of deterministic loading, the additional stress induced by the stretching of the string reduces the mean squared deflection at every point compared with that for the equivalent linear string.

Formulation

Consider an elastic string, clamped at its ends subjected to a random loading. The nomenclature used is as follows:

u = transverse deflection of string
T_0 = initial tension in string
ρ = linear density of string
$\rho\beta$ = viscous damping coefficient
A = cross-sectional area of string
E = elastic modulus of string
L = length of string
$f(x,t)$ = loading on string

If the deflections and slopes are considered to be moderately small (consistent with the string remaining elastic) the equation of motion of the string is

$$\rho\left(\frac{\partial^2 u}{\partial t^2}+\beta\frac{\partial u}{\partial t}\right)=\left[T_0+\frac{AE}{2L}\int_0^L\left(\frac{\partial u}{\partial x}\right)^2 dx\right]\frac{\partial^2 u}{\partial x^2}+f(x,t) \quad (1)$$

subject to the boundary conditions that

$$u(0,t)=u(L,t)=0 \quad (2)$$

In the analysis that follows it will be assumed that $f(x,t)$ is a randomly varying force with a clipped Gaussian white spectrum and has the following cross correlation:

$$\overline{f(x,t_1)f(\eta,t_2)}=4D\delta(x-\eta)\frac{\sin\omega_c\tau}{\tau} \quad (3)$$

where

$$\tau=t_1-t_2$$

Since the eigenmodes for equation (1) are sine waves, let

$$f(x,t)=\sum_{i=1}^{\infty}a_i(t)\sin\frac{i\pi x}{L}$$
$$u(x,t)=\sum_{i=1}^{N}b_i(t)\sin\frac{i\pi x}{L} \quad (4)$$

where N is chosen such that $\omega_N<\omega_c<\omega_{N+1}$.

As a consequence of the assumed form of the cross correlation (3), the a_i in (4) are uncorrelated and the power spectrum $g_i(\omega)$ of a_i is given by

$$g_i(\omega)=\frac{2}{L}\frac{4D}{2\pi}\quad 0<\omega<\omega_c$$
$$=0\qquad\omega>\omega_c \quad (5)$$

Substituting (4) into (1)

$$\frac{d^2b_n}{dt^2}+\beta\frac{db_n}{dt}+\left(\frac{n\pi}{L}\right)^2\frac{T_0}{\rho}\left[1+\frac{AE}{2LT_0}\times\int_0^L\left(\sum_{i=1}^{N}b_i\frac{i\pi}{L}\cos\frac{i\pi x}{L}\right)^2 dx\right]b_n=a_n(t)/\rho \quad (6)$$

Using the orthogonality of the circular functions, equation (6) becomes

$$\frac{d^2b_n}{dt^2}+\beta\frac{db_n}{dt}+\left(\frac{n\pi}{L}\right)^2\frac{T_0}{\rho}\left(1+\alpha\sum_{i=1}^{N}i^2b_i^2\right)b_n=a_n/\rho \quad (7)$$

where

$$\alpha=\frac{AE}{4T_0L}\left(\frac{\pi}{L}\right)^2 \quad (8)$$

Equivalent Linear Form of Equation (7)

The method of equivalent linearization has been applied successfully in the past to nonlinear differential equations with harmonic excitation. It will now be shown that, by a slightly different approach to the problem, this method may be applied to equation (7).

Rewriting equation (7) in the form

[1] G. F. Carrier, "On the Nonlinear Vibration Problem of the Elastic String," *Quarterly of Applied Mathematics*, vol. 3, 1945, pp. 157–165.

[2] G. F. Carrier, "A Note on the Vibrating String," *Quarterly of Applied Mathematics*, vol. 7, 1949, pp. 97–101.

[3] E. W. Lee, "Nonlinear Forced Vibrations of a Stretched String," *British Journal of Applied Physics*, vol. 8, 1957, pp. 411–413.

[4] T. K. Caughey, unpublished CalTech Report No. 85, 1956.

Presented at the West Coast Conference of the Applied Mechanics Division, Stanford, Calif., September 9–11, 1959, of THE AMERICAN SOCIETY OF MECHANICAL ENGINEERS.

Discussion of this paper should be addressed to the Secretary, ASME, 29 West 39th Street, New York, N. Y., and will be accepted until October 10, 1959, for publication at a later date. Discussion received after the closing date will be returned.

NOTE: Statements and opinions advanced in papers are to be understood as individual expressions of their authors and not those of the Society. Manuscript received by ASME Applied Mechanics Division, November 18, 1957. Paper No. 59—APMW-4.

$$\frac{d^2b_n}{dt^2} + \beta\frac{db_n}{dt} + \left(\frac{n\pi}{L}\right)^2\frac{T_0}{\rho}K_nb_n + \epsilon(b_1, b_2, \ldots b_N) = \frac{a_n}{\rho} \quad (9)$$

If in (9), $\epsilon(b_1, b_2, \ldots b_N)$ is neglected, (9) is linear and can be solved readily. The smaller $\epsilon(b_1, b_2, \ldots b_N)$ is, the smaller the error in neglecting it. The logical choice of K_n is, therefore, that value of K_n which minimizes $\epsilon(b_1, b_2, \ldots b_N)$.

The choice of minimization procedure is somewhat arbitrary, but by analogy with Galerkin's method, and for mathematical expediency, it is desirable to use the minimization of the mean squared error

$$\overline{\epsilon^2} = \frac{1}{2T}\int_{-T}^{T}\left[\left(\frac{n\pi}{L}\right)^2\frac{T_0}{\rho}\right]^2 \left\{\left[1 + \alpha\sum_{i=1}^{N} i^2b_i^2\right]b_n - K_nb_n\right\}^2 dt \quad (10)$$

If the process is an ergodic one, then equation (10) may be replaced by the stochastic average. Further, since the a_i are uncorrelated

$$\therefore\overline{\epsilon^2} = \int_{-\infty\ N\text{-fold}}^{\infty}\int_{-\infty}^{\infty}\left[\left(\frac{n\pi}{L}\right)^2\frac{T_0}{\rho}\right]^2 \left\{\left[1 + \alpha\sum_{i=1}^{N} i^2b_i^2\right] - K_n\right\}^2 b_n^2\prod_{i=1}^{N}\left\{p(b_i)db_i\right\} \quad (11)$$

where $p(b_i)$ is the first probability density function of b_i.

If in (9), $\epsilon(b_1, b_2, \ldots b_N)$ is neglected, b_n is Gaussian since a_n is Gaussian.

Thus

$$\left.\begin{aligned} p(b_i) &= \frac{1}{(2\pi)^{1/2}\sigma_i}\exp\left(-b_i^2/2\sigma_i^2\right) \\ \text{where} \qquad \sigma_i^2 &= \overline{b_i^2} \end{aligned}\right\} \quad (12)$$

$$\therefore\overline{\epsilon^2} = \left[\prod_{i=1}^{N}(2\pi)^{1/2}\sigma_i\right]^{-1}\int_{-\infty\ N\text{-fold}}^{\infty}\int_{-\infty}^{\infty}\left[\left(\frac{n\pi}{L}\right)^2\frac{T_0}{\rho}\right]^2\left[1 + \alpha\sum_{i=1}^{N} i^2b_i^2 - K_n\right]^2 b_n^2\prod_{i=1}^{N}\left[\exp\left(-b_i^2/2\sigma_i^2\right)db_i\right] \quad (13)$$

Minimizing $\overline{\epsilon^2}$ with respect to K_n:

$$K_n = \left[\int_{-\infty\ N\text{-fold}}^{\infty}\int_{-\infty}^{\infty} b_n^2\prod_{i=1}^{N}\left\{\exp\left(-b_i^2/2\sigma_i^2\right)db_i\right\}\right]^{-1} \int_{-\infty\ N\text{ fold}}^{\infty}\int_{-\infty}^{\infty}\left[1 + \alpha\sum_{i=1}^{N} i^2b_i^2\right]b_n^2 \prod_{i=1}^{N}\left[\exp\left(-b_i^2/2\sigma_i^2\right)db_i\right] \quad (14)$$

Evaluating the integrals:

$$K_n = 1 + \alpha\left[\sum_{i=1}^{N} i^2\sigma_i^2 + 2n^2\sigma_n^2\right] \quad (15)$$

If in equation (9) $\epsilon(\ )$ is neglected, then

$$\frac{d^2b_n}{dt^2} + \beta\frac{db_n}{dt} + \left(\frac{n\pi}{L}\right)^2\frac{T_0}{\rho}K_nb_n = \frac{a_n(t)}{\rho} \quad (16)$$

The power spectrum of b_n is therefore given by

$$B_n(\omega) = g_n(\omega)\rho^{-2}\left\{\left[\left(\frac{n\pi}{L}\right)^2\frac{T_0}{\rho}K_n - \omega^2\right]^2 + [\omega\beta]^2\right\}^{-1} \quad (17)$$

where $g_n(\omega)$ is given by equation (5).

The mean squared value of b_n is readily computed from (17). Thus

$$\sigma_n^2 = \overline{b_n^2} = \int_0^{\infty} B_n(\omega)dw$$

$$= \int_0^{\infty}\frac{2^2}{\rho^2L}\frac{D}{\pi}\left\{\left[\left(\frac{n\pi}{L}\right)^2\frac{T_0}{\rho}K_n - \omega^2\right]^2 + [w\beta]^2\right\}^{-1}dw \quad (18)$$

If β is small and

$$\left(\frac{n\pi}{L}\right)^2\frac{T_0}{\rho}K_n < \omega_c^2$$

$$\sigma_n^2 \doteq \frac{2}{\rho^2L}D\left\{\left(\frac{n\pi}{L}\right)^2\frac{T_0}{\rho}K_n\beta\right\}^{-1} \quad (19)^5$$

The main contribution to the integral (18) coming from a small region close to

$$\omega^2 = \left(\frac{n\pi}{L}\right)^2\frac{T_0}{\rho}K_n$$

By the same token it will be seen that if

$$\left(\frac{i\pi}{L}\right)^2\frac{T_0}{\rho}K_i > \omega_c^2$$

the integral (18) will be very small, thus justifying the approximate representation of u in (4).

Substituting K_n from (15) into (19)

$$\sigma_n^2 = \frac{2}{\rho L}D\left\{n^2\left(\frac{\pi}{L}\right)^2\frac{T_0}{\rho}\beta \left(1 + \alpha\left[\sum_{i=1}^{N} i^2\sigma_i^2 + 2n^2\sigma_n^2\right]\right)\right\}^{-1} \quad (20)$$

Noting that

$$\frac{2}{\rho L}D\left[\left(\frac{\pi}{L}\right)^2\frac{T_0}{\rho}\beta\right]^{-1} = \sigma_{1,0}^2 \quad (21)$$

the mean squared deflection in the first mode of the linearized problem obtained by setting $\alpha = 0$ in (7). Thus

$$n^2\frac{\sigma_n^2}{\sigma_{1,0}^2} = \left\{1 + \alpha\sigma_{1,0}^2\left[\sum_{i=1}^{N} i^2\frac{\sigma_i^2}{\sigma_{1,0}^2} + 2n^2\frac{\sigma_n^2}{\sigma_{1,0}^2}\right]\right\}^{-1} \quad (22)$$

Denoting

$$\left.\begin{aligned} i^2\frac{\sigma_i^2}{\sigma_{1,0}^2} &= y_i \\ \alpha\sigma_{1,0}^2 &= z \\ \sum_{i=1}^{N} i^2\frac{\sigma_i^2}{\sigma_{1,0}^2} &= \sum_{i=1}^{N} y_i = S \end{aligned}\right\} \quad (23)$$

Equation (22) becomes

$$2zy_n^2 + [1 + zS]y_n - 1 = 0 \quad (24)$$

Solving:

$$y_n = \left\{-(1 + zS) + [(1 + zS)^2 + 8z]^{1/2}\right\}[4z]^{-1} \quad (25)$$

[5] See Appendix.

The positive root being taken in (25) since y_n by definition is positive. Multiplying both sides of (25) by $4z$, and summing on n

$$4zS = -N(1 + zS) + N[(1 + zS)^2 + 8z]^{1/2} \tag{26}$$

Rearranging terms and squaring

$$\left[1 + z\left(1 + \frac{4}{N}\right)S\right]^2 = (1 + zS)^2 + 8z \tag{27}$$

Solving for zS:

$$zS = \tfrac{1}{2}\{-1 + [1 + 4(N + 2)z]^{1/2}\}\left[2\left(1 + \frac{2}{N}\right)\right]^{-1} \tag{28}$$

Since zS is positive, the positive radical is taken.

Substituting (28) into (25), y_n may be calculated. It will be observed from (25) that y_n is independent of n; thus there is equipartition of energy among the modes.

Calculation of Mean Squared Deflection $\overline{U^2}$

Using equation (4)

$$\overline{u^2} = \overline{\left[\sum_{i=1}^{N} b_i \sin\frac{i\pi x}{L}\right]^2} \tag{29}$$

$$\overline{U^2} = \sum_{i,j}^{N} \overline{b_i b_j} \sin\frac{i\pi x}{L} \sin\frac{jx\pi}{L} \tag{30}$$

Owing to the particular cross correlation function (3), the b_i are uncorrelated; thus

$$b_i b_j = 0 \quad i \neq j \tag{31}$$

Equation (30) therefore becomes

$$\overline{U^2} = \sum_{i=1}^{N} \overline{b_i^2} \sin^2\frac{i\pi x}{L} \tag{32}$$

From equations (23) and (25)

$$\overline{b_i^2} = \sigma_i^2 = y_i \frac{\sigma_{1,0}^2}{i^2}$$

$$= \frac{\sigma_{1,0}^2}{i^2}\{-(1 + zS) + [(1 + zS)^2 + 8z]^{1/2}\}[4z]^{-1} \tag{33}$$

Substituting (33) into (32)

$$\overline{U^2} = \sigma_{1,0}^2\{-(1 + zS) + [(1 + zS)^2 + 8z]^{1/2}\}[4z]^{-1}\sum_{i=1}^{N}\frac{1}{i^2}\sin^2\frac{i\pi x}{L} \tag{34}$$

In the linearized problem given by setting $\alpha = 0$ in (7), the mean squared deflection $\overline{U_0^2}$ is given by

$$\overline{U_0^2} = \sigma_{1,0}^2 \sum_{i=1}^{N} \frac{1}{i^2}\sin^2\frac{i\pi x}{L} \tag{35}$$

Thus

$$\frac{\overline{U^2}}{\overline{U_0^2}} = \{-(1 + zS) + [(1 + zS)^2 + 8z]^{1/2}\}[4z]^{-1} \tag{36}$$

where zS is given by equation (28).

If in (36) $z \ll 1$, (36) reduces to

$$\frac{\overline{U^2}}{\overline{U_0^2}} \doteq [1 + zS]^{-1} \leq 1 \tag{37}$$

Further, if in (28) N is large,

$$zS \doteq {}^1/_z[-1 + (1 + 4Nz)^{1/2}] \tag{38}$$

Using (38), equation (37) becomes

$$\frac{\overline{U^2}}{\overline{U_0^2}} \doteq 2[1 + (1 + 4Nz)^{1/2}]^{-1} \leq 1 \tag{39}$$

Thus the mean squared deflection in the nonlinear case is always less than the mean squared deflection in the equivalent linear string.

Conclusions

From the foregoing analysis it is clearly seen that the effect of the stress induced by the stretching of the string is to reduce the mean squared deflection at every point in the string compared with the corresponding mean squared deflection in the equivalent linear string.

APPENDIX

(a) Evaluation of integral (18). Let

$$\left(\frac{n\pi}{L}\right)^2 \frac{T_0}{\rho} K_n = \tilde{\omega}_n^2$$

Thus

$$\sigma_n^2 = 2^3 D/\rho L\pi \int_0^{\omega_c} \{[\tilde{\omega}_n^2 - \omega^2]^2 + [\beta w]^2\}^{-1} dw \tag{40}$$

Using integral 211.16c of "Integraltaffel, Ester Teil, Unbestimmte Integral," by W. Grobner and N. Hofreiter (Springer, 1949), equation (40) becomes

$$\sigma_n^2 = 2D/\rho L\pi\tilde{\omega}_n\{\sin\phi_0 \ln[(\tilde{\omega}_n^2 + \omega_c^2 + 2\tilde{\omega}_n\omega_c\cos\phi_0)/(\tilde{\omega}_n^2 + \omega_c^2 - 2\tilde{\omega}_n\omega_c\cos\phi_0)] + \cos\phi_0 \tan^{-1}[2\tilde{\omega}_n\omega_c \sin\phi_0/(\tilde{\omega}_n^2 - \omega_c^2)]\}\{\beta^2(\tilde{\omega}_n^2 - \beta^2/4)\}^{-1/2} \tag{41}$$

where

$$\tan 2\phi_0 = \{\beta^2(\tilde{\omega}_n^2 - \beta^2/4)\}^{1/2}\{\tilde{\omega}_n^2 - \beta^2/2\}^{-1} \tag{42}$$

If β is small compared to $\tilde{\omega}_n$, equation (41) reduces to

$$\sigma_n^2 \simeq 2D/\rho L\pi\tilde{\omega}_n^2\beta\{\tan^{-1}[\omega_c\beta/(\tilde{\omega}_n^2 - \omega_c^2)] + 0[\beta/2\tilde{\omega}_n \ln(2\tilde{\omega}_n/\beta)]\} \tag{43}$$

For $\beta/\tilde{\omega}_n$ very small, the second term may be neglected entirely. Thus

$$\sigma_n^2 \doteq 2D/\rho L\pi\tilde{\omega}_n^2\beta\{\tan^{-1}[\omega_c\beta/(\tilde{\omega}_n^2 - \omega_c^2)]\} \tag{44}$$

If $\omega_c > \tilde{\omega}_n$

$$\sigma_n^2 \doteq 2D/\rho L\tilde{\omega}_n^2\beta \tag{45}$$

If $\tilde{\omega}_n > \omega_c$

$$\sigma_n^2 \doteq 2D/\rho L\pi\tilde{\omega}_n^2\beta\{\omega_c\beta/(\tilde{\omega}_n^2 - \omega_c^2)\} = 2\beta D\omega_c/\rho L\pi\beta\tilde{\omega}_n^2(\tilde{\omega}_n^2 - \omega_c^2) \ll 2D/\rho L\pi\beta\tilde{\omega}_n^2 \quad \text{for} \quad \beta/\tilde{\omega}_n \ll 1 \tag{46}$$

This justifies the approximate representation of u in equation (4)

(b) Justification for neglecting term $z\sum_{N+1}^{\infty} i^2(\sigma_n^2/\sigma_{1,0}^2)$. As is shown in (46), for $\tilde{\omega}_i^2 > \omega_c^2$

$$\sigma_i^2 \doteq 2D\omega_c[\rho L\pi\tilde{\omega}_i^2(\tilde{\omega}_i^2 - \omega_c^2)]^{-1} \tag{47}$$

i.e.,

$$i^2 \frac{\sigma_i^2}{\sigma_{1,0}^2} \doteq \omega_0 \beta [\pi(\omega_i^2 K_i - \omega_e^2)]^{-1} \tag{48}$$

$$\therefore \sum_{N+1}^{\infty} i^2 \frac{\sigma_i^2}{\sigma_{1,0}^2} \simeq \frac{\omega_0 \beta}{\pi \omega_0^2 K_{N+1}} \sum_{N+1}^{\infty} \left(i^2 - \frac{\omega_e^2}{\omega_0^2 K_{N+1}} \right)^{-1} \tag{49}$$

$$\leq \frac{\beta}{2\pi\omega_0 K_{N+1}^{1/2}} \int_{N+1}^{\infty} \left[\left(i - \frac{\omega_e}{\omega_0 K_{N+1}^{1/2}} \right)^{-1} - \left(i + \frac{\omega_e}{\omega_0 K_{N+1}^{1/2}} \right)^{-1} \right] di \tag{50}$$

$$\leq \frac{\beta}{2\pi\omega_0 K_{N+1}^{1/2}} \ln \left[(N + 1 + \omega_e/\omega_0 K_{N+1}^{1/2}) / (N + 1 - \omega_e/\omega_0 K_{N+1}^{1/2}) \right] \tag{51}$$

$$\doteq \frac{\beta}{2\pi\omega_0 K_{N+1}^{1/2}} \ln [(N + 2)/N] \tag{52}$$

Comparing

$$\sum_{N+1}^{\infty} i^2 \frac{\sigma_i^2}{\sigma_{1,0}^2} \quad \text{with} \quad \sum_{i=1}^{N} i^2 \frac{\sigma_i^2}{\sigma_{1,0}^2}$$

$$\sum_{N+1}^{\infty} i^2 \frac{\sigma_i^2}{\sigma_{1,0}^2} \Big/ \sum_{1}^{N} i^2 \frac{\sigma_i^2}{\sigma_{1,0}^2} \doteq \frac{2\beta \left(1 + \frac{2}{N}\right) z \ln [(N + 2)/N]}{2\pi\omega_0 K_{N+1}^{1/2} \{-1 + [1 + 4(N + 2)z]^{1/2}\}} \tag{53}$$

For z small

$$\sum_{N+1}^{\infty} i^2 \frac{\sigma_i^2}{\sigma_{1,0}^2} \Big/ \sum_{1}^{N} i^2 \frac{\sigma_i^2}{\sigma_{1,0}^2} \leq \frac{\beta z^{1/2}}{\omega_0} 0 \left[\frac{\ln (1 + 2/N)}{N} \right] \tag{54}$$

If β is small and N is large, this ratio becomes very small and may be neglected, thus justifying the treatment given in the paper.

T. K. CAUGHEY
Assistant Professor of Applied Mechanics, Division of Engineering, California Institute of Technology, Pasadena, Calif.

Response of Van Der Pol's Oscillator to Random Excitation

This paper considers the response of Van der Pol's oscillator to random excitation. It is shown that the output of the oscillator consists of a periodic term, plus a narrow band noise term centered at the natural frequency of the oscillator. The root-mean-square amplitude of this noise term is shown to be proportional to the square root of the spectral density of the excitation, and inversely proportional to the amplitude of self-oscillation.

In recent years considerable interest has been aroused in the response of nonlinear systems to various types of excitation. Most of the recent work has been in the field of servomechanisms and feedback systems, where the equivalent linearization technique of nonlinear mechanics has been used in various guises and under various names. With the exception of Garstens' paper,[1] the analytical studies have been on the response of systems to either periodic excitation alone or to random excitation alone. In this paper an analysis will be presented on a self-excited oscillator acted upon by an external random excitation. Because of the self-excitation, the solution will contain periodic terms and, owing to the random excitation, the solution also will contain random terms. The results of this study show that the noise component of the solution decreases with increasing amplitude of self-excited oscillation; however, the band width of the noise increases with increasing amplitude of self-oscillation.

To verify the results of the analysis, the problem was simulated on an analog computer. The results of this study are in good agreement with the theory.

Equation of Oscillator With Noise as Driving Force

The equation of a Van der Pol oscillator acted upon by noise is

$$\frac{d^2V}{dt^2} - (\alpha - \gamma V^2)\frac{dV}{dt} + \omega_0^2 V + \gamma \frac{d}{dt}(V^3) = N(t) = \frac{1}{2\pi}\int_{-\infty}^{\infty} A_N(\omega) e^{i\omega t} d\omega \quad (1)$$

where $N(t)$ is a small Gaussian noise force, assumed to have a white power spectrum of density $4D$/cycle. Let

$$V(t) = V_p(t) + V_N(t)$$

where $V_p(t) = A \sin \omega_0 t$ is the periodic part of the solution and $V_N(t)$ is the randomly varying part of the solution.

If equation (1) was linear, the noise component $V_N(t)$ would be Gaussian since $N(t)$ is Gaussian; further, if the damping is small the noise component $V_N(t)$ is confined to a narrow band of frequencies close to ω_0. In a nonlinear system the noise component in general will not be Gaussian; however, if the nonlinearity is small the assumption of a Gaussian distribution is a fairly good one.

If the assumption is made that the noise component V_N is narrow band Gaussian noise, then the power spectrum $W(\omega)$ of V^3 can be calculated easily by the method of Rice[2] and Bennett.[3]

Power Spectrum of $[V_p(t) + V_N(t)]^3$

The power spectrum $W(\omega)$ of a function $V_1(t)$ representing a random voltage or force is given by

$$W(\omega) = 4\int_0^\infty \Psi(\tau)\cos(\omega\tau)d\tau \quad (2)$$

where the autocorrelation function $\Psi(\tau)$ is defined as the time average of $V_1(t)V_1(t+\tau)$. It is convenient to express $V_1(\tau)$ as a contour integral of an exponential since the averaging required to obtain $\Psi(\tau)$ is relatively easily done. Thus, following the method of Rice,[2] set

$$V_1(t) = V^3 = (V_p + V_N)^3 = \frac{3!}{2\pi}\int_c \frac{e^{tV_N}}{u^4}\,du \quad (3)$$

where the path of integration is a positive loop around $u = 0$. Thus

$$\begin{aligned}\Psi(\tau) &= \langle V_1(t)V_1(t+\tau)\rangle_{av} \\ &= \operatorname*{Lim}_{T\to\infty}\frac{1}{T}\int_0^T V_1(t)V_1(t+\tau)dt \\ &= \frac{1}{4\pi^2}\int_c \frac{6}{u^4}\,du\int_c \frac{6}{v^4}\,dv \operatorname*{Lim}_{T}\frac{1}{T} \\ &\quad \left\{\int_0^T \exp\left[iuV_1(t) + iv V_1(t+\tau)\right]dt\right\} \quad (4)\end{aligned}$$

In the present case, that of a sine wave plus noise, equation (4) can be reduced to an expression of the form (see Rice,[2] section 4.9):

$$\Psi = \sum_{n=0}^{\infty}\sum_{k=0}^{\infty}\frac{1}{k!}\psi_\tau^k h_{nk}^2 \epsilon_n \cos n\omega_0\tau \quad (5)$$

where

$$h_{nk} = \frac{j^{n+k}}{2\pi}\int_c \frac{6}{u^4}\,u^k J_n(Au)\exp\left(\frac{-\psi_0}{2}u\right)^3 \quad (6)$$

$$\epsilon_0 = 1, \quad \epsilon_n = 2 \quad \text{for} \quad n \geq 1$$

J_n is a Bessel function of the first kind order n, and $\psi_\tau = \psi(\tau)$

[1] M. A. Garstens, "Noise in Non-Linear Oscillators," *Journal of Applied Physics*, vol. 28, 1957, pp. 353–356.

Presented at the West Coast Conference of the Applied Mechanics Division, Stanford, Calif., September 9–11, 1959, of The American Society of Mechanical Engineers.

Discussion of this paper should be addressed to the Secretary, ASME, 29 West 39th Street, New York, N. Y., and will be accepted until October 10, 1959, for publication at a later date. Discussion received after the closing date will be returned.

Note: Statements and opinions advanced in papers are to be understood as individual expressions of their authors and not those of the Society. Manuscript received by ASME Applied Mechanics Division, November 18, 1957. Paper No. 59—APMW-5.

[2] S. O. Rice, *Bell System Technical Journal*, vol. 23, 1944, p. 283, and vol. 24, 1945, p. 46; also "Noise and Stochastic Processes," edited by N. Wax, Dover Publications, Inc., New York, N. Y., 1954, pp. 133–293, sections 4.8 and 4.9.

[3] W. R. Bennett, "Response of a Linear Rectifier to Signal and Noise," *Journal of The Acoustical Society of America*, vol. 15, 1944, pp. 164–172.

is the correlation function of $V_N(t)$. In order to determine the spectral distribution of V^2, h_{nk} must be evaluated; $\Psi(\tau)$ can then be calculated and finally by means of equation (2), $W(\omega)$ can be evaluated. The reduction of the autocorrelation function in equation (4) to the form given by Rice in equation (5) allows a selection in the modulation products of the solution, of those components whose frequencies fall near ω_0 and are largest in magnitude.

Examination of equation (6) shows that:

$$h_{nk} = 0 \text{ if } n + k \geqslant 4$$

A table of h_{nk} for $n + k \leq 3$ follows:

$$\left.\begin{aligned} &h_{00} = 0 && h_{10} = \frac{A}{2}\left(3\psi_0 + \frac{3A^2}{4}\right); && h_{21} = \frac{3}{2}A^2 \\ &h_{01} = 3\left(\frac{A^2}{2} + \psi_0\right) && h_{11} = 0 && h_{30} = \frac{A^3}{8} \\ &h_{02} = 0 && h_{12} = 3A \\ &h_{02} = 6 \end{aligned}\right\} \quad (7)$$

Substituting (7) into (5) one finds that:

(i) h_{21} and h_{30} have no contribution at ω_0.

(ii) If $A^2 > A > \psi_0$ the largest contribution to Ψ comes from h_{01} and h_{10}.

Substituting equation (5) into equation (2)

$$W(\omega) \simeq 4h_{01}^2 \int_0^\infty \psi_\tau \cos \omega\tau d\tau + 2h_{10}^2 \int_0^\infty \cos \omega\tau \cos \omega_0\tau d\tau \quad (8)$$

Therefore the power spectrum of V_1^2 is given by

$$W(\omega) \simeq h_{01}^2 W_n(\omega) + 2h_{10}^2\delta(\omega_0) \quad (9)$$

where $Wn(\omega)$ is the power spectrum of $V_N(\tau)$. Substituting into (9) the values of h_{01} and h_{10} given in (7)

$$W(\omega) = (3\psi_0 + {}^3/_2A^2)^2 W_n(\omega) + \frac{A^2}{2}(3\psi_0 + {}^3/_4A^2)^2\delta(\omega_0) \quad (10)$$

It is to be noted that

$$\left.\begin{aligned} &Wn(\omega) \text{ is the power spectrum of } V_N(t) \\ &\frac{A^2}{2}\delta(\omega_0) \text{ is the power spectrum of } A \sin \omega_0 t \end{aligned}\right\} \quad (11)$$

Thus the power spectrum of V^2 as given by equation (10) is the same as would have been obtained by passing the noise component through a linear device with a gain of $(3\psi_0 + {}^3/_2A^2)$ and passing the periodic part of the solution through a linear device with a gain of $(3\psi_0 + {}^3/_4A^2)$. This result is in complete agreement with that obtained by a straightforward application of Van der Pol's method neglecting higher-order cross-modulation terms.

Equivalent Linear Form of Equation (1)

Equation (1) may now be replaced by an equivalent linear equation having the same first-order power spectrum. Equation (1) becomes

$$\left[\frac{d^2V_p}{dt^2} - \left\{\alpha - r - \gamma(3\psi_0 + 3A^2/4)\right\}\frac{dV_p}{dt} + \omega_0^2 V_p\right] + \left[\frac{d^2V_n}{dt^2} - \left\{\alpha - r - \gamma(3\psi_0 + {}^3/_2A^2)\right\}\frac{dV_n}{dt} + \omega_0^2 V_n\right] = N(t) \quad (12)$$

The terms in the first bracket are all periodic, none of the other terms are periodic, hence the terms in the first bracket must be zero. Equation (12) therefore splits into two separate linear equations:

$$\frac{d^2V_p}{dt^2} - \left\{\alpha - r - \gamma(3\psi_0 + 3A^2/4)\right\}\frac{dV_p}{dt} + \omega_0^2 V_p = 0 \quad (13)$$

and

$$\frac{d^2V_N}{dt^2} - \left\{\alpha - r - \gamma(3\psi_0 + {}^3/_2A^2)\right\}\frac{dV_N}{dt} + \omega_0^2 V_N = N(t) \quad (14)$$

Solution of Equations (13) and (14)

Consider equation (13); two stable solutions are possible:
(*a*) $V_p = A \sin \omega_0 t \quad A \neq 0$. In this case

$$\alpha - r - \gamma(3\psi_0 + 3A^2/4) = 0.$$

Hence

$$A^2 = \frac{\alpha - r}{{}^3/_4\gamma} - 4\psi_0 \quad (15)$$

But $(\alpha - r)/{}^3/_4 = A_0^2$, where A_0 is the amplitude of oscillation in the absence of noise

$$\therefore A^2 = A_0^2 - 4\psi_0 \quad (16)$$

Equation (16) requires that $A_0^2 > 4\psi_0$; this condition will naturally be satisfied if $N(t)$ is kept sufficiently small.

(*b*) Another possibility is that $V_p = 0$. If this is to be a stable solution

$$\alpha - r - \gamma(3\psi_0) < 0 \quad (17)$$

i.e.,

$$\psi_0 > {}^1/_4\frac{\alpha - r}{{}^3/_4} = {}^1/_4A_0^2 \quad (18)$$

In deriving equation (9) it was assumed that $A^2 > \psi_0$; since this condition is violated in case (*b*) the analysis breaks down. For this reason, and also for the reason that the effect of small noise is of more practical interest, further analysis will be restricted to case (*a*).

Using the results of (*a*), substitute equation (15) into equation (12):

$$\frac{d^2V_N}{dt^2} - \left\{\alpha - r - \gamma\left(3\psi_0 + 2\frac{(\alpha - r)}{\gamma} - 6\psi_0\right)\right\}\frac{dV_N}{dt} + \omega_0^2 V_N = N(t) \quad (19)$$

i.e.,

$$\frac{d^2V_N}{dt^2} + \{\alpha - r - 3\gamma\psi_0\}\frac{dV_N}{dt} + \omega_0^2 V_N = N(t) \quad (20)$$

Let

$$\beta = \alpha - r - 3\gamma\psi_0 \quad (21)$$

by equation (15) $\beta \geqslant 0$. Equation (20) is therefore identical with the Langevin equation for the Brownian motion of a simple harmonic oscillator.

Since $N(t)$ is Gaussian, it is clear that $V_N(t)$ will also be a Gaussian random process with a spectrum:

$$W_N(\omega) = \frac{4D}{|\omega_0^2 - \omega^2 + i\omega\beta|^2} \tag{22}$$

from which it follows that

$$\psi(\tau) = \langle V_N(t)V_N(t+\tau)\rangle_{av} = \frac{2D}{\pi}\int_0^\infty \frac{\cos\omega\tau}{(\omega^2-\omega_0^2)^2+\beta^2\omega^2}\,d\omega$$

$$\therefore \psi(\tau) = \frac{D}{\beta\omega_0^2}\exp\left(-\frac{\beta\tau}{2}\right)\left(\cos\omega_1\tau + \frac{\beta}{2\omega_1}\sin\omega_1\tau\right) \tag{23}$$

where $\omega_1^2 = \omega_0^2 - \beta^2/4$.

In particular, when $\tau = 0$

$$\psi_0 = \sigma^2 = \langle V_N(t)^2\rangle_{av} = \frac{D}{\beta\omega_0^2} \tag{24}$$

Thus, substituting for β, a quadratic equation in ψ_0 is obtained; viz.,

$$3\gamma\psi_0^2 - (\alpha - r)\psi_0 + \frac{D}{\omega_0^2} = 0 \tag{25}$$

$$\therefore \psi_0 = {}^1/_8 A_0^2 \pm \left[({}^1/_8 A_0^2)^2 - \frac{D}{3\gamma\omega_0^2}\right]^{1/2} \tag{26}$$

where

$$A_0 = \left(\frac{\alpha - r}{{}^3/_4\gamma}\right)^{1/2}$$

is the amplitude of self-oscillation in the absence of noise.

The positive root in equation (26) can be eliminated on physical grounds, since ψ_0 must tend to zero as D tends to zero.

$$\therefore \psi_0 = {}^1/_8 A_0^2 - \left[({}^1/_8 A_0^2)^2 - \frac{D}{3\gamma\omega_0^2}\right]^{1/2} \tag{27}$$

In particular if

$$\frac{D}{3\gamma\omega_0^2} \ll ({}^1/_8 A_0^2)^2$$

equation (27) reduces to

$$\psi_0 \simeq \frac{4}{3\gamma}\frac{D}{A_0^2\omega_0^2} \tag{28}$$

Hence

$$\sqrt{\psi_0} = \sigma = \frac{1}{A_0}\left(\frac{4D}{3\gamma\omega_0^2}\right)^{1/2} \tag{29}$$

Thus for small noise, the rms amplitude of the noise component of $V(t)$ is proportional to the square root of the spectral density and inversely proportional to the amplitude of self-oscillator in the absence of noise. The effect of the noise on the amplitude of self-oscillator can be seen by substituting (27) into (16). Thus

$$A^2 = {}^1/_2 A_0^2 + {}^1/_2 A_0^2\left\{\left(1 - \frac{64D}{3\gamma A_0^4\omega_0^2}\right)^{1/2}\right\} \tag{30}$$

For a given A_0, A will decrease as the spectral density D of the noise is increased.

Bandwidth of $V_N(t)$

The power spectrum of the noise component $V_N(t)$ of the solution is given by (22)

$$W_n(\omega) = \frac{4D}{(\omega_0^2 - \omega^2) + (\omega\beta)^2}$$

Thus the bandwidth to the half-power points is given by

$$\Delta\omega = \beta \tag{31}$$

But by (21) $\beta = \alpha - r - 3\gamma\psi_0$, and if D is small

$$\psi_0 \simeq \frac{4}{3\gamma}\frac{D}{A_0^2\omega_0^2}$$

by (28).

Thus

$$\beta = {}^3/_4\gamma\frac{\alpha - r}{{}^3/_4\gamma} - \frac{4D}{A_0^2\omega_0^2}$$

$$\therefore \beta = {}^3/_4\,\gamma A_0^2 - \frac{4D}{A_0^2\omega_0^2} \tag{32}$$

Thus, if A_0 increases, β increases, and hence the bandwidth $\Delta\omega$ also increases.

Summary of Results of Analysis

The results of the analysis may be summarized as follows: If a Van der Pol oscillator is excited by a small Gaussian noise force, then:

(i) The amplitude of self-oscillation decreases with increasing $N(t)$.

(ii) The largest part of the noise component of the signal is narrow band Gaussian, centered at the frequency of self-oscillation, with a bandwidth increasing with increasing amplitude of self-oscillation.

(iii) The mean-squared amplitude of the noise component is proportional to the input noise power, but inversely proportional to the square of the amplitude of self-oscillation.

The result (iii) is in disagreement with the results obtained by Garstens[1] who finds that the noise component increases rapidly with the amplitude of self-oscillation. To resolve this problem, equation (1) was simulated on an electronic differential analyzer, and a study was made of the effect of the amplitude of self-oscillation on the magnitude of the noise component of the output.

Summary of Results of Computer Studies

The following results were obtained from a computer study of equation (1) for small $N(t)$:

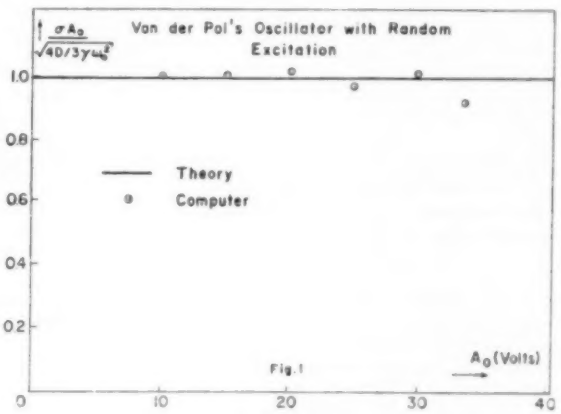

Fig. 1

(*a*) The amplitude of self-oscillation decreases only slightly with increasing noise power.

(*b*) The noise component of the output consists of narrow band noise centered at ω_0, the frequency of self-oscillation, together with a much smaller noise component at $3\omega_0$. The bandwidth of the noise increased as the amplitude of self-oscillation was increased. (In these experiments, A_0 was varied by varying $\alpha - r$ keeping γ constant.)

(*c*) The root-mean-squared amplitude of the noise component was found to vary proportionally with the root mean square of the noise input, but inversely with the amplitude of self-oscillation. Fig. 1 shows the results of one such test, in which the input was maintained constant while the amplitude of self-oscillation was varied. The results show that $A_0\sigma$ is constant, within ± 5 per cent, thus verifying the results of the analysis.

Conclusions

The main findings of the theory were confirmed by the computer studies, thereby proving Garstens' conclusions incorrect. As Garstens points out, however, actual oscillators do exhibit increasing noise with increasing amplitude of self-oscillation, from which one is forced to conclude that the model of the oscillator described by equation (1), in which the noise $N(t)$ remains constant, is incorrect. A more realistic model would require that the noise increase with increasing self-oscillation.

ROBERT GOODSTEIN[1]
Research Specialist,
Pilotless Aircraft Division,
Boeing Airplane Company,
Seattle, Wash.

A Perturbation Solution of the Equations of Motion of a Gyroscope

A perturbation method of solution is outlined for the nonlinear equations of motion of free and forced vibration of a two-gimbal gyro. Results are given for the term displayed in the solution which indicates that the outer gimbal of the gyro will not oscillate about its initial center position, but will acquire a steady rate of change of position.

Solutions of the equations of motion of a balanced, frictionless gyro will be outlined and results given for three problems:

1 Motion due to an impulse on the outer gimbal, with the gyro housing or case considered fixed.

2 Motion due to a sinusoidal torque applied to the outer gimbal, with the gyro housing considered fixed.

3 Motion due to a sinusoidal displacement of the gyro housing.

A sketch of the system, with co-ordinates and parts labeled, is shown in Fig. 1.

The method for obtaining solutions of the simultaneous nonlinear equations of motion will be a form of the perturbation method.[2] This method assumes solutions for the time variables as power series in a suitable small parameter of the problem. Substitution of the assumed series in the equations of motion and equating of like powers of the parameter yield relations for the coefficients of the assumed series. The results which are obtained in this paper are justified by their ability to yield values of the correct magnitude and variation with independent variables to verify experimental test results.

Equations of Motion

The equations of motion of the system may be obtained by applying Euler's equations for the motion of a rigid body about a fixed point to each of the four rigid bodies of the problem and combining them to eliminate the bearing forces, or applying Lagrange's equations and eliminating the constraints automatically.[3,4] Either way, the equations may be reduced to a pair of equations with φ and θ unknown.

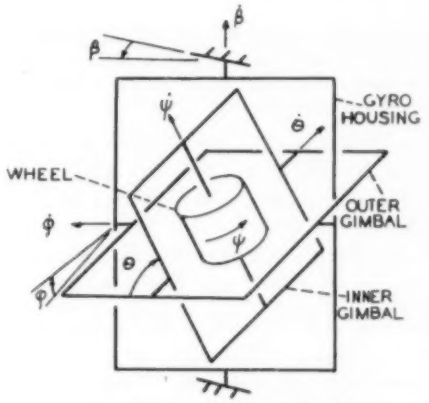

Fig. 1 Schematic of gyro assembly

[1] Formerly, Assistant Professor of Engineering Mechanics, Ohio State University, Columbus, Ohio.

[2] N. Minorsky, "Introduction to Non-Linear Mechanics," Edwards Brothers, Inc., Ann Arbor, Mich., 1947, pp. 182-185.

Contributed by the Applied Mechanics Division for presentation at the Annual Meeting, Atlantic City, N. J., November 29–December 4, 1959, of THE AMERICAN SOCIETY OF MECHANICAL ENGINEERS.

Discussion of this paper should be addressed to the Secretary, ASME, 29 West 39th Street, New York, N. Y., and will be accepted until January 11, 1960, for publication at a later date. Discussion received after the closing date will be returned.

NOTE: Statements and opinions advanced in papers are to be understood as individual expressions of their authors and not those of the Society. Manuscript received by ASME Applied Mechanics Division November 29, 1957. Paper No. 59—A-5.

[3] H. Poritsky, "Topics in Gyroscopic Motion," JOURNAL OF APPLIED MECHANICS, vol. 20, TRANS. ASME, vol. 75, 1953, pp. 1–8.

[4] E. J. Routh, "The Advanced Part of a Treatise on the Dynamics of a System of Rigid Bodies," Dover Publications, New York, N. Y., sixth edition, 1905, pp. 41–42.

Nomenclature

A = moment of inertia of outer gimbal or Cardan ring about outer gimbal axis

B = moment of inertia of outer gimbal about inner gimbal axis

C = moment of inertia of outer gimbal about an axis perpendicular to inner and outer gimbal axes

D = moment of inertia of inner gimbal about inner gimbal axis

E = moment of inertia of inner gimbal about wheel spin axis

F = moment of inertia of inner gimbal about an axis perpendicular to inner gimbal and wheel spin axes

G = moment of inertia of wheel about wheel spin axis

H = moment of inertia of wheel about any axis in plane of symmetry of wheel which is perpendicular to spin axis

J = moment of inertia of gyro case about axis of input displacement

t = time

φ = angular position of outer gimbal relative to gyro case

θ = angular position of inner gimbal relative to outer gimbal

ψ = angular position of wheel relative to inner gimbal

β = angular position of gyro case about axis of input displacement

ω_n = natural or nutation frequency

ω = forcing frequency of applied torque or angular displacement

Dots indicate differentiation with respect to time.

The moments of inertia are assumed to be principal moments of inertia, so that the wheel and gimbals are described completely for rotation about the geometric center of the wheel.

For the first two problems, in which the housing is considered fixed, the equations of motion are

$$[A + E + (F + H - E)\sin^2\theta]\ddot{\varphi} - Gs\dot{\theta}\sin\theta + 2(F + H - E)\dot{\varphi}\dot{\theta}\sin\theta\cos\theta = Q_\varphi \quad (1)$$

$$(D + H)\ddot{\theta} + Gs\dot{\varphi}\sin\theta - (F + H - E)\dot{\varphi}^2\sin\theta\cos\theta = Q_\theta \quad (2)$$

$$\dot{\psi} + \dot{\varphi}\cos\theta = \text{const} = s \quad (3)$$

Equations (1) and (2) are the equations to be solved; (3) is the expression for the so-called spin velocity of the wheel, and aids in the simplification of (1) and (2). Q_φ and Q_θ are the generalized forces, in this case torques, for co-ordinates φ and θ, respectively.

For the problem in which the gyro housing is subjected to a sinusoidal angular displacement, such as from the motion of a missile or other carrier vibrating as an elastic body, the equations of motion can be reduced to

$$\begin{aligned}[A + E + (F + H - E)\sin^2\theta]\ddot{\varphi} + 2(F + H - E)\dot{\varphi}\dot{\theta}\sin\theta\cos\theta - Gs\dot{\theta}\sin\theta &= (F + H - E)(\ddot{\beta}\cos\varphi\cos\theta\sin\theta + \dot{\beta}\dot{\theta}\cos\varphi\cos^2\theta - \dot{\beta}\dot{\theta}\cos\varphi\sin^2\theta) \\ &+ (B + D + H)\dot{\beta}^2\sin\varphi\cos\varphi - C\dot{\beta}^2\sin\varphi\cos\varphi \\ &- E\dot{\beta}^2\sin\varphi\cos\varphi\sin^2\theta - (F + H)\dot{\beta}^2\sin\varphi\cos\varphi\cos^2\theta \\ &- (D + H)\dot{\theta}\dot{\beta}\cos\varphi - Gs\dot{\beta}\sin\varphi\sin\theta + Q_\varphi\end{aligned} \quad (4)$$

$$\begin{aligned}(D + H)\ddot{\theta} - (F + H - E)\dot{\varphi}^2\sin\theta\cos\theta + Gs\dot{\varphi}\sin\theta &= (D + H)(\ddot{\beta}\sin\varphi + \dot{\beta}\dot{\varphi}\cos\varphi) - (F + H - E)\dot{\beta}^2 \\ &\cos^2\varphi\cos\theta\sin\theta - (F + H - E)\dot{\varphi}\dot{\beta}\cos\varphi \\ &(\cos^2\theta - \sin^2\theta) + Gs\dot{\beta}\cos\varphi\cos\theta + Q_\theta\end{aligned} \quad (5)$$

$$\dot{\psi} + \dot{\varphi}\cos\theta + \dot{\beta}\cos\varphi\sin\theta = \text{const} = s \quad (6)$$

Again, the third equation of motion (6) is used in simplifying (4) and (5). Equations (4) and (5) have been arranged to have the same left sides as (1) and (2), respectively, so that all terms in β and its derivatives appear on the right sides of (4) and (5).

To complete the formulations of the three problems, initial conditions and applied torques must be specified. For the first problem, that of the motion due to an impulse on the outer gimbal, the applied torques Q_φ and Q_θ will be considered as vanishingly small and

$$\text{at} \quad t = 0, \qquad \varphi = \varphi_0 \qquad \dot{\varphi} = \Omega \qquad \theta = \theta_0 \qquad \dot{\theta} = 0$$

This represents the sudden acquisition of an angular velocity Ω by the outer gimbal. For the second problem, that of the response to an applied torque about the outer gimbal axis, $Q_\varphi = M\sin\omega t$, $Q_\theta = 0$, and

$$\text{at} \quad t = 0, \qquad \varphi = \varphi_0 \qquad \dot{\varphi} = \dot{\varphi}_0 \qquad \theta = \theta_0 \qquad \dot{\theta} = \dot{\theta}_0$$

For the third problem, that of the response to a displacement of the housing, the torque about the housing axis will be assumed to be that required to produce the motion $\beta = \beta_0\sin\omega t$, with the conditions that

$$\text{at} \quad t = 0, \qquad \varphi = \varphi_0 \qquad \dot{\varphi} = \dot{\varphi}_0 \qquad \theta = \theta_0 \qquad \dot{\theta} = \dot{\theta}_0$$

Thus examination of (4) and (5) indicates that their right sides contain several forcing terms of frequency ω. It will be assumed that $Q_\varphi = Q_\theta = 0$ for this problem as in the first problem.

Method of Solution

For the problem of the motion of the system when subjected to an impulse, there will be no motion of the gimbals if there is no impulse. For small magnitudes of Ω, the imparted angular velocity, the motion will depend on the magnitude of the impulse. Therefore the solutions assumed for φ and θ will be

$$\varphi = \varphi^\circ + \varphi'\Omega + \varphi''\Omega^2 + \ldots \quad (7)$$

$$\theta = \theta^\circ + \theta'\Omega + \theta''\Omega^2 + \ldots \quad (8)$$

where $\varphi^\circ, \varphi', \varphi'', \ldots, \theta^\circ, \theta', \theta'', \ldots$, are unknown functions of time to be determined from substitution of (7) and (8) in the equations of motion. The terms in Ω to powers higher than the second will be neglected; carrying more terms increases the algebraic difficulties tremendously, and the retention of terms in Ω to the second power is sufficient to display the significant features of the motion.

For the problem of the response to a torque $M\sin\omega t$ about the outer gimbal axis, the perturbation parameter chosen is M, the amplitude of the torque. For M equal to zero, there will be no motion, and for increasing M there should be increasingly larger motion amplitudes. The assumed form of solutions will be

$$\varphi = \varphi^\circ + \varphi'M + \varphi''M^2 + \ldots \quad (9)$$

$$\theta = \theta^\circ + \theta'M + \theta''M^2 + \ldots \quad (10)$$

where again $\varphi^\circ, \varphi', \varphi'', \ldots, \theta^\circ, \theta', \theta'', \ldots$ are unknown functions of time, and terms in powers of M greater than 2 will be neglected.

Finally, application of the same method to the problem of determining the response to the input displacement $\beta_0\sin\omega t$ indicates that β_0, the magnitude of the input-angle amplitude, is the choice for the perturbation parameter. The assumed solutions are

$$\varphi = \varphi^\circ + \varphi'\beta_0 + \varphi''\beta_0^2 + \ldots \quad (11)$$

$$\theta = \theta^\circ + \theta'\beta_0 + \theta''\beta_0^2 + \ldots \quad (12)$$

where, as before, $\varphi^\circ, \varphi', \varphi'', \ldots, \theta^\circ, \theta', \theta'', \ldots$ are unknown functions of time to be determined.

In the early use of the perturbation method by Poincaré and others, a difficulty arose which is due to the use of a finite number of terms of the assumed infinite-series solution. Terms of the form $t\sin\omega t$ and $t\cos\omega t$, so-called "secular" terms, can appear in the solutions, indicating oscillations of increasing amplitude for systems which, from energy considerations, cannot possibly develop these oscillation amplitudes. For systems in which the solutions are assumed to be periodic, methods have been developed which eliminate these secular terms, and essentially account for them as small changes in frequency with changes in amplitude. However, if one is not sure that the solutions to be obtained are periodic, the periodicity condition invoked which eliminates the secular terms may disguise or lose some other feature of the motion. This is the essence of the problem at hand; the gyro is neutrally stable, in that it will remain in any position it starts in, but prefers none. Hence the motion of the gimbals is expected to be of an oscillatory nature in all the problems, but not necessarily about the initial center positions of the gimbals, there being no unique static equilibrium position. Thus the assumed solutions will be substituted into the equations of motion with no assumption that the results for φ and θ are periodic.

The details of carrying out the solutions for all the problems are quite lengthy. In each case, approximate expressions for the trigonometric terms such as $\sin\theta$, $\cos\theta$ and $\sin\theta\cos\theta$ are prepared and, with the assumed solution forms, they are substituted in the equations of motion. Terms in the perturbation parameter to the zero power are collected in each motion equation to form a pair of differential equations with the unknown functions φ° and θ° as variables. By choosing initial conditions for φ° and θ° which are compatible with the initial conditions for φ and θ and the assumed solution forms, results for φ° and θ° are obtained as functions of time. Then, using these results, terms in the perturbation parameter to the first power are collected and another

pair of differential equations is obtained, now with φ' and θ' as unknowns. Application of suitable initial conditions yields results for φ' and θ' as functions of time in each case. Finally, inserting all the results obtained, the collection of terms in the perturbation parameter to the second power yields another (considerably lengthier) pair of differential equations, and their solution yields φ'' and φ'', to complete the approximate solution of the problems.

Solution of Free-Vibration Problem

In order to clarify the details of the method proposed for all three problems, the first, or free-vibration problem will be solved in detail.

The equations of motion for this problem are (1) and (2) with $Q_\varphi = Q_\theta = 0$. The assumed forms of solution are

$$\varphi = \varphi^\circ + \varphi'\Omega + \varphi''\Omega^2 \tag{13}$$

$$\theta = \theta^\circ + \theta'\Omega + \theta''\Omega^2 \tag{14}$$

and the initial conditions are

$$\text{at} \quad t = 0, \qquad \varphi = \varphi_0 \qquad \dot{\varphi} = \Omega \qquad \theta = \theta_0 \qquad \dot{\theta} = 0$$

The trigonometric functions are approximated by

$$\begin{aligned}\sin\theta &\approx \sin(\theta^\circ + \theta'\Omega + \theta''\Omega^2)\\ &\approx \sin\theta^\circ\cos(\theta'\Omega + \theta''\Omega^2) + \cos\theta^\circ\sin(\theta'\Omega + \theta''\Omega^2)\\ &\approx \sin\theta^\circ(1 - {}^1/_2\theta'^2\Omega^2) + \cos\theta^\circ(\theta'\Omega + \theta''\Omega^2)\end{aligned} \tag{15}$$

Similarly,

$$\cos\theta \approx \cos\theta^\circ(1 - {}^1/_2\theta'^2\Omega^2) - \sin\theta^\circ(\theta'\Omega + \theta''\Omega^2) \tag{16}$$

Expressions for $\sin\theta\cos\theta$ and $\sin^2\theta$ are obtained from (15) and (16), neglecting terms in Ω to the third power and higher.

Substitution of the assumed solution forms and approximate trigonometric expressions results in

$$\begin{aligned}&\tfrac{1}{2}(A + E) + (F + H - E)[\sin^2\theta^\circ + 2\sin\theta^\circ\cos\theta^\circ(\theta'\Omega + \theta''\Omega^2)\\ &\quad + \cos^2\theta^\circ(\theta'^2\Omega^2)]\{(\ddot{\varphi}^\circ + \ddot{\varphi}'\Omega + \ddot{\varphi}''\Omega^2) - Gs(\dot{\theta}^\circ + \dot{\theta}'\Omega\\ &\quad + \dot{\theta}''\Omega^2)[\sin\theta^\circ(1 - {}^1/_2\theta'^2\Omega^2) + \cos\theta^\circ(\theta'\Omega + \theta''\Omega^2)] + 2(F\\ &\quad + H - E)(\dot{\varphi}^\circ + \dot{\varphi}'\Omega + \dot{\varphi}''\Omega^2)(\dot{\theta}^\circ + \dot{\theta}'\Omega + \dot{\theta}''\Omega^2)[\sin\theta^\circ\cos\\ &\quad \theta^\circ(1 - 2\theta'^2\Omega^2) + (\cos^2\theta^\circ - \sin^2\theta^\circ)(\theta'\Omega + \theta''\Omega^2)] = 0\end{aligned} \tag{17}$$

$$\begin{aligned}&(D + H)(\ddot{\theta}^\circ + \ddot{\theta}'\Omega + \ddot{\theta}''\Omega^2) + Gs(\dot{\varphi}^\circ + \dot{\varphi}'\Omega + \dot{\varphi}''\Omega^2)\\ &\qquad [\sin\theta^\circ(1 - {}^1/_2\theta'^2\Omega^2) + \cos\theta^\circ(\theta'\Omega + \theta''\Omega^2)]\\ &- (F + H - E)(\dot{\varphi}^\circ + \dot{\varphi}'\Omega + \dot{\varphi}''\Omega^2)^2[\sin\theta^\circ\cos\theta^\circ(1 - 2\theta'^2\Omega^2)\\ &\qquad + (\cos^2\theta^\circ - \sin^2\theta^\circ)(\theta'\Omega + \theta''\Omega^2)] = 0\end{aligned} \tag{18}$$

Recalling that φ°, φ', φ'', θ°, θ', and θ'' are unknown functions of time which are to be determined so as to satisfy the actual equations of motion approximately by satisfying (17) and (18) exactly, the left and right-hand side coefficients of terms in (17) and (18) in Ω to the zero power are equated. Collecting these coefficients leads to

$$\begin{aligned}&[(A + E) + (F + H - E)\sin^2\theta^\circ]\ddot{\varphi}^\circ - Gs\sin\theta^\circ\dot{\theta}^\circ\\ &\qquad + 2(F + H - E)\dot{\varphi}^\circ\dot{\theta}^\circ\sin\theta^\circ\cos\theta^\circ = 0\end{aligned} \tag{19}$$

$$\begin{aligned}&(D + H)\ddot{\theta}^\circ + Gs\dot{\varphi}^\circ\sin\theta^\circ\\ &\qquad - (F + H - E)\dot{\varphi}^{\circ 2}\sin\theta^\circ\cos\theta^\circ = 0\end{aligned} \tag{20}$$

To satisfy the initial conditions for the problem and the assumed solution forms, the functions φ° and θ° must themselves satisfy

$$\text{at} \quad t = 0, \qquad \varphi^\circ = \varphi_0 \qquad \dot{\varphi}^\circ = 0 \qquad \theta^\circ = \theta_0 \qquad \dot{\theta}^\circ = 0$$

The solutions of the differential equations (19) and (20) in unknowns φ° and θ° are

$$\varphi^\circ = \varphi_0 \tag{21}$$

$$\theta^\circ = \theta_0 \tag{22}$$

Collecting terms of (17) and (18) in Ω to the first power and using the results (21) and (22) for φ° and θ° lead to

$$I_0\ddot{\varphi}' - Gs\sin\theta_0\dot{\theta}' = 0 \tag{23}$$

$$I_i\ddot{\theta}' + Gs\sin\theta_0\dot{\varphi}' = 0 \tag{24}$$

where

$$I_0 = A + E + (F + H - E)\sin^2\theta^\circ \tag{25}$$

$$I_i = D + H \tag{26}$$

The pair of linear differential equations with constant coefficients (23) and (24) in unknowns φ' and θ' has initial conditions

$$\begin{aligned}&\text{at} \quad t = 0, \qquad \varphi' = 0 \qquad \dot{\varphi}' = 1\\ &\qquad\qquad\quad \theta' = 0 \qquad \dot{\theta}' = 0\end{aligned}$$

Solutions to (23) and (24) may be written as

$$\varphi' = \sin\omega_n t/\omega_n \tag{27}$$

$$\theta' = \frac{I_0}{Gs\sin\theta_0}(\cos\omega_n t - 1) \tag{28}$$

where

$$\omega_n = \frac{Gs\sin\theta_0}{(I_0 I_i)^{1/2}} \tag{29}$$

These results indicate a sinusoidal-type oscillation of each gimbal at a frequency which varies with the initial inner gimbal angle. This deviates from the result for a single rigid rotator, which oscillates at the same frequency regardless of its initial orientation. For vanishingly small gimbal inertias, (29) reduces to

$$\omega_n = Gs/H, \tag{30}$$

the result for a single rigid rotator.

The collection of terms in Ω to the second power and insertion of results for φ°, φ', θ°, and θ' lead to

$$\begin{aligned}I_0\ddot{\varphi}'' - Gs\sin\theta_0\dot{\theta}'' &= \frac{I_0\omega_n}{Gs\sin\theta_0}\\ &\left\{\left[(F + H - E)2\sin\theta_0\cos\theta_0 - \frac{I_0\cot\theta_0}{2}\right]\sin 2\omega_n t\right.\\ &\left. + [I_0\cot\theta_0 - (F + H - E)2\sin\theta_0\cos\theta_0]\sin\omega_n t\right\}\end{aligned} \tag{31}$$

$$\begin{aligned}&I_i\ddot{\theta}'' + Gs\sin\theta_0\dot{\varphi}''\\ &\quad = {}^1/_2[(F + H - E)\sin\theta_0\cos\theta_0 - I_0\cot\theta_0]\\ &\quad + {}^1/_2[(F + H - E)\sin\theta_0\cos\theta_0 - I_0\cot\theta_0]\cos 2\omega_n t\\ &\quad + I_0\cot\theta_0\cos\omega_n t\end{aligned} \tag{32}$$

This pair of linear differential equations with constant coefficients in φ'' and θ'' unknown has initial conditions

$$\text{at} \quad t = 0, \qquad \varphi'' = 0 \qquad \dot{\varphi}'' = 0 \qquad \theta'' = 0 \qquad \dot{\theta}'' = 0$$

Solutions to (31) and (32) may be written as

$$\begin{aligned}\varphi'' = {}&\frac{\sin\omega_n t}{Gs\sin\theta_0\omega_n}[2I_0\cot\theta_0 - 3(F + H - E)\sin\theta_0\cos\theta_0] + \frac{\sin 2\omega_n t}{Gs\sin\theta_0\omega_n}[{}^3/_4(F + H - E)\sin\theta_0\cos\theta_0 - {}^1/_4 I_0\cot\theta_0]\\ &+ \frac{t\cos\omega_n t}{Gs\sin\theta_0}[(F + H - E)\sin\theta_0\cos\theta_0 - I_0\cot\theta_0] - \frac{t(A + E)\cos\theta_0}{2Gs\sin^2\theta_0}\end{aligned} \tag{33}$$

$$\theta'' = \frac{1}{I_i\omega_n^2}\ [^3/_2(F + H - E)\sin\theta_0\cos\theta_0 - {}^5/_4\cot\theta_0]$$

$$+ \frac{\cos\omega_n t}{I_i\omega_n^2}\ [-(F + H - E)\sin\theta_0\cos\theta_0 + I_o\cot\theta_0]$$

$$+ \frac{\cos 2\omega_n t}{I_i\omega_n^2}\ [-^1/_2(F + H - E)\sin\theta_0\cos\theta_0 + {}^1/_4 I_o\cot\theta_0]$$

$$- \frac{t\sin\omega_n t}{I_i\omega_n}\ [-(F + H - E)\sin\theta_0\cos\theta_0 + I_o\cot\theta_0] \quad (34)$$

The approximate solutions then are as indicated by the assumed solution forms (13) and (14) with the functions φ°, θ°, φ', θ', φ'', θ'', given by (21), (22), (27), (28), (33), and (34), respectively.

The solutions for φ and θ display motions of the gimbals which start at the initial gimbal-angle positions, contain a fundamental harmonic at the frequency ω_n, and a variety of smaller second-order effects, indicated by the solutions for φ'' and θ''. The second-order terms in $\sin\omega_n t$, $\cos\omega_n t$, $\sin 2\omega_n t$, $\cos 2\omega_n t$ indicate a deviation from pure sinusoidal motion of the gimbal angles. The so-called secular terms of the form $t\sin\omega_n t$ and $t\cos\omega_n t$ arise because of the approximation-type solution. The term of main interest is the term in the solution for φ'' which is proportional to time, and indicates a steady rate of change of the central position of the oscillations of the outer gimbal. This steady-rate term $\bar{\dot{\varphi}}$ is given by

$$\bar{\dot{\varphi}} = -\frac{(A + E)\cos\theta_0}{2Gs\sin^2\theta_0}\,\Omega^2 \quad (35)$$

and is noted to increase with the square of the amplitude, and vanish if the gimbals are inertialess ($A = E = 0$) or are initially perpendicular ($\cos\pi/2 = 0$). At $\theta = 0$, the co-ordinates used are inadequate to describe the position of the system due to a redundancy between φ and ψ and, physically, the gyro goes into "gimbal lock." The solutions are not to be considered near $\theta = 0$; for an estimated 15 deg away from the $\theta = 0$ position, the results should be valid.

When the gyro is subjected to the torque $M\sin\omega t$ about the outer gimbal axis, the perturbation analysis yields results which in some respects are analogous to those obtained in a spring-mass system subjected to a sinusoidal force. The solutions for φ' and θ' of the assumed solution forms (9) and (10) indicate, neglecting the transient, sinusoidal-type motions at the forcing frequency, with a resonant build-up at $\omega \approx \omega_n$. Then, in the solution for φ'' and θ'', a steady-rate term again arises for φ'', along with the higher harmonic and secular terms. This term indicates that there will be a steady rate for the outer gimbal at all frequencies if the gimbals are not initially perpendicular, but there is a sharp resonance effect for $\omega \approx \omega_n$. For this case, the result reduces to

$$\bar{\dot{\varphi}} \approx -\frac{M^2}{2I_o\omega_n^2}(\mathrm{RR})^2\left[\frac{(A + E)\cos\theta_0}{Gs\sin^2\theta_0}\right] \quad (36)$$

where RR is termed "resonant-rise" and is given by

$$\mathrm{RR} = \frac{1}{[1 - (\omega/\omega_n)^2]} \quad (37)$$

Ever-present small dissipative torques will limit RR in actual gyros; values of 20–50 are not uncommon. The case of the response to the sinusoidal angular input can be carried out as outlined with rapidly increasing algebraic difficulty. All the results obtained for this case are similar to those for the input-torque problem; namely, a sinusoidal-type oscillation of the gimbals at the forcing frequency, with a resonant build-up at $\omega \approx \omega_n$, smaller harmonic distortion terms, secular terms, and a steady-rate term for φ'', which displays a sharp resonant build-up. The expression for the magnitude of the steady-rate term is

$$\bar{\dot{\varphi}} \approx \frac{B_0^2(\mathrm{RR})^2}{2Gs\sin\theta_0\omega_n^4}\left\{(F + H - E)\sin\theta_0\cos\theta_0\omega^2\right.$$

$$\left[\frac{(F + H - E)}{I_o}\sin\theta_0\cos\theta_0\omega^2 - G^2s^2\sin\theta_0\cos\theta_0\right]^{1/2}$$

$$- Gs\cos\theta_0\omega\left[\frac{(F + H - E)}{I_o}\sin\theta_0\cos\theta_0\omega^2\right.$$

$$\left.\left. - \frac{G^2s^2\sin\theta_0\cos\theta_0}{I_oI_i}\right]\left[\frac{Gs\cos\theta_0\omega}{I_i}\right.\right.$$

$$\left.\left.\left(\frac{(F + H - E)\sin^2\theta_0}{I_o} - 1\right)\right]\right\} \quad (38)$$

Conclusions

In a long series of test programs on gyros similar to the one under consideration in this paper, it was discovered that, for well-balanced, low-friction gyros which displayed a drift rate of only 1 or 2 deg per min when sitting on a bench, the mildest application of a sinusoidal angular input at the nutation frequency could produce outer gimbal rates on the order of 100 deg per sec! The search for the tremendous forcing torque required to explain this effect was finally narrowed down to the inertial effects of the gimbals, and subsequent tests revealed the steady rate of the outer gimbal in free vibrations. The analytical results listed in this paper yield the correct orders of magnitude and correct variation with independent parameters to explain the observed results. Although the steady rate and varying natural frequency effects for free vibration are difficult to detect and measure on rapidly spinning gyros of natural frequency 50–100 cps, a specially constructed gyro with a natural frequency of 5–10 cps has repeatedly displayed the results predicted by (35) and (29) in the free-vibration case.

Thus the following conclusions appear to be in order:

1 For nonlinear systems with neutral stability, the assumption of periodicity in a perturbation solution for an expected oscillatory-type motion may mask some feature of the result. Although unwanted secular terms may arise, they may be grouped to display a variation of natural frequency with amplitude, or recognized as part of an infinite series which is convergent if more terms are included in the analysis.

2 If the gimbals carrying a gyro may vary from the perpendicular in its normal operation, as, for instance, in the case of an aircraft or missile vertical or azimuth-gyro indicator during maneuvers, the possibility of sinusoidal excitation at the gyro natural frequency must be considered as a possibly ruinous input.

3 Since the natural frequency of the gyro varies with inner gimbal initial angle, if vibration isolators are used to protect the gyro, the isolator designer should not increase the possibility of having the gyro lose its reference or initial orientation by amplifying external excitations at possible gyro natural frequencies.

Acknowledgments

The author wishes to acknowledge the skill and efforts of Messrs. B. C. Muzzey, B. T. Plymale, and C. M. Ablow of the Physical Research Staff, Boeing Airplane Company, who encountered the gyro problems described in connection with a large missile development program.

The method and results of this paper have been condensed from the author's dissertation, written under the capable direction of Prof. C. T. West, Chairman, Department of Engineering Mechanics, The Ohio State University.

T. C. YEN
Senior Staff Engineer,
Nuclear Engineering Division,
The Franklin Institute Laboratories
for Research and Development,
Philadelphia, Pa.
Assoc. Mem. ASME

S. KAO
Development Engineer,
Engineering Development Division,
The M. W. Kellogg Company,
New York, N. Y.
Mem. ASME

Vibration of Beam-Mass Systems With Time-Dependent Boundary Conditions

Vibration problems of beams with time-dependent boundary conditions are solved by the method of Laplace transforms. The problems treated include the simply supported, cantilevered, and fixed beams carrying a single arbitrarily placed mass; two equal masses symmetrically placed on a simply supported or fixed-end beam and a beam carrying a mass at the center and two equal masses at tips, striking a spring.

THE vibration problem of a beam with time-dependent boundary conditions can be solved by using Laplace transforms [1],[1] or by transforming the nonhomogeneous boundary conditions into homogeneous ones and thus solving a nonhomogeneous differential equation [2, 3].

The fundamental frequency of a simply supported beam with a concentrated mass at mid-point [4] and a cantilever with a concentrated mass at the free end [5] can be obtained by classical methods. For a beam with an arbitrarily located concentrated mass, the natural frequencies have been obtained by making use of series expansion [6]. By using Laplace transforms, employed for the solution of problems presented in this paper, closed-form frequency equations can be obtained readily for a beam with several concentrated masses.

The present analysis is related to numerous practical engineering problems. Typical among these are the vibration of piping systems carrying large valves, structures with heavy machinery subjected to earthquake or other excitation, and problems in a moving vehicle such as truck frames and airplane-wing assemblies.

Vibration of a Beam With Ends Uniformly Accelerated

Since the solutions for the different cases are essentially similar, they are illustrated briefly by solving the case of a simply supported beam with a concentrated mass.

[1] Numbers in brackets designate References at end of paper.

Presented at the Summer Conference of the Applied Mechanics Division, Troy, N. Y., June 18–20, 1959, of THE AMERICAN SOCIETY OF MECHANICAL ENGINEERS.

Discussion of this paper should be addressed to the Secretary, ASME, 29 West 39th Street, New York, N. Y., and will be accepted until October 10, 1959, for publication at a later date. Discussion received after the closing date will be returned.

NOTE: Statements and opinions advanced in papers are to be understood as individual expressions of their authors and not those of the Society. Manuscript received by ASME Applied Mechanics Division, December 9, 1957. Paper No. 59—APM-22.

Case 1. In Fig. 1(*a*), the motion of the support of the beam with a concentrated mass is defined by $f(t)$. Let the beam be initially at rest, so that $y(x, 0) = \dot{y}(x, 0) = z(x, 0) = \dot{z}(x, 0) = 0$. The differential equations governing the left and right parts of the beam, Fig. 1(*b*), and their corresponding Laplace transforms are, respectively,

$$y^{iv}(x, t) + a^2\ddot{y}(x, t) = 0 \quad Y^{iv}(x, s) - q^4Y(x, s) = 0 \quad (1a)$$

$$z^{iv}(x, t) + a^2\ddot{z}(x, t) = 0 \quad Z^{i}(x, s) - q^4Z(x, s) = 0 \quad (1b)$$

where $q^4 = -a^2s^2$, Y and Z are Laplace transforms of the y and z-functions, dots represent time differentials while primes stand for differentials with respect to x.

The boundary conditions for the left and right ends of the beam are

$$y(0, t) = z(c, t) = f(t)$$
$$y'(0, t) = z'(c, t) = 0 \quad (2)$$

Compatibility conditions at the junction of the left and right parts of the beam require

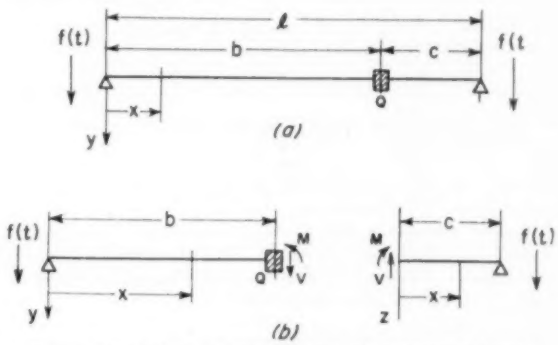

Fig. 1 Case 1; Simply supported beam, one concentrated mass

Nomenclature

$a = \sqrt{m/EI}$
b, c = location of the concentrated mass, Figs. 1 to 5
E = Young's modulus
$f(t), F(s)$ = displacement of beam support and its Laplace transform
I = moment of inertia of beam cross section
$2k$ = spring constant as defined
l = beam length as defined in Figs. 1 to 5
M = moment
m = uniform mass of beam per unit length
Q, R = concentrated mass
s = parameter in Laplace integral
t = time
V = shear
v = velocity
x = distance from left hand support
$y(x, t), z(x, t)$ = beam displacement

$$
\left.\begin{aligned}
y''(b,t) &= -M/EI = z''(0,t)\\
y'''(b,t) &= \frac{Q}{EI}\,\ddot{y}(b,t) - \frac{V}{EI} = -\frac{Q}{m}\,y^{iv}(b,t) + z'''(0,t)\\
z(0,t) &= y(b,t)\\
z'(0,t) &= y'(b,t)
\end{aligned}\right\} \quad (3)
$$

The Laplace transforms corresponding to Equations (2) and (3) become

$$
\left.\begin{aligned}
&Y(0,s) = Z(c,s) = F(s) \qquad Y''(0,s) = Z''(c,s) = 0\\
&Y''(b,s) = Z''(0,s) \qquad Y'''(b,s) = -\frac{Q}{m}\,Y^{iv}(b,s) + Z'''(0,s)\\
&Z(0,s) = Y(b,s) \qquad Z'(0,s) = Y'(b,s)
\end{aligned}\right\} \quad (4)
$$

The solutions of Equations (1a) and (1b) are given by

$$
\begin{aligned}
Y(x,s) &= C_1\cos qx + C_2\sin qx + C_3\cosh qx + C_4\sinh qx\\
Z(x,s) &= c_1\cos qx + c_2\sin qx + c_3\cosh qx + c_4\sinh qx
\end{aligned} \quad (5)
$$

Determining the C and c-functions in terms of s from the eight boundary conditions of Equation (5), we obtain for $0 \le x \le b$

$$
y(x,s) = F(s)\left[\frac{1}{2}\,(\cos qx + \cosh qx) + \frac{1}{D}\,(N_1\sin qx + N_2\sinh qx)\right] \quad (6)
$$

where

$$
\begin{aligned}
D &= -2\sin ql\sinh ql + \frac{Qq}{m}\,(-\sinh qb\sinh qc\sin ql + \sin qb\sin qc\sinh ql)\\
N_1 &= \sinh ql\,(\cos ql - 1) - \frac{Qq}{2m}\,[\sinh qb\,(\sin qc + \sinh qc)\\
&\quad + \sin qc\sinh qc + \sin qc\cos qb\sinh ql - \sinh qc\sinh qb\cos ql]\\
N_2 &= \sin ql(\cosh ql - 1) + \frac{Qq}{2m}\,[\sin qb(\sin qc + \sinh qc)\\
&\quad + \sin qc\sinh qc + \sinh qc\cos qb\sin ql - \sin qc\sin qb\cosh ql]
\end{aligned}
$$

Natural frequencies are characterized by $D = 0$, yielding

$$
\frac{Q}{2ml} = \frac{\sin ql\sinh ql}{ql(\sin qb\sin qc\sinh ql - \sinh qb\sinh qc\sin ql)} \quad (7)
$$

The solution of Equation (1a) can be obtained [1] by finding the inverse of Equation (6). Such mathematical procedures are well known. For the case of uniform acceleration $f(t) = \alpha t^2/2$, and the solution of Equation (1a) for $0 \le x \le b$ is,

$$
\left.\begin{aligned}
y(x,t) &= y_1(x,t) + y_2(x,t)\\
&= \alpha a^2 l^4\left\{\frac{1}{2}\left(\frac{t}{al^2}\right)^2 - \frac{1}{24}\left[\left(\frac{x}{l}\right)^4 + \frac{x}{l} - 2\left(\frac{x}{l}\right)^3\right]\right.\\
&\quad \left. - \frac{Qc}{6ml^2}\left[\left(1 - \left(\frac{c}{l}\right)^2\right)\frac{x}{l} - \left(\frac{x}{l}\right)^3\right]\right\}\\
&\quad + 2\alpha a^2 l^4\sum_{n=1}^{\infty}\frac{\cos(q_n^2\,t/a)}{q_n^{\,6}U(q_n)}\,[N_1(q_n)\sin q_n x + N_2(q_n)\sinh q_n x]\\
y''(x,t) &= \alpha a^2 l^2\left\{\left[\frac{x}{2l}\left(1 - \frac{x}{l}\right) + \frac{Qcx}{ml^3}\right]\right.\\
&\quad \left. + 2\sum_{n=1}^{\infty}\frac{\cos(q_n^2\,t/a)}{q_n^{\,2}U(q_n)}\,[-N_1(q_n)\sin q_n x + N_2(q_n)\sinh q_n x]\right\}
\end{aligned}\right\} \quad (8)\ (cont.)
$$

where $N_1(q_n)$ and $N_2(q_n)$ are as defined in Equation (6) with q_n representing the roots of Equation (7) and $U(q_n) = dD/dq$, $q = q_n$. For $b \le x \le l$, x is to be replaced by $(l - x)$ and b by c in the foregoing equations.

Similar solutions for the cantilever and fixed-ends beam also can be obtained by observing appropriate boundary conditions. For beam-mass systems symmetrical about the center line only half of the beam needs to be investigated. The boundary conditions and the resulting frequency equations for the various cases treated can be listed briefly as follows:

Case 2. Simply supported beam, two symmetrical concentrated masses, Fig. 2:

$$
\begin{aligned}
&y(0,t) = f(t)\\
&y''(0,t) = z'(c,t) = z'''(c,t) = 0
\end{aligned}
$$

$$
\frac{Q}{2ml} = \frac{\cos ql\cosh ql}{ql(\sin qb\cos qc\cosh ql - \sinh qb\cosh qc\cos ql)} \quad (9)
$$

Case 3. Cantilever beam, one concentrated mass, Fig. 3:

$$
\begin{aligned}
&y(0,t) = f(t)\\
&y'(0,t) = z''(c,t) = z'''(c,t) = 0
\end{aligned}
$$

$$
\begin{aligned}
\frac{Q}{ml} &= \frac{2}{ql}\,(1 + \cosh ql\cos ql)\\
&\quad [(1 - \cosh qb\cos qb)(\sinh qc\cos qc - \cosh qc\sin qc)\\
&\quad - (1 + \cosh qc\cos qc)(\sinh qb\cos qb - \cosh qb\sin qb)]^{-1}
\end{aligned} \quad (10)
$$

Case 4. Fixed-ends beam, single concentrated mass, Fig. 4:

$$
\begin{aligned}
&y(0,t) = z(c,t) = f(t)\\
&y'(0,t) = z'(c,t) = 0
\end{aligned}
$$

$$
\begin{aligned}
\frac{Q}{ml} &= -\frac{2}{ql}\,(1 - \cosh ql\cos ql)\\
&\quad [(1 - \cosh qb\cos qb)(\sinh qc\cos qc - \cosh qc\sin qc)\\
&\quad + (1 - \cosh qc\cos qc)(\sinh qb\cos qb - \cosh qb\sin qb)]^{-1}
\end{aligned} \quad (11)
$$

Case 5. Fixed-ends beam, two concentrated masses, Fig. 5:

$$
\begin{aligned}
&y(0,t) = f(t)\\
&y'(0,t) = z'(c,t) = z'''(c,t) = 0
\end{aligned}
$$

$$
\begin{aligned}
\frac{Q}{ml} &= \frac{2}{ql}\,(\sinh ql\cos ql + \cosh ql\sin ql)\\
&\quad [\cos qc\,(\cosh qc - \cosh ql\cos qb + \sinh ql\sin qb)\\
&\quad + \cosh qc\,(\cos qc - \cosh qb\cos ql - \sinh qb\sin ql)]^{-1}
\end{aligned} \quad (12)
$$

It is interesting to note that if in Fig. 1, $c = b$, or in Fig. 2, $c = 0$, $b = l$ while Q is replaced by $Q/2$, both Equations (7) and (9) can be reduced to

$$
\frac{Q}{4mb} = \frac{\cos qb\cosh qb}{qb(\sin qb\cosh qb - \cos qb\sinh qb)} \quad (13)
$$

which is the expression obtained by von Karman and Biot [4] for the simply supported beam with one center mass. The frequency equation for a single center mass on a fixed beam can be in a similar manner obtained from Equation (11) or (12).

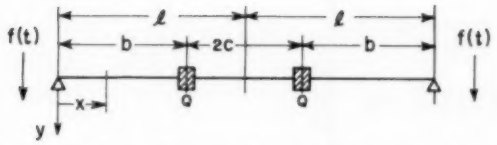

Fig. 2 Case 2; simply supported beam, two concentrated masses

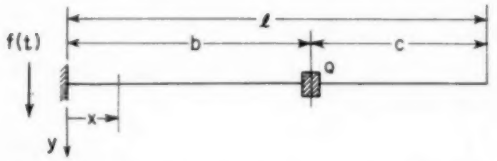

Fig. 3 Case 3; cantilever beam, one concentrated mass

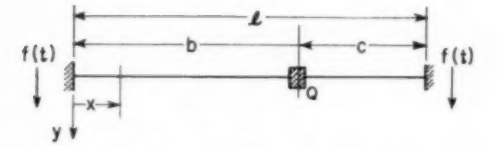

Fig. 4 Case 4; fixed-ends beam, one concentrated mass

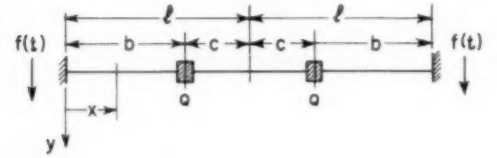

Fig. 5 Case 5; fixed-ends beam, two concentrated masses

$$\frac{Q}{2ml} = \frac{\sin ql \cosh ql + \cos ql \sinh ql}{ql(1 - \cos ql \cosh ql)} \tag{14}$$

while for the cantilever beam with an end mass, Equation (10), setting $c = 0$,

$$\frac{Q}{ml} = \frac{1 + \cos ql \cosh ql}{ql(\sin ql \cosh ql - \cos ql \sinh ql)} \tag{15}$$

which is in agreement with Prescott's result [5].

Beam With Other Time-Dependent Boundary Conditions

In the foregoing derivations, only the case of uniform acceleration at the supports has been illustrated. However, the method can be applied to any time-dependent boundary conditions, provided that their Laplace transforms can be found. Let the case be that shown in Fig. 6 where a uniform beam, carrying concentrated masses $2Q$ at the center and R at each end, strikes a spring (spring constant $2k$) with an initial velocity v. The initial conditions are $\dot{y}(x, 0) = v$ and $y(x, 0) = 0$. The Laplace transform of Equation (1a) becomes

$$Y^{iv}(x, s) - q^4 Y(x, s) = a^2 v$$

The boundary conditions (before the beam-mass system is separated from the spring) are

$$Q\bar{y}(0, t) + \int_0^l \bar{y}(x, t)m dx + ky(0, t) + R\bar{y}(x, l) = 0$$

$$y'(0, t) = y''(l, t) = y'''(l, t) + \frac{R}{m} y^{iv}(l, t) = 0$$

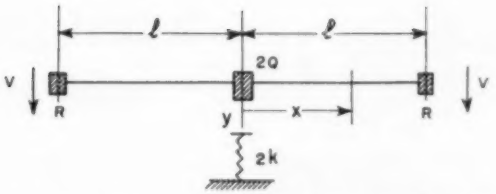

Fig. 6 Beam with concentrated masses strikes a spring with spring constant 2k

or, in transformed presentation:

$$Q[s^2Y(0, s) - v] + m\int_0^l [s^2Y(x, s) - v]dx + kY(0, s) + R[s^2Y(l, s) - v] = 0$$

$$Y'(0, s) = Y''(l, s) = Y'''(l, s) + \frac{R}{m} Y^{iv}(l, s) = 0$$

Following the procedure outlined, $Y(x, s)$ can be solved and the frequency equation determined as

$$\frac{Rq}{m} = \frac{\dfrac{m}{Qq}(\sinh ql \cos ql + \cosh ql \sin ql) + (1 + \cosh ql \cos ql)\left(1 - \dfrac{Ka^2}{Qq^4}\right)}{-\dfrac{2m}{Qq}\cosh ql \cos ql - (\sinh ql \cos ql - \cosh ql \sin ql)\left(1 - \dfrac{ka^2}{Qq^4}\right)} \tag{16}$$

It can be shown that if $k \ll Q$ and $m \ll Q$, Equation (16) reduces to that of a cantilever beam with an end mass. On the other hand, if $k \ll Q \ll R$, Equation (16) approaches that of the simply supported beam with a concentrated mass at the center.

Discussion

The investigation presented here for beam-mass systems can be extended to multimass cases with various other boundary conditions, although the algebraic manipulations may become quite tedious.

The $y_2(x, t)$ function of Equation (8) shows that the deflections and amplitudes are directly related to frequencies. Frequencies up to the fifth modes, as obtained for the various cases from Equations (7), (9), (10), (11), (12), are plotted as function of Q/ml in Figs. 7 and 8 for various positions of the concentrated mass. From the plots, the following observations can be made.

As Q/ml increases, approaching the case of the weightless beam as a limit, the frequency tends to decrease. For $Q/ml > 5$, the high-mode frequencies seem to remain constant if the mass is sufficiently far removed from the supports while the fundamental frequencies of all cases can be predicted with the simple energy method (spring suspended mass) with minor error. The fundamental frequencies are lowest when maximum static deflections are produced; i.e., the mass is at the mid-point of the two-support system and at the end for the cantilever case. This is in agreement with the principles of Rayleigh's method. However, this statement no longer holds beyond the fundamental mode.

It should be pointed out that, in Fig. 7 of Cases 1 and 4, the mass locations $c/l = 0.25$ or 0.5 are only approximate. When c/l is exactly 0.50, these cases require special treatment, calling for the use of Equations (13) and (14); the even modes will then be missing. Similarly, the 4th, 8th, ... modes of Case 1 are missing when $c/l = 0.25$. Similar phenomena also can be observed in the two-mass systems when $c/l = 0$. The possible coincidence of

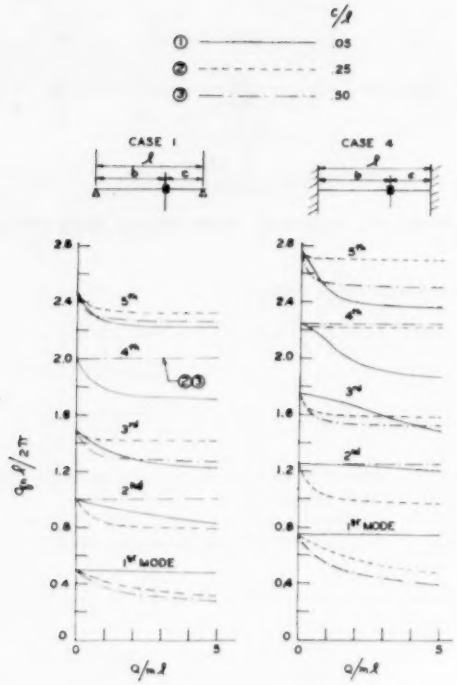

Fig. 7 Frequency curves, cases 1 and 4

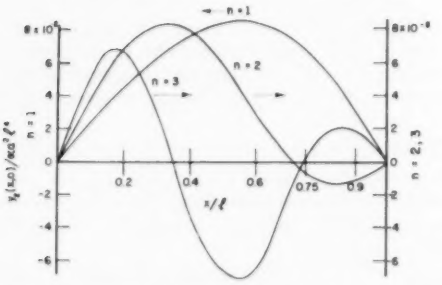

Fig. 9 First three modes of vibration $Q/ml = 5$, $c/l = 0.25$ $t = 0$

Fig. 8 Frequency curves, cases 2, 3, and 5

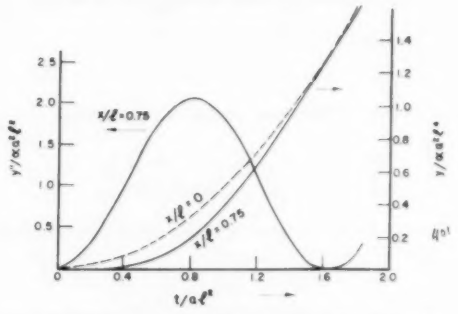

Fig. 10 Beam movement and bending moment $Q/ml = 5$, $c/l = 0.25$

the mass location and nodal points at the particular modes are suspected to be the cause.

A numerical example of Equation (8) is evaluated with $Q/ml = 5$ and $c/l = 0.25$. The first three frequencies become $q_1 l = 1.9596$, $q_2 l = 4.9666$, and $q_3 l = 8.8658$. Beam displacement, bending moment, and time are expressed in dimensionless parameters as $y/\alpha a^{2}l^{4}$, $y''/\alpha a^{2}l^{2}$, and t/al^{2}, respectively. The first three modes of vibration are shown in Fig. 9; beam movement and bending moment at the location of the mass are plotted against time in Fig. 10. It is seen that the vibratory amplitude of the mass Q, $(x/l = 0.75)$ is very small at the higher modes, which is in line with the conclusion of von Karman and Biot [4]. The infinite series of Equation (8) converges rapidly, so that carrying the summation to the first term is adequately accurate in this particular case.

Acknowledgments

The authors wish to express their gratitude to Dr. N. A. Weil, manager of the Mechanical Development Division of The M. W. Kellogg Company, for his encouragement and guidance. Valuable comments and suggestions by Drs. D. H. Cheng and M. Yachter are acknowledged also.

References

1 G. A. Nothmann, "Vibration of a Cantilever Beam With Prescribed End Motion," JOURNAL OF APPLIED MECHANICS, vol. 15, TRANS. ASME, vol. 70, 1948, pp. 327–334.

2 R. D. Mindlin and L. E. Goodman, "Beam Vibrations With Time-Dependent Boundary Conditions," JOURNAL OF APPLIED MECHANICS, vol. 17, TRANS. ASME, vol. 72, 1950, pp. 377–380.

3 J. G. Berry and P. M. Naghdi, "On the Vibration of Elastic Bodies Having Time-Dependent Boundary Conditions," *Quarterly of Applied Mathematics*, vol. 14, 1956, 43–50.

4 T. von Karman and M. A. Biot, "Mathematical Method in Engineering," McGraw-Hill Book Company, Inc., New York, N. Y., 1940.

5 John Prescott, "Applied Elasticity," Dover Publications, New York, N. Y., 1946, p. 213.

6 Dana Young, "Vibration of a Beam With Concentrated Mass, Spring, and Dashpot," JOURNAL OF APPLIED MECHANICS, vol. 15, TRANS. ASME, vol. 70, 1948, pp. 65–72.

7 S. Timoshenko, "Vibration Problems in Engineering," third edition, D. Van Nostrand Company, New York, N. Y., 1955.

8 R. V. Churchill, "Modern Operational Mathematics in Engineering," McGraw-Hill Book Company, Inc., New York, N. Y., 1944.

E. A. RIPPERGER
Professor,
Department of Engineering Mechanics,
University of Texas, Austin, Tex.
Mem. ASME

W. R. BARTON
Supervisor,
Drogue Research,
Sandia Corporation,
Albuquerque, N. Mex.

Dynamic Loading Tests of an Aircraft-Type Beam

Experimental tests were conducted to determine the failure characteristics of simplified box-type wing structures loaded dynamically, as compared to those of similar beams loaded statically. It was found that under dynamic loading, of the type applied, failure occurred at essentially the same loads and deflections observed at failure under static loading conditions. Tip deflections and accelerations were calculated using the force-deflection relationship determined by static loading, and compared to measured values. Agreement between measured and calculated values was only fair.

Introduction

THE relatively meager amount of information available regarding failure of materials subjected to dynamic loads makes the establishment of a suitable criterion of failure difficult. Usually, in design calculations for dynamic loading, a factor called the dynamic load factor is introduced. This factor, which is defined as the ratio between the failure loads for dynamic and static loading conditions, is assigned a value between 1 and 2. The factor is assumed to be greater than 1 because of the known fact that many materials, when loaded quickly, support a much larger load without failure than they do under static loading conditions. The choice of a specific value is based primarily on good engineering judgment. The validity of this procedure for obtaining a design load for dynamic conditions is open to question, not only because of the uncertainty involved in selecting a load factor, but also because it has not yet been shown that peak load is the most reliable criterion of failure.

The mechanism by which built-up structures fail under dynamic loading is more complicated than that of simple rods and beams. Consequently, a satisfactory criterion of failure is more difficult to establish for such structures. To obtain information directly applicable to this problem, the study reported here has been made of the response of a built-up aircraft-type beam to dynamic loads of sufficient intensity to cause failure of the beam by any definition.

Test Beam Details

Ten beams of the type shown in Fig. 1 were loaded dynamically to destruction. These beams, which were 48 in. long, 13 in. wide, and 6 in. deep, were made up of a curved 24S-T aluminum-alloy skin, 0.025 in. thick, stiffened with $^1/_2 \times {}^1/_2 \times 0.0625$-in. aluminum angles on 2-in. centers, and spars consisting of $^1/_2$-in-sq aluminum caps and a 0.040-in. aluminum web. Rivets in the stiffeners and spar caps were on $^3/_4$-in. centers. The weight of each beam was about 12 lb and the moment of inertia of the typical cross section was 11.76 in.[4] Beams of this same type had been used for a previous study of behavior under static loading. Some of the results of that study will be introduced later in this paper for comparison with the results of the dynamic-loading tests.

Test Procedure

The dynamic tests were conducted by attaching equal weights at the ends of the beam to be tested, raising the beam to a given height, dropping it, and then suddenly arresting the fall at the mid-point of the beam. Under these conditions, the beam acts essentially as two tip-loaded falling cantilevers suddenly arrested at the roots. Beams were lifted for the drop by means of a pull-bar attached at the center of the beam as shown in Fig. 2. This steel pull-bar, $1^3/_4$ in. diam, and about 25 ft long, passes through an opening at the top of a tower. By using a chain hoist attached through a quick-disconnect link to the upper end of the bar, the beam was raised to the required height for the drop. When the link was opened, the entire assembly, including the pull-bar, fell as a unit. The fall was arrested when a collar on the upper end of the pull-bar came in contact with a neoprene-rubber pad supported by the drop-tower framework. The shock of the impact was cushioned, to some extent, by the rubber pad. The falling beam was constrained to move in the vertical plane by guides at the ends of the beam moving in slots in the steel framework which may be seen in Fig. 2.

Measurements

All of the physical quantities believed to be involved significantly in the dynamic failure of a beam were detected by suitable electrical transducers and recorded with a 12-channel recorder. These quantities are:

1 Deflections—measured at the root, mid-point, and tip of each cantilever. Measurements were made by means of strip potentiometers supported on steel angles which may be seen behind the beam in Fig. 2.

2 Accelerations—measured at each tip and at the center of the beam. Statham 100g accelerometers with natural frequencies of about 700 cps were used for the measurements.

3 Strains—measured by six SR-4 strain gages of the post-yield type (PA-3), mounted on the top skin of each beam; three on each side of the supporting yoke at the center of the beam, $1^1/_2$ in. from the mid-line. One of the three gages on each side was placed on the longitudinal center line and the other two were located 1 in. from the edges of the beam.

4 Skin rupture—rupture was indicated by the interruption of a current carried in annealed copper wires, 0.001 in. diam, insulated with Formvar and cemented to the upper surface of the beam and to the upper spar caps. Tests have indicated that these

Presented at the West Coast Conference of the Applied Mechanics Division, Los Angeles, Calif., September 8–10, 1958, of THE AMERICAN SOCIETY OF MECHANICAL ENGINEERS. This paper was not preprinted.

Discussion of this paper should be addressed to the Secretary, ASME, 29 West 39th Street, New York, N. Y., and will be accepted until October 10, 1959, for publication at a later date. Discussion received after the closing date will be returned.

NOTE: Statements and opinions advanced in papers are to be understood as individual expressions of their authors and not those of the Society. Manuscript received by ASME Applied Mechanics Division, May 19, 1958.

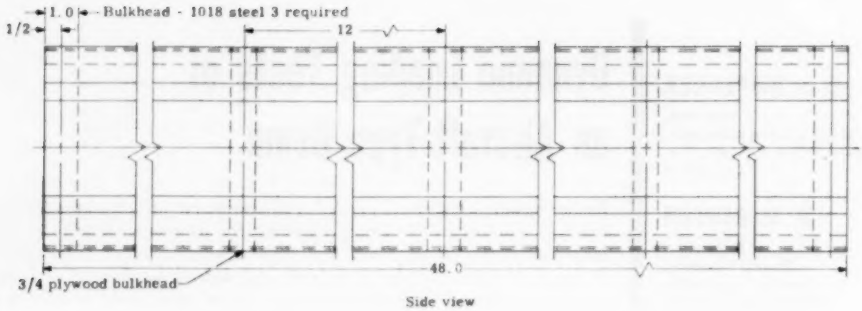

Side view

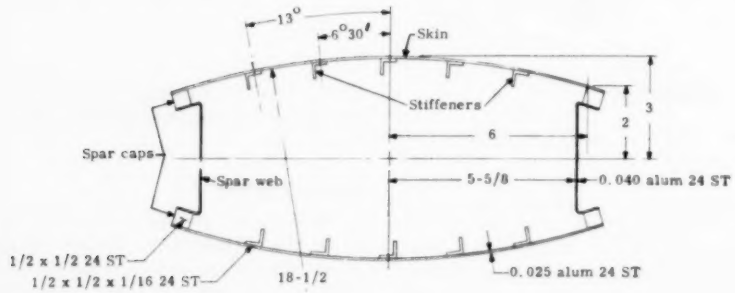

End view

Fig. 1 Beam description

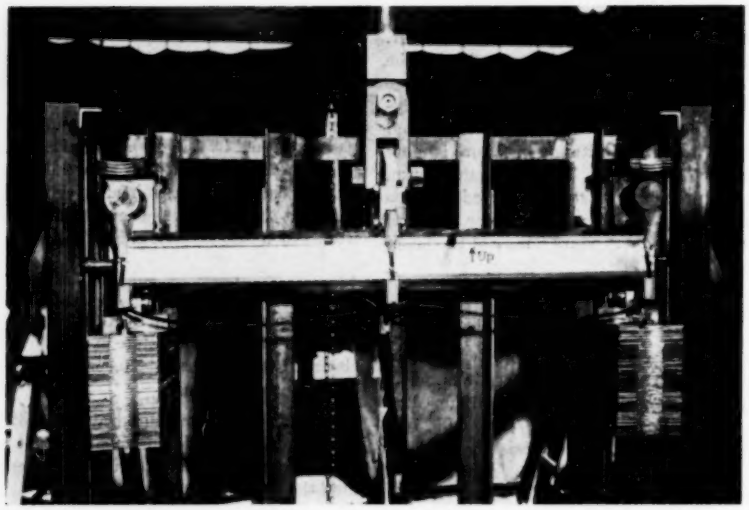

Fig. 2 Beam arrangement before release

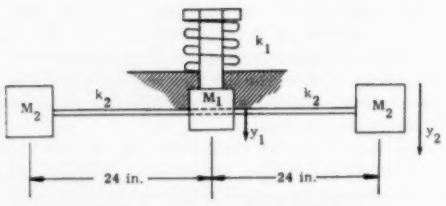

Fig. 3 Simplified schematic of the beam

wires break at practically the same strain as the 24S-T aluminum from which the beams were made.[1]

Simplified Analysis of Beam Motion

The beam with its tip weights, the pull-bar, and the rubber cushion can be regarded as a two-degree-of-freedom system, the

[1] H. W. Foster, "A Method of Detecting Incipient Fatigue Failure," *Proceedings of The Society for Experimental Stress Analysis*, vol. 4, 1957, p. 25.

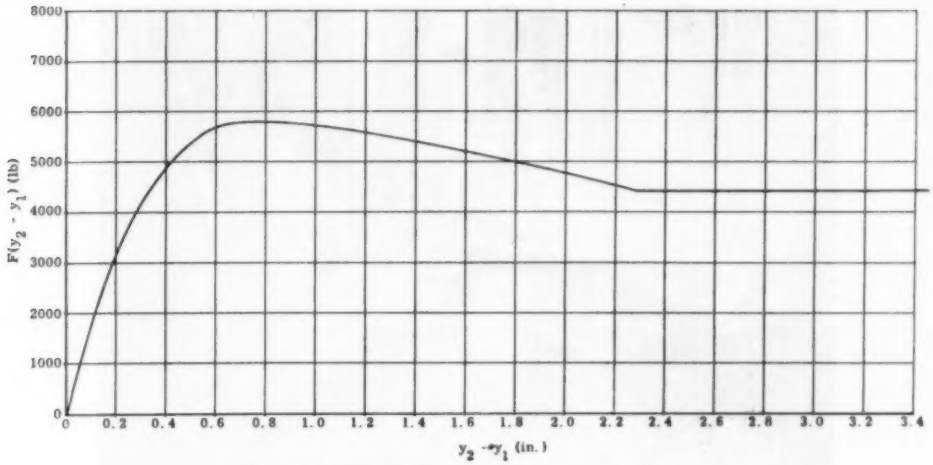

Fig. 4 Tip load versus tip deflection, cantilever test beam

essential elements of which are shown in Fig. 3. The equations of motion of this system, assuming complete linearity, are:

$$M_1\ddot{y}_1 + k_1y_1 - k_2(y_2 - y_1) = 0$$

$$M_2\ddot{y}_2 + k_2(y_2 - y_1) = 0$$

For large values of $y_2 - y_1$, the force-deflection relationship for the tip mass becomes nonlinear. The equations of motion are then more correctly written as:

$$M_1\ddot{y}_1 + k_1y_1 - F(y_2 - y_1) = 0$$

$$M_2\ddot{y}_2 + F(y_2 - y_1) = 0$$

The initial conditions for the conditions of the test described are taken as follows:

$$y_1 = y_2 = 0$$

$$\dot{y}_1 = \dot{y}_2 = V_0$$

where V_0 represents the impact velocity.

The function $F(y_2 - y_1)$ obtained from static loading tests is shown in Fig. 4. Solutions of the equations of motion have been obtained for y_1, y_2, $\dot{y}_1$, $\dot{y}_2$, and $y_2 - y_1$ by means of an analog computer using $F(y_2 - y_1)$ as shown in Fig. 4. It is understood that the function $F(y_2 - y_1)$ obtained from static loading tests may differ significantly from the corresponding function for dynamic conditions. However, one of the purposes of this investigation has been to determine the degree of accuracy which may be obtained in the calculation of such quantities as deflection and acceleration using statically determined, but nonlinear load-deflection curves in the simplified equations of motion for a system with an infinite number of degrees of freedom. Methods which provide an accurate prediction of deflection and accelerations, when combined with a suitable criterion of failure, should allow accurate predictions to be made concerning failure or nonfailure of a given structure subjected to a transient loading.

Basic Test Parameters

The mass M_1, which includes a bulkhead at the center of the beam, the pull-bar, and an attachment fixture, was 416 lb for each of the ten beams. The tip mass M_2 was one of the variables in the test. It ranged in value from 250 to 402 lb.

The stiffness of the rubber pad which formed the spring indicated at the center of the beam in Fig. 3 varied somewhat depending upon the temperature at the time of test. Its value was taken as 11,000 lb per in. for the first four beams tested and 8750 lb per in. for the last six to be tested.

The spring constant k_2, for the beam, is not required in the calculations, since it enters the solution in the function $F(y_2 - y_1)$.

The tip weights, drop heights, impact velocities, and kinetic energy at impact for the ten test beams are shown in Table 1 along with the fundamental periods of vibration for the two halves of the beam treated as tip-loaded cantilevers.

For beams Nos. 1 through 4, the choice of tip weights and drop heights was made to insure a definite failure. For the remaining six beams, drop heights and tip weights were selected so as to bracket the conditions which led to failure. It may be noted that

Table 1 Data for test beams

Beam no.	Tip weight, lb	Drop height, in.	Impact velocity, fps	Total energy, ft-lb	Fundamental period of beam, sec
1[a]	402	33	13.3	1105	40×10^{-3}
2[a]	402	33	13.3	1105	40×10^{-3}
3[a]	402	33	13.3	1105	40×10^{-3}
4[a]	402	33	13.3	1105	40×10^{-3}
5	200	38.5	14.4	640	28×10^{-3}
6[a]	262	38.5	14.4	845	32×10^{-3}
7[a]	263	33	13.3	724	32×10^{-3}
8	290	29	12.4	700	35×10^{-3}
9	350	29	12.4	844	37×10^{-3}
10	250	33	13.3	690	32×10^{-3}

[a] These beams ruptured. The remaining beams showed varying signs of distress, but did not fail.

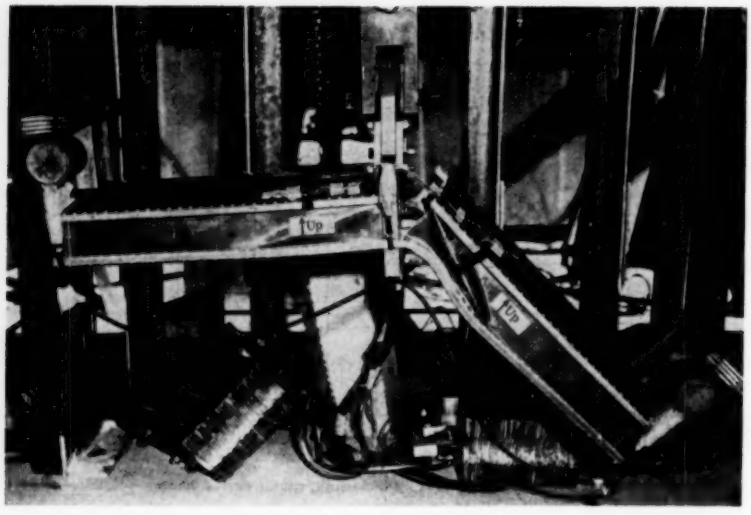

Fig. 5 Beam 2 after failure

for beam No. 5, the load was decreased to one half that used on the first four beams, but the drop height was increased to 38.5 in. which happened to be the maximum available height. Since this beam did not fail, the kinetic energy at impact for beam No. 6 was increased by about 32 per cent by increasing the tip load and using the maximum drop height. These parameters produced failure so the kinetic energy of beam No. 7 was decreased by reducing the drop height.

The results of the tests of beams Nos. 5, 6, and 7 indicated that the critical kinetic energy at impact was about 700 ft-lb. Consequently, the parameters for the three remaining tests were chosen to make the product of tip weight and drop height approximately 700 ft-lb. Beam No. 9 falls somewhat outside this pattern because of an error in setting the drop height. It is interesting to note, however, that this beam did not fail even though the kinetic energy at impact was 21 per cent greater than the 700-ft-lb figure previously quoted as the energy required to cause failure.

Beam No. 2 (tip load 402 lb, impact velocity 13.3 fps) is shown in Fig. 5 as it appeared after failure. It is evident that, despite the symmetry of the beam, the right side has undergone a great deal more distortion than the left side.

Note that the spar caps and stiffeners, as well as the skin, have failed in tension. Considerable buckling has occurred in the web on the right side because of diagonal compression as the beam deflected. The buckling on the left side of center appears to be equally severe even though the upper and lower spar caps are practically unbent.

Experimental Results

The results obtained in these tests are summarized in the following series of tables. In Table 2 the deflection of the cantilever tips relative to the center ($y_2 - y_1$) and the static load which would have been required to give the same deflection are shown. For those tests in which failure occurred, the deflection given is that observed at the time of failure. For the beams which did not fail, the deflection given is the maximum deflection observed. The static load corresponding to the deflection $y_2 - y_1$ was obtained from the curve shown in Fig. 4.

The load at the time the tension skin failed, shown in column 6 of Table 2, is the product of the tip weight and measured acceleration at the time of failure. The exaggerated influence of higher frequency components in the motion of the accelerometer made it advisable to hand-smooth the recorded curve before reading the accelerations, thus the measured accelerations are subject to considerable error. Calculated results based on these measurements vary considerably and probably have a limited reliability.

The static-load deflections of three similar beams at failure were 2.2, 1.7, and 2.3 in. It is evident that the deflections at failure of the six beams which failed are somewhat lower than the failure deflections for static-load tests. It is significant, no doubt, that, with one exception, the deflections of the beams which failed exceeded the maximum deflections of the four beams which did not fail. These results indicate that, in general, failure will occur at somewhat smaller deformations or displacements when the

Table 2 Tip deflection $y_2 - y_1$

Beam no.	Impact velocity, fps	Tip weight, lb	$y_2 - y_1$, in.	Static load to give same deflection, lb	Peak acceleration, g	Load lb
1[a]	13.3	402	...	...	11.8	4700
2[a]	13.3	402	1.58	5200	15.9	6400
3[a]	13.3	402	1.65	5150	7.5	3000
4[a]	13.3	402	1.26	5550	12.3	4950
5	14.4	200	1.38	5400	25.0	5000
6[a]	14.4	262	2.00	4750	19.0	5000
7[a]	13.3	263	1.46	5350	22.0	5800
8	12.4	290	0.77	5800	17.5	5100
9	12.4	350	1.06	5700	14.5	5100
10	13.3	250	0.75	5800	19.5	4900

[a] See Table 1 for note.

Table 3 Measured strain in the tension skin at failure

Wing no.	Impact velocity, fps	Tip weight, lb	Strain at center, in./in.	Average strain—sides, in./in.
1[a]	13.3	402	No strain gages	.....
2[a]	13.3	402	No strain gages	.....
3[a]	13.3	402	13560×10^{-6}	10000×10^{-6}
4[a]	13.3	402	17720×10^{-6}	No measurement
5	14.4	200	15800×10^{-6}	10150×10^{-6}
6[a]	14.4	262	24200×10^{-6}	12950×10^{-6}
7[a]	13.3	263	13500×10^{-6}	13065×10^{-6}
8	12.4	300	4018×10^{-6}	3230×10^{-6}
9	12.4	350	7378×10^{-6}	6495×10^{-6}
10	11.6	250	4164×10^{-6}	3266×10^{-6}

[a] See note, Table 1.

Table 4 Time between impact and tension skin failure

Wing no.	Tip weight, lb	Time of failure or maximum strain, sec	Fundamental period sec	Ratio
1[a]	402	16×10^{-3}	40×10^{-3}	0.40
2[a]	402	20	40	0.50
3[a]	402	22	40	0.55
4[a]	402	23	40	0.57
5	200	35	28	1.25
6[a]	262	27.5	32	0.86
7[a]	263	22.0	32	0.69
8	300	37.5	35	1.07
9	350	43	37	1.16
10	250	35	32	1.09

[a] See note, Table 1.

loads are applied dynamically than in those tests where the load is applied very slowly.

In the static tests, the failure loads were 5300, 5640, and 5450 lb. Only two of the dynamic loads exceeded these values. Also, it should be noted that the maximum computed loads for the beams that did not fail are higher than the peak loads for all except two of the beams that failed. These results indicate that load may be an unreliable criterion of failure. It must be remembered, however, that the difficulties encountered in measuring accelerations cause the values given here for the loads to have a limited reliability. If the load is used as the primary criterion of failure, certainly a dynamic-load factor greater than unity should not be used if the rate of loading is not expected to be appreciably greater than that developed in these tests.

The measured strains in the tension skin at failure are shown in Table 3. It will be recalled that there were six strain gages mounted on the beam, three on each side of the mid-line, which is also the root of each of the two cantilevers. A great deal of variation was observed in the strains at the six gaging points, but the strains on one side of the mid-line were always appreciably higher than those on the other. Also, the strain along the longitudinal axis was always higher than the strain at either of the side gages. In this tabulation, the strains given are those measured on the side of the mid-line where failure occurred, or if failure did not occur, that side on which the strains were greater. The strains measured by the two side gages have been averaged.

In the static-load tests, the maximum strain at failure was $21{,}500 \times 10^{-6}$ in./in. The dynamic strains are consistent in one respect with the loads shown in Table 3. With one exception, they are all lower than the static strain. The extreme variations seen in these records probably should be expected in view of the nature of the beams. Local buckling, and high stress concentration in the vicinity of rivets are certainly to be expected and these would have a significant effect on strains. Clearly, the strain in the tension skin cannot be used as a satisfactory criterion of failure when conditions exist which tend to produce local buckling and high stress concentrations.

The time between the beginning of the loading and the first tension skin failure, or the development of maximum strain, is shown in Table 4. For comparison, the fundamental period of each beam considering it to be an elastic, tip-loaded cantilever, is shown.

For an elastic single-degree-of-freedom system, the maximum deflection, and hence the maximum force, would be reached at a time equal to one fourth of the fundamental period after the start of the loading. The lack of any sort of agreement between the times at which maximum strain developed and the quarter periods of the cantilever probably can be attributed largely to the fact that the beams and the rubber pad on which they were dropped comprise a two-degree-of-freedom, nonlinear system, rather than the single-degree-of-freedom, elastic system for which the periods were computed.

Comparisons of Calculated and Measured Results

Comparisons between the computer solutions and the measured results are shown in Figs. 6 through 14. For proper evaluation of the significance of these comparisons, it should be noted that deflection measurements are probably the most accurate of the experimental results since these quantities are least influenced by high-frequency vibrations in the beam and the supporting structure. Also, the measured deflections were of the order of 1 in. or more, a relatively large quantity. On the other hand, the accelerations are probably the least accurate of the measured quantities owing to the exaggerated influence which the high-frequency vibration components have on accelerations. The procedure which was followed for reading the accelerations from the recorded results consisted of sketching by hand, on the record, a smooth curve to represent the average acceleration, and then reading the amplitude of this curve. Justification for ignoring the numerous sharp peaks and dips in the acceleration records must rest on (1) the smoothness of the deflection records, and (2) the short duration of the individual peaks in the acceleration records.

The comparisons show that, in general, the best agreement is obtained between the computed and measured values of the ab-

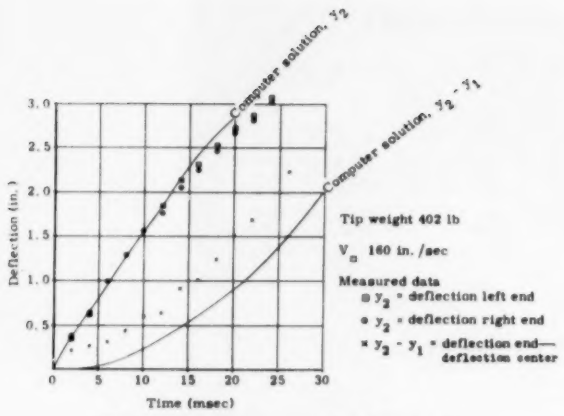

Fig. 6(a) Deflection versus time for wing 2

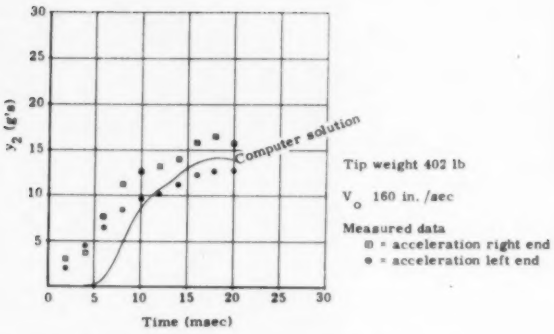

Fig. 6(b) Tip acceleration versus time for wing 2

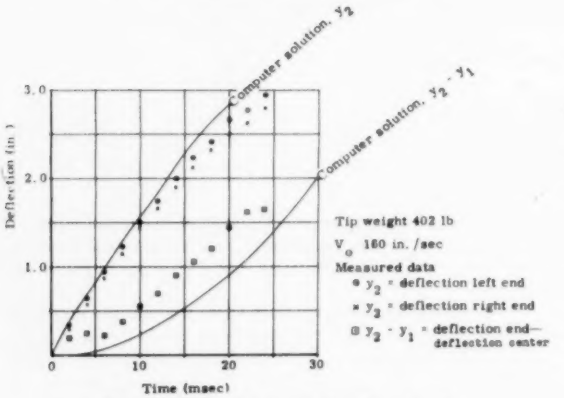

Fig. 7(a) Deflection versus time for wing 3

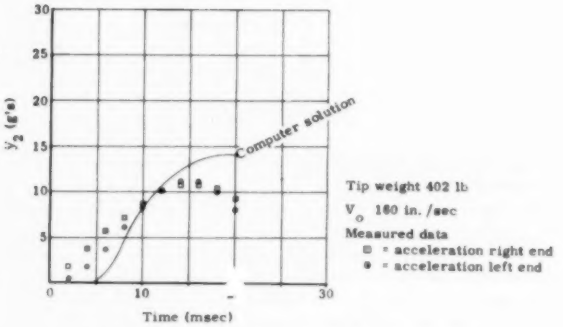

Fig. 7(b) Tip acceleration versus time for wing 3

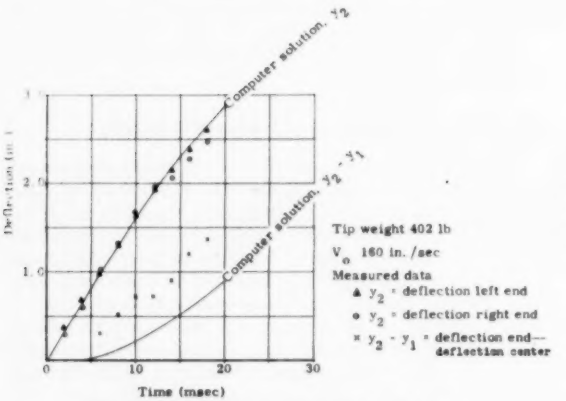
Computer solution, y_2
Computer solution, $y_2 - y_1$
Time (msec)
Tip weight 402 lb
V_o 160 in./sec
Measured data
y_2 = deflection left end
y_2 = deflection right end
$y_2 - y_1$ = deflection end—deflection center

Fig. 8(a) Deflection versus time for wing 4

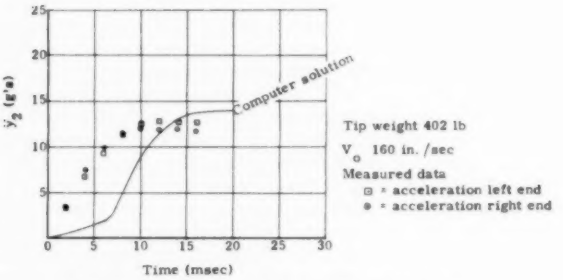

Fig. 8(b) Tip acceleration versus time for wing 4

solute tip deflection, y_2. The tip deflections $y_2 - y_1$, relative to the center, show the next best agreement and the accelerations $\ddot{y}_2$ show the poorest agreement. This is the sort of relationship that might be expected in view of the relative accuracies of the quantities involved. It also might be pointed out that the relative deflection $y_2 - y_1$ is less accurate, particularly at the lower deflections than the absolute deflection y_2 since y_1 and y_2 are almost equal at the beginning of the impact when both are small. It is interesting to note in many of these records, Fig. 7 for example, that a slight shift in the time origin will bring the computed and the experimental results for the relative deflection, $y_2 - y_1$ into excellent agreement. In Fig. 7, a shift of 5 millisec suffices. However, such a shift makes the agreement for the absolute deflection y_2 worse, and neither improves nor impairs the acceleration comparison. For beam No. 5, Fig. 9, the agreement between measured and computed values of both deflections is

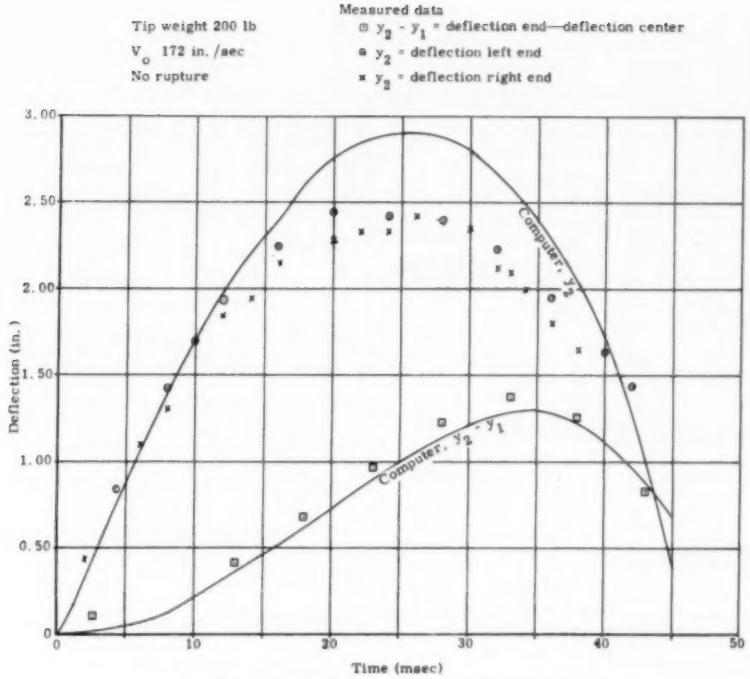

Fig. 9(a) Deflection versus time for wing 5

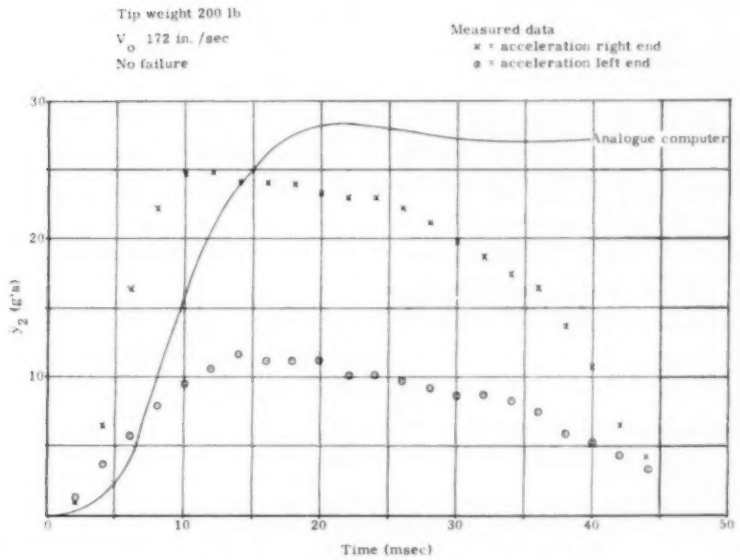

Fig. 9(b) Tip acceleration versus time for wing 5

reasonably good without any shift in the origin. However, there is very poor agreement for the accelerations, and also a considerable difference between the measured accelerations at the two tips. In a few instances, notably wing No. 7, Fig. 11(*b*), a slight shift in both the time origin and the absolute level of the acceleration brings the measured and computed values of acceleration at the tips into reasonably good agreement.

In general, these comparisons indicate that the deflections and accelerations of such beams can be computed with a fair degree of accuracy by introducing an average force-deflection curve obtained from static tests. However, it must be recognized that built-up structures of the type involved here will probably always show a significant amount of variation from one test to another, thus precluding the possibility of obtaining extremely accurate predictions from the solution of the simplified differential equations.

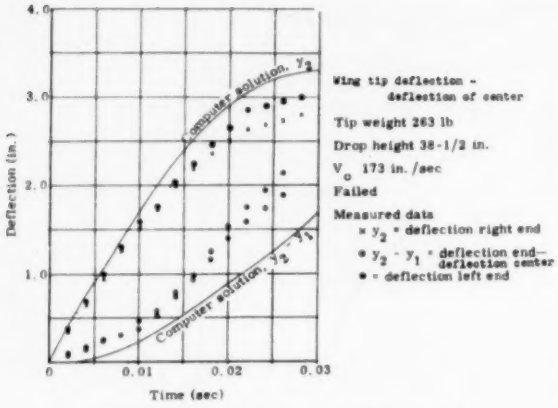
Deflection (in.)
Time (sec)
Computer solution, y_2
Computer solution, $y_2 - y_1$
Wing tip deflection - deflection of center
Tip weight 263 lb
Drop height 38-1/2 in.
V_o 173 in./sec
Failed
Measured data
× y_2 = deflection right end
⊕ $y_2 - y_1$ = deflection end—deflection center
• = deflection left end

Fig. 10(a) Deflection versus time for wing 6

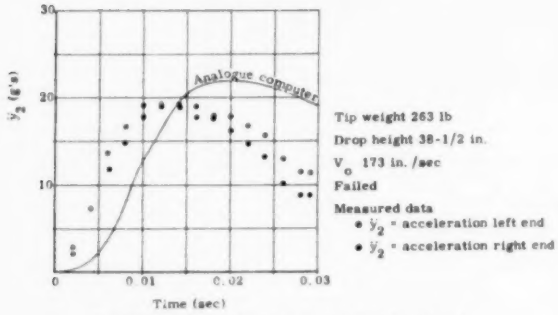

Fig. 10(b) Tip acceleration versus time for wing 6

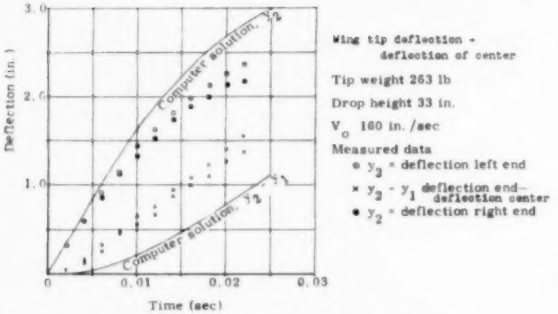
Deflection (in.)
Time (sec)
Computer solution, y_2
Computer solution, $y_2 - y_1$
Wing tip deflection - deflection of center
Tip weight 263 lb
Drop height 33 in.
V_o 160 in./sec
Measured data
• y_2 = deflection left end
× $y_2 - y_1$ deflection end—deflection center
• y_2 = deflection right end

Fig. 11(a) Deflection versus time for wing 7

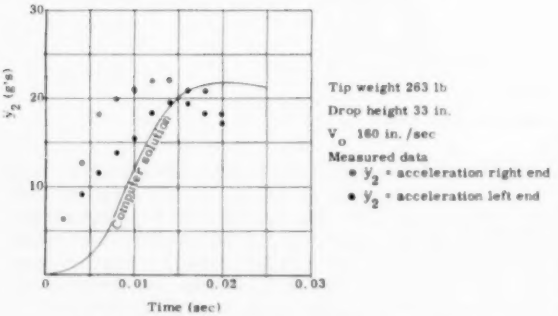

Fig. 11(b) Tip acceleration versus time for wing 7

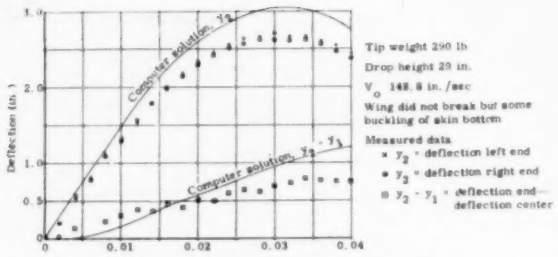
Deflection (in.)
Time (sec)
Computer solution, y_2
Computer solution, $y_2 - y_1$
Tip weight 290 lb
Drop height 29 in.
V_o 148.8 in./sec
Wing did not break but some buckling of skin bottom
Measured data
× y_2 = deflection left end
• y_2 = deflection right end
⊞ $y_2 - y_1$ = deflection end—deflection center

Fig. 12(a) Deflection versus time for wing 8

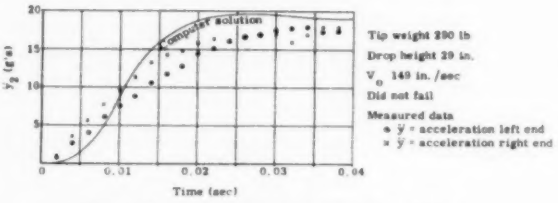

Fig. 12(b) Tip acceleration versus time for wing 8

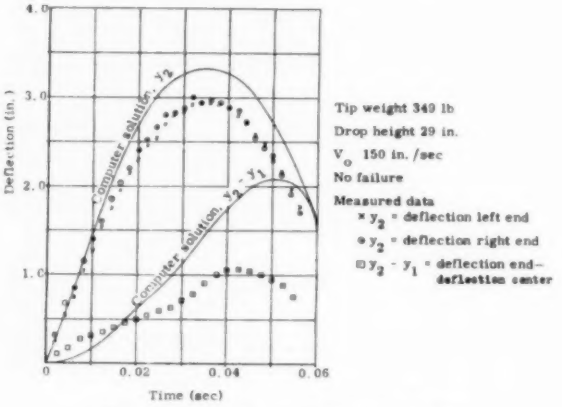

Fig. 13(a) Deflection versus time for wing 9

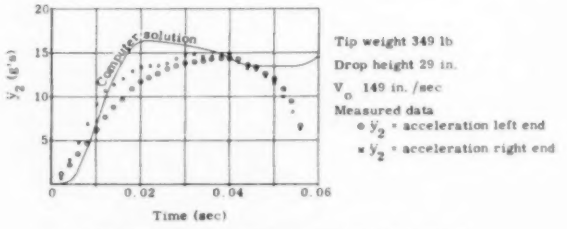

Fig. 13(b) Tip acceleration versus time for wing 9

Summary

In order to emphasize the more important results of the simplified wing-structure tests, the following points are noted:

1 The most consistent indication of the likelihood that failure will occur in tests of the type conducted in this investigation is the kinetic energy which must be absorbed at impact. With one exception, when the kinetic energy of the tip weight of the beam exceeded 700 ft-lb, failure occurred. This figure as-

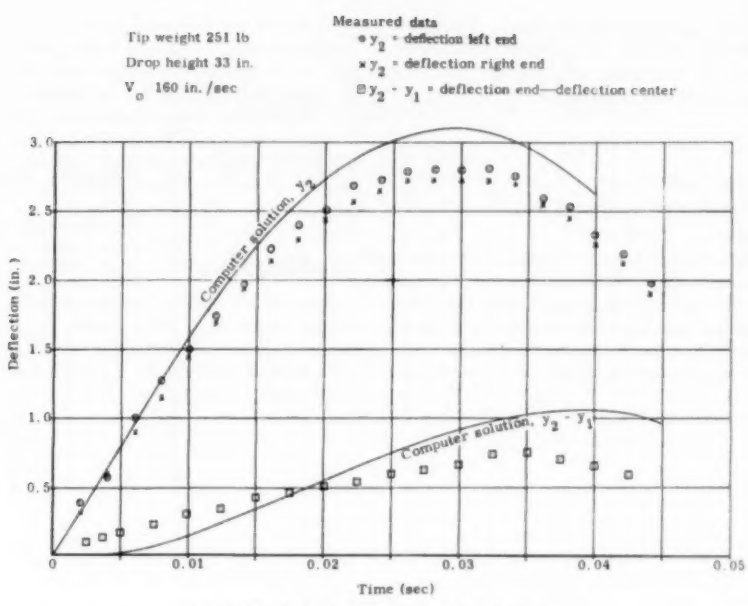
Measured data
Tip weight 251 lb
Drop height 33 in.
V_o 160 in. /sec
• y_2 = deflection left end
× y_2 = deflection right end
⊡ $y_2 - y_1$ = deflection end—deflection center
Computer solution, y_2
Computer solution, $y_2 - y_1$
Deflection (in.)
Time (sec)

Fig. 14(a) Deflection versus time for wing 10

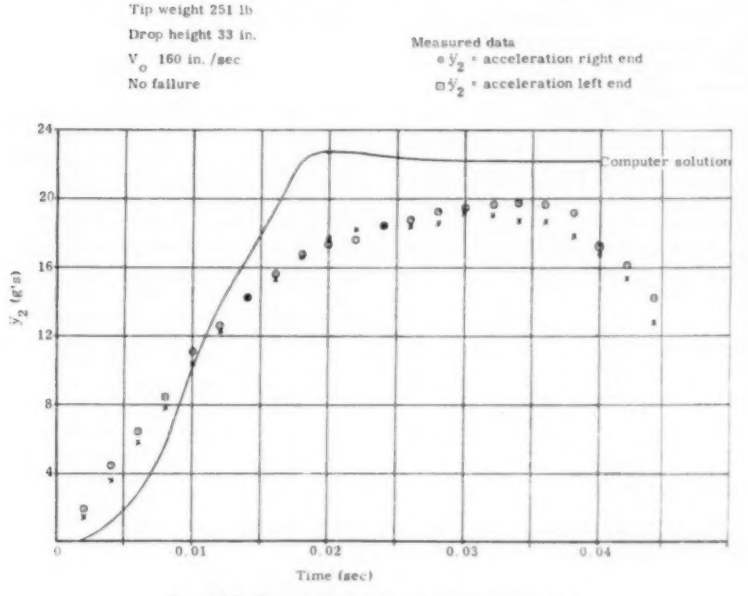

Fig. 14(b) Tip acceleration versus time for wing 10

sumes added significance, when compared with the average energy of 750 ft-lb absorbed at failure in static tests.

2 Tip deflections at failure were moderately consistent but slightly lower, on the average, than the tip deflections observed in the static tests. Thus, if tip deflection were to be used as a criterion of failure, a dynamic-load factor greater than unity should not be used. On the basis of the data presented here, the reliability of deflection as a criterion would be questionable.

3 The maximum load at failure as computed from measured accelerations and tip weights is, in general, somewhat lower than the failure loads observed in the static-loading studies. The last five beams tested, however, supported loads which were approximately the same as the failure loads in the static tests. Certainly, there is no evidence in the results obtained that loads can be sustained in the dynamic tests that are higher than the static loads that cause failure. If load is used as a criterion for failure of a beam under dynamic loading conditions where the rate of load application is such that peak load is reached in a time interval between $^1/_4$ and $^1/_2$ the fundamental period of the beam, the amplification factor should be taken as unity.

4 The time required for failure to occur, or for maximum strain to develop in the tension skin, varied from 0.40 to 1.16

times the natural period of the beams being tested. The absolute time varied from 20 to 39 millisec. It is evident that the rate of load application was not extremely fast; probably not fast enough to introduce rate, or inertia effects.

Conclusions

After comparison of the results of the static tests of a previous investigation and the dynamic tests reported here, the following conclusions were reached:

1 If the rate of application of a dynamic load is such that a load required to cause failure in static tests is reached in a time equal to or greater than $^1/_4$ the fundamental period of the structure, the structure will fail at essentially the same load as would be required to cause failure under static loading conditions. The dynamic-load amplification factor should be unity under such conditions.

2 The work which must be done on a beam or a structure to produce failure under static-loading conditions is essentially the same as the energy required to produce failure under dynamic-loading conditions if the rate of loading is as indicated above.

3 Deflections and accelerations during dynamic loading of a complete structure with nonlinear characteristics can be computed with moderate accuracy by using simplified equations of motion and the static load-deflection relationship for the structure.

Acknowledgments

The work reported here was performed in the laboratories of the Sandia Corporation. Many people contributed to the success of the investigation. In particular, the authors wish to acknowledge the contributions of Mr. W. B. Stephenson, former staff member at the Sandia Corporation.

Viscous Damping in Flexural Vibrations of Bars

M. K. NEWMAN

Professor and Head,
Department of Mechanical Engineering,
University of Notre Dame,
Notre Dame, Ind.
Mem. ASME

Energy dissipation in flexural vibrations is considered by introducing into the Timoshenko beam equation viscous-damping terms proportional to the time rate of extensional strain. Two modes of wave transmission arise from the roots of a quartic equation. On the lower mode, a solution is indicated in terms of characteristic functions which represent the damped natural vibrations. For a specified range of values of damping, the amplitudes of natural vibrations are governed by characteristic damping factors which exhibit a maximum in the region of frequencies where wave velocities are dispersed. There can be no frequency cut-offs. In the higher mode of wave motion, the characteristic damping factors exhibit a monotone increase toward short wave-length limits analogous to those obtained in the Bernoulli-Euler-Sezawa equation.

EARLIER attempts at a theory of beam vibrations with viscous damping were based on the Bernoulli-Euler beam equation. Sezawa [1][1] used a damping term proportional to the time rate of extensional strain in the Bernoulli-Euler equation.

Later, others [2] used the same Bernoulli-Euler equation with "Sezawa" damping to approximate the response of damped elastic systems to transient disturbances.

It was found that on such a theory the damping factor β increases indefinitely with the frequency of vibration. β is defined as the fraction of critical damping, a nondimensional ratio of the viscous damping constant to the critical damping constant. An indefinite increase of β with frequency leads, of course, to eventual suppression of the higher natural modes of vibration, a fact not in agreement with experimental evidence.

The Bernoulli-Euler equation is an approximation to flexural vibrations in beams which does not include important effects of shear and rotatory inertia and leads to infinite phase velocities for short wave-length vibrations. It was pointed out quite early by W. Flügge [3] that the contributions of rotatory inertia and shear are essential in order to have finite phase velocities of propagation for short wave-length vibrations. Later, H. Schirmer [4] showed that contributions of rotatory inertia and shear lead to two modes of wave propagation. The well-known partial differential equations are such that coupling terms occur between the transverse displacement w of the beam element and the angle of rotation ψ. The resulting wave forms are not pure rotations and pure shears, but combinations of the two.

Results of Schirmer's analysis are shown in Fig. 1, where the phase velocities c_1 and c_2 are plotted for undamped vibrations as functions of nondimensional frequency ratios $\omega/\omega_0 = \alpha$. ω and ω_0 are circular frequencies in radians per sec (rps). Included in this figure is also a graph of the phase velocity for pure rotations.

Of special interest is the lower mode of wave transmission c_1. Near the origin and in the range of frequencies where $0 \leq \alpha \leq 3$ the phase velocities are dispersed and wave shapes approach those of the Bernoulli-Euler theory. In the range of higher frequencies where $\alpha > 3$, wave shapes and phase velocities approach those of pure shear waves. The lower mode therefore tends to transmit predominantly flexural waves when $\alpha \leq 3$, and shear waves when $\alpha > 3$. When frequencies become very high, no flexural waves can be transmitted in this mode.

In the higher mode of wave motion, c_2, all waves are approximately rotational and approach for high frequencies the phase velocities for pure rotations. This mode will transmit primarily flexural waves. According to this theory, wave motion in the higher mode is possible only for frequencies in the range where $1 \leq \alpha \leq \infty$. There can be no wave transmission when $\alpha < 1$.

The effect of viscous flexural damping on the behavior of β as function of wave length or frequency can be analyzed readily. In the lower mode c_1 flexural dissipation will be most effective for frequencies where predominantly flexural waves are transmitted.

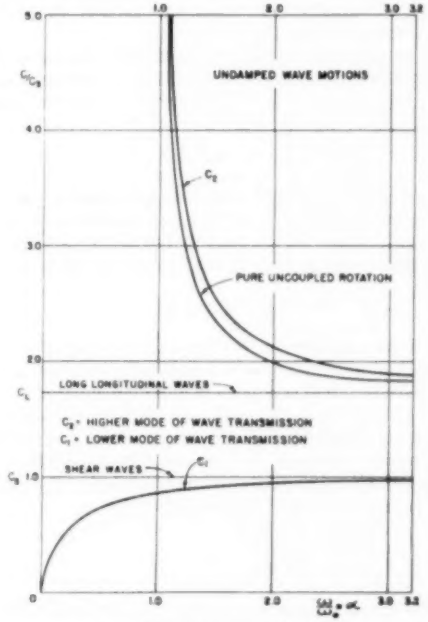
UNDAMPED WAVE MOTIONS
PURE UNCOUPLED ROTATION
LONG LONGITUDINAL WAVES
C_2 = HIGHER MODE OF WAVE TRANSMISSION
C_1 = LOWER MODE OF WAVE TRANSMISSION
SHEAR WAVES

Fig. 1 Dispersion curves for beam

[1] Numbers in brackets designate References at end of paper.

Presented at the West Coast Conference of the Applied Mechanics Division, Stanford, Calif., September 9–11, 1959, of THE AMERICAN SOCIETY OF MECHANICAL ENGINEERS.

Discussion of this paper should be addressed to the Secretary, ASME, 29 West 39th Street, New York, N. Y., and will be accepted until October 10, 1959, for publication at a later date. Discussion received after the closing date will be returned.

NOTE: Statements and opinions advanced in papers are to be understood as individual expressions of their authors and not those of the Society. Manuscript received by ASME Applied Mechanics Division, May 7, 1958. Paper No. 59—APMW-8.

Therefore flexural dissipation and β should pass through a maximum in the region of frequencies where $0 \leq \alpha \leq 3$ and go to zero when $\alpha > 3$. In the higher mode which transmits flexural waves from $1 \leq \alpha \leq \infty$, and no shears at the higher frequencies, flexural dissipation and β are expected to rise indefinitely as wave lengths diminish.

Experimental results have in fact been reported by a number of investigators [5, 6, 7] confirming a maximum of β. This is interpreted as an interplay of intensive and extensive parameters such that, at certain frequencies, a maximum dissipation of energy is achieved. The intensive parameter in this case may be the flexural moment applied, and the extensive parameter the flexural waves in the lower mode c_1 which are transmitted over a band of frequencies of roughly a range where $0 \leq \alpha \leq 3$.

The lower mode c_1 appears to be suitable for use in an approximate theory of vibrations with viscous flexural damping as it covers adequately the complete spectrum of wave lengths of flexural and shear waves for all frequencies from $0 \leq \alpha \leq \infty$. In the higher mode c_2, there can be no wave propagation for frequencies $\alpha < 1$.

Although the algebraic work associated with this solution is relatively great, this extension of the beam equation, including effects of rotatory inertia, shear, and flexural viscous damping, overcomes the shortcoming of the Bernoulli-Euler-Sezawa equation where the damping factor β is proportional to the frequency. It offers an approximation to the behavior of materials in viscous damping also at higher frequencies.

Therefore, a solution is presented of the beam equation including contributions due to rotatory inertia, shear, and flexural energy dissipation. It is written for the case of a half-period sine excitation applied to the root of a cantilever beam. This excitation is chosen because it yields a transient solution in terms of characteristic frequencies that can be compared with already existing solutions [8, 9].

Equations of Motion and Boundary Conditions for Cantilever Bar

The appropriate differential equations and boundary conditions are obtained conveniently from the equations of motion for undamped vibrations [4, 8, 9].

In the derivation of the equation of flexural vibrations of bars, the assumption is made that the axial stress σ is directly proportional to the axial strain ϵ. The constant of proportionality is Young's modulus E. Thus

$$\sigma = E\epsilon \tag{1a}$$

Viscous internal damping in an elastic solid may be introduced into the beam equation and into the end conditions by assuming that Stokes' law may be extended to a "viscous" solid [2]. The stress is thus taken to be a linear function of strain and strain rate; i.e.,

$$\sigma = E\epsilon + \zeta\dot{\epsilon} \tag{1b}$$

where ζ is the coefficient of viscosity and $\dot{\epsilon}$ is the strain rate. To pass from (1a) to (1b), it is only necessary to replace E in (1a) by $[E + \zeta(\partial/\partial t)]$. If this is done in the differential equations of undamped motion and in the end conditions [8], the desired equations and end conditions for damped vibrations are obtained.

Let w be the transverse displacement of the beam element, and ψ the angle of rotation of the element due to bending, then the slope of the neutral axis of the bar is given by

$$\frac{\partial w}{\partial x} = \psi + \gamma \tag{2}$$

where x is the co-ordinate parallel to the axis of the beam and γ is the shearing strain.

The bending moment is

$$M = EI\left(1 + \frac{\zeta\partial}{E\partial t}\right)\frac{\partial \psi}{\partial x} \tag{3}$$

where EI is the flexural rigidity of the bar and $\partial\psi/\partial x$ is a first approximation to the curvature for small values of ψ.

The shearing force is

$$Q = K'AG\gamma = K'AG\left(\frac{\partial w}{\partial x} - \psi\right) \tag{4}$$

where $K'A$ measures the effective shear area and G is the shear modulus.

The differential equations of motion are

$$-\rho A\frac{\partial^2 w}{\partial t^2} + K'AG\left(\frac{\partial^2 w}{\partial x^2} - \frac{\partial \psi}{\partial x}\right) = 0 \tag{5}$$

$$-K^2\rho A\frac{\partial^2 \psi}{\partial t^2} + EI\left(1 + \frac{\zeta\partial}{E\partial t}\right)\frac{\partial^2 \psi}{\partial x^2} + K'AG\left(\frac{\partial w}{\partial x} - \psi\right) = 0 \tag{6}$$

where K is the radius of gyration of the cross section of the bar with respect to the horizontal principal axis through the centroid of the section, and ρ the mass density of the bar material.

Equations (5) and (6) may be combined. The result is the equation

$$\frac{\partial^4 w}{\partial x^4} - \frac{1+\epsilon}{c_l^2}\frac{\partial^4 w}{\partial x^2 \partial t^2} + \frac{\epsilon}{c_l^4}\frac{\partial^4 w}{\partial t^4} + \frac{1}{K^2 c_l^2}\frac{\partial^2 w}{\partial t^2} + f_i\frac{\partial^5 w}{\partial x^4 \partial t} - f_i\frac{\epsilon}{c_l^2}\frac{\partial^5 w}{\partial x^2 \partial t^3} = 0 \tag{7}$$

In this equation, c_l is the velocity of long extensional waves, i.e., $c_l = [E/\rho]^{1/2}$, and ϵ is a nondimensional constant defined by

$$\epsilon = \frac{E}{K'G} = \frac{2(1+\nu)}{K'} \tag{8}$$

where ν is Poisson's ratio.

ϵ is adjusted so that the limiting velocity of wave transmission for short waves in the lower mode approaches that of Rayleigh's surface waves. For $\nu = 0.3$ the value of $\epsilon = 3$; f_i is the damping constant, defined by

$$f_i = \zeta/E \tag{9}$$

The initial and end conditions for excitation of the cantilever of length l in a drop test, taking the origin of co-ordinates at the free end, are

$$[w]_{t=0} = 0 \tag{10a}$$

$$\left[\frac{\partial w}{\partial t}\right]_{t=0} = -V \tag{10b}$$

$$[w]_{x=l} = -\frac{V}{\omega}\sin\omega t\, M\left(\frac{\pi}{\omega} - t\right) + V\left(t - \frac{\pi}{\omega}\right)M\left(t - \frac{\pi}{\omega}\right) \tag{10c}$$

$$[\psi]_{x=l} = 0 \tag{10d}$$

Equation (10d) may be written in terms of the transverse displacement w. The result is

$$\left(\frac{\partial^3 w}{\partial x^3} - \frac{\epsilon}{c_i^2}\frac{\partial^3 w}{\partial x \partial t^2} + \frac{1}{\epsilon K^2}\frac{\partial w}{\partial x} + f_i\frac{\partial^4 w}{\partial x^3 \partial t} - f_i\frac{\epsilon}{c_i^2}\frac{\partial^4 w}{\partial x \partial t^3}\right)_{x=l} = 0 \quad (10e)$$

At the free end of the bar, $x = 0$, the moment and shear must be zero.

The condition of zero moment is

$$EI\left(1 + \frac{\xi}{E}\frac{\partial}{\partial t}\right)\frac{\partial \psi}{\partial x} = 0 \quad (10f)$$

This becomes in terms of w

$$\left(\frac{\partial^2 w}{\partial x^2} - \frac{\epsilon}{c_i^2}\frac{\partial^2 w}{\partial t^2} + f_i\frac{\partial^2 w}{\partial x^2 \partial t} - f_i\frac{\epsilon}{c_i^2}\frac{\partial^3 w}{\partial t^3}\right)_{x=0} = 0 \quad (10g)$$

The condition of zero shear is

$$\left(\frac{\partial w}{\partial x} - \psi\right) = 0 \quad (10h)$$

In terms of w this becomes

$$\left(\frac{\partial^3 w}{\partial x^3} - \frac{1+\epsilon}{c_i^2}\frac{\partial^3 w}{\partial x \partial t^2} + f_i\frac{\partial^4 w}{\partial x^3 \partial t} - f_i\frac{\epsilon}{c_i^2}\frac{\partial^4 w}{\partial x \partial t^3}\right)_{x=0} = 0 \quad (10i)$$

In Equation (10c), M is the unit step function

$$M\left(\frac{\pi}{\omega} - t\right) = 1 \quad \text{when} \quad \left(\frac{\pi}{\omega} - t\right) > 0$$

$$M\left(\frac{\pi}{\omega} - t\right) = 0 \quad \text{when} \quad \left(\frac{\pi}{\omega} - t\right) < 0$$

V is the initial velocity of the beam at the instant of impact. It is of such magnitude that the maximum acceleration $V\omega$ is very large in comparison with the acceleration g of gravity, so that the latter may be neglected.

The solution of the problem is readily accomplished by means of the Laplace transform

$$Y(x, p) = \int_0^\infty e^{-pt} w(x, t)\, dt \quad (11)$$

where $p = \xi + i\eta$ and $Y(x, p)$ are complex.

Applying the so-called infinite integral to the partial differential Equation (7) and integrating by parts, certain restrictions are placed on $w(x, t)$ and its time derivatives.

$w(x, t)$ and its time derivatives must be of exponential order. A positive real constant M and a real constant γ must exist such that, as $t \to \infty$

$$|w(x, t)| < Me^{\gamma t} \quad (12)$$

The initial conditions on $w(x, t)$ and its time derivatives are

$$w(0) = 0, \quad \dot{w}(0) = -V, \quad \ddot{w}(0) = 0, \quad \dddot{w}(0) = 0 \quad (13)$$

With these conditions, the Laplace transform is an analytic function of p in the half plane $\xi > \gamma$. The Laplace integral converges absolutely and uniformly with respect to ξ and η in that half plane.

The partial differential Equation (7) and the initial and boundary-conditions Equations (10a) to (10i) are thus converted to the following equations in $Y(x, p)$:

$$\frac{d^4 Y}{dx^4} - \frac{[\epsilon(1 + f_i p) + 1]}{(1 + f_i p)}\frac{p^2}{c_i^2}\frac{d^2 Y}{dx^2} + \frac{p^2}{K^2 c_i^4}\frac{(\epsilon p^2 K^2 + c_i^2)}{(1 + f_i p)} Y = -\frac{V}{K^2 c_i^4}\frac{(\epsilon p^2 K^2 + c_i^2)}{(1 + f_i p)} \quad (14)$$

At $x = 0$

$$\frac{d^2 Y}{dx^2} - \frac{\epsilon p^2}{c_i^2} Y = \frac{\epsilon V}{c_i^2} \quad (15a)$$

$$\frac{d^3 Y}{dx^3} - \frac{[\epsilon(1 + f_i p) + 1]}{(1 + f_i p)}\frac{p^2}{c_i^2}\frac{dY}{dx} = 0 \quad (15b)$$

At $x = l$

$$Y = Ve^{-p\frac{x}{\omega}}\frac{\omega^2}{p^2(p^2 + \omega^2)} - \frac{V}{(p^2 + \omega^2)} \quad (15c)$$

$$\frac{d^2 Y}{dx^2} - \left[\frac{\epsilon p^2}{c_i^2} - \frac{1}{\epsilon K^2(1 + f_i p)}\right]\frac{dY}{dx} = 0 \quad (15d)$$

Equation (14) is an ordinary differential equation with constant coefficients. Its solution is written in the form

$$Y_{(x,p)} = A_1 e^{m_1 x} + A_2 e^{-m_1 x} + A_3 e^{m_2 x} + A_4 e^{-m_2 x} - \frac{V}{p^2} \quad (16)$$

where m_1, $-m_1$, m_2, and $-m_2$ are the four roots of the biquadratic equation in m

$$m^4 - \frac{[\epsilon(1 + f_i p) + 1]p^2}{(1 + f_i p)c_i^2} m^2 + \frac{p^2}{K^2 c_i^4}\frac{(\epsilon p^2 K^2 + c_i^2)}{(1 + f_i p)} = 0 \quad (17)$$

These roots may be presented in various convenient forms. For purpose of numerical computation, one form is as follows:

$$m_1 = F_1(p)[F_2(p) - [F_3(p)]^{1/2}]^{1/2} \quad (18a)$$

$$m_2 = F_1(p)[F_2(p) + [F_3(p)]^{1/2}]^{1/2} \quad (18b)$$

where

$$F_1(p) = \frac{p}{c_i[2(1 + f_i p)]^{1/2}};$$

$$F_2(p) = [\epsilon(1 + f_i p) + 1];$$

$$F_3(p) = [\epsilon(1 + f_i p) - 1]^2 - \frac{4c_i^2}{K^2}\frac{(1 + f_i p)}{p^2};$$

In order to identify the harmonic terms in Equation (16), the following notation is introduced:

$$m_1 = \mu_1 \text{ and } m_2 = i\mu_2$$

where $\mu_2 = 2\pi/\lambda$ is a real number and λ is the wave length. This locates p in Equation (18b) to the left of the imaginary axis. Equation (16) then takes the form

$$Y = c_1 \sin h\mu_1 x + c_2 \cosh \mu_1 x + c_3 \sin \mu_2 x + c_4 \cos \mu_2 x - \frac{V}{p^2} \quad (19)$$

where

$$\mu_1 = F_1(p)[F_2(p) - G_1(p)[G_2(p)]^{1/2}]^{1/2} \quad (20a)$$

$$\mu_2 = -iF_1(p)[F_2(p) + G_1(p)[G_2(p)]^{1/2}]^{1/2} \quad (20b)$$

where $F_1(p)$ and $F_2(p)$ are as in (18a) and (18b) and

$$G_1(p) = [\epsilon(1 + f_i p) - 1];$$

$$G_2(p) = 1 - \frac{4c_i^2}{K^2}\frac{(1 + f_i p)}{[G_1(p)]^2 p^2};$$

Applying the boundary conditions (15a) to (15d) to the general solution (19), the Laplace transform $Y(x, p)$ of the solution $w(x, t)$ is obtained

$$Y(x, p) = \frac{V\omega^2\left(1 + e^{-p\frac{\pi}{\omega}}\right)\phi}{p^2(p^2 + \omega^2)\Delta} - \frac{V}{p^2} \tag{21}$$

where

$$\phi = \phi_1 + \phi_2 + \phi_3 \tag{22}$$

and

$$\phi_1 = \mu_1\mu_2 \frac{c_l^2}{K^2} [\cosh \mu_1(l - x) + \cos \mu_2(l - x)]$$

$$\phi_2 = \mu_1\mu_2 \left[\left\{ [\epsilon(1 + f_s p) - 1](\mu_1^2 c_l^2 - \epsilon p^2) + \frac{c_l^2}{K^2} \right\} \cosh \mu_1 l \cos \mu_2 x + \left\{ [1 - \epsilon(1 + f_s p)](\mu_2^2 c_l^2 + \epsilon p^2) + \frac{c_l^2}{K^2} \right\} \cos \mu_2 l \cosh \mu_1 x \right]$$

$$\phi_3 = \frac{\mu_1^2 c_l^2}{K^2} \sin \mu_2 l \sinh \mu_1 x - \frac{\mu_2^2 c_l^2}{K^2} \sinh \mu_1 l \sin \mu_2 x$$

and

$$\Delta = \Delta_1 + \Delta_2 + \Delta_3 \tag{23}$$

$$\Delta_1 = \mu_1\mu_2 \frac{2c_l^2}{K^2}$$

$$\Delta_2 = \mu_1\mu_2 \left[\frac{2c_l^2}{K^2} - \frac{[\epsilon(1 + f_s p) - 1]^2 p^2}{(1 + f_s p)} \right] \cosh \mu_1 l \cos \mu_2 l$$

$$\Delta_3 = \frac{[\epsilon(1 + f_s p) + 1]p^2}{K^2(1 + f_s p)} \sinh \mu_1 l \sin \mu_2 l$$

It may be shown readily that for $x = l$

$$\phi(l, p) = \Delta(l, p)$$

Also, as $f_s = 0$, both $\phi(l, p)$ and $\Delta(l, p)$ reduce to the form appropriate to the Timoshenko equation. In addition, ϕ/Δ is of zero order in p, thus insuring that the Laplace transform $Y(x, p)$ is of order $0(p^{-k})$ where $K > 1$.

$Y(x, p)$ A Single-Valued Function of p

The Laplace transform is a single-valued function of p at all points of the complex plane. It is analytic except at certain simple poles located on and to the left of the axis of imaginaries and has a double pole at $p = 0$.

To show this, we examine the behavior of the parameters μ_1 and μ_2 which occur in $Y(x, p)$. They are defined by Equations (20*a*) and (20*b*) and may be written in the form

$$\mu_1 = [f(p) - [f_1(p)]^{1/2}]^{1/2} \tag{24a}$$

$$\mu_2 = -i[f(p) + [f_1(p)]^{1/2}]^{1/2} \tag{24b}$$

where

$$f(p) = \frac{[\epsilon(1 + f_s p) + 1]p^2}{2c_l^2(1 + f_s p)} \tag{25a}$$

$$f_1(p) = \frac{[\epsilon(1 + f_s p) - 1]^2}{4c_l^4(1 + f_s p)^2} p^4 - \frac{p^2}{K^2 c_l^2(1 + f_s p)} \tag{25b}$$

Consider the function $w = [f_1(p)]^{1/2}$ which occurs in both μ_1 and μ_2, but with opposite sign. At any point in the complex plane, $[f_1(p)]^{1/2}$ has two values which are the roots of the quadratic in w

$$w^2 = f_1(p)$$

These roots are

$$w_{1,2} = \pm[f_1(p)]^{1/2}$$

$[f_1(p)]^{1/2}$ has four branch points. These branch points are the values of p which reduce $f_1(p)$ to zero. They are the roots of the quartic in p

$$p^4 + \frac{2(\epsilon - 1)}{\epsilon f_s} p^3 + \frac{(\epsilon - 1)^2}{\epsilon^2 f_s^2} p^2 - \frac{4c_l^2}{K^2\epsilon^2 f_s} p - \frac{4c_l^2}{K^2\epsilon^2 f_s^2} = 0 \tag{26a}$$

which in nondimensional form is

$$z^4 + \frac{2(\epsilon - 1)}{\rho_1\epsilon} z^3 + \frac{(\epsilon - 1)^2}{\rho_1^2\epsilon^2} z^2 - \frac{4}{\rho_1\epsilon} z - \frac{4}{\rho_1^2\epsilon} = 0 \tag{26b}$$

where

$$\rho_1 = \frac{c_l f_s}{K\sqrt{\epsilon}} \quad \text{and} \quad z = \frac{K\sqrt{\epsilon}}{c_l} p$$

For $\rho_1 = 1$ and $\epsilon = 3$, the roots are

$$z_{1,2} = -0.686 \pm i0.979 \quad \text{and} \quad z_{3,4} = 0.019 \pm 0.966$$

A change in sign of $[f_1(p)]^{1/2}$ will change μ_1 and μ_2 such that

$$\mu_1 \to i\mu_2 \quad \text{and} \quad \mu_2 \to -i\mu_1$$

In a similar manner, at any point p in the complex plane, μ_1 and μ_2 have two values of opposite sign. They are the roots of the quadratic equations

$$\mu_1^2 = f(p) - [f_1(p)]^{1/2}$$

and

$$-\mu_2^2 = f(p) + [f_1(p)]^{1/2}$$

where $f(p)$ and $f_1(p)$ are defined in Equations (25*a*) and (25*b*), respectively.

The three branch points of μ_1 are

$$p = 0, \quad p = i\frac{c_l}{K\sqrt{\epsilon}}, \quad p = -i\frac{c_l}{K\sqrt{\epsilon}}$$

The branch point of μ_2 is $p = 0$.

It should be noted that μ_1 and μ_2 have the branch point $p = 0$ in common.

ϕ/Δ and $(d/dp)(\phi/\Delta)$ are single-valued functions of p if their value remains unchanged when p returns to its original value for any arbitrary closed path in the complex plane enclosing any or all of the branch points of μ_1, μ_2 and $[f_1(p)]^{1/2}$. This is a necessary and sufficient condition.

It is apparent from this discussion that the points

$$p = \pm i\frac{c_l}{K\sqrt{\epsilon}}$$

affect only μ_1, while all other points mentioned in the foregoing will affect both μ_1 and μ_2 together.

A single closed circuit around

$$p = +i\frac{c_l}{K\sqrt{\epsilon}}$$

for example, will change the sign of μ_1 only, thus reversing the sign of ϕ and also of Δ. This, however, will leave ϕ/Δ unchanged. On the other hand, a single closed circuit around $p = 0$

will change the signs of both μ_1 and μ_2. Consequently, the sign of ϕ and also of Δ will remain the same. A single closed circuit around any of the roots of $f_i(p) = 0$ will change μ_1 into $i\mu_2$ and μ_2 into $-i\mu_1$. If these values are substituted into ϕ and Δ, it will be noted that both ϕ and Δ remain the same. For any arbitrary closed circuit, ϕ/Δ will return to its original value.

(ϕ/Δ) is therefore a single-valued function of p at all points of the complex plane. The same can be shown to be true for the derivative $(d/dp)(\phi/\Delta)$.

(ϕ/Δ), and $(d/dp)(\phi/\Delta)$ Are Finite at Branch Points of μ_1, μ_2, $[f_1(p)]^{1/2}$ and at $p = -(1/f_i)$

Consider the branch point of μ_1 at

$$p = +i\frac{c_i}{K\sqrt{\epsilon}}$$

or at

$$p = -i\frac{c_i}{K\sqrt{\epsilon}}$$

In either case, the value of μ_1 is zero. This can be seen by substituting either value of p into Equations (20*a*) and (20*b*).

The corresponding value of μ_2 will be for

$$p = +i\frac{c_i}{K\sqrt{\epsilon}}$$

$$\mu_2 = \left[\frac{[\epsilon(1 + i\rho_1) + 1]}{K^2\epsilon(1 + i\rho_1)}\right]^{1/2}$$

For small values of μ_1 both ϕ and Δ will have a common factor $\mu_1(c_i^2/K^2)$, which cancels in the quantity ϕ/Δ. As μ_1 approaches zero, ϕ/Δ approaches the finite and single-valued limit ϕ_0/Δ_0 where

$$\phi_0 = \phi_{01} + \phi_{02} + \phi_{03} \tag{27a}$$

and

$$\Delta_0 = \Delta_{01} + \Delta_{02} + \Delta_{03} \tag{27b}$$

and where

$$\phi_{01} = \mu_2[1 + \cos\mu_2(l - x)];$$

$$\phi_{02} = \mu_2\left[\epsilon(1 + f_ip)\cos\mu_2 x + \frac{1}{\epsilon(1 + f_ip)}\cos\mu_2 l\right];$$

$$\phi_{03} = -l\frac{[1 + \epsilon(1 + f_ip)]}{\epsilon K^2(1 + f_ip)}\sin\mu_2 x;$$

$$\Delta_{01} = 2\mu_2;$$

$$\Delta_{02} = \mu_2\frac{[1 + \epsilon^2(1 + f_ip)^2]}{\epsilon(1 + f_ip)}\cos\mu_2 l;$$

$$\Delta_{03} = -l\frac{[1 + \epsilon(1 + f_ip)]}{\epsilon K^2(1 + f_ip)}\sin\mu_2 l;$$

The derivative of ϕ/Δ may be written in the form

$$\frac{d}{dp}\left(\frac{\phi}{\Delta}\right) = \frac{\phi}{\Delta}\left[\frac{\phi'}{\phi} - \frac{\Delta'}{\Delta}\right] \tag{28}$$

where ϕ' and Δ' are derivatives with respect to p of ϕ and Δ.

In the limit as $\mu_1 \to 0$; $(d\mu_1/dp) \to \infty$.

Those terms in ϕ' and Δ' having $(d\mu_1/dp)$ as coefficients are infinite and produce identical cancellation as follows:

$$\operatorname*{Lim}_{\frac{d\mu_1}{dp} = \infty}\left[\frac{\phi_\infty'}{\phi} - \frac{\Delta_\infty'}{\Delta}\right] = 0$$

where

$$\frac{\phi_\infty'}{\phi} = \frac{\frac{d\mu_1}{dp}\phi_0}{\mu_1\phi_0};$$

and

$$\frac{\Delta_\infty'}{\Delta} = \frac{\frac{d\mu_1}{dp}\Delta_0}{\mu_1\Delta_0};$$

The finite terms ϕ_n' and Δ_n' of ϕ_0' and Δ_0' approach a limit such that the derivative

$$\operatorname*{Lim}_{\mu_1 = 0}\frac{d}{dp}\left(\frac{\phi}{\Delta}\right) = \frac{\phi_0}{\Delta_0}\left[\frac{\phi_0'}{\phi_0} - \frac{\Delta_0'}{\Delta_0}\right]$$

is finite and single-valued at the points

$$p = \pm i\frac{c_i}{K\sqrt{\epsilon}}$$

Consider the roots of $f_i(p) = 0$. These are the branch points of $[f_i(p)]^{1/2}$. At these points

$$\mu_1 = \left[\frac{[1 + \epsilon(1 + f_ip)]}{2c_i^2(1 + f_ip)}\right]^{1/2}p = \beta$$

$$\mu_2 = -i\left[\frac{[1 + \epsilon(1 + f_ip)]}{2c_i^2(1 + f_ip)}\right]^{1/2}p = -i\beta$$

$$\mu_1\mu_2 = -i\frac{[1 + \epsilon(1 + f_ip)]}{2c_i^2(1 + f_ip)}p^2 = -i\beta^2$$

Since these points are the roots of the quartic

$$p^4 + \frac{2(\epsilon - 1)}{\epsilon f_i}p^3 + \frac{(\epsilon - 1)^2}{\epsilon^2 f_i^2}p^2 - \frac{4c_i^2}{f_i\epsilon^2K^2}p - \frac{4c_i^2}{\epsilon^2f_i^2K^2} = 0$$

the following relation is satisfied:

$$\left[-\frac{[\epsilon(1 + f_ip) - 1]^2}{2(1 + f_ip)}p^2 + \frac{c_i^2}{K^2}\right] = -\frac{c_i^2}{K^2} \tag{29}$$

Using this relation, it is found that both ϕ and Δ become zero, leaving the quantity ϕ/Δ in the indeterminate form

$$\frac{\phi}{\Delta} = \frac{0}{0}$$

After some algebraic simplifications and cancellation of identical infinities, the value of ϕ/Δ is found to be

$$\frac{\phi_{Br}}{\Delta_{Br}} = \frac{\phi'_{Br}}{\Delta'_{Br}} = \frac{A_{Br}\sinh\beta l\sinh\beta x + B_{Br}\cosh\beta l\cosh\beta x}{A_{Br}\sinh^2\beta l + B_{Br}\cosh^2\beta l} \tag{30}$$

where the subscript Br refers to the particular branch point and

$$A_{Br} = \frac{4\epsilon p}{K^2[1 + \epsilon(1 + f_ip)]} - \frac{[1 + \epsilon(1 + f_ip)](2p + f_ip^2) + 2f_i\epsilon p^2(1 + f_ip)}{2K^2(1 + f_ip)^2} \tag{30a}$$

$$B_{Br} = \frac{[\epsilon^2(1 + f_ip)^2 - 1]p^2}{2c_i^2(1 + f_ip)} \frac{[\epsilon(1 + f_ip) - 1](2p + f_ip^2) + 2f_i\epsilon p^2(1 + f_ip)}{(1 + f_ip)^2} \tag{30b}$$

$(\phi_{B_r}/\Delta_{B_r})$ reduces to the value appropriate to the Timoshenko equation when f_i is zero. The derivative $(d/dp)(\phi/\Delta)$ is an identical zero at the branch points of $[f_i(p)]^{1/2}$.

At the point $p = 0$, μ_1 and μ_2 become zero and ϕ reduces to

$$\phi_0 = \mu_1\mu_2 4 \frac{c_i^2}{K^2}$$

and Δ to

$$\Delta_0 = \mu_1\mu_2 4 \frac{c_i^2}{K^2}$$

Consequently

$$\operatorname*{Lim}_{p=0} \frac{\phi_0}{\Delta_0} = 1$$

The derivative with respect to p of ϕ/Δ approaches zero; i.e.,

$$\operatorname*{Lim}_{p=0} \frac{d}{dp}\left(\frac{\phi}{\Delta}\right) = 0$$

This limit may be found by writing the derivative in the form

$$\operatorname*{Lim}_{p=0} \frac{d}{dp}\left(\frac{\phi}{\Delta}\right) = \frac{\phi_0}{\Delta_0}\left[\frac{\phi_0'}{\phi_0} - \frac{\Delta_0'}{\Delta_0}\right]$$

where corresponding terms of ϕ_0' and Δ_0' in the bracket cancel identically or approach zero.

Another point of interest is $p = -(1/f_i)$ for which $(1 + f_i p) = 0$. At this point $\mu_1 = \infty$ and $\mu_2 = iq$ where q is finite, real, and constant.

It can be shown that for these values of p, μ_1, and μ_2

$$\operatorname*{Lim}_{p=-(1/f_i)} (\phi/\Delta) = (\cosh qx)/(\cosh ql)$$

This limit of ϕ/Δ is obviously finite and single-valued. (ϕ/Δ) is also analytic at $p = -(1/f_i)$. The derivative with respect to p of ϕ/Δ approaches zero; i.e.,

$$\operatorname*{Lim}_{p=-(1/f_i)} \frac{d}{dp}\left(\frac{\phi}{\Delta}\right) = \frac{\phi}{\Delta}\left[\frac{\phi'}{\phi} - \frac{\Delta'}{\Delta}\right] \equiv 0$$

This may be shown by calculating the large terms in ϕ' and ϕ and also in Δ' and Δ finding that

$$(\phi'/\phi) - (\Delta'/\Delta) \equiv 0$$

Solution by Inversion Integral

$Y(x, p)$ is analytic and of the order $0(p^{-K})$ in the half plane $R(p) \geq x_0$, where x_0 and K are real constants and $K > 1$. The solution of the problem is then obtained by the inversion integral

$$w(x, t) = \frac{1}{2\pi i}\int_{\gamma-i\infty}^{\gamma+i\infty} e^{pt}Y(x, p)dp \qquad (31a)$$

or

$$w(x, t) = \frac{V\omega^2}{2\pi i}\int_{\gamma-i\infty}^{\gamma+i\infty} \frac{e^{pt}\left(1 + e^{-p\frac{\pi}{\omega}}\right)}{p^2(p^2+\omega^2)}\frac{\phi(x, p)}{\Delta(l, p)}\,dp - \frac{V}{2\pi i}\int_{\gamma-i\infty}^{\gamma+i\infty}\frac{e^{pt}}{p^2}\,dp \qquad (31b)$$

The inversion integral along the line $x = \gamma$, where $\gamma \geq x_0$ converges to $w(x, t)$ and is independent of γ. Furthermore, the function $w(x, t)$ is continuous for each $t \geq 0$, and $w(x, 0) = 0$.

In addition, $w(x, t)$ is of order $0(e^{\gamma t})$ for all $t \geq 0$.

The inversion process is unique and $w(x, t)$ is the exact solution of the differential Equation (7), the initial conditions, and the boundary conditions (10*a*) to (10*i*).

Since e^{pt} is analytic and not zero, the singularities of the product $e^{pt}Y(x, p)$ in Equation (31*a*) are precisely the poles p_n of $Y(x, p)$. Let $r_n(t)$ denote the residue of that product at p_n for any fixed t; i.e.,

$$r_n(t) = \text{residue of } [e^{pt}Y(x, p)] \text{ at } p = p_n$$

According to Cauchy's residue theorem, the integral of $e^{pt}Y(x, p)$ around a closed path including all the points $p_1, p_2, \ldots p_n$ has the value

$$\oint e^{pt}Y(x, p)dp = 2\pi i \sum_{n=1}^{n=\infty} r_n(t) \qquad (32a)$$

The closed contour is chosen to be made up of the infinite straight-line segment from $\gamma - i\infty$ to $\gamma + i\infty$ parallel to the axis of imaginaries and of the infinite semicircle C_∞ to the left. The contour integral in Equation (32*a*) is then divided into the sum of two integrals, one along the straight-line segment and the other along the infinite semicircle to the left; i.e.,

$$\frac{1}{2\pi i}\int_{\gamma-i\infty}^{\gamma+i\infty} e^{pt}\,Y(x, p)dp + \frac{1}{2\pi i}\int_{c_\infty} e^{pt}\,Y(x, p)dp = \sum_{n=1}^{n=\infty} r_n(t) \qquad (32b)$$

The integral along the straight-line segment is the inversion integral (31*a*) which converges to $w(x, t)$. The integral along the infinite semicircle to the left is zero.

This can be shown by considering the behavior of the integrand $e^{pt}Y(x, p)$ along the infinite semicircle to the left of the straight-line segment $\gamma - i\infty \leq y \leq \gamma + i\infty$. If $Y(x, p)$ remains finite, then the integral along such a half circle evidently will be zero unless an appreciable contribution is obtained from the portion of the path immediately adjacent to the axis of imaginaries, for remote from this axis, the integrand approaches zero exponentially as the radius of the circle is increased beyond limits.

The quantity $\phi/[p^2(p^2 + \omega^2)\Delta]$ which is a part of $Y(x, p)$, approaches zero at all points of the infinite circle, including the points on the imaginary axis, $p = \pm i\infty$.

To show this, it is noted that for large values of p, μ_1 and μ_2 reduce to

$$\mu_1 = \frac{p}{c_i[1 + f_i p]^{1/2}}; \quad \mu_2 = -i\frac{\epsilon^{1/2}}{c_i}p;$$

Let p be on the imaginary axis; i.e., $p = i\beta$; then

$$\mu_1 = (1 + i)b\beta^{1/2}, \quad \mu_2 = a\beta$$

where

$$b = \frac{1}{(2f_i)^{1/2}c_i}; \quad \text{and} \quad a = \frac{\epsilon^{1/2}}{c_i};$$

and a, b, and β are positive real numbers. As β is allowed to increase indefinitely, μ_1 and μ_2 go to infinity.

The quantity ϕ/Δ is found by dividing out the large identical quantities

$$\mu_1\mu_2[\exp(b\beta^{1/2}l)]\beta^3$$

The result is

$$\phi/\Delta = (\cos ax\beta)/(\cos al\beta) \qquad (33)$$

where

$$ax = \text{const}$$

$$al = \text{const}$$

For large values of β, (ϕ/Δ) becomes highly oscillatory; however, $Y(x, p)$ approaches zero because $Y(x, p)$ is of the order $0(p^{-K})$, where $K = 4$; i.e.,

$$\lim_{p=\pm i\infty} \frac{(\phi/\Delta)}{p^2(p^2+\omega^2)} = 0$$

It also can be shown that

$$\lim_{p=\pm i\infty} \frac{d}{dp}\frac{(\phi/\Delta)}{p^2(p^2+\omega^2)} = 0$$

The integrand is analytic at $p = \pm i\infty$ where $p = \pm i\infty$ are not zeros of $(p^2 + \omega^2)$.

At all other points on the infinite circle ϕ/Δ vanishes exponentially; i.e.,

$$\lim_{d=\infty} \frac{\phi}{\Delta} = \lim_{d=\infty} e^{-|d|(l-x)} = 0$$

where the absolute value of d is defined by

$$|d| = \frac{\epsilon^{1/2}}{c_l} r\,|\cos\theta|$$

r is the radius of the large circle, and θ is the angle which the vector from the origin to the point on the circle makes with the direction of the positive x-axis.

In the special cases when $\theta = 90$ or 270 deg, the point on the large circle will be on the imaginary axis. In that case, the value of d reduces to zero and ϕ/Δ approaches the value given in Equation (33).

It may be stated that, if $f_i = 0$, the problem is reduced to the solution of the Timoshenko beam Equation (8).

The solution of the problem is written as the sum of the residues at the poles of the integrands of Equation (32*b*). In addition to the double pole at $p = 0$ and to the poles at $p = \pm i\omega$, there exist zeros of $\Delta(l, p)$ which yield the characteristic values for free vibrations.

Consider the equation

$$\Delta(l, p) = 0 \tag{34}$$

In nondimensional form $\Delta(l, p)$ appears as a function of parameters $K\mu_1$ and $K\mu_2$ where

$$\Delta(l, z, K\mu_1, K\mu_2) = \Delta_1 + \Delta_2 + \Delta_3$$

and

$$\Delta_1 = (K\mu_1)(K\mu_2)2\epsilon$$

$$\Delta_2 = (K\mu_1)(K\mu_2)\left[2\epsilon - \frac{[\epsilon(1+\rho_1 z)-1]^2 z^2}{(1+\rho_1 z)}\right]\cosh\mu_1 l\cos\mu_2 l$$

$$\Delta_3 = \frac{[\epsilon(1+\rho_1 z)+1]z^2}{(1+\rho_1 z)}\sinh\mu_1 l\sin\mu_2 l$$

$$z = x + iy; \quad p = \frac{c_l}{K\sqrt{\epsilon}}z; \quad \rho_1 = \frac{f_i c_l}{K\sqrt{\epsilon}};$$

$$K\mu_1 = f_1(z)[f_2(z) - [f_3(z)]^{1/2}]^{1/2} \tag{35a}$$

$$K\mu_2 = -if_1(z)[f_2(z) + [f_3(z)]^{1/2}]^{1/2} \tag{35b}$$

$$f_1(z) = \left[\frac{z}{2\epsilon(1+\rho_1 z)}\right]^{1/2}$$

$$f_2(z) = [\epsilon(1+\rho_1 z)+1]z$$

$$f_3(z) = [\epsilon(1+\rho_1 z)-1]^2 z^2 - 4\epsilon(1+\rho_1 z)$$

It is not feasible to solve Equation (34) explicitly for the roots. Instead, the value of $\Delta(l, z, K\mu_1, K\mu_2)$ may be computed for appropriate values of the parameters and the zeros approximated by interpolation.

The Laplace transform, Equation (21), was chosen harmonic in $\mu_2 x$ and $\mu_2 l$ in order to exhibit the wave solution for real values of μ_2, where

$$\mu_2 = 2\pi/\lambda$$

and λ is the wave length.

The wave function $Y(x, p) = e^{i\mu_2 x}$ satisfies the transformed and homogeneous differential Equation (14), provided the following quartic equation in p is satisfied:

$$p^4 + f_i\mu_2^3 c_l^2 p^3 + \left[\frac{\epsilon+1}{\epsilon}\mu_2^2 c_l^2 + \frac{c_l^2}{\epsilon K^2}\right]p^2 + \frac{f_i\mu_2^4 c_l^4}{\epsilon}p + \frac{\mu_2^4 c_l^4}{\epsilon} = 0 \tag{36a}$$

The appropriate nondimensional form of this equation is

$$z^4 + \rho_1\epsilon(K^2\mu_2^2)z^3 + [(1+\epsilon)(K^2\mu_2^2)+1]z^2 + \rho_1\epsilon(K^4\mu_2^4)z + \epsilon(K^4\mu_2^4) = 0 \tag{36b}$$

A wave solution will therefore exist when all coefficients of this quartic equation are positive and real.

On the other hand, the complete criterion for stability of the solution satisfying a quartic of the form

$$z^4 + a_1 z^3 + a_2 z^2 + a_3 z + a_4 = 0 \tag{36c}$$

is that all the coefficients a must be real and positive and that

$$a_1 a_2 a_3 > a_3^2 + a_1^2 a_4$$

In terms of the coefficients of Equation (36*b*), this means that $(K\mu_2)^2$ and ρ_1 must be real and positive; i.e.,

$$(K\mu_2)^2 > 0, \quad \rho_1 > 0$$

Therefore, for every real value of $K\mu_2$ and for every positive real ρ_1, the four roots of Equation (36*b*) occur either in complex conjugate pairs with negative real parts, or as pairs of negative real numbers, or as one pair of negative real numbers and another pair of complex conjugate numbers with negative real parts.

These roots may be computed by the method of Ferrari and Cardan in terms of radicals of the coefficients. The complex roots also may be found by iteration and Horner's method as suggested by R. Ludwig [10].

The complex roots appear in the form

$$\begin{aligned} z_{1,2} &= -\alpha_1\beta_1 \pm i\alpha_1(1-\beta_1^2)^{1/2} \\ z_{3,4} &= -\alpha_2\beta_2 \pm i\alpha_2(1-\beta_2^2)^{1/2} \end{aligned} \tag{37a}$$

where the α are nondimensional frequencies defined by

$$\alpha = \frac{\omega}{\omega_0} \quad \text{and} \quad \omega_0 = \frac{c_l}{K\sqrt{\epsilon}}$$

and the β are nondimensional fractions of critical damping.

When any of the values of β in Equations (37*a*) become larger than unity, the roots become negative real numbers of the form

$$z_{1,2} = -\alpha_1\beta_1 \mp \alpha_1\beta_1\left(1 - \frac{1}{\beta_1^2}\right)^{1/2}$$

$$z_{3,4} = -\alpha_2\beta_2 \mp \alpha_2\beta_2\left(1 - \frac{1}{\beta_2^2}\right)^{1/2}$$

These roots correspond to the case of overdamping when free vibrations cannot exist.

When damping is neglected, the quartic (36*b*) reduces to the biquadratic

$$z^4 + [(1 + \epsilon)(K^2\mu_2^2) + 1]z^2 + \epsilon K^4\mu_2^4 = 0 \qquad (36d)$$

The four roots of (36*d*) are imaginary and of the form

$$z_{1,2} = \pm i\alpha_1;\ z_{3,4} = \pm i\alpha_2$$

These pairs of roots represent the two modes of wave-transmission characteristic of the Timoshenko beam equation.

Physically, it is to be expected that, for undamped vibrations, the roots will be on the imaginary axis, while in the case of damped vibrations the beam may be looked upon as a dissipative network. The roots should then lie to the left of the axis of imaginaries.

The complex roots given in Equations (37*a*) define the two modes of wave motion c_1 and c_2 for damped vibrations. $z_{1,2}$ is associated with the lower mode c_1 and $z_{3,4}$ with the higher mode c_2.

The wave velocity c for damped vibrations satisfies the relation

$$c = \Omega/\mu_2 \qquad (38)$$

where

$$\Omega = \omega_0\alpha(1 - \beta^2)^{1/2}$$

is the circular frequency of damped vibrations and

$$\omega_0^2 = \frac{K'G}{\rho K^2}$$

It is instructive to write the phase velocity in terms of c_i which is defined by

$$c_s^2 = \frac{c_i^2}{\epsilon} = \frac{K'G}{\rho}$$

This relation is

$$\frac{c}{c_s} = \frac{\alpha(1 - \beta^2)^{1/2}}{K\mu_2} \qquad (39)$$

Term (c/c_s) is plotted as function of $K\mu_2$ in Fig. 2 for both modes of wave motion and for widely different values ρ_1 of damping. Fig. 3 shows the behavior of β as function of $K\mu_2$, also for both modes and for the same values of the damping coefficient ρ_1. The values of ρ_1 chosen in these illustrations are arbitrary. However, it is of interest to note that for a rod with $K = 1$ in., the value of $\rho_1 = 10^{-8}$ corresponds to a viscosity coefficient $\zeta = 17.9$ cp and $\rho_1 = 1$ corresponds to 17.9×10^8 poise. A small value of damping represented by $\rho_1 = 10^{-8}$ approximates the results of this theory to the case of undamped vibrations.

Of special interest is the behavior of the roots $z_{1,2}$ of the quartic Equation (36*b*) in the lower mode c_1. An upper limit M_1 exists of ρ_1 such that for a large range of values $\rho_1 < M_1$ the roots $z_{1,2}$ of this quartic are a pair of complex conjugate numbers for all real values of $K\mu_2$, where $-\infty \leq K\mu_2 \leq \infty$. The damping factor β remains less than unity for all values of $K\mu_2$. In fact, β as function of $K\mu_2$ rises from zero to a maximum and returns to zero for large values of $K\mu_2$. There are no frequency cut-offs and no short-wave-length limits in this mode for the range of damping specified.

The situation is different in the upper mode c_2 of wave transmission. No upper limit M exists for values of ρ_1 such that when $\rho_1 < M$ the roots $z_{3,4}$ will be pairs of complex conjugates for all real values of $K\mu_2$. On the other hand, for any fixed small values of $\rho_1 > 0$, there exists a lower limit M_2 for real values of $K\mu_2$ such that when $|K\mu_2| \geq M_2$ the roots $z_{3,4}$ become pairs of negative real numbers. This leads to overdamped solutions in the higher mode c_2 as wave lengths diminish indefinitely. It is illustrated in Fig. 3 although the limiting values of β_2 for very short wave lengths are not shown.

Reference to Fig. 2 shows that the dispersion curves for a range of damping where $10^{-8} \leq \rho_1 \leq 10^{-1}$ coincide within the accuracy of the calculations in spite of the great range of values of damping. There is similar agreement with the curves for undamped vibra-

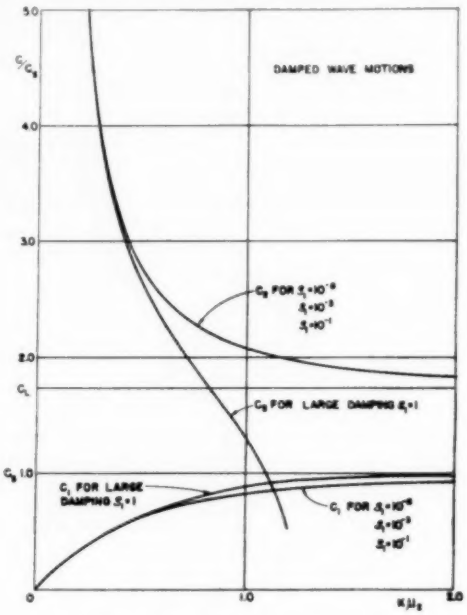

Fig. 2 Dispersion curves with damping

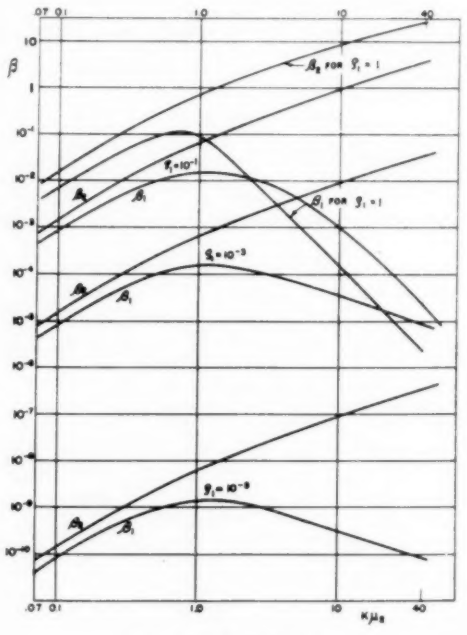

Fig. 3 Damping factor

tions shown in Fig. 1. This is due to the fact that the values of β remain sufficiently small in the range of values of $K\mu_2$ shown. In the case when $\rho_1 = 1$, which is also shown in Figs. 2 and 3, the damping factors β become sufficiently large to affect values of the phase velocities noticeably in both modes of wave motion.

In the lower mode c_1 the phase velocity for short wave lengths approaches asymptotically a value $c_1 = c_s$ when ρ_1 is limited to $\rho_1 < M_1$. In the higher mode c_2 and for a range of values of $K\mu_2$, where $|K\mu_2| < M_2$, phase velocities tend to approach a value $c_2 = c_l$. If the range of $K\mu_2$ is extended indefinitely, c_2 tends to zero producing short-wave-length vibration cut-offs. This is not indicated in Fig. 2.

Confining attention to the lower mode c_1 and to values of damping in the range $0 \leq \rho_1 < M_1$, the zeros of $\Delta(l, z, K\mu_1, K\mu_2)$ may be found for real values of $K\mu_2$. These zeros are the poles of $Y(x, p)$ that are associated with the characteristic values for free vibrations. For a wave solution, to each real value of $K\mu_2$ belongs a pair of complex conjugate roots $z_{1,2}$ of the quartic Equation (36*b*) and a pair of complex conjugate values of $K\mu_1$ according to Equation (35*a*). Equation (35*b*) yields real values of $K\mu_2$ for the complex roots $z_{1,2}$. In general, the values of $\Delta(l, z, K\mu_1, K\mu_2)$ are complex; however, they may be real and also imaginary.

For example, when damping is zero $\Delta(l, z, K\mu_1, K\mu_2)$ oscillates for real $K\mu_2$ through positive and negative real or imaginary values, as $z_{1,2} = \pm i\alpha$ passes through values on the axis of imaginaries which are exact roots of the biquadratic Equation (36*d*). When $0 \leq \alpha_1 < 1$, $K\mu_1$ is real and the imaginary part of $\Delta(l, z, K\mu_1, K\mu_2)$ vanishes. When $1 < \alpha_1 \leq \infty$, $K\mu_1$ is imaginary, and the real part of $\Delta(l, z, K\mu_1, K\mu_2)$ becomes zero. When damping is present $\Delta(l, z, K\mu_1, K\mu_2)$ is complex. The characteristic values $K\mu_{2n}$ for real $K\mu_2$ are located at the zeros of the modulus of $\Delta(l, z, K\mu_1, K\mu_2)$.

To insure free oscillations, it is necessary that damping be limited to values where $0 \leq \rho_1 < M_1$. The existence of damping for real $K\mu_2$ is reflected in the appearance of the quartic Equation (36*b*). The complex conjugate roots $z_{1,2}$ of this quartic are approximate values that are located to the left of the imaginary axis.

Characteristic values $K\mu_{2n}$ were computed for the first six modes of natural vibrations for values of $\rho_1 = 10^{-8}$, $\rho_1 = 10^{-1}$, $\epsilon = 3$, and $l/K = 30$. Small differences $\delta K\mu_{2n}$ occurring between values $K\mu_{2n}$ obtained from the zeros of the real and imaginary parts of $\Delta(l, z, K\mu_1, K\mu_2)$ were well within limits of precision inherent in the algebraic equations used. These results are listed in Table 1.

Those values of z at the branch points of $K\mu_1$, $K\mu_2$, and $[f_1(p)]^{1/2}$ which reduce $\Delta(l, z, K\mu_1, K\mu_2)$ and $\phi(x, z, K\mu_1, K\mu_2)$ to zero are not roots of

$$\Delta(l, z, K\mu_1, K\mu_2) = 0$$

At these points, the quantity (ϕ/Δ) and $Y(x, p)$ approach finite limits as shown in an earlier section.

To every characteristic value $K\mu_{2n}$ corresponds a value of $\mu_{2n}l$, $(\mu_{1n}l)_R$, $(\mu_{1n}l)_I$, $\alpha_{1n}\beta_{1n}$, $\alpha_{1n}(1 - \beta_{1n}^2)^{1/2}$. The subscripts R and I of $\mu_{1n}l$ refer to the real and imaginary parts. These quantities are listed in Table 2. Values for zero damping and $\epsilon = 2.9$ are also listed.

The natural frequencies for the cantilever are given by

$$f_n = \frac{c_l}{K\sqrt{\epsilon}} \frac{\alpha_n(1 - \beta_n^2)^{1/2}}{2\pi} \tag{40}$$

The values obtained by this theory agree well with results reported for the first three modes by E. T. Kruszewski [9]. In fact, it was found that, for a slender bar, the first six natural frequencies are slightly lower than those obtained from the Bernoulli-

Table 1 Differences between values of $K\mu_{2n}$

$\rho_1 = 10^{-8}$			$\rho_1 = 10^{-1}$		
Real part $\Delta_R = 0$ $K\mu_{2n}$	Im. part $\Delta_I = 0$ $K\mu_{2n}$	$\delta K\mu_{2n}$	Real part $\Delta_R = 0$ $K\mu_{2n}$	Im. part $\Delta_I = 0$ $K\mu_{2n}$	$\delta K\mu_{2n}$
0.06242	0.06463	0.00221	0.06242	0.06468	0.00226
0.15473	0.15654	0.0018	0.15483	0.15654	0.0017
0.25793	0.25977	0.00184	0.25793	0.25909	0.00116
0.35956	0.36120	0.00164	0.35960	0.36110	0.00150
0.46104	0.46281	0.00177	0.46103	0.46280	0.00177
0.56247	0.56397	0.00150	0.56245	0.56386	0.00141

Table 2 Approximate characteristic values for cantilever $l/K = 30$

$\alpha_{1n}\beta_{1n}$	$\alpha_{1n}(1 - \beta_{1n}^2)^{1/2}$	$(\mu_{1n}l)_R$	$(\mu_{1n}l)_I$	$\mu_{2n}l$
Zero damping, $\beta = 0$, $\zeta = 0$, $\epsilon = 2.9$				
0	0.0064	1.834	0	1.872
0	0.0390	4.440	0	4.632
0	0.1014	6.861	0	7.740
0	0.1783	8.775	0	10.644
0	0.2704	10.011	0	13.740
0	0.3646	10.764	0	16.629
$\zeta = 17.9$ cp, $\rho_1 = 10^{-8}$, $\epsilon = 3$				
0.222×10^{-12}	0.0067	1.858	-0.7164×10^{-12}	1.873
0.735×10^{-11}	0.0396	4.434	-0.578×10^{-10}	4.642
0.449×10^{-10}	0.1028	6.869	-0.568×10^{-9}	7.738
0.128×10^{-9}	0.1839	8.706	-0.217×10^{-8}	10.787
0.256×10^{-9}	0.2764	9.980	-0.533×10^{-8}	13.831
0.419×10^{-9}	0.3760	10.728	-0.1018×10^{-7}	16.874
$\zeta = 1.79 \times 10^6$ p, $\rho_1 = 10^{-1}$, $\epsilon = 3$				
0.222×10^{-5}	0.0067	1.858	-0.709×10^{-5}	1.873
0.737×10^{-4}	0.0397	4.436	-0.575×10^{-3}	4.645
0.449×10^{-3}	0.1028	6.869	-0.568×10^{-2}	7.738
0.128×10^{-2}	0.1839	8.706	-0.217×10^{-1}	10.788
0.256×10^{-2}	0.2764	9.980	-0.533×10^{-1}	13.831
0.419×10^{-2}	0.3760	10.728	-0.1019	16.874

Euler equation. The effect of rotatory inertia and shear is to reduce these frequencies, the reduction increasing with frequency. In the case of thick bars, this reduction becomes very substantial in the higher modes.

The effect of damping on the natural frequencies and wave lengths appears insignificant for the values of viscosity chosen.

The solution for the period of the disturbance when $0 \leq t \leq \pi/\omega$ is given in terms of the transverse displacement $w(x, t)$

$$w(x, t) = -\frac{V}{\omega}\,[\xi(x)\cos\omega t + \eta(x)\sin\omega t] - 2V\omega^2 \sum_{n=1}^{n=\infty} e^{-\beta_n p_n t} \frac{\varphi_{1n}(x)\cos(p_n' t + \gamma_n) - \varphi_{2n}(x)\sin(p_n' t + \gamma_n)}{p_n^2[(C_n'^2 + D_n'^2)[(\omega^2 - p_n^2)^2 + 4p_n^2\beta_n^2\omega^2]^{1/2}}; \quad (41)$$

where the individual terms in (41) are the residues at the poles of the integrands of Equation (32*b*).

At the poles $p = \pm i\omega$ the values of μ_1 and μ_2, $\phi(x, i\omega)$, and $\Delta(l, i\omega)$ are complex. Let

$$\phi(x, i\omega) = A(x) + iB(x)$$

$$\Delta(l, i\omega) = C(l) + iD(l)$$

then

$$\xi(x) = \frac{B(x)C(l) - A(x)D(l)}{C^2(l) + D^2(l)}$$

$$\eta(x) = \frac{A(x)C(l) + B(x)D(l)}{C^2(l) + D^2(l)}$$

At the poles n, $p = -p_n\beta_n \pm ip_n'$

where

p_n = the natural frequency of undamped vibrations
$p_n' = p_n(1 - \beta_n^2)^{1/2}$ is the corresponding natural frequency of damped vibrations

$\mu_2 = \mu_{2n}$ is real, however, $\mu_1 = \mu_{1n}$ and $\phi(x, p) = \phi_n(x, p)$ are complex. $\Delta(l, p) = \Delta_n(l, p)$ passes through zero as required by the frequency equation.

The residues at these poles appear in terms of the derivatives of $\Delta(l, p)$

$$\text{Res} = \lim_{p \to -p_n\beta_n \pm ip_n'} \frac{e^{pt}\phi(x, p)}{p^2(p^2 + \omega^2)\Delta'(l, p)}$$

where $\Delta_n'(l, p)$, the value of the derivative at the pole n, is complex.

Let

$$\Delta_n'(l, p) = C_n' + iD_n'$$

then $C_n'^2 + D_n'^2$ is the square of the absolute value of the derivative at the pole n.

Similarly

$$\varphi_{1n}(x) = [A_n(x)C_n' + B_n(x)D_n'](1 - 2\beta_n^2) + [B_n(x)C_n' - A_n(x)D_n'](2\beta_n(1 - \beta_n^2)^{1/2};$$

$$\varphi_{2n}(x) = [B_n(x)C_n' - A_n(x)D_n'](1 - 2\beta_n^2) - [A_n(x)C_n' + B_n(x)D_n'](2\beta_n(1 - \beta_n^2)^{1/2}$$

$$\tan\gamma_n = \frac{2p_n^2\beta_n(1 - \beta_n^2)^{1/2}}{\omega^2 - p_n^2(1 - 2\beta_n^2)}$$

The solution for the time after the disturbance has ceased to exist, i.e., when $(\pi/\omega) \leq t \leq \infty$, is obtained from Equation (41) by means of the transfer operator

$$e^{-p\frac{\pi}{\omega}} f(t) = f\left(t - \frac{\pi}{\omega}\right)$$

For the time $(\pi/\omega) \leq t \leq \infty$ the displacement is given by

$$w(x, t) = V\left(t - \frac{\pi}{\omega}\right) - 4V\omega^2 \sum_{n=1}^{n=\infty} \frac{e^{-\beta_n p_n\left(t - \frac{\pi}{2\omega}\right)}\left[\sinh^2\frac{\beta_n p_n \pi}{2\omega} + \cos^2\frac{p_n'\pi}{2\omega}\right]^{1/2}}{p_n^2[C_n'^2 + D_n'^2][(\omega^2 - p_n^2)^2 + 4\beta_n^2 p_n^2\omega^2]^{1/2}} [\varphi_{1n}(x)\cos(p_n' t + \delta_n) - \varphi_{2n}(x)\sin(p_n' t + \delta_n)] \quad (42)$$

where

$$\tan\delta_n = \frac{\sin\gamma_n e^{-\beta_n p\frac{\pi}{\omega}} - \sin\left(p_n'\frac{\pi}{\omega} - \gamma_n\right)}{\cos\gamma_n e^{-\beta_n p_n\frac{\pi}{\omega}} + \cos\left(p_n'\frac{\pi}{\omega} - \gamma_n\right)}$$

The solutions (41) and (42) satisfy the differential Equation (7) and the initial conditions and boundary conditions (10*a*) to (10*i*), inclusive.

Conclusion

A solution has been indicated of the beam equation in flexural vibrations including effects of shear, rotatory inertia, and viscous flexural damping. Separation of variables is obtained by using the Laplace transform. The free vibrations appear as an expansion in terms of characteristic functions satisfying the initial and boundary conditions and representing the characteristic flexural shapes as they appear under the influence of viscous flexural damping.

Acknowledgment

The present study is a part of a research program entitled "Thermo-Elastic Damping in Impact Vibrations of Beams," sponsored by the National Science Foundation under Contract NSF G3498 with the University of Notre Dame. Their financial assistance is hereby gratefully acknowledged.

References

1 K. Sezawa, "On the Decay of Waves in Visco-Elastic Solid Bodies," Bulletin of the Earthquake Research Institute, Tokyo Imperial University, vol. 3, 1927, p. 50.

2 R. D. Mindlin, F. W. Stubner, and H. L. Cooper, "Response of Damped Elastic Systems to Transient Disturbances," *Proceedings*, The Society for Experimental Stress Analysis, vol. 5, 1948, pp. 69–87.

3 W. Flügge, "Die Ausbreitung von Biegewellen in Stäben," *Zeitschrift für Angewandte Mathematik und Mechanik*, vol. 22, 1942, p. 312.

4 H. Schirmer, "Über Biegewellen in Staben," *Ingenieur-Archiv*, vol. 20, 1952, pp. 247–257.

5 C. Zener, "Internal Friction in Solids—I, Theory of Internal Friction in Reeds," *Physical Review*, vol. 52, 1937, pp. 230–235.

6 C. Zener, "Internal Friction in Solids—II, General Theory of Thermo-Elastic Internal Friction," *Physical Review*, vol. 53, 1938, pp. 90–99.

7 C. Zener, W. Otis, and R. Nuckolls, "Internal Friction in Solids—III, Experimental Demonstration of Thermo-Elastic Internal Friction," *Physical Review*, vol. 53, 1938, pp. 100–101.

8 M. K. Newman, "Effect of Rotatory Inertia and Shear on Maximum Strain in Cantilever Impact Excitation," *Journal of the Aeronautical Sciences*, vol. 22, 1955, pp. 313–320.

9 E. T. Kruszewski, "Effect of Transverse Shear and Rotary Inertia on the Natural Frequency of a Uniform Beam," NACA TN 1909, July, 1949.

10 Rudolf Ludwig, "Ein praktisches Verfahren zur Lösung Biquadratischer Gleichuugen mit nur Komplexen Wurzeln," *Zeitschrift für Angewandte Mathematik und Mechanik*, vol. 35, 1955, p. 401.

On the Natural Modes and Their Stability in Nonlinear Two-Degree-of-Freedom Systems

R. M. ROSENBERG
Professor of Engineering Mechanics,
University of California,
Berkeley, Calif.

C. P. ATKINSON
Assistant Professor of Engineering Design,
University of California,
Berkeley, Calif.

The natural modes of free vibrations of a symmetrical two-degree-of-freedom system are analyzed theoretically and experimentally. This system has two natural modes, one in-phase and the other out-of-phase. In contradistinction to the comparable single-degree-of-freedom system where the free vibrations are always orbitally stable, the natural modes of the symmetrical two-degree-of-freedom system are frequently unstable. The stability properties depend on two parameters and are easily deduced from a stability chart. For sufficiently small amplitudes both modes are, in general, stable. When the coupling spring is linear, both modes are always stable at all amplitudes. For other conditions, either mode may become unstable at certain amplitudes. In particular, if there is a single value of frequency and amplitude at which the system can vibrate in either mode, the out-of-phase mode experiences a change of stability. The experimental investigation has generally confirmed the theoretical predictions.

In a discussion following the presentation of a paper by T. C. Huang [1][1] and of a prepared discussion of that paper [2], Dr. Gabriel Horvay of the General Electric Company posed a question which has motivated the investigation reported here, and whose answer forms a part of its content. Horvay's question suggests itself readily when one considers, simultaneously, the properties of linear vibrating two-degree-of-freedom systems, and of the effect which spring nonlinearity has on systems with one or more degrees of freedom.

It is well known that linear two-degree-of-freedom systems in forced vibrations show two "resonance peaks" in the amplitude-frequency plane; what Klotter [3] calls the "backbones" of these peaks are the amplitude-frequency relations of the system in free vibrations. Moreover, it is well known [4] that the effect of spring nonlinearity on single-degree-of-freedom systems is to bend the (single) resonance peak to the right or left depending on the character of the nonlinearity. Huang [1], Sethna [5], Arnold [6], and others have shown that, in two-degree-of-freedom systems, both peaks are bent to the right or left in the presence of nonlinear spring forces. Horvay's question was this: "If the resonance peaks of two-degree-of-freedom systems, or their backbones, are bent in the presence of spring nonlinearities, do they ever intersect and, if so, what is the physical implication of the points of intersection?" An examination of this problem has led to the present investigation.

The System

We consider the free vibrations of the two-degree-of-freedom system shown in Fig. 1. It consists of two masses m_1 and m_2 and three springs S_1, S_2, S_3. Each mass is constrained to a single degree of freedom consisting of a translation in the direction of the (coincident) spring center lines, and the co-ordinates of the configuration are $x_1 = x_1(t)$, $x_2 = x_2(t)$ denoting displacements from a position of static equilibrium of the two masses. All springs have the following characteristics: It requires a force $\bar{f}_i(u)$, $(i = 1, 2, 3)$ to deflect a spring by an amount u; the $\bar{f}_i(u)$ are single-valued, analytic, and odd in u and, although this restriction is easily removed, we also prescribe $\bar{f}_i(0) = 0$. The equations of motion of the system are

$$\begin{aligned} m_1\ddot{x}_1 &= -\bar{f}_1(x_1) - \bar{f}_2(x_1 - x_2) \\ m_2\ddot{x}_2 &= -\bar{f}_3(x_2) + \bar{f}_2(x_1 - x_2) \end{aligned} \tag{1}$$

It is known that free vibrations of this system may take place in either of two modes, and with each mode there is associated a backbone curve in the amplitude-frequency plane. If all springs are linear, the backbones are distinct, straight lines in the amplitude-frequency plane, each parallel to the amplitude axis. If one or more springs are not linear, the backbones become curved and, in each mode, the frequency of free vibrations becomes a unique function of amplitude. The backbones may, or may not, intersect one another depending on the character of the functions $\bar{f}_i$.

If one is concerned with properties associated with the possible intersection of the backbones, one need not consider a system of such generality as (1). A system of the type (1) exists which possesses, in the amplitude-frequency plane, the necessary characteristics and for which the analysis becomes particularly simple. This is the "symmetrical" system for which

$$\begin{aligned} m_1 &= m_2 = m \\ \bar{f}_1(u) &= \bar{f}_3(u) = \bar{f}(u) \\ \bar{f}_2(u) &= F(u) \end{aligned} \tag{2}$$

If one writes

$$\begin{aligned} \bar{f}(u)/m &= f(u) \\ F(u)/m &= F(u) \end{aligned}$$

the system (1) reduces to

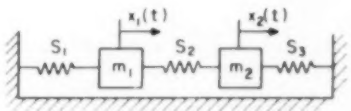

Fig. 1 The two-degree-of-freedom system. All springs are nonlinear.

[1] Numbers in brackets designate References at end of paper.

Contributed by the Applied Mechanics Division and presented at the Annual Meeting, November 30–December 5, 1958, New York, N. Y., of THE AMERICAN SOCIETY OF MECHANICAL ENGINEERS.

Discussion of this paper should be addressed to the Secretary, ASME, 29 West 39th Street, New York, N. Y., and will be accepted until October 10, 1959, for publication at a later date. Discussion received after the closing date will be returned.

NOTE: Statements and opinions advanced in papers are to be understood as individual expressions of their authors and not those of the Society. Manuscript received by ASME Applied Mechanics Division, May 23, 1958. Paper No. 58—A-57.

$$\ddot{x}_1 = -f(x_1) - F(x_1 - x_2)$$
$$\ddot{x}_2 = -f(x_2) + F(x_1 - x_2) \tag{3}$$

In view of the fact that the functions $f(u)$ and $F(u)$ are odd, it may readily be ascertained by substitution that solutions of (3) have the following property:

If a fundamental set of solutions

$$x_1 = x_{1i}^*(t) \quad \text{and} \quad x_1 = x_{10}^*(t)$$

is known, then the two corresponding solutions for x_2 are

$$x_2 = x_{1i}^*(t) \quad \text{and} \quad x_2 = -x_{10}^*(t)$$

These equations will be called the "mode relations." Their physical interpretation is that the free vibrations of the system consist of an "in-phase" mode when $x_2 = x_1$ and an "out-of-phase" mode when $x_2 = -x_1$. The former is realized by the initial conditions $x_1(0) = x_2(0)$, and the latter by $x_1(0) = -x_2(0)$. Clearly, one need concern oneself only with the motion of one of the masses, say $x_1(t)$, and the other motion is then found simply by making use of the mode relations. Therefore, the number subscripts 1 and 2 henceforth will be omitted wherever possible. When no such subscripts are given, the results apply to the motion of either mass.

The motions $x_i = x_i^*(t)$ and $x_0 = x_0^*(t)$ are the solutions, respectively, of

$$\ddot{x}_i = -f(x_i)$$
$$\ddot{x}_0 = -f(x_0) - F(2x_0) \tag{4}$$

These are the equations which one obtains by substituting the mode relations in (3). They will be called the "modal equations." The solutions of (4) can always be reduced to quadratures. However, they can be written in closed form when the functions f and F are cubic polynomials. If one puts

$$f(u) = a_1u + a_3u^3$$
$$F(u) = A_1u + A_3u^3 \tag{5}$$

the equations of motion (3) become

$$\ddot{x}_1 = -(a_1x_1 + a_3x_1^3) - [A_1(x_1 - x_2) + A_3(x_1 - x_2)^3]$$
$$\ddot{x}_2 = -(a_1x_2 + a_3x_2^3) + [A_1(x_1 - x_2) + A_3(x_1 - x_2)^3] \tag{6}$$

It is these equations on which all further development is based.

The modal equations (4) become

$$\ddot{x}_i + a_1x_i + a_3x_i^3 = 0$$
$$\ddot{x}_0 + (a_1 + 2A_1)x_0 + (a_3 + 8A_3)x_0^3 = 0 \tag{7}$$

But these are Duffing equations without forcing terms and they are widely discussed in the literature [4, 7]. A necessary condition of the existence of periodic solutions, of small amplitudes at least, is that

$$a_1 > 0, \quad A_1 > -a_1/2 \tag{8}$$

and these restrictions will be observed throughout the paper.

The Backbone Curves

The backbones are curves in the amplitude-frequency plane. If the amplitudes of in-phase and out-of-phase modes, respectively, are denoted by y_i and y_0, the backbone curves are given by [7]

$$\omega_i(y_i) = \frac{\pi}{2}(a_1 + a_3y_i^2)^{1/2}K^{-1}(k_i)$$
$$\omega_0(y_0) = \frac{\pi}{2}(b_1 + b_3y_0^2)^{1/2}K^{-1}(k_0) \tag{9}$$

where $K(k)$ is the complete elliptic integral of the first kind,

$$k_i = \frac{a_3y_i^2}{2(a_1 + a_3y_i^2)}, \qquad b_1 = a_1 + 2A_1,$$
$$k_0 = \frac{b_3y_0^2}{2(b_1 + b_3y_0^2)}, \qquad b_3 = a_3 + 8A_3$$

If one puts $y_i = 0$ in (9) one finds

$$\omega_i(0) = \sqrt{a_1}$$

This permits the transformation of the relations (9) into the convenient nondimensional form

$$\nu_i(y_i) = \frac{\omega_i(y_i)}{\omega_i(0)} = \frac{\pi}{2}\left(1 + \frac{4}{3}\eta_i\right)^{1/2}K^{-1}\left[\frac{\frac{4}{3}\eta_i}{2\left(1 + \frac{4}{3}\eta_i\right)}\right]$$
$$\nu_0(y_0) = \frac{\omega_0(y_0)}{\omega_i(0)} = \frac{\pi}{2}\left[(1 + 2\alpha_1) + (1 + 8\alpha_3)\frac{4}{3}\eta_0\right]^{1/2}K^{-1}\left[\frac{(1 + 8\alpha_3)\frac{4}{3}\eta_0}{2\left[(1 + 2\alpha_1) + (1 + 8\alpha_3)\frac{4}{3}\eta_0\right]}\right] \tag{10}$$

where

$$\alpha_1 = A_1/a_1,$$
$$\alpha_3 = A_3/a_3,$$
$$^2\eta_{i,0} = \frac{3}{4}\frac{a_3}{a_1}y_{i,0}^2$$

Equations (9) and (10) are the equations of the backbones. They and their first derivatives with respect to the y, or η, are monotonic in these variables. Therefore the backbones, at most, can have one intersection. This intersection, if it exists, occurs when $y_{i,0} = y_{cr}$ (or $\eta_{i,0} = \eta_{cr}$) and when $\omega_{i,0} = \omega_{cr}$ (or $\nu_{i,0} = \nu_{cr}$), where the subscript cr denotes the "crossover" value of amplitude and frequency. The crossover amplitude is the real root y_{cr} (or η_{cr}) of the equation obtained when the two equations (9) or the two equations (10) are equated, and the subscripts i and 0 are replaced by the subscript cr.

Evidently, the resulting equations are highly transcendental and cannot be solved explicitly for the crossover amplitude. However, one can obtain a very useful, approximate equation for the backbones and for the crossover amplitudes by using the Duffing relation [4] connecting the frequency and amplitude in systems of the form (7). The Duffing approximation gives in place of (9)

$$\omega_i^2 = a_1 + \frac{3}{4}a_3y_i^2$$
$$\omega_0^2 = (a_1 + 2A_1) + \frac{3}{4}(a_3 + 8A_3)y_0^2 \tag{11}$$

and in nondimensional form

$$\nu_i^2 = 1 + \eta_i$$
$$\nu_0^2 = (1 + 2\alpha_1) + (1 + 8\alpha_3)\eta_0 \tag{12}$$

[2] Reason for introducing the factor 3/4 into the definition of $\eta_{i,0}$ will become apparent later.

To find the crossover point in the amplitude-frequency plane, one puts $\omega_i = \omega_0 = \omega_{cr}$ and $y_i = y_0 = y_{cr}$. It is found that

$$y_{cr}^2 = -\frac{1}{3}\,A_1/A_3 \qquad \omega_{cr}^2 = a_1 - \frac{1}{4}\,a \quad /A_3 \tag{13}$$

Thus real values of crossover amplitude and frequency occur if, and only if

$$\begin{gathered} A_1/A_3 \leq 0, \quad a_1/a_3 \geq \frac{1}{4}\,A_1/A_3 \quad \text{if} \quad a_3 > 0 \\ a_1/a_3 \leq \frac{1}{4}\,A_1/A_3 \quad \text{if} \quad a_3 < 0 \end{gathered} \tag{14}$$

From the first of the inequalities (14), it is seen that the crossover amplitude depends only on the properties of the coupling spring. In fact, if the coupling spring is restoring at small amplitudes ($A_1 > 0$), the crossover amplitude is real only if the spring is soft[3] ($A_3 < 0$), and conversely if the spring is exciting at small amplitudes ($A_1 < 0$), the existence of a real crossover amplitude requires that the coupling spring be hard[3] ($A_3 > 0$). It is of interest to observe that the force $F(u) = A_1u + A_3u^3$ in the coupling spring has zero slope at

$$u^2 = -\frac{1}{3}\,\frac{A_1}{A_3}$$

which is the same as the crossover amplitude. Thus real crossover amplitude can occur only in systems in which the slope of the coupling spring force has a change in sign.

While the system under discussion is always subject to the inequalities (8), those in (14) are not necessarily satisfied in the subsequent treatment. Thus we include systems in which the backbones intersect, as well as those in which they do not.

The Stability

A stability investigation of the vibrations of the nonlinear two-mode system discussed here yields many interesting results. It is, however, not the first time that the stability of free vibrations of two-degree-of-freedom systems has been investigated by the methods used here. Tobias [8], for instance, has studied the nonlinear vibrations of circular disks capable of vibrating in two modes, and he has encountered results similar to some of those reported here.

When raising the question of stability of free vibrations of a conservative system (such as the one treated here) one must discuss the implications of lack of stability. Clearly, since energy is conserved, one cannot expect instabilities in which the amplitudes become unbounded with $t \to \infty$. However, as will be seen, unstable solutions which are not orbitally stable either are encountered frequently. One would expect the instability to be a breakdown of the solution in either one, or in a combination of the following two ways: The zeroes of the amplitudes occur at intervals which are not constant, or the amplitude ceases to be constant. However, the amplitude will not become a monotonic function of time.

We examine the stability of the in-phase mode by substituting

$$x_2 = x_{1i}^* + \xi_i, \quad x_1 = x_{2i}^* + \zeta_i, \quad |\xi_i|, |\zeta_i| \text{ small} \tag{15}$$

and that of the out-of-phase mode by substituting

$$x_2 = -(x_{10}^* + \xi_0), \quad x_1 = -(x_{20}^* + \zeta_0), \quad |\xi_0|, |\zeta_0| \text{ small} \tag{16}$$

into the second of (6) where x_{1i}^* and x_{2i}^* are the periodic solutions of the first of (7), while x_{10}^* and x_{20}^* are periodic and satisfy the second of (7). When simple harmonic solutions are adopted, i.e., when

$$x_{1i}^* = x_{2i}^* = y_i \cos \omega_i t$$

$$x_{10}^* = -x_{20}^* = y_0 \cos \omega_0 t$$

it is found that the $\xi_{i,0}$ must satisfy Mathieu equations

$$\xi'' + (\delta + \epsilon \cos z)\xi = 0$$

where, for the in-phase mode

$$\begin{aligned} \epsilon = \epsilon_i(y_i) &= \frac{3}{8}\,a_3 \left(\frac{y_i}{\omega_i(y_i)}\right)^2 \\ \delta = \delta_i(y_i) &= \frac{1}{4}\,\frac{a_1 + A_1}{[\omega_i(y_i)]^2} + \epsilon_i(y_i) \end{aligned} \tag{17}$$

and, for the out-of-phase mode

$$\begin{aligned} \epsilon = \epsilon_0(y_0) &= \frac{3}{8}\,(a_3 + 4A_3) \left(\frac{y_0}{\omega_0(y_0)}\right)^2 \\ \delta = \delta_0(y_0) &= \frac{1}{4}\,\frac{a_1 + A_1}{[\omega_0(y_0)]^2} + \epsilon_0(y_0) \end{aligned} \tag{18}$$

It turns out that ζ_i must satisfy

$$\begin{aligned} A_1\zeta_i &= 0 \quad \text{if} \quad A_1 \neq 0 \\ \zeta_i &\equiv 0 \quad \text{if} \quad A_1 = 0 \end{aligned}$$

and ζ_0 is the solution of

$$(-A_1 + 12A_3y_0^2 \cos^2 \omega_0 t)\zeta_0 = 0$$

Evidently, the $\zeta_{i,0}$ have as their only solutions $\zeta_1 = \zeta_0 \equiv 0$; this carries the physical implication [in view of the second of (15) and (16)] that the stability of $x_1(t)$ is the same as that of $x_2(t)$. Therefore only one of them, say the latter, need be considered. The stability of the vibration modes depends, then, on those of Mathieu equations whose parameters are given in (17) and (18).

Each of the pairs (17) and (18) defines a line in the $\epsilon\delta$-plane called a "stability characteristic," the first giving the characteristic of the in-phase mode, the second that of the out-of-phase mode. Since the stability characteristics are analytic in $y_{i,0}^2$, given amplitudes $y_{i,0}$ define unique points on the stability characteristics and, conversely, given points on the stability characteristics define unique amplitudes $|y_{i,0}|$. Now it is well known that the stability of solutions of a Mathieu equation may be deduced from a stability chart in the $\epsilon\delta$-plane. This chart consists of a set of curves dividing the $\epsilon\delta$-plane into stable and unstable domains. For values (ϵ, δ) which define a point imbedded in a stable region, the solutions of the Mathieu equation are stable. For values $(\epsilon \neq 0, \delta)$ defining a point on the boundary of, or imbedded in an unstable region, the solutions of the Mathieu equation are unstable.

If the stability characteristics (17) and (18) are mapped on the stability chart, they will, in general, cut across stable and unstable domains. It follows that any point on a characteristic lying in, or on the boundary of an unstable region, defines an amplitude of vibration at which the mode in question is unstable. All other points on the stability characteristic define amplitudes of stable vibration. Therefore the "course" of the stability characteristics through the stability chart is of paramount importance for the stability properties of the modes.

[3] A spring is called "hard" if the slope of the spring force increases with increasing deflection, "soft" if the slope decreases with increasing deflection. This is the nomenclature used by Stoker [4]. Klotter [3] prefers the terms "hardening" and "softening"; the latter are perhaps more descriptive of the physical process taking place, but they are less concise.

Certain properties are common to the stability characteristics of both modes. For instance, they lie either entirely in the upper half-plane ($\epsilon \geq 0$) of the stability chart, or entirely in the lower ($\epsilon \leq 0$) as is readily seen from the equations of the $\epsilon_{i,0}$. To deduce their other properties, one must have expressions for the frequencies $\omega_{i,0}$. Exact expressions (9), or approximate ones (11) might be used. We propose to use the Duffing approximations (11) rather than the exact forms. This has the obvious advantage that (17) and (18) will be algebraic, rather than transcendental, in the amplitudes $y_{i,0}$. However, the actual motive for using the Duffing approximations is that the degree of precision in deriving them is consistent with that applied in the derivation of (17) and (18) themselves. Both, (11) as well as (17) and (18), are the results of first-order theories in which simple harmonic motion is adopted for the time histories of the displacements, but not for their time derivatives. Thus no improvement in accuracy can be expected from using the exact frequencies (9) in place of the Duffing frequencies (11).

When (11) has been substituted in (17) and (18), one can easily find expressions for the slopes of the characteristics in the $\epsilon\delta$-plane. They are

$$\frac{d\epsilon_i}{d\delta_i} = \frac{2}{1 - \alpha_1} = s_i(\alpha_1)$$
$$\frac{d\epsilon_0}{d\delta_0} = 2\left(1 - \frac{\alpha_1 - 4\alpha_3}{1 + 3\alpha_1 + 8\alpha_1\alpha_3}\right) = s_0(\alpha_1, \alpha_3) \tag{19}$$

Since both s_i and s_0 are constants, both stability characteristics are straight lines in the $\epsilon\delta$-plane.

Finally, it is seen from the second of (17) and (18) that $\delta_{i,0}(0)$ can never be nonpositive [under the restrictions (8)], and that $\epsilon_{i,0}(y_{i,0}) \to 0$ with $y_{i,0} \to 0$. Therefore, points on the stability characteristic lie, for sufficiently small vibrational amplitudes, always in the neighborhood of the positive δ-axis. As such points are in general stable, it follows that either mode is, in general, stable for sufficiently small amplitudes of vibration.

In all other significant respects, the stability characteristics differ for the two modes. Therefore these characteristics must be discussed separately.

The In-Phase Stability Characteristic

In examining the in-phase stability characteristic, it is advantageous to make use of the nondimensional forms. One finds

$$\epsilon_i(\eta_i) = \frac{1}{2}\,\frac{\eta_i}{\nu_i^3}$$
$$\delta_i(\eta) = \frac{1}{4}\,\frac{1 + \alpha_1}{\nu_i^3} + \epsilon_i \tag{20}$$

These equations, together with the first of (12) and of (19), are sufficient to describe the properties of the stability characteristic in question.

It will be seen from the first of (20) that the characteristic lies entirely in the upper half of the $\epsilon\delta$-plane if $\eta_i \geq 0$, in the lower if $\eta_i \leq 0$, and in the δ-axis if $\eta_i \equiv 0$. But, in view of the definition of η_i [see (10)] and of the first of the inequalities (8), η_i has the same sign as a_4. It follows that the characteristic lies entirely in the upper half-plane if the "outer" springs of the system are hard, in the lower if the outer springs are soft and, in the δ-axis if the outer springs are linear. Moreover, characteristics lying in the δ-axis degenerate to a point on that axis in the in-phase mode.

The first of (19) shows that the slope s_i is independent of α_3 (or a_3) and is a function of α_1 only. Thus for a given α_1 the slope is the same whether the characteristic lies in the upper half-plane ($a_3 > 0$) or in the lower half ($a_3 < 0$) of the $\epsilon\delta$-plane.

The intersection of the characteristic with the δ-axis is found from

$$\delta_i(0) = \frac{1}{4}\,\frac{1 + \alpha_1}{1 + 2\alpha_1} \tag{21}$$

Since the intersection, as well as the slope s_i is independent of α_3, the characteristic is continuous at $\eta_i = 0$; i.e., the characteristic is a straight line cutting across the δ-axis. The largest value of $\delta_i(0)$ is obtained when α_1 takes on its smallest value $\alpha_1 = -1/2$. In view of (21), $\delta_i(0)|_{\alpha_1 = -1/2} = \infty$. The smallest value of $\delta_i(0)$ occurs at $\alpha_1 = \infty$ for which $\delta_{i(0)}|_{\alpha_1 = \infty} = 1/8$. Thus the intersection of the stability characteristic with the δ-axis occurs at, or to the right of $\delta = 1/8$.

Finally, when $a_3 > 0$, and only then, one has the limits

$$a_3 > 0: \qquad \lim_{\eta_i \to \infty} \frac{\nu_i^3}{\eta_i} = 1; \quad \lim_{\eta_i \to \infty} \nu_i^3 = \infty$$

From this it follows, in view of (20), that

$$a_3 > 0: \qquad \epsilon_i(\infty) = \delta_i(\infty) = \frac{1}{2} \tag{22}$$

or, all stability characteristics consist of portions of straight lines, terminating on the point (1/2, 1/2) in the $\epsilon\delta$-plane.

When $a_3 < 0$, ν_i decreases with increasing η_i, and there exists a maximum (nondimensional) amplitude $\eta_{im} = -1$ for which $\nu_i = 0$. For that case one finds the limits

$$a_3 < 0: \qquad \lim_{\eta_i \to \eta_{im}} \frac{\nu_i^3}{\eta_i} = 0; \quad \lim_{\eta_i \to \eta_{im}} \nu_i^3 = 0$$

From this it follows that

$$a_3 < 0: \qquad -\epsilon_i(\eta_{im}) = |\delta_i(\eta_{im})| = \infty \tag{23}$$

or, stability characteristic lying in the lower half of the $\epsilon\delta$-plane extend infinitely far.

From this information, one can construct the entire family of in-phase stability characteristics in the stability chart. This is shown in Fig. 2(*a*). The characteristics have the following properties:

1 They are rays converging on the point (1/2, 1/2).

2 They all lie in a sector bounded by the lines of slope 4/3 and 0, respectively.

3 Points on them near the δ-axis correspond for all a_3 to small vibrational amplitudes.

4 The finite segments lying above the δ-axis correspond to the characteristics of systems in which the outer springs are hard.

5 The infinitely long segments below the δ-axis correspond to systems in which the outer springs are soft.

In Fig. 2(*b*), the curves on the stability chart which separate stable from unstable regions have been numbered from right to left in the order in which they intersect an imaginary line drawn parallel to, and below, the δ-axis; these numbers will be used to characterize the lines. Since each line is representative of an equation in the $\epsilon\delta$-plane, we shall write for them

$$\delta_j = \delta_j(\epsilon_j), \quad (j = 1, 2, \ldots) \tag{24}$$

Thus, for instance, $\delta_2 = \delta_2(\epsilon_2)$ is the equation of the line which passes from the upper right to the lower left through the δ-axis at $\delta = 1/4$. It is important to identify these lines because their intersections with a stability characteristic define special values y_{ij}, ($j = 1, 2, \ldots$) of the vibrational amplitude at which the in-phase mode experiences a change of stability. These special

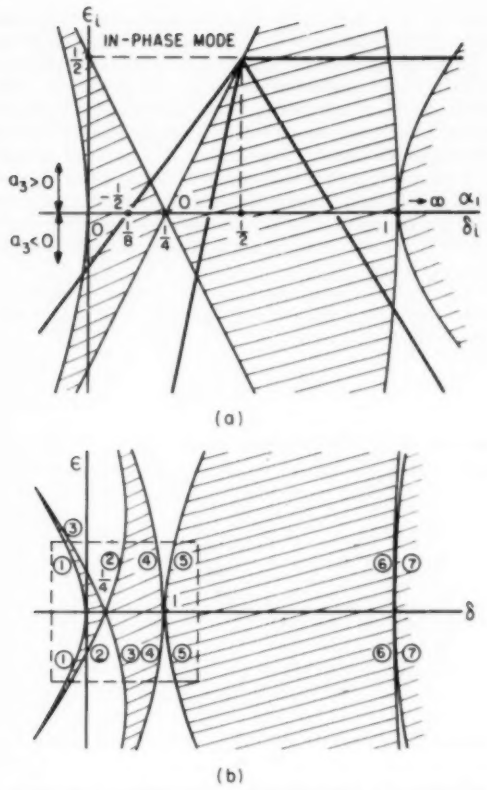

Fig. 2 (a) The stability characteristics of the in-phase mode in the stability chart. (b) The coding of the stability threshold lines in the stability chart. The area surrounded by the dotted line is used in (a).

amplitudes will be designated as "threshold amplitudes." Similarly, there exist nondimensional threshold amplitudes

$$\eta_{ij} = \frac{3}{4}\frac{a_1}{a_3} y_{ij}^2$$

One can easily find an equation of the form

$$g_i(\eta_{ij}) = 0, \quad (j = 1, 2, \ldots) \tag{25}$$

whose real roots, if they exist, are the nondimensional threshold amplitudes. For instance, equating the second of (20) and (24) yields an equation in ϵ_{ij}, i.e., in that value of ϵ at which the jth line of the stability chart intersects the in-phase characteristic. When ϵ_{ij} is eliminated between that equation and the first of (20) (where the latter is written for $\epsilon_i = \epsilon_{ij}$, $\eta_i = \eta_{ij}$) one finds for (25)

$$g_i = \delta_i\left(\frac{1}{2}\frac{\eta_{ij}}{\nu_{ij}^2}\right) - \frac{1}{4}\frac{1+\alpha_1}{\nu_{ij}^2} - \frac{1}{2}\frac{\eta_{ij}}{\nu_{ij}^2} = 0, \quad (j = 1, 2, \ldots) \tag{26}$$

Stoker [4] has given simple equations for some of the lines in the stability chart which are ". . . quite good for not too large values of ϵ." Each is a polynomial in ϵ and is accurate to powers in ϵ higher by one degree than the highest power appearing in the equations. These equations are

$$\left.\begin{aligned}
\delta_1 &= -\frac{1}{2}\epsilon_1^2 \\
\delta_2 &= \frac{1}{4} + \frac{1}{2}\epsilon_2 \\
\delta_3 &= \frac{1}{4} - \frac{1}{2}\epsilon_3 \\
\delta_4 &= 1 - \frac{1}{12}\epsilon_4^2 \\
\delta_5 &= 1 + \frac{5}{12}\epsilon_5^2
\end{aligned}\right\} \tag{27}$$

When the first of (27) and of (12) are substituted in (26), there results

$$\frac{1}{2}\frac{\eta_{i1}}{1+\eta_{i1}} = -1 \pm \left[1 - \frac{1+\alpha_1}{2(1+\eta_{i1})}\right]^{1/2} \tag{28}$$

which is easily solved for η_{i1}. It has no real roots if $\alpha_1 > 0$.

When use is made of the second of (27), one finds

$$\frac{\alpha_1}{1+\eta_{i2}} = 0 \tag{29}$$

which is satisfied by $\eta_{i2} = \pm\infty$ if $\alpha_1 \neq 0$, and by every value of η_{i2} if $\alpha_1 = 0$. The interpretation of this result is that the in-phase stability characteristics do not intersect line 2 at finite vibrational amplitudes except in the singular case when the characteristic coincides with that line. But in that case the solutions are orbitally stable [4].

By means of the third of (27) one finds

$$\eta_{i3} = -\frac{1}{2}\alpha_1 \tag{30}$$

or, in dimensional form,

$$y_{i3}^2 = -\frac{2}{3}\frac{A_1}{a_3}$$

For real roots one must have $A_1/a_3 < 0$. The physical implication of this result is that stability changes produced by the intersection of the characteristic with line 3, occur in the case of hard outer springs if the "center" spring is exciting at small amplitudes and, in the case of soft outer springs, if the center spring is restoring at small amplitudes.

By means of the fourth and fifth of (29), one obtains for the threshold amplitudes, respectively,

$$\frac{\eta_{i4}}{1+\eta_{i4}} = 12\left[-1 \pm \left(\frac{4}{3} - \frac{1}{12}\frac{1+\alpha_1}{1+\eta_{i4}}\right)^{1/2}\right] \tag{31}$$

and

$$\frac{\eta_{i5}}{1+\eta_{i5}} = \frac{12}{5}\left[1 \pm \left(-\frac{2}{3} + \frac{1}{6}\frac{1+\alpha_1}{1+\eta_{i5}}\right)^{1/2}\right] \tag{32}$$

An interesting property of the nondimensional threshold amplitudes is that they depend on α_1 only, i.e., on the linear terms in the spring forces, while the dimensional threshold amplitudes depend on the nonlinearity in the outer springs as well. One would hardly have expected this result because the position of the characteristics in the stability chart—whether above or below the δ-axis—is decided by the sign of a_3.

Finally, it is of interest to consider the stability of the in-phase mode when all springs are linear. In that case, the characteristic is a point on the δ-axis and, therefore, always stable.

The Out-of-Phase Stability Characteristic

The stability characteristics of the out-of-phase mode are more complex than those of the in-phase mode. While the latter could have been discussed easily in terms of the dimensional quantities, this is no longer feasible in the out-of-phase mode.

The nondimensional forms of (18) are

$$\epsilon_0(\eta_0) = \frac{1}{2}\frac{(1+4\alpha_3)\eta_0}{\nu_0^2}$$
$$\delta_0(\eta_0) = \frac{1}{4}\frac{1+\alpha_1}{\nu_0^2} + \epsilon_0 \tag{33}$$

These equations together with the second of (12) and of (19) are suitable to deduce the properties of the stability characteristics in the out-of-phase mode. While (33) seem to reduce to the comparable equations in the in-phase mode when one puts $\alpha_2 = 0$, this is not the case because $\nu_0^2|_{\alpha_2=0} \neq \nu_0^2$.

If the out-of-phase mode is hard ($a_3(1+8\alpha_3) > 0$), but only in that case, one finds

$$a_3(1+8\alpha_3) > 0: \quad \lim_{\eta_0 \to \infty}\frac{\eta_0}{\nu_0^2} = \frac{1}{1+8\alpha_3}$$
$$\epsilon_0(\infty) = \frac{1}{2}\frac{1+4\alpha_3}{1+8\alpha_3}, \quad \delta_0(\infty) = \epsilon_0(\infty) \tag{34}$$

and it follows from the last two of (34) that the stability characteristics of the hard out-of-phase mode terminate always on a point of the line which passes with slope 1 through the origin of the $\epsilon\delta$-plane; the position of that point depends on the value of α_3. Evaluation of the second of (34) shows that, when

$$\left.\begin{aligned}
\alpha_3 &= -\frac{1}{8}, && \epsilon_0(\infty) = \pm\infty,\\
0 > \alpha_3 &> -\frac{1}{8}, && \frac{1}{2} < \epsilon_0(\infty) < +\infty,\\
\alpha_3 &= 0, && \epsilon_0(\infty) = \frac{1}{2},\\
\infty > \alpha_3 &> 0, && \frac{1}{4} < \epsilon_0(\infty) < \frac{1}{2},\\
-\frac{1}{4} > \alpha_3 &> -\infty, && 0 < \epsilon_0(\infty) < \frac{1}{4},\\
\alpha_3 &= \frac{1}{4}, && \epsilon_0(\infty) = 0,\\
-\frac{1}{8} > \alpha_3 &> -\frac{1}{4}, && -\infty < \epsilon_0(\infty) < 0.
\end{aligned}\right\} \tag{35}$$

Four exceptional cases arise when $\alpha_3 = \pm\infty$. Two of these may be encountered easily in physical systems when $a_3 = 0$, $A_3 \neq 0$; i.e., when the outer springs are linear while the center spring is not. In that case the nondimensional amplitude $\eta_0 \equiv 0$ for every value of the vibrational amplitude y_0. But $\eta_0 \equiv 0$ implies $\epsilon_0 \equiv 0$; therefore, the characteristic is a point on the positive[4] δ-axis. Since all points on the positive δ-axis lie in stable regions, the out-of-phase mode is always stable when the outer springs are linear. Two more exceptional cases arise from $A_3 = \pm\infty$, $|a_3| \neq \infty$. The first of these corresponds to an infinitely stiff center spring; i.e., the masses of the system are rigidly interconnected. In that case, out-of-phase motion cannot occur, and a discussion of its stability is meaningless. In the second of these, the center spring develops an infinitely large exciting force for sufficiently large displacements; here, the system is, indeed, unstable for these sufficiently large displacements. However, these last two cases cannot arise in physically realizable systems.

Although only linear or hard out-of-phase modes, defined by $a_3(1+8\alpha_3) \geq 0$, have been considered, these stability characteristics may lie entirely in the lower, as well as entirely in the upper, half of the $\epsilon\delta$-plane. This is quite different from the in-phase mode where the characteristic always lies in the upper half-plane if the mode is hard.

One finds easily the value of δ at which the characteristic of the out-of-phase mode originates on the δ-axis by forming from the second of (33)

$$\delta_0(0) = \frac{1}{4}\frac{1+\alpha_1}{1+2\alpha_1} \tag{36}$$

Evaluating this quantity it turns out that, when

$$\left.\begin{aligned}
\alpha_1 &= \infty, && \delta_0(0) = \frac{1}{8},\\
0 < \alpha_1 &< \infty, && \frac{1}{4} > \delta_0(0) > \frac{1}{8},\\
\alpha_1 &= 0, && \delta_0(0) = \frac{1}{4},\\
-\frac{1}{2} < \alpha_1 &< 0, && \infty > \delta_0(0) > \frac{1}{4}.
\end{aligned}\right\} \tag{37}$$

It follows that the out-of-phase characteristics intersect the δ-axis at, or to the right of, $\delta = 1/8$. In this respect, the characteristics of the in and out-of-phase modes are similar. However, there exist differences as well. In the out-of-phase mode, the characteristics are horizontal when α_1 takes on its least value $\alpha_1 = -1/2$, while they are horizontal in the in-phase mode when $\alpha_1 = \infty$. A similar exchange takes place when one considers the intersection of the characteristics with the δ-axis at $\delta = 1/8$.

Since the equations for the slope s_0 [see the second of (19)] and for the intersection with the δ-axis [see (36)] are independent of the question of hardness of the out-of-phase mode, the characteristics for given values of α_1 and $\alpha_2 \neq \infty$ are portions of straight lines which originate at the same point on the δ-axis and which have the same slopes. That portion which terminates on a line of slope unity passing through the origin of the $\epsilon\delta$-plane, is the characteristic of the hard out-of-phase mode; the other portion is that of a soft mode. The latter portion extends to infinity. This is easily seen by noting that the maximum amplitude of a soft out-of-phase mode is given by

$$a_3(1+8\alpha_3) < 0: \quad \eta_{0m} = -\frac{1+2\alpha_1}{1+8\alpha_3} \tag{38}$$

and, at that amplitude, the frequency ν_0 vanishes. In the case of a soft outer mode one finds

$$a_3(1+8\alpha_3) < 0; \quad \lim_{\eta_0 \to \eta_{0m}}\frac{\eta_0}{\nu_0^2} = \infty,$$
$$\epsilon_0(\eta_{0m}) = \infty, \quad \delta_0(\eta_{0m}) = \epsilon_0(\eta_{0m}) \tag{39}$$

With this information, one can describe the entire family of out-of-phase stability characteristics in the stability chart; they have the appearance shown in Fig. 3. The characteristics have the following properties:

1 They are rays intersecting the δ-axis and converging on a

[4] The fact that the point lies on the δ-axis at $\delta \geq 1/8$ follows from (36).

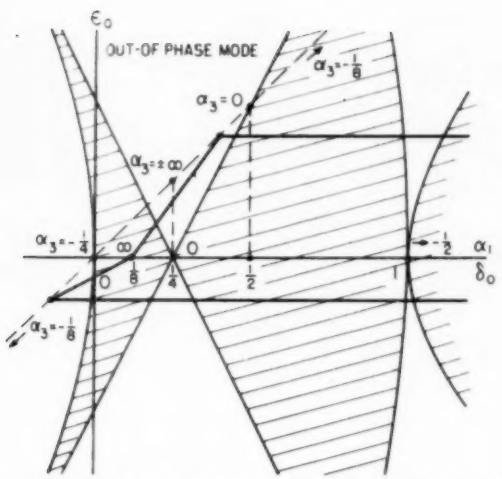

Fig. 3 The stability characteristics of out-of-phase mode in stability chart

point of that line which passes with unity slope through the origin of the $\epsilon\delta$-plane.

2 The point of convergence may lie above, below, or on the δ-axis. Its position is determined by the parameter $|\alpha_3| \neq \infty$ only; i.e., by the nonlinear properties of the springs.

3 The characteristics originate on the δ-axis at a point $\delta_0(0) \geq 1/8$ whose position is determined by the parameter α_1 only; i.e., by the linear terms of the spring forces.

4 The segments of the characteristics lying between the δ-axis and the point of convergence are those of hard modes $a_3(1 + 8\alpha_3) > 0$.

5 The segments, originating on the δ-axis and extending infinitely far, belong to the soft modes for which $a_3(1 + 8\alpha_3) < 0$.

6 Points on the stability characteristic near the δ-axis correspond always to small amplitudes of vibration and these are in general, stable.

The threshold amplitudes at which out-of-phase vibrations experience a change in stability are the real roots of

$$g_0 = \delta_j \left(\frac{1}{2} \frac{(1 + \alpha_3)\eta_{0j}}{\nu_{0j}^2} \right) - \frac{1}{4} \frac{1 + \alpha_1}{\nu_{0j}^2} - \frac{1}{2} \frac{(1 + \alpha_3)\eta_{0j}}{\nu_{0j}^2} = 0, \quad (j = 1, 2, \ldots) \quad (40)$$

For sufficiently small ϵ_j, the δ_j, $(j = 1, 2, \ldots)$ are given in (27). The threshold amplitudes of the out-of-phase modes are obtained from

$$\frac{1}{2}\left[\frac{(1 + 4\alpha_3)\eta_{01}}{(1 + 2\alpha_1) + (1 + 8\alpha_3)\eta_{01}}\right] = -1 \pm \left\{1 - \frac{1}{2}\left[\frac{1 + \alpha_1}{(1 + 2\alpha_1) + (1 + 8\alpha_3)\eta_{01}}\right]\right\}^{1/2} \quad (41)$$

$$\eta_{02} = -\frac{1}{4}\frac{\alpha_1}{\alpha_3} \quad (42)$$

$$\eta_{03} = \frac{1}{2}\frac{\alpha_1}{1 + 2\alpha_3} \quad (43)$$

$$\frac{1}{2}\left[\frac{(1 + 4\alpha_3)\eta_{04}}{(1 + 2\alpha_1) + (1 + 8\alpha_3)\eta_{04}}\right] = 6\left\{-1 \pm \left\langle \frac{4}{3} - \frac{1}{12}\left[\frac{1 + \alpha_1}{(1 + 2\alpha_1) + (1 + 8\alpha_3)\eta_{04}}\right]\right\rangle^{1/2}\right\} \quad (44)$$

$$\frac{1}{2}\left[\frac{(1 + 4\alpha_3)\eta_{05}}{(1 + 2\alpha_1) + (1 + 8\alpha_3)\eta_{05}}\right] = \frac{1}{5}\left\{6 \pm \left\langle -24 + 15\left[\frac{1 + \alpha_1}{(1 + 2\alpha_1) + (1 + 8\alpha_3)\eta_{05}}\right]\right\rangle^{1/2}\right\} \quad (45)$$

The equation for η_{05} is of special interest. That particular threshold amplitude is identical with the nondimensional amplitude η_{cr} at which the backbones in the frequency-amplitude plane intersect. This will be seen by transforming either (13) to nondimensional, or (42) to dimensional form. The physical interpretation of this equality of the two amplitudes is that the out-of-phase mode experiences always a change of stability at the amplitude and frequency at which the backbones intersect. Moreover, since this change of stability is intimately connected with the zero-slope point of the force in the coupling spring, it is suggested that the mechanism of the instability at crossover amplitudes is different from the others and is closely linked to the action of the coupling spring.

Experimental Results

The differential equations (6) contain the four constants a_1, a_3, A_1, A_2 which, when assigned particular magnitudes and signs, will yield 18 different configurations of backbone curves in the amplitude-frequency plane. Because of this variety, a coding technique was developed that is based on the shape of these backbone curves and their relative positions in the amplitude-frequency plane. The springs may be hard, soft, or linear, and the phase "in" or "out"; thus the backbones will bend to the right, the left, or be vertical, and the out-of-phase backbones may originate to the left or the right of that of the in-phase curve.

Fig. 4(*a*) shows the backbones for a representative configuration as an example of the coding technique. In Fig. 4(*a*) the in-phase backbone is that of a hard mode; this condition is expressed by the letters IH for "in hard." The out-of-phase backbone in Fig. 4(*a*) is characteristic of a soft mode; this is expressed by OS, "out soft." The code word for the configuration is IH-OS with IH on the left since $\omega_1(0) < \omega_0(0)$. Fig. 4(*b*) is a composite of backbones any two of which will represent a configuration defined by specified values of the parameters of (6).

The differential equations (6) were solved by an electronic analog computer for such values of the constants that a representative number of configurations was studied experimentally. The computer circuit is sketched in Fig. 5. The solution curves $x_1(t)$, $x_2(t)$ were plotted on a Sanborn recorder. Data from these records were used to construct backbone curves for a comparison of the form and stability of the experimental solutions with the theoretical results.

Instability is displayed in a computer solution by the departure of the solutions $x_1(t)$, $x_2(t)$ from an established periodic pattern. The instability may be "mild" or "violent," depending on the number of stable cycles before instability sets in. The appearance of the instability suggests an energy transfer between the two masses. Fig. 6(*a*) shows a record of a computer run for

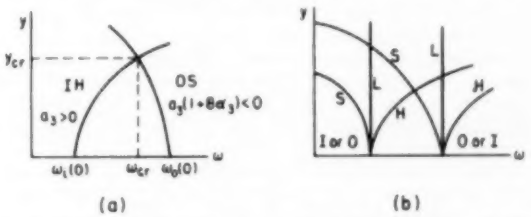

Fig. 4 Explanation of coding technique for classifying special cases

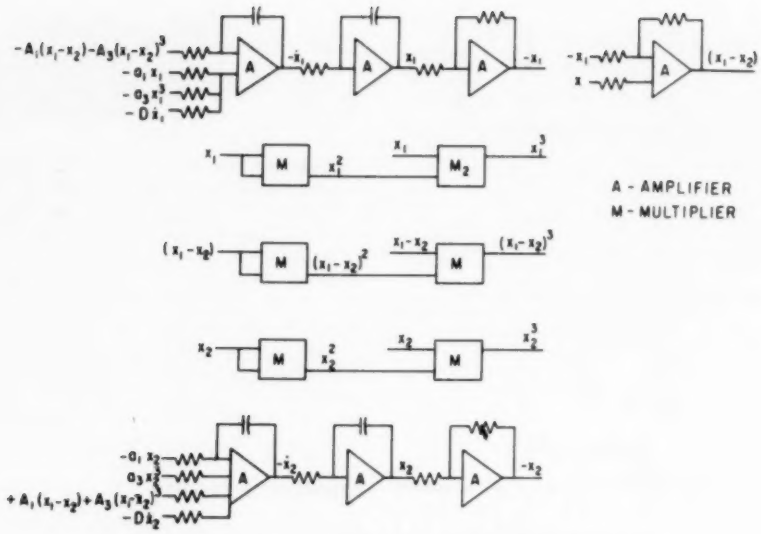

Fig. 5 Elements of computer circuit used to test the theoretical development

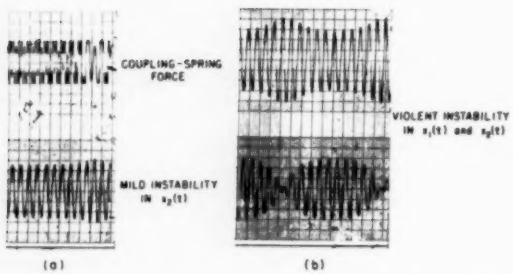

Fig. 6 (a) Experimental data showing a mild instability and action of the coupling spring. (b) Experimental evidence of violent instability.

configuration IH-OH (with crossover). The initial conditions are such that the solutions are out of phase. A mild instability occurs after eight cycles. Fig. 6(*b*) shows instability in an IH-OH configuration (without crossover); this is an example of violent instability.

As stated earlier, the instability of the out-of-phase mode at the crossover amplitude is intimately connected with the force in the coupling spring; therefore it is of interest to observe the behavior of this spring at the amplitude in question. A record of the coupling-spring force as a function of time is shown in Fig. 6-(*a*). It is observed that the spring force is periodic at the period of the motion but displays a dominant third harmonic.

Fig. 7 shows a summary of a comparison between experimental results obtained by the electronic computer and theoretical results predicted by the stability characteristics. The summary presents the backbones in the amplitude-frequency planes for the different configurations studied. The backbones are drawn as double lines. Full lines represent stable regions, dashed lines represent unstable regions. The heavy lines are based on the theoretical results. The light lines give experimental results. The values for the constants a_1, a_3, A_1, A_3 for each configuration are given in Fig. 7.

In nine of the thirteen configurations of Fig. 7, there is complete agreement between the theoretical and the experimental results. An examination of the stability characteristics in the remaining four cases shows that there is no fundamental discrepancy between theory and experiment. Fig. 7(7) indicates instability of the computer solution where the theoretical results predict stable behavior. As shown in Fig. 8, the stability characteristic for this mode is a line coinciding with the δ-axis and extending from a value $\delta = 3/8$ to $\delta = 0$. However, Fig. 3 shows that the position of the endpoint of this characteristic for $\alpha_3 \cong -1/4$ is very sensitive to the value of α_3. This endpoint lies between $\delta = 0$ and $\delta = -\infty$ for values of α_3 between $\alpha_3 = -1/4$ and $\alpha_3 = -1/8$. If the value of α_3 in the computer solution is slightly different from $-1/4$, the characteristic no longer has zero slope, and an unstable range will be encountered.

In Fig. 8 there are also shown the stability characteristics for the two cases OL-IS and OS-IS where there exists a discrepancy between experimental and theoretical results. In the case OL-IS, the theoretical and experimental results are easily brought into conformity by an argument similar to that used for the configuration OH-IS. In the case OS-IS, conformity between theory and experiment is produced when the straight lines of the stability chart in Fig. 8 are replaced by the more accurate curved lines which the straight lines approximate.

There remains the discrepancy between theory and experiment in the case IS-OH. In this case $a_3 = -1/7$ or the outer springs are nearly linear. If they were altogether linear, the theory would predict stability of the out-of-phase mode. We suspect that the instability in this case was so mild as to have been overlooked. It probably could be discovered by a sufficiently protracted observation of the behavior of the system. However, errors in the performance of the computer which accumulate with time do not permit such an extended observation.

Concluding Remarks

We have discussed the free vibrations of a conservative system consisting of springs and masses. When this system is linear, questions concerning the stability of the motion do not normally arise, whether the system has one or several degrees of freedom. When the system is nonlinear and possesses only a single degree of freedom, an examination of the stability of free vibrations is usually restricted to the demonstration that the motion is orbitally stable.

The situation is quite different in nonlinear systems having two degrees of freedom. Here, the question of stability is of cen-

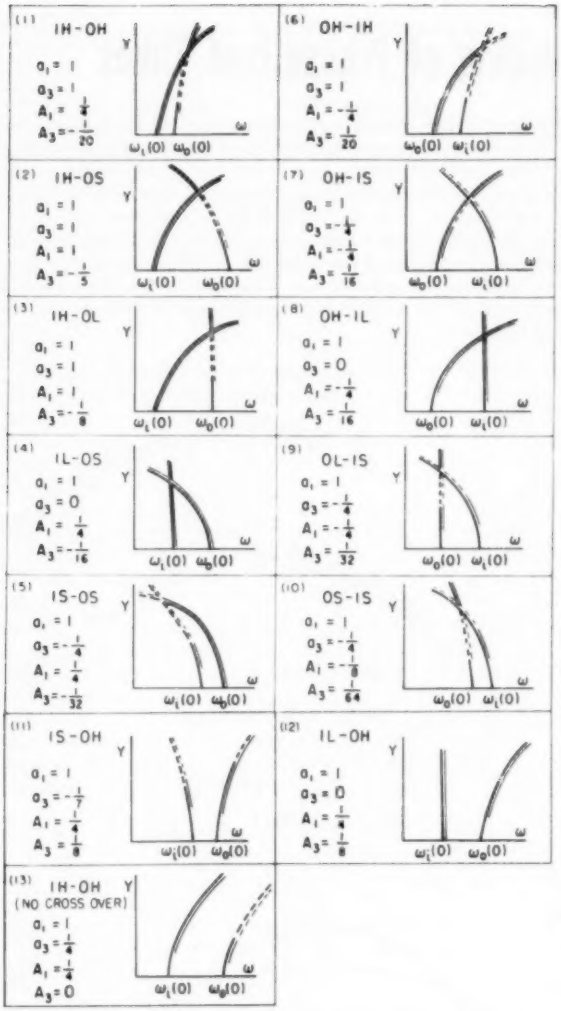

Fig. 7 Comparison between theoretical and experimental data. Heavy lines are theoretical results, light lines are experimental results. Dotted lines represent instability.

tral importance because its resolution decides on the existence, in a physical sense, of the periodic solutions. It has been demonstrated that the free vibrations are frequently unstable, and changes of stability take place at threshold amplitudes whose magnitudes cannot be estimated from heuristic arguments based on physical intuition.

It is not difficult to extend the theory of this paper in two directions. One of these is concerned with forced vibrations. For sufficiently large amplitudes, the amplitude-frequency curves of forced vibrations lie in the neighborhood of the backbones, and for sufficiently small amplitudes of vibration they lie in the neighborhood of the frequency-axis. But, the frequency axis maps into the δ-axis of the stability chart, and the backbones map into the stability characteristics of free vibrations. Thus one can discuss the stability of forced vibrations in terms of continuity arguments with reference to the amplitude of the forcing function. The general appearance of the stability characteristics in the $\epsilon\delta$-plane is shown in Fig. 9. It is observed that the intersection of the stability characteristic of free vibrations with the δ-axis is a saddle point in the $\epsilon\delta$-plane.

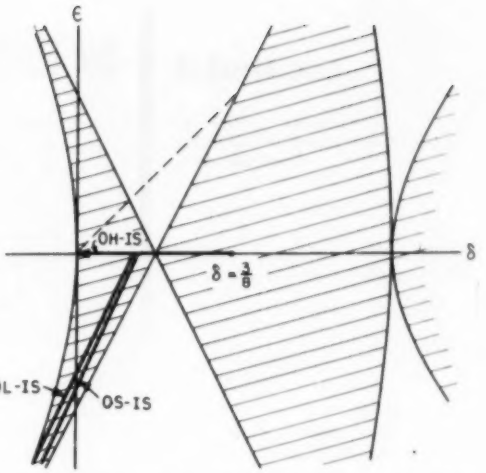

Fig. 8 Stability characteristics of three cases where the experiment seems to counterindicate theoretical results

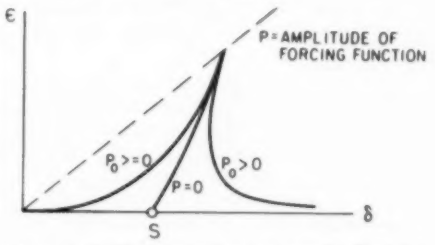

Fig. 9 Stability characteristics of forced vibrations

The extension of the present theory to unsymmetrical systems is accomplished by the demonstration that the modal relations in the general two-degree-of-freedom case are of the type $x_1 = cx_2$ where c = const is given by the roots of an equation involving c and the parameters of the problem. In the symmetrical case these roots were $c = \pm 1$.

Reports on these extensions of the theory will be given in the near future.

References

1 T. C. Huang, "Harmonic Oscillations of Nonlinear Two-Degree-of-Freedom Systems," JOURNAL OF APPLIED MECHANICS, vol. 22, TRANS. ASME, vol. 77, 1955, pp. 107–110.

2 R. M. Rosenberg, Discussion of [1], JOURNAL OF APPLIED MECHANICS, vol. 22, TRANS. ASME, vol. 77, 1955, pp. 602–603.

3 K. Klotter, "Steady State Vibrations in Systems Having Arbitrary Restoring and Arbitrary Damping Forces," Proceedings of the Symposium on Nonlinear Circuit Analysis, Polytechnic Institute of Brooklyn, 1953, pp. 234–257.

4 J. J. Stoker, "Nonlinear Vibrations," Interscience Publishers, Inc., New York, N. Y., 1950.

5 P. R. Sethna, "Steady State Motion of One and Two-Degrees-of-Freedom Vibrating Systems With a Nonlinear Restoring Force," Proceedings of the Second U. S. National Congress of Applied Mechanics, University of Michigan, 1954, pp. 69–78.

6 F. R. Arnold, "Steady-State Behavior of Systems Provided With Nonlinear Dynamic Vibration Absorbers," JOURNAL OF APPLIED MECHANICS, vol. 22, TRANS. ASME, vol. 77, 1955, pp. 487–492.

7 N. W. McLachlan, "Ordinary Non-Linear Differential Equations in Engineering and Physical Sciences," Clarendon Press, 1950.

8 S. A. Tobias, "Free Undamped Non-Linear Vibrations of Imperfect Circular Disks," The Institution of Mechanical Engineers, preprint, 1957.

ERIC REISSNER

Professor of Mathematics,
Massachusetts Institute of Technology,
Cambridge, Mass.

On Finite Bending of Pressurized Tubes[1]

A unified treatment is presented of two well-known problems which have until now been considered separately. The two problems are: (a) the linear problem of pure bending of curved tubes, and (b) the nonlinear problem of pure bending of straight tubes. In both problems the effect of uniform internal pressure is included. The essential step in the present analysis is the treatment of the flattening of the cross sections of the tube by means of a theory of finite bending of circular rings. The general results of the paper are used to obtain improved values for the stability parameters in the problem of flattening instability of originally straight tubes acted upon by end bending moments, and also to obtain results on the effect of slight original curvature of the beam axis in the problem of flattening instability.

THE present paper is concerned with the linear problem of pure bending of curved tubes as considered by von Karman [1],[2] Thuloup [2], and others, and with the nonlinear problem of pure bending of straight tubes as considered by Brazier [3] and others. In both problems the effect of internal tube pressure is included. We consider these two problems from a unified point of view and in this way obtain additional results of the following kind:

1 We show that the results of Brazier [3] and Wood [4] for originally straight tubes may be considered as a first approximation to the solution of their problem, in so far as expansion in powers of a suitable parameter is concerned. We establish the nature of this expansion and obtain the corresponding second approximation.

2 We obtain first-order, nonlinear corrections to the results of the linear theory of originally curved tubes, and in this way delimit the range of validity of linear theory.

3 We generalize the known, first-approximation nonlinear theory for originally straight tubes to the case of tubes possessing a slight initial curvature, under the assumption that the order of magnitude of this initial curvature is the same as the critical curvature for originally straight tubes.

Formulation of Problem

We consider a tube with center-line radius a, wall thickness h, and cross-sectional radius b, which is subjected to an internal pressure p, Fig. 1. A moment M is applied to the ends of the tube which changes the center-line radius from a to R. At the same time the circular cross section of the tube deforms into a doubly symmetrical noncircular shape, Fig. 2.

Application of the moment M causes a longitudinal fiber stress σ and a longitudinal fiber strain ϵ. We designate by y and by

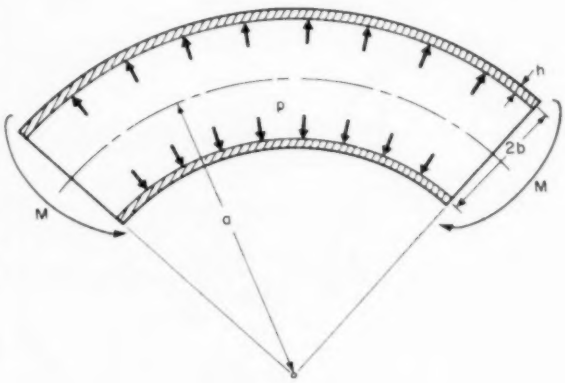

Fig. 1

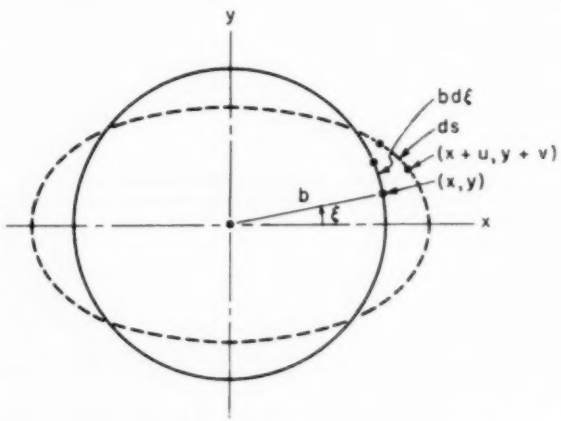

Fig. 2

$y + v$, the distances of the points of the middle surface of the tube wall from the neutral surface of the tube, before and after deformation. The relation between moment M and fiber stress σ is then

$$M = \int h\sigma(y + v)ds \tag{1}$$

where ds is the element of arc of the deformed meridian curve of the tube wall.

[1] A report on work carried out as part of a project supported by the Office of Naval Research of the United States Navy. Some of the ideas incorporated in this report were arrived at during a consulting appointment, in August, 1957, with the Mechanics Department of the Guided Missiles Research Division of the Ramo-Wooldridge Corporation.

[2] Numbers in brackets designate References at end of paper.

Presented at the Summer Conference of the Applied Mechanics Division, Troy, N. Y., June 18–20, 1959, of THE AMERICAN SOCIETY OF MECHANICAL ENGINEERS.

Discussion of this paper should be addressed to the Secretary, ASME, 29 West 39th Street, New York, N. Y., and will be accepted until October 10, 1959, for publication at a later date. Discussion received after the closing date will be returned.

NOTE: Statements and opinions advanced in papers are to be understood as individual expressions of their authors and not those of the Society. Manuscript received by ASME Applied Mechanics Division, May 7, 1958. Paper No. 59—APM-5.

The relation between fiber stress σ and fiber strain ϵ is

$$\sigma = E\epsilon \tag{2}$$

where E is Young's modulus of the tube material.

The fiber strain ϵ is a function of the radius change $R - a$ and of the displacement component v. We limit ourselves to the consideration of tubes for which

$$b/a \ll 1 \tag{3}$$

For such tubes we have that the neutral surface of the tube is the cylinder with radius R and the expression for ϵ is found to be

$$\epsilon = \left(\frac{1}{R} - \frac{1}{a}\right) y + \frac{v}{R} \tag{4}$$

In order to determine the displacement function v we consider the problem of the deformation of the tube cross section as a problem of the cylindrical deformation of an infinite pressurized circular cylinder or, except for a factor $1 - \nu^2$ in the appropriate stiffness coefficient, as a problem of plane deformations of a circular ring.

Let ξ be the angular co-ordinate of the points of the middle surface of the cross section before deformation, Fig. 2. The corresponding Cartesian co-ordinates are

$$x = b\cos\xi, \quad y = b\sin\xi \tag{5}$$

Because of deformation the co-ordinates x and y change to $x + u$ and $y + v$, and the original radius of curvature b changes to a variable radius ρ, Fig. 3. The original tangent angle ϕ changes into $\phi + \beta$.

We may assume that the deformation of the cross section takes place with negligible extension so that the arc length ds of the deformed element is the same as the corresponding undeformed arc length $bd\xi$. We then have

$$\rho d(\phi + \beta) = ds = bd\xi = bd\phi \tag{6}$$

and

$$\frac{1}{\rho} = \frac{1}{b}(1 + \beta') \tag{7}$$

where the prime indicates differentiation with respect to ξ.

The components of displacement u and v follow from the relations

$$\frac{d(x+u)}{ds} = -\cos(\phi + \beta), \quad \frac{d(y+v)}{ds} = \sin(\phi + \beta) \tag{8}$$

Since $\phi = \xi + {}^1/_2\pi$ and $ds = bd\xi$, equations (8) may be written in the following form:

$$\begin{aligned} \frac{du}{d\xi} &= b[\sin(\xi + \beta) - \sin\xi] \\ \frac{dv}{d\xi} &= b[\cos(\xi + \beta) - \cos\xi] \end{aligned} \tag{9}$$

The second of equations (9) and the symmetry condition $v(0) = 0$ leads to the formula

$$v = b\int_0^\xi [\cos(\xi + \beta) - \cos\xi]d\xi \tag{10}$$

In order to relate the deformation variable β and the fiber stress σ we consider the equilibrium equations and stress-strain relations of the meridional rings of which the tube is composed.

Introducing forces, moments, and load intensities in accordance with Fig 4, we have the following system of equilibrium equations:

$$\frac{N'}{b} - \frac{Q}{\rho} + p_t = 0 \tag{11}$$

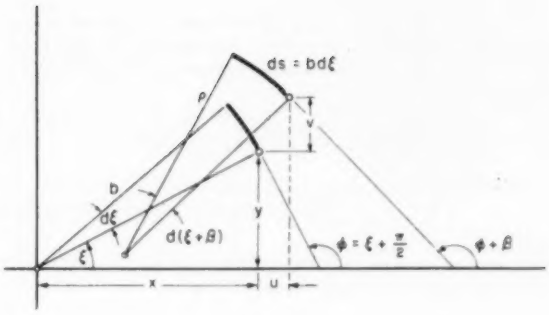

Fig. 3

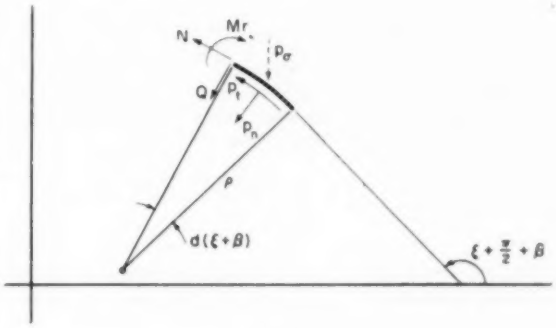

Fig. 4

$$\frac{Q'}{b} + \frac{N}{\rho} + p_n = 0 \tag{12}$$

$$\frac{M_r'}{b} - Q = 0 \tag{13}$$

In view of the assumed inextensibility of the ring sections, the system (11) to (13) is complemented by one stress-strain relation only, which is of the form

$$\frac{M_r}{D} = \frac{1}{b} - \frac{1}{\rho} = -\frac{\beta'}{b} \tag{14}$$

It will be assumed that the tube material is isotropic so that

$$D = \frac{Eh^3}{12(1 - \nu^2)} \tag{15}$$

It is, however, equally well possible to consider D as a stiffness constant for an anisotropic tube material, in which case equation (15) is replaced by a different relation.

A final system of relations expresses the components of load intensity p_n and p_t in terms of the internal pressure p and in terms of the ring-load intensity p_σ which is due to the relative inclination of the fiber stresses σ, as caused by the curvature $1/R$ of the center line of the tube. The load intensity p_σ is in the direction of the axis y and is of magnitude

$$p_\sigma = \sigma\frac{h}{R} \tag{16}$$

The load intensities p_n and p_t are then

$$p_n = -p + p_\sigma\sin(\xi + \beta) \tag{17}$$

$$p_t = -p_\sigma\cos(\xi + \beta) \tag{18}$$

The system of equations (11) to (18) may be reduced to one differential equation for β and σ. Introducing (12) into (11), and (14) into (13) we have first as a system of two equations for Q and β

$$\left(\frac{\rho}{b}\,Q'\right)' + \frac{b}{\rho}\,Q = bp_t - (\rho p_n)' \tag{19}$$

$$\frac{D}{b^3}\,\beta'' + Q = 0 \tag{20}$$

With ρ from equation (7) and p_n and p_t from equations (17) and (18) there follows as equation relating β and σ,

$$\frac{D}{b^3}\left[\left(\frac{\beta'''}{1+\beta'}\right)' + (1+\beta')\beta'' + \frac{pb^3}{D}\left(\frac{1}{1+\beta'}\right)'\right] = \frac{h}{R}\left[\sigma\cos(\xi+\beta) + \left(\frac{\sigma\sin(\xi+\beta)}{1+\beta'}\right)'\right] \tag{21}$$

A second equation relating β and σ is given by the stress-strain relation (2) upon introducing v from equation (10), and y from equation (5) into equation (4) for ϵ,

$$\frac{\sigma}{E} = \left(\frac{b}{R} - \frac{b}{a}\right)\sin\xi + \frac{b}{R}\int_0^\xi [\cos(\xi+\beta) - \cos\xi]d\xi \tag{22}$$

Equations (21) and (22) are to be solved subject to suitable boundary conditions for the function β. Because of symmetry, β as well as Q must vanish for $\xi = 0, \pi/2, \pi$, and $3\pi/2$. This means that it is sufficient to determine β in the quadrant $0 \leq \xi \leq \pi/2$ subject to the boundary conditions

$$\beta(0) = \beta''(0) = \beta(\pi/2) = \beta''(\pi/2) = 0 \tag{23}$$

In addition to the longitudinal fiber stress σ, as given by (22), and the displacement v as given by (10), quantities of interest are the meridional bending stress σ_B given by

$$\sigma_B = \pm\frac{6M_r}{h^2} = \mp\frac{6D}{bh^2}\,\beta' \tag{24}$$

and the applied bending moment M which may be written in the form

$$\frac{M}{EI} = \left(\frac{1}{R} - \frac{1}{a}\right)\left[1 + \frac{1}{\pi}\int_0^{2\pi}\frac{v}{b}\sin\xi\,d\xi\right] + \frac{1}{R}\,\frac{1}{\pi}\int_0^{2\pi}\left[\frac{v}{b}\sin\xi + \left(\frac{v}{b}\right)^2\right]d\xi \tag{25}$$

where $I = \pi hb^3$ is the moment of inertia of the tube cross section in the undeformed state.

First and Second-Order Nonlinear Theories

For the application of the results to specific cases we write

$$\cos(\xi+\beta) = \cos\xi - \beta\sin\xi - \frac{1}{2}\,\beta^2\cos\xi + O(\beta^3) \tag{26}$$

$$\sin(\xi+\beta) = \sin\xi + \beta\cos\xi - \frac{1}{2}\,\beta^2\sin\xi + O(\beta^3) \tag{27}$$

and, except for higher-order terms,

$$\frac{v}{b} = -\int_0^\xi\left(\beta\sin\xi + \frac{1}{2}\,\beta^2\cos\xi\right)d\xi \tag{28}$$

$$\frac{\sigma}{E} = \left(\frac{b}{R} - \frac{b}{a}\right)\sin\xi - \frac{b}{R}\int_0^\xi\left(\beta\sin\xi + \frac{1}{2}\,\beta^2\cos\xi\right)d\xi \tag{29}$$

A corresponding approximation for the differential equation (21) results in the relation

$$\frac{D}{b^3}\left\{\beta^{iv} + \left(1 - \frac{pb^3}{D}\right)\beta'' - \left[\beta'\beta^{iv} + \beta''\beta''' - \left(1 + 2\,\frac{pb^3}{D}\right)\beta'\beta''\right]\right\} = \frac{h}{R}\left\{\sigma[2\cos\xi - (2\beta + \beta'')\sin\xi] + \sigma'[\sin\xi + \beta\cos\xi - \beta'\sin\xi]\right\} \tag{30}$$

which, upon introduction of σ from equation (29), is further reduced to the following form:

$$\begin{aligned}\frac{D}{b^3}\Big\{&\beta^{iv} + \left(1 - \frac{pb^3}{D}\right)\beta'' - \beta'\left[\beta^{iv} - \left(1 + 2\,\frac{pb^3}{D}\right)\beta''\right] - \beta''\beta'''\Big\} \\ = \frac{hE}{R}\Big\{&\left(\frac{b}{R} - \frac{b}{a}\right)[3\cos\xi\sin\xi + (\cos^2\xi - 2\sin^2\xi)\beta \\ &- \beta'\sin\xi\cos\xi - \beta''\sin^2\xi] \\ &- \frac{b}{R}\left[2\cos\xi\int_0^\xi\beta\sin\xi d\xi + \beta\sin^2\xi\right. \\ &-(2\beta + \beta'')\sin\xi\int_0^\xi\beta\sin\xi d\xi + \cos\xi\int_0^\xi\beta^2\cos\xi d\xi \\ &\left.+\frac{3}{2}\,\beta^2\cos\xi\sin\xi - \beta\beta'\sin^2\xi\right]\Big\}\end{aligned} \tag{31}$$

Inasmuch as $b/R - b/a$ may be small compared with b/R, we have included in equation (31) terms of order β^2 in the second bracket on the right but terms of order β only in the first bracket on the right. Consistent with this, terms of order β^2 will be retained in the second integral on the right of the moment-curvature change relation (25).

First and Second-Order Nonlinear Theory for an Originally Straight Tube

For an originally straight tube we have

$$\frac{1}{a} = 0 \tag{32}$$

and since in this case $b/R - b/a$ is the same as b/R, we may further delete all terms of order β^2 on the right of the differential equation (31). In this way (31) reduces to

$$\begin{aligned}\frac{D}{b^3}\Big\{&\beta^{iv} + \left(1 - \frac{pb^3}{D}\right)\beta'' - \beta'\left[\beta^{iv} - \left(1 + 2\,\frac{pb^3}{D}\right)\beta''\right] - \beta''\beta'''\Big\} \\ = \frac{hbE}{R^2}\Big\{&\frac{3}{2}\sin 2\xi - 2\cos\xi\int_0^\xi\beta\sin\xi d\xi \\ &+ (\cos^2\xi - 3\sin^2\xi)\beta - \frac{1}{2}\,\beta'\sin 2\xi - \beta''\sin^2\xi\Big\}\end{aligned} \tag{33}$$

Equation (29) for the fiber stress σ becomes

$$\frac{\sigma}{E} = \frac{b}{R}\left\{\sin\xi - \int_0^\xi \left(\beta \sin\xi + \frac{1}{2}\beta^2 \cos\xi\right) d\xi\right\} \quad (34)$$

and equation (25) for the moment-curvature change relation becomes

$$\frac{M}{EI} = \frac{1}{R}\left\{1 - \frac{2}{\pi}\int_0^{2\pi}\left[\int_0^\xi \beta \sin\xi\, d\xi\right]\sin\xi\, d\xi - \frac{1}{\pi}\int_0^{2\pi}\left[\left(\int_0^\xi \beta^2 \cos\xi\, d\xi\right)\sin\xi - \left(\int_0^\xi \beta \sin\xi\, d\xi\right)^2\right] d\xi\right\} \quad (35)$$

The form of the differential equation (33) indicates that β depends on two parameters α^2 and λ, defined as follows:

$$\alpha^2 = \frac{hEb^4}{DR^2}, \quad \lambda = \frac{pb^2}{D} \quad (36)$$

For an isotropic tube, with D given by equation (15), the forms of α and λ are

$$\alpha = [12(1-\nu^2)]^{1/3}\frac{b^2}{hR}, \quad \lambda = 12(1-\nu^2)\frac{pb^3}{Eh^2} \quad (37)$$

The solution β of equation (33) may be expanded in powers of α, as follows:

$$\beta = \alpha^2\beta_1 + \alpha^4\beta_2 + \ldots \quad (38)$$

However, the first two terms only of this expansion are meaningful. Determination of β_n for $n \geq 3$ requires that higher powers of β and its derivatives be taken into account, in accordance with the complete equations (21) and (22).

Introducing (38) into equation (33) we are led to the following two equations:

$$\beta_1^{iv} + (1-\lambda)\beta_1'' = \frac{3}{2}\sin 2\xi \quad (39)$$

$$\beta_2^{iv} + (1-\lambda)\beta_2'' = \beta_1'[\beta_1^{iv} - (1+2\lambda)\beta_1''] + \beta_1''\beta_1''' - 2\cos\xi\int_0^\xi \beta_1 \sin\xi\, d\xi + (2\cos 2\xi - 1)\beta_1 - \frac{1}{2}\beta_1' \sin 2\xi - \frac{1}{2}\beta_1''(1-\cos 2\xi) \quad (40)$$

Both β_1 and β_2 must satisfy the boundary conditions (23).

Introduction of (38) into equation (28) gives for the displacement v

$$\frac{v}{b} = \alpha^2\frac{v_1}{b} + \alpha^4\frac{v_2}{b} + \ldots \quad (41)$$

where

$$\frac{v_1}{b} = -\int_0^\xi \beta_1 \sin\xi\, d\xi \quad (42)$$

$$\frac{v_2}{b} = -\int_0^\xi \left(\beta_2 \sin\xi + \frac{1}{2}\beta_1^2\cos\xi\right) d\xi \quad (43)$$

Finally, introduction of (41) into the moment curvature relation (25) leads to the formula

$$\frac{M}{EI} = \frac{1}{R}\{1 + c_1\alpha^2 + c_2\alpha^4 + \ldots\} \quad (44)$$

where

$$c_1 = \frac{2}{\pi}\int_0^{2\pi}\frac{v_1}{b}\sin\xi\, d\xi \quad (45)$$

$$c_2 = \frac{2}{\pi}\int_0^{2\pi}\left[\frac{v_2}{b}\sin\xi + \frac{1}{2}\left(\frac{v_1}{b}\right)^2\right] d\xi \quad (46)$$

The solution of the differential equations (39) and (40) is readily carried out. We find

$$\beta_1 = A_1 \sin 2\xi, \quad A_1 = \frac{3/2}{12+4\lambda} \quad (47)$$

$$\beta_2 = A_2 \sin 2\xi + B_2 \sin 4\xi$$

$$A_2 = \frac{4}{9}A_1^2, \quad B_2 = \frac{(36+8\lambda)A_1^2 - A_1/3}{240+16\lambda} \quad (48)$$

Introduction of (47) and (48) into (42) and (43) gives

$$\frac{v_1}{b} = -\frac{1}{2}A_1 \sin\xi + \frac{1}{6}A_1 \sin 3\xi \quad (49)$$

$$\frac{v_2}{b} = -\left(\frac{1}{2}A_2 + \frac{1}{4}A_1^2\right)\sin\xi + \left(\frac{1}{6}A_2 - \frac{1}{6}B_2 + \frac{1}{24}A_1^2\right)\sin 3\xi + \left(\frac{1}{10}B_2 + \frac{1}{40}A_1^2\right)\sin 5\xi \quad (50)$$

Introduction of (49) and (50) into (45) and (46) gives

$$c_1 = -A_1, \quad c_2 = -A_2 - \frac{2}{9}A_1^2 = -\frac{2}{3}A_1^2 \quad (51)$$

and therewith

$$\frac{M}{EI} = \frac{1}{R}\left[1 - A_1\alpha^2 - \frac{2}{3}(A_1\alpha^2)^2 + \ldots\right] \quad (52)$$

where, according to (47) and (37)

$$A_1\alpha^2 = \frac{18(1-\nu^2)}{12+4\lambda}\frac{b^4}{h^2R^2} \quad (53)$$

Retention of two terms only on the right of equation (52) leads to the result of Wood [4]. Specialization of this result to the case $\lambda = 0$ represents Brazier's result [3].

Letting $A_1\alpha^2 = x^2$ we may write (52) in the dimensionless form

$$m = x\left(1 - x^2 - \frac{2}{3}x^4\right) \quad (54)$$

where

$$m = \frac{M}{EI}\frac{b^2}{h}\left[\frac{18(1-\nu^2)}{(12+4\lambda)}\right]^{1/2}$$

According to Brazier and Wood the value of m is largest when

$$x = x_{BW} = \frac{1}{\sqrt{3}} = 0.577 \quad (55)$$

According to equation (54) the value of m is largest when

$$x = x_c = \frac{1}{2}\left(\frac{\sqrt{201}-9}{5}\right)^{1/2} = 0.509 \quad (56)$$

that is, when

$$\frac{b^2}{hR_c} = 0.509\left(\frac{2}{3}\cdot\frac{1+\lambda/3}{1-\nu^2}\right)^{1/2} = 0.415\left(\frac{1+\lambda/3}{1-\nu^2}\right)^{1/2} \quad (57)$$

Corresponding to the factor 0.415 in equation (57) the analogous formula by Brazier and Wood has a factor $\sqrt{2}/3 = 0.471$. The corresponding values of the moment function m are

$$m_{BW} = \frac{1}{\sqrt{3}}\cdot\frac{2}{3} = 0.385 \quad (58)$$

$$m_c = 0.509\,(1 - 0.259 - 0.049) = 0.354 \quad (59)$$

We note that consideration of the α^4-term in the expansion of the present solution results in a 15 per cent decrease of the critical value of the curvature $1/R$ and in a 10 per cent decrease of the corresponding critical value of the moment M.

The critical values of $1/R$ according to (55) or (57) may be compared with a corresponding value obtained by Chwalla [5] by means of a minimum-energy analysis of the finite-deflection problem. Chwalla assumes as an approximation that the shape of the cross section is truly elliptical after deformation and finds for the case $\lambda = 0$ that $b^2/hR_c = 0.806$. This differs from Brazier's value 0.471 by about 70 per cent and from the present value 0.415 by nearly 80 per cent.

We may determine further the amount of flattening δ of the cross section associated with the critical value of $1/R$. According to equations (41), (49), and (50)

$$\delta = \frac{v(\pi/2)}{b} = -\frac{2}{3}A_1\alpha^2 - \left(\frac{2}{3}A_2 + \frac{4}{15}A_1^2 - \frac{4}{15}B_2\right)\alpha^4 \quad (60)$$

With A_1, A_2, and B_2 as given by equations (47) and (48), this may be written in the form

$$\delta = -\frac{2}{3}A_1\alpha^2 - \frac{71+4\lambda}{135+9\lambda}(A_1\alpha^2)^2 \quad (61)$$

Retaining the first term on the right of (61) we obtain, with $A_1\alpha^2 = x_{BW}^2 = 1/3$, for the amount of flattening associated with the critical value $1/R_{BW}$, independent of pressurization

$$\delta_{BW} = -\frac{2}{9} = -0.222 \quad (62)$$

If we retain both terms in (61) we obtain

$$\delta_c = -\frac{2}{3}x_c^2 - \frac{71+4\lambda}{135+9\lambda}x_c^4 \quad (63)$$

where $x_c = 0.509$. Equation (63) indicates that, in second approximation, pressurization tends to decrease the amount of flattening to a very small extent. We find

$$(\delta_c)_{\lambda=0} = -0.207, \quad (\delta_c)_{\lambda=\infty} = -0.202 \quad (64)$$

which is about 10 per cent less than Brazier and Wood's values.

Nonlinear Corrections for Originally Curved Tubes

We write

$$\frac{1}{R} = \frac{1}{a} + \left(\frac{1}{R} - \frac{1}{a}\right) \quad (65)$$

and

$$\frac{1/R - 1/a}{1/a} = k \quad (66)$$

and we consider an expansion of the solution of the problem in powers of k. For this purpose we write the differential equation (31) in the form

$$\beta^{iv} + (1-\lambda)\beta'' - \beta'[\beta^{iv} - (1+2\lambda)\beta''] - \beta''\beta''' = \frac{hEb^4}{Da^2}(1+k)\left\{k\left[\frac{3}{2}\sin 2\xi + (\cos^2\xi - 2\sin^2\xi)\beta - \frac{1}{2}\beta'\sin 2\xi - \beta''\sin^2\xi\right] - (1+k)\left[2\cos\xi\int_0^\xi \beta\sin\xi\,d\xi + \beta\sin^2\xi - (2\beta+\beta'')\sin\xi\int_0^\xi\beta\sin\xi\,d\xi + \cos\xi\int_0^\xi\beta^2\cos\xi\,d\xi + \frac{3}{4}\beta^2\sin 2\xi - \beta\beta''\sin^2\xi\right]\right\} \quad (67)$$

Setting further

$$\frac{hEb^4}{Da^2} = 12(1-\nu^2)\frac{b^4}{h^2a^2} = \mu^2 \quad (68)$$

and assuming

$$\beta = k\beta_1 + k^2\beta_2 + \ldots \quad (69)$$

we obtain by equating corresponding powers of k in equation (67) a system of successive differential equations for the functions β_n. The first two of these are

$$\beta_1^{iv} + (1-\lambda)\beta_1'' + \mu^2\left[2\cos\xi\int_0^\xi\beta_1\sin\xi\,d\xi + \beta_1\sin^2\xi\right] = \frac{3}{2}\mu^2\sin 2\xi \quad (70)$$

$$\beta_2^{iv} + (1-\lambda)\beta_2'' + \mu^2\left[2\cos\xi\int_0^\xi\beta_2\sin\xi\,d\xi + \beta_2\sin^2\xi\right] = \frac{3}{2}\mu^2\sin 2\xi + \beta_1'[\beta_1^{iv} - (1+2\lambda)\beta_1''] + \beta_1''\beta_1''' + \mu^2\left\{(\cos^2\xi - 2\sin^2\xi)\beta_1 - \frac{1}{2}\beta_1'\sin 2\xi - \beta_1''\sin^2\xi - 4\cos\xi\int_0^\xi\beta_1\sin\xi\,d\xi - 2\beta_1\sin^2\xi + (2\beta_1+\beta_1'')\sin\xi\int_0^\xi\beta_1\sin\xi\,d\xi - \cos\xi\int_0^\xi\beta_1^2\cos\xi\,d\xi - \frac{3}{4}\beta_1^2\sin 2\xi + \beta_1\beta_1''\sin^2\xi\right\} \quad (71)$$

Equations (28) and (29) for displacement v and stress σ become

$$\frac{v}{b} = k\frac{v_1}{b} + k^2\frac{v_2}{b} + \ldots = -k\int_0^\xi\beta_1\sin\xi\,d\xi - k^2\int_0^\xi\left(\beta_2\sin\xi + \frac{1}{2}\beta_1^2\cos\xi\right)d\xi + \ldots \quad (72)$$

$$\frac{\sigma}{E} = \frac{b}{a}\left\{k\left[\sin\xi - \int_0^\xi\beta_1\sin\xi\,d\xi\right] - k^2\int_0^\xi\left[(\beta_1+\beta_2)\sin\xi + \frac{1}{2}\beta_1^2\cos\xi\right]d\xi + \ldots\right\} \quad (73)$$

Equation (25) for the applied moment M becomes

$$\frac{Ma}{EI} = k\left[1 + \frac{1}{\pi}\int_0^{2\pi}\frac{v_1}{b}\sin\xi\,d\xi\right] + \frac{k^2}{\pi}\int_0^{2\pi}\left[\left(2\frac{v_1}{b} + \frac{v_2}{b}\right)\sin\xi + \left(\frac{v_1}{b}\right)^2\right]d\xi + \ldots \quad (74)$$

The form of equations (70) to (74) allows two qualitative conclusions without further analysis. These are: (*a*) Nonlinear corrections to the linear theory are negligible provided the relative change of curvature k, as defined by (66), is small compared to unity; and (*b*) the effect of the nonlinear corrections differs, depending on whether k is positive or negative.

Trigonometric Series Solution for Initially Curved Tubes

Suitable series solutions of equations (70) and (71) which satisfy the boundary conditions (23) term by term are

$$\beta_m = \Sigma A_{mn}\sin 2n\xi \quad (75)$$

In what follows we are limiting ourselves to a consideration of the equations of the linear theory, for which the results are not new. We do, however, obtain an approximate formula for the rigidity of the tube which seems more suitable for interpretation than previous forms of this result.

Writing

$$A_{1n} = A_n \quad (76)$$

we find from equation (70) the following system of recurrence relations for the coefficients A_n:

$$A_1\left[12 + 4\lambda + \frac{5}{6}\mu^2\right] - A_2\frac{\mu^2}{12} = \frac{3}{2}\mu^2 \quad (77)$$

$$-A_{n-1}\frac{2n+1}{2n-1}\frac{\mu^2}{4} + A_n\left[16n^4 - 4(1-\lambda)n^2 + \frac{4n^2+1}{4n^2-1}\frac{\mu^2}{2}\right] - A_{n+1}\frac{2n-1}{2n+1}\frac{\mu^2}{4} = 0, \quad n = 2,3,\ldots \quad (78)$$

Introduction of β_1 into equation (72) gives for the displacement v_1

$$\frac{v_1}{b} = -\sum\frac{1}{2}A_n\left[\frac{\sin(2n-1)\xi}{2n-1} - \frac{\sin(2n+1)\xi}{2n+1}\right] \quad (79)$$

Introduction of v_1 into equation (74) gives within the range of applicability of linear theory the following moment-curvature relation:

$$\frac{M}{EI} = \frac{k}{a}\left[1 - \frac{1}{2}A_1\right] \quad (80)$$

The quantity $[1 - {}^1/_2A_1]$ represents the effect of the initial curvature on the effective rigidity of the tube. For moderate values of the parameter μ we may obtain successively closer approximations to the true value of $[1 - {}^1/_2A_1]$ by solving the system (77) and (78) by sectionalization, as follows: Disregarding all coefficients except A_1 we obtain in first approximation

$$1 - \frac{1}{2}A_1^{(1)} = \frac{1 + \frac{1}{3}\lambda + \frac{1}{144}\mu^2}{1 + \frac{1}{3}\lambda + \frac{10}{144}\mu^2} \quad (81)$$

Disregarding all coefficients, except the first two, we obtain

$$1 - \frac{1}{2}A_1^{(2)} = \frac{1 + \frac{1}{3}\lambda + \frac{1}{144}\mu^2 - \frac{\frac{5}{1728}\mu^4}{240 + 16\lambda + \frac{17}{30}\mu^2}}{1 + \frac{1}{3}\lambda + \frac{10}{144}\mu^2 - \frac{\frac{5}{1728}\mu^4}{240 + 16\lambda + \frac{17}{30}\mu^2}} \quad (82)$$

When $\lambda = 0$ equations (81) and (82) reduce to formulas given by von Karman [1]. When $\lambda \neq 0$ they are equivalent to results obtained by Thuloup [2] and Barthélémy [6]. Equation (82) represents the effect of initial curvature with sufficient accuracy for values of μ up to about 10. For larger values of μ equation (82) may be replaced by simple asymptotic formulas which for the case $\lambda = 0$ were obtained by Clark and the present author [7], and for finite but not too large values of λ by Crandall and Dahl [8].

Tubes With Slight Initial Curvature

We now consider tubes for which the initial curvature $1/a$ is of the same order of magnitude as the critical curvature of an initially straight tube. In particular we derive a moment-curvature-change relation for such tube which is an appropriate generalization of Brazier's formula for the initially straight tube and which has the same range of applicability as Brazier's formula.

The basic equations which are needed for this problem follow by specialization of equations (31), (29), (28), and (25) in the form

$$\frac{D}{b^2}\left\{\beta^{IV} + \left(1 - \frac{pb^2}{D}\right)\beta''\right\} = \frac{Eh}{R}\left(\frac{b}{R} - \frac{b}{a}\right)\frac{3}{2}\sin 2\xi \quad (83)$$

$$\frac{\sigma}{E} = \left(\frac{b}{R} - \frac{b}{a}\right)\sin\xi - \frac{b}{R}\int_0^\xi\beta\sin\xi\,d\xi \quad (84)$$

$$\frac{v}{b} = -\int_0^\xi\beta\sin\xi\,d\xi \quad (85)$$

$$\frac{Mb}{EI} = \left(\frac{b}{R} - \frac{b}{a}\right)\left[1 + \frac{1}{\pi}\int_0^{2\pi}\frac{v}{b}\sin\xi\,d\xi\right] + \frac{b}{R}\frac{1}{\pi}\int_0^{2\pi}\frac{v}{b}\sin\xi\,d\xi \quad (86)$$

The solution of (83) is

$$\beta = \frac{hEb^2}{D}\frac{b}{R}\left(\frac{b}{R} - \frac{b}{a}\right)\frac{(3/2)\sin 2\xi}{12 + 4\lambda} \quad (87)$$

where λ is defined in equation (37).

The displacement function v becomes

$$\frac{v}{b} = -\frac{Ehb^2}{D}\frac{b}{R}\left(\frac{b}{R} - \frac{b}{a}\right)\frac{3/2}{12 + 4\lambda}\left(\frac{\sin\xi}{2} - \frac{\sin 3\xi}{6}\right) \quad (88)$$

Introduction of (88) into (86) gives as relation between moment M and curvature change $R^{-1} - a^{-1}$

$$\frac{M}{EI} = \left(\frac{1}{R} - \frac{1}{a}\right)\left[1 - \frac{3/4}{12 + 4\lambda}\frac{hEb^2}{D}\frac{b}{R}\left(2\frac{b}{R} - \frac{b}{a}\right)\right] \quad (89)$$

When $b/a = 0$ equation (89) reduces to the corresponding formula by Brazier and Wood.

For the purpose of further discussion we write

$$\frac{b}{R} - \frac{b}{a} = z, \quad \frac{b}{a} = z_0 \tag{90}$$

$$\frac{3/4}{12 + 4\lambda} \frac{hEb^2}{D} = \frac{3(1 - \nu^2)/4}{1 + \lambda/3} \frac{b^2}{h^2} = \gamma \tag{91}$$

and

$$\frac{Mb}{E} = (1 - \gamma z_0^2)z - 3\gamma z_0 z^2 - 2\gamma z^3 \tag{92}$$

In addition to including the formulas of Brazier and Wood, equation (92) also includes the appropriate formula of linear theory in so far as the first term on the right of (92) is equivalent to the first two terms on the right of (81) and (82) if these formulas are expanded in powers of μ^2.

According to Brazier and Wood we have a critical value z_{BW} such that $6\gamma z_{BW}^2 = 1$. In view of this fact our original assumption concerning the order of magnitude of $1/a$ may be expressed in the form

$$\gamma z_0^2 = O(1) \tag{93}$$

However, in order that equation (92) remain significant within the range of applicability of linear theory, we must assume somewhat more restrictively that

$$\gamma z_0^2 = \frac{3}{4} \frac{1 - \nu^2}{1 + \lambda/3} \frac{b^4}{h^2 a^2} \lesssim \frac{1}{4} \tag{94}$$

Critical values of z are again obtained from the relation $\partial M/\partial z = 0$, that is, from

$$1 - \gamma z_0^2 - 6\gamma z_0 z - 6\gamma z^2 = 0 \tag{95}$$

We find

$$z_c = -\frac{1}{2} z_0 \pm \frac{1}{(6\gamma)^{1/2}} \left(1 + \frac{1}{2} \gamma z_0^2\right)^{1/2} \tag{96}$$

or

$$6\gamma z_c^2 = 1 + 2\gamma z_0^2 \pm (6\gamma z_0^2)^{1/2} \left(1 + \frac{1}{2} \gamma z_0^2\right)^{1/2} \simeq 1 + 2\gamma z_0^2 \pm (6\gamma z_0^2)^{1/2} \tag{97}$$

Equation (97) may be written in the equivalent form

$$\left(\frac{b}{R_c} - \frac{b}{a}\right)^2 = \frac{2}{9} \cdot \frac{1 + \lambda/3}{1 - \nu^2} \frac{h^2}{b^2} + \frac{1}{3} \frac{b^2}{a^2} \pm \left(\frac{2}{9} \cdot \frac{1 + \lambda/3}{1 - \nu^2}\right)^{1/2} \frac{h}{a} \tag{98}$$

The validity of equation (98) requires according to (94) that $1/a$ satisfy the inequality

$$\frac{b}{a} \lesssim \left(\frac{1 + \lambda/3}{3(1 - \nu^2)}\right)^{1/2} \frac{h}{b} \tag{99}$$

When b/a is larger than the right-hand side of equation (99) then a more accurate analysis of the problem is required.

References

1 Th. von Karman, "Über die Formänderung dünnwandiger Rohre," *Zeit. des Vereines deutscher Ingenieure*, vol. 55, 1911, pp. 1889–1895.

2 M. A. Thuloup, "Fatigue des tuyaux minces," *Bulletin de l'Association Tech. Maritime et Aéronautique*, vol. 32, 1928, pp. 643–680.

3 L. G. Brazier, "On the Flexure of Thin Cylindrical Shells and Other 'Thin' Sections," *Proceedings of the Royal Society*, series A, vol. 116, 1927, pp. 104–114.

4 J. D. Wood, "The Flexure of a Uniformly Pressurized, Circular, Cylindrical Shell," JOURNAL OF APPLIED MECHANICS, vol. 25, TRANS. ASME, vol. 80, 1958, pp. 453–458.

5 E. Chwalla, "Reine Biegung schlanker, dünnwandiger Rohre mit gerader Achse," *Zeit. für Angewandte Mathematik und Mechanik*, vol. 13, 1933, pp. 48–53.

6 J. Barthélémy, "Déformation et tensions internes des tuyaux à ligne moyenne planne," *Bulletin de l'Association Tech. Maritime et Aéronautique*, vol. 46, 1947, pp. 411–458.

7 R. A. Clark and E. Reissner, "Bending of Curved Tubes," *Advances in Applied Mechanics*, vol. 2, 1951, pp. 93–122.

8 S. H. Crandall and N. C. Dahl, "The Influence of Pressure on Bending of Curved Tubes," *Proceedings of the Ninth International Congress of Applica Mechanics*, 1956.

On the Instability and Folding Deformation of a Layered Viscoelastic Medium in Compression

M. A. BIOT
Consultant, Shell Development Company, New York, N. Y.
Mem. ASME

When a layer of material embedded in an infinite medium is subject to a compression parallel with the layer an instability tends to develop which manifests itself in the folding of the layer. This phenomenon is examined here for the general case where the layer and the surrounding medium are both viscoelastic. This problem which was examined in preliminary form in an earlier publication [6][1] is treated here with particular attention to the effect of interfacial adherence of the layer and the medium, and to an evaluation of the amplitude of the folding. In general there is a lower and upper-critical value of the compressive load between which folding occurs with a finite rate of deformation. There appears also a dominant wave length, for which the rate of folding is maximum under a given load. The dominant wave length may or may not depend on the load. The effect of interfacial adherence while not negligible is not generally significant. The rate of folding increases very rapidly beyond a certain value of the viscosity ratio of the two media. A brief discussion is also included of the thermodynamic implications of incremental stress-strain relations in prestressed media.

Consider an inhomogeneous elastic medium of infinite extent containing a layer of material of higher rigidity. It is well known that such a system when subject to a compression parallel with the layer will buckle beyond a certain critical value of the load. This buckling instability manifests itself through a folding of the layer which appears suddenly with a characteristic wave length at the critical load.[2] The nature of the phenomenon is typified in the elementary treatment of the buckling of a beam or an elastic foundation. It is clear that this phenomenon is a particular case of the much more general one where the layer and the medium are viscoelastic. In this case we shall not in general observe a sharp buckling, but a folding of the layer will appear with a rate of folding and a wave-length content which are dependent on the physical properties, the compressive load, and the initial irregularities of the layer.

The present paper is one in a series presenting the results of an investigation of these phenomena carried out at the Shell Development Company during the past 10 years. The subject is of course of primary interest to the geologist since it furnishes for the first time a quantitative basis for the evaluation of folding and other tectonic features of stratified rock formations. There are also interesting technological applications connected with the buckling failure of inhomogeneous structural material such as sandwich panels under conditions of creep and the deformation due to instability of materials in general in the viscoelastic temperature range when there is a high-temperature gradient. The result also throws light on the behavior of such engineering components as an axially compressed rod in a viscoelastic fluid, and so on.

A discussion of the fundamental aspects of the theory is given in [6]. This makes use of the general results established previously for the viscoelastic behavior of solids on the basis of irreversible thermodynamics [4, 5]. In the present paper we have emphasized a more exact approach which takes into account the adherence between the layer and the surrounding medium. While this adherence does not affect the phenomenon qualitatively, it does introduce considerably more complication in the analysis. We also have given a more complete discussion of some aspects of the phenomenon, and in particular of the magnitude of the instability as represented by the rate of growth of the folding. The theory is developed here by representing the layer as a viscoelastic plate obeying the equations derived from a straightforward generalization of the classical equations for elastic plates by a correspondence rule [5]. A more rigorous treatment of the problem on the basis of a continuum also has been completed [7]. This more rigorous treatment takes into account the existence of a compression in the surrounding medium which is neglected in the present theory. Results indicate that use of the plate equations is satisfactory for most practical purposes. In more recent work the effect of gravity has also been introduced [13].

In Section 1 we derive the equations of flexure of a viscoelastic plate under compression, and Section 2 derives the properties of the surrounding medium. These results are combined in Section 3 and equations are established for an embedded layer with perfect or imperfect adherence at the interface. We assume that if an interfacial slip occurs the friction is proportional to the rate of slip. Section 4 develops quantitatively the results for the case where the layer and the surrounding medium are both incompressible viscous solids under the assumption of perfect adherence. Particular attention is paid to a comparison with the case of perfect slip and to the rate of growth of the folding.

Section 5 discusses briefly other cases such as the elastic layer in a viscous medium, and two Maxwell materials. These other cases were treated in more detail in reference [6].

[1] Numbers in brackets designate References at end of paper.

[2] The buckling of layered elastic media was investigated by Biljaard [1, 2], Gough, Elam, and DeBruyne [3], Goodier [12], and others.

Presented at the Summer Conference of the Applied Mechanics Division, Troy, N. Y., June 18–20, 1959, of The American Society of Mechanical Engineers.

Discussion of this paper should be addressed to the Secretary, ASME, 29 West 39th Street, New York, N. Y., and will be accepted until October 10, 1959, for publication at a later date. Discussion received after the closing date will be returned.

Note: Statements and opinions advanced in papers are to be understood as individual expressions of their authors and not those of the Society. Manuscript received by ASME Applied Mechanics Division, March 11, 1958. Paper No. 59—APM-21.

In Section 6 a few remarks are presented regarding the incremental stress-strain relations in nonlinear rheology and it is pointed out that an essential distinction is to be made between thermodynamic systems in the vicinity of equilibrium or in a steady state of flow.

It is pointed out that there exists, in general, a lower and higher limit for the critical compressive load. Between these limits the folding takes place with a dominant wave length; i.e., one for which under a given load there is a maximum rate of growth. The dominant wave length may or may not depend on the load. The latter case is true for two viscous fluids and in general for two materials with the same relaxation time. The rate of growth of the folds which is evaluated for the particular case of two viscous fluids becomes large and very wave-length-selective for values of the viscosity ratio μ/μ_1, of the order of about 70 or higher. The influence of interfacial adherence is found to be very small in the range where the magnitude of the instability becomes significant.

1 Equations for Deformation of a Viscoelastic Plate

We shall first derive the approximate equations for an elastic plate under the assumption that the wave length of the deformation is large relative to the thickness h of the plate. We consider a two-dimensional deformation such that the upward displacement of the plate is, Fig. 1,

$$v = v' \cos lx \tag{1}$$

The assumption stated above corresponds to the conditions $lh \ll 1$.

The upward plate deflection may be derived in terms of the bending moment M per unit width. We may write the differential equation

$$\frac{Bh^3}{12}\frac{d^2v}{dx^2} = -M \tag{2}$$

The sign of M is taken positive clockwise when matter is located to the left of the cross section. The coefficient B is

$$B = \frac{4G(G+\lambda)}{2G+\lambda} \tag{3}$$

The Lamé constants of the plate are denoted by λ and G.[3]

The bending moment M will now be determined. We assume that the plate is subject to a total compressive load Ph acting in its plane. In addition we assume a vertical load q per unit area taken positive upward and a tangential force τ per unit area on the surface of the plate acting positively to the right on the upper surface and to the left on the lower surface, Fig. 1. These loads are distributed sinusoidally according to

$$q = q_0 \cos lx$$
$$\tau = \tau_0 \sin lx \tag{4}$$

If we call M_1 the bending moment due to q, we may write

$$\frac{d^2M_1}{dx^2} = -q \tag{5}$$

[3] The shear modulus G is also generally represented by μ but we prefer to reserve the latter symbol for the viscosity coefficient.

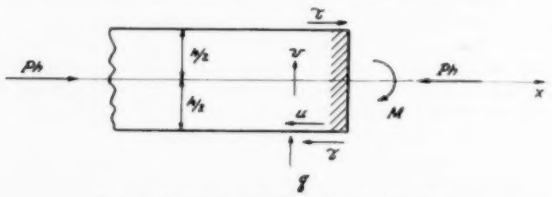

Fig. 1 Forces and displacements for the plate

The moment M_2 due to the tangential load must satisfy

$$h\int_0^x \tau dx + M_2 = M_0 \tag{6}$$

where M_0 is the moment at a cross section $x = 0$ where $\tau = 0$; i.e., the total shear also vanishes at that cross section. Differentiating (6) we find

$$\frac{dM_2}{dx} = -\tau h \tag{7}$$

Finally, we must evaluate the bending moment due to the axial compressive load Ph. This bending moment depends on the deformation and is equal to

$$M_3 = Phv \tag{8}$$

The total bending moment is

$$M = M_1 + M_2 + M_3 \tag{9}$$

Combining (5), (7), (8), and (9) we derive

$$\frac{d^2M}{dx^2} = -q - h\frac{d\tau}{dx} + Ph\frac{dv^2}{dx^2} \tag{10}$$

and substituting in (2) we find the differential equation for the plate deflection as

$$\frac{1}{12}Bh^3\frac{d^4v}{dx^4} + Ph\frac{d^2v}{dx^2} = q + h\frac{d\tau}{dx} \tag{11}$$

In addition to the plate deflection we also need for our present purpose the displacement u of the plate tangentially to the surface. The sign of u is chosen positive to the right on the upper surface. The displacement u is due to the rotation $(dv)/(dx)$ of the cross section and in addition to the shearing deformation of the plate produced by the tangential force τ. The sum of these two effects is

$$u = -\frac{h}{2}\frac{dv}{dx} + \frac{h}{2}\frac{\tau}{G} \tag{12}$$

It should be noted that in establishing the last relation we have assumed that the shearing deformation of the plate is solely due to τ. There is, of course, an additional transverse shear associated with the bending which we have neglected. Although these two assumptions are not quite consistent, we are concerned here mainly with the separate evaluation of the effect of interfacial adherence and therefore we wish to introduce this effect as the sole correction to the approximate theory of reference [6] for the purpose of comparison. A consistent assumption would be to neglect the shear deformation of the plate. This is easily done by putting $G = \infty$ in relation (12) and $Q = \infty$ in all relations derived in the following. Further remarks on this point will be found in Section 4. It should be added that the effect of shearing deformation associated with bending is evaluated implicitly in the exact treatment of reference [7] based on equations for the prestressed continuum. The magnitude of the effect is found to be not very significant.

Putting

$$u = U \sin lx$$
$$v = V \cos lx \tag{13}$$

we find

$$q_0 = \left(\frac{1}{12}Bh^2l^2 - P + G\right)hl^2V - 2GlU$$
$$2\tau_0 = -2GlV + \frac{4G}{h}U \tag{14}$$

As we have pointed out in earlier publications [4, 5, 6], equations obtained for an elastic body can be extended readily to a viscoelastic continuum by replacing the elastic constants by their corresponding operators. We have called this the "correspondence rule." This rule holds for the most general case of anisotropy and is valid for relations derived by energy or variational methods. For an isotropic viscoelastic material Hooke's law is replaced by

$$\sigma_{ij} = 2\bar{Q}e_{ij} + \delta_{ij}\bar{R}e \tag{15}$$

Where σ_{ij} and e_{ij} are the stress and strain tensors, δ_{ij} is the Kronecker symbol and

$$e = e_{xx} + e_{yy} + e_{zz} \tag{16}$$

is the dilatation. The symbols $\bar{Q}$ and $\bar{R}$ represent operators. They replace the Lamé constants G and λ. We have shown [4] from linear irreversible thermodynamics that these operators are of the form

$$\bar{Q} = \int_0^\infty \frac{p}{p+r} Q(r)\gamma(r)dr + Q + pQ' \tag{17}$$

$$\bar{R} = \int_0^\infty \frac{p}{p+r} R(r)\gamma(r)dr + R + p\bar{R}' \tag{18}$$

In these expressions p is a differential time operator

$$p = \frac{d}{dt} \tag{19}$$

The variable of integration r is a relaxation constant with a spectral density $\gamma(r)$. We have written the function $Q(r)\gamma(r)$ and $R(r)\gamma(r)$ with the spectral density function $\gamma(r)$ as a common factor in order to bring out the common properties of these functions as regards their singularities. In case of relaxation with a discrete spectrum the integrals are replaced by summations,

$$\bar{Q} = \sum^s \frac{p}{p+r_s} Q_s + Q + pQ'$$
$$\bar{R} = \sum^s \frac{p}{p+r_s} R_s + R + pR' \tag{20}$$

It was also shown that the constants in the operator $\bar{Q}$ are all positive. In addition, we must have $\bar{R} + \bar{Q} > 0$. The applicability of these operators for incremental stresses in a linear or nonlinear prestressed medium is discussed in Section 6.

The significance of the operational stress-strain law (15) is multifold. It may be interpreted as a relation between Laplace or Fourier transforms of the stress and strain components. For instance, if the strain components are harmonic functions of time and represented by $e_{ij}e^{i\omega t}$ then the stress tensor is $\sigma_{ij}e^{i\omega t}$ where e_{ij} is related to σ_{ij} by equations (15) after putting $p = i\omega$ in the expression of the operators.

Relations (15) may also be considered as giving directly the response to an arbitrary function of time by operational rules or Fourier integrals. For instance, assume a relation for pure shear

$$\sigma_s = 2\bar{Q}e_s \tag{21}$$

and assume the shear strain to be of constant unit value and suddenly applied at $t = 0$

$$e_s = 1(t) \begin{cases} = 0 & t < 0 \\ = 1 & t > 0 \end{cases} \tag{22}$$

We have the operational rule

$$\frac{p}{p+r} 1(t) = e^{-rt} \tag{23}$$

$$p1(t) = \frac{d}{dt} 1(t) = \delta(t) \tag{24}$$

Hence applying the complete operator $\bar{Q}$ as given by (17) to e_s we find

$$\sigma_s = \int_0^\infty e^{-rt}Q(r)\gamma(r)dr + Q + Q'\delta(t) \tag{25}$$

The time history of the stress contains a distribution of exponential stress relaxations. The Dirac function $\delta(t)$ corresponds to infinite shear rate at $t = 0$. The coefficient Q' is equivalent to a viscosity coefficient since

$$Q'pe_s = Q'\frac{de_s}{dt} \tag{26}$$

More generally, if the strain $e_s(t)$ is an arbitrary function of time the significance of the operator is given by

$$\frac{p}{p+r} e_s(t) = e^{-rt}\int_0^t e^{r\tau}de_s(\tau) \tag{27}$$

The complete stress-strain law expressed by the operational equation (21) is therefore

$$\frac{1}{2}\sigma_s = \int_0^\infty Q(r)\gamma(r)dr \int_0^t e^{-r(t-\tau)}de_s(\tau) + Qe_s(t) + Q'\frac{de_s(t)}{dt} \tag{28}$$

The coefficient Q is pure elastic modulus. Putting

$$Q(r)\gamma(r) = F(r)$$
$$h(t) = \int_0^\infty F(r)e^{-rt}dr \tag{29}$$

we write (28) in the form

$$\frac{1}{2}\sigma_s = \int_0^t h(t-\tau)de_s(\tau) + Qe_s(t) + Q'\frac{de_s(t)}{dt} \tag{30}$$

which brings out an heredity function $h(t)$.

By the correspondence rule we may apply immediately the elastic-plate relations (14) to the case of a viscoelastic plate. The Lamé constants G and λ are replaced by the corresponding operators $\bar{Q}$ and $\bar{R}$. The coefficient B becomes the operator

$$\bar{B} = \frac{4\bar{Q}(\bar{Q}+\bar{R})}{2\bar{Q}+\bar{R}} \tag{31}$$

and equations (14) are transformed into the operational relations

$$q_0 = \left(\frac{1}{12}\bar{B}h^3l^2 - P + \bar{Q}\right)hl^2V - 2\bar{Q}lU$$
$$2\tau_0 = -2\bar{Q}lV + \frac{4\bar{Q}}{h}U \tag{32}$$

Again, these may be considered as relations between Fourier or Laplace transforms or as differential and integral operations relating the quantities U, V, to q_0 and τ_0.

We should finally add a remark concerning the deformation produced by the compressive load P. If the material tends to flow indefinitely under load the compression P will be associated with a constant rate of compressional deformation of the plate. This deformation, however, will be disregarded as we are interested in cases where the deflection normal to the plate is the preponderant effect.

2 Deflection of a Semi-Infinite Viscoelastic Medium Under Normal and Tangential Surface Load

We have pointed out that from the correspondence rule we may proceed exactly as in the theory of elasticity provided we replace the elastic coefficients by the corresponding operators. We shall therefore proceed directly by using operational equations throughout. The semi-infinite medium is represented in Fig. 2. It has a boundary at $y = 0$ on which the normal and tangential loads are q' and τ. The solid half space is in the region $y > 0$. We write Lamé's equations for the displacement components u and v of the solid after replacing the elastic coefficients G and λ by the operators $\bar{Q}$ and $\bar{R}$. We have

$$\bar{Q}\nabla^2 u + (\bar{Q} + \bar{R})\frac{\partial e}{\partial x} = 0$$
$$\bar{Q}\nabla^2 v + (\bar{Q} + \bar{R})\frac{\partial e}{\partial y} = 0 \tag{33}$$

with

$$\nabla^2 = \frac{\partial^2}{\partial x^2} + \frac{\partial^2}{\partial y^2}$$
$$e = \frac{\partial u}{\partial x} + \frac{\partial v}{\partial y} \tag{34}$$

The Papkovitch-Boussinesq solution of these equations is

$$\vec{u} = -\text{grad}(\psi_0 + \vec{r}\cdot\vec{\psi}) + 2\frac{(2\bar{Q} + \bar{R})}{\bar{Q} + \bar{R}}\vec{\psi} \tag{35}$$

The field displacement vector is

$$\vec{u} = (u, v) \tag{36}$$

and the co-ordinate vector is

$$\vec{r} = (x, y) \tag{37}$$

The vector $\vec{\psi}$ and the scalar ψ_0 satisfy Laplace's equation

$$\nabla^2\psi_0 = \nabla^2\vec{\psi} = 0 \tag{38}$$

We shall choose the vector $\vec{\psi}$ to be oriented along y and put

$$\vec{\psi} = (0, \psi_y) \tag{39}$$

The component ψ_y also satisfied Laplace's equation

$$\nabla^2\psi_y = 0 \tag{40}$$

We are seeking here a solution which will match that of the plate at the boundary. We therefore assume a sinusoidal distribution of the surface load, i.e.

$$\tau = \tau_0 \sin lx$$
$$q' = q_0' \cos lx \tag{41}$$

We also choose Boussinesq potentials ψ_0 and ψ_y which contain the same trigonometric factors, and write

$$\psi_0 = Ae^{-ly}\cos lx$$
$$\psi_y = Ce^{-ly}\cos lx \tag{42}$$

These functions satisfy Laplace's equation in compliance with (38) and (40). Substituting ψ_0 and ψ_y in (35) yields the displacement field,

$$u = l(A + Cy)e^{-ly}\sin lx$$
$$v = \left\{lA + C\left[ly - 1 + \frac{2(2\bar{Q} + \bar{R})}{\bar{Q} + \bar{R}}\right]\right\}e^{-ly}\cos lx \tag{43}$$

From stress-strain relations (I5) we derive the relevant stress components at the boundary $y = 0$. We find

$$q' = \sigma_{yy} = 2\left[-Al - \frac{2\bar{Q} + \bar{R}}{\bar{Q} + \bar{R}}C\right]Ql\cos lx$$
$$\tau = \sigma_{xy} = 2\left[-Al - \frac{\bar{Q}}{\bar{Q} + \bar{R}}C\right]Ql\sin lx \tag{44}$$

The displacement u, v at the boundary is found by putting $y = 0$ in (43). We write the boundary displacement as

$$u = U\sin lx$$
$$v = V\cos lx \tag{45}$$

and the boundary stresses as

$$q' = q_0'\cos lx$$
$$\tau = \tau_0\sin lx \tag{46}$$

Then eliminating A and C in equations (43) and (44) (with $y = 0$) yields the following relation between surface stress and displacement:

$$\frac{1}{2\bar{Q}l}q_0' = -\frac{\bar{Q}}{3\bar{Q} + \bar{R}}U - \frac{2\bar{Q} + \bar{R}}{3\bar{Q} + \bar{R}}V$$
$$\frac{1}{2\bar{Q}l}\tau_0 = -\frac{2\bar{Q} + \bar{R}}{3\bar{Q} + \bar{R}}U - \frac{\bar{Q}}{3\bar{Q} + \bar{R}}V \tag{47}$$

It is of interest to call attention to the particular case of the incompressible material. This is the case for which $\bar{R} = \infty$ while $e = 0$ and $\bar{R}e$ remains finite. If we substitute $\bar{R} = \infty$ in relations (47) they simplify to

$$q_0' = -2\bar{Q}lV$$
$$\tau_0 = -2\bar{Q}lU \tag{48}$$

In this case the vertical and horizontal displacements are uncoupled.

We must remember that the significance of these relations is operational. For instance, if the material is elastic and incompressible then relations (48) are proportionality relations with $\bar{Q}$ replaced by the shear modulus G. If the material is an incompressible viscous fluid of viscosity μ then

$$\bar{Q} = \mu p \tag{49}$$

and equations (48) become differential relations

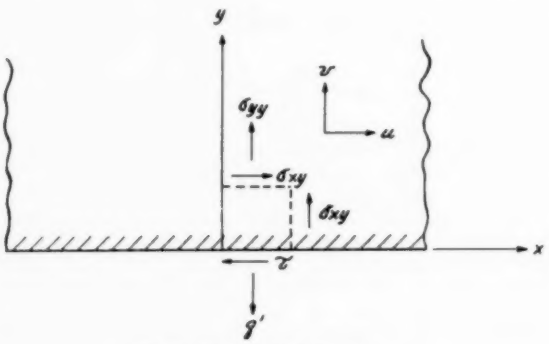

Fig. 2 Viscoelastic half-space

$$q_0' = -2\mu l \frac{dV}{dt}$$
$$\tau_0 = -2\mu l \frac{dU}{dt} \tag{50}$$

If the material is elastic in pure compression with an elastic bulk modulus K, we have shown [4] that the operator $\bar{R}$ is given in terms of $\bar{Q}$ by

$$\bar{R} = K - \frac{2}{3}\bar{Q}$$

In this case, even for a viscous fluid relations (47) imply both integrations and differentiations.

3 Unstable Deformation of the Embedded Layer

We are now in a position to consider the case of the embedded layer by putting together the foregoing results. We will first assume the case of perfect adherence between the layer and the embedding medium, Fig. 3. We will then follow with a brief discussion of the case of imperfect adherence.

Assuming perfect adherence the displacements U and V are equal at the interface for both media. The stresses also are continuous, the value of the shear τ_0 being the same at each boundary and the normal load q_0 on the layer being equal to twice the normal traction q_0' at the boundary

$$q_0 = 2q_0' \tag{51}$$

From (32) and taking into account (51) we may write the stress at the boundary of the layer as

$$q_0' = (\bar{A}_{11}V + \bar{A}_{12}U)l$$
$$\tau_0 = (\bar{A}_{12}V + \bar{A}_{22}U)l \tag{52}$$

with the operators

$$\bar{A}_{11} = {}^1/_2({}^1/_{12}\bar{B}h^2l^2 - P + \bar{Q})lh$$
$$\bar{A}_{12} = -\bar{Q} \tag{53}$$
$$\bar{A}_{22} = 2\bar{Q}/lh$$

The stress at the boundary of the embedding medium is given by (47). We replace $\bar{Q}$ and $\bar{R}$ by $\bar{Q}_1$ and $\bar{R}_1$, the latter referring to the viscoelastic properties of the embedding medium while the former refer to the properties of the layer. We write, for the stress at the boundary of the half space,

$$q_0' = -(\bar{C}_1V + \bar{C}_2U)l$$
$$\tau_0 = -(\bar{C}_2V + \bar{C}_1U)l \tag{54}$$

with the operators

$$\bar{C}_1 = 2\bar{Q}_1\frac{2\bar{Q}_1 + \bar{R}_1}{3\bar{Q}_1 + \bar{R}_1}$$
$$\bar{C}_2 = 2\bar{Q}_1\frac{\bar{Q}_1}{3\bar{Q}_1 + \bar{R}_1} \tag{55}$$

The condition that the stresses are continuous at the interface is obtained by equating expressions (52) and (54), i.e.

$$(\bar{A}_{11} + \bar{C}_1)V + (\bar{A}_{12} + \bar{C}_2)U = 0$$
$$(\bar{A}_{12} + \bar{C}_2)V + (\bar{A}_{22} + \bar{C}_1)U = 0 \tag{56}$$

At this point we must call attention to a property of the operators which is implicit in some remarks made previously concerning their significance. All the operational equations derived here are valid if the variables vary with time proportionally to an exponential factor e^{pt}. In that case all operators are simply algebraic quantities and p instead of being the differential operator d/dt is the algebraic value of the coefficient of time in the exponential factor. If we now consider equations (56) we conclude that instability of the layer will appear whenever there are positive values of p for which the determinant vanishes,

$$\begin{vmatrix} \bar{A}_{11} + \bar{C}_1 & \bar{A}_{12} + \bar{C}_2 \\ \bar{A}_{12} + \bar{C}_2 & \bar{A}_{22} + \bar{C}_1 \end{vmatrix} = 0 \tag{57}$$

In that case any initial value of U and V no matter how small will increase exponentially with time proportionally to e^{pt}. An instability of the layer will appear in the form of sinusoidal folding. In principle, a range of wave lengths will be unstable but not all wave lengths will grow at the same rate. For a given value of the load P equation (57) may be considered as a relation between p and lh. The latter parameter being related to the wave length L of the folding by the relation

$$\frac{L}{h} = 2\pi/lh \tag{58}$$

The wave length for which the value of p is maximum will tend to grow faster than others and will generally be the observed one. We have called it the "dominant wave length" L_d, the corresponding value of l being denoted by l_d. We have discussed the behavior of the folding and the value of the dominant wave length for various types of materials in reference [6] for the case of perfect slip. In the next section we shall discuss in more detail the case for which the layer and the embedding medium are both incompressible viscous solids with perfect adherence.

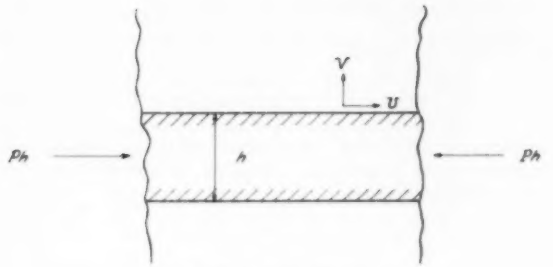

Fig. 3 Embedded layer

Before concluding this section let us formulate the case of imperfect adherence. In this case it is assumed that slipping may occur at the interface of the layer and the embedding medium. The slip layer is assumed to be a thin viscous layer of thickness h_s and viscosity coefficient μ_s. The interface displacements of the folding layer and the medium are denoted, respectively, by $U \sin lx$ and $U_1 \sin lx$. The shearing stress τ_0 at the interface is proportional to the rate of slip, according to the equation

$$\tau_0 = bp(U_1 - U) \tag{59}$$

with a coefficient of slip resistance

$$b = \mu_s/h_s \tag{60}$$

Expressing that there is continuity of stress and normal displacement V, we find the three equations

$$(\bar{A}_{11} + \bar{C}_1)V + \bar{A}_{12}U + \bar{C}_2U_1 = 0$$
$$(\bar{A}_{12} + \bar{C}_2)V + \bar{A}_{22}U + \bar{C}_1U_1 = 0$$
$$\bar{C}_2V - p\frac{b}{l}U + \left(\frac{pb}{l} + \bar{C}_1\right)U_1 = 0 \tag{61}$$

Equating to zero the determinant yields

$$\bar{C}_1(\bar{A}_{11}\bar{A}_{22} - \bar{A}_{12}^2) + \bar{A}_{22}(\bar{C}_1^2 - \bar{C}_2^2) \cdot$$

$$+ \frac{pb}{l}\left[(\bar{A}_{11} + \bar{C}_1)(\bar{A}_{22} + \bar{C}_1) - (\bar{A}_{12} + \bar{C}_2)^2\right] = 0 \quad (62)$$

The particular case of perfect adherence at the interface corresponds to $b = \infty$ giving again equation (57), while the case of perfect slip $b = 0$ yields

$$\bar{A}_{11} - \frac{\bar{A}_{12}^2}{\bar{A}_{22}} + \bar{C}_1 - \frac{\bar{C}_2^2}{\bar{C}_1} = 0 \quad (63)$$

This case was considered previously [6]. We note that

$$\bar{C}_1 - \frac{\bar{C}_2^2}{\bar{C}_1} = \frac{2\bar{Q}_1(\bar{Q}_1 + \bar{R}_1)}{2\bar{Q}_1 + \bar{R}_1} = \frac{1}{2}\,\bar{B}_1 \quad (64)$$

while

$$\bar{A}_{11} - \frac{\bar{A}_{12}^2}{\bar{A}_{22}} = \frac{1}{2}\left(\frac{1}{12}\,\bar{B}h^2l^2 - P\right)lh \quad (65)$$

Hence equation (63) becomes

$$P = \frac{1}{12}\,\bar{B}h^2l^2 + \frac{\bar{B}_1}{lh} \quad (66)$$

It is readily seen that for every value of p the load P plotted as a function of lh goes through a minimum which corresponds to the dominant wave length for that load. This last equation coincides with relation (3.1) of reference [6] where it was the object of a detailed discussion.

4 The Case of Two Incompressible Viscous Solids

We shall now consider the particular case of a layer of incompressible purely viscous solid embedded in a medium which is also incompressible and purely viscous. Perfect adherence is assumed at the interface. Incompressibility of the medium is expressed by the condition $\bar{R}_1 = \infty$ hence from (55)

$$\begin{aligned} \bar{C}_1 &= 2\bar{Q}_1 \\ \bar{C}_2 &= 0 \end{aligned} \quad (67)$$

Also for the layer

$$\bar{B} = 4\bar{Q} \quad (68)$$

For the case of pure viscosity the operators become

$$\begin{aligned} \bar{Q} &= \mu p \\ \bar{Q}_1 &= \mu_1 p \end{aligned} \quad (69)$$

where μ is the viscosity coefficient of the layer and μ_1 that of the medium. The stability equation (57) becomes

$$(\bar{A}_{11} + \bar{C}_1)(A_{22} + \bar{C}_1) - \bar{A}_{12}^2 = 0 \quad (70)$$

This yields

$$P = \frac{1}{12}\,\bar{B}h^2l^2 + \frac{4\bar{Q}_1}{lh} + \frac{\bar{Q}_1 lh}{1 + \dfrac{\mu_1}{\mu}\,lh} \quad (71)$$

The two first terms in this expression correspond to the case of perfect interfacial slip. The third term represents the correction due to perfect interfacial adherence.

Let us substitute expressions (68) and (69) for the operators. Equation (71) becomes

$$\frac{P}{\mu p} = \frac{1}{3}\,(lh)^2 + 4\,\frac{\mu_1}{\mu}\,\frac{1}{lh} + \frac{\mu_1}{\mu}\,\frac{lh}{1 + \dfrac{\mu_1}{\mu}\,lh} \quad (72)$$

The dominant wave length is determined by considering the minimum value of this expression as a function of lh. Equating to zero the derivative of this expression with respect to lh yields an equation for the value $l_d h$ corresponding to the dominant wave length. We may write this equation

$$(l_d h)^3 = 6\,\frac{\mu_1}{\mu}\left[1 - \frac{1}{4}\left(\frac{l_d h}{1 + \dfrac{\mu_1}{\mu}\,l_d h}\right)^2\right] \quad (73)$$

We note that the dominant wave length for the case of two incompressible viscous solids is independent of the load P. This is a particular case of a general rule for systems with a homogeneous spectrum as already discussed in reference (6).

The second term in the bracket of equation (73) represents the effect of the imperfect adherence at the interface. In order to evaluate the importance of this adherence let us consider the case of perfect interfacial slip. This corresponds to neglecting the second term in the bracket of equation (73). The equation then gives immediately the value of $l_d h$. Denoting by l_d' the value of l_d for perfect slip we find

$$l_d' h = \left(\frac{6\mu_1}{\mu}\right)^{1/3} \quad (74)$$

The corresponding dominant wave length for perfect slip is

$$L_d' = \frac{2\pi}{l_d'} = 2\pi h\left(\frac{\mu}{6\mu_1}\right)^{1/3} \quad (75)$$

We denote by

$$L_d = \frac{2\pi}{l_d} \quad (76)$$

the dominant wave length for the case of perfect adherence as determined by equation (73). We may solve equation (73) for $l_d h$ as a function of μ/μ_1 and derive the value of L/L_d'. Values of this ratio are shown in Table 1 along with $l_d' h$ and L_d'/h.

Table 1

$\frac{\mu}{\mu_1}$	$l_d' h$	L_d'/h	L_d/L_d'	$\exp(pt_1)$
6	1.000	6.28	1.062	2.7
12	0.793	7.90	1.046	4.9
36	0.551	11.4	1.025	27.0
72	0.437	14.4	1.015	221
144	0.347	18.2	1.010	4440

Values of L_d/L_d' show the influence of interfacial adherence on the dominant wave length. We can see that the effect of adherence is to lengthen the dominant wave length by amounts up to about 6 per cent. The effect however becomes vanishingly small for viscosity ratios $\mu/\mu_1 > 70$. This corresponds to ratios of the dominant wave length to the thickness larger than 14.

That the wave length increases due to adherence follows immediately from inspection of equation (73) since the bracketed factor which represents the effect of adherence amounts to an increase in the viscosity μ of the layer.

As already pointed out in Section 1, we have assumed that a shearing deformation occurs due to the interfacial stress τ. If we neglect this shearing deformation, i.e., if we assume that all normal cross sections of the layer remain normal to the middle surface (neutral axis of the beam theory) this amounts to putting $\bar{Q} = \infty$ while retaining $\bar{B}$ finite in equation (70), hence replacing the bracket of relation (73) by

$$\left[1 - \frac{1}{4}\,(l_d h)^2\right]$$

The correction of the dominant wave length due to adherence will in that case be increased, but only by an insignificant amount.

An important feature to be considered is the "degree of instability" as represented by the amplitude of the folding observed after a given time. Consider that a total time t_1 has elapsed such that under the load P the compressive strain of the layer is ϵ. We may write

$$P = \frac{\bar{B}}{p}\frac{\epsilon}{t_1} = 4\mu\frac{\epsilon}{t_1} \tag{77}$$

If the compressive strain is 25 per cent during this time t_1,

$$P = \frac{\mu}{t_1} \tag{78}$$

Let us go back to equation (72) and neglect the effect of the adherence, i.e., let us drop the third term in this equation. Substituting in this equation the value (78) for P we find

$$\frac{1}{pt_1} = \frac{4}{12}\mu l^2 h^2 + \frac{4\mu_1}{lh} \tag{79}$$

Introducing the value $l = l_d'$ from (74) corresponding to the dominant wave length yields

$$pt_1 = \frac{1}{(l_d'h)^2} = \left(\frac{\mu}{6\mu_1}\right)^{2/3} \tag{80}$$

The factor e^{pt_1} is an amplification factor. During a compressive strain of 25 per cent the amplitude of a dominant wave length initially present as an irregularity in the layer will be multiplied by e^{pt_1}. It may therefore be considered as a measure of the instability. Values of e^{pt_1} are also shown in Table 1 against μ/μ_1.

We notice that the amplification factor e^{pt_1} and hence the instability itself become large for values of the viscosity ratio μ/μ_1 of the order of 70. For $\mu/\mu_1 = 70$ the dominant wave length is about 14 times the layer thickness. An initial disturbance of the layer with this wave length is amplified by a factor of about 200 in a compressive deformation of 25 per cent.

Another interesting point brought out by Table 1 is the fact that outside the range of the viscosity ratio μ/μ_1, for which the instability is mild, the influence of the interfacial adherence on the dominant wave length becomes negligible.

5 Discussion of the More General Case

In the previous section we have considered the folding of a viscous layer in a viscous medium. We shall now consider the case where one or both materials is not only viscous but viscoelastic in the more general sense. In order to simplify the derivation we shall neglect the influence of interface adherence. From our discussion in the previous section we may infer that neglecting adherence will not affect substantially the results. Since these cases have been treated in more detail in another publication [6], we shall simply outline briefly the results.

The essential result is furnished by equation (66) which gives P as a function of lh for every value of the rate coefficient p in the time factor $\exp(pt)$. The variable p appears in $\bar{B}$ and $\bar{B}_1$.

The dominant wave length L_d is found by taking the derivative of equation (66) with respect to lh. We find

$$L_d = 2\pi h\left(\frac{\bar{B}}{6\bar{B}_1}\right)^{1/3} \tag{81}$$

The corresponding load

$$P = \frac{3}{2}\bar{B}_1\left(\frac{\bar{B}}{6\bar{B}_1}\right)^{1/3} \tag{82}$$

Eliminating p between those two relations yields the dominant wave length as a function of the load P. It can be seen that, in general, there is a lower critical load obtained by putting $p = 0$ in equation (82). At this load instability is incipient. The higher critical load is a buckling load obtained by putting $p = \infty$. This load corresponds to elastic buckling. The case of two incompressible viscous fluids examined in the foregoing corresponds to

$$\begin{aligned}\bar{B} &= 4\mu p\\ \bar{B}_1 &= 4\mu_1 p\end{aligned} \tag{83}$$

We find expression (75) independent of p. Hence in this case the dominant wave length is independent of the load.

For an elastic layer in a viscous medium both incompressible we have

$$\begin{aligned}\bar{B} &= 4G\\ \bar{B}_1 &= 4\mu_1 p\end{aligned} \tag{84}$$

where G is the shear modulus of the layer. Applying expressions (81) and (82) and eliminating p between them we find

$$L_d = \pi h\left(\frac{4G}{P}\right)^{1/2} \tag{85}$$

In this case the dominant wave length decreases as the load increases. It is interesting to compare L_d with the wave length of elastic buckling of the layer assumed free. It is found that L_d is $\sqrt{3}$ times the wave length of free elastic buckling under the same load P. It is independent of the viscosity.

Another case is that of a viscous layer in an elastic medium. The layer of course must be sufficiently viscous to sustain the load. Assuming again incompressibility of both media, we find

$$L_d = \frac{4}{3}\pi h\frac{P}{4G_1} \tag{86}$$

where G_1 is the shear modulus of the surrounding medium. The dominant wave length (86) is independent of the viscosity and increases with the load.

The case of two Maxwell media is also examined in reference [6] and it is found that the ratio of relaxation times of the two media is an important parameter which controls the dependence of the dominant wave length on the load.

6 Nonlinear and Incremental Stress-Strain Relations

As mentioned in the previous work [6] there is a lot more to be said if we wish to apply irreversible thermodynamics to relations between incremental stresses and incremental strains. This is of course closely related to the problem of nonlinear rheology since a deformation may be considered as a succession of incremental states.[4] While this appears to be quite a complex problem in general there is, however, one case which can be immediately analyzed by combining the thermodynamics of linear rheology [4] with those of the theory of elasticity for incremental stresses [8, 9]. Consider a solid which is in a state of thermodynamic equilibrium under a stress field S_{ij}. Then for small deviations from this equilibrium state we may assume Onsager's relations to apply to the incremental strains and stresses. We must be careful, however, to express the stress components t_{ij} as forces per unit area before incremental deformation [8, 9]. This is necessary because application of thermodynamic principles requires the use of conjugate variables in such a way that

$$W = \frac{1}{2}e_{ij}t_{ij} \tag{87}$$

[4] The somewhat arbitrary assumption proposed by Ziegler [11] that linear viscoelasticity is directly applicable to plasticity overlooks the asymmetry of the operators.

represents the work done by t_{ij} with e_{ij} the incremental strains. Then the relation between e_{ij} and t_{ij} is of the same general type as for the unstressed system

$$t_{ij} = P_{ij}{}^{kl} e_{kl} \tag{88}$$

where $P_{ij}{}^{kl}$ is the tensor operator derived in reference [4].

The actual incremental stresses σ_{ij} as referred to areas after deformation are related to t_{ij} by the relations [9]

$$t_{ij} = \sigma_{ij} + eS_{ij} - \frac{1}{2}(e_{il}S_{jl} + e_{jl}S_{il}) \tag{89}$$

which may also be written

$$t_{ij} = \sigma_{ij} + B_{ij}{}^{lk} e_{lk} \tag{90}$$

with

$$B_{ij}{}^{lk} = \delta_{lk}S_{ij} - \frac{1}{2}(\delta_{ik}S_{jl} + \delta_{jk}S_{il}) - \frac{1}{2}(\delta_{il}S_{jk} + \delta_{jl}S_{ik}) \tag{91}$$

Note that this is not generally a symmetric tensor, i.e.,

$$B_{ij}{}^{lk} \neq B_{lk}{}^{ij} \tag{92}$$

For instance, if we start from a two-dimensional state of principal stresses

$$S_{ij} = \begin{vmatrix} S_{11} & 0 \\ 0 & S_{22} \end{vmatrix} \tag{93}$$

Then

$$B_{11}{}^{22} = S_{22}$$
$$B_{22}{}^{11} = S_{11} \tag{94}$$

Hence the tensor is symmetric only if we have

$$S_{22} = S_{11} \tag{95}$$

i.e., if the initial state is isotropic. In three dimensions this will be the case if the initial stress is hydrostatic. Substitution of (90) in (88) yields

$$\sigma_{ij} = (P_{ij}{}^{lk} + B_{ij}{}^{lk})e_{lk} \tag{96}$$

We conclude that under our assumptions the relation between the actual incremental stress and strain is not, in general, expressed by a symmetric tensor operator except if the initial stress is hydrostatic.

We see therefore that the stress-strain relation (15) which involves a symmetric matrix is in contradiction with (96). The error, however, will be small if the initial stress is sufficiently small relative to the incremental matrix $P_{ij}{}^{lk}$ (incremental moduli in the elastic case). This contradiction does not arise if the material is not assumed to satisfy the condition that it is initially in thermodynamic equilibrium subject to small perturbations, e.g., if the state of prestress produces a steady state of flow. Similar considerations may be applied to the more general case of perturbation in the vicinity of a steady or near-steady creep. In this case, the creep rate is coupled to the deformation because of temperature changes due to the thermoelastic effect[5] and the Onsager relations are not satisfied for the incremental quantities.

If the body is such that for infinitely slow deformations it becomes elastic whether linear or nonlinear, then it is probably legitimate to assume that Onsager's relations are satisfied for incremental deformations and to use relations of the type (96). The operator, however, is restricted in this case and must be such that an incremental stress produces no steady-state creep. Hence it must be of a form such that

$$P_{ij}{}^{lk} \neq 0 \quad \text{for} \quad p = 0 \tag{97}$$

These simple remarks are presented here to indicate some of the deeper implications which are involved if we wish to extend linear viscoelasticity to incremental deformations.

References

1 P. P. Bijlaard, "On the Elastic Stability of Thin Plates Supported by a Continuous Medium," Proc. Koninklijke Nederlandsche Akademie van Wetenschappen, vol. 49, 1946, pp. 1189–1199.

2 P. P. Bijlaard, "On the Elastic Stability of Sandwich Plates," Proc. Koninklijke Nederlandsche Akademie van Wetenschappen, vol. 50, 1947, pp. 79–193.

3 G. S. Gough, C. F. Elam, and N. A. De Bruyne, "The Stabilization of a Thin Sheet by a Continuous Supporting Medium," *Journal of The Royal Aeronautical Society*, vol. 44, 1940, pp. 12–43.

4 M. A. Biot, "Theory of Stress-Strain Relations in Anisotropic Viscoelasticity and Relaxation Phenomena," *Journal of Applied Physics*, vol. 25, 1954, pp. 1385–1391.

5 M. A. Biot, "Variational and Lagrangian Methods in Viscoelasticity," Proceedings IUTAM Colloquium on the Deformation and Flow of Solids, Madrid, 1955, Springer, Berlin, 1956.

6 M. A. Biot, "Folding Instability of a Layered Viscoelastic Medium under Compression," *Proceedings of the Royal Society*, series A, vol. 242, 1957, pp. 444–454.

7 M. A. Biot, "Folding of a Layered Viscoelastic Medium Derived From an Exact Stability Theory of a Continuum Under Initial Stress," *Quarterly of Applied Mathematics*, vol. 17, 1959, pp. 185–204.

8 M. A. Biot, "Nonlinear Theory of Elasticity and the Linearized Case for a Body Under Initial Stress," *Philosophical Magazine* vol. 27, 1939, pp. 468–489.

9 M. A. Biot, "Elastizitats Theorie Zweiter Ordnung mit Anwendungen," *Zeitschrift für angewandte Mathematik und Mechanik*, vol. 20, 1940, pp. 89–99.

10 R. Mazet, "On a Suitable Model for Thermoelastic Vibrations of a Test Specimen Undergoing Creep," Ninth International Congress of Applied Mechanics, Brussels, 1956.

11 H. Ziegler, "An Attempt to Generalize Onsager's Principle and its Significance for Rheological Problems," Technical Report No. 13, Division of Applied Mathematics, Brown University, March 1957.

12 J. N. Goodier, "Cylindrical Buckling of Sandwich Plates," JOURNAL OF APPLIED MECHANICS, vol. 13, TRANS. ASME, vol. 68, 1946, pp. 253–260

13. M. A. Biot, "The Influence of Gravity on the Folding of a Layered Viscoelastic Medium Under Compression," *Journal of the Franklin Institute*, vol. 267, 1959, pp. 211–228.

[5] Equations for one-dimensional oscillations of a simple model of this type were given by Mazet [10].

The Stress Distribution in a Semi-Infinite Strip Subjected to a Concentrated Load[1]

P. S. THEOCARIS
Visiting Assistant Professor,
Division of Engineering,
Brown University, Providence, R. I.
Mem. ASME

A solution is presented for the stress distribution in a semi-infinite strip subjected to an axial concentrated compressive load. The problem is solved by using the function $z = f(w)$ defining the Schwarz-Christoffel transformation. All the boundary conditions are satisfied except along the two longitudinal edges of the strip. Normal stresses along these boundaries are present which are eliminated by applying the minimum-strain-energy principle at a part of the strip. The stress components are calculated along all the boundaries and the axis of symmetry, as well as along three transverse sections in the neighborhood of the applied load. The theoretical results are compared with experimental results obtained by using photoelasticity and the electrical analogy method for the tracing of isostatics.

THE problem of a semi-infinite strip compressed by a concentrated load was first studied experimentally by Filon [1],[2] Favre [2], Tesar [3], and others. The models they used for their experiments were loaded uniformly over a small portion at the middle of the transverse boundary of the strip. Thus the problem can be easily related to the problem of a concentrated load.

Theoretical solutions of a similar problem of a finite plate compressed by two symmetrical concentrated loads are given by Timoshenko [4], Coker and Filon [5], Goodier [6], Foeppl [7], Pickett [8], and others. All these solutions, which are presented as applications of general methods for solving plane elasticity problems, give approximate results for the stress distribution in this particular problem.

While the solution of related problems has been considered extensively, there appears to have been no theoretical investigation of the specific problem of the stress distribution in a semi-infinite strip loaded along its transverse edge. The object of this paper is to present such a solution for the limiting case when the applied load is concentrated on the longitudinal axis of the strip.

It has been shown [11] that it is possible to derive a solution in certain plane elasticity problems by determining a function $\zeta(z)$ of the complex variable $z = (x + iy)$ representing the field of isostatics. The problem is solved by using the analytic function $\zeta(z)$ defining the field of isostatics in the case when a normal concentrated load is applied at the straight boundary of a semi-infinite plate. The Schwarz-Christoffel transformation defined by the function $z = f(w)$ maps the foregoing field of isostatics to the corresponding field in the semi-infinite strip.

Since the field of isostatics in the strip is determined, the stress components can be calculated all over the strip by using the previously established formulas [11].

Analytical Solution

We consider the semi-infinite plane (w) with a normal load P applied on the point O of its boundary, Fig. 1(*a*).

The Schwarz-Christoffel transformation for mapping of this plane into the semi-infinite strip is given by the relation [10]

$$\frac{dz}{dw} = \frac{c}{(w^2 - 1)^{1/2}} \tag{1}$$

From the relation (1) it can be deduced that the points (-1)

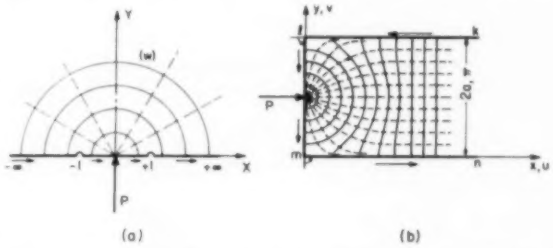

Fig. 1 Conformal mapping of semi-infinite plane into semi-infinite strip

[1] The results presented in this paper were obtained in the course of research sponsored by the National Academy of Sciences under the Scientific Research Project TA-01-101-3006.

[2] Numbers in brackets designate References at end of paper.

Presented at the Summer Conference of the Applied Mechanics Division, Troy, N. Y., June 18–20, 1959, of THE AMERICAN SOCIETY OF MECHANICAL ENGINEERS.

Discussion of this paper should be addressed to the Secretary, ASME, 29 West 39th Street, New York, N. Y., and will be accepted until October 10, 1959, for publication at a later date. Discussion received after the closing date will be returned.

NOTE: Statements and opinions advanced in papers are to be understood as individual expressions of their authors and not those of the Society. Manuscript received by ASME Applied Mechanics Division, April 14, 1958. Paper No. 59—APM-17.

Nomenclature

$w = (X + iY)$, complex variable at semi-infinite plane

$z = (x + iy)$ complex variable at semi-infinite strip

$\varphi(u, v)$ = a complex variable related to the u, v-system of co-ordinates for which we have $(u + iv) = \left(\frac{\pi x}{2a} + i\,\frac{\pi y}{2a}\right)$

$\zeta(z)$ = an analytic function of complex variable $z = (x + iy)$

σ = semisum of principal stresses $(2\sigma = \sigma_1 + \sigma_2)$

$\mu = \mu(x, y)$ = an analytic function expressed by relation: $\mu = \mu(x, y) = -[a + bx + cy + d(x^2 + y^2)]$

$\sigma_{xa}, \sigma_{ya}, \tau_{xya}$ = Cartesian components of supplementary stresses at part of strip where $0 \leqslant u \leqslant \pi/2$

$\sigma_{xb}, \sigma_{yb}, \tau_{xyb}$ = Cartesian components of supplementary stresses at part of strip where $\pi/2 < u < \infty$

and $(+1)$ on the X-axis of the semi-infinite plane correspond to the points l and m of the strip, respectively, and the regions $-\infty < w < -1$, $-1 < w < +1$ and $+1 < w < +\infty$ of the w-axis to the (kl), (lm), and (mn) boundaries of the strip, Fig. 1(*b*). By integrating Equation (1) we obtain the following relation:

$$z = c_1 \log[w + (w^2 - 1)^{1/2}] + c_2 \tag{2}$$

where c_1 and c_2 are constants. From the conditions of the problem, we can place

$$c_1 = 2a/\pi \quad \text{and} \quad c_2 = 0$$

then relation (2) becomes

$$z = \frac{2a}{\pi} \log[w + (w^2 - 1)^{1/2}] = \frac{2a}{\pi} \cosh^{-1} w \tag{3}$$

Equation (3) can be also written as follows:

$$w = \cosh\left(\frac{\pi z}{2a}\right) \tag{4}$$

On the other hand, it is known that the curves $\zeta(z)$ representing the two families of isostatics in the case of the semi-infinite plane w are given by the relation

$$\zeta(w) = \log(w) \tag{5}$$

These curves are defined in the plane z by the equation

$$\zeta(z) = \log\left[\cosh\left(\frac{\pi z}{2a}\right)\right] \tag{6}$$

We now change variables by letting

$$\frac{\pi z}{2a} = \varphi(u, v) = u + iv$$

and we have $$\zeta(z) = \log[\cosh \varphi] \tag{7}$$

The Cartesian components of stresses are given by the following relations [11]:

$$\begin{aligned} \sigma_x &= \sigma + \mu R[-h^2(z)] \\ \sigma_y &= \sigma - \mu R[-h^2(z)] \\ \tau_{xy} &= 2\mu I[-h^2(z)] \end{aligned} \tag{8}$$

where R and I are the real and imaginary parts of the function $[-h^2(z)]$ and σ is the semisum of principal stresses given by the relation

$$\sigma(z) = -R\left\{\int_{z_0}^{z} (2dz + b + ic)\left(\frac{\partial \zeta}{\partial z}\right)^2 dz + p\right\} \tag{9}$$

and μ is an analytic function given by the relation

$$\mu = \mu(x, y) = -[a + bx + cy + d(x^2 + y^2)] \tag{10}$$

In these relations a, b, c, and d are arbitrary constants depending on the applied load and the geometry and R in (9) is the real part of the function

$$\int f(z) \frac{\partial \zeta}{\partial z} dz$$

In the special case of this problem the constants $a = c = d = 0$ and the function μ is reduced to the following

$$\mu = -bx \tag{11}$$

herewith Equation (9) becomes

$$\sigma(z) = -R\left[b \int \left(\frac{\partial \zeta}{\partial z}\right)^2 dz\right] = R\left[\frac{\pi b}{2a}\left(\frac{\pi z}{2a} - \tanh\frac{\pi z}{2a}\right)\right]$$

and consequently

$$\sigma(u, v) = \frac{\pi b}{2a}\left[u - \frac{\sinh u \cosh u}{(\cosh^2 u - \sin^2 v)}\right] \tag{12}$$

But we have also that

$$h = \frac{\partial \zeta}{\partial z} = \frac{\pi}{2a} \frac{\sinh u \cosh u + i \sin v \cos v}{\cosh^2 u - \sin^2 v} \tag{13}$$

which gives

$$\begin{aligned} R[-h^2(z)] &= -\frac{\pi^2}{4a^2} \frac{\sinh^2 u \cosh^2 u - \sin^2 v \cos^2 v}{(\cosh^2 u - \sin^2 v)^2} \\ I[-h^2(z)] &= -\frac{\pi^2}{8a^2} \frac{\sinh 2u \sin 2v}{(\cosh^2 u - \sin^2 v)^2} \end{aligned} \tag{14}$$

By introducing the values of $\sigma(z)$ and $R[-h^2(z)]$, $I[-h^2(z)]$ given by (12) and (14) into relations (8) we obtain the Cartesian components of stresses:

$$\begin{aligned} \sigma_x &= \frac{\pi b}{2a}\left\{u\left[\frac{\cosh^2 u \cos^2 v - \sinh^2 u \sin^2 v}{(\cosh^2 u - \sin^2 v)^2}\right] - \frac{\sinh u \cosh u}{\cosh^2 u - \sin^2 v}\right\} \\ \sigma_y &= \frac{\pi b}{2a}\left\{2u - u\left[\frac{\cosh^2 u \cos^2 v - \sinh^2 u \sin^2 v}{(\cosh^2 u - \sin^2 v)^2}\right] - \frac{\sinh u \cosh u}{\cosh^2 u - \sin^2 v}\right\} \\ \tau_{xy} &= -\frac{\pi b}{4a} u \frac{\sinh 2u \sin 2v}{(\cosh^2 u - \sin^2 v)^2} \end{aligned} \tag{15}$$

From Equations (15) we have for the transverse boundary of the strip that for $u = 0$ $\sigma_x = 0$ all over this boundary with the exception of the point $v = \pi/2$ where we have $\sigma_x = -\infty$.

For $u = \infty$ the stress σ_x becomes

$$\sigma_x = -\frac{\pi b}{2a} = -\frac{P}{2a}$$

consequently, the constant b is

$$b = P/\pi \tag{16}$$

and the relations (15) become

$$\begin{aligned} \sigma_x &= \frac{P}{2a}\left\{u\left[\frac{\cosh^2 u \cos^2 v - \sinh^2 u \sin^2 v}{(\cosh^2 u - \sin^2 v)^2}\right] - \frac{\sinh u \cosh u}{\cosh^2 u - \sin^2 v}\right\} \\ \sigma_y &= \frac{P}{2a}\left\{2u - u\left[\frac{\cosh^2 u \cos^2 v - \sinh^2 u \sin^2 v}{(\cosh^2 u - \sin^2 v)^2}\right] - \frac{\sinh u \cosh u}{\cosh^2 u - \sin^2 v}\right\} \\ \tau_{xy} &= -\frac{P}{4a} u \frac{\sinh 2u \sin 2v}{(\cosh^2 u - \sin^2 v)^2} \end{aligned} \tag{17}$$

The stresses at the longitudinal edges where $v = 0, \pi$ become

$$\sigma_x = \frac{P}{2a}\,[u - u\tanh^2 u - \tanh u]$$

$$\sigma_y = \frac{P}{2a}\,[u + u\tanh^2 u - \tanh u] \qquad (18)$$

$$\tau_{xy} = 0$$

From Equations (18) it follows that along the longitudinal edges of the strip there exists not only stresses σ_x parallel to the edges but also stresses σ_y normal to these edges. In order to cancel these stresses we introduce a stress function ϕ which gives the appropriate stresses along the boundaries of the strip. The examination of the distribution of the normal stresses σ_y shows that their variation along the longitudinal edges becomes almost proportional to the co-ordinate u for values beyond $\pi/2$.

Thus the domain of the strip can be divided into two parts, for the determination of ϕ. The one corresponds to values of u defined by $0 \leqslant u \leqslant \pi/2$ and the second corresponds to values of u between $\pi/2 < u < \infty$. In the second part of the strip, the stresses σ_y remain constant along any section parallel to the v-axis. In order to cancel these stresses we must simply add a function ϕ_b giving values of stresses differing only in sign with those given by (18) for $u > \pi/2$. For values of $\pi/2 < u < \pi$ this function has the form

$$\phi_b = \frac{P}{4a}\left[1.333u^2 - \frac{2.106}{3}\,u^3\right] \qquad (19)$$

and gives stresses

$$\sigma_{xb} = \tau_{xyb} = 0 \quad \text{and} \quad \sigma_{yb} = \frac{P}{2a}\,[1.333 - 2.106u]$$

For values of $u > \pi$ the function ϕ_b is expressed as follows:

$$\phi_b = \frac{P}{12a}\,[3u^2 - 2u^3] \qquad (19a)$$

and gives values of stresses

$$\sigma_{xb} = \tau_{xyb} = 0, \quad \sigma_{yb} = \frac{P}{2a}\,[1 - 2u]$$

The maximum residual stresses σ_{yb} introduced along the longitudinal boundaries $v = 0$ and π by accepting the functions ϕ_b are of the order of less than $0.02P/2a$ (actually they are $\sigma_{yb} = 0.0175\,P/2a$ at $v = 2\pi/3$ and $\sigma_{yb} = 0.0195\,P/2a$ at $v = \pi$).

In order to obtain the function ϕ_a in the first part of the strip ($0 \leqslant u \leqslant \pi/2$) we must express the boundary conditions in a suitable form. We call first the stress function giving the stresses σ_y, expressed by Equation (18) as ϕ_{a1}. This function is given by the equation

$$\phi_{a1} = \frac{P}{2a}\left\{\frac{u^2}{3} + \frac{u^2}{2} - u\log(1 + e^{2u}) + \sum_{p=1}^{\infty}(-1)^{p+1}\frac{e^{2pu}}{2p^2}\right\} \qquad (20)$$

Next we add to this function a supplementary function ϕ_{a2} given by the relation

$$\phi_{a2} = \frac{P}{4a}\left\{1.3330u^2 - \frac{2.0160u^3}{3}\right\} \qquad (20a)$$

This function introduces only stresses σ_y and as a result annuls the stresses σ_y at the point $u = \pi/2$.

Finally, we consider the double of the first part of the strip as a square plate loaded along half its opposite sides ($v = 0, \pi$) with a normal load equal and of opposite sign of the stresses σ_y introduced by the sum of functions ($\phi_{a1} + \phi_{a2}$). This load is given by the relation

$$\sigma_{ya} = -\frac{P}{2a}\,[1.3330 - 1.0160u + u\tanh^2 u - \tanh u] \qquad (21)$$

By application of the minimum-strain-energy principle to this plate we can determine the function ϕ_a which satisfies all the boundary conditions of the plate, i.e., it gives zero shear stresses along all the boundaries, zero stresses σ_x along the transverse boundaries ($u = 0, \pi$), and furthermore it gives the appropriate stresses σ_y, expressed by Equation (21), for $v = 0, \pi$.

The stress function ϕ_a is given in a form of series of functions of which we retain only the four first terms [4, 9].

This function is given by the relation

$$\phi_a = \frac{P}{2a}\left\{\left[2.3330\,\frac{u^2}{2} - \frac{0.0160}{6}\,u^3 - u\log(1 + e^{2u}) + \sum_{p=0}^{\infty}(-1)^{p+1}\frac{e^{2pu}}{2p^2}\right] + u^2v^2(u - \pi)^2(v - \pi)^2[\lambda_1 + \lambda_2/4(2u - \pi)^2 + \lambda_3/4(2v - \pi)^2 + \lambda_4/16(2u - \pi)^2(2v - \pi)^2]\right\} \qquad (22)$$

The last term, which expresses the correction function in Equation (22), is truncated after the fourth term λ_4. The contribution of the fourth term to the stresses σ_{xa} along the longitudinal boundaries is calculated to be of the order of 2 per cent in the regions where the stresses take significant values. Near the corners, where the stresses are very small, the contribution of the term λ_4 is greater but there the stresses are insignificant.

Since the next term is expected to contribute much less than the term λ_4, truncation of the series at this term does not affect significantly the stress distribution.

Application of the minimum-strain-energy principle to this plate, as it is described by Goodier [6], gives the following four relations from which we evaluate the four coefficients λ_1, λ_2, λ_3, and λ_4:

$$164.5714\lambda_1 + 3.7403\pi^2(\lambda_2 + \lambda_3) + 0.1039\pi^4\lambda_4 = -\frac{2^8.5.5.7.9}{\pi^{14}}\int_0^{\pi/2}\int_0^{\pi/2}\sigma_y v^2(v - \pi)^2(6u^2 - 6\pi u + \pi^2)\,du\,dv$$

$$14.9611\lambda_1 + 8.0240\pi^2\lambda_2 + 0.4156\pi^2\lambda_3 + 0.1678\pi^4\lambda_4 = -\frac{2^8.5.5.7.9}{\pi^{16}}\int_0^{\pi/2}\int_0^{\pi/2}\sigma_y v^2(v - \pi)^2(480u^4 - 240u^3 + 624\pi^2u^2 - 144\pi^3u + 8\pi^4)\,du\,dv \qquad (23)$$

$$14.9611\lambda_1 + 0.4156\pi^2\lambda_2 + 8.0240\pi^2\lambda_3 + 0.1678\pi^4\lambda_4 = -\frac{2^8.5.5.7.9}{\pi^{16}}\int_0^{\pi/2}\int_0^{\pi/2}\sigma_y v^2(v - \pi)^2(2u - \pi)^2(6u^2 - 6\pi u + \pi^2)\,du\,dv$$

$$128\lambda_1 + 51.6923\pi^2(\lambda_2 + \lambda_3) + 6.9930\pi^4\lambda_4 = -\frac{2^8.5.5.7.7.9.11}{\pi^{16}}\int_0^{\pi/2}\int_0^{\pi/2}\sigma_y v^2(v - \pi)^2(2v - \pi)^2(480u^4 - 240\pi u^3 + 624\pi^2u^2 - 144\pi^3u + 8\pi^4)\,du\,dv$$

where σ_y is given by the relation (21). After the evaluation of the integrals and rearrangement of its terms the system of equations (23) becomes

Table 1 Values of principal stresses along boundaries and longitudinal axis of strip

$x/a, y/a$	0	$\pi/12$	$\pi/6$	$\pi/3$	$\pi/2$	$2\pi/3$	$5\pi/6$	$11\pi/12$	π
					v-axis ($x/a = 0$)				
σ_x	0	0	0	0	$-\infty$	0	0	0	0
σ_y	0	0.076	0.212	0.419	0.478	0.419	0.212	0.076	0
					u-axis ($y/a = 0, \pi$)				
σ_x	0	+0.058	+0.101	−0.085	−0.383	−0.771	−0.934	−0.961	−0.973
σ_y	0	0	0	0	0	0	0	0	0
					axis $y/a = \pi/2$				
σ_x	$-\infty$	−7.629	−3.831	−2.020	−1.452	−1.164	−1.076	−1.080	−1.027
σ_y	0.478	0.503	0.508	0.486	0.310	0.175	0.082	0.057	0.040

Table 2 Values of Cartesian components of stresses along three transverse sections of strip

$x/a, y/a$	0	$\pi/6$	$\pi/3$	$\pi/2$	$2\pi/3$	$5\pi/6$	π
				I-I Section ($x/a = \pi/12$)			
σ_x	0.058	−0.041	−0.303	−7.629	−0.303	−0.047	0.058
σ_y	0	−0.120	−0.816	0.503	−0.816	−0.120	0
τ_{xy}	0	−0.100	−0.248	0	0.248	0.100	0
				II-II Section ($x/a = \pi/6$)			
σ_x	0.101	−0.180	−1.169	−3.831	−1.169	−0.180	0.101
σ_y	0	−0.168	−0.298	0.507	−0.298	−0.168	0
τ_{xy}	0	−0.336	−0.988	0	0.988	0.336	0
				III-III Section ($x/a = \pi/3$)			
σ_x	−0.085	−0.606	−1.357	−2.020	−1.357	−0.606	−0.085
σ_y	0	−0.012	0.179	0.486	0.179	−0.012	0
τ_{xy}	0	−0.378	−0.601	0	0.601	0.378	0

$$164.5714\lambda_1 + 3.7403\pi^2(\lambda_2 + \lambda_3) + 0.1039\pi^4\lambda_4 = \frac{1}{\pi^6} \times 362.6703$$

$$29.9222\lambda_1 + 8.4396\pi^2(\lambda_2 + \lambda_3) + 0.3357\pi^4\lambda_4 = \frac{1}{\pi^4} \times 150.6397$$

$$7.6084\pi^2(\lambda_2 - \lambda_3) = \frac{1}{\pi^6} \times 47.0196 \quad (24)$$

$$128\lambda_1 + 51.6923\pi^2(\lambda_2 + \lambda_3) + 6.9930\pi^4\lambda_4 = \frac{1}{\pi^6} \times 1087.1267$$

From the solution of system (24) we find the following values for the coefficients λ_1, λ_2, λ_3, and λ_4:

$$\lambda_1 = \frac{1}{\pi^6} \times 1.9722 \qquad \pi^2\lambda_3 = \frac{1}{\pi^6} \times 1.2319$$
$$\pi^2\lambda_2 = \frac{1}{\pi^6} \times 7.4127 \qquad \pi^4\lambda_4 = \frac{1}{\pi^6} \times 55.4435 \quad (25)$$

The Cartesian components of stresses due to the function ϕ_a, in the first part of the strip ($0 \leq u \leq \pi/2$), are

$$\sigma_{xa} = \frac{P}{2a} u^2(u - \pi)^2\{(3v^2 - 3\pi v + \pi^2/2)[4\lambda_1 + \lambda_3(2u - \pi)^2] + 2^{-6}[480v^4 - 240\pi v^3 + 624\pi^2v^2 - 144\pi^3v + 8\pi^4][4\lambda_2 + \lambda_4(2u - \pi)^2]\}$$

$$\sigma_{ya} = \frac{P}{2a} v^2(v - \pi)^2\{(3u^2 - 3\pi u + \pi^2/2)[4\lambda_1 + \lambda_4(2v - \pi)^2] + 2^{-6}[480u^4 - 240\pi u^3 + 624\pi^2u^2 - 144\pi^3u + 8\pi^4][4\lambda_2 + \lambda_4(2v - \pi)^2]\} \quad (26)$$

$$\tau_{xya} = \frac{P}{2a} uv(u - \pi)(v - \pi)(2u - \pi)(2v - \pi)$$

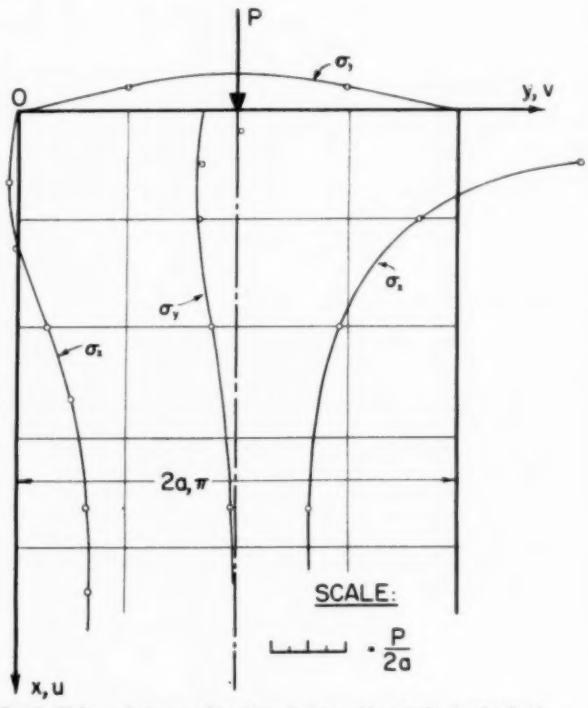

Fig. 2 Values of stresses along boundaries and longitudinal axis of strip (experimental values are represented by small circles)

$$\{4\lambda_1 + \lambda_2(6u^2 - 6\pi u + \pi^2) + \lambda_3(6v^2 - 6\pi v + \pi^2) + \lambda_4/4(6u^2 - 6\pi u + \pi^2)(6v^2 - 6\pi v + \pi^2)\}$$

From relations (17) with (19) or (26) we can evaluate the Cartesian components of stress all over the strip. These stresses are calculated along all boundaries, the longitudinal axis of symmetry ($v = \pi/2$) as well as along three transverse sections at dis-

tances of $u = \pi/12, \pi/6$, and $\pi/3$ from the v-axis. These stresses are tabulated in Tables 1 and 2 and plotted in Figs. 2 and 5.

Photoelastic Tests

The foregoing analytical work was complemented by a series of photoelastic tests, using Columbia Resin CR-39 and plexiglas models and the graphited-paper analogy for the tracing of isostatics [12].

The Columbia resin models are used for the determination of isochromatics and the difference of principal stresses. The models are loaded with a symmetrical concentrated load applied over a small portion of the transverse boundary of the model. Thus the stress distribution in the strip can simulate closely the

Fig. 3 Isochromatics for semi-infinite strip

Fig. 4 Family of isostatics for semi-infinite strip. Left half of strip is shown.

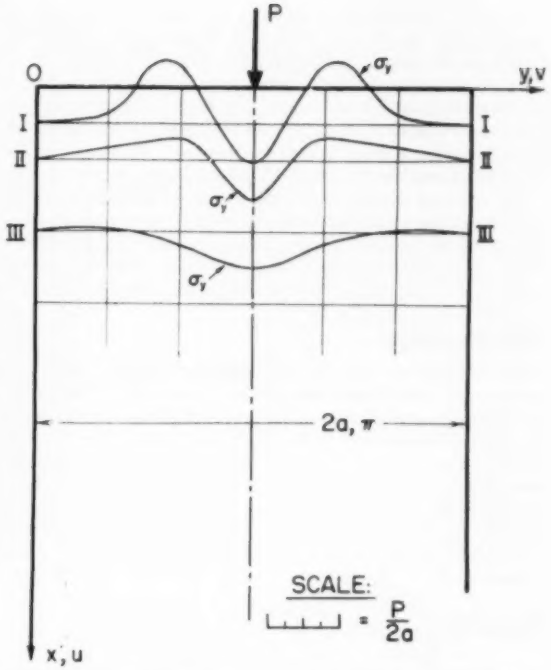

Fig. 5 Stresses σ_y along three transverse sections of strip where $x/a = \pi/12, \pi/6, \pi/3$

distribution produced by a concentrated load with the exception of a small area near the application of the load.

The stress along the free boundaries is obtained from the foregoing stress patterns, Fig. 3. These experimental values are also plotted in Fig. 2. The comparison with the analytical results shows a good agreement between the results over all boundaries except near the point of load application, as is to be expected.

An isotropic point is also determined on the longitudinal boundaries and at a distance 0.3π from the transverse boundary. Experimental determination of this point placed it at a distance of 0.32π.

Extensive study of isoclinics at the region near the transverse boundary with models made by plexiglas revealed a second isotropic point at the interior of the strip and at a distance from the corners $u = 0.0314\pi$ and $v = 0.178\pi$.

The determination of the isotropic points and the separation of the boundaries into two groups of families of isostatics provide the means for the tracing of isostatics by the electrical analogy method [12]. In Fig. 4 the one family of isostatics is shown.

By using data from the isochromatics and isostatics in the adapted Lamé-Maxwell equations of equilibrium, we separate the principal stresses along the longitudinal axis of the strip. The values of stresses obtained are plotted in Fig. 2 and they are in good agreement with analytical results.

Conclusions

An analytic solution of the stress distribution in a semi-infinite strip loaded by a concentrated symmetric load is given by using conformal mapping and the properties of isostatics.

The theoretical results are compared with experimental results obtained using photoelasticity and the electrical analogy method for the tracing of isostatics; good agreement was found, except in the neighborhood of the point of application.

A maximum compression stress σ_x is presented at the point of application of the load. A maximum tensile stress σ_y exists on the longitudinal axis $v = \pi/2$ and at a distance $u = \pi/6$.

The boundaries are divided into two parts by the isotropic points at the longitudinal boundaries. These isotropic points are found at a distance of about $u = \pi/3$ from the transverse boundary. Two other isotropic points are detected at the interior of the strip placed near the transverse boundary.

The principal stresses σ_1 are compression stresses over the entire strip except the small regions at the two free corners of the strip. The principal stresses σ_2 are tensile stresses throughout the strip, except in the two regions surrounding the interior isotropic points. At these domains stresses σ_2 are compression stresses.

Acknowledgments

The assistance of Prof. E. I. Fiesenheiser, Director of the Department of Civil Engineering of Illinois Institute of Technology, in obtaining some of the equipment used in the experiments is gratefully acknowledged. The author is also greatly indebted to Prof. August J. Durelli and to the Armour Research Foundation for the use of their laboratories to carry out the experimental work. Finally, the author wishes to express his gratitude to Messrs. W. F. Riley and T. W. Dally of the Armour Research Foundation for their helpful assistances in organizing the experimental work.

References

1 L. N. G. Filon, "On an Approximate Solution for the Bending of a Beam of a Rectangular Cross-Section Under Any System of Load," *Philosophical Transactions*, The Royal Society, London, vol. 201, series A, 1903, pp. 63–155.

2 H. Favre, "Sur une Nouvelle Méthode Optique de Détermination des Tensions Intérieures," *La Revue d'Optique Théorique et Instrumentale*, Paris, 1929.

3 V. Tesar, "Détermination Expérimentale des Tensions dans les Extrémités des Pièces Prismatiques Munies d'une Semi-articulation," Mémoires de l'Association Internationale des Ponts et Charpentes, 1e vol., 1931, pp. 497–506.

4 S. Timoshenko, "Theory of Elasticity," McGraw-Hill Book Company, Inc., New York, N. Y., first edition, 1934, pp. 48–51.

5 E. G. Coker and L. N. G. Filon, "A Treatise on Photoelasticity," Cambridge University Press, second edition, 1957, pp. 358–361.

6 J. N. Goodier, "Compression of Rectangular Blocks and the Bending of Beams by Non-Linear Distributions of Bending Forces," Trans. ASME, vol. 54, 1932, pp. 173–183.

7 L. Foeppl, "Drang und Zwang," erster Band, R. Oldenbourg, editor, zweite Auflage, 1924, section 56, pp. 344–354.

8 G. Pickett, "Application of the Fourier Method of the Solution of Certain Boundary Problems in the Theory of Elasticity," Journal of Applied Mechanics, vol. 11, Trans. ASME, vol. 66, 1944, pp. A-176–A-182.

9 S. Timoshenko, "The Approximate Solution of Two-Dimensional Problems in Elasticity," *Philosophical Magazine*, series 6, vol. 47, 1924, pp. 1095–1104.

10 R. V. Churchill, "Introduction to Complex Variables and Applications," McGraw-Hill Book Company, Inc., New York, N. Y., 1948, pp. 171–176.

11 P. S. Theocaris, "Direct Determination of Stresses in Plane Elasticity Problems Based on the Properties of Isostatics," Journal of Applied Mechanics, vol. 26, Trans. ASME, vol. 81, Series E, 1959, pp. 227–234.

12 P. S. Theocaris, "On an Electrical Analogy Method for the Separation of Principal Stresses Along Stress Trajectories," *Proceedings*, The Society for Experimental Stress Analysis, vol. 14, 1957, pp. 11–20.

Postbuckling Behavior of Rectangular Plates With Small Initial Curvature Loaded in Edge Compression

NOBORU YAMAKI

Assistant Professor,
Institute of High Speed Mechanics,
Tohoku University,
Sendai, Japan

The solution of Marguerre's fundamental equations for large deflections of thin plates with slight initial curvature is presented for the case of a rectangular plate subjected to edge compression. The problem is solved under eight different boundary conditions, combining two kinds of loading conditions and four kinds of supporting conditions. Numerical solutions are obtained for square plates with and without initial deflection, and the connections of deflection, edge shortening, and effective width of the plate with applied loads are clarified. The solutions here obtained include as special cases those investigated by Levy and Coan.

It is a well-known phenomenon that the failing strength of a thin plate can exceed appreciably the buckling stress when the latter occurs in the elastic range. Thus it will be of technical importance to clarify the postbuckling behavior of the plate, accompanied with large deflections.

The fundamental equations for the large deflection of thin flat plates have been derived by von Karman [1],[1] and the extension to the plate with small initial curvature has been achieved by Marguerre [2]. Using these equations, the postbuckling behavior of rectangular plates under edge compression has been investigated by several researchers. For example, approximate solutions have been obtained by Schnadel [3], Cox [4], Timoshenko [5], and Marguerre [6]; and solutions of theoretically exact nature by Levy [7] and Coan [8]. However, most of these studies seem to be confined to the simplest case where the plate is simply supported.

In this paper, the extension of Levy and Coan's works is attempted and the problem is solved extensively under various boundary conditions. Numerical solutions are obtained for the deflection, edge shortening, and effective width of the square plate, and the results are graphed and discussed.[2]

Statement of Problem

We will first derive the fundamental equations for large deflection of a thin elastic plate with small initial deflection. Denoting by w_0 and w the initial and additional deflections, respectively, the strain components in the middle surface of the plate become[3]

$$\epsilon_x = u_{,x} + 1/2\, w_{,x}^2 + w_{0,x}w_{,x}, \quad \epsilon_y = v_{,y} + 1/2\, w_{,y}^2 + w_{0,y}w_{,y},$$
$$\gamma_{xy} = u_{,y} + v_{,x} + w_{,x}w_{,y} + w_{0,x}w_{,y} + w_{0,y}w_{,x}, \quad (1)$$

and the connections with membrane stresses are expressed as

$$E\epsilon_x = \sigma_x - \nu\sigma_y, \quad E\epsilon_y = \sigma_y - \nu\sigma_x, \quad E\gamma_{xy} = 2(1+\nu)\tau_{xy} \quad (2)$$

Introducing the Airy stress function F defined by

$$\sigma_x = F_{,yy}, \quad \sigma_y = F_{,xx}, \quad \tau_{xy} = -F_{,xy}, \quad (3)$$

and eliminating displacement functions u and v from the preceding equations, we obtain the following compatibility equation:

$$\nabla^4 F = E(w_{,xy}^2 - w_{,xx}w_{,yy} + 2w_{0,xy}w_{,xy} - w_{0,xx}w_{,yy} - w_{0,yy}w_{,xx}) \quad (4)$$

The equilibrium equation in the z-direction, taking account of the initial deflection, becomes

[1] Numbers in brackets designate References at end of paper.

Contributed by the Applied Mechanics Division and presented at the Annual Meeting, November 30–December 5, 1958, New York, N. Y., of THE AMERICAN SOCIETY OF MECHANICAL ENGINEERS.

Discussion of this paper should be addressed to the Secretary, ASME, 29 West 39th Street, New York, N. Y., and will be accepted until October 10, 1959, for publication at a later date. Discussion received after the closing date will be returned.

NOTE: Statements and opinions advanced in papers are to be understood as individual expressions of their authors and not those of the Society. Manuscript received by ASME Applied Mechanics Division, May 21, 1958. Paper No. 58—A-59.

[2] Numerical results for stress distributions have been reserved for another report.

[3] Subscripts following a comma stand for differentiation; e.g., $w_{,x} = \partial w/\partial x$, $w_{,xy} = \partial^2 w/\partial x \partial y$, etc.

Nomenclature

x, y, z = co-ordinates of a point; origin at center of plate, Fig. 1
a = length of plate in x-direction
b = width of plate in y-direction
h = plate thickness
$\beta = a/b$ = aspect ratio
u, v, w = displacements of a point in x, y and z-directions, respectively
w_0 = initial deflection
$\epsilon_x, \epsilon_y, \gamma_{xy}$ = median-fiber strains
$\sigma_x, \sigma_y, \tau_{xy}$ = median-fiber stresses
E = Young's modulus
ν = Poisson's ratio
$D = Eh^3/12(1-\nu^2)$ = flexural rigidity of plate
F = Airy's stress function
$\nabla^4 = \partial^4/\partial x^4 + 2\partial^4/\partial x^2\partial y^2 + \partial^4/\partial^4 y$
P_x, P_y = total loads in x and y-directions, respectively
p_y = average compressive stress in y-direction
a_{mn} = given coefficient concerning initial deflection
b_{mn} = unknown coefficient concerning net deflection
$\lambda = p_y a^2/\pi^2 Eh^2$ = nondimensional load factor
w_m = maximum net deflection
δ_y = edge shortening in y-direction
R = ratio of effective width to actual width

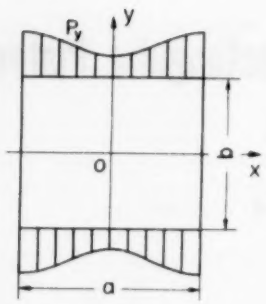

Fig. 1 Rectangular plate loaded in edge compression

$$\nabla^4 w = (h/D)[F_{,yy}(w + w_0)_{,xx} + F_{,xx}(w + w_0)_{,yy} - 2F_{,xy}(w + w_0)_{,xy}] \quad (5)$$

Equations (4) and (5) are Marguerre's fundamental equations governing the finite deflection of initially deflected thin plates.

Next, we will state the boundary conditions for the problems here treated, Fig. 1. They consist of the loading and supporting conditions along the edges. Concerning the loading conditions along the side edges, $x = \pm a/2$, we will consider the following two cases:

$$\text{Case } (a): \quad [u]_{x=\pm a/2} = \int_0^{\pm a/2} \left[\frac{1}{E} (F_{,yy} - \nu F_{,xx}) - \frac{1}{2} w_{,x}{}^2 - w_{0,x} w_{,x} \right] dx = \text{const},$$

$$P_x = h \int_{-b/2}^{b/2} F_{,yy} dy = 0, \quad F_{,xy} = 0, \quad (6a)$$

$$\text{Case } (b): \qquad F_{,yy} = F_{,xy} = 0 \qquad (6b)$$

In Case (a), the edges are kept straight by a distribution of normal stresses, the resultant of which is zero, while in Case (b), the edges are free from stresses. Assuming that the plate is compressed by frictionless loading heads, the conditions along the loaded edges, $y = \pm b/2$, become

$$[v]_{y=\pm b/2} = \int_0^{\pm b/2} \left[\frac{1}{E} (F_{,xx} - \nu F_{,yy}) - \frac{1}{2} w_{,y}{}^2 - w_{0,y} w_{,y} \right] dy = \text{const},$$

$$P_y = h \int_{-a/2}^{a/2} F_{,xx} dx = -p_y ah, \quad F_{,xy} = 0, \quad (7)$$

where p_y is the average compressive stress in the y-direction.

As for the supporting conditions, we will treat the following four cases: I—All edges simply supported; II—loaded edges simply supported, the other edges clamped; III—loaded edges clamped, the other edges simply supported; IV—all edges clamped. These conditions can be expressed as follows:

	along $x = \pm a/2$,	along $y = \pm b/2$	
I:	$w = w_{,xx} + \nu w_{,yy} = 0$,	$w = w_{,yy} + \nu w_{,xx} = 0$,	(8)
II:	$w = w_{,x} = 0$,	$w = w_{,yy} + \nu w_{,xx} = 0$,	(9)
III:	$w = w_{,xx} + \nu w_{,yy} = 0$,	$w = w_{,y} = 0$,	(10)
IV:	$w = w_{,x} = 0$,	$w = w_{,y} = 0$	(11)

Further, the initial deflection w_0 is assumed to satisfy the same conditions as w in each case.

Now the problem consists in determining the functions F and w which satisfy the fundamental equations, together with the given boundary conditions.

Theoretical Analysis

The initial and additional deflections in each case, which satisfy the corresponding conditions in (8) to (11), may be expressed as[4]

$$w_0 = h \sum_m \sum_n a_{mn} f_m(x) g_n(y), \qquad w = h \sum_m \sum_n b_{mn} f_m(x) g_n(y), \quad (12)$$

where

$$f_m(x) = \begin{cases} \cos(m\pi/a)x, & m = 1, 3, 5 \ldots \\ & \text{for Cases I and III,} \\ (-1)^{m+1} + \cos(2m\pi/a)x, & m = 1, 2, 3 \ldots \\ & \text{for Cases II and IV,} \end{cases} \quad (13)$$

$$g_n(y) = \begin{cases} \cos(n\pi/b)y, & n = 1, 3, 5 \ldots \\ \text{or } \sin(n\pi/b)y, & n = 2, 4, 6 \ldots \\ & \text{for Cases I and II,} \\ (-1)^{n+1} + \cos(2n\pi/b)y, & n = 1, 2, 3 \ldots \\ & \text{for Cases III and IV} \end{cases} \quad (14)$$

In Equations (12), a_{mn} and b_{mn} represent the prescribed and undetermined coefficients, respectively. Substituting these expressions in Equation (4), the results can be generally expressed in the following form

$$\nabla^4 F = \frac{\pi^4 E h^2}{a^2 b^2} \sum_{p=0,1}^{\infty} \sum_{q=0,1}^{\infty} c_{pq} \cos \frac{2p\pi}{a} x \cos \frac{2q\pi}{b} y, \quad (15)$$

where c_{pq} are the quadratic functions of a_{mn} and b_{mn}, differing in each case obviously.

A particular solution F_1 of the foregoing equation is given as

$$F_1 = Eh^2 \sum_{p=0,1}^{\infty} \sum_{q=0,1}^{\infty} \varphi_{pq} \cos \frac{2p\pi}{a} x \cos \frac{2q\pi}{b} y, \quad (16)$$

where

$$\varphi_{pq} = \frac{1}{16(p^2 + \beta^2 q^2)^2} \beta^2 c_{pq}, \quad \beta = \frac{a}{b} \quad (17)$$

Letting

$$F_a = -(1/2)\, p_y x^2 + F_1, \quad (18)$$

it will be verified that F_a satisfies Equations (4), (6a), and (7); hence F_a is the stress function corresponding to Case (a).

To obtain the stress function F_b for Case (b), we put

$$F_b = -\frac{1}{2} p_y x^2 + F_1 + F_2 \quad (19)$$

Substitution of this expression in Equations (4), (6b), and (7) yields the following conditions for F_2:

$$\nabla^4 F_2 = 0, \quad (20)$$

[4] In Cases I and II, both symmetric and antisymmetric deflection surfaces with respect to the x-axis are considered.

At $x = \pm a/2$:

$$F_{2,xy} = 0, \quad F_{2,yy} = \frac{4\pi^2}{b^2} \sum_{p=0,\,1}^{\infty} \sum_{q=0,\,1}^{\infty} (-1)^p q^2 \varphi_{pq} \cos \frac{2q\pi}{b} y, \tag{21}$$

At $y = \pm b/2$:

$$\int_0^{\pm b/2} (F_{2,xx} - \nu F_{2,yy}) dy = 0, \quad \int_{-a/2}^{a/2} F_{2,xx} dx = 0, \quad F_{2,xy} = 0 \tag{22}$$

Noting that F_2 should be an even function in x and y, the general solution of Equation (20) can be expressed as

$$F_2 = A_0 x^2 + C_0 y^2 + Eh^2 \sum_{n=1,\,2}^{\infty} \left[\left(A_n \cosh \frac{2n\pi}{a} y + B_n y \sinh \frac{2n\pi}{a} y \right) \cos \frac{2n\pi}{a} x + \left(C_n \cosh \frac{2n\pi}{b} x + D_n x \sinh \frac{2n\pi}{b} x \right) \cos \frac{2n\pi}{b} y \right],$$

where A_n, B_n, C_n, and D_n are unknown constants. Determining these constants by conditions (21) and (22), we are led to

$$F_2 = Eh^2 \sum_{n=1,\,2}^{\infty} E_n \left[(\sinh n\pi\beta + n\pi\beta \cosh n\pi\beta) \cosh \frac{2n\pi}{b} x - \frac{2n\pi}{b} x \sinh n\pi\beta \sinh \frac{2n\pi}{b} x \right] \cos \frac{2n\pi}{b} y, \tag{23}$$

where

$$E_n = (\sinh n\pi\beta \cosh n\pi\beta + n\pi\beta)^{-1} \sum_{m=0,\,1}^{\infty} (-1)^{m+1} \varphi_{mn} \tag{24}$$

To facilitate the calculation hereafter, we expand the foregoing expression in the Fourier series, which gives

$$F_2 = Eh^2 \sum_{p=0,\,1}^{\infty} \sum_{q=0,\,1}^{\infty} \psi_{pq} \cos \frac{2p\pi}{a} x \cos \frac{2q\pi}{b} y, \tag{25}$$

where

$$\psi_{pq} = \frac{4\epsilon_p (-1)^{p+1} q^2 \beta^2}{\pi (p^2 + \beta^2 q^2)^2} \frac{\sinh^2 q\pi\beta}{\sinh q\pi\beta \cosh q\pi\beta + q\pi\beta} \sum_{m=0,\,1}^{\infty} (-1)^m \varphi_{mq}, \tag{26}$$

and where $\epsilon_0 = 1/2$ and $\epsilon_p (p \geq 1) = 1$. Thus the stress function F may be generally expressed as

$$F = -\frac{1}{2} p_y x^2 + Eh^2 \sum_{p=0,\,1}^{\infty} \sum_{q=0,\,1}^{\infty} \Phi_{pq} \cos \frac{2p\pi}{a} x \cos \frac{2q\pi}{b} y, \tag{27}$$

where

$$\Phi_{pq} = \begin{cases} \varphi_{pq} & \text{for Case } (a), \\ \varphi_{pq} + \psi_{pq} & \text{for Case } (b) \end{cases} \tag{28}$$

It will be noted that Φ_{pq} are, as c_{pq}, quadratic functions of a_{mn} and b_{ms}.

For the determination of the unknown coefficients b_{ms} contained in the expressions of w and F, we will apply the Galerkin's method to the remaining equation (5). This leads to the requirement that the following conditions be satisfied by each function $f_r(x)g_s(y)$, in terms of which the deflection w is represented.

$$\int_0^{a/2} \int_0^{b/2} \left\{ \nabla^4 w - \frac{h}{D} [F_{,yy}(w + w_0)_{,xx} + F_{,xx}(w + w_0)_{,yy} - 2F_{,xy}(w + w_0)_{,xy}] \right\} f_r(x) g_s(y) dx dy = 0 \tag{29}$$

Substituting the expressions of w, w_0, and F above obtained and integrating, Equation (29) yields the following general equations in each case:

$$\text{I:} \quad 4s^2\lambda(a_{rs} + b_{rs}) - [3(1 - \nu^2)\beta^2]^{-1}(r^2 + \beta^2 s^2)^2 b_{rs} + \sum_m \sum_n (a_{mn} + b_{mn}) \left[(ms - nr)^2 \left(\Phi_{\frac{m-r}{2}, \frac{n-s}{2}} + \Phi_{\frac{m-r}{2}, \frac{n-s}{2}} + \Phi_{\frac{r-m}{2}, \frac{n-s}{2}} + \Phi_{\frac{r-m}{2}, \frac{s-n}{2}} \pm \Phi_{\frac{m+r}{2}, \frac{n+s}{2}} \right) + (ms + nr)^2 \left(\Phi_{\frac{m+r}{2}, \frac{n-s}{2}} + \Phi_{\frac{m+r}{2}, \frac{s-n}{2}} \pm \Phi_{\frac{m-r}{2}, \frac{n+s}{2}} \pm \Phi_{\frac{r-m}{2}, \frac{n+s}{2}} \right) \right] = 0,$$

$$m, r = 1, 3, 5 \ldots, \quad n, s = \begin{cases} 1, 3, 5 \ldots \text{ for upper signs,} \\ 2, 4, 6 \ldots \text{ for lower signs} \end{cases} \tag{30}$$

$$\text{II:} \quad s^2\lambda \sum_m (a_{ms} + b_{ms})[2(-1)^{m+r} + \delta_{mr}] - [12(1 - \nu^2)\beta^2]^{-1} \sum_m b_{ms}[2(-1)^{m+r}\beta^4 s^4 + (4r^2 + \beta^2 s^2)^2 \delta_{mr}] + \sum_m \sum_n (a_{mn} + b_{mn}) \left[2(-1)^{r+1} m^2 s^2 \left(\Phi_{m, \frac{n-s}{2}} + \Phi_{m, \frac{s-n}{2}} \pm \Phi_{m, \frac{n+s}{2}} \right) + 2(-1)^{m+1} n^2 r^2 \left(\Phi_{r, \frac{n-s}{2}} + \Phi_{r, \frac{s-n}{2}} \pm \Phi_{r, \frac{n+s}{2}} \right) + (ms - nr)^2 \left(\Phi_{m-r, \frac{n-s}{2}} + \Phi_{m-r, \frac{s-n}{2}} + \Phi_{r-m, \frac{n-s}{2}} + \Phi_{r-m, \frac{s-n}{2}} \pm \Phi_{m+r, \frac{n+s}{2}} \right) + (ms + nr)^2 \left(\Phi_{m+r, \frac{n-s}{2}} + \Phi_{m+r, \frac{s-n}{2}} \pm \Phi_{m-r, \frac{n+s}{2}} \pm \Phi_{r-m, \frac{n+s}{2}} \right) \right] = 0,$$

$$m, r = 1, 2, 3 \ldots, \quad n, s = \begin{cases} 1, 3, 5 \ldots \text{ for upper signs,} \\ 2, 4, 6 \ldots \text{ for lower signs} \end{cases} \tag{31}$$

$$\text{III:} \quad 4s^2\lambda(a_{rs} + b_{rs}) - [12(1 - \nu^2)\beta^2]^{-1} \sum_n b_{rn}[2(-1)^{n+s} r^4 + (r^2 + 4\beta^2 s^2)^2 \delta_{ns}] + \sum_m \sum_n (a_{mn} + b_{mn}) \left[2(-1)^{n+1} m^2 s^2 \left(\Phi_{\frac{m-r}{2}, s} + \Phi_{\frac{r-m}{2}, s} + \Phi_{\frac{m+r}{2}, s} \right) + 2(-1)^{s+1} n^2 r^2 \left(\Phi_{\frac{m-r}{2}, n} + \Phi_{\frac{r-m}{2}, n} + \Phi_{\frac{m+r}{2}, n} \right) + (ms - nr)^2 \left(\Phi_{\frac{m-r}{2}, n-s} + \Phi_{\frac{m-r}{2}, s-n} + \Phi_{\frac{r-m}{2}, n-s} + \Phi_{\frac{r-m}{2}, s-n} + \Phi_{\frac{m+r}{2}, n+s} \right) + (ms + nr)^2 \left(\Phi_{\frac{m-r}{2}, n+s} + \Phi_{\frac{r-m}{2}, n+s} + \Phi_{\frac{m+r}{2}, n-s} + \Phi_{\frac{m+r}{2}, s-n} \right) \right] = 0,$$

$$m, r = 1, 3, 5 \ldots, \quad n, s = 1, 2, 3 \ldots. \tag{32}$$

$$\text{IV:}\quad s^2\lambda \sum_m (a_{ms} + b_{ms})[2(-1)^{m+r} + \delta_{mr}]$$
$$- [3(1-\nu^2)\beta^2]^{-1} \sum_m \sum_n b_{mn}[2(-1)^{n+r}r^4\delta_{mr}$$
$$+ 2(-1)^{m+r}\beta^4 s^4\delta_{ns} + (r^2 + \beta^2 s^2)^2\delta_{mr}\delta_{ns}]$$
$$+ \sum_m \sum_n (a_{mn} + b_{mn})\{2(-1)^{n+1}m^2s^2\,[2(-1)^{r+1}\Phi_{m,s} + \Phi_{m+r,s}$$
$$+ \Phi_{m-r,s} + \Phi_{r-m,s}] + 2(-1)^{m+1}n^2r^2[2(-1)^{s+1}\Phi_{r,n} + \Phi_{r,n+s}$$
$$+ \Phi_{r,n-s} + \Phi_{r,s-n}] + 2(-1)^{r+1}m^2s^2(\Phi_{m,n-s} + \Phi_{m,s-n} + \Phi_{m,n+s})$$
$$+ 2(-1)^{s+1}n^2r^2(\Phi_{m-r,n} + \Phi_{r-m,n} + \Phi_{m+r,n})$$
$$+ (ms - nr)^2(\Phi_{m-r,n-s} + \Phi_{m-r,s-n} + \Phi_{r-m,n-s}$$
$$+ \Phi_{r-m,s-n} + \Phi_{m+r,n+s}) + (ms + nr)^2(\Phi_{m+r,n-s}$$
$$+ \Phi_{m+r,s-n} + \Phi_{m-r,n+s} + \Phi_{r-m,n+s})\} = 0,$$
$$m, n, r, s = 1, 2, 3 \ldots \quad (33)$$

In these equations, λ is the nondimensional load factor defined as

$$\lambda = p_y a^2 / \pi^2 E h^2 \quad (34)$$

and δ_{ij} is the Kronecker delta. Further Φ_{ij} is to be taken zero if either i or j is negative.

It will be noted that these equations, in each case, give a set of simultaneous equations involving cubic products of b_{mn}. Solving these equations for each prescribed value of λ, the corresponding deflection and stress functions can be determined, thus the problem is solved.

The present solutions for Cases I(a) and I(b) are ascertained to be mathematically identical with those obtained by Levy [7] and Coan [8], respectively, through somewhat different procedures.

Table 1 Nonzero deflection coefficients in equations (12) for each case

Case	a_{mn}	b_{mn}			
I	a_{11}	b_{11},	b_{13},	b_{31},	b_{33}
II	a_{12}	b_{12},	b_{22},	b_{32},	b_{34}
III	a_{11}	b_{11},	b_{13},	b_{31},	b_{33}
IV	a_{11}	b_{11},	b_{12},	b_{21},	b_{22}

Table 2 Values of deflection coefficients b_{mn} for cases I(a) and I(b): $\nu = 1/3$

Case I(a)					Case I(b)				
λ	b_{11}	$-b_{13}$	$-b_{31}$	b_{33}	λ	b_{11}	$-b_{13}$	$-b_{31}$	b_{33}
		$a_{11} = 0$					$a_{11} = 0$		
0.375	0	0	0	0	0.375	0	0	0	0
0.406	0.5	0.0^{2}130*	0.0^{3}84	0.0^{4}12	0.396	0.5	0.0^{2}127	0.0^{2}135	0.0^{4}76
0.497	1	0.0103	0.0^{3}608	0.0^{3}35	0.457	1	0.0^{3}95	0.0101	0.0^{3}88
0.643	1.5	0.0347	0.0180	0.0^{2}25	0.549	1.5	0.0290	0.0312	0.0^{2}38
0.839	2	0.0829	0.0355	0.0100	0.664	2	0.0612	0.0668	0.0115
1.079	2.5	0.1651	0.0629	0.0298	0.798	2.5	0.1054	0.1169	0.0264
1.364	3	0.294	0.0953	0.0716	0.945	3	0.160	0.180	0.0505
1.703	3.5	0.482	0.127	0.146	1.103	3.5	0.220	0.254	0.0839
					1.273	4	0.283	0.336	0.125
		$a_{11} = 0.1$			1.456	4.5	0.345	0.423	0.172
0	0	0	0	0					
0.213	0.125	0.0^{4}76	0.0^{4}62	0.0^{5}11			$a_{11} = 0.1$		
0.282	0.25	0.0^{3}35	0.0^{3}27	0.0^{3}15	0	0	0	0	0
0.356	0.5	0.0^{2}199	0.0^{2}138	0.0^{2}25	0.212	0.125	0.0^{4}76	0.0^{4}99	0.0^{5}46
0.418	0.75	0.0^{2}595	0.0^{2}378	0.0^{2}15	0.278	0.25	0.0^{3}35	0.0^{3}43	0.0^{4}21
0.487	1	0.0129	0.0^{2}782	0.0^{2}53	0.342	0.5	0.0^{3}193	0.0^{2}224	0.0^{3}13
0.654	1.5	0.0404	0.0211	0.0^{2}331	0.390	0.75	0.0^{2}561	0.0^{2}623	0.0^{2}45
0.865	2	0.0933	0.0414	0.0124	0.438	1	0.0117	0.0131	0.0^{2}115
1.118	2.5	0.182	0.0688	0.0352	0.546	1.5	0.0332	0.0370	0.0^{2}478
1.414	3	0.320	0.102	0.0820	0.672	2	0.0673	0.0755	0.0135
1.767	3.5	0.519	0.132	0.162	0.812	2.5	0.1134	0.1284	0.0301
					0.963	3	0.169	0.194	0.0559
					1.126	3.5	0.230	0.270	0.0908
					1.300	4	0.293	0.353	0.133
					1.486	4.5	0.354	0.442	0.181

* The following abbreviation is used in Tables 2 to 5: 0.0^{2}130 = 0.00130, etc.

Table 3 Values of deflection coefficients b_{mn} for cases II(a) and II(b): $\nu = 1/3$

Case II(a)					Case II(b)				
λ	b_{12}	$-b_{22}$	b_{32}	b_{34}	λ	b_{12}	$-b_{22}$	b_{32}	b_{34}
		$a_{12} = 0$					$a_{12} = 0$		
0.724	0	0	0	0	0.724	0	0	0	0
0.781	0.2	0.0206	0.0^{3}452	0.0^{4}47	0.781	0.2	0.0206	0.0^{3}450	0.0^{4}51
0.951	0.4	0.0566	0.0115	0.0^{3}33	0.949	0.4	0.0569	0.0112	0.0^{3}38
1.235	0.6	0.1213	0.0235	0.0^{3}91	1.231	0.6	0.1228	0.0239	0.0^{3}110
1.646	0.8	0.221	0.0469	0.0^{3}185	1.637	0.8	0.227	0.0488	0.0^{3}242
2.204	1.0	0.350	0.0857	0.0^{3}35	2.189	1.0	0.364	0.0921	0.0^{3}50
		$a_{12} = 0.05$					$a_{12} = 0.05$		
0	0	0	0	0	0	0	0	0	0
0.386	0.05	0.0^{3}439	0.0^{3}103	0.0^{4}46	0.386	0.05	0.0^{3}440	0.0^{3}103	0.0^{4}50
0.524	0.1	0.0^{3}948	0.0^{3}214	0.0^{4}18	0.524	0.1	0.0^{3}949	0.0^{3}214	0.0^{4}20
0.676	0.2	0.0222	0.0^{3}467	0.0^{4}96	0.675	0.2	0.0223	0.0^{3}467	0.0^{4}96
0.800	0.3	0.0398	0.0^{3}784	0.0^{3}23	0.799	0.3	0.0399	0.0^{3}787	0.0^{3}25
0.937	0.4	0.0640	0.0122	0.0^{3}44	0.934	0.4	0.0643	0.0122	0.0^{3}51
1.275	0.6	0.1373	0.0266	0.0^{3}110	1.269	0.6	0.1391	0.0271	0.0^{3}134
1.733	0.8	0.246	0.0536	0.0^{3}22	1.721	0.8	0.252	0.0559	0.0^{3}29
2.335	1.0	0.380	0.0949	0.0^{3}40	2.320	1.0	0.397	0.104	0.0^{3}58

Numerical Solutions

The method of solution outlined in the foregoing will be applied to investigate the postbuckling behavior of square plates. Noticing that a good approximation will be obtained by retaining only a few terms of the deflection function, Equation (12), we will take the nonzero coefficients a_{mn} and b_{mn} as shown in Table 1. In each case, a_{mn} corresponds to the fundamental mode of the deflection and b_{mn} is chosen so as to minimize the buckling load. Thus in Case II, we have chosen the coefficients corresponding to the deflection surface with two half-waves in the y-direction.

In what follows, numerical solutions will be obtained for initially flat plates and plates with initial deflection, the magnitude of which is 0.1 h. Further we assume the value of the Poisson's ratio ν as 1/3.

(a) Evaluation of the Deflection Coefficient. To illustrate the procedure for the determination of the coefficients b_{mn}, we will treat Case I(a); i.e., the case where the plate is simply supported and the side edges are held straight. From Equations (12) to (14) and Table 1, we have

$$w_0 = ha_{11} \cos \frac{\pi}{a} x \cos \frac{\pi}{b} y,$$

$$w = h\left(b_{11} \cos \frac{\pi}{a} x \cos \frac{\pi}{b} y + b_{12} \cos \frac{\pi}{a} x \cos \frac{3\pi}{b} y + b_{21} \cos \frac{3\pi}{a} x \cos \frac{\pi}{b} y + b_{22} \cos \frac{3\pi}{a} x \cos \frac{3\pi}{b} y\right)$$

Substituting these expressions in Equation (4) and noting Equations (15), (17), and (28), the stress coefficients Φ_{rq} for $\beta = 1$ are obtained as

$$\left.\begin{aligned} \Phi_{01} &= -0.03125(2a_{11} + b_{11})b_{11} - 0.0625(a_{11} + b_{11})b_{12} \\ &\quad - 0.28125b_{21}(b_{21} + 2b_{12}), \\ \Phi_{02} &= -0.015625(a_{11} + b_{11})b_{12} - 0.140625b_{21}b_{22}, \\ &\cdot \\ &\cdot \\ &\cdot \\ &\text{etc.} \end{aligned}\right\}$$

Table 4 Values of deflection coefficients b_{mn} for cases III(a) and III(b): $\nu = 1/3$

		Case III(a)					Case III(b)		
λ	b_{11}	b_{12}	$-b_{21}$	$-b_{22}$	λ	b_{11}	b_{12}	$-b_{21}$	b_{22}
		$a_{11} = 0$					$a_{11} = 0$		
0.632	0	0	0	0	0.632	0	0	0	0
0.666	0.25	$0.0^{2}269$	$0.0^{2}927$	$0.0^{3}103$	0.661	0.25	$0.0^{2}240$	$0.0^{3}118$	$-0.0^{3}38$
0.765	0.5	$0.0^{2}536$	$0.0^{2}659$	$0.0^{2}743$	0.740	0.5	$0.0^{2}301$	$0.0^{3}861$	$-0.0^{3}158$
0.925	0.75	$0.0^{2}878$	0.0187	$0.0^{2}215$	0.860	0.75	$0.0^{2}53$	0.0252	$0.0^{3}15$
1.143	1	0.0147	0.0365	$0.0^{3}442$	1.013	1	$-0.0^{2}642$	0.0506	$0.0^{2}219$
1.419	1.25	0.0265	0.0590	$0.0^{2}815$	1.192	1.25	−0.0201	0.0822	$0.0^{2}803$
1.755	1.5	0.0545	0.0841	0.0144	1.392	1.5	−0.0449	0.1170	0.0206
					1.610	1.75	−0.0849	0.1525	0.0429
		$a_{11} = 0.05$			1.843	2	−0.142	0.185	0.0774
0	0	0	0	0			$a_{11} = 0.05$		
0.357	0.0625	$0.0^{3}537$	$0.0^{4}65$	$0.0^{5}6$					
0.467	0.125	$0.0^{3}115$	$0.0^{3}286$	$0.0^{4}28$	0	0	0	0	0
0.574	0.25	$0.0^{2}242$	$0.0^{3}148$	$0.0^{3}136$	0.356	0.0625	$0.0^{3}521$	$0.0^{4}84$	$-0.0^{4}15$
0.654	0.375	$0.0^{3}370$	$0.0^{3}409$	$0.0^{3}431$	0.465	0.125	$0.0^{3}108$	$0.0^{3}366$	$-0.0^{4}84$
0.734	0.5	$0.0^{3}504$	$0.0^{3}832$	$0.0^{3}894$	0.566	0.25	$0.0^{3}198$	$0.0^{3}192$	$-0.0^{4}45$
0.924	0.75	$0.0^{2}868$	0.0216	$0.0^{2}242$	0.636	0.375	$0.0^{2}239$	$0.0^{3}532$	$-0.0^{3}101$
1.163	1	0.0151	0.0403	$0.0^{3}481$	0.703	0.5	$0.0^{2}213$	0.0110	$-0.0^{3}12$
1.456	1.25	0.0279	0.0627	$0.0^{3}847$	0.849	0.75	$-0.0^{3}105$	0.0288	$0.0^{3}58$
1.806	1.5	0.0564	0.0889	0.0153	1.016	1	$-0.0^{2}885$	0.0562	$0.0^{3}300$
					1.205	1.25	−0.0241	0.0887	$0.0^{3}989$
					1.413	1.5	−0.0508	0.1242	0.0239
					1.638	1.75	−0.0938	0.1589	0.0485
					1.876	2	−0.153	0.191	0.0850

Table 5 Values of deflection coefficients b_{mn} for cases IV(a) and IV(b): $\nu = 1/3$

		Case IV(a)					Case IV(b)		
λ	b_{11}	b_{12}	$-b_{21}$	$-b_{22}$	λ	b_{11}	b_{12}	$-b_{21}$	$-b_{22}$
		$a_{11} = 0$					$a_{11} = 0$		
0.956	0	0	0	0	0.956	0	0	0	0
1.009	0.125	$0.0^{3}805$	$0.0^{3}962$	$0.0^{2}209$	1.006	0.125	$0.0^{3}792$	$0.0^{3}961$	$0.0^{2}200$
1.162	0.25	0.0165	0.0241	$0.0^{3}520$	1.150	0.25	0.0153	0.0239	$0.0^{3}458$
1.417	0.375	0.0277	0.0469	0.0103	1.383	0.375	0.0224	0.0461	$0.0^{3}772$
1.585	0.4375	0.0364	0.0619	0.0141	1.702	0.5	0.0300	0.0768	0.0105
1.783	0.5	0.0506	0.0805	0.0198	1.891	0.5625	0.0339	0.0947	0.0112
2.036	0.5625	0.0827	0.1050	0.0307	2.098	0.625	0.0366	0.1135	0.0100
		$a_{11} = 0.025$					$a_{11} = 0.025$		
0	0	0	0	0	0	0	0	0	0
0.554	0.03125	$0.0^{2}132$	$0.0^{2}212$	$0.0^{3}36$	0.554	0.03125	$0.0^{3}132$	$0.0^{2}212$	$0.0^{3}35$
0.719	0.0625	$0.0^{3}300$	$0.0^{3}447$	$0.0^{3}82$	0.718	0.0625	$0.0^{2}298$	$0.0^{3}446$	$0.0^{3}80$
0.879	0.125	$0.0^{3}667$	$0.0^{3}994$	$0.0^{2}192$	0.874	0.125	$0.0^{3}650$	$0.0^{3}990$	$0.0^{2}182$
0.999	0.1875	0.0106	0.0169	$0.0^{3}333$	0.989	0.1875	$0.0^{3}998$	0.0168	$0.0^{2}299$
1.122	0.25	0.0147	0.0257	$0.0^{3}513$	1.105	0.25	0.0133	0.0254	$0.0^{3}433$
1.422	0.375	0.0255	0.0502	0.0105	1.381	0.375	0.0196	0.0491	$0.0^{3}722$
1.822	0.5	0.0497	0.0857	0.0206	1.726	0.5	0.0255	0.0808	$0.0^{3}912$
2.096	0.5625	0.0848	0.1116	0.0324	1.925	0.5625	0.0276	0.0988	$0.0^{3}861$
					2.134	0.625	0.0263	0.1167	$0.0^{3}544$

Letting $r = s = 1$ in Equations (30) and recalling that $\nu = 1/3$, it follows

$$4\lambda(a_{11} + b_{11}) - 1.5b_{11} + 8(a_{11} + b_{11})(\Phi_{01} + \Phi_{10}) + 4b_{12}(2\Phi_{01} + 8\Phi_{02} + 4\Phi_{11} + \Phi_{12}) + 4b_{21}(2\Phi_{10} + 4\Phi_{11} + 8\Phi_{20} + \Phi_{21}) + 36b_{33}(\Phi_{12} + \Phi_{21}) = 0,$$

and substitution of Φ_{pq} in the foregoing gives

$$4\lambda(a_{11} + b_{11}) - 1.5b_{11} - 0.5(3a_{11} + b_{11})b_{11}^2 - 0.5a_{11}^2(2b_{11} + b_{13} + b_{31}) - 0.75b_{11}(2a_{11} + b_{11})(b_{12} + b_{31}) - 4.26(a_{11} + b_{11})(b_{12}^2 + b_{31}^2) - 2(a_{11} + b_{11})b_{13}b_{31} - 4.68b_{33}(a_{11} + b_{11})(b_{13} + b_{31}) - 1.62(a_{11} + b_{11})b_{33}^2 - 6.5b_{13}b_{31}(b_{13} + b_{31}) - 22.5b_{12}b_{31}b_{33} = 0$$

Similar equations can be obtained by taking $rs = 13$, 31, and 33, respectively. The method of obtaining a solution of this set of cubic equations consists in assuming values of b_{11} and determining by successive approximation from their respective equations the corresponding values of λ, b_{13}, b_{31}, and b_{33}.

Other cases can be treated in the same manner. The results are shown in Tables 2, 3, 4, and 5. Observing that, in each case, the fourth coefficient is much smaller than the others, fairly good approximation will be expected in the following calculations.

Critical values of λ corresponding to the buckling loads for flat square plates are obtained by letting $a_{mn} = 0$ and $b_{mn} \to 0$ in the cubic equations and by solving the resulting set of linear equations. The results are shown in Table 6, together with the exact ones. It will be seen that the approximation is satisfactorily good.

(b) Relation Between Load and Maximum Deflection. Denoting by w_m the maximum net deflection, it is easy to see that

$$\frac{w_m}{h} = \begin{cases} b_{11} + b_{13} + b_{31} + b_{33} & \text{for Case I,} \\ 2(b_{12} + b_{32} - b_{16}) & \text{for Case II,} \\ 2(b_{11} + b_{31}) & \text{for Case III,} \\ 4b_{11} & \text{for Case IV} \end{cases} \tag{35}$$

Substituting the values of b_{mn} given above, the relations between λ and w_m/h are obtained with the results shown in Figs. 2 and 3. In the figures hereafter, including these, full lines correspond to the initially flat plates and dotted lines to the plates with initial deflection, the magnitude of which is 0.1 h.

From these figures, the following may be observed:

1 The deflection for Case (a) is always smaller than the corresponding one for Case (b). This seems to be due to the fact that for Case (a), tensile stresses act along the central portion of the side edges to constrain them straight.

2 For Case II, the effect of the edge constraint discussed in the foregoing is very small, but it is to be recalled that in this case the plate buckles in two half-waves in the y-direction.

3 Under loads much greater than the criticals, the net deflection for the initially deflected plate is smaller than that for the initially flat plate. But it should be noted that the total deflection $w_m + 0.1\,h$ of the former is always larger than that of the latter.

4 The inflection point of the load-deflection curve for the initially deflected plate almost corresponds to the critical load.

Levy [7] calculated the deflection of an initially flat square plate for Case I(a), assuming that the Poisson's ratio ν is 0.316 and taking the six coefficients b_{11}, b_{13}, b_{31}, b_{33}, b_{15}, and b_{51} different from zero. His results are shown in Fig. 2. It is seen that both the results agree within about 1 per cent. Noticing the slight difference in the value of ν, this seems to prove the accuracy of the present solution. Assuming the same value for ν, Coan [8] obtained the solutions for Case I(b) when $a_{11} = 0$ and 0.1 by using the three nonzero coefficients b_{11}, b_{13}, and b_{31}. His results are plotted in Fig. 3. The deviations appreciable at large deflections are examined to be due to the neglect of the fourth coefficient b_{33}.

Table 6 Critical values of λ in equation (34): $\nu = 1/3$

Case	Approx.	Exact	Error, per cent
I	0.3750	0.3750[a]	0
II	0.7242	0.7206[b]	+0.5
III	0.6323	0.6322[c]	+0.02
IV	0.9559	0.9444[d]	+1.2

[a,b,c] See reference [9a, b, c], respectively.
[d] See reference [10].

(c) Relation Between Load and Edge Shortening. As given in Equations (7), the displacements v along the loaded edges are

$$[v]_{y=\pm\frac{b}{2}} = \int_0^{\pm b/2} \left[\frac{1}{E}(F_{,xx} - \nu F_{,yy}) - \frac{1}{2}w_{,y}^2 - w_{0,y}w_{,y} \right] dy$$

Substituting the general expressions of w, w_0, and F, and integrating, we obtain the following formulas for v at $y = \pm b/2$ in each case:

$$\text{I:} \quad \mp\left[\frac{p_y b}{2E} + \frac{\pi^2 h^2}{16b} \sum_{m=1,3}^{\infty} \sum_{\substack{n=1,3 \\ \text{or } 2,4}}^{\infty} n^2(2a_{mn} + b_{mn})b_{mn} \right],$$

$$\text{II:} \quad \mp\left\{ \frac{p_y b}{2E} + \frac{\pi^2 h^2}{16b} \sum_{m=1,2}^{\infty} \sum_{r=1,2}^{\infty} \sum_{\substack{n=1,3 \\ \text{or } 2,4}}^{\infty} n^2(2a_{mn} + b_{mn})b_{rn}[2(-1)^{m+r} + \delta_{mr}] \right\}, \tag{36}$$

$$\text{III:} \quad \mp\left[\frac{p_y b}{2E} + \frac{\pi^2 h^2}{4b} \sum_{m=1,3}^{\infty} \sum_{n=1,2}^{\infty} n^2(2a_{mn} + b_{mn})b_{mn} \right],$$

$$\text{IV:} \quad \mp\left\{ \frac{p_y b}{2E} + \frac{\pi^2 h^2}{4b} \sum_{m=1,2}^{\infty} \sum_{r=1,2}^{\infty} \sum_{n=1,2}^{\infty} n^2(2a_{mn} + b_{mn})b_{rn}[2(-1)^{m+r} + \delta_{mr}] \right\}$$

These check the uniform displacement along the loaded edges. Denoting by δ_y the edge shortening in the y-direction and recalling the Definition (34), it will be seen that $\delta_y b/\pi^2 h^2$ in each case becomes

$$\text{I:} \quad \lambda + (1/8)(2a_{11}b_{11} + b_{11}^2 + 9b_{13}^2 + b_{31}^2 + 9b_{33}^2),$$

$$\text{II:} \quad \lambda + a_{12}(3b_{12} - 2b_{22} + 2b_{32}) + 1.5(b_{12}^2 + b_{22}^2 + b_{32}^2 + 9b_{16}^2) - 2(b_{12}b_{22} - b_{12}b_{32} + b_{22}b_{32}), \tag{37}$$

$$\text{III:} \quad \lambda + a_{11}b_{11} + 0.5(b_{11}^2 + b_{31}^2) + 2(b_{12}^2 + b_{32}^2),$$

$$\text{IV:} \quad \lambda + a_{11}(3b_{11} - 2b_{21}) + 1.5(b_{11}^2 + b_{21}^2) + 6(b_{12}^2 + b_{22}^2) - 2b_{11}b_{21} - 8b_{12}b_{22}$$

The relations between λ and $\delta_y b/h^2$ are shown in Figs. 4 and 5. For the initially flat plate, the curve consists of two parts joining at the buckling load. The first straight line obviously corresponds to the simple compression and the second line represents the increase of shortening due to deflection. The apparent

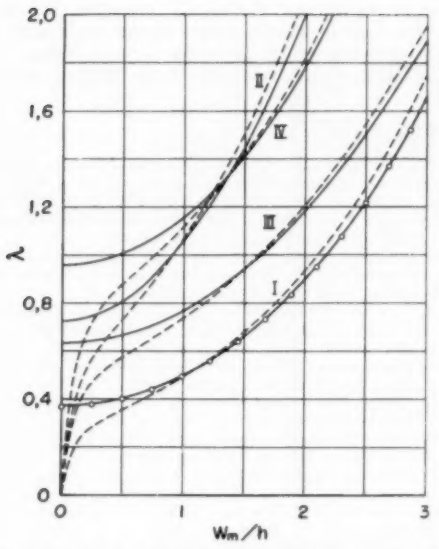

Fig. 2 Relation between load and maximum deflection for Case (a): $\nu = 1/3$ (O denotes the Levy results obtained for Case I(a) with $\alpha_{11} = 0$, $\nu = 0.316$)

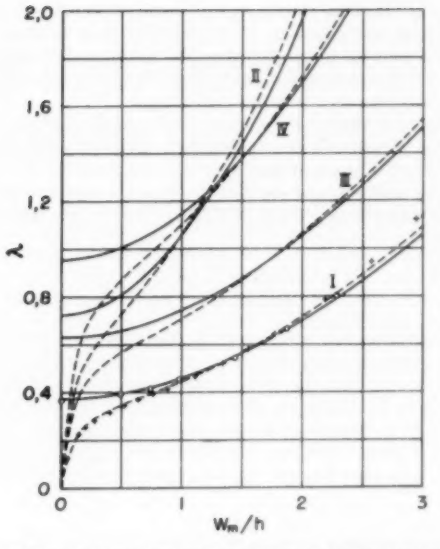

Fig. 3 Relation between load and maximum deflection for Case (b): $\nu = 1/3$ (O and + denote the Coan results obtained for Case I(b) with $\alpha_{11} = 0$ and 0.1, respectively; $\nu = 0.316$)

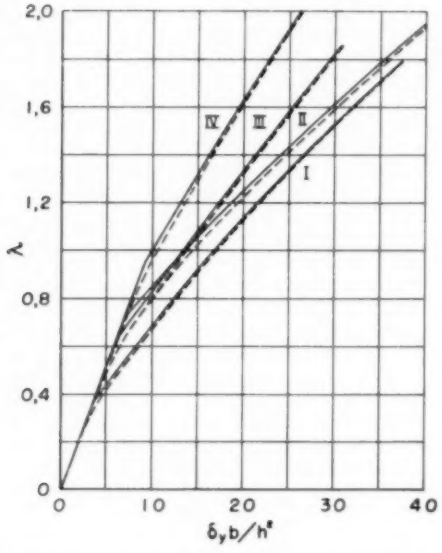

Fig. 4 Relation between load and edge shortening for Case (a)

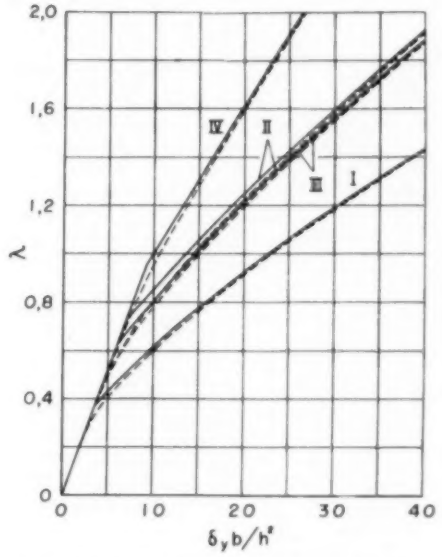

Fig. 5 Relation between load and edge shortening for Case (b)

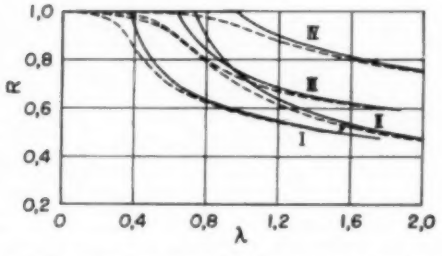

Fig. 6 Relation between load and effective width for Case (a)

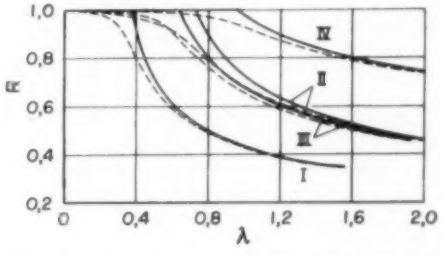

Fig. 7 Relation between load and effective width for Case (b)

rigidity of the plate after buckling is seen to be 0.4 to 0.6 times the original one, according to the various edge constraints. It is also seen that the initial deflection has the effect of reducing the rigidity of the plate and that the plate with undistorted edges is more rigid than that with stress-free edges.

(d) Effective Width. The ratio of the effective width to the initial width will be defined as the ratio of the actual load carried by the plate to the load the plate would have carried if the stress had been uniform, and equal to the Young's modulus times the average edge strain. Hence denoting by R the ratio stated above, we have

$$R = \frac{p_y}{E(\delta_y/b)} = \frac{\lambda}{(\delta_y b/\pi^2 h^2)\beta^2} \tag{38}$$

Using the preceding results for δ_y, the relations between λ and R are easily obtained with the results shown in Figs. 6 and 7. It will be seen that the effect of the assumed initial deflection is remarkable in the vicinity of the critical load, and that the effective width in case of a clamped plate is much greater than those for other cases. Further, it is ascertained that the results here obtained for Case I(a) are in good agreement with those obtained by Levy [7].

Acknowledgment

The author wishes to express his hearty thanks to Professor Emeritus S. Higuchi and Professor F. Numachi, Tōhoku University, for their invaluable advice during the course of the present work. The author also wishes to acknowledge a grant for science research given by the Education Ministry of Japan.

References

1 Th. von Karman, "Festigkeitsprobleme im Maschinenbau," *Encyklopädie der Mathematischen Wissenschaften*, vol. 4, 1910, p. 349.

2 K. Marguerre, "Zur Theorie der gekrümmten Platte grosser Formänderung," Proceedings of the Fifth International Congress for Applied Mechanics, Cambridge, 1938, pp. 93–101.

3 G. Schnadel, "Die Überschreitung der Knickgrenze bei dünnen Platten," Proceedings of the Third International Congress for Applied Mechanics, Stockholm, vol. 3, 1930 , pp. 73–81.

4 H. L. Cox, "The Buckling of Thin Plates in Compression," Technical Report of the Aeronautical Committee, 1933–1934, pp 443–463.

5 S. Timoshenko, "Theory of Elastic Stability," McGraw-Hill Book Co., Inc., New York, N. Y., 1936, p. 390.

6 K. Marguerre, "Die mittragende Breite der gedrückten Platte," *Luftfahrtforschung*, vol. 14, 1937, pp. 121–128.

7 S. Levy, "Bending of Rectangular Plates with Large Deflections," NACA Report No. 737, 1942, pp. 139–157.

8 J. M. Coan, "Large Deflection Theory for Plates with Small Initial Curvature Loaded in Edge Compression," JOURNAL OF APPLIED MECHANICS, vol. 18, TRANS. ASME, vol. 73, 1951, pp. 143–151.

9 Reference 5, (a) p. 332; (b) p. 345; (c) p. 364.

10 S. Levy, "Buckling of Rectangular Plates with Built-In Edges," JOURNAL OF APPLIED MECHANICS, vol. 9, TRANS. ASME, vol. 64, 1942, pp. 171–174.

A New Theory of Elastic Sandwich Plates—One-Dimensional Case[1]

YI-YUAN YU

Professor,
Department of Mechanical Engineering,
Polytechnic Institute of Brooklyn,
Brooklyn, N. Y.
Assoc. Mem. ASME

A new flexural theory of isotropic elastic sandwich plates is deduced from the theory of elasticity. The one-dimensional case is presented in this paper. The theory includes the effects of transverse-shear deformation and rotatory inertia in both the core and faces of the sandwich, and no limitation is imposed upon the magnitudes of the ratios between the thicknesses, material densities, and elastic constants of the core and faces of the sandwich. The method used is an extension of one due to Mindlin [1],[2] and the results reduce to those of his for the corresponding homogeneous plates as special limiting cases. A final equation also may be simplified and reduced to the corresponding results of Reissner [2], Hoff [3], and Eringen [4] for the bending of ordinary sandwich plates that have thin faces. Results of the theory are applied to the problem of bending of a cantilever plate subjected to load at the unsupported end and to the problem of propagation of straight-crested waves in an infinite plate.

Sandwich plates have been studied by many authors. The type of sandwich construction investigated consists of comparatively thin faces covering a thick core, the material of the faces being much heavier and more rigid than that of the core. Thus, in an investigation carried out by Reissner [2], the faces were taken to be membranes, although the transverse-shear deformation in the core was taken care of. Hoff [3] later considered also the flexural rigidity of the faces, and Eringen [4] further included in his investigation the flexural rigidity of the core, but the transverse-shear deformation in the faces has never been taken into consideration in the sandwich-plate problem by any previous author. Then, the investigation has been limited to the bending and buckling of such plates; no publication on the vibration of sandwich plates is known to be available.

In this paper an exploratory study aiming to attack the vibration problem of sandwich plates is carried out, for the one-dimensional plane-strain case. Guided by our knowledge on the vibration of homogeneous plates [5], we shall consider the effects of transverse-shear deformation and rotatory inertia in both the core and the faces. Besides, we shall impose no restriction on the magnitude of the ratios between the thicknesses, material densities, and elastic constants of the core and faces. The treatment is therefore more inclusive than any others that could be effected by adapting the existing bending theories of sandwich plates to the vibration study. Inversely, a new set of equilibrium equations is obtained as a by-product, which is more complete than and reducible to previous bending equations such as those given by Reissner, Hoff, and Eringen. The method of approach used here is an extension of one employed by Mindlin [1] in a systematic treatment of the vibration of homogeneous plates, and the results for the sandwich plates reduce to those of his for the homogeneous plates as special limiting cases. To illustrate the use of the results of the present theory, two problems are solved in this paper; namely, the problem of bending of a cantilever plate subjected to loading at the unsupported end, and the problem of propagation of straight-crested waves in an infinite plate.

Stress Equations of Motion

We consider the sandwich plate the cross section of which is shown in Fig. 1. The section lies in the xz-plane; and, since our discussion will be restricted to the plane-strain case, only a unit length of the plate in the y-direction need be taken. As shown in Fig. 1, the two faces of the sandwich have the same dimensions; they are also of the same material.

The variational equations of motion in the theory of elasticity yield for the plane-strain case

$$\int_V \left(\frac{\partial \sigma_x}{\partial x} + \frac{\partial \tau_{xz}}{\partial z} - \rho \frac{\partial^2 u}{\partial t^2} \right) \delta u \, dV = 0 \tag{1}$$

$$\int_V \left(\frac{\partial \tau_{xz}}{\partial x} + \frac{\partial \sigma_z}{\partial z} - \rho \frac{\partial^2 w}{\partial t^2} \right) \delta w \, dV = 0 \tag{2}$$

where the integrals are to be taken over the volume of the body under consideration. These equations will now be applied to the core and faces of the sandwich plate, each of the three layers being bounded by two end sections ($x = 0$ and $x = l$), two plane surfaces

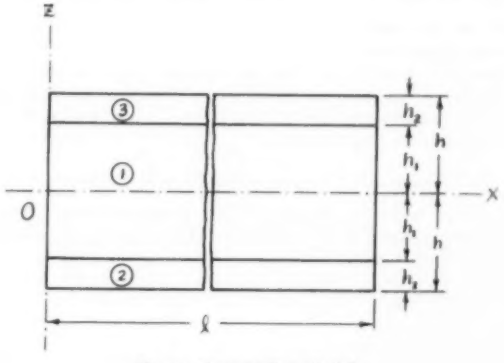

Fig. 1 Cross section of plate

[1] This research was supported in part by the United States Air Force under Contract No. AF49(638)-453 monitored by the Air Force Office of Scientific Research of the Air Research and Development Command.

[2] Numbers in brackets designate References at end of paper.

Presented at the Summer Conference of the Applied Mechanics Division, Troy, N. Y., June 18–20, 1959, of The American Society of Mechanical Engineers.

Discussion of this paper should be addressed to the Secretary, ASME, 29 West 39th Street, New York, N. Y., and will be accepted until October 10, 1959, for publication at a later date. Discussion received after the closing date will be returned.

Note: Statements and opinions advanced in papers are to be understood as individual expressions of their authors and not those of the Society. Manuscript received by ASME Applied Mechanics Division, March 28, 1958. Paper No. 59-APM-23.

at the top and bottom (z = const), and two planes parallel to the xz-plane at a unit distance apart.

Consider, first, Equation (1). The various quantities, in general, will be different for the core, the lower face, and the upper face, which will be distinguished from each other by the subscripts 1, 2, and 3, respectively. The displacements in the x-direction in the three layers are assumed in the form

$$\begin{aligned} u_1(x,z,t) &= zu_1^{(1)}(x,t) \\ u_2(x,z,t) &= u_2^{(0)}(x,t) + zu_2^{(1)}(x,t) \\ u_3(x,z,t) &= u_3^{(0)}(x,t) + zu_3^{(1)}(x,t) \end{aligned} \tag{3}$$

where the superscripts in parentheses are used to indicate the order of the displacement components in the manner of Mindlin [1]. With the displacements chosen in this form, it will be seen to be possible to maintain their continuity at the interfaces between the core and the faces; also, the effects of transverse-shear deformation and rotatory inertia may thereby be included in both the core and the faces. Equations (3) are now substituted in (1) for the various layers. After integrating with respect to z and putting to zero the coefficients of the variations of the displacement components in the integrand, we find

$$M_{x1}' - Q_{x1} + [z\tau_{xz1}]_{-h_1}^{h_1} - \rho_1 \frac{2h_1^3}{3} \ddot{u}_1^{(1)} = 0 \tag{4}$$

$$M_{x2}' - Q_{x2} + [z\tau_{xz2}]_{-h}^{-h_1} - \rho_2 \frac{h_1^2 - h^2}{2} \ddot{u}_2^{(0)} - \rho_2 \frac{h^3 - h_1^3}{3} \ddot{u}_2^{(1)} = 0 \tag{5}$$

$$M_{x3}' - Q_{x3} + [z\tau_{xz3}]_{h_1}^{h} - \rho_3 \frac{h^2 - h_1^2}{2} \ddot{u}_3^{(0)} - \rho_3 \frac{h^3 - h_1^3}{3} \ddot{u}_3^{(1)} = 0 \tag{6}$$

$$N_{x1}' + [\tau_{xz2}]_{-h}^{-h_1} - \rho_2 h_2 \ddot{u}_2^{(0)} - \rho_2 \frac{h_1^2 - h^2}{2} \ddot{u}_2^{(1)} = 0 \tag{7}$$

$$N_{x3}' + [\tau_{xz3}]_{h_1}^{h} - \rho_3 h_3 \ddot{u}_3^{(0)} - \rho_3 \frac{h^2 - h_1^2}{2} \ddot{u}_3^{(1)} = 0 \tag{8}$$

where we have introduced the following plate-stress components:

$$\begin{aligned} M_{x1} &= \int_{-h_1}^{h_1} \sigma_{x1} z dz, \quad M_{x2} = \int_{-h}^{-h_1} \sigma_{x2} z dz, \quad M_{x3} = \int_{h_1}^{h} \sigma_{x3} z dz \\ N_{x2} &= \int_{-h}^{-h_1} \sigma_{x2} dz, \quad N_{x3} = \int_{h_1}^{h} \sigma_{x3} dz \\ Q_{x1} &= \int_{-h_1}^{h_1} \tau_{xz1} dz, \quad Q_{x2} = \int_{-h}^{-h_1} \tau_{xz2} dz, \quad Q_{x3} = \int_{h_1}^{h} \tau_{xz3} dz \end{aligned} \tag{9}$$

which are the usual bending moments, forces in the plane, and shearing forces, respectively.

Equations (4) to (8) are valid for the individual core and faces of the plate. In the composite plate, however, the shearing stress τ_{xzi} must be the same for the faces and the core at the interfaces between them, namely,

$$(\tau_{xz1})_{z=-h_1} = (\tau_{xz2})_{z=-h_1}, \quad (\tau_{xz1})_{z=h_1} = (\tau_{xz3})_{z=h_1}$$

which may hence be eliminated from these equations. Thus, adding Equations (4), (5), and (6) and noting that $\rho_2 = \rho_3$ for the identical faces, we find

$$M_x' - Q_x + hp_x = \rho_1 \frac{2h_1^3}{3} \ddot{u}_1^{(1)} + \rho_2 \frac{h^2 - h_1^2}{2} (\ddot{u}_2^{(0)} - \ddot{u}_3^{(0)}) + \rho_2 \frac{h^3 - h_1^3}{3} (\ddot{u}_3^{(1)} + \ddot{u}_2^{(1)}) \tag{10}$$

where

$$M_x = M_{x1} + M_{x2} + M_{x3}$$

$$Q_x = Q_{x1} + Q_{x2} + Q_{x3}$$

are the resultant bending moment and shearing force for the sandwich plate, and

$$p_x = (\tau_{xz2})_{z=-h} + (\tau_{xz3})_{z=h}$$

is given by the surface traction in the x-direction acting on the top and bottom surfaces of the sandwich plate. Similarly, adding to Equation (4) the difference between Equations (8) and (7) first multiplied by h_1, we obtain

$$M_{x1}' - Q_{x1} + h_1(N_{x3}' - N_{x2}') + h_1 p_x = \rho_1 \frac{2h_1^3}{3} \ddot{u}_1^{(1)} + \rho_2 h_1 \frac{h^2 - h_1^2}{2} (\ddot{u}_3^{(1)} + \ddot{u}_2^{(1)}) + \rho_2 h_1 h_2 (\ddot{u}_3^{(0)} - \ddot{u}_2^{(0)}) \tag{11}$$

In an entirely similar but simpler manner, Equation (2) is made use of in the derivation of another stress equation of motion for the sandwich plate. It is now sufficient to assume for the three layers of the plate

$$w_i(z,x,t) = w_i^{(0)}(x,t) \tag{12}$$

where the subscript i takes in turn the values 1, 2, and 3, as will also be used hereafter throughout this paper. Since continuity in the normal stresses at the interfaces requires that

$$(\sigma_{z1})_{z=-h_1} = (\sigma_{z2})_{z=-h_1}, \quad (\sigma_{z1})_{z=h_1} = (\sigma_{z3})_{z=h_1}$$

the equations derived from Equation (2) for the individual layers may be added to yield for the composite plate

$$Q_x' + p_z = 2\rho_1 h_1 \ddot{w}_1^{(0)} + \rho_2 h_2 w_2^{(0)} + \rho_3 h_3 \ddot{w}_3^{(0)} \tag{13}$$

where

$$p_z = (\sigma_{z3})_{z=h} - (\sigma_{z2})_{z=-h}$$

represents the resultant surface traction in the z-direction acting on the top and bottom surfaces of the sandwich plate.

We add here that further refinement of the theory of the sandwich plate may be made by including higher-order components in the displacement expressions in Equations (3) and (12), as was done by Mindlin [1] in the case of homogeneous plates. For instance, compression of the layers in the thickness direction may be included by introducing in Equation (12) additional first-order terms.

Displacements, Strains, and Stresses

The displacements in the core and faces are now written in the following form:

$$\begin{aligned} u_1 &= z\psi_1 \\ u_2 &= -h_1(\psi_1 - \psi_2) + z\psi_2 \\ u_3 &= h_1(\psi_1 - \psi_2) + z\psi_2 \\ v_i &= 0 \\ w_i &= w \end{aligned} \tag{14}$$

that is, the nonzero displacement components are

$$\begin{aligned} u_1^{(1)} &= \psi_1 \\ u_2^{(1)} &= u_3^{(1)} = \psi_2 \\ u_2^{(0)} &= -u_3^{(0)} = -h_1(\psi_1 - \psi_2) \\ w_i^{(0)} &= w \end{aligned} \tag{15}$$

In these expressions, w is the transverse deflection of the plate, assumed to be constant for each cross section (x = const), and ψ_1 and ψ_2 are the changes of slope of the normal to the middle plane of the plate in the core and faces, respectively. The quantities w, ψ_1, and ψ_2 will be referred to as the plate displacements. It may now be seen that the displacements are continuous at the interfaces between the core and faces of the plate, as was pointed out before.

It follows from Equations (14) that the strains are

$$\begin{aligned} \epsilon_{z1} &= z\psi_1' \\ \epsilon_{z2} &= -h_1(\psi_1' - \psi_2') + z\psi_2' \\ \epsilon_{z3} &= h_1(\psi_1' - \psi_2') + z\psi_2' \end{aligned} \tag{16}$$

$$\begin{aligned} \gamma_{xz1} &= \psi_1 + w' \\ \gamma_{xz2} &= \gamma_{xz3} = \psi_2 + w' \end{aligned}$$

$$\epsilon_{yi} = \epsilon_{zi} = \gamma_{xyi} = \gamma_{yzi} = 0 \tag{17}$$

Since the strains in Equations (16) are related to their components by

$$\epsilon_{xi} = \epsilon_i^{(0)} + z\epsilon_i^{(1)}, \quad \gamma_{xzi} = \gamma_i^{(0)} \tag{18}$$

the strain components are

$$\begin{aligned} &\epsilon_1^{(0)} = 0, \quad \epsilon_2^{(0)} = -\epsilon_3^{(0)} = -h_1(\psi_1' - \psi_2') \\ &\epsilon_1^{(1)} = \psi_1', \quad \epsilon_2^{(1)} = \epsilon_3^{(1)} = \psi_2' \\ &\gamma_1^{(0)} = \psi_1 + w', \quad \gamma_2^{(0)} = \gamma_3^{(0)} = \psi_2 + w' \end{aligned} \tag{19}$$

where, as in the case of the displacement components, the superscripts refer to the order of the strain components.

It is now observed that $\epsilon_{zi} = 0$ in Equations (17) would lead to an unrealistic and undesirable situation, for it implies that no strain of any kind is permitted to develop in the thickness direction of the plate. The following expression of ϵ_{zi} will simulate the true situation more appropriately:

$$\epsilon_{zi} = \epsilon_{zi}^{(0)} + z\epsilon_{zi}^{(1)} \tag{20}$$

where the zero-order term represents the type of strain that occurs in the thickness direction when the plate is under extension in its plane, and the first-order term is associated with flexure of the plate, both reflecting Poisson's effect. To be consistent with the assumed form of the displacement w_i in Equations (14), however, the presence of $\epsilon_{zi}^{(0)}$ and $\epsilon_{zi}^{(1)}$ is made implicit in the manner described in the following.

According to Hooke's law, the following stresses correspond to the strains in Equations (18) and (20):

$$\sigma_{xi} = (\lambda_i + 2\mu_i)(\epsilon_i^{(0)} + z\epsilon_i^{(1)}) + \lambda_i(\epsilon_{zi}^{(0)} + z\epsilon_{zi}^{(1)}) \tag{21}$$

$$\sigma_{zi} = (\lambda_i + 2\mu_i)(\epsilon_{zi}^{(0)} + z\epsilon_{zi}^{(1)}) + \lambda_i(\epsilon_i^{(0)} + z\epsilon_i^{(1)}) \tag{22}$$

$$\tau_{xzi} = \mu_i\gamma_i^{(0)} \tag{23}$$

where λ_i and μ_i are Lamé's constants. To these we could add σ_{yi}, which is also nonzero but will not concern us in the present discussion of the one-dimensional case. The stresses σ_{xi} and τ_{xzi} in Equations (21) and (23) are next integrated in accordance with Equations (9), to yield the plate-stresses:

$$\left.\begin{aligned} M_{xi} &= \int_{a_i}^{b} \sigma_{xi} z\,dz = \frac{b_i^2 - a_i^2}{2}[(\lambda_i + 2\mu_i)\epsilon_i^{(0)} + \lambda_i\epsilon_{zi}^{(0)}] + \frac{b_i^3 - a_i^3}{3}[(\lambda_i + 2\mu_i)\epsilon_i^{(1)} + \lambda_i\epsilon_{zi}^{(1)}] \\ N_{xi} &= \int_{a_i}^{b_i} \sigma_{xi}\,dz = (b_i - a_i)[(\lambda_i + 2\mu_i)\epsilon_i^{(0)} + \lambda_i\epsilon_{zi}^{(0)}] + \frac{b_i^2 - a_i^2}{2}[(\lambda_i + 2\mu_i)\epsilon_i^{(1)} + \lambda_i\epsilon_{zi}^{(1)}] \\ Q_{xi} &= \int_{a_i}^{b} \tau_{xzi}\,dz = (b_i - a_i)\,\mu_i\gamma_i^{(0)} \end{aligned}\right\} \tag{24}$$

where a_i and b_i are the lower and upper limits of the z-value of the respective layers. The stress σ_{zi} in Equation (22) may similarly be integrated as follows:

$$\begin{aligned} \int_{a_i}^{b_i} \sigma_{zi} z\,dz &= \frac{b_i^2 - a_i^2}{2}[(\lambda_i + 2\mu_i)\epsilon_{zi}^{(0)} + \lambda_i\epsilon_i^{(0)}] \\ &\quad + \frac{b_i^3 - a_i^3}{3}[(\lambda_i + 2\mu_i)\epsilon_{zi}^{(1)} + \lambda_i\epsilon_i^{(1)}] \\ \int_{a_i}^{b_i} \sigma_{zi}\,dz &= (b_i - a_i)[(\lambda_i + 2\mu_i)\epsilon_{zi}^{(0)} + \lambda_i\epsilon_i^{(0)}] \\ &\quad + \frac{b_i^2 - a_i^2}{2}[(\lambda_i + 2\mu_i)\epsilon_{zi}^{(1)} + \lambda_i\epsilon_i^{(1)}] \end{aligned} \tag{25}$$

The integrals in Equations (25) are associated with the transverse normal stress σ_{zi} which is, in general, much smaller than the other normal stresses σ_{xi} and σ_{yi} except at locations where the transverse load is highly concentrated. Furthermore, they do not occur in the stress equations of motion of the plate. It is therefore assumed that these integrals are equal to zero, which leads to the relations

$$\epsilon_{zi}^{(0)} = -\frac{\lambda_i}{\lambda_i + 2\mu_i}\epsilon_i^{(0)}, \quad \epsilon_{zi}^{(1)} = -\frac{\lambda_i}{\lambda_i + 2\mu_i}\epsilon_i^{(1)}$$

By means of these relations the strain components $\epsilon_{zi}^{(0)}$ and $\epsilon_{zi}^{(1)}$ may now be eliminated from Equations (24). The results are

$$\begin{aligned} M_{xi} &= \frac{E_i^*}{1 - \nu_i^2}\left[\frac{b_i^2 - a_i^2}{2}\epsilon_i^{(0)} + \frac{b_i^3 - a_i^3}{3}\epsilon_i^{(1)}\right] \\ N_{xi} &= \frac{E_i^*}{1 - \nu_i^2}\left[(b_i - a_i)\epsilon_i^{(0)} + \frac{b_i^2 - a_i^2}{2}\epsilon_i^{(1)}\right] \\ Q_{xi} &= \mu_i(b_i - a_i)\gamma_i^{(0)} \end{aligned}$$

where E_i^* and ν_i are Young's modulus and Poisson's ratio, respectively. By virtue of Equations (19), these results may further be written as

$$\begin{aligned} M_{x1} &= D_1\epsilon_1^{(1)} = D_1\psi_1' \\ M_{x2} &= -F_2\epsilon_2^{(0)} + D_2\epsilon_2^{(1)} = F_2h_1(\psi_1' - \psi_2') + D_2\psi_2' \\ M_{x3} &= F_3\epsilon_3^{(0)} + D_3\epsilon_3^{(1)} = F_3h_1(\psi_1' - \psi_2') + D_3\psi_2' \\ N_{x2} &= E_2\epsilon_2^{(0)} - F_2\epsilon_2^{(1)} = -E_2h_1(\psi_1' - \psi_2') - F_2\psi_2' \\ N_{x3} &= E_3\epsilon_3^{(0)} + F_3\epsilon_3^{(1)} = E_3h_1(\psi_1' - \psi_2') + F_3\psi_2' \\ Q_{x1} &= G_1\gamma_1^{(0)} = G_1(\psi_1 + w') \\ Q_{x2} &= G_2\gamma_2^{(0)} = G_2(\psi_2 + w') \\ Q_{x3} &= G_3\gamma_3^{(0)} = G_3(\psi_2 + w') \end{aligned} \tag{26}$$

where

$$D_1 = \frac{E_1^*}{1 - \nu_1^2}\frac{2h_1^3}{3}$$

$$D_2 = D_3 = \frac{E_2^*}{1 - \nu_2^2}\frac{h^3 - h_1^3}{3}$$

$$E_2 = E_3 = \frac{E_2^*}{1 - \nu_2^2} h_2$$

$$F_2 = F_3 = \frac{E_2^*}{1 - \nu_2^2} \frac{h^2 - h_1^2}{2}$$

$$G_1 = 2\kappa\mu_1 h_1$$

$$G_2 = G_3 = \kappa\mu_2 h_2$$

It follows that

$$M_{x2} = M_{x3}, \quad N_{x2} = -N_{x3}, \quad Q_{x2} = Q_{x3}$$

The factor κ in G_i is a shear coefficient introduced in the manner of Mindlin; choice of its value will be discussed later.

Initial and Boundary Conditions

Subject to certain restrictions concerning continuity, single-valuedness, and singularities, initial and boundary conditions sufficient to insure a unique solution of the stress equations of motion and the displacement-strain-stress relations in the theory of elasticity may be obtained from Neumann's theorem [6], which is applicable to the sandwich-plate problem. Following the procedure used by Mindlin [1], we find that the initial conditions consist of the specification of the initial values of w, ψ_1, ψ_2, and their time derivatives. Similarly, the boundary conditions can be shown to be specified by prescribing for the entire plate between $x = 0$ and $x = l$ one member of each of the two products

$$p_x(u_3)_{z=\pm h}, \quad p_z(w_3)_{z=h} \tag{27}$$

and by prescribing at the end sections $x = 0$ and $x = l$ one member of each of the three products

$$[M_{x1} + h_1(N_{x3} - N_{x2})]\psi_1,$$
$$[M_{x2} + M_{x3} - h_1(N_{x3} - N_{x2})]\psi_2, \; Q_x w \tag{28}$$

or, alternatively, the three products

$$M_x\psi_1, \; [M_{x2} + M_{x3} - h_1(N_{x3} - N_{x2})](\psi_2 - \psi_1), \; Q_x w \tag{29}$$

Displacement Equations of Motion

The following displacement equations of motion are obtained by substituting Equations (15) and (26) in Equations (10), (11), and (13):

$$\begin{aligned} &D_1\psi_1'' + 2D_3\psi_2'' + 2F_2h_1(\psi_1'' - \psi_2'') - G_1(\psi_1 + w') - \\ &2G_2(\psi_2 + w') + hp_x = \rho_1 I_{11}\ddot{\psi}_1 + \rho_2 I_{22}\ddot{\psi}_2 + \rho_2 I_{12}(\ddot{\psi}_1 - \ddot{\psi}_2) \\ &D_1\psi_1'' - G_1(\psi_1 + w') + 2F_2h_1\psi_2'' + 2E_2h_1^2(\psi_1'' - \psi_2'') \\ &\qquad + h_1 p_x = \rho_1 I_{11}\ddot{\psi}_1 + \rho_2 I_{12}\ddot{\psi}_2 + \rho_2 I_{21}(\ddot{\psi}_1 - \ddot{\psi}_2) \\ &G_1(\psi_1' + w'') + 2G_2(\psi_2' + w'') + p_z = 2(\rho_1 h_1 + \rho_2 h_2)\ddot{w} \end{aligned} \tag{30}$$

where

$$I_{11} = \frac{2h_1^2}{3}, \quad I_{22} = \frac{2(h^3 - h_1^3)}{3}, \quad I_{12} = h_1(h^2 - h_1^2), \quad I_{21} = 2h_1^2 h_2$$

A single equation involving only w may further be derived by differentiation and elimination; thus,

$$\begin{aligned} &[L_1][2(\rho_1 h_1 + \rho_2 h_2)\ddot{w} - (G_1 + 2G_2)w''] \\ &\qquad + [L_2][2(\rho_1 h_1 + \rho_2 h_2)\ddot{w}] - [L_3][2G_1G_2w''] \\ &\quad + 2G_1G_2[2(\rho_1 h_1 + \rho_2 h_2)\ddot{w}] - \{[L_1] + [L_2] + 2G_1G_2\}p_z \\ &\qquad + \{[L_4]h - [L_5]h_1 - 2G_1G_2h\}p_x' = 0 \end{aligned} \tag{31}$$

where the operators are

$$[L_1] = \left[(\rho_1 I_{11} + \rho_2 I_{21})\frac{\partial^2}{\partial t^2} - (D_1 + 2E_2h_1^2)\frac{\partial^2}{\partial x^2}\right]$$

$$\left[(\rho_2 I_{22} - \rho_2 I_{12})\frac{\partial^2}{\partial t^2} - (2D_2 - 2F_2h_1)\frac{\partial^2}{\partial x^2}\right]$$
$$- \left[(\rho_1 I_{11} + \rho_2 I_{12})\frac{\partial^2}{\partial t^2} - (D_1 + 2F_2h_1)\frac{\partial^2}{\partial x^2}\right]$$
$$\left[(\rho_2 I_{12} - \rho_2 I_{21})\frac{\partial^2}{\partial t^2} - (2F_2h_1 - 2E_2h_1^2)\frac{\partial^2}{\partial x^2}\right]$$

$$[L_2] = [G_1(\rho_2 I_{22} - 2\rho_2 I_{12} + \rho_2 I_{21}) + 2G_2(\rho_1 I_{11} + \rho_2 I_{21})]\frac{\partial^2}{\partial t^2}$$
$$- [G_1(2D_2 - 4F_2h_1 + 2E_2h_1^2)$$
$$+ 2G_2(D_1 + 2E_2h_1^2)]\frac{\partial^2}{\partial x^2}$$

$$[L_3] = \left[(\rho_1 I_{11} + \rho_2 I_{22})\frac{\partial^2}{\partial t^2} - (D_1 + 2D_2)\frac{\partial^2}{\partial x^2}\right]$$

$$[L_4] = [G_1(\rho_2 I_{12} - \rho_2 I_{21}) - 2G_2(\rho_1 I_{11} + \rho_2 I_{21})]\frac{\partial^2}{\partial t^2}$$
$$- [G_1(2F_2h_1 - 2E_2h_1^2) - 2G_2(D_1 + 2E_2h_1^2)]\frac{\partial^2}{\partial x^2}$$

$$[L_5] = [G_1(\rho_2 I_{22} - \rho_2 I_{12}) - 2G_2(\rho_1 I_{11} + \rho_2 I_{12})]\frac{\partial^2}{\partial t^2}$$
$$- [G_1(2D_2 - 2F_2h_1) - 2G_2(D_1 + 2F_2h_1)]\frac{\partial^2}{\partial x^2}$$

When the faces are absent, the various operators in Equation (31) become

$$[L_1] = 0$$

$$[L_2] = \left(\rho_1 I_{11}\frac{\partial^2}{\partial t^2} - D_1\frac{\partial^2}{\partial x^2}\right)$$

$$[L_3] = -[L_4] = -[L_5] = 2G_2\left(\rho_1 I_{11}\frac{\partial^2}{\partial t^2} - D_1\frac{\partial^2}{\partial x^2}\right)$$

and Equation (31) reduces to

$$\left(\rho_1 I_{11}\frac{\partial^2}{\partial t^2} - D_1\frac{\partial^2}{\partial x^2}\right)(2\rho_1 h_1 w - G_1 w'' - p_z)$$
$$+ G_1(2\rho_1 h_1\ddot{w} - p_z - hp_x') = 0 \tag{32}$$

Similarly, when the core is absent, the operators become

$$[L_1] = [L_4] = 0$$

$$[L_2] = \left(\rho_2 I_{22}\frac{\partial^2}{\partial t^2} - 2D_2\frac{\partial^2}{\partial x^2}\right)$$

$$[L_3] = [L_5] = G_1\left(\rho_2 I_{22}\frac{\partial^2}{\partial t^2} - 2D_2\frac{\partial^2}{\partial x^2}\right)$$

and Equation (31) takes the form

$$\left(\rho_2 I_{22}\frac{\partial^2}{\partial t^2} - 2D_2\frac{\partial^2}{\partial x^2}\right)(2\rho_2 h_2\ddot{w} - 2G_2 w'' - p_z)$$
$$+ 2G_2(2\rho_2 h_2\ddot{w} - p_z - hp_x') = 0 \tag{33}$$

Equations (32) and (33) are seen to agree with Mindlin's result for a homogeneous plate; namely, Equation (37) of reference (5) with the y-dependent terms neglected, if in Equations (32) and (33) we disregard the p_x-terms and choose the shear coefficient κ to have the same value $\pi^2/12$ as given by Mindlin. By so adopting the value of κ, the limiting frequency for very long

waves for the second flexural mode (which approaches the fundamental simple thickness-shear mode) in the reduced core or face plate is made identical with the result derived from the exact elasticity theory.[3]

When Equations (30) and (31) are applied to bending problems of sandwich plates, the time-dependent terms are not needed. The value of $\kappa = \pi^2/12$ may still be used from the standpoint of considering the equilibrium equations to be a special case of the equations of motion, or we may use Reissner's value of $\kappa = {}^5/_6$ for homogeneous plates, which was specifically derived for the bending case [8] and differs only slightly from the value $\pi^2/12$.

If the effect of transverse-shear deformation in the face layers is suppressed, by taking $2G_2 = \infty$, Equation (31) in its static form may be shown to be comparable to Eringen's result; namely, Equation (30) of reference [4]. When the bending rigidity D_1 of the core is further neglected, Equation (31) in its static form becomes comparable to Hoff's result for a sandwich plate, Equation (19) of reference [3], or his result for a sandwich beam [7]. In both of these cases, comparison should be made only when the faces are thin, for only then can Eringen's and Hoff's results apply. Finally, if the difference between h and h_1 is completely ignored, Equation (31) in its static form is then comparable to Reissner's result for a sandwich plate; namely, Equation (79) of reference [2].[4] It should be noted that, in references [2], [3], [4], and [7], no shear coefficient such as κ was employed.

Bending of Long Cantilever Plate

The foregoing results will first be employed to solve the problem of bending of a long (in the y-direction) cantilever plate subjected to a line load at the unsupported end, as shown in Fig. 2. The problem is essentially the same as that of a cantilever beam under a concentrated force at the unsupported end, as was solved by Hoff [7]. For the plate shown in Fig. 2, P is the load per unit length of the plate in the y-direction.

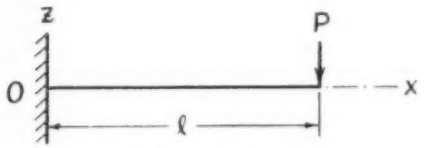

Fig. 2 Cantilever plate

Equation (31) for w is simplified into the following form for the present problem of equilibrium in which no distributed lateral load is acting:

$$(G_1 + 2G_2)[(D_1 + 2E_2h_1^2)(2D_2 - 2F_2h_1) - (D_1 + 2F_2h_1)(2F_2h_1 - 2E_2h_1^2)]w^{vi} - 2G_1G_2(D_1 + 2D_2)w^{iv} = 0 \quad (34)$$

Another equation convenient for use is obtained by solving for ψ_1 from the third of Equations (30) and substituting the result into the first, also for the equilibrium case,

$$[G_1(2D_2 - 2F_2h_1) - 2G_2(D_1 + 2F_2h_1)]\psi_2''' = (G_1 + 2G_2)(D_1 + 2F_2h_1)w^{iv} \quad (35)$$

For convenience, Equations (34) and (35) will be put in the following abbreviated form:

$$w^{vi} - p^2w^{iv} = 0 \quad (36)$$

$$\psi_2''' = Kw^{iv} \quad (37)$$

The coefficients p^2 and K are thereby introduced. A third equation for the equilibrium case is deduced from the third of Equations (30) itself:

$$G_1(\psi_1' + w'') + 2G_2(\psi_2' + w'') = 0 \quad (38)$$

Solving now Equations (36), (37) and (38) in turn for w, ψ_2 and ψ_1, we find

$$\begin{aligned} w &= C_0 + C_1x + C_2x^2 + C_3x^3 + C_4\cosh px + C_5\sinh px \\ \psi_2 &= B_0 + B_1x + B_2x^2 + C_4Kp\sinh px + C_5Kp\cosh px \\ \psi_1 &= A_0 - \frac{G_1 + 2G_2}{G_1}(2C_2x + 3C_3x^2 + C_4p\sinh px \\ &\quad + C_5p\cosh px) - \frac{2G_2}{G_1}(B_1x + B_2x^2 + C_4Kp\sinh px \\ &\quad + C_5Kp\cosh px) \end{aligned} \quad (39)$$

Four of the ten integration constants in Equations (39) are not independent ones. Their dependence on the others may be determined by substituting Equations (39) into the first two of Equations (30) (with time-dependent terms omitted) and equating to zero the sum of the constant terms, the coefficients of the x-terms, and those of the x^2-terms; thus,

$$\begin{aligned} &(D_1 + 2E_2h_1^2)\left(6\frac{G_1 + 2G_2}{G_1}C_3 + 2\frac{2G_2}{G_1}B_2\right) \\ &\quad - 2(2F_2h_1 - 2E_2h_1^2)B_2 + G_1(A_0 + C_1) = 0 \\ &(D_1 + 2F_2h_1)\left(6\frac{G_1 + 2G_2}{G_1}C_3 + 2\frac{2G_2}{G_1}B_2\right) \\ &\quad - 2(2D_2 - 2F_2h_1)B_2 + G_1A_0 + 2G_2B_0 \\ &\quad + (G_1 + 2G_2)C_1 = 0 \\ &B_1 = -2C_2 \\ &B_2 = -3C_3 \end{aligned} \quad (40)$$

In addition to the four Equations (40), another six equations also needed for the determination of the ten constants are from the boundary conditions written for the end sections of the plate:

$$w = \psi_1 = \psi_2 = 0 \qquad (x = 0) \quad (41)$$

$$\left.\begin{aligned} M_x &= 0 \\ Q_x &= -P \\ M_{x2} + M_{s2} - h_1(N_{x2} - N_{s2}) &= 0 \end{aligned}\right\} \quad (x = l) \quad (42)$$

Substitution of Equations (39) in (41) yields

$$\begin{aligned} &C_0 + C_4 = 0 \\ &A_0 - \frac{G_1 + 2G_2}{G_1}pC_5 - \frac{2G_2}{G_1}KpC_4 = 0 \\ &B_0 + KpC_5 = 0 \end{aligned} \quad (43)$$

By making use of Equations (39), (40), and (43), the following relations are derived from Equations (42):

$$\begin{aligned} &C_4\cosh pl + C_5\sinh pl = 0 \\ &(G_1 + 2G_2)(pC_5 + C_1) = -P \\ &2C_2 + 6C_3l = 0 \end{aligned} \quad (44)$$

[3] Further discussion on the value of κ for sandwich plates in the case of vibration is given in the paper, "Simple Thickness-Shear Modes of Vibration of Infinite Sandwich Plates," by Yi-Yuan Yu, to be published in the JOURNAL OF APPLIED MECHANICS.

[4] In Equation (79) of reference [2], m_x and m_y should be replaced by $2m_x$ and $2m_y$, respectively.

The ten constants may now be determined from the ten Equations (40), (43), and (44), with the results given by

$$A_0 = \frac{G_1 + 2G_2(1 + K)}{G_1} pC_5$$

$$B_0 = -KpC_5$$

$$B_1 = \frac{Pl}{D_1 + 2D_2}$$

$$B_2 = -\frac{P}{2(D_1 + 2D_2)}$$

$$C_0 = -C_4 = C_5 \tanh pl$$

$$C_1 = -C_5 p - \frac{P}{G_1 + 2G_2}$$

$$C_2 = -\frac{Pl}{2(D_1 + 2D_2)}$$

$$C_3 = \frac{P}{6(D_1 + 2D_2)}$$

$$C_5 = \frac{P}{2G_2 p(1 + K)} \left(\frac{G_1}{G_1 + 2G_2} - \frac{D_1 + 2F_2h_1}{D_1 + 2D_2} \right)$$

w, ψ_1, and ψ_2 are thus completely determined.

We are particularly interested in the maximum deflection at the unsupported end of the plate, which is

$$w_{x=l} = -\frac{Pl^3}{3(D_1 + 2D_2)} - \frac{Pl}{G_1 + 2G_2} - \frac{Pl}{(D_1 + 2D_2)^2} \left(1 - \frac{\tanh pl}{pl}\right) \frac{2G_1G_2}{G_1 + 2G_2} \left(\frac{D_1 + 2F_2h_1}{G_1} - \frac{2D_2 - 2F_2h_1}{2G_2} \right)^2 \quad (45)$$

where

$$p^2 = 2G_1G_2(D_1 + 2D_2)/(G_1 + 2G_2)[(D_1 + 2E_2h_1^2)(2D_2 - 2F_2h_1) - (D_1 + 2F_2h_1)(2F_2h_1 - 2E_2h_1^2)]$$

It is observed that the first term on the right side of Equation (45) is the usual bending term. The second is a shear-correction term similar in form to that usually given for a homogeneous cantilever beam [9]. The last term involves the effects of both bending and shear deformation. Equation (45) is for the general case. When the bending and shearing rigidities of the faces are so much higher than those of the core that D_1 may be neglected and $2G_2$ may be put equal to infinity, the equation reduces to

$$w_{x=l} = -\frac{Pl^3}{3(2D_2)} - \frac{Pl}{G_1} \left(1 - \frac{\tanh pl}{p}\right) \left(\frac{2F_2h_1}{2D_2}\right)^2 \quad (46)$$

where we now have

$$p^2 = \frac{G_1(2D_2)}{2E_2h_1^2(2D_2 - 2F_2h_1)}$$

Equation (46) is still for arbitrary dimensions of the core and faces of the sandwich plate. In the case of thin faces, the result may be shown to be comparable to Hoff's result for the analogous problem of a cantilever sandwich beam [7]. As was pointed out before, no shear coefficient such as κ was employed in Hoff's work.

Propagation of Straight-Crested Waves

We will now apply Equation (31) to the problem of propagation of straight-crested waves along the x-direction in an infinite sandwich plate. For this purpose, the lateral-load terms in the equation are not needed, and we put in the remaining part of the equation the following form of w:

$$w = \sin \frac{2\pi x}{L} \sin \omega t$$

where L is the wave length and ω the circular frequency. The result gives

$$\left\{ \left[(\rho_1 I_{11} + \rho_2 I_{21})\omega^2 - (D_1 + 2E_2h_1^2) \left(\frac{2\pi}{L}\right)^2 \right] \left[(\rho_2 I_{22} - \rho_2 I_{12})\omega^2 - (2D_2 - 2F_2h_1) \left(\frac{2\pi}{L}\right)^2 \right] - \left[(\rho_1 I_{11} + \rho_2 I_{12})\omega^2 - (D_1 + 2F_2h_1) \left(\frac{2\pi}{L}\right)^2 \right] \left[(\rho_2 I_{12} - \rho_2 I_{21})\omega^2 - (2F_2h_1 - 2E_2h_1^2) \left(\frac{2\pi}{L}\right)^2 \right] \right\} \left[2(\rho_1 h_1 + \rho_2 h_2)\omega^2 - (G_1 + 2G_2) \left(\frac{2\pi}{L}\right)^2 \right] - \{ [G_1(\rho_2 I_{22} - 2\rho_2 I_{12} + \rho_2 I_{21}) + 2G_2(\rho_1 I_{11} + \rho_2 I_{21})]\omega^2 - [G_1(2D_2 - 4F_2h_1 + 2E_2h_1^2) + 2G_2(D_1 + 2E_2h_1^2)] \left(\frac{2\pi}{L}\right)^2 \} \left\{ 2(\rho_1 h_1 + \rho_2 h_2)\omega^2 + \left[(\rho_1 I_{11} + \rho_2 I_{22})\omega^2 - (D_1 + 2D_2) \left(\frac{2\pi}{L}\right)^2 \right] 2G_1G_2 \left(\frac{2\pi}{L}\right)^2 + 2G_1G_2 2(\rho_1 h_1 + \rho_2 h_2)\omega^2 = 0 \quad (47)$$

which is the frequency equation. Once the frequency becomes known, the phase velocity c may be calculated from

$$c = \frac{\omega L}{2\pi}$$

It is seen that there are three branches of the frequency or phase-velocity curve. The detailed discussion of these modes will however not be given here, and we shall concern ourselves for the time being with a study of the general effect of neglecting the transverse-shear deformation and rotatory inertia. When the transverse-shear deformation is neglected in the faces, Equation (47) reduces to

$$\left\{ \left[(\rho_1 I_{11} + \rho_2 I_{21})\omega^2 - (D_1 + 2E_2h_1^2) \left(\frac{2\pi}{L}\right)^2 \right] \left[(\rho_2 I_{22} - \rho_2 I_{12})\omega^2 - (2D_2 - 2F_2h_1) \left(\frac{2\pi}{L}\right)^2 \right] - \left[(\rho_1 I_{11} + \rho_2 I_{12})\omega^2 - (D_1 + 2F_2h_1) \left(\frac{2\pi}{L}\right)^2 \right] \left[(\rho_2 I_{12} - \rho_2 I_{21})\omega^2 - (2F_2h_1 - 2E_2h_1^2) \left(\frac{2\pi}{L}\right)^2 \right] \right\} \left(\frac{2\pi}{L}\right)^2 + \left[(\rho_1 I_{11} + \rho_2 I_{21})\omega^2 - (D_1 + 2E_2h_1^2) \left(\frac{2\pi}{L}\right)^2 \right] 2(\rho_1 h_1 + \rho_2 h_2)\omega^2 - G_1 \left[(\rho_1 I_{11} + \rho_2 I_{22})\omega^2 - (D_1 + 2D_2) \left(\frac{2\pi}{L}\right)^2 \right] \left(\frac{2\pi}{L}\right)^2 - G_1 2(\rho_1 h_1 + \rho_2 h_2)\omega^2 = 0 \quad (48)$$

The number of branches is seen to have been reduced to two. When the shear effect is also neglected in the core, we find

$$\left[(\rho_1 I_{11} + \rho_2 I_{22})\omega^2 - (D_1 + 2D_2) \left(\frac{2\pi}{L}\right)^2 \right] \left(\frac{2\pi}{L}\right)^2 + 2(\rho_1 h_1 + \rho_2 h_2)\omega^2 = 0 \quad (49)$$

Table 1 Limiting values of ω^2 and c^2

		Equation (47) Nothing neglected	Equation (48) Shear neglected in faces	Equation (49) Shear neglected in faces and core	Equation (50) Shear and rotation all neglected
[b]	ω_1^2	0	0	0	0
	c_1^2	0	0	0	0
	ω_2^2	$\dfrac{G_1{}^a}{\rho_1 I_{11} + \rho_2 I_{21}}$	$\dfrac{G_1}{\rho_1 I_{11} + \rho_2 I_{21}}$	–	–
	c_2^2	∞	∞	–	–
	ω_3^2	$\dfrac{2G_2{}^a}{\rho_2 I_{22} - \rho_2 I_{21}}$	–	–	–
	c_3^2	∞	–	–	–
[c]	ω_1^2	∞	∞	∞	∞
	c_1^2	$\dfrac{D_1 + 2E_2 h_1{}^{2\,a}}{\rho_1 I_{11} + \rho_2 I_{21}}$	$\dfrac{D_1 + 2E_2 h_1{}^{2\,a}}{\rho_1 I_{11} + \rho_2 I_{21}}$	$\dfrac{D_1 + 2D_2}{\rho_1 I_{11} + \rho_2 I_{22}}$	∞
	ω_2^2	∞	∞	–	–
	c_2^2	$\dfrac{2D_2 - 2F_2 h_1{}^a}{\rho_2 I_{22} - \rho_2 I_{12}}$	$\dfrac{2D_2 - 2F_2 h_1{}^a}{\rho_2 I_{22} - \rho_2 I_{12}}$	–	–
	ω_3^2	∞	–	–	–
	c_3^2	$\dfrac{G_1 + 2G_2}{2(\rho_1 h + \rho_2 h_2)}$	–	–	–

[a] Approximate value, for the case of thin faces ($h_2 \ll h_1$).
[b] Very long waves $L = \infty$.
[c] Very short waves $L = 0$.

and there is now only one branch left. Finally, if the rotatory-inertia effect is further suppressed, the result becomes

$$2(\rho_1 h_1 + \rho_2 h_2)\omega^2 - (D_1 + 2D_2)\left(\frac{2\pi}{L}\right)^4 = 0 \qquad (50)$$

The limiting values of ω^2 and c^2 when the waves are very long or very short may be determined readily from Equations (47) to (50) for the various cases. The results are summarized in Table 1.

Aside from the fact that one value of the frequency or phase velocity is lost through neglecting shear in the faces, we see that the remaining values of the frequency and phase velocity calculated from Equation (48) are all comparable to those from Equation (47) when the faces are thin. On the other hand, results from Equations (49) and (50) may hardly be considered satisfactory from the standpoint of the more complete Equation (47). It should be emphasized, however, that these observations are based upon only the limiting cases of very long and very short waves. Over the entire range of the wave length, comparison among the various cases can only be made through detailed numerical evaluation of Equations (47) to (50).

References

1 R. D. Mindlin, "An Introduction to the Mathematical Theory of Vibrations of Elastic Plates," a monograph prepared for U. S. Army Signal Corps Engineering Laboratories, 1955.

2 Eric Reissner, "Small Bending and Stretching of Sandwich-Type Shells," NACA Report 975, 1950.

3 N. J. Hoff, "Bending and Buckling of Rectangular Sandwich Plates," NACA TN 2225, November, 1950.

4 A. C. Eringen, "Bending and Buckling of Rectangular Sandwich Plates," Proceedings of the First U. S. National Congress of Applied Mechanics, 1951, pp. 381–390.

5 R. D. Mindlin, "Influence of Rotatory Inertia and Shear on Flexural Motions of Isotropic, Elastic Plates," JOURNAL OF APPLIED MECHANICS, vol. 18, TRANS. ASME, vol. 73, 1951, pp. 31–38.

6 A. E. H. Love, "A Treatise on the Mathematical Theory of Elasticity," Cambridge University Press, London, England, 1927, p. 176.

7 N. J. Hoff, "The Analysis of Structures," John Wiley & Sons, Inc., New York, N. Y., 1956, pp. 180–194.

8 Eric Reissner, "The Effect of Transverse Shear Deformation on the Bending of Elastic Plates," JOURNAL OF APPLIED MECHANICS, vol. 12, TRANS. ASME, vol. 67, 1945, pp. A69–A77.

9 S. Timoshenko, "Strength of Materials," Part 1, third edition, D. Van Nostrand Company, Inc., New York, N. Y., 1955, pp. 318–319.

On Invariant Perforation in an Infinite Strip

CHIH-BING LING

Director,
Aeronautical Research Laboratory,
Taichung; concurrently, Acting Director,
Institute of Mathematics,
Academia Sinica, Taipei,
Taiwan, China

The invariant perforation in an infinite strip can be classified into two groups. One is the finite group and the other is the infinite group. There are five cases in the finite group and nine cases in the infinite group. All the cases can be solved by the method of images. This method has, in fact, been used by the author to solve the stresses in an infinite strip containing either an unsymmetrically located single hole or a series of uniformly distributed equal holes. The solution is illustrated by working out in detail one of the cases in the infinite group, in which the strip contains two series of equal holes symmetrically staggered along the strip. The stress function is constructed by using a class of periodic harmonic functions derived from Weierstrass' sigma function. Numerical examples also are given to show the effect of such a perforation on the stresses in the strip.

In a previous paper [1][1] the author presented an analytic solution of the classical problem dealing with the stresses in an infinite strip containing an unsymmetrically located perforating hole. The method used, though not specifically mentioned in the paper, is in fact a method of "images." It appears that the method of solution can be extended to solve the stresses in an infinite strip containing any number of nonoverlapping perforating holes, of equal or unequal radii, in the same way as was done by Green [2] for a perforated plate. Naturally, such a solution for the general perforation, as inferred from Green's solution, is exceedingly complicated.

The simplest of the general perforation is the invariant perforation in which all the holes are of equal radii and symmetrically located in the strip in such a manner that, under the given stress system acting in the strip, the properties of all the holes are alike. Consequently, the required solution must satisfy this invariant property. In other words, if the solution satisfies the boundary conditions on any one of the holes, then by symmetry the corresponding conditions on all the remaining holes are automatically satisfied. The solution thus becomes greatly simplified.

The invariant perforation in a strip can be classified into two groups: One consists of a finite number of equal holes only, while the other consists of an infinite number of equal holes. Various cases of the two groups are shown in Figs. 1 and 2, respectively. It appears that there are, in all, five cases in the finite group and nine cases in the infinite group.

It may be mentioned that the cases (i), (ii), and (v) in the finite group as shown in Fig. 1, in which the strip is perforated by one pair or two pairs of equal holes, respectively, have been investigated by Howland and Knight [3] by using a special method previously developed by the authors. The case (ii) was also investigated recently by Atsumi [4]. Again, the case (i) in the infinite group as shown in Fig. 2, in which the strip is perforated by an infinite series of equal holes uniformly distributed along the strip, has been solved by the author and his associates [5]. In the present paper, the solution of case (vii) in the infinite group as shown in Fig. 2 will be given, in which the strip is perforated by two infinite series of equal holes symmetrically staggered along the strip. The following two fundamental stress systems will be considered: (*a*) When the strip is under a longitudinal tension, and (*b*) when the strip is under a transverse bending.

The present solution at the same time would throw ample light on the solutions of the remaining cases in the infinite group for such cases can be solved by essentially the same method. As will be seen later, the class of special harmonic functions used in constructing the present solution is derived from Weierstrass' sigma function. The cases in the finite group can also be solved in a similar way, except that a hyperbolic sine function is used in place of the Weierstrass sigma function and a biharmonic integral in place of the biharmonic series.

In what follows, the solution of case (vii) in the infinite group will first be presented and then numerical values will be given to show the effect of such a perforation on the stresses in the strip.

A Class of Special Harmonic Functions

The given strip is here shown again in Fig. 3. Let the strip be

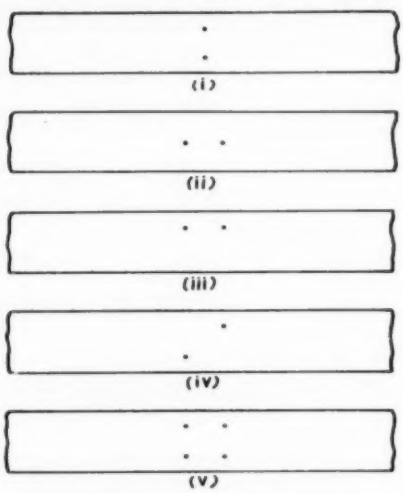

Fig. 1 Finite group of invariant perforation

[1] Numbers in brackets designate References at end of paper.

Presented at the Summer Conference of the Applied Mechanics Division, Troy, N. Y., June 18–20, 1959, of The American Society of Mechanical Engineers.

Discussion of this paper should be addressed to the Secretary, ASME, 29 West 39th Street, New York, N. Y., and will be accepted until October 10, 1959, for publication at a later date. Discussion received after the closing date will be returned.

Note: Statements and opinions advanced in papers are to be understood as individual expressions of their authors and not those of the Society. Manuscript received by ASME Applied Mechanics Division, May 7, 1958. Paper No. 59—APM-20.

of width $2b$ and each perforating hole be of radius λb. The two series of perforating holes are equally spaced with their centers symmetrically staggered along the strip. Let a pair of rectangular axes be orientated as shown in Fig. 3. For convenience, the co-ordinates x and y will be regarded as dimensionless variables referring to a typical length b or the half width of the strip. Let the centers of holes be at the points $(x, y) = (2ma, 0)$ and $(2ma + a, -2c)$, respectively, where m takes all positive and negative integral values including zero. The edges of the strip are represented by $y = 1 - c$ and $y = -1 - c$, respectively.

By reflection about the edges, the strip forms an infinite set of images as shown in Fig. 4. The strip in which the origin of co-ordinates is orientated represents the given strip and is marked by a positive sign as shown. The remaining strips marked by positive signs represent the images formed by an even number of reflections, while those marked by negative signs represent the images formed by an odd number of reflections. Note that any two adjacent strips have alternate signs. The set of points in each strip represents the images of the centers of holes in the given strip.

Consider the xy-plane in Fig. 3 or 4 as an Argand plane of a complex variable z where

$$z = x + iy \tag{1}$$

The affixes of the image points in the positive strips, including the points in the given strip, are then given by

$$P_{mn} = 2ma + 4ni$$

and

$$P_{mn}^{*} = (2m + 1)a + 2(2n - c)i = P_{mn} + a - 2ci \tag{2}$$

where m and n are extended to all positive and negative integral and zero values. Again, the affixes of the image points in the negative strips are given by

$$Q_{mn} = 2ma + 2(2n + 1 - c)i = P_{mn} + 2i - 2ci$$

and (3)

$$Q_{mn}^{*} = (2m + 1)a + 2(2n - 1)i = P_{mn} + a - 2i$$

where m and n are also extended to all positive and negative integral and zero values.

Now, define a function W_0 with logarithmic singularities at these image points, including the points in the given strip, by

$$W_0(z) = -\log\{\sigma(z)\sigma_1(z)\sigma_2(z)\sigma_3(z)\} \tag{4}$$

where

$$\begin{aligned}
\sigma(z) &= z \prod_{m,n=-\infty}^{\infty}{}' \left\{\left(1 - \frac{z}{P_{mn}}\right)\exp\left(\frac{z}{P_{mn}} + \frac{z^2}{2P_{mn}^2}\right)\right\} \\
\sigma_1(z) &= \prod_{m,n=-\infty}^{\infty} \left\{\left(1 - \frac{z}{P_{mn}^{*}}\right)\exp\left(\frac{z}{P_{mn}^{*}} + \frac{z^2}{2P_{mn}^{*2}}\right)\right\} \\
\sigma_2(z) &= \prod_{m,n=-\infty}^{\infty} \left\{\left(1 - \frac{z}{Q_{mn}}\right)\exp\left(\frac{z}{Q_{mn}} + \frac{z^2}{2Q_{mn}^2}\right)\right\} \\
\sigma_3(z) &= \prod_{m,n=-\infty}^{\infty} \left\{\left(1 - \frac{z}{Q_{mn}^{*}}\right)\exp\left(\frac{z}{Q_{mn}^{*}} + \frac{z^2}{2Q_{mn}^{*2}}\right)\right\}
\end{aligned} \tag{5}$$

σ is Weierstrass' sigma function. The accent on the multiplication sign denotes the omission of simultaneous zeros of m and n from the double multiplication. The remaining functions are related to σ by [6]

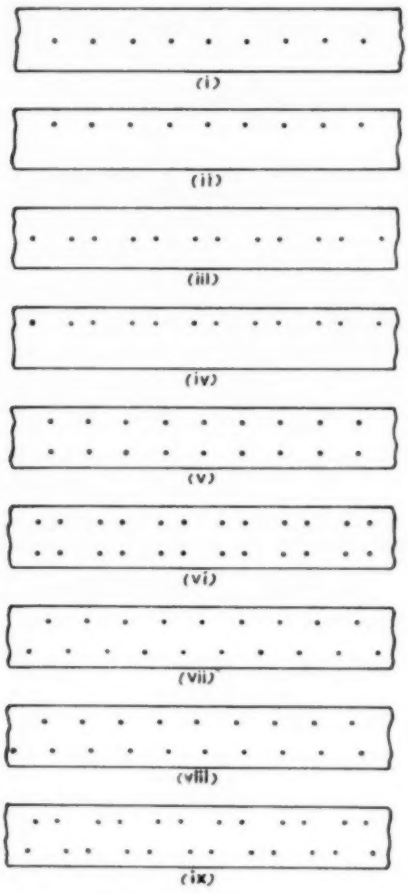

Fig. 2 Infinite group of invariant perforation

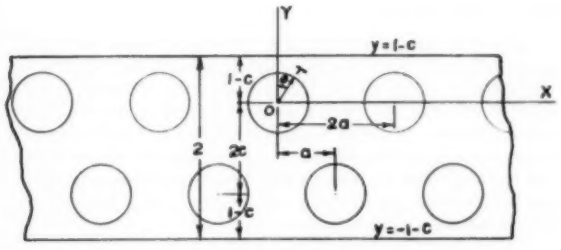

Fig. 3 The given strip, lengths measured in unit b

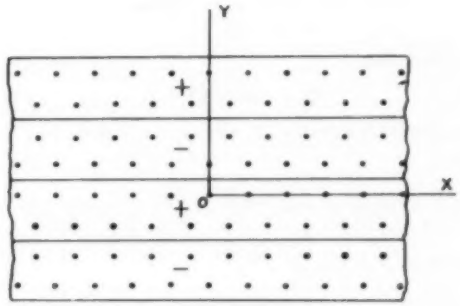

Fig. 4 An infinite set of images

$$\prod_{m,n=-\infty}^{\infty} \left\{\left(1 - \frac{z}{P_{mn} + \alpha}\right) \exp\left(\frac{z}{P_{mn} + \alpha} + \frac{z^2}{2(P_{mn} + \alpha)^2}\right)\right\} = \frac{\sigma(z - \alpha)}{\sigma(-\alpha)} \exp\left\{z\zeta(\alpha) + \frac{z^2}{2} p(\alpha)\right\} \quad (6)$$

where ζ and p are Weierstrass' zeta and elliptic functions, respectively, defined by

$$\begin{aligned} \zeta(z) &= \frac{d}{dz} \log \sigma(z) \\ &= \frac{1}{z} + \sum_{m,n=-\infty}^{\infty}{}' \left(\frac{1}{z - P_{mn}} + \frac{1}{P_{mn}} + \frac{z}{P_{mn}^2}\right) \\ p(z) &= -\frac{d}{dz} \zeta(z) \\ &= \frac{1}{z^2} + \sum_{m,n=-\infty}^{\infty}{}' \left(\frac{1}{(z - P_{mn})^2} - \frac{1}{P_{mn}^2}\right) \end{aligned} \quad (7)$$

in which the accent on each summation sign denotes the omission of simultaneous zeros of m and n from the double summation.

We thus find, except for a constant,

$$W_0(z) = -\log(-iz) + \sum_{k=3}^{\infty} \frac{1}{k} \omega_k (-iz)^k \quad (8)$$

where, for $k \geqslant 3$,

$$\omega_k = i^k \sum_{m,n=-\infty}^{\infty}{}' \frac{1}{P_{mn}^k} + i^k \sum_{m,n=-\infty}^{\infty} \left(\frac{1}{P_{mn}^{*k}} + \frac{1}{Q_{mn}^k} + \frac{1}{Q_{mn}^{*k}}\right) \quad (9)$$

By symmetry with respect to the y-axis, it can be shown readily that the coefficients ω_k, for $k \geqslant 3$, are all real.

Again, define a class of analytic functions with poles of integral orders at all the image points, including the points in the given strip, by

$$W_s(z) = \frac{(-i)^s}{(s-1)!} \frac{d^s}{dz^s} W_0(z) \quad (10)$$

where s is the order of poles of the functions. Consequently, we have

$$W_s(z) = \frac{1}{(-iz)^s} + (-1)^s \sum_{n=0}^{\infty} {}^n\Omega_s (-iz)^n \quad (11)$$

where, for $n + s \geqslant 3$,

$${}^n\Omega_s = \binom{n+s-1}{n} \omega_{n+s}$$

and in particular,

$${}^0\Omega_1 = {}^0\Omega_2 = {}^1\Omega_1 = 0 \quad (12)$$

For uniformity in notation, W_0 may be rewritten in the following form

$$W_0(z) = -\log(-iz) + \sum_{n=3}^{\infty} {}^n\Omega_0 (-iz)^n, \quad (13)$$

where, for $n \geqslant 3$,

$${}^n\Omega_0 = \frac{1}{n} \omega_n \quad (14)$$

Now, split W_s into real and imaginary parts as follows: For $s \geqslant 0$,

$$W_s(z) = S_s(x, y) + iT_s(x, y) \quad (15)$$

Also, define a pair of polar co-ordinates (r, θ) by

$$z = ire^{-i\theta}$$

that is,

$$x = r \sin\theta, \quad y = r \cos\theta \quad (16)$$

We thus have, since ${}^n\Omega_s$ is real,

$$\begin{aligned} S_0 &= -\log r + \sum_{n=3}^{\infty} {}^n\Omega_0 r^n \cos n\theta \\ T_0 &= \theta - \sum_{n=3}^{\infty} {}^n\Omega_0 r^n \sin n\theta \\ S_s &= \frac{\cos s\theta}{r^s} + (-1)^s \sum_{n=0}^{\infty} {}^n\Omega_s r^n \cos n\theta \\ T_s &= \frac{\sin s\theta}{r^s} - (-1)^s \sum_{n=1}^{\infty} {}^n\Omega_s r^n \sin n\theta \end{aligned} \quad (17)$$

It is obvious that these functions satisfy the harmonic equation $\nabla^2 = 0$, where $\nabla^2 = \partial^2/\partial x^2 + \partial^2/\partial y^2$.

Cauchy-Riemann equations give the following relations:

$$\begin{aligned} \frac{\partial S_0}{\partial x} &= \frac{\partial T_0}{\partial y} = -T_1, & \frac{\partial T_0}{\partial x} &= -\frac{\partial S_0}{\partial y} = S_1 \\ \frac{\partial S_s}{\partial x} &= \frac{\partial T_s}{\partial y} = -sT_{s+1}, & \frac{\partial T_s}{\partial x} &= -\frac{\partial S_s}{\partial y} = sS_{s+1} \end{aligned} \quad (18)$$

The functions S_s are even in x while T_s are odd in x. It also can be shown that when $x = na$, where n is an integer or zero,

$$T_1 = \text{const}, \qquad T_s = 0, \quad (s \geqslant 2) \quad (19)$$

and when $y = 4n \pm 1 - c$,

$$S_1 = \text{const}, \quad S_{2s+1} = 0, \quad T_{2s} = 0. \quad (s \geqslant 1) \quad (20)$$

Here the constants are not absolute constants but are linear functions of n. In particular,

$$\begin{aligned} T_1(\pm a, y) &= \pm 4\zeta(a) \pm a\omega_2 \\ S_1(x, \pm 1 - c) &= \pm 2i\zeta(2i) - (\pm 1 - c)\omega_2 + \omega_1 \end{aligned} \quad (21)$$

where

$$\begin{aligned} \omega_1 &= RP\{i\zeta(a - 2ci) + i\zeta(2i - 2ci) + i\zeta(a - 2i)\} \\ \omega_2 &= p(a - 2ci) + p(2i - 2ci) + p(a - 2i) \end{aligned} \quad (22)$$

The Stress Function

Suppose that in the absence of the holes the stresses in the strip are derived from a basic stress function χ_0. In order to allow for the effect of the holes an auxiliary stress function χ_1 is constructed by using the special harmonic functions defined previously. Besides, series of suitable biharmonic functions which possess no singularities within the entire strip are added so that the resulting auxiliary stress function yields no normal and tangential tractions along either edge of the strip. The required stress function is thus given by

$$\chi = \chi_0 + \chi_1. \quad (23)$$

Suppose further that the basic stress function is even in x. Consequently, the auxiliary stress function is also even in x. On account of the periodic property of the given strip the auxiliary stress function is here constructed as follows:

$$\chi_1 = b^2 \sum_{s=0}^{\infty} A_{2s} S_{2s}(x, y) + b^2 \sum_{s=1}^{\infty} D_{2s} S_{2s-1}(x, y) + b^2 \sum_{s=1}^{\infty} (y + c) B_{2s} S_{2s-1}(x, y) + b^2 \sum_{s=1}^{\infty} C_{2s} \left\{ (y + c) S_{2s}(x, y) + \frac{1}{2s - 1} S_{2s-1}(x, y) \right\} + b^2 \sum_{n=1}^{\infty} \left\{ A_n^* \cosh \frac{n\pi(y + c)}{a} + (y + c) B_n^* \sinh \frac{n\pi(y + c)}{a} + C_n^* \sinh \frac{n\pi(y + c)}{a} + (y + c) D_n^* \cosh \frac{n\pi(y + c)}{a} \right\} \cos \frac{n\pi x}{a} \tag{24}$$

where A_{2s}, B_{2s}, C_{2s}, D_{2s}, A_n^*, B_n^* C_n^*, and D_n^* are coefficients of superposition. The auxiliary stress function thus constructed satisfies the biharmonic equation $\nabla^4 = 0$. It is noted that the first four series involving S_s are of the same form as in the previous solution for a strip containing an unsymmetrically located hole [1], but the subsequent biharmonic integral is here replaced by a biharmonic series. Provided that all the series converge, the stress function thus constructed gives univalued displacements and stresses in the entire strip except the singularities at the centers of holes.

The following normal and tangential stresses along the edges $y = \pm 1 - c$ are derived from χ_1.

$$\sigma_y = \frac{1}{b^2} \left[\frac{\partial^2 \chi_1}{\partial x^2} \right]_{y = \pm 1 - c} = -A_0 S_2(x, \pm 1 - c) - \sum_{s=1}^{\infty} 2s(2s + 1)(A_{2s} \pm C_{2s}) S_{2s+2}(x, \pm 1 - c) - \sum_{n=1}^{\infty} \frac{n^2\pi^2}{a^2} \left\{ (A_n^* \pm D_n^*) \cosh \frac{n\pi}{a} + (B_n^* \pm C_n^*) \sinh \frac{n\pi}{a} \right\} \cos \frac{n\pi x}{a} \tag{25}$$

$$\tau_{xy} = -\frac{1}{b^2} \left[\frac{\partial^2 \chi_1}{\partial x \partial y} \right]_{y = \pm 1 - c} = \mp \sum_{s=1}^{\infty} 2s(2s - 1)(B_{2s} \pm D_{2s}) T_{2s+1}(x, \pm 1 - c) \pm \sum_{n=1}^{\infty} \frac{n\pi}{a} \left\{ \frac{n\pi}{a} A_n^* \sinh \frac{n\pi}{a} + B_n^* \left(\sinh \frac{n\pi}{a} + \frac{n\pi}{a} \cosh \frac{n\pi}{a} \right) \pm \frac{n\pi}{a} C_n^* \cosh \frac{n\pi}{a} \pm D_n^* \left(\cosh \frac{n\pi}{a} + \frac{n\pi}{a} \sinh \frac{n\pi}{a} \right) \right\} \sin \frac{n\pi x}{a} \tag{26}$$

Whenever the sign is in ambiguity, the upper one goes with the upper edge and the lower with the lower edge. These stresses vanish identically along both edges provided that by Fourier transforms the following relations are satisfied:

$$\frac{n^2\pi^2}{a^2} \left\{ (A_n^* \pm D_n^*) \cosh \frac{n\pi}{a} + (B_n^* \pm C_n^*) \sinh \frac{n\pi}{a} \right\} = -A_0 U_2(\pm 1 - c) - \sum_{s=1}^{\infty} 2s(2s + 1) \times (A_{2s} \pm C_{2s}) U_{2s+2}(\pm 1 - c),$$

$$\frac{n\pi}{a} \left\{ \frac{n\pi}{a} A_n^* \sinh \frac{n\pi}{a} + B_n^* \left(\sinh \frac{n\pi}{a} + \frac{n\pi}{a} \cosh \frac{n\pi}{a} \right) \pm \frac{n\pi}{a} C_n^* \cosh \frac{n\pi}{a} \pm D_n^* \left(\cosh \frac{n\pi}{a} + \frac{n\pi}{a} \sinh \frac{n\pi}{a} \right) \right\} = \sum_{s=1}^{\infty} 2s(2s - 1)(B_{2s} \pm D_{2s}) U_{2s+1}(\pm 1 - c) \tag{27}$$

where, for $n \geqslant 1$,

$$U_{2s+1}(\pm 1 - c) = \frac{1}{a} \int_{-a}^{a} T_{2s+1}(x, \pm 1 - c) \sin \frac{n\pi x}{a} \, dx$$
$$U_{2s+2}(\pm 1 - c) = \frac{1}{a} \int_{-a}^{a} S_{2s+2}(x, \pm 1 - c) \cos \frac{n\pi x}{a} \, dx \tag{28}$$

Since $T_{2s+1}(x, \pm 1 - c)$, for $s \geqslant 1$, vanishes identically when $x = \pm a$, we find by integrating by parts,

$$U_{2s+1}(\pm 1 - c) = \frac{1}{(2s)!} \left(\frac{n\pi}{a} \right)^{2s-1} U_2(\pm 1 - c)$$
$$U_{2s+2}(\pm 1 - c) = \frac{1}{(2s + 1)!} \left(\frac{n\pi}{a} \right)^{2s} U_2(\pm 1 - c) \tag{29}$$

In evaluating U_2, it may be recalled that $S_2(x, y)$ is the real part of $W_2(z)$ and in turn $W_2(z)$ is equal to

$$W_2(z) = \omega_2 - p(z) - p(z - a + 2ci) - p(z - 2i + 2ci) - p(z - a + 2i) \tag{30}$$

where ω_2 is defined in the second equation of (22). The Weierstrass elliptic function $p(z)$ can be expressed by the following series [7]:

$$p(z) = \left(\frac{\pi}{2a} \right)^2 \left\{ -\frac{1}{3} + \sum_{m=-\infty}^{\infty} \csc^2 \frac{\pi(z - 4mi)}{2a} - \sum_{m=-\infty}^{\infty}{}' \csc^2 \frac{2m\pi i}{a} \right\} \tag{31}$$

Now, for convenience, let u stand for 0 or a as the case may be, and v for a real quantity. Then, for $n \geqslant 1$,

$$\int_{-a}^{a} RP \, p(x - u + iv) \cos \frac{n\pi x}{a} \, dx = \int_{-a}^{a} \left(\frac{\pi}{2a} \right)^2 \times RP \sum_{m=-\infty}^{\infty} \csc^2 \frac{\pi(x - u + iv - 4mi)}{2a} \cos \frac{n\pi x}{a} \, dx = \frac{\pi}{2a} \sum_{m=-\infty}^{\infty} \int_{-\pi}^{\pi} \left\{ \frac{\cosh \alpha}{\cosh \alpha \mp \cos \phi} - \frac{\sinh^2 \alpha}{(\cosh \alpha \mp \cos \phi)^2} \right\} \cos n\phi \, d\phi \tag{32}$$

where

$$\phi = \frac{\pi x}{a}, \quad \alpha = \frac{\pi}{a} |4m - v| \tag{33}$$

The upper sign goes with $u = 0$ and the lower with $u = a$. Integrals of this type can be evaluated by Cauchy's theorem of residues [8]. It is found that for $\alpha > 0$,

$$\int_{-\pi}^{\pi} \frac{\cos n\phi \, d\phi}{\cosh \alpha \mp \cos \phi} = (\pm 1)^n \frac{2\pi e^{-n\alpha}}{\sinh \alpha}$$

$$\int_{-\pi}^{\pi} \frac{\cos n\phi d\phi}{(\cosh\alpha \mp \cos\phi)^2} = (\pm 1)^n \frac{2\pi e^{-n\alpha}}{\sinh^3\alpha}(n\sinh\alpha + \cosh\alpha) \tag{34}$$

It turns out that the values of $U_s(\pm 1 - c)$ are different according as n is odd or even. When n is odd,

$$U_s(\pm 1 - c) = \pm\frac{2n\pi^2}{a^2}\sinh\frac{n\pi c}{a}\Big/\cosh\frac{n\pi}{a} \tag{35}$$

and when n is even,

$$U_s(\pm 1 - c) = \frac{2n\pi^2}{a^2}\cosh\frac{n\pi c}{a}\Big/\sinh\frac{n\pi}{a} \tag{36}$$

With these values the values of $U_s(\pm 1 - c)$ are readily obtained from Equations (29). Consequently, we solve when n is odd

$$A_n^* = -\frac{4}{n}\sinh\frac{n\pi c}{a}\left\{\left(\frac{n\pi}{a} + \tanh\frac{n\pi}{a}\right)\sum_{s=1}^{\infty}\frac{C_{2s}}{(2s-1)!}\left(\frac{n\pi}{a}\right)^{2s} + \tanh\frac{n\pi}{a}\sum_{s=1}^{\infty}\frac{D_{2s}}{(2s-2)!}\left(\frac{n\pi}{a}\right)^{2s}\right\}\Big/\left(\sinh\frac{2n\pi}{a} + \frac{2n\pi}{a}\right)$$

$$B_n^* = \frac{4\pi}{a}\sinh\frac{n\pi c}{a}\left\{\tanh\frac{n\pi}{a}\sum_{s=1}^{\infty}\frac{C_{2s}}{(2s-1)!}\left(\frac{n\pi}{a}\right)^{2s} + \sum_{s=1}^{\infty}\frac{D_{2s}}{(2s-2)!}\left(\frac{n\pi}{a}\right)^{2s-1}\right\}\Big/\left(\sinh\frac{2n\pi}{a} + \frac{2n\pi}{a}\right)$$

$$C_n^* = -\frac{4}{\pi}\sinh\frac{n\pi c}{a}\left[\left(1 + \frac{n\pi}{a}\tanh\frac{n\pi}{a}\right)\times\left\{A_0 + \sum_{s=1}^{\infty}\frac{A_{2s}}{(2s-1)!}\left(\frac{n\pi}{a}\right)^{2s}\right\} + \sum_{s=1}^{\infty}\frac{B_{2s}}{(2s-2)!}\left(\frac{n\pi}{a}\right)^{2s}\right]\Big/\left(\sinh\frac{2n\pi}{a} - \frac{2n\pi}{a}\right)$$

$$D_n^* = \frac{4\pi}{a}\sinh\frac{n\pi c}{a}\left\{A_0 + \sum_{s=1}^{\infty}\frac{A_{2s}}{(2s-1)!}\left(\frac{n\pi}{a}\right)^{2s} + \tanh\frac{n\pi}{a}\sum_{s=1}^{\infty}\frac{B_{2s}}{(2s-2)!}\left(\frac{n\pi}{a}\right)^{2s-1}\right\}\Big/\left(\sinh\frac{2n\pi}{a} - \frac{2n\pi}{a}\right) \tag{37}$$

and when n is even

$$A_n^* = -\frac{4}{n}\cosh\frac{n\pi c}{a}\left[\left(1 + \frac{n\pi}{a}\coth\frac{n\pi}{a}\right)\times\left\{A_0 + \sum_{s=1}^{\infty}\frac{A_{2s}}{(2s-1)!}\left(\frac{n\pi}{a}\right)^{2s}\right\} + \sum_{s=1}^{\infty}\frac{B_{2s}}{(2s-2)!}\left(\frac{n\pi}{a}\right)^{2s}\right]\Big/\left(\sinh\frac{2n\pi}{a} + \frac{2n\pi}{a}\right)$$

$$B_n^* = \frac{4\pi}{a}\cosh\frac{n\pi c}{a}\left\{A_0 + \sum_{s=1}^{\infty}\frac{A_{2s}}{(2s-1)!}\left(\frac{n\pi}{a}\right)^{2s} + \coth\frac{n\pi}{a}\sum_{s=1}^{\infty}\frac{B_{2s}}{(2s-2)!}\left(\frac{n\pi}{a}\right)^{2s-1}\right\}\Big/\left(\sinh\frac{2n\pi}{a} + \frac{2n\pi}{a}\right)$$

$$C_n^* = -\frac{4}{n}\cosh\frac{n\pi c}{a}\left\{\left(\frac{n\pi}{a} + \coth\frac{n\pi}{a}\right)\sum_{s=1}^{\infty}\frac{C_{2s}}{(2s-1)!}\left(\frac{n\pi}{a}\right)^{2s} + \coth\frac{n\pi}{a}\sum_{s=1}^{\infty}\frac{D_{2s}}{(2s-2)!}\left(\frac{n\pi}{a}\right)^{2s}\right\}\Big/\left(\sinh\frac{2n\pi}{a} - \frac{2n\pi}{a}\right)$$

$$D_n^* = \frac{4\pi}{a}\cosh\frac{n\pi c}{a}\left\{\coth\frac{n\pi}{a}\sum_{s=1}^{\infty}\frac{C_{2s}}{(2s-1)!}\left(\frac{n\pi}{a}\right)^{2s} + \sum_{s=1}^{\infty}\frac{D_{2s}}{(2s-2)!}\left(\frac{n\pi}{a}\right)^{2s-1}\right\}\Big/\left(\sinh\frac{2n\pi}{a} - \frac{2n\pi}{a}\right) \tag{38}$$

These are the conditions of zero tractions along both edges. Since the stresses derived from χ_0 do not vanish at x infinity, it is therefore necessary to investigate the resultant tension across any section of the strip. It is mentioned that by symmetry the resultant shear and transverse bending moment derived from χ_0 are both zero across any section of the strip. If we denote the resultant tension by bT^*, we have

$$T^* = \int_{-1-c}^{1-c}\sigma_x dy = \frac{1}{b^2}\int_{-1-c}^{1-c}\frac{\partial^2\chi_0}{\partial y^2}dy = \frac{1}{b^2}\left[\frac{\partial\chi_0}{\partial y}\right]_{-1-c}^{1-c}$$
$$= (B_2 - A_0)\{S_0(x, 1-c) - S_0(x, -1-c)\} - \sum_{s=1}^{\infty}(2s-1)\{(B_{2s} + D_{2s})S_{2s}(x, 1-c) + (B_{2s} - D_{2s})S_{2s}(x, -1-c)\} + 2\sum_{n=1}^{\infty}\left\{\frac{n\pi}{a}A_n^*\sinh\frac{n\pi}{a} + B_n^*\left(\sinh\frac{n\pi}{a} + \frac{n\pi}{a}\cosh\frac{n\pi}{a}\right)\right\}\cos\frac{n\pi x}{a} \tag{39}$$

By Equations (27), (28), and (29),

$$2\sum_{n=1}^{\infty}\left\{\frac{n\pi}{a}A_n^*\sinh\frac{n\pi}{a} + B_n^*\left(\sinh\frac{n\pi}{a} + \frac{n\pi}{a}\cosh\frac{n\pi}{a}\right)\right\}\cos\frac{n\pi x}{a} = \sum_{s=1}^{\infty}(2s-1)\sum_{n=1}^{\infty}\{(B_{2s} + D_{2s})U_{2s}(1-c) + (B_{2s} - D_{2s})U_{2s}(-1-c)\}\cos\frac{n\pi x}{a} \tag{40}$$

Again, by Fourier expansion,

$$S_{2s}(x, \pm 1 - c) = \frac{1}{(2s-1)a}T_{2s-1}(a, \pm 1 - c) + \sum_{n=1}^{\infty}U_{2s}(\pm 1 - c)\cos\frac{n\pi x}{a} \tag{41}$$

Also, with the aid of Equation (21) and the relation [6]

$$2\zeta(a) + ai\zeta(2i) = \frac{1}{2}\pi \tag{42}$$

we find

$$T^* = -\frac{\pi}{a}A_0 - (A_0 - 2B_2)\left\{\frac{\pi}{a} - \frac{8}{a}\zeta(a) - 2\omega_2\right\} \tag{43}$$

which is a constant. Hence the resultant tension will be annulled if a biharmonic function χ^* of the following form is added to χ_0:

$$\chi^* = -\frac{1}{2} b^2 T^* y^2 \quad . \tag{44}$$

It is obvious that such a modification on χ_1 does not affect the boundary conditions of zero tractions along the edges.

Boundary Conditions on the Holes

To adjust the remaining boundary conditions of zero tractions on the holes, it is necessary to express the function χ_1 thus modified in polar co-ordinates (r, θ) as defined in Equation (16). By Equation (17) and the following expansions:

$$\cosh \frac{m\pi(y+c)}{a} \cos \frac{m\pi x}{a} = \sum_{n=0}^{\infty} \left\{ \cosh \frac{m\pi c}{a} \left(\frac{m\pi r}{a}\right)^{2n} \frac{\cos 2n\theta}{(2n)!} + \sinh \frac{m\pi c}{a} \left(\frac{m\pi r}{a}\right)^{2n+1} \frac{\cos (2n+1)\theta}{(2n+1)!} \right\}$$

$$\sinh \frac{m\pi(y+c)}{a} \cos \frac{m\pi x}{a} = \sum_{n=0}^{\infty} \left\{ \sinh \frac{m\pi c}{a} \left(\frac{m\pi r}{a}\right)^{2n} \frac{\cos 2n\theta}{(2n)!} + \cosh \frac{m\pi c}{a} \left(\frac{m\pi r}{a}\right)^{2n+1} \frac{\cos (2n+1)\theta}{(2n+1)!} \right\} \tag{45}$$

we find through a lengthy, though straightforward, reduction that the modified stress function χ_1 is expanded into the following condensed form:

$$\chi_1 = b^2(-E_0 \log r + Q_0 r^2) + b^2 \sum_{n=1}^{\infty} \{(E_n + F_n r^2) r^{-n} + (P_n + Q_n r^2) r^n\} \cos n\theta \tag{46}$$

where, save for F_1 and P_1, the coefficients of the trivial term $r \cos \theta$, the following notations are used:

$$E_0 = A_0, \quad E_{2n} = A_{2n} + \frac{1}{2} B_{2n+2} + cC_{2n},$$

$$E_{2n-1} = D_{2n} + \frac{2n+1}{2(2n-1)} C_{2n} + cB_{2n}, \tag{47}$$

$$F_{2n} = \frac{1}{2} B_{2n}, \quad F_{2n+1} = \frac{1}{2} C_{2n}$$

and

$$P_n = -{}^n\alpha_n A_0 - \sum_{s=1}^{\infty} ({}^n\alpha_{2s} A_{2s} + {}^n\beta_{2s} B_{2s} + {}^n\gamma_{2s} C_{2s} + {}^n\delta_{2s} D_{2s})$$

$$Q_n = {}^n\alpha_0{}^* A_0 + \sum_{s=1}^{\infty} ({}^n\alpha_{2s}{}^* A_{2s} + {}^n\beta_{2s}{}^* B_{2s} + {}^n\gamma_{2s}{}^* C_{2s} + {}^n\delta_{2s}{}^* D_{2s}) \tag{48}$$

in which

$${}^n\alpha_0 = -{}^n\Omega_0 + \frac{2(K_n{}^* - cK_n)}{(2-2c)^{n+1}} - \frac{(n-2)K_{n-1}}{n(2-2c)^n},$$

$${}^n\alpha_{2s} = -{}^n\Omega_{2s} + \binom{n+2s-1}{n} \frac{2(n+2s)(K_{n+2s}{}^* - cK_{n+2s})}{(2-2c)^{n+2s+1}} - \frac{n-2}{n} \binom{n+2s-2}{n-1} \frac{(n+2s-1)K_{n+2s-1}}{(2-2c)^{n+2s}},$$

$${}^n\beta_{2s} = \frac{1}{2} ({}^{n-1}\Omega_{2s-1} + 2c\,{}^n\Omega_{2s-1}) + \binom{n+2s-2}{n} \frac{2(n+2s-1)(K_{n+2s-1} - cK_{n+2s-1}{}^*)}{(2-2c)^{n+2s}} - \binom{n+2s-3}{n-1} \frac{(n+2s-2)K_{n+2s-2}{}^*}{(2-2c)^{n+2s-1}}$$

$${}^n\gamma_{2s} = -\frac{1}{2} \left(\frac{n-2}{n} {}^{n-1}\Omega_{2s} + 2c\,{}^n\Omega_{2s} \right) + \binom{n+2s-1}{n} \frac{2(n+2s)(J_{n+2s}{}^* - cJ_{n+2s})}{(2-2c)^{n+2s+1}} - \frac{n-2}{n} \binom{n+2s-2}{n-1} \frac{(n+2s-1)J_{n+2s-1}}{(2-2c)^{n+2s}}$$

$${}^n\delta_{2s} = {}^n\Omega_{2s-1} + \binom{n+2s-2}{n} \frac{2(n+2s-1)(J_{n+2s-1} - cJ_{n+2s-1}{}^*)}{(2-2c)^{n+2s}} - \binom{n+2s-3}{n-1} \frac{(n+2s-2)J_{n+2s-2}{}^*}{(2-2c)^{n+2s-1}}, \tag{49}$$

and

$${}^n\alpha_0{}^* = \frac{K_{n+1}}{(2-2c)^{n+2}}$$

$${}^n\alpha_{2s}{}^* = \binom{n+2s}{n+1} \frac{(n+2s+1)K_{n+2s+1}}{(2-2c)^{n+2s+2}}$$

$${}^n\beta_{2s}{}^* = -\frac{1}{2} {}^{n+1}\Omega_{2s-1} + \binom{n+2s-1}{n+1} \frac{(n+2s)K_{n+2s}{}^*}{(2-2c)^{n+2s+1}}$$

$${}^n\gamma_{2s}{}^* = \frac{1}{2} {}^{n+1}\Omega_{2s} + \binom{n+2s}{n+1} \frac{(n+2s+1)J_{n+2s+1}}{(2-2c)^{n+2s+2}}$$

$${}^n\delta_{2s}{}^* = \binom{n+2s-1}{n+1} \frac{(n+2s)J_{n+2s}{}^*}{(2-2c)^{n+2s+1}} \tag{50}$$

Besides, due to χ^*, values

$$\pm \left\{ \frac{\pi}{2a} - \frac{2}{a} \zeta(a) - \frac{1}{2} \omega_2 \right\} \quad \text{and} \quad \mp \left\{ \frac{\pi}{2a} - \frac{4}{a} \zeta(a) - \omega_2 \right\}$$

are to be added to ${}^0\alpha_0{}^*$, ${}^2\alpha_0$, ${}^0\beta_2{}^*$, and ${}^2\beta_2$, respectively. The coefficients K_k, J_k, $K_k{}^*$, and $J_k{}^*$ are defined by the following series:

$$\frac{K_{2k}}{J_{2k}{}^*} = \frac{(1-c)^{2k+1}}{(2k)!} \left(\frac{2\pi}{a}\right)^{2k+1} \times \left\{ \sum_{n=1,3,5,\ldots}^{\infty} \frac{n^{2k} \sinh (2n\pi c/a)}{\sinh (2n\pi/a) \mp (2n\pi/a)} + \sum_{n=2,4,6,\ldots}^{\infty} \frac{n^{2k} \sinh (2n\pi c/a)}{\sinh (2n\pi/a) \pm (2n\pi/a)} \right\}$$

$$\frac{K_{2k+1}}{J_{2k+1}{}^*} = \frac{2(1-c)^{2k+2}}{(2k+1)!} \left(\frac{2\pi}{a}\right)^{2k+2} \times \left\{ \sum_{n=1,3,5,\ldots}^{\infty} \frac{n^{2k+1} \sinh^2 (n\pi c/a)}{\sinh (2n\pi/a) \mp (2n\pi/a)} + \sum_{n=2,4,6,\ldots}^{\infty} \frac{n^{2k+1} \cosh^2 (n\pi c/a)}{\sinh (2n\pi/a) \pm (2n\pi/a)} \right\}$$

$$\frac{K_{2k}^*}{J_{2k}} = \frac{2(1-c)^{2k+1}}{(2k)!}\left(\frac{2\pi}{a}\right)^{2k+1} \times \left\{\sum_{n=1,3,5,\ldots}^{\infty} \frac{n^{2k}\tanh(n\pi/a)\sinh^2(n\pi c/a)}{\sinh(2n\pi/a) \mp (2n\pi/a)} + \sum_{n=2,4,6,\ldots}^{\infty} \frac{n^{2k}\coth(n\pi/a)\cosh^2(n\pi c/a)}{\sinh(2n\pi/a) \pm (2n\pi/a)}\right\}$$

$$\frac{K_{2k+1}^*}{J_{2k+1}} = \frac{(1-c)^{2k+2}}{(2k+1)!}\left(\frac{2\pi}{a}\right)^{2k+2} \times \left\{\sum_{n=1,3,5,\ldots}^{\infty} \frac{n^{2k+1}\tanh(n\pi/a)\sinh(2n\pi c/a)}{\sinh(2n\pi/a) \mp (2n\pi/a)} + \sum_{n=2,4,6,\ldots}^{\infty} \frac{n^{2k+1}\coth(n\pi/a)\sinh(2n\pi c/a)}{\sinh(2n\pi/a) \pm (2n\pi/a)}\right\} \quad (51)$$

Suppose now that the normal and tangential stresses derived from the basic stress function χ_0 take the following values on the hole $r = \lambda$:

$$[\sigma_r]_0 = \sum_{n=0}^{\infty} a_n \cos n\theta, \quad [\tau_{r\theta}]_0 = \sum_{n=1}^{\infty} c_n \sin n\theta \quad (52)$$

Note that the equality $a_1 = c_1$ implies the condition of zero force resultant on this hole. In order to satisfy the boundary conditions of zero tractions, these stresses must be annulled by the corresponding stresses derived from the modified function χ_1. Now, from the latter the normal and tangential stresses in polar co-ordinates are derived as follows:

$$\sigma_r = \frac{1}{b^2}\left(\frac{1}{r}\frac{\partial\chi_1}{\partial r} + \frac{1}{r^2}\frac{\partial^2\chi_1}{\partial\theta^2}\right)$$

$$= -E_0 r^{-2} + 2Q_0 - \sum_{n=1}^{\infty} [\{n(n+1)E_n + (n-1)(n+2)F_n r^2\} r^{-n-2} + \{n(n-1)P_n + (n-2)(n+1)Q_n r^2\} r^{n-2}] \cos n\theta \quad (53)$$

$$\tau_{r\theta} = -\frac{1}{b^2}\frac{\partial}{\partial r}\left(\frac{1}{r}\frac{\partial\chi_1}{\partial\theta}\right)$$

$$= -\sum_{n=1}^{\infty} [\{n(n+1)E_n + n(n-1)F_n r^2\} r^{-n-2} - \{n(n-1)P_n + n(n+1)Q_n r^2\} r^{n-2}] \sin n\theta$$

It can be shown that the boundary conditions of zero tractions on the hole $r = \lambda$ are satisfied provided that

$$E_0 = a_0\lambda^2 + 2Q_0\lambda^2$$

$$E_n = \frac{(n+2)c_n - na_n}{2n(n+1)}\lambda^{n+2} + (n-1)P_n\lambda^{2n} + nQ_n\lambda^{2n+2}, \quad (n \geqslant 1) \quad (54)$$

$$F_n = \frac{a_n - c_n}{2(n-1)}\lambda^n - nP_n\lambda^{2n-2} - (n+1)Q_n\lambda^{2n}, \quad (n \geqslant 2)$$

The set of linear equations may be solved in a similar manner by the method of successive approximations as described in the previous paper for a strip containing an unsymmetrically located hole [1]. It is mentioned that the validity of this method depends upon the value of λ. The larger the value of λ the slower will be the convergence. From physical consideration alone, it seems likely that there will be convergence as long as each perforating hole does not touch the adjacent boundaries. By the method previously used by Howland [9] and Knight [10], a considerable range of convergence can be established for λ corresponding to any given pair of values of c and a. However, for the sake of brevity, the convergence will only be illustrated later by numerical examples.

Because of periodicity, if the boundary conditions of zero tractions on the hole $r = \lambda$ are satisfied, the corresponding conditions on all the remaining holes are automatically satisfied.

It is now rather straightforward to calculate the stresses at any point in the strip. In particular, the stress on the hole $r = \lambda$ is given by

$$[\sigma_\theta]_{r=\lambda} = \frac{1}{b^2}\left[\frac{\partial^2\chi}{\partial r^2}\right]_{r=\lambda} = \frac{1}{b^2}[\nabla^2\chi]_{r=\lambda}$$

$$= \frac{1}{b^2}[\nabla^2\chi_0]_{r=\lambda} + 4Q_0 - 4\sum_{n=1}^{\infty}\{(n-1)F_n\lambda^{-n} - (n+1)Q_n\lambda^n\}\cos n\theta \quad (55)$$

Numerical Examples

The foregoing solution will be illustrated numerically by solving a perforated strip specified by the following values:

$$a = 0.5, \quad c = 0.4, \quad \lambda = 0.3$$

Two fundamental stress systems acting in the strip will be considered: (*a*) When it is under a longitudinal tension; and (*b*) when it is under a transverse bending.

The coefficients in Equations (49) and (50) are first computed with the aid of the values in Tables 1 and 2. The results are shown in Tables 3 and 4.

When the strip is under a longitudinal tension of T per unit width, the basic stress function χ_0 is given by

$$\chi_0 = \frac{1}{2}Tb^2y^2 \quad (56)$$

By comparing the stresses at $r = \lambda$ derived from this function with Equations (52), we find

$$a_0 = -a_2 = c_2 = \frac{1}{2}T, \quad (57)$$

the rest of a_n and c_n being all zero.

Again, when the strip is under a transverse bending of total moment $-Mb^2$, the basic stress function is given by

$$\chi_0 = \frac{1}{4}Mb^2(y+c)^2 \quad (58)$$

Similarly, we find

$$-a_0 = -a_2 = c_2 = \frac{3}{4}Mc$$

$$a_1 = -a_3 = c_1 = c_3 = \frac{3}{8}M\lambda \quad (59)$$

the rest of a_n and c_n being all zero.

With these values of a_n and c_n, the coefficients E_n, F_n, P_n, and Q_n are computed in each case for $\lambda = 0.3$ by the method of successive approximations. The results are shown in Table 5. Each computation has been carried out up to the sixth approxi-

Table 1 Coefficients, for $a = 0.5$ and $c = 0.4$

k	J_{2k}	J_{2k+1}	K_{2k}	K_{2k+1}	J^*_{2k}	J^*_{2k+1}	K^*_{2k}	K^*_{2k+1}
0	0.00395670	0.0302427	0.00400966	0.0298543	0.00400896	0.0298491	0.00395739	0.0302480
1	0.1126488	0.287459	0.1141544	0.283779	0.1141344	0.283729	0.1126686	0.287510
2	0.537117	0.827517	0.544249	0.817057	0.544154	0.816916	0.537210	0.827660
3	1.044094	1.176888	1.057608	1.162735	1.057426	1.162544	1.044271	1.177081
4	1.167582	1.111053	1.181291	1.099894	1.181109	1.099743	1.167762	1.111206
5	1.014999	0.961373	1.023636	0.955637	1.023520	0.955559	1.015113	0.961452
6	0.936604	0.952305	0.940284	0.950261	0.940235	0.950233	0.936653	0.952334
7	0.977995	1.003491	0.979095	1.002986	0.979079	1.002979	0.978010	1.003498
8	1.016247	1.017348	1.016460	1.017322	1.016456	1.017282	1.016250	1.017350

Table 2 Functions, for $a = 0.5$ and $c = 0.4$

k	ω^*_k	$f_k(a-2a_1)$	$f_k(2_1-2a_1)$	$f_k(a-2_1)$	ω_k
1	-	1.6x4934 +0.4687401	0.8029081	1.644934 -3.4301443	2.166496
2	-	-3.034300	-3.3 0674	-3.289593	-9.634667
3	0	0.7927314	0.0560561	0	0.858790
4	2.16464, 5474	-1.616866	0.13 653	-0.071812	0.684622
5	0	-2.405131	-0.2187031	0	2.624015
6	2.03468, 6111	2.092163	-0.277183	0.003576	-4.453842
7	0	2.150234	0.2951331	0	2.445367
8	2.00815, 4724	-0.708971	0.273753	-0.003360	1.488577
9	0	1.030694	-0.2289241	0	-0.801970
10	2.00196, 9144	-2.744130	-0.179467	0.001840	0.919768
11	0	-3.764701	0.1377911	0	-3.626909
12	2.00049, 2175	3.677670	0.107633	-0.000657	3.785338
13	0	2.301222	-0.0878601	0	-2.293342
14	2.00012, 2496	-0.150866	-0.074174	0.000163	-1.775246
15	0	2.402941	0.0633421	0	2.466192
16	2.00003, 0365	-4.409425	0.034277	-0.000028	-2.439145
17	0	-3.371221	-0.0456171	0	5.417237

mation. The coefficients are readily converted to A_n, B_n, C_n, and D_n by Equations (47).

The most important are the stresses on the rims of the holes. For the hole $r = \lambda$, the values found from Equation (55) are shown in Table 6 and also plotted in Fig. 5. It appears that in both examples there are three points of maximum tensile stress on the rim of each hole, among which the point nearest to the adjacent straight boundary, where $\theta = 0$, is of the greatest magnitude. In the longitudinal tension case the two remaining maximum points occur at $\theta = \pm 148°0'$ which are nearest to the adjacent circular boundaries and are each of the magnitude 3.081 T. In the transverse-bending case the two remaining points occur at $\theta = \pm 135°19'$ and are each of the magnitude 0.838 M.

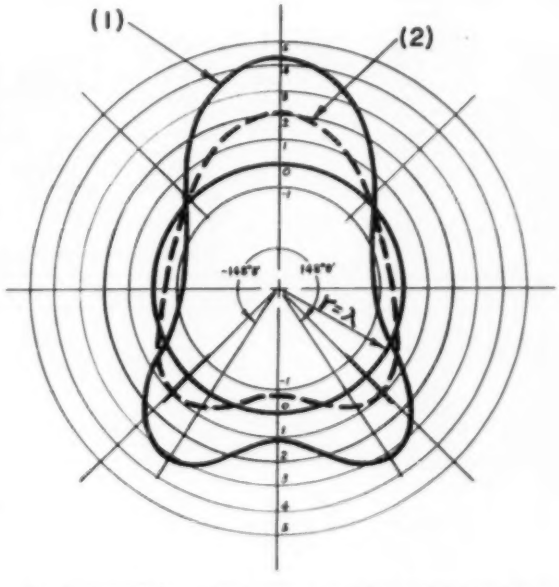

Fig. 5 Stress $[\sigma\theta]_{r=\lambda}$, for the case $a = 0.5$, $c = 0.4$, $\lambda = 0.3$. (1) Longitudinal tension, for $T = 1$; (2) transverse bending, for $M = 1$.

References

1 C. B. Ling, "Stresses in a Perforated Strip," JOURNAL OF APPLIED MECHANICS, vol. 24, TRANS. ASME, vol. 79, 1957, pp. 365–375.

2 A. E. Green, "General Biharmonic Analysis for a Plate Containing Circular Holes," *Proceedings of The Royal Society*, London, England, series A, vol. 176, 1940, pp. 121–139.

3 R. C. J. Howland and R. C. Knight, "Stress Functions for a Plate Containing Groups of Circular Circles," *Philosophical Transactions of The Royal Society*, London, England, series A, vol. 238, 1939, pp. 357–392.

4 A. Atsumi, "Stresses in a Strip With Two Circular Holes," JOURNAL OF APPLIED MECHANICS, vol. 23, TRANS. ASME, vol. 78, 1956, pp. 555–562.

5 C. B. Ling, P. S. Wang, and K. S. Jing, "Stresses in a Perforated Strip Containing a Series of Circular Holes Under Tension,"

Table 3 Coefficients, for $a = 0.5$ and $c = 0.4$

Coeff.	2s	n=0	n=1	n=2	n=3	n=4	n=5	n=6	n=7	n=8
${}^{n}\alpha_{1s}$	0	–	–	-1.3016	-1.4046×10^{-1}	1.7226×10^{-2}	-3.2058×10^{-1}	9.0653×10^{-1}	-2.2900×10^{-1}	-1.1940×10^{-1}
	2	–	–	1.0278	-4.6618	2.9932×10	-6.0759×10^{-1}	-2.9004	$1.2869\times10_{2}$	-3.1978
	4	–	–	6.5337×10	-8.4466	4.4270	1.1573×10^{2}	0.3024×10^{-2}	5.2406×10^{2}	-8.5322×10^{2}
	6	–	–	1.4014×10	1.4137×10^{2}	$4.4760\times10_{3}$	1.1700×10^{3}	-2.2900×10^{3}	2.3861×10^{3}	3.0847×10^{3}
	8	–	–	2.5579×10	5.9019×10^{2}	-4.5660×10^{3}	2.5253×10^{3}	4.3669×10^{3}	-6.2013×10^{3}	1.9234×10^{4}
${}^{n}\beta_{1s}$	2	–	–	3.1826×10^{-1}	1.3462	2.1559	2.8781×10^{-1}	-7.4429×10^{-1}	2.1165	5.1829×10^{-1}
	4	–	–	1.4499×10	3.1737	8.7118	4.8608×10^{2}	2.1976×10	$1.6638\times10_{2}$	-3.4505×10
	6	–	–	2.8588×10	$8.7948\times10_{2}$	7.3600×10	1.1469×10^{2}	-1.2296×10^{2}	5.5244×10^{2}	7.2452×10^{2}
	8	–	–	3.6904×10	1.1409×10^{2}	-8.4892×10	1.0254×10^{3}	1.0687×10^{3}	-1.3356×10^{3}	2.8460×10^{3}
${}^{n}\gamma_{1s}$	2	–	–	2.3546	1.1050	1.4224×10	9.0806	-1.2226	5.0342	4.3649
	4	–	–	3.9239×10	2.7080×10	2.5274×10	7.1003×10	6.3400×10	2.3361×10^{2}	$-1.1603\times10_{2}$
	6	–	–	3.3996×10	1.0677×10^{2}	1.2909×10^{2}	5.8260×10^{2}	-3.7759×10^{2}	3.3838×10^{2}	2.3973×10^{3}
	8	–	–	4.6595×10	3.2125×10^{2}	-3.0735×10^{2}	8.5887×10^{2}	3.1482×10^{3}	-4.8824×10	6.6594×10^{3}
${}^{n}\delta_{1s}$	2	–	–	1.2301	1.3012	3.4263	-3.7410	2.9925	1.7515	-6.8211×10^{-1}
	4	–	–	2.3182×10	-3.1939×10	5.3741×10	$4.8138\times10_{2}$	-6.2802	$4.7036\times10_{3}$	-1.4850×10^{2}
	6	–	–	6.2595×10	$9.9156\times10_{2}$	$1.6346\times10_{2}$	2.0939×10^{2}	-6.3515×10^{3}	2.0765×10^{3}	-9.0962×10^{2}
	8	–	–	1.9357×10	1.6943×10^{2}	-5.7727×10^{2}	3.0061×10^{3}	-1.5356×10^{3}	-2.1067×10^{3}	8.8151×10^{3}

Table 4 Coefficients, for $a = 0.5$ and $c = 0.4$

Coeff.	2s	n=0	n=1	n=2	n=3	n=4	n=5	n=6	n=7	n=8
${}^{n}\alpha^{*}_{1s}$	0	1.3999	6.6062×10^{-2}	1.3685×10^{-1}	2.1872×10^{-1}	2.7363×10^{-1}	2.9516×10^{-1}	2.7042×10^{-1}	2.2894×10^{-1}	1.7764×10^{-1}
	2	8.2112×10^{-1}	2.6247	5.4726	8.8546	1.1357x10	1.2821x10	$1.2790\times10_{2}$	$1.2399\times10_{2}$	1.1750×10
	4	5.4726	1.7710×10	3.7858×10	6.4104×10	$8.9530\times10_{2}$	1.1573×10^{2}	1.4148×10^{2}	1.7401×10^{3}	2.1168×10^{2}
	6	1.1357×10	3.8462×10	$8.9530\times10_{2}$	1.7359×10^{2}	2.9711×10^{2}	4.6722×10^{2}	7.6203×10^{2}	1.1450×10^{3}	1.6291×10^{3}
	8	1.2790×10	4.9597×10	1.4148×10^{2}	3.4802×10^{2}	7.6203×10^{2}	1.5267×10^{3}	2.7928×10^{3}	4.7171×10^{3}	7.4314×10^{3}
${}^{n}\beta^{*}_{1s}$	2	3.1362×10^{-1}	-1.3438×10^{-2}	5.2126×10^{-1}	7.3900×10^{-2}	3.9752	6.9358×10^{-1}	1.0663	2.0162	9.0634×10^{-1}
	4	1.5638	4.4340×10^{-1}	3.9752x10	1.0404x10	2.2392×10	5.6453x10	$3.2628\times10_{2}$	1.3498×10^{2}	-1.0132×10^{2}
	6	1.9876x10	1.0404x10	3.7320×10	1.4113×10^{2}	1.1420×10^{2}	6.2992×10^{2}	-6.0791×10^{2}	1.0449×10^{3}	1.2701×10^{3}
	8	7.4639	5.6453x10	7.6132×10	6.2992×10^{2}	-8.5107×10^{2}	1.9505×10^{3}	3.0482×10^{3}	-1.2585×10^{3}	9.7621×10^{3}
${}^{n}\gamma^{*}_{1s}$	2	1.6906	3.6172	1.0791×10	-2.3915	1.8832×10	1.7882×10	9.7119	$1.6434\times10_{2}$	-6.2739
	4	1.0791×10	-4.7830	6.2773×10	$8.9410\times10_{2}$	$6.7983\times10_{2}$	1.5338×10^{2}	$-7.5286\times10_{2}$	6.5062×10^{2}	$-4.0136\times10_{3}$
	6	1.8832×10	5.3646×10	6.7983×10	2.3007×10^{2}	-1.5810×10^{2}	1.8217×10^{3}	-1.4449×10^{2}	1.3616	4.0989×10^{3}
	8	9.7119	6.5734×10	-7.5286×10	1.3012×10^{3}	-1.4449×10^{2}	1.8155	7.0267×10^{3}	-3.1189×10^{3}	3.8418×10^{4}
${}^{n}\delta^{*}_{1s}$	2	1.3210×10^{-1}	4.1049×10^{-1}	8.7473×10^{-1}	1.3679	1.7707	1.8926	1.8313	1.5985	1.3775
	4	2.6242	8.2075	1.7707×10	$2.8389\times10_{2}$	$3.8456\times10_{2}$	$4.4759\times10_{2}$	$4.8591\times10_{2}$	$5.3050\times10_{2}$	$5.7999\times10_{2}$
	6	8.6533	2.8389×10	$6.4094\times10_{2}$	1.1190×10^{2}	1.7357×10^{2}	2.4757×10^{2}	3.4800×10^{2}	4.7626×10^{2}	6.3611×10^{2}
	8	1.2819×10	4.4759×10	1.1571×10^{2}	2.4757×10^{2}	4.8720×10^{2}	8.8901×10^{2}	1.5267×10^{3}	2.4436×10^{3}	3.6689×10^{3}

Table 5 Coefficients, for case $a = 0.5$, $c = 0.4$, $\lambda = 0.3$

n	Longitudinal tension case (T=1)				Transverse bending case (L=1)			
	E_n	F_n	P_n	Q_n	E_n	F_n	P_n	Q_n
0	4.7516×10^{-2}	–	–	1.3976×10^{-2}	-4.0488×10^{-2}	–	–	-7.4935×10^{-2}
1	1.4608×10^{-4}	–	–	1.3035×10^{-2}	1.4951×10^{-3}	–	–	-2.9215×10^{-3}
2	2.2624×10^{-3}	-5.0583×10^{-2}	3.6134×10^{-2}	-3.7915×10^{-2}	6.4662×10^{-4}	-1.4044×10^{-2}	-6.4079×10^{-2}	-3.3840×10^{-2}
3	1.9418×10^{-4}	-3.1901×10^{-3}	1.1604×10^{-1}	1.2696×10^{-1}	1.4267×10^{-4}	-2.3593×10^{-3}	2.8495×10^{-2}	5.0787×10^{-2}
4	-1.1308×10^{-5}	1.5970×10^{-4}	-1.4542×10^{-2}	-3.5757×10^{-1}	-7.0103×10^{-6}	1.0066×10^{-4}	-1.6081×10^{-2}	-1.4612×10^{-1}
5	6.4405×10^{-6}	-8.9450×10^{-5}	2.7264×10^{-1}	2.4528×10^{-4}	2.3241×10^{-6}	-3.2332×10^{-5}	1.0248×10^{-1}	-3.6316×10^{-2}
6	-6.7329×10^{-7}	8.9795×10^{-6}	-2.5601×10^{-1}	2.4339×10^{-2}	-1.1531×10^{-7}	1.5373×10^{-6}	-4.3181×10^{-2}	-2.0010×10^{-3}
7	2.2941×10^{-8}	-2.9894×10^{-7}	1.0036×10^{-1}	-1.9451×10^{-1}	-1.6963×10^{-9}	2.1310×10^{-8}	3.0452×10^{-3}	-8.5296×10^{-2}
8	6.6111×10^{-9}	-8.3892×10^{-8}	2.0943×10^{-1}	9.6888×10^{-2}	2.8611×10^{-9}	-3.6301×10^{-8}	8.9908×10^{-2}	4.9003×10^{-2}

Technical Report No. 9, Bureau of Aeronautical Research, China, 1944.

6 E. T. Copson, "Theory of Functions of a Complex Variable," Oxford University Press, 1935, compare with example 13, p. 378. For the general theory of the functions, see chapter 13.

7 Ibid., example 19, p. 379.

8 E. T. Whittaker and G. N. Watson, "Modern Analysis," Cambridge University Press, American edition, 1945, p. 112.

9 R. C. J. Howland, "Stresses in a Plate Containing an Infinite Row of Holes," *Proceedings of The Royal Society*, London, England, series A, vol. 148, 1935, pp. 471–491.

10 R. C. Knight, "On the Stresses in a Perforated Strip," *Quarterly Journal of Mathematics*, Oxford series, vol. 5, 1934, pp. 255–268.

11 C. B. Ling, Doctoral thesis presented to London University, England, 1937, p. 28.

12 Reference [8], example 23, p. 459; also p. 441.

APPENDIX

Evaluation of Coefficients

The coefficients K_k, K_k^*, J_k, J_k^* in Equations (51) can conveniently be computed by direct summation of the series which are in general rapidly convergent. The values corresponding to $a = 0.5$ and $c = 0.4$ are shown in Table 1.

To evaluate the coefficients ω_k in Equation (9), we denote for $k \geqslant 3$,

$$\omega_k^* = \sum_{m,n=-\infty}^{\infty}{}' \frac{1}{P_{mn}^k}, \qquad f_k(z) = \sum_{m,n=-\infty}^{\infty} \frac{1}{(z + P_{mn})^k}, \tag{60}$$

so that

$$(-1)^k\omega_k = \omega_k^* + f_k(a - 2ri) + f_k(2i - 2ci) + f_k(a - 2i) \tag{61}$$

The coefficients ω_k^* vanish identically when k is odd. A recurrence relation for ω_{2k}^* is as follows: For $k \geqslant 4$,

$$\frac{1}{3}(k-3)(2k+1)G_{2k} = G_4G_{2k-4} + G_6G_{2k-6} + G_8G_{2k-8} + \ldots + G_{2k-4}G_4 \tag{62}$$

where

$$G_{2k} = (2k-1)\omega_{2k}^* \tag{63}$$

The values of ω_{2k}^* corresponding to $a = 0.5$ have been computed to 10 digits by the author [11] some time ago and are reproduced in Table 2.

For convenience, we also denote

$$f_1(z) = \zeta(z) = \frac{1}{z} - \sum_{n=1}^{\infty} \omega_{2n+2}^* z^{2n+1},$$
$$f_2(z) = p(z) = \frac{1}{z^2} + \sum_{n=1}^{\infty} (2n+1)\omega_{2n+2}^* z^{2n} \tag{64}$$

Table 6 Stress $[\sigma_\theta]_{r=\lambda}$, for case $a = 0.5$, $c = 0.4$, $\lambda = 0.3$

θ, degs	Longitudinal tension Case ($T = 1$)	Transverse bending Case ($M = 1$)
0	4.423	2.087
15	3.695	1.731
30	2.035	0.932
45	0.316	0.141
60	−0.833	−0.366
75	−1.178	−0.515
90	−1.164	−0.429
105	−0.863	−0.137
120	0.504	0.425
135	2.457	0.836
150	3.034	0.525
165	1.909	−0.255
180	1.095	−0.657

Each expansion is valid near the origin. If the convergence of the series is slow, the following two duplication formulas [12] are useful:

$$f_1(2z) = 2f_1(z) - \frac{3f_3(z)}{2f_3(z)}$$
$$f_2(2z) = \left\{\frac{3f_3(z)}{2f_3(z)}\right\}^2 - 2f_2(z) \tag{65}$$

unless $2z$ is a period. Again, the following two addition theorems are useful especially when $z_1 + z_2$ is a complex quantity.

$$f_1(z_1 + z_2) = f_1(z_1) + f_1(z_2) - \frac{f_3(z_1) - f_3(z_2)}{f_2(z_1) - f_2(z_2)},$$
$$f_2(z_1 + z_2) = \left\{\frac{f_3(z_1) - f_3(z_2)}{f_2(z_1) - f_2(z_2)}\right\}^2 - f_2(z_1) - f_2(z_2) \tag{66}$$

The function f_3 and f_4 may be computed from the following:

$$f_3(z) = \left\{4f_2^3(z) - 15\omega_4^* f_2(z) - 35\omega_6^*\right\}^{1/2}$$
$$f_4(z) = f_2^2(z) - 5\omega_4^* \tag{67}$$

and the subsequent functions from the recurrence relation, for $k \geqslant 5$,

$$\frac{1}{6}(k-2)(k-3)H_k = H_2H_{k-2} + H_3H_{k-3} + H_4H_{k-4} + \ldots + H_{k-2}H_2 \tag{68}$$

where

$$H_k = (k-1)f_k(z) \tag{69}$$

The values of f_k and therefore ω_k are shown in Table 2, ω_1 and ω_2 being defined in Equations (22).

Thermal Stresses in Moderately Thick Elastic Plates

B. E. GATEWOOD

Research Co-ordinator and Research Professor, Air Force Institute of Technology, Wright-Patterson Air Force Base, Ohio. Mem. ASME

The three-dimensional stresses in the plate are investigated without using the plane-stress or plane-strain assumptions, the thickness of the plate being limited so that the normal stress in the thickness direction can be taken as a polynomial in the thickness variable. The temperature is taken as a polynomial in the thickness variable but with relatively large, though restricted, gradients with respect to the co-ordinates of the plane of the plate. For the case of the temperature constant in thickness variable, the stresses in the plane of the plate are presented as the plane-stress solution plus correcting terms due to the plate thickness, where the correcting terms involve the product of the temperature gradient and the ratio of the plate thickness to the plate length in the direction of the temperature gradient. In many cases the corrections are small even for moderately thick plates.

In the plane-stress problem of elasticity theory the stresses σ_z, τ_{yz}, and τ_{xz} associated with the thickness direction, z, of the plate are taken as zero. Under this assumption the strains γ_{yz} and γ_{xz} are zero but the strain e_z and the two-dimensional stresses and strains are functions of the co-ordinate z as well as the co-ordinates x and y. However, if average values over the thickness of the plate are used for the two-dimensional stresses and if the thickness is small, the stresses may be regarded as two-dimensional, Sokolnikoff [1].[1]

If there are large temperature gradients in the plane of the plate or through the thickness of the plate, the question arises as to whether the plane-stress assumption is permissible with regard not only to the magnitude of the stresses σ_z, τ_{xz}, and τ_{yz} but also to the stresses in the plane. Even though the stresses σ_z, τ_{xz}, and τ_{yz} may be relatively small for a thin plate, the effect on the stresses in the plane may be relatively large. Langhaar [2] and Hilton [3] have pointed out that these effects may be large unless the temperature gradients are small. However, it should be noted that Hilton's argument is based on comparing two differential equations for the circular plate, one of which is based on the plane-stress assumption and the other on both the plane-stress and the plane-strain (e_z = const) assumptions. The latter assumption of both plane stress and plane strain does not appear to be physically possible in a plate. Even the plane-strain assumption alone cannot be realized in a plate without using external restraints, which will produce a completely different stress system in the plate.

The purpose of this paper is to investigate the three-dimensional stresses in the plate without using the plane-stress and plane-strain assumptions. However, the thickness of the plate will be limited so that the stress σ_z can be expressed as a polynomial in the co-ordinate z and the temperature will be taken as a polynomial in z but with relatively large, though restricted, gradients with respect to the x and y-co-ordinates.

The general thermoelastic equations are given in Sokolnikoff [4] and in Gatewood [5]. The compatibility equations can be written in terms of the stresses as follows [4, 6]:

$$\nabla^2 X_{ij} + \frac{1}{1+\nu}\frac{\partial^2 \theta}{\partial x_i \partial x_j} = -\frac{\alpha E}{1-\nu}\nabla^2 T \delta_{ij} - \frac{\alpha E}{1+\nu}\frac{\partial^2 T}{\partial x_i \partial x_j} \tag{1}$$

where $i, j = 1, 2, 3$, $X_{11} = \sigma_x$, $X_{22} = \sigma_y$, $X_{33} = \sigma_z$, $X_{12} = \tau_{xy}$, $X_{13} = \tau_{xz}$, $X_{23} = \tau_{yz}$, $x_1 = x$, $x_2 = y$, $x_3 = z$, ν is Poisson's ratio, E is modulus of elasticity, α is coefficient of thermal expansion, T is temperature in body, δ_{ij} is the Kronecker delta, and

[1] Numbers in brackets designate References at end of paper.

Presented at the Summer Conference of the Applied Mechanics Division, Troy, N. Y., June 18–20, 1959, of THE AMERICAN SOCIETY OF MECHANICAL ENGINEERS.

Discussion of this paper should be addressed to the Secretary, ASME, 29 West 39th Street, New York, N. Y., and will be accepted until October 10, 1959, for publication at a later date. Discussion received after the closing date will be returned.

NOTE: Statements and opinions advanced in papers are to be understood as individual expressions of their authors and not those of the Society. Manuscript received by ASME Applied Mechanics Division, June 2, 1958. Paper No. 59—APM-7.

Nomenclature

b = radius of circular plate
E = modulus of elasticity
e_x, e_y, e_z = normal strains
$\sigma_r, \sigma_\vartheta, \tau_{r\theta}$ = stresses in polar co-ordinates r, θ
$\sigma_x, \sigma_y, \sigma_z$ = normal stresses in x, y, z-directions, respectively
f_1, f_2 = functions of integration, Equation (17)
H = parameter, Equation (28)
$\bar{m}_x, \bar{m}_y, \bar{m}_{xy}$ = moments at edge of plate
P = parameter, Equation (14)
$\bar{P}$ = average of P over plate thickness
T = temperature change in body
x, y, z = rectangular co-ordinates
α = coefficient of thermal expansion
$\gamma_{xy}, \gamma_{xz}, \gamma_{yz}$ = shear strains
θ = sum of normal stresses
ν = Poisson's ratio
$\tau_{xy}, \tau_{xz}, \tau_{yz}$ = shear stresses
φ = stress function
$2a, 2b$ = rectangular plate dimensions in plane
$2h$ = plate thickness in z-direction
$\nabla^2 = \frac{\partial^2}{\partial x^2} + \frac{\partial^2}{\partial y^2} + \frac{\partial^2}{\partial z^2}$, operator
$\nabla_1^2 = \frac{\partial^2}{\partial x^2} + \frac{\partial^2}{\partial y^2}$, operator
∂ = partial differentiation symbol

$$\theta = \sigma_x + \sigma_y + \sigma_z, \nabla^2\theta = -\frac{2\alpha E}{1-\nu}\nabla^2 T \tag{2}$$

Take the temperature distribution as

$$T = T_0(x, y) + zT_1(x, y) + T_H, T_H = \sum_{i=2}^{n} T_i(x, y)z^i \tag{3}$$

For the case of $T_H = 0$, Sokolnikoff [4] gives the normal stress σ_z through the plate thickness as

$$\sigma_z = \frac{\alpha E}{24(1-\nu)}(z^2 - h^2)^2\left[\nabla_1^4 T_0 - \frac{z}{5}\nabla_1^4 T_1 + \frac{z^2 - 3h^2}{15}\nabla_1^6 T_0 + \frac{5z^3 - 11h^2 z}{525}\nabla_1^6 T_1 - \frac{9z^4 - 66z^2h^2 + 41h^4}{7!}\nabla_1^8 T_0\right] \tag{4}$$

$$\nabla_1^2 = \frac{\partial^2}{\partial x^2} + \frac{\partial^2}{\partial y^2}$$

where $2h$ is the plate thickness and it is assumed that $\nabla_1^{10} T_0 = 0$ and $\nabla_1^8 T_1 = 0$. In the derivation of Equation (4) it is assumed that σ_z can be expressed as a polynomial in z. The restrictions on T_0 and T_1 allow rather large temperature gradients in the plane of the plate, since T_0 can be a polynomial of degree nine and T_1 of degree seven.

Shear Stresses τ_{xz}, τ_{yz}

If T is taken as in Equation (3) then from Equation (1)

$$\frac{\partial^2}{\partial z^2}\left[\sigma_z + \frac{2\alpha E T_H}{1-\nu^2} + \frac{\theta}{1+\nu}\right] = -\nabla_1^2\left[\sigma_z + \frac{\alpha E T}{1-\nu}\right] \tag{5}$$

whence

$$\frac{\theta}{1+\nu} = -\sigma_z - \frac{2\alpha E T_H}{1-\nu^2} - \iint \nabla_1^2\left(\sigma_z + \frac{\alpha E T}{1-\nu}\right) dz\, dz - z\theta_1 - \theta_0 \tag{6}$$

To evaluate θ_1 and θ_0 operate on Equation (6) with

$$\nabla^2 = \nabla_1^2 + \frac{\partial^2}{\partial z^2}$$

and use the relations

$$\nabla^4\sigma_z = \frac{\alpha E}{1-\nu}\left(\frac{\partial^2}{\partial z^2}\nabla^2 T - \nabla^4 T\right) \tag{7}$$

$$\nabla^4 = \nabla_1^4 + 2\frac{\partial^2}{\partial z^2}\nabla_1^2 + \frac{\partial^4}{\partial z^4} \tag{8}$$

to obtain $\theta_0 = \dfrac{\alpha E T_0}{1+\nu} + \theta_{00}$, $\theta_1 = \dfrac{\alpha E T_1}{1+\nu} + \theta_{11}$ (9)

$$\nabla_1^2\theta_{00} = \nabla_1^2\theta_{11} = 0 \tag{10}$$

Thus Equation (6) becomes

$$\theta = -\alpha E T_0 - \alpha E T_1 z - \frac{2\alpha E T_H}{1-\nu} - (1+\nu)\left[\sigma_z + \nabla_1^2\iint\left(\sigma_z + \frac{\alpha E T}{1-\nu}\right) dz\, dz + z\theta_{11} + \theta_{00}\right] \tag{11}$$

From Equation (10.8) in Sokolnikoff [4]

$$\frac{\partial^2\tau_{yz}}{\partial z^2} = -\frac{1}{1+\nu}\frac{\partial^2\theta}{\partial y\partial z} - \frac{\alpha E}{1+\nu}\frac{\partial^2 T}{\partial y\partial z} + \frac{\partial^2\sigma_z}{\partial y\partial z} \tag{12}$$

where the condition $\partial\sigma_z/\partial z = 0$ on $z = \pm h$ was used to discard a harmonic function in the first approximation. Note that Equation (4) satisfies this condition. Equation (12) can be expressed as

$$\frac{\partial^2\tau_{yz}}{\partial z^2} = \frac{\partial P}{\partial y\partial z} \tag{13}$$

where

$$P = \sigma_z - \frac{\alpha E T}{1+\nu} - \frac{\theta}{1+\nu} = 2\sigma_z + \frac{\alpha E T_H}{1-\nu} + \nabla_1^2\iint\left(\sigma_z + \frac{\alpha E T}{1-\nu}\right) dz\, dz + z\theta_{11} + \theta_{00} \tag{14}$$

Thus

$$\left.\begin{aligned}\tau_{yz} &= \int_0^z \frac{\partial P}{\partial y}\, dz + zf_3(x, y) + f_4(x, y)\\ \tau_{xz} &= \int_0^z \frac{\partial P}{\partial x}\, dz + zf_1(x, y) + f_2(x, y)\end{aligned}\right\} \tag{15}$$

With the conditions

$$\tau_{xz} = \tau_{yz} = 0, \text{ on } z = \pm h \tag{16}$$

there follows

$$\left.\begin{aligned} f_1 &= -\frac{1}{2h}\int_{-h}^{h}\frac{\partial P}{\partial x}\, dz = -\frac{\partial\bar{P}}{\partial x}\\ f_2 &= -\frac{1}{2}\left[\int_0^h \frac{\partial P}{\partial x}\, dz + \int_0^{-h}\frac{\partial P}{\partial x}\, dz\right]\\ \bar{P} &= +\frac{1}{2h}\int_{-h}^{h} P\, dz\end{aligned}\right\} \tag{17}$$

with similar expressions for f_3 and f_4.

Stress Function for Stresses σ_x, σ_y, τ_{xy}

By using Equation (15) in the equilibrium equations with no body forces there results[2]

$$\left.\begin{aligned}\frac{\partial\sigma_x}{\partial x} + \frac{\partial\tau_{xy}}{\partial y} + \frac{\partial P}{\partial x} - \frac{\partial\bar{P}}{\partial x} &= 0\\ \frac{\partial\tau_{xy}}{\partial x} + \frac{\partial\sigma_y}{\partial y} + \frac{\partial P}{\partial y} - \frac{\partial\bar{P}}{\partial y} &= 0\end{aligned}\right\} \tag{18}$$

If a stress function φ is defined by

$$\left.\begin{aligned}\sigma_x &= \frac{\partial^2\varphi}{\partial y^2} - P + \bar{P}\\ \sigma_y &= \frac{\partial^2\varphi}{\partial x^2} - P + \bar{P}\\ \tau_{xy} &= -\frac{\partial^2\varphi}{\partial x\partial y}\end{aligned}\right\} \tag{19}$$

then Equations (18) are satisfied.

Since from Equation (2) $\sigma_x + \sigma_y = \theta - \sigma_z$, it follows from Equations (19), (14), and (11) that

$$\nabla_1^2\varphi = 2P - 2\bar{P} + \theta - \sigma_z = (1-\nu)P - 2\bar{P} - \alpha E T + \nu\sigma_z \tag{20}$$

Also from Equation (19)

[2] Gatewood [5], equations (1-30).

$$\nabla^2\sigma_z = \frac{\partial^2}{\partial y^2}(\nabla^2\varphi) - \nabla^2 P + \nabla_1^2\bar{P} \tag{21}$$

By using Equations (7), (8), and (14)

$$\nabla_1^2 P = -\frac{\partial^2\sigma_z}{\partial z^2}, \quad \nabla_1^2 P = 0$$
$$\nabla^2 P = \frac{\partial^2}{\partial z^2}[P - \sigma_z] = -\frac{\partial^2}{\partial z^2}\left[\frac{\theta + \alpha E T_H}{1+\nu}\right] \tag{22}$$

so that Equation (21) becomes

$$\nabla^2\sigma_z = \frac{\partial^2}{\partial y^2}(\nabla^2\varphi) + \frac{\partial^2}{\partial z^2}\left[\frac{\theta + \alpha E T_H}{1+\nu}\right] \tag{23}$$

Put this value of $\nabla^2\sigma_z$ in Equation (1) to get

$$\frac{\partial^2}{\partial y^2}(\nabla^2\varphi) + \frac{1}{1+\nu}\left(\frac{\partial^2\theta}{\partial x^2} + \frac{\partial^2[\theta + \alpha E T_H]}{\partial z^2}\right)$$
$$= -\frac{\alpha E}{1+\nu}\left(\frac{\partial^2 T}{\partial x^2}\right) - \frac{\alpha E}{1-\nu}(\nabla_1^2 T) - \frac{\alpha E}{1-\nu}\left(\frac{\partial^2 T_H}{\partial z^2}\right) \tag{24}$$

By use of Equation (2), Equation (24) reduces to

$$\frac{\partial^2}{\partial y^2}\left[\frac{\partial^2\varphi}{\partial z^2} + \nabla_1^2\varphi - \frac{\theta + \alpha E T}{1+\nu}\right] = 0 \tag{25}$$

In a similar way by putting $\nabla^2\sigma_y$ and $\nabla^2\tau_{xy}$ in Equation (1) there results

$$\frac{\partial^2}{\partial x^2}\left[\frac{\partial^2\varphi}{\partial z^2} + \nabla_1^2\varphi - \frac{\theta + \alpha E T}{1+\nu}\right] = 0$$
$$\frac{\partial^2}{\partial x\partial y}\left[\frac{\partial^2\varphi}{\partial z^2} + \nabla_1^2\varphi - \frac{\theta + \alpha E T}{1+\nu}\right] = 0 \tag{26}$$

Thus the expressions in brackets in Equations (25) and (26) can at most be linear in x and y. Since linear terms will not affect the stresses in Equation (19), the bracket expression may be taken as zero. Hence by Equations (14) and (20)

$$\frac{\partial^2\varphi}{\partial z^2} = \sigma_z - P - \nabla_1^2\varphi = (1-\nu)\sigma_z - (2-\nu)P + 2P + \alpha E T \tag{27}$$

Integration of Equation (27) and use of Equation (20) to obtain the form of the constants of integration gives

$$\varphi = \int\int[(1-\nu)\sigma_z - (2-\nu)P + \alpha E T]\,dz\,dz + Pz^2 + \varphi_1 z + \varphi_0 = H + \varphi_1 z + \varphi_0 \tag{28}$$

where
$$\nabla_1^2\varphi_0 = -\alpha E T_0 + (1-\nu)\theta_{00} - 2\bar{P}$$
$$\nabla_1^2\varphi_1 = -\alpha E T_1 + (1-\nu)\theta_{11} \tag{29}$$

Furthermore,
$$\nabla_1^4\varphi_0 = -\alpha E\nabla_1^2 T_0$$
$$\nabla_1^4\varphi_1 = -\alpha E\nabla_1^2 T_1 \tag{30}$$

so that φ_0 and φ_1 are the stress functions for the plane-stress problem.[3] Once they are obtained, the plane harmonic functions θ_{00} and θ_{11} can be determined from Equation (29).

Stresses σ_x, σ_y, τ_{xy}

The stresses σ_x, σ_y, and τ_{xy} in the plane of the plate are given by Equation (19) with φ from Equation (28) and P from Equation (14). The plane-stress functions φ_0 and φ_1 occurring in these expressions for the stress must be determined from Equation (30) and the boundary conditions of the finite plate:[4]

$$\sigma_x\cos(nx) + \tau_{xy}\cos(ny) = X_s$$
$$\tau_{xy}\cos(nx) + \sigma_y\cos(ny) = Y_s \tag{31}$$

Since the stress functions φ_0 and φ_1 are not functions of z while the stresses σ_x, σ_y, and τ_{xy} are functions of z, it is not possible to satisfy Equation (31) for arbitrary X_s and Y_s. Either X_s and Y_s must contain all the z-terms of second order and higher occurring on the left side of Equation (31), which is not likely in an actual plate, or some approximation must be made in the boundary conditions. If the stresses and their moments on the boundary are averaged with respect to the plate thickness, then by Saint Venant's principle the stresses at a sufficient distance from the boundary will be correct to a high order of magnitude.

From Equations (19) and (28) write

$$\sigma_x = \frac{\partial^2(\varphi_1 z + \varphi_0)}{\partial y^2} + \frac{\partial^2 H}{\partial y^2} - P + \bar{P}$$
$$\sigma_y = \frac{\partial^2(\varphi_1 z + \varphi_0)}{\partial x^2} + \frac{\partial^2 H}{\partial x^2} - P + \bar{P} \tag{32}$$
$$\tau_{xy} = -\frac{\partial^2(\varphi_1 z + \varphi_0)}{\partial x\partial y} - \frac{\partial^2 H}{\partial x\partial y}$$

and at the boundary take

$$\bar{\sigma}_x = \frac{\partial^2}{\partial y^2}(\varphi_0 + \bar{H}), \quad \bar{\sigma}_y = \frac{\partial^2}{\partial x^2}(\varphi_0 + \bar{H}),$$
$$\bar{\tau}_{xy} = -\frac{\partial^2}{\partial x\partial y}(\varphi_0 + \bar{H}), \quad \bar{H} = \frac{1}{2h}\int_{-h}^{h} H\,dz \tag{33}$$

for the function φ_0 and

$$\frac{3\bar{m}_x}{2h^3} = \frac{\partial^2}{\partial y^2}(\varphi_1 + \bar{H}z) - \bar{P}z$$
$$\frac{3\bar{m}_y}{2h^3} = \frac{\partial^2}{\partial x^2}(\varphi_1 + \bar{H}z) - \bar{P}z, \quad \frac{3\bar{m}_{xy}}{2h^3} = \frac{\partial^2}{\partial x\partial y}(\varphi_1 + \bar{H}z) \tag{34}$$
$$\bar{H}z = \frac{3}{2h^3}\int_{-h}^{h} Hz\,dz, \quad \bar{P}z = \frac{3}{2h^3}\int_{-h}^{h} Pz\,dz$$

for the function φ_1.

Order of Magnitude of Stresses Due to Plate Thickness

In the foregoing formulas for the stresses, take $T_1 = T_H = 0$ and consider terms to the fourth order in h and z. Assume that in a rectangular plate of dimensions $2a$ by $2b$ ($x = \pm a$, $y = \pm b$) the temperature T_0 is

$$T_0 = T_{0m}\left[\left(\frac{x}{a}\right)^m + \left(\frac{y}{b}\right)^n\right] \tag{35}$$

From Equation (4)

$$\sigma_z = \frac{\alpha E T_{0m}}{24(1-\nu)}\left(\frac{h}{a}\right)^4\left[\left(\frac{z}{h}\right)^2 - 1\right]^2 \times \left[m(m-1)(m-2)(m-3)\left(\frac{x}{a}\right)^{m-4} + \left(\frac{a}{b}\right)^4(n)(n-1)(n-2)(n-3)\left(\frac{y}{b}\right)^{n-4}\right] \tag{36}$$

[3] See reference [5], page 201.

[4] See reference [5], equations (1–40).

which is zero if $m \leq 3$ and $n \leq 3$. If $m = n = 9$, which gives steep temperature gradients, then the maximum value of σ_x in Equation (36) for $a = b$ and $\nu = 0.3$ is

$$(\sigma_x)_{max} = 360 \left(\frac{h}{a}\right)^4 \alpha E T_{0m} \tag{37}$$

For metals as used in aircraft and missile structures, thermal stresses of the order of $0.05\,\alpha E T_{0m}$ are usually considered to be within the approximations of the other factors in the problem. Hence in the foregoing particular case h/a can be of the order of 0.11 which will correspond to a relatively thick plate.

To write expressions for the other stresses in Equations (15) and (19) it is necessary to obtain the expressions for the functions P and φ using the foregoing assumptions. From Equation (14)

$$P = \frac{\alpha E}{12(1-\nu)}(z^2 - h^2)^2 \nabla_1^4 T_0 + \frac{\alpha E \nabla_1^2 T_0}{1-\nu}\frac{z^2}{2} + \theta_{0c} \tag{38}$$

whence from Equation (17)

$$\bar{P} = \frac{2h^4 \alpha E}{45(1-\nu)} \nabla_1^4 T_0 + \frac{h^2 \alpha E}{6(1-\nu)} \nabla_1^2 T_0 + \theta_{0c}$$

$$f_1 = -\frac{\partial \bar{P}}{\partial x} \tag{39}$$

$$f_2 = 0$$

From Equation (28)

$$\varphi = \alpha E T_0 \frac{z^2}{2} + \frac{\alpha E \nabla_1^2 T_0}{1-\nu}\frac{h^2 z^2}{6} - \frac{(2-\nu)}{1-\nu}\alpha E \nabla_1^2 T_0 \frac{z^4}{24} + \varphi_0 + \frac{\nu}{2}\theta_{0c} z^2 \tag{40}$$

Using these expressions in Equation (15) gives

$$\tau_{xz} = \frac{\partial}{\partial x}\frac{\alpha E}{1-\nu}\nabla_1^2 T_0 \frac{z}{6}(z^2 - h^2)$$

$$= \frac{\alpha E T_{0m}}{6(1-\nu)}\left(\frac{h}{a}\right)^2 \left(\frac{z}{h}\right)\left[\left(\frac{z}{h}\right)^2 - 1\right]\left[m(m-1)(m-2)\left(\frac{x}{a}\right)^{m-3}\right] \tag{41}$$

with a similar expression for τ_{yz}.

The maximum values for $m = n = 9$, $a = b$, and $\nu = 0.3$ are

$$(\tau_{xz})_{max} = (\tau_{yz})_{max} = 46.2\left(\frac{h}{a}\right)^3 \alpha E T_{0m} \tag{42}$$

and for the stresses of order $0.05\,\alpha E T_{0m}$, $h/a = 0.10$.

From Equation (19)

$$\sigma_z = \frac{\partial^2}{\partial y^2}\left[\alpha E T_0 \frac{z^2}{2} + \nu\theta_{0c}\frac{z^2}{2} - \frac{\alpha E \nabla_1^2 T_0}{1-\nu}\left\{\frac{(2-\nu)}{24}z^4 - \frac{h^2 z^2}{6}\right\}\right] + \frac{\partial^2 \varphi_0}{\partial y^2} - \frac{\alpha E \nabla_1^4 T_0}{1-\nu}\left[\frac{1}{12}(z^2 - h^2)^2 - \frac{2h^4}{45}\right] + \frac{\alpha E \nabla_1^2 T_0}{1-\nu}\left(\frac{h^2}{6} - \frac{z^2}{2}\right) \tag{43}$$

The coefficient of the second-order terms in h and z depend upon θ_{0c} and upon the h^2-terms in φ_0 so that its value cannot be obtained except for particular problems for which φ_0 and θ_{0c} have been obtained from the boundary conditions. However, this coefficient is probably of the order of the stress itself, so that the correction to the two-dimensional stress is

$$(\sigma_z)_e < \frac{h^2}{3}\left[\frac{\partial^2}{\partial y^2}(\alpha E T_0) + \alpha E \nabla_1^2 T_0\right]$$

$$< \frac{\alpha E T_{0m}}{3}\left(\frac{h}{b}\right)^2\left[n(n-1) + n(n-1) + m(m-1)\left(\frac{a}{b}\right)^2\right]$$

$$= 72\,\alpha E T_{0m}\left(\frac{h}{a}\right)^2, \quad n = m = 9, \quad a = b \tag{44}$$

Thus for the stresses of order $0.05\,\alpha E T_{0m}$, $h/a \approx 0.03$. If the gradient is smaller, say $m = n = 3$, then $h/a \approx 0.09$.

The foregoing approximations indicate that the effect of the thickness of the plate on the thermal stresses may be negligible for the stresses associated with the thickness direction on the plate but may have considerable effect on the stresses in the plane of the plate. An approximate criterion for determining whether the stresses in the plane should be corrected for the thickness effects may be taken as

$$\frac{h}{a}(m) = 0.2 \tag{45}$$

where m is a measure of the temperature gradient, Equation (35), h is plate thickness, and a is plate width in direction of the temperature gradient.

Example of Circular Plate

Consider a circular plate of radius b with the temperature T_0 a function of the radius and take $T_1 = T_H = 0$. Consider terms to the fourth order in z and h so that the stress function φ in Equation (40) is applicable. From Equations (33) and (40)

$$\bar{H} = \frac{\alpha E T_0 h^2}{6} + \frac{\nu}{6}\theta_{0c}h^2 + \frac{\alpha E \nabla_1^2 T_0}{1-\nu}h^4\left(\frac{14 + 3\nu}{360}\right) \tag{46}$$

From [5][a] take $\varphi_0 = U - V$ and in Equation (33) take $\bar{\sigma}_r = 0$ on $r = b$, whence

$$\frac{\partial}{\partial r}(U - V + \bar{H}) = 0 \text{ on } r = b, \quad \frac{\partial U}{\partial r} = M - N \text{ on } r = b$$

$$M = \frac{\alpha E}{b}\int_0^b r T_0 dr, \; N = \left[\frac{\partial \bar{H}}{\partial r}\right]_{r=b} \tag{47}$$

From [5][a]

$$\sigma_{r0} = \frac{M-N}{b} - \frac{\alpha E}{r^2}\int_0^r r T_0 dr = \sigma_{r\theta c} - \frac{N}{b}$$

$$\sigma_{\theta 0} = \frac{M-N}{b} + \frac{\alpha E}{r^2}\int_0^r r T_0 dr - \alpha E T_0 = \sigma_{\theta c} - \frac{N}{b} \tag{48}$$

$$\tau_{r\theta 0} = 0 = \tau_{r\theta 0c}$$

where σ_{r0}, $\sigma_{\theta 0}$, $\tau_{r\theta 0}$ are the stresses for the stress function φ_0 while σ_{r0c}, $\sigma_{\theta 0c}$ are the two-dimensional stresses neglecting any thickness effects. From Equation (29)

$$\theta_{0c} = -\frac{2(M-N)}{b(1+\nu)} - \frac{4h^4 \alpha E \nabla_1^4 T_0}{45(1-\nu^2)} - \frac{h^2 \alpha E \nabla_1^2 T_0}{3(1-\nu^2)} \tag{49}$$

[a] Reference [5], p. 101.

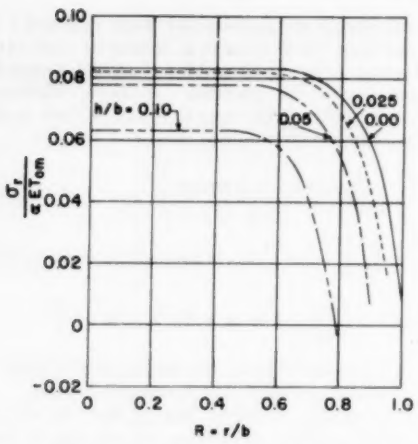

Fig. 1 Radial thermal stresses in circular plates for $T_0 = T_{0m}R^{10}$

From Equation (43) with

$$T = \frac{T_0}{T_{0m}}, \quad R = \frac{r}{b}, \quad Z = \frac{z}{h} \tag{50}$$

the stresses in the plane are

$$\sigma_r = \alpha E T_{0m} \left(\frac{h}{b}\right)^2 \left[\frac{1}{R}\frac{\partial T}{\partial R}\left(\frac{Z^2}{2}\right) - \left(\frac{h}{b}\right)^2 \left(\frac{1}{1-\nu}\right) \frac{1}{R}\frac{\partial}{\partial R}(\nabla_1^2 T)\left\{\frac{2-\nu}{24} Z^4 - \frac{Z^2}{6(1+\nu)}\right\} + \frac{\nabla_1^2 T}{1-\nu}\left(\frac{1}{6} - \frac{Z^2}{2}\right) - \left(\frac{h}{b}\right)^2 \frac{\nabla_1^4 T}{1-\nu}\left\{\frac{1}{12}(Z^2-1)^2 - \frac{2}{45}\right\} - \frac{1}{6}\left[\frac{\partial T}{\partial R}\right]_{R=1} - \left(\frac{h}{b}\right)^2 \frac{14 + 3\nu^2 - 3\nu}{360(1-\nu^2)}\left[\frac{\partial \nabla_1^2 T}{\partial R}\right]_{R=1}\right] + \sigma_{r00} \tag{51}$$

with a similar expression for σ_θ. Here $\tau_{r\theta} = 0$.

Fig. 1 shows a graph of Equation (51) for the case of $Z = 1$, $\nu = 0.3$, and $T = R^{10}$. The figure shows that, for this large temperature gradient, values of h/b must be of the order of 0.10 to have an appreciable effect on the plane-stress solution ($h/b = 0$ case in Fig. 1). As terms in Equation (51) involving h/b are not applicable at the edge of the plate, the solutions have been stopped at a distance of $2h/b$ from the edge (equivalent distance equal to plate thickness).

Conclusions

The results of this paper show that the thermal stresses in the plane of moderately thick elastic plates can be expressed as a function of two plane-stress functions, the normal stress in the thickness direction, and the temperature. For the case of the temperature a function of the co-ordinates in the plane, the stresses reduce to the plane-stress solution plus corrections because of the plate thickness. In many cases, these corrections are so small that the stresses can be approximated closely by the two-dimensional plane-stress solutions for the thermal stresses. The corrections to the plane-stress solutions involve the product of the temperature gradient and the plate-thickness ratio (plate thickness divided by length of plate in direction of temperature gradient), instead of just the temperature gradient as in the discussion by Langhaar [2] and Hilton [3]. The corrections are largest for the stresses in the plane of the plate and least for the normal stress in the thickness direction. If the thickness ratio is large or the temperature gradient is unusually large, corrections should be made for the stresses in the plane; the stresses associated with the thickness direction may yet be small. If the plate is thin, the temperature gradient must be extremely large to have any effect on the plane-stress solution.

References

1 I. S. Sokolnikoff, "Mathematical Theory of Elasticity," McGraw-Hill Book Company, Inc., New York, N. Y., 2nd edition, 1956.

2 H. L. Langhaar, discussion of the paper, "Axisymmetric Flexural Temperature Stresses in Circular Plates," by J. E. Goldberg, JOURNAL OF APPLIED MECHANICS, vol. 20, TRANS. ASME, vol. 75, 1953, pp. 257–260, 575.

3 H. H. Hilton, "Thermal Stresses in Bodies Exhibiting Temperature-Dependent Elastic Properties," JOURNAL OF APPLIED MECHANICS, vol. 19, TRANS. ASME, vol. 74, 1952, pp. 350–354.

4 I. S. Sokolnikoff and E. S. Sokolnikoff, "Thermal Stresses in Elastic Plates," *Transactions American Mathematical Society*, vol. 45, 1939, pp. 235–255.

5 B. E. Gatewood, "Thermal Stresses," McGraw-Hill Book Company, Inc., New York, N. Y., 1957.

6 A. E. H. Love, "Mathematical Theory of Elasticity," 4th edition, Dover Publications, New York, N. Y., 1944.

H. D. CONWAY

Julius Stone Visiting Professor,
Department of Engineering Mechanics,
Ohio State University,
Columbus, Ohio

Analysis of Plane Stress in Polar Co-ordinates and With Varying Thickness

The biharmonic stress-function equation for plane stress in polar co-ordinates is generalized by assuming that the thickness varies with the radius. In order to make this equation tractable, the thickness is assumed to be proportional to an arbitrary power of the radius. Michell's general solution for the constant-thickness case is then generalized for this variation of thickness. As a numerical example, the solution is given for the problem of a segmental plate bent by end couples, the constant-thickness version of this well-known problem being due to Golovin.[1]

Most calculations of plane-stress problems are made assuming that the thickness is constant. However, if the thickness is everywhere small, the method of analysis may be extended to plates of varying thickness. For the axisymmetrical case of a rotating disk of variable thickness proportional to a power of the radius, a solution utilizing stress functions is outlined by Timoshenko and Goodier.[2]

In that which follows, the general, nonaxisymmetrical problem is considered, the thickness at any point being assumed to be proportional to a power of the radius of the point.

Analysis

Fig. 1 shows a stationary element of a disk of variable thickness $h = f(r)$, bounded by two radial surfaces, inclined at angle $d\theta$ to one another, and by two circumferential surfaces of radii r and $r + dr$, respectively. By resolving radially and tangentially, the equations of equilibrium are

$$\frac{\partial}{\partial r}(rh\sigma_r) - h\sigma_\theta + h\frac{\partial \tau_{r\theta}}{\partial \theta} = 0$$
$$\frac{\partial}{\partial r}(r^2 h\tau_{r\theta}) + rh\frac{\partial \sigma_\theta}{\partial \theta} = 0 \tag{1}$$

Introducing a stress function $\phi(r, \theta)$, it may be shown that the foregoing equilibrium conditions are satisfied by equations similar to those in the constant-thickness case; viz.

$$h\sigma_r = \frac{1}{r}\frac{\partial \phi}{\partial r} + \frac{1}{r^2}\frac{\partial^2 \phi}{\partial \theta^2}$$
$$h\sigma_\theta = \frac{\partial^2 \phi}{\partial r^2} \tag{2}$$
$$h\tau_{r\theta} = -\frac{\partial}{\partial r}\left(\frac{1}{r}\frac{\partial \phi}{\partial \theta}\right)$$

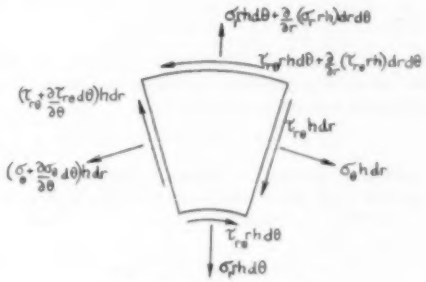
$\sigma_r rh d\theta + \frac{\partial}{\partial r}(\sigma_r rh)dr d\theta$
$\tau_{r\theta} rh d\theta + \frac{\partial}{\partial r}(\tau_{r\theta} rh)dr d\theta$
$(\tau_{r\theta} + \frac{\partial \tau_{r\theta}}{\partial \theta} d\theta)h dr$
$\tau_{r\theta} h dr$
$(\sigma_\theta + \frac{\partial \sigma_\theta}{\partial \theta} d\theta)h dr$
$\sigma_\theta h dr$
$\tau_{r\theta} rh d\theta$
$\sigma_r h dr d\theta$

Fig. 1 Element of plate

The direct and shearing-strain equations in polar co-ordinates are

$$e_r = \frac{\partial u}{\partial r}$$
$$e_\theta = \frac{u}{r} + \frac{1}{r}\frac{\partial v}{\partial \theta} \tag{3}$$
$$\gamma_{r\theta} = \frac{1}{r}\frac{\partial u}{\partial \theta} + \frac{\partial v}{\partial r} - \frac{v}{r}$$

and from these it may be shown that the compatibility strain equation is

$$\frac{\partial}{\partial r}\left(r\frac{\partial \gamma_{r\theta}}{\partial \theta} - r^2\frac{\partial e_\theta}{\partial r}\right) + r\frac{\partial e_r}{\partial r} - \frac{\partial^2 e_\theta}{\partial \theta^2} = 0 \tag{4}$$

Introducing the stress-strain equations

$$Ee_r = \sigma_r - \nu\sigma_\theta$$
$$Ee_\theta = \sigma_\theta - \nu\sigma_r \tag{5}$$
$$G\gamma_{r\theta} = \tau_{r\theta}$$

in Equation (4) and with the use of Equations (2), the resulting compatibility equation is shown after some simplification to be

$$\left(r^2\frac{\partial^2}{\partial r^2} + [2+\nu]r\frac{\partial}{\partial r} - \nu\frac{\partial^2}{\partial \theta^2}\right)\left(\frac{1}{h}\frac{\partial^2 \phi}{\partial r^2}\right)$$
$$-\left(\nu r^2\frac{\partial^2}{\partial r^2} + [2\nu+1]r\frac{\partial}{\partial r} - \frac{\partial^2}{\partial \theta^2}\right)\left(\frac{1}{hr}\frac{\partial \phi}{\partial r} + \frac{1}{hr^2}\frac{\partial^2 \phi}{\partial \theta^2}\right)$$
$$+ 2(1+\nu)\frac{\partial}{\partial r}\left(r\frac{\partial}{\partial \theta}\left[\frac{1}{h}\frac{\partial}{\partial r}\left(\frac{1}{r}\frac{\partial \phi}{\partial \theta}\right)\right]\right) = 0 \tag{6}$$

[1] H. Golovin, Transactions of the Institute of Technology, St. Petersburg, 1891.

[2] S. Timoshenko and J. N. Goodier, "Theory of Elasticity," McGraw-Hill Book Company, Inc., New York, N. Y., 1951, p. 72.

Presented at the Summer Conference of the Applied Mechanics Division, Troy, N. Y., June 18–20, 1959, of THE AMERICAN SOCIETY OF MECHANICAL ENGINEERS.

Discussion of this paper should be addressed to the Secretary, ASME, 29 West 39th Street, New York, N. Y., and will be accepted until October 10, 1959, for publication at a later date. Discussion received after the closing date will be returned.

NOTE: Statements and opinions advanced in papers are to be understood as individual expressions of their authors and not those of the Society. Manuscript received by ASME Applied Mechanics Division, May 12, 1958. Paper No. 59-APM-1.

If h is a constant, this naturally reduces to

$$\nabla^2\nabla^2\phi = \left(\frac{\partial^2}{\partial r^2} + \frac{1}{r}\frac{\partial}{\partial r} + \frac{1}{r^2}\frac{\partial^2}{\partial\theta^2}\right)^2 \phi = 0 \qquad (7)$$

the well-known biharmonic equation in polar co-ordinates.

The general solution of Equation (7) due to Michell[3] is

$$\begin{aligned}\phi = {} & A_0 \log r + B_0 r^2 + C_0 r^2 \log r + D_0 r^2\theta + A_0'\theta + \frac{A_1}{2} r\theta \sin\theta \\ & + (B_1 r^3 + A_1' r^{-1} + B_1' r \log r) \cos\theta - \frac{C_1}{2} r\theta \cos\theta \\ & + (D_1 r^3 + C_1' r^{-1} + D_1' r \log r) \sin\theta \\ & + \sum_{n=2}^{\infty} (A_n r^n + B_n r^{n+2} + A'_n r^{-n} + B'_n r^{-n+2}) \cos n\theta \\ & + \sum_{n=2}^{\infty} (C_n r^n + D_n r^{n+2} + C_n' r^{-n} + D_n' r^{-n+2}) \sin n\theta \qquad (8)\end{aligned}$$

In order to find tractable solutions of Equation (6) which are also useful in solving practical problems, we assume that the thickness may be written in the form

$$h = h_0 r^{-m} \qquad (9)$$

where h_0 and m are arbitrary constants. Since such an equation means that the thickness is either zero or infinite at $r = 0$, depending on whether m is negative or positive, it is only of value for plates with a hole.

Paralleling part of the constant-thickness general solution in Equation (8), we substitute (9) in (6) and write

$$\phi = R_0 + \sum_{n=1}^{\infty} R_n \sin n\theta + \sum_{n=1}^{\infty} S_n \cos n\theta \qquad (10)$$

The following Euler equation is then obtained:

$$\begin{aligned}r^4 R_n^{iv} + 2(m+1) r^3 R_n''' - (1 + \nu m + 2n^2 - m - m^2) r^2 R_n'' \\ - (m-1)(1 + \nu m + 2n^2) r R_n' \\ - n^2(4 + \nu m - 3m - \nu m^2 - n^2) R_n = 0 \qquad (11)\end{aligned}$$

which, by the change of variable $r = e^z$, becomes

$$\begin{aligned}\frac{d^4 R_n}{dz^4} + 2(m-2)\frac{d^3 R_n}{dz^3} + (4 - 5m - \nu m - 2n^2 + m^2)\frac{d^2 R_n}{dz^2} \\ - (m-2)(m + \nu m + 2n^2)\frac{dR_n}{dz} \\ - n^2(4 + \nu m - 3m - \nu m^2 - n^2) R_n = 0 \qquad (12)\end{aligned}$$

A similar equation is obtained for S_n. Hence the characteristic equation to be solved is

$$\begin{aligned}\lambda^4 + 2(m-2)\lambda^3 + (4 - 5m - \nu m - 2n^2 + m^2)\lambda^2 \\ - (m-2)(m + \nu m + 2n^2)\lambda \\ - n^2(4 + \nu m - 3m - \nu m^2 - n^2) = 0 \qquad (13)\end{aligned}$$

To find the roots, we tentatively write

$$(\lambda + \alpha + \beta_1)(\lambda + \alpha - \beta_1)(\lambda + \alpha + \beta_2)(\lambda + \alpha - \beta_2) = 0$$

where $\alpha = (m-2)/2$ and obtain, after multiplication

$$\begin{aligned}\lambda^4 + 2(m-2)\lambda^3 + [3(m-2)^2/2 - \beta_1^2 - \beta_2^2]\lambda^2 \\ + (m-2)[(m-2)^2/2 - \beta_1^2 - \beta_2^2]\lambda \\ + [(m-2)^2/4 - \beta_1^2][(m-2)^2/4 - \beta_2^2] = 0 \qquad (14)\end{aligned}$$

Comparing the coefficients of λ^2 and λ in Equation (13) with the corresponding ones in Equation (14), it is seen that in both cases

$$\beta_1^2 + \beta_2^2 = (m-2)^2/2 + m(1+\nu) + 2n^2 \qquad (15)$$

The other equation for the determination of β_1 and β_2 is, of course, found by equating the terms independent of λ in Equations (13) and (14). It is

$$\begin{aligned}[(m-2)^2/4 - \beta_1^2][(m-2)^2/4 - \beta_2^2] \\ = -n^2(4 + \nu m - 3m - \nu m^2 - n^2) \qquad (16)\end{aligned}$$

In forms best suited for computation, the equations for the determination of β_1 and β_2 are then

$$\beta_1^2 + \beta_2^2 = (m-2)^2/2 + m(1+\nu) + 2n^2$$

$$(\beta_1^2 - \beta_2^2)^2 = m^2(1+\nu)^2 - 4n^2 m(2 - 2\nu + \nu m) + 16n^2 \qquad (17)$$

and, with $\alpha = (m-2)/2$, the roots of Equation (13) are obtained.

A simple and interesting solution of the characteristic equation occurs when $m = 2$ and the thickness thus given by $h = h_0 r^{-2}$. The coefficients of λ^3 and λ in Equation (13) then disappear, leaving a quadratic in λ^2

$$\lambda^4 - 2(n^2 + 1 + \nu)\lambda^2 + n^2(n^2 + 2 + 2\nu) = 0 \qquad (18)$$

The roots of this equation are

$$\lambda = \pm n, \quad \pm(n^2 + 2 + 2\nu)^{1/2} \qquad (19)$$

For the constant-thickness case, $m = 0$ and roots are

$$\lambda = \pm n, \quad 2 \pm n \qquad (20)$$

For the axisymmetrical case, $n = 0$ and the roots are

$$\lambda = 0,\ 2 - m,\ -(m-2)/2 \pm [(m-2)^2 + 4m(1+\nu)]^{1/2}/2 \qquad (21)$$

The equation for R_n is finally obtained as

$$R_n = (A_n r^{\lambda_1} + B_n r^{\lambda_2} + C_n r^{\lambda_3} + D_n r^{\lambda_4}) \qquad (22)$$

with a corresponding equation for S_n. However, for the multiple-roots cases, such as Equation (21) with $m = 2$

$$R_0 = (A_0 + B_0 \log r + C_0 r^{\lambda_3} + D_0 r^{\lambda_4}) \qquad (23)$$

Following Michell's solution for the constant-thickness case we next write

$$\phi = E[r\theta \sin\theta + F(r) \cos\theta] \qquad (24)$$

and substituting in Equation (6) with $h = h_0 r^{-m}$, obtain

$$\begin{aligned}r^4 F^{iv} + 2(m+1) r^3 F''' - (3 + \nu m - m - m^2) r^2 F'' \\ + (3 + \nu m - 3m - \nu m^2) r F' - (3 + \nu m - 3m - \nu m^2) F \\ = (2\nu m - 2m - 2\nu m^2) r \qquad (25)\end{aligned}$$

whence the particular solution is

$$F(r) = 2m(\nu - 1 - \nu m)(r \log r)/(3 + m + \nu m - m^2) \qquad (26)$$

The complementary solution of Equation (25) is accounted for in Equation (10), and the companion solution to Equation (24) obtained in a similar manner is

$$\phi = G[r\theta \cos\theta + F(r) \sin\theta] \qquad (27)$$

Finally, we assume with $h = h_0 r^{-m}$ a solution of Equation (6) in the form

$$\phi = \theta H(r) \qquad (28)$$

and obtain

$$H(r) = [Ar^{\lambda_1} + Br^{\lambda_2} + Cr^{\lambda_3} + Dr^{\lambda_4}] \qquad (29)$$

[3] S. Timoshenko and J. N. Goodier, "Theory of Elasticity," McGraw-Hill Book Company, Inc., New York, N. Y., 1951, p. 116.

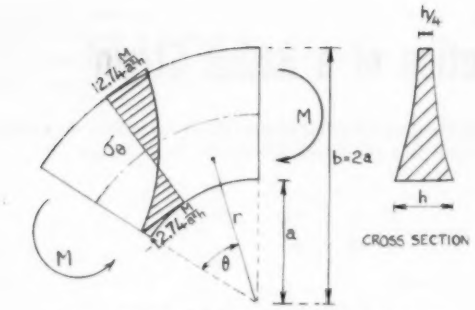

Fig. 2 Circumferential stress distribution of segment

where the λ are given by Equation (21); that is, the axisymmetrical case.

Example

As a numerical example, we consider the problem shown diagrammatically in Fig. 2, the well-known solution of the constant-thickness version of which is attributed by Timoshenko and Goodier[4] to Golovin.[1]

Assuming that the thickness is given by $h = h_0 r^{-2}$, that is, $m = 2$, and noting that the first term in Equation (23) produces no stresses, we select the stress function

$$\phi = B \log r + Cr^{\lambda} + Dr^{-\lambda}; \quad \lambda = (2 + 2\nu)^{1/2} \tag{30}$$

and obtain

$$\begin{aligned} \sigma_r &= (B + C\lambda r^{\lambda} - D\lambda r^{-\lambda})/h_0 \\ \sigma_\theta &= [-B + C\lambda(\lambda - 1)r^{\lambda} + D\lambda(\lambda + 1)r^{-\lambda}]/h_0 \\ \tau_{r\theta} &= 0 \end{aligned} \tag{31}$$

Since the radial stress vanishes on $r = a$ and $r = b$

$$B + C\lambda a^{\lambda} - D\lambda a^{-\lambda} = 0, \quad B + C\lambda b^{\lambda} - D\lambda b^{-\lambda} = 0 \tag{32}$$

For zero normal force on any radial cross section

$$\int_a^b \sigma_\theta h dr = \int_a^b \frac{\partial^2 \phi}{\partial r^2}\, dr = \left| \frac{\partial \phi}{\partial r} \right|_a^b = [Br^{-1} + C\lambda r^{\lambda - 1} - D\lambda r^{-\lambda - 1}]_a^b = 0 \tag{33}$$

from Equations (32). This condition is satisfied if each of Equations (32) is satisfied. Similarly

$$\int_a^b \sigma_r h dr = \int_a^b r \frac{\partial^2 \phi}{\partial r^2}\, dr = \left| r \frac{\partial \phi}{\partial r} \right|_a^b - |\phi|_a^b = -B \log \frac{b}{a} - C(b^{\lambda} - a^{\lambda}) - D(b^{-\lambda} - a^{-\lambda}) = M \tag{34}$$

The constants B, C, and D are now determined from Equations (32) and (34) and, after some simplification, it may be shown that the stresses are

$$\begin{aligned} \sigma_r = \frac{M\lambda}{h_0 N} \Bigg\{ &\left(\frac{b}{a}\right)^{\lambda} - \left(\frac{a}{b}\right)^{\lambda} + \left(\frac{r}{a}\right)^{\lambda} \left[\left(\frac{a}{b}\right)^{\lambda} - 1\right] \\ &- \left(\frac{r}{a}\right)^{-\lambda} \left[\left(\frac{b}{a}\right)^{\lambda} - 1\right] \Bigg\} \\ \sigma_\theta = \frac{M\lambda}{h_0 N} \Bigg\{ &-\left(\frac{b}{a}\right)^{\lambda} + \left(\frac{a}{b}\right)^{\lambda} + (\lambda - 1)\left(\frac{r}{a}\right)^{\lambda} \left[\left(\frac{a}{b}\right)^{\lambda} - 1\right] \\ &+ (\lambda + 1)\left(\frac{r}{a}\right)^{-\lambda} \left[\left(\frac{b}{a}\right)^{\lambda} - 1\right] \Bigg\} \end{aligned} \tag{35}$$

where

$$N = 2\left(\frac{a}{b}\right)^{\lambda} + 2\left(\frac{b}{a}\right)^{\lambda} - 4 + \lambda\left[\left(\frac{a}{b}\right)^{\lambda} - \left(\frac{b}{a}\right)^{\lambda}\right] \log \frac{b}{a} \tag{36}$$

From the foregoing it may be shown that

$$\sigma_{\theta\, r=a} = -\sigma_{\theta\, r=b} = \frac{-M\lambda^2 \left[\left(\frac{b}{a}\right)^{\lambda/2} - \left(\frac{a}{b}\right)^{\lambda/2}\right]}{h_0 \left\{\left[\left(\frac{b}{a}\right)^{\lambda/2} + \left(\frac{a}{b}\right)^{\lambda/2}\right] \lambda \log \frac{b}{a} - 2\left[\left(\frac{b}{a}\right)^{\lambda/2} - \left(\frac{a}{b}\right)^{\lambda/2}\right]\right\}} \tag{37}$$

The circumferential stress in the constant-thickness version of this problem is greatest at the inner radius, and thus it appears that the thickness variation $h = h_0/r^2$ produces the most efficient stress distribution. A graph of circumferential stress for $b/a = 2$, $\nu = 0.28$, is given in Fig. 2. For the case of constant thickness h, the circumferential stresses at radii a and $2a$ are $-7.76\ M/a^2h$ and $4.91\ M/a^2h$, respectively.

It is interesting to compare the foregoing results with those given by the elementary theory of curved bars reproduced in practically all texts on strength of materials. Equating the second of Equations (35) to zero, we obtain a quadratic equation in $(r/a)^{\lambda}$ for the determination of the position of the neutral axis. Assuming $\nu = 0.28$, $\lambda = (2 + 2\nu)^{1/2} = 1.6$, $b = 2a$, we further obtain $r/a = 1.3323$; this compares very favorably with $r/a = 1^1/_3$ from the elementary, curved-bar theory. Also the stresses at $r = a$, $2a$ from this latter theory are $\pm 12.586\ M/a^2h$ as compared with $\pm 12.740\ M/a^2h$ from the present theory—a difference of only just over 1 per cent.

[4] S. Timoshenko and J. N. Goodier, "Theory of Elasticity," McGraw-Hill Book Company, Inc., New York, N. Y., 1951, p. 61.

F. GODED
Ingeniero de Caminos,
General Eléctrica Española,
Madrid, Spain

The Stress Function of a Radial Strain

A stress function which permits the study of radial strain and, in particular, the manner of determining this stress function in a given cone, are derived in this paper.

In this development, spherical co-ordinates are used throughout the paper and are shown in Fig. 1, where

u = displacement in direction of radius
v = displacement normal to radius plane
ω = displacement normal to uv-plane
i, j, k = unit vectors in direction of u, v, and ω, respectively
$\rho = ui + vj + \omega k$ = displacement vector
ν = Poisson's coefficient
$\mu = \dfrac{E}{2(1+\nu)}$

The stresses σ_R, σ_θ, σ_ψ, $\tau_{R\theta}$, $\tau_{R\psi}$, $\tau_{\theta\psi}$, and the corresponding strains are used in a conventional manner.

The three possible cases arising from nullifying two of the components of the displacement are represented by the following relationships:

$$(a) - \begin{cases} u \neq 0 \\ v = \omega = 0 \end{cases} \quad (b) - \begin{cases} v \neq 0 \\ u = \omega = 0 \end{cases} \quad (c) - \begin{cases} \omega \neq 0 \\ u = v = 0 \end{cases} \tag{1}$$

The first of these cases indicates the existence of a radial strain. The derivation of the stress function for this case is shown in this paper.

The second set of relationships leads to J. H. Michell's stress function for problems concerning the torsion of axially symmetric straight bars of variable cross section.[1]

The third case does not possess a stress function, the only solution for the system being:

$$u = v = 0$$

$$\omega = R^{2-4\nu}(\sin\psi)^{4\nu-2}[A\cos 4(1-\nu)\theta + B\sin 4(1-\nu)\theta] \tag{2}$$

If we make $v = w = 0$, case (a) of equation (1), in the equilibrium equations, and in the components of the strain tensor[2] we obtain the following system:

$$(a)\quad \epsilon_R = \frac{\partial u}{\partial R} = \frac{\sigma_R - 2\nu\sigma_\theta}{E}$$

$$(b)\quad \epsilon_\theta = \epsilon_\psi = \frac{u}{R} = \frac{\sigma_\theta(1-\nu) - \nu\sigma_R}{E}$$

$$(c)\quad \gamma_{R\theta} = \frac{1}{R\sin\psi}\frac{\partial u}{\partial\theta} = \frac{\tau_{R\theta}}{\mu}$$

$$(d)\quad \gamma_{R\psi} = \frac{1}{R}\frac{\partial u}{\partial\psi} = \frac{\tau_{R\psi}}{\mu}$$

$$(e)\quad \gamma_{\psi\theta} = 0 \tag{3}$$

$$(f)\quad \frac{\partial\sigma_R}{\partial R} + \frac{1}{R\sin\psi}\frac{\partial\tau_{R\theta}}{\partial\theta} + \frac{1}{R}\frac{\partial\tau_{R\psi}}{\partial\psi} + \frac{2\sigma_R - 2\sigma_\theta}{R} + \frac{\tau_{R\psi}}{R}\operatorname{ctg}\psi = 0$$

$$(g)\quad \frac{\partial\tau_{R\theta}}{\partial R} + \frac{1}{R\sin\psi}\frac{\partial\sigma_\theta}{\partial\theta} + \frac{3\tau_{R\theta}}{R} = 0$$

$$(h)\quad \frac{\partial\tau_{R\psi}}{\partial R} + \frac{1}{R}\frac{\partial\sigma_\psi}{\partial\psi} + \frac{3\tau_{R\psi}}{R} = 0$$

Since $\epsilon_\psi = \epsilon_\theta$ and therefore $\sigma_\psi = \sigma_\theta$, Equations $(3g)$ and $(3h)$ may be written as follows:

$$(a)\quad \frac{\partial}{\partial R}[R^3\sin\psi\tau_{R\theta}] + \frac{\partial}{\partial\theta}[\sigma_\theta R^3] = 0$$

$$(b)\quad \frac{\partial}{\partial R}[R^3\tau_{R\psi}] + \frac{\partial}{\partial\psi}[\sigma_\theta R^3] = 0 \tag{4}$$

The second of these equations is satisfied when

$$(a)\quad \sigma_\theta R^3 = -\phi_R'$$

$$(b)\quad \tau_{R\psi}R^3 = \phi_\psi' \tag{5}$$

By substituting equation $(5a)$ into $(4a)$, one obtains:

$$\frac{\partial}{\partial R}[R^3\sin\psi\tau_{R\theta}] - \phi_{R\theta}'' = 0 \tag{6}$$

Integration of this equation yields

$$\tau_{R\theta} = \frac{1}{R^3\sin\psi}\phi_\theta' \tag{7}$$

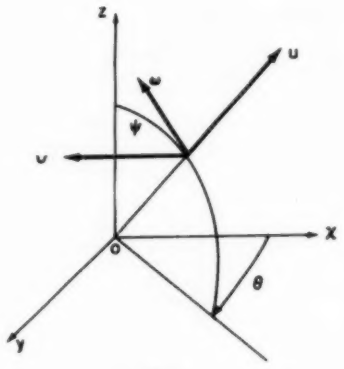

Fig. 1

[1] J. H. Michell, "The Uniform Torsion and Flexure of Incomplete Tores With Application to Helical Springs," Proceedings of the London Mathematical Society, vol. 31, 1900, p. 140.

[2] I. S. Sokolnikoff, "Mathematical Theory of Elasticity," McGraw-Hill Book Company, Inc., New York, N. Y., second edition, 1956.

Presented at the Summer Conference of the Applied Mechanics Division, Troy, N. Y., June 18–20, 1959, of The American Society of Mechanical Engineers.

Discussion of this paper should be addressed to the Secretary, ASME, 29 West 39th Street, New York, N. Y., and will be accepted until October 10, 1959, for publication at a later date. Discussion received after the closing date will be returned.

Note: Statements and opinions advanced in papers are to be understood as individual expressions of their authors and not those of the Society. Manuscript received by ASME Applied Mechanics Division, March 7, 1958. Paper No. 59—APM-25.

it not being necessary to add any arbitrary function of θ and ψ, as this is already included in ϕ.

By substituting equations (5*b*) and (7) into (3*c*) and (3*d*), the following equations are obtained:

$$\frac{1}{R \sin \psi} \frac{\partial u}{\partial \theta} = \frac{1}{\mu R^3 \sin \psi} \phi_\theta' \qquad \frac{1}{R} \frac{\partial u}{\partial \psi} = \frac{1}{\mu R^3} \phi_\psi' \tag{8}$$

Each of these equations yields

$$u = \frac{\phi}{\mu R^2} = \frac{2(1+\nu)}{E} \frac{\phi}{R^2} \tag{9}$$

For the same reason given previously it will not be necessary to add any arbitrary functions to the integrations performed in (9).

Solving equations (3*a*) and (3*b*) for σ_R and σ_θ, we have:

$$(a) \quad \sigma_\theta = \frac{E}{(1+\nu)(1-2\nu)} \left[\nu \frac{\partial u}{\partial R} + \frac{u}{R} \right]$$
$$(b) \quad \sigma_\psi = \frac{E}{(1+\nu)(1-2\nu)} \left[(1-\nu) \frac{\partial u}{\partial R} + 2\nu \frac{u}{R} \right] \tag{10}$$

and substituting in the first of these equations the values of u and σ_θ from equations (9) and (5*a*), we obtain, after simplification, the following differential equation:

$$\phi_R' = -2(1-2\nu) R^{-1} \phi \tag{11}$$

Integration yields

$$\phi = R^{4\nu-2} \cdot \varphi(\theta\psi) \tag{12}$$

Substituting this value of ϕ in the expressions for σ_R, $\tau_{R\theta}$, $\tau_{R\psi}$, σ_θ, and u of equations (10*a*), (7), (5*b*), (5*a*), and (9), respectively, one obtains

$$(a) \quad u = \frac{2(1+\nu)}{E} R^{4\nu-4} \varphi(\theta\psi)$$
$$(b) \quad \sigma_R = 4(\nu-2) R^{4\nu-5} \varphi(\theta\psi)$$
$$(c) \quad \sigma_\theta = \sigma_\psi = 2(1-2\nu) R^{4\nu-5} \varphi(\theta\psi)$$
$$(d) \quad \tau_{R\theta} = R^{4\nu-5} \frac{\varphi_\theta'(\theta\psi)}{\sin \psi} \tag{13}$$
$$(e) \quad \tau_{R\psi} = R^{4\nu-5} \varphi_\psi'(\theta\psi)$$
$$(f) \quad \tau_{\psi\theta} = 0$$

The equation to be satisfied by the stress function is obtained through the substitution of the foregoing expressions of the stresses in equation (3*f*). After simplifying, we have

$$\varphi_{\theta\theta}'' + \varphi_\psi' \sin \psi \cos \psi + \beta \cdot \varphi \sin^2 \psi + \varphi_{\psi\psi}'' \sin^2 \psi = 0 \tag{14}$$

in which

$$\beta = 4(1-\nu)(5-4\nu) \tag{15}$$

The stresses in (13) will satisfy both the equilibrium and the compatibility equations provided φ is a solution of equation (14).

The stress field (13) permits the determination of φ in such a way that no tangential stresses operate on the cone surface. This will be true if the resultant of the stresses $\tau_{R\theta}$ and $\tau_{R\psi}$ of Fig. 2 is parallel to ds at all points on the curve C. This curve C

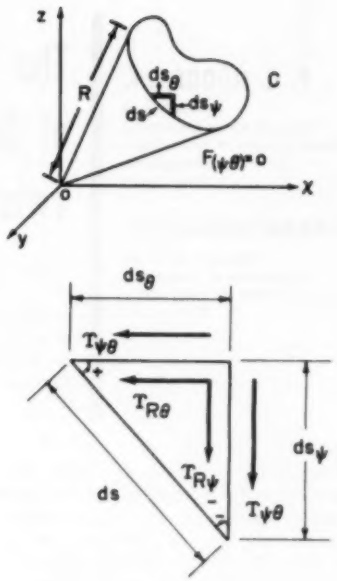

Fig. 2

is the intersection of the cone with a sphere whose center is the origin and whose radius is R.

The condition that the resultant shear stress be parallel to the arc element ds may be expressed as

$$\tau_{R\psi} \cos(n, ds_\psi) + \tau_{R\theta} \cos(n, ds_\theta) = 0 \tag{16}$$

or

$$\tau_{R\psi} \cos(ds, ds_\theta) + \tau_{R\theta} \cos(ds, ds_\psi) = 0 \tag{17}$$

where n is the outward normal to the boundary C of the cone section.

From Fig. 2 it may be seen that:

$$\cos(ds, ds_\psi) = \frac{ds_\psi}{ds} = R \frac{d\psi}{ds}$$
$$\cos(ds, ds_\theta) = -\frac{ds_\theta}{ds} = -R \frac{\sin \psi d\theta}{ds} \tag{18}$$

Substituting the foregoing values into (17), we have

$$\tau_{R\psi} \sin \psi d\theta - \tau_{R\theta} d\psi = 0 \tag{19}$$

and substituting here the expressions for $\tau_{R\theta}$ and $\tau_{R\psi}$ from (13) leads to

$$\varphi_\psi' \sin^3 \psi d\theta - \varphi_\theta' d\psi = 0 \quad \text{in } C \tag{20}$$

Function φ is therefore completely determined except for an arbitrary constant, by the following two conditions:

1 φ be a solution of equation (14)

2 φ to verify (20) at all points of the surface of the cone $F(\theta, \psi) = 0$

On the boundary surface, the only stresses caused by field (13) are the following:

$$\sigma_\theta = \sigma_\psi = 2(1-2\nu) R^{4\nu-5} K_1 \text{ in } D$$

P. G. HODGE, JR.
Professor,
Department of Mechanics,
Illinois Institute of Technology,
Chicago, Ill.
Mem. ASME

R. SANKARANARAYANAN
Research Assistant,
Department of Mechanics,
Illinois Institute of Technology,
Chicago, Ill.

The Determination of Safe Loads of Beams Subjected to Combined Twisting and Biaxial Bending Moments[1]

Using the lower-bound theorem of limit analysis, a yield criterion is obtained in terms of the stress resultants for a beam, subjected to combined twisting and biaxial bending moments. Based on a piecewise linear approximate yield condition, the "collapse load" is determined for a right-angle bent, subjected to a load in an arbitrary direction applied to the mid-point of one leg. Such a collapse load, which is a 'safe load" for the beam, is plotted as a function of a suitable parameter.

THERE appears to be no published work on the application of the theorems of limit analysis for structures subjected to a combination of a bending moment in an arbitrary plane and a twisting moment; i.e., bending moments in two perpendicular planes and a torque. The works of Hill and Siebel [1][2] and Steele [2] on thin tubes and of Heyman on beams [3] were restricted to the consideration of the simultaneous action of a twisting couple and a bending moment in a fixed plane. The present paper is concerned with a beam subjected to bending moments in two planes plus a twisting moment.

The lower-bound theorem of limit analysis states that a structure will not fail under any load for which some statically admissible stress field can be found. A statically admissible stress field is one which is in internal and external equilibrium and does not violate the yield condition. Applied to the problem of determining an interaction curve, the theorem states that any stress resultants which are in equilibrium with a statically admissible set of stresses in the cross section will not cause failure. Therefore a curve or surface in stress space composed entirely of such statically admissible stress resultants will lie on, or within, the true yield curve or surface.

The formulation of an approximate interaction surface for combined twisting and biaxial bending moments of a square section is presented in the next section. The following section is concerned with a right-angle bent, subjected to a load in an arbitrary direction applied to the mid-point of one leg. Finally, the conclusions of the paper are summarized.

Formulation of Interaction Surface

We consider for definiteness a beam of solid square section, Fig. 1, subjected to the simultaneous action of bending moments in two planes and a twisting moment. However, the methods can be easily generalized to apply to any section.

We consider first the case of bending without twist. The only nonzero stress component is the axial one σ. When the section is fully plastic, σ will be equal to the yield stress in tension or compression. When both moments are positive, the tensile and compressive yield stresses will be distributed qualitatively in the manner indicated in Fig. 1. Let $y = f(x)$ denote the surface which separates tensile from compressive stress. Then the two bending moments M and N are given by

$$M = \int_{-h}^{h}\left[\int_{-h}^{f(x)} x(-Y)dy + \int_{f(x)}^{h} x(Y)dy\right]dx$$

$$= -2Y\int_{-h}^{h} xf(x)dx \qquad (1)$$

$$N = Y\int_{-h}^{h}[h^2 - f(x)^2]dx$$

Equations (1) give a pair of statically admissible bending moments, and hence a lower bound on the interaction curve, for any function $f(x)$. To determine the best lower bound, we try to maximize N for a given value of M. By use of variational calculus, it can be shown that this is equivalent to finding a stationary value of the quantity

$$\delta N + \lambda\delta M = -2Y\int_{-h}^{h}[f(x) + \lambda x]\delta f(x)\,dx$$

If this is to be equal to zero for all choices of the variation $\delta f(x)$, the quantity in brackets in the integrand must be equal to zero. Thus $f(x)$ must be a straight line through the origin

$$f(x) = -\lambda x \qquad (2)$$

The moments in Equations (1) are now easily evaluated in terms of the parameter λ

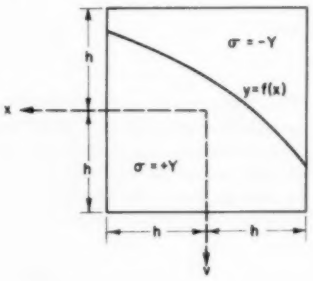

Fig. 1 Square section with two bending moments

[1] The research described in this paper was begun while the authors were at the Polytechnic Institute of Brooklyn and concluded at the Illinois Institute of Technology. The support of the Office of Naval Research in both phases is gratefully acknowledged. This paper is part of a thesis submitted by one of the authors (RS) in partial fulfillment of the requirements for the degree of Doctor of Philosophy in Mechanics at the Illinois Institute of Technology.

[2] Numbers in brackets designate References at end of paper.

Presented at the Summer Conference of the Applied Mechanics Division, Troy, N. Y., June 18–20, 1959, of THE AMERICAN SOCIETY OF MECHANICAL ENGINEERS.

Discussion of this paper should be addressed to the Secretary, ASME, 29 West 39th Street, New York, N. Y., and will be accepted until October 10, 1959, for publication at a later date. Discussion received after the closing date will be returned.

NOTE: Statements and opinions advanced in papers are to be understood as individual expressions of their authors and not those of the Society. Manuscript received by ASME Applied Mechanics Division, May 8, 1958. Paper No. 59—APM-26.

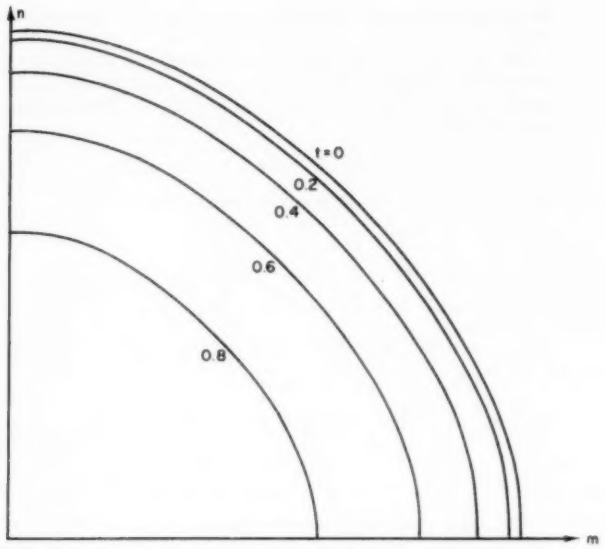

Fig. 2 Level curves for combined twisting and biaxial bending of a square section

$$M = (4/3)Yh^2\lambda, \quad N = (2/3)Yh^2(3 - \lambda^2) \tag{3a}$$

At this point it is convenient to introduce dimensionless moments

$$m = M/M_0, \quad n = N/M_0, \quad \text{where} \quad M_0 = 2Yh^2 \tag{3b}$$

Elimination of the parameter λ from Equations (3) then leads to

$$(3/4)m^2 + n = 1 \tag{4}$$

Equations (3) implicitly assume that the line $y = -\lambda x$ extends from $x = -h$ to $x = +h$; i.e., that $|\lambda| \leqslant 1$ and hence is only valid for $0 \leqslant m \leqslant 2/3$. The case $|\lambda| > 1$ as well as the cases of negative moments are easily obtained by symmetry. The level curve $t = 0$ in Fig. 2 shows the first quadrant of the interaction curve for combined bending with no twist of a square section.

An approach to the problem of twist combined with bending in one plane has been given by Hill and Siebel [1] and can easily be generalized to the present problem. We assume a distribution of normal stress similar to that encountered in pure bending. Thus tensile and compressive stresses of magnitude σ are distributed as in the absence of twist, but the magnitude is such that

$$(3/4)(mY/\sigma)^2 + (nY/\sigma) = 1 \tag{5a}$$

At the same time, a distribution of shearing stress is assumed similar to the fully plastic distribution for pure torsion [4], but of magnitude τ. The dimensionless torque is then

$$t = T/T_0 = 2\tau/Y, \quad T_0 = (4/3)Yh^3 \tag{5b}$$

Finally, the magnitudes σ and τ are related so that the Tresca yield condition[3]

$$\sigma^2 + 4\tau^2 = Y^2 \tag{5c}$$

is satisfied throughout the cross section. Elimination of σ and τ between Equations (5) then leads to the yield condition

$$(3/4)m^2 + n(1 - t^2)^{1/2} + t^2 = 1 \quad |m| < n \tag{6}$$

with similar expressions for the other octants. Typical level curves are shown in Fig. 2.

For the purpose of solving problems, it is convenient to replace Equation (6) with a piecewise linear approximation. In view of the symmetry and the generally spherical character of Equation (6), it appears reasonable to use an essentially octagonal approach. To this end, we take the symmetric points $(0, \pm 1)$, $(\pm 1, 0)$, $(\pm 2/3, \pm 2/3)$ on the level curves $t = 0$ together with corresponding points on the plane $t = \pm 1/\sqrt{2}$. These points determine 32 plane faces as shown in Figs. 3 and 4. The equations of the planes and the corresponding flow rules are given in Table 1. In each case, the upper sign goes with the first numbered face, the lower with the second.

[3] The Mises condition $\sigma^2 + 3\tau^2 = Y^2$ could equally well be used.

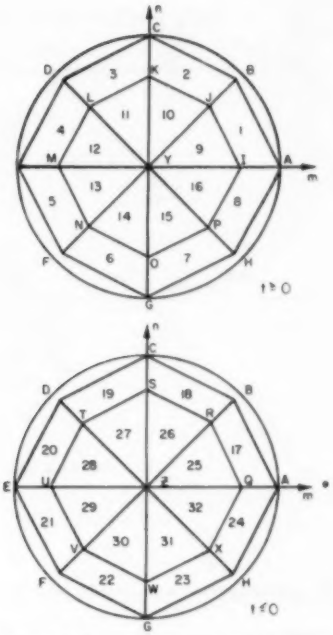

Fig. 3 Faces of yield polyhedron for combined twisting and biaxial bending of square section

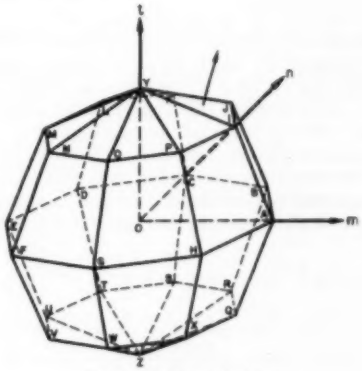

Fig. 4 Yield polyhedron

Strain-rate variables must be associated with the dimensionless stress resultants so that the dissipation of energy D_i is proportional to the scalar product of stress times strain rate [5]. If θ and ϕ are the two bending rates and χ the rate of twist, the unit dissipation is

$$D_i = M\theta + N\phi + T\chi = M_0[m\theta + n\phi + (T_0/M_0)\chi]$$

For a square section it is obvious from Equations (3b) and (5b)

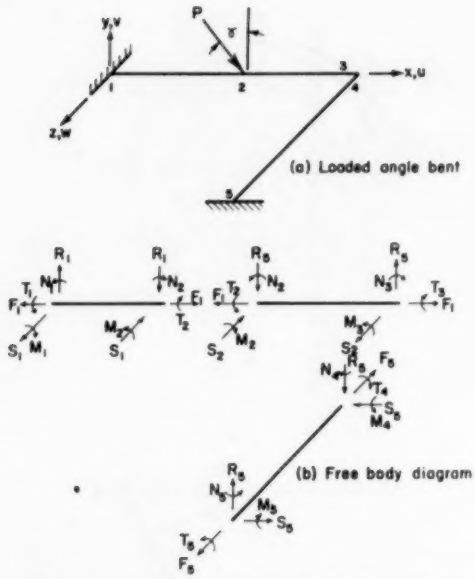

Fig. 5 Right-angle bent with arbitrary load direction

that $T_0/M_0 = 2/3$; hence a proper choice of strain variables is θ, ϕ and $\psi = (2/3)\chi$ [6].

Example

As an example, we consider the right-angle bent shown in Fig. 5, the load P acting at the mid-point of one leg and being applied at an arbitrary angle γ, $(0 \leqslant \gamma \leqslant \pi/2)$ to the normal to the plane of the bent. It is assumed that the effect of the induced axial forces on the yield condition can be neglected.

Hinges can occur only at the ends, corner, or under the loads. Hence the free-body diagram shown in Fig. 5 is appropriate. Subscripts are used to indicate possible hinge locations.

Equilibrium of the free bodies and joints in Fig. 5 leads to the relations

$$\begin{gathered} R_1L/2 = M_2 - M_1 \qquad S_1L/2 = N_1 - N_2 \qquad T_1 = T_2 \\ R_2L/2 = M_2 - M_3 \qquad S_2L/2 = N_2 - N_3 \qquad T_2 = T_3 \\ R_5L = M_4 - M_5 \qquad S_5L = N_4 - N_5 \qquad T_4 = T_5 \\ S_1 + S_2 = P \sin\gamma;\ R_1 + R_5 = P\cos\gamma \\ F_1 = S_5, \quad S_2 = F_5 \\ N_2 = N_4, \quad M_2 = T_4, \quad T_3 = M_4 \end{gathered} \tag{7}$$

We introduce dimensionless quantities defined by

$$\begin{gathered} r_i = R_iL/M_0, \quad \sigma_i = S_iL/M_0, \quad f_i = F_iL/M_0, \quad \omega = PL/M_0 \\ m_i = M_i/M_0, \quad n_i = N_i/M_0, \quad t_i = T_i/T_0 = 3T_i/2M_0 \end{gathered} \tag{8}$$

Equations (7) can then be written in the form

$$\begin{gathered} t_1 = t_2 = t_3 = {}^2/_3m_4; \quad t_4 = t_5 = {}^2/_3m_3; \quad n_3 = n_4; \\ 2m_2 - 2m_3 - m_4 + m_5 = 0; \quad -2m_1 + 2m_2 + m_4 - m_5 = \\ \omega\cos\gamma; \quad 2n_1 - 4n_2 + 2n_3 = \omega\sin\gamma; \\ f_1 = \sigma_5 = (n_4 - n_5); \quad \sigma_2 = f_5 = 2(n_3 - n_2); \\ r_1 = 2(m_2 - m_1); \quad r_5 = (m_4 - m_5); \quad \sigma_1 = 2(n_1 - n_2) \end{gathered} \tag{9}$$

Any set of moments satisfying Equation (9) and not violating the yield condition may be used to find a lower bound on the collapse load ω.

The exact solution also must produce strain rates which lead to compatible velocities. The velocity components at each joint computed from either end of the bent must agree. Thus denoting velocities by

$$U_i = u_i/L, \quad V_i = v_i/L, \quad W_i = w_i/L$$

in the directions x, y, z, respectively, we obtain

$$\begin{aligned} u_1 &= u_2 = u_3 = u_4 = \phi_5 = 0 \\ u_5 &= \phi_1 + \phi_2 + \phi_3 + \phi_4 = 0 \\ v_1 &= \theta_5 + \theta_3 + {}^1/_2\theta_2 + \chi_3 + \chi_4 = 0 \\ v_2 &= {}^1/_2\theta_1 = \theta_5 + {}^1/_2\theta_3 + {}^1/_2(\chi_3 + \chi_4) \\ v_3 &= v_4 = \theta_1 + {}^1/_2\theta_2 = \theta_5 \\ v_5 &= \theta_1 + {}^1/_2\theta_2 + \theta_4 + \chi_1 + \chi_2 + \chi_3 = 0 \\ w_1 &= -(\phi_5 + \phi_4 + \phi_3 + {}^1/_2\phi_2) = 0 \\ w_2 &= -{}^1/_2\phi_1 = -{}^1/_2(\phi_5 + \phi_4 + \phi_3) \\ w_3 &= w_4 = w_5 = 0 = -(\phi_1 + {}^1/_2\phi_2) \end{aligned}$$

Not all of the foregoing equations are independent. Replacing χ_i by $(3/2)\psi_i$, the independent relations may be written in the form

$$\begin{gathered} \phi_1 = \phi;\ \phi_2 = -2\phi;\ \phi_3 + \phi_4 = \phi;\ \phi_5 = 0; \\ 4\theta_5 + 2\theta_3 - 2\theta_1 + 3(\psi_4 + \psi_5) = 0 \\ 2\theta_5 - \theta_2 - 2\theta_1 = 0 \\ 2\theta_4 + \theta_2 + 2\theta_1 + 3(\psi_1 + \psi_2 + \psi_3) = 0 \end{gathered} \tag{10}$$

If the strain-rate variables are all known, then the collapse load is determined from the principle of virtual work. The external rate of energy dissipation is

$$D_e/M_0 = {}^1/_2\omega[-\theta_1\cos\gamma + \phi\sin\gamma] \tag{11}$$

The actual mode of collapse depends on the inclination γ of the load P to the normal to the plane of the bent. For values of γ near 90 deg it is intuitively plausible that there will be hinges at 1, 2, and 3 and that there will be no twisting moment in either leg. Hence the points 1, 2, and 3 should lie on the plane $t = 0$ of the yield surface. Further, the compatibility relations $\phi_1 = \phi$, $\phi_2 = -2\phi$, $\phi_3 + \phi_4 = \phi$, suggest that 1 and 3 are associated with positive values of n, whereas 2 is associated with a negative n-value. The equilibrium equations $t_4 = t_5 = (3/2)m_3$ require 3 to stay at corner C. Therefore it seems reasonable to assume the following locations for the hinges:

$$1 \text{ on } CD, \quad 2 \text{ on } GH, \quad 3 \text{ at } C$$

The plastic strain-rate vector corresponding to a stress point on a given face of the yield polyhedron is given in Table 1. For a point at the intersection of two or more faces, the vector may be any positive combination of the vectors for the intersecting faces. Thus the strain-rate vector for point 1 on edge CD is

$$\begin{aligned} E_1 = (\theta_1, \phi_1, \psi_1) = \lambda_3[-{}^1/_2, 1, (\sqrt{2} - 1)] \\ + \lambda_{19}[-{}^1/_2, 1, -(\sqrt{2} - 1)] \end{aligned} \tag{12a}$$

where λ_3 and λ_{19} are arbitrary positive multipliers. Similarly, the strain-rate vectors for points 2 and 3 are

$$\begin{aligned} E_2 &= \mu_7[{}^1/_2, -1, (\sqrt{2} - 1)] + \mu_{23}[{}^1/_2, -1, -(\sqrt{2} - 1)] \\ E_3 &= \nu_3[{}^1/_3, 1, (\sqrt{2} - 1)] + \nu_9[-{}^1/_3, 1, (\sqrt{2} - 1)] \\ &\quad + \nu_{18}[{}^1/_2, 1, -(\sqrt{2} - 1)] + \nu_{19}[-{}^1/_2, 1, -(\sqrt{2} - 1)] \end{aligned} \tag{12b}$$

Table 1 Yield condition and flow rule for combined twisting and biaxial bending of square section

Face	Equation	Strain-rate vector (θ, ϕ, ψ)
1, 17	$m + \frac{1}{2}n \pm (\sqrt{2} - 1)t = 1$	$\Lambda[1, \frac{1}{2}, \pm(\sqrt{2} - 1)]$
2, 18	$\frac{1}{2}m + n \pm (\sqrt{2} - 1)t = 1$	$\Lambda[\frac{1}{2}, 1, \pm(\sqrt{2} - 1)]$
3, 19	$-\frac{1}{2}m + n \pm (\sqrt{2} - 1)t = 1$	$\Lambda[-\frac{1}{2}, 1, \pm(\sqrt{2} - 1)]$
4, 20	$-m + \frac{1}{2}n \pm (\sqrt{2} - 1)t = 1$	$\Lambda[-1, \frac{1}{2}, \pm(\sqrt{2} - 1)]$
5, 21	$-m - \frac{1}{2}n \pm (\sqrt{2} - 1)t = 1$	$\Lambda[-1, -\frac{1}{2}, \pm(\sqrt{2} - 1)]$
6, 22	$-\frac{1}{2}m - n \pm (\sqrt{2} - 1)t = 1$	$\Lambda[-\frac{1}{2}, -1, \pm(\sqrt{2} - 1)]$
7, 23	$\frac{1}{2}m - n \pm (\sqrt{2} - 1)t = 1$	$\Lambda[\frac{1}{2}, -1, \pm(\sqrt{2} - 1)]$
8, 24	$m - \frac{1}{2}n \pm (\sqrt{2} - 1)t = 1$	$\Lambda[1, -\frac{1}{2}, \pm(\sqrt{2} - 1)]$
9, 25	$(\sqrt{2} - 1)(m + \frac{1}{2}n) \pm t = 1$	$\Lambda[1, \frac{1}{2}, \pm(\sqrt{2} + 1)]$
10, 26	$(\sqrt{2} - 1)(\frac{1}{2}m + n) \pm t = 1$	$\Lambda[\frac{1}{2}, 1, \pm(\sqrt{2} + 1)]$
11, 27	$(\sqrt{2} - 1)(-\frac{1}{2}m + n) \pm t = 1$	$\Lambda[-\frac{1}{2}, 1, \pm(\sqrt{2} + 1)]$
12, 28	$(\sqrt{2} - 1)(-m + \frac{1}{2}n) \pm t = 1$	$\Lambda[-1, \frac{1}{2}, \pm(\sqrt{2} + 1)]$
13, 29	$(\sqrt{2} - 1)(-m - \frac{1}{2}n) \pm t = 1$	$\Lambda[-1, -\frac{1}{2}, \pm(\sqrt{2} + 1)]$
14, 30	$(\sqrt{2} - 1)(-\frac{1}{2}m - n) \pm t = 1$	$\Lambda[-\frac{1}{2}, -1, \pm(\sqrt{2} + 1)]$
15, 31	$(\sqrt{2} - 1)(\frac{1}{2}m - n) \pm t = 1$	$\Lambda[\frac{1}{2}, -1, \pm(\sqrt{2} + 1)]$
16, 32	$(\sqrt{2} - 1)(m - \frac{1}{2}n) \pm t = 1$	$\Lambda[1, -\frac{1}{2}, \pm(\sqrt{2} + 1)]$

The components of the strain-rate vectors at the points 1, 2, and 3 are then seen to be

$$\theta_1 = -\tfrac{1}{2}(\lambda_3 + \lambda_{19}); \quad \phi_1 = (\lambda_3 + \lambda_{19}); \quad \psi_1 = (\sqrt{2} - 1)(\lambda_3 - \lambda_{19})$$

$$\theta_2 = \tfrac{1}{2}(\mu_7 + \mu_{23}); \quad \phi_2 = -(\mu_7 + \mu_{23}); \quad \psi_2 = (\sqrt{2} - 1)(\mu_7 - \mu_{23}) \tag{12c}$$

$$\theta_3 = \tfrac{1}{2}(\nu_2 - \nu_3 + \nu_{18} - \nu_{19}); \quad \phi_3 = (\nu_2 + \nu_3 + \nu_{18} + \nu_{19}); \quad \psi_3 = (\sqrt{2} - 1)(\nu_2 + \nu_3 - \nu_{18} - \nu_{19})$$

It then follows from Equations (10) and (12c) that

$$\theta_1 = -\frac{\phi}{2}; \quad \theta_2 = \phi; \quad \theta_3 = -\frac{\phi}{2} \tag{12d}$$

$$\phi_1 = \phi; \quad \phi_2 = -2\phi; \quad \phi_3 = \phi$$

If the foregoing solution is to be an upper bound, then the arbitrary factors of the strain-rate vectors should all be positive and this is found to be the case provided

$$\psi_1 = \psi_2 = \psi_3 = 0 \tag{12e}$$

The rate of dissipation of internal energy is given by

$$D_i = M_0[m\theta + n\phi + t\psi] = 4M_0\phi$$

Equating this value to the external energy Equation (11) the collapse load is found to be

$$\omega = \frac{16}{\cos\gamma + 2\sin\gamma} \tag{12f}$$

The set of moments should be in equilibrium with the given load P. Since there is no twisting moment on either leg, it follows that

$$t_1 = t_2 = t_3 = t_4 = t_5 = m_3 = m_4 = 0 \tag{13a}$$

For the assumed position of the hinges

$$-\tfrac{1}{2}m_1 + n_1 = 1; \quad \tfrac{1}{2}m_2 - n_2 = 1; \quad n_3 = n_4 = 1 \tag{13b}$$

Equations (9), (13a) and (13b) do not uniquely determine the remaining stresses. However, they do lead to the unique value of the collapse load given by Equation (12f).

The foregoing solution is valid only if the following requirements are satisfied:

(ia) The strain-rate vector at the point 1 must lie between the limiting normals associated with faces 3 and 19.

(ib) Point 1 must remain on the finite edge CD. Reference to Table 1 shows that the requirement (ia) is equivalent to

$$\frac{\theta_1}{\phi_1} = -\tfrac{1}{2} \quad \text{and} \quad -0.414 \leqslant \frac{\psi_1}{\phi_1} \leqslant 0.414$$

Obviously, these are true by virtue of Equations (12d) and (12e). The requirement (ib) can be written as

$$-\tfrac{2}{3} \leqslant m_1 \leqslant 0 \tag{14a}$$

(iia) The strain-rate vector at 2 should lie between the limiting normals associated with faces 7 and 23.

(iib) Point 2 must remain on the finite edge GH.

Requirement (iia) is equivalent to

$$\frac{\theta_2}{\phi_2} = -\tfrac{1}{2} \quad \text{and} \quad -0.414 \leqslant \frac{\psi_2}{\phi_2} \leqslant 0.414$$

These are satisfied in view of Equations (12d) and (12e). If we make use of Equations (9), requirement (iib) can be written

$$-\frac{\omega}{2}\cos\gamma \leqslant m_1 \leqslant \frac{4}{3} - \frac{\omega}{2}\cos\gamma \tag{14b}$$

(iii) The strain-rate vector at 3 should lie between the limiting normals associated with faces 2, 3, 18 and 19. Thus

$$-\tfrac{1}{2} < \frac{\theta_3}{\phi_3} < \tfrac{1}{2} \quad \text{and} \quad -0.414 < \frac{\psi_3}{\phi_3} < 0.414$$

These are satisfied in view of Equations (12d) and (12e).

(iv) Point 4 should lie within the yield surface. Equations (9) and (13a) determine

$$m_4 = 0, \quad n_4 = 1.0, \quad t_4 = 0$$

Hence point 4 is at the corner C and this requirement is satisfied.

(v) Point 5 is not uniquely determined, but it must be possible to find some location for point 5 which satisfies the equilibrium equations and does not violate the yield condition. To this end, we arbitrarily set $n_5 = 0$; since $t_5 = 0$ the yield condition reduces to

$$-1 \leqslant m_5 \leqslant 1$$

In view of Equations (9) and (14a) the right-hand inequality is always satisfied and m_1 must satisfy

$$m_1 \leqslant 1 - \tfrac{1}{4}\omega\cos\gamma \tag{14c}$$

The foregoing solution will be valid provided some value of m_1 can be found which satisfies all of Equations (14). A necessary and sufficient condition that this be true is that each left side of the continued inequalities (14) be less than each right side.

Table 2 Location of points on the yield surface and values of the collapse load for $90° \geq \gamma \geq 0°$

Range of values of γ	Location of the points 1	2	3	4	5	Collapse load, ω
$\gamma_0 = 90°$	C	G	C	C	Interior	8
$\gamma_0 < \gamma < \gamma_1$	CD	GH	C	C	Interior	$16(\cos\gamma + 2\sin\gamma)^{-1}$
$\gamma_1 = 62° 14'$	D	GH	C	C	E	7.16
$\gamma_1 < \gamma < \gamma_2$	DE	GH	C	Interior	E	$13(2\cos\gamma + \sin\gamma)^{-1}$
$\gamma_2 = 51° 20'$	E	GH	C	C	E	6.401
$\gamma_2 < \gamma < \gamma_3$	E	GH	Interior	CK	EM	$18.83(3.457\cos\gamma + \sin\gamma)^{-1}$
$\gamma_3 = 46° 13'$	E	H	Interior	CK	EM	6.046
$\gamma_3 < \gamma < \gamma_4$	E	HA	Interior	CK	EM	$41.66(8.914\cos\gamma + \sin\gamma)^{-1}$
$\gamma_4 = 32° 51'$	E	HA	Interior	K	M	5.187
$\gamma_4 < \gamma < \gamma_5$	EM	Face 8	Interior	KJ	M	$60.10(13.15\cos\gamma + \sin\gamma)^{-1}$
$\gamma_5 = 15° 42'$	EM	IA	Interior	KJ	M	4.648
$\gamma_6 < \gamma < \gamma_4$	EM	IA	Interior	Interior	M	$4.475(\cos\gamma)^{-1}$
$\gamma_6 = 0°$	EM	IA	Interior	Interior	M	4.475

Therefore m_1 is eliminated from (14) by setting up six inequalities expressing this condition:

$$-{}^{2}/_{3} < 0 \tag{15a}$$

$$-\frac{2}{3} < \frac{4}{3} - \frac{\omega}{2}\cos\gamma \tag{15b}$$

$$-\frac{2}{3} < 1 - \frac{\omega}{2}\cos\gamma \tag{15c}$$

$$-\frac{\omega}{2}\cos\gamma < 0 \tag{15d}$$

$$-\frac{\omega}{2}\cos\gamma < \frac{4}{3} - \frac{\omega}{2}\cos\gamma \tag{15e}$$

$$-\frac{\omega}{2}\cos\gamma < 1 - \frac{\omega}{2}\cos\gamma \tag{15f}$$

Three of these (15*a*, *e*, *f*) are identically satisfied. From the remaining inequalities we find the most restrictive ones to be

$$0 < \omega\cos\gamma < \frac{10}{3} \tag{16a}$$

Substituting the value of ω from Equation (12*f*) into (16*a*), the solution is seen to be valid for

$$62° 14' < \gamma < 90° \tag{16b}$$

At $\gamma = 62° 14'$, the values of the moments and the positions of the points on the yield surface are as shown in line 3 of Table 2.

For γ slightly less than 62° 14′, point 1 leaves the edge CD and point 5 just comes into contact with the yield surface at E. Therefore it seems reasonable to try a four-hinge mechanism with hinges at 1, 2, 3 and 5, the corresponding locations being DE, GH, C, and E, respectively.

For the assumed arrangement of hinges, a solution can be found as under the previous hypothesis. In the present case, all stresses are uniquely determined. The collapse load, computed by the principle of virtual work or by the equilibrium equations, turns out to be

$$\omega = \frac{13}{2\cos\gamma + \sin\gamma} \tag{17}$$

Details of this and other solutions may be found in [7].

As before, the solution is valid only for values of γ such that the strain-rate vectors lie between the limiting normals associated with the corresponding adjacent sides and as long as the points 1 and 2 remain on the finite edges DE and GH, respectively, and point 4 does not leave the yield polyhedron. It can be shown that the most restrictive condition is the one on point 1; namely,

$$-1.0 < m_1 < -0.667 \tag{18a}$$

and that this restriction is satisfied for all γ such that

$$51° 20' < \gamma < 62° 14' \tag{18b}$$

At $\gamma = 51° 20'$, the values of the moments and the positions of the points on the yield surface are as shown in line 5 of Table 2.

For values of γ less than 51° 20′, we may anticipate some torsional moment on the leg 4–5, and hence we move the point 5 upward along the edge EM of the yield surface. As the equilibrium Equations (9) require that $t_4 = t_5$, we also move the point 4 upward along CK of the yield surface. Further, the hinge at the corner of the bent is now at the point 4, rather than point 3. Finally, the hinges at points 1 and 2 stay at the corner E and on the edge GH, respectively.

The resulting solution and similar solutions for each of the ranges of γ may be obtained as shown in Table 2. In each case, the arrangement of hinges is first suggested by the reason for which the previous solution becomes invalid and is then verified by constructing a statically and kinematically admissible stress and velocity field. The solutions are summarized in Table 2; details may be found in [7]. The resulting collapse load ω is shown in Fig. 6 as a function of the angle of inclination of the oad γ.

Conclusion

A plastic analysis has been made of a square beam subjected to combined twisting and biaxial bending moments. The material of the beam is rigid-plastic and satisfies Tresca's yield condition and the associated flow rule.

The yield surface is defined in a three-dimensional space. In this space the two bending moments and the twisting moment, all made suitably nondimensional, are taken as rectangular Cartesian co-ordinates. The yield surface is closed, convex, and nonlinear in character. Accordingly, there is considerable complexity in the yield condition and the flow rule appropriate to any plastic regime. Therefore the yield condition has been replaced by a piecewise linear approximation based on an octagonal approach. Based on this approximate yield condition, the collapse load of an angle bent (which is a safe load for the structure) has been determined for a variety of combinations of bending and twisting moments.

The difficulty arising in two and three stress-dimensional problems is that the number of permissible independent static solutions, each of which determines a lower bound, is multiply infinite; hence a good solution may be difficult to recognize. The same difficulty is also present in a kinematic approach leading to an upper bound. Further, since simplifying physical assumptions and inexact physical constants must be used in any event, it is not always worth while engaging in the large effort required for an exact mathematical solution. In such cases, an approxi-

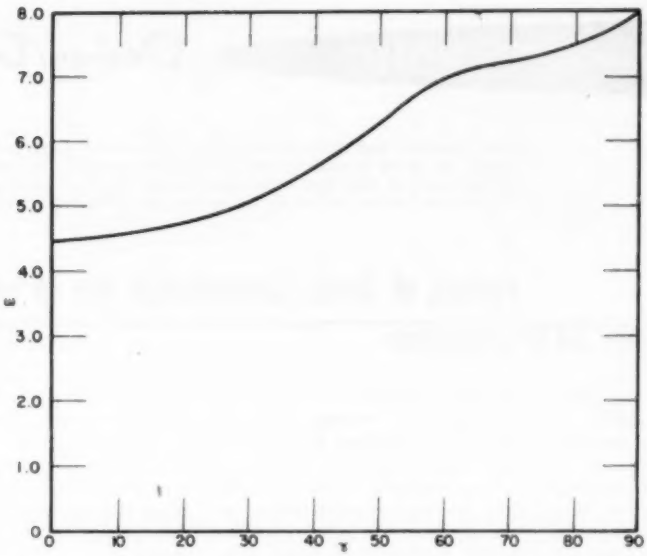

Fig. 6 Collapse load ω versus angle of inclination γ

mate linear method, such as the one suggested herein, may be sufficiently simple to obtain solutions easily, and at the same time be sufficiently accurate for practical applications.

References

1 R. Hill and M. P. L. Siebel, "On Combined Bending and Twisting of Thin Tubes in the Plastic Range," *Philosophical Magazine*, series 7, vol. 42, 1951, pp. 722–733.

2 M. C. Steele, "The Plastic Bending and Twisting of Square Section Members," *Journal of the Mechanics and Physics of Solids*, vol. 3, 1954, pp. 156–166.

3 Jacques Heyman, "The Limit Design of Space Frames," JOURNAL OF APPLIED MECHANICS, vol. 18, TRANS. ASME, vol. 73, 1951, pp. 157–162.

4 W. Prager and P. G. Hodge, Jr., "Theory of Perfectly Plastic Solids," John Wiley & Sons, New York, N. Y., 1951, pp. 55–94.

5 W. Prager, "General Theory of Limit Design," Proceedings of the Eighth International Congress of Theoretical and Applied Mechanics, Istanbul, Turkey, 1952.

6 P. G. Hodge, Jr., "Plastic Analysis of Structures," McGraw-Hill Book Company, Inc., New York, N. Y., 1959.

7 P. G. Hodge, Jr., and R. Sankaranarayanan, "The Determination of Safe Loads of Beams Subjected to Combined Bending, Bending and Twisting Moments," Illinois Institute of Technology, DOMIIT Report 1–2, 1958.

It is important that the data contained in technical papers be made readily available to design engineers. In order to satisfy these needs of industry, this section of the Journal includes a concise presentation of data and information drawn chiefly from papers previously published by the Applied Mechanics Division of The American Society of Mechanical Engineers.

Factors of Stress Concentration Due to Elliptical Fillets[1]

M. M. FROCHT[2] and D. LANDSBERG[3]

It is well known that circular fillets can produce rather high stress concentrations in tension as well as in bending. One way to reduce these stress concentrations is to increase the radius of the fillet. However, this is not always feasible since there are cases in which the design requires a shoulder which limits the radius of the fillet. In such cases the stress concentration can be mitigated by the use of elliptical fillets with the major axis of the ellipse parallel to the axis of the bar. Specifically, for given ratios of D/d and h/b, Fig. 1, elliptical fillets will produce smaller stress concentrations than circular fillets. A limited amount of data is already available on this subject [1, 2, 3, 4].[4] The following curves give additional design data for two-dimensional cases in uniform tension and in pure bending for several ratios of D/d, a/b, and h/b. These data were obtained from photoelastic tests using Castolite models. The fillets were machined with small end mills the centers of which were made to follow a calculated co-ordinate system to produce an exact elliptical contour. The size of the end mill was chosen to be smaller than the minimum radius of curvature of the particular ellipse being cut and was kept constant for each ellipse. In the models used the cutters ranged from $^1/_{16}$ in. to $^3/_{16}$-in. diam.

Definitions: The factor of stress concentration k is defined in the usual way,

$$k = \sigma_{max}/\sigma_{nom}$$

where σ_{max} is the maximum stress at the discontinuity, and σ_{nom} is the nominal stress based on elementary formulas.

For fillets in tension,

$$\sigma_{nom} = P/A$$

where P is the applied axial load, and A is the cross-sectional area of the smaller shank.

For fillets in pure bending,

$$\sigma_{nom} = Mc/I$$

where M is the maximum bending moment at the discontinuity, I is the moment of inertia of the cross section of the smaller shank about the neutral axis, and c is the distance from the neutral axis to the extreme fibers of the smaller shank.

The experimental data are presented in Figs. 1–8. Fig. 9 is a typical stress pattern showing the rather sharp reduction in the factor of stress concentration when a circular fillet is replaced by an elliptical fillet. In Figs. 1 and 3 the upper curves represent the values of k for circular fillets for different values of D/d. It is seen that, as the ellipse increases in length, or more precisely as a/b increases, the values of k drop sharply. Inspection of the curves shows that it is not necessary to go to extremely long ellipses in order to produce substantial mitigation of stress concentration. Thus, in Fig. 1 for $D/d = 1.5$ and $b/h = 2$, the value of k drops by approximately 30 per cent when a/b is changed from 1 to 2. It will also be noticed that as a/b goes from 2 to 3 the drop in k is only about 14 per cent.

It is well known that the stress concentrations produced by circular fillets are substantially greater in tension than in bending. Figs. 5–8 show that elliptical fillets tend to equalize the stress concentration in tension and bending.

Acknowledgment

The assistance of Messrs. Cheng, Thomson, and Wang in pre-

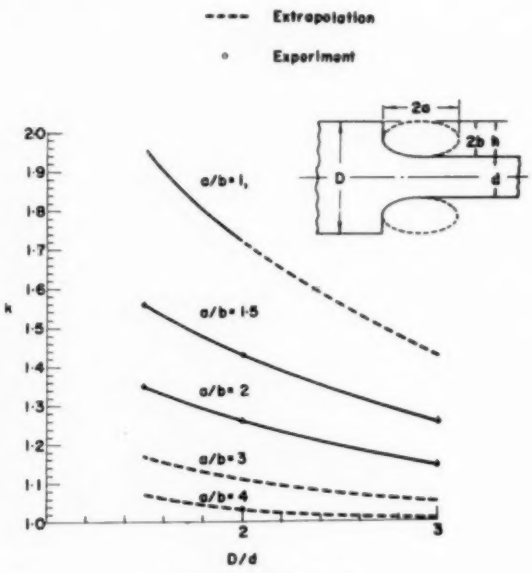

Fig. 1 Tension, $b = h/2$

[1] The results presented in this paper were obtained in the course of research sponsored by the United States Air Force, Wright Air Development Center, Wright-Patterson Air Force Base, Ohio, under contract No. AF33(616)-2831 with Illinois Institute of Technology.

[2] Research Professor of Mechanics and Director of Experimental Stress Analysis, Illinois Institute of Technology, Chicago, Ill.

[3] Associate Research Engineer, Department of Mechanics, Illinois Institute of Technology, Chicago, Ill.

[4] Numbers in brackets indicate References at end of paper.

Discussion of this paper should be addressed to the Secretary, ASME, 29 West 39th Street, New York, N. Y., and will be accepted until October 10, 1959, for publication at a later date. Discussion received after the closing date will be returned.

NOTE: Statements and opinions advanced in papers are to be understood as individual expressions of their authors and not those of the Society. Manuscript received by ASME Applied Mechanics Division, March 27, 1959.

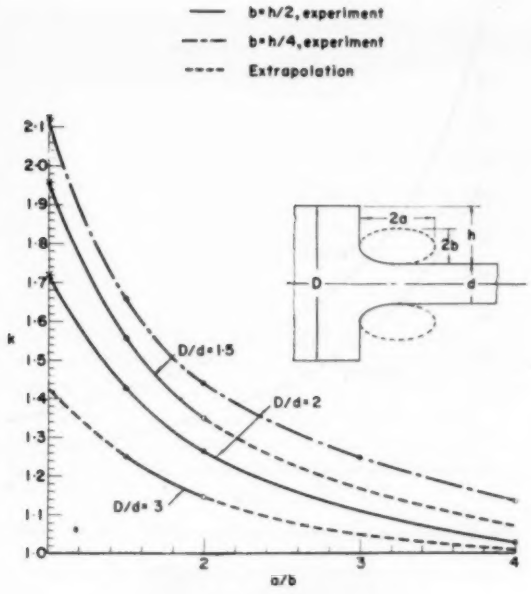

Fig. 2 Tension

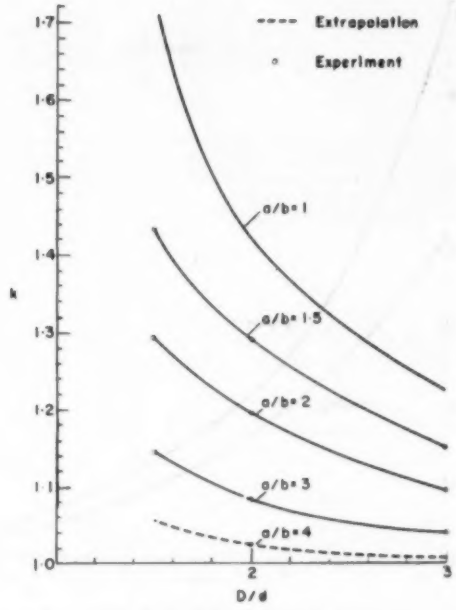

Fig. 3 Bending, $b = h/2$

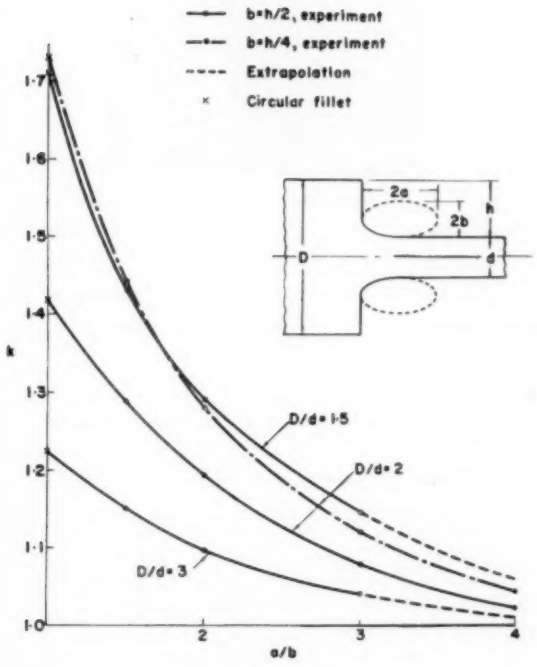

Fig. 4 Bending

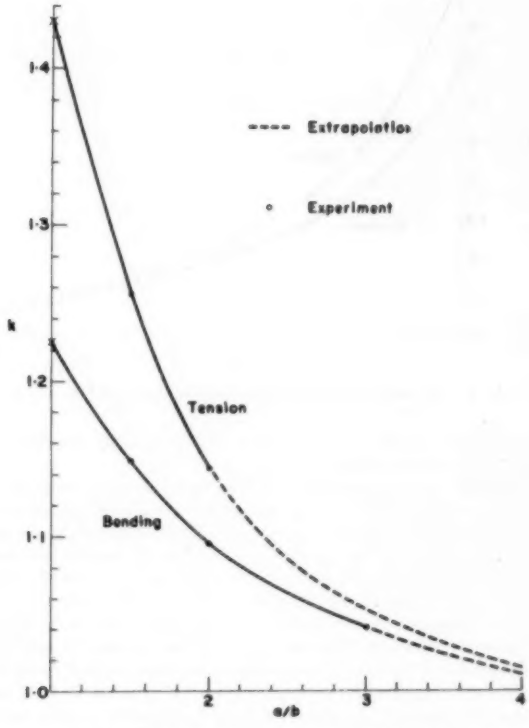

Fig. 5 Comparison of tension and bending, $D/d = 3$, $b = h/2$

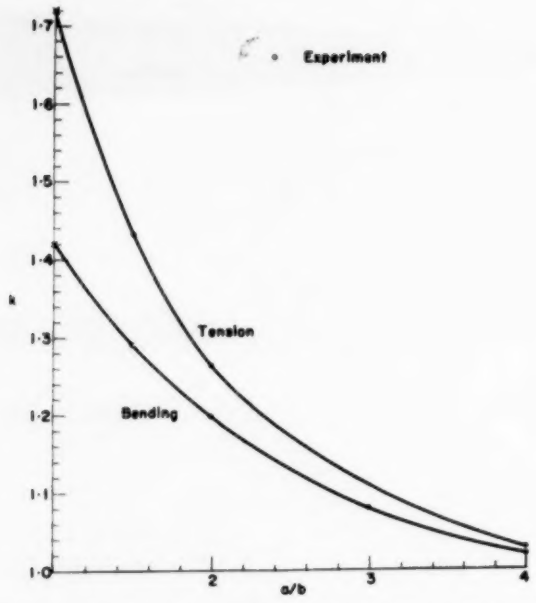

Fig. 6 Comparison of tension and bending, $D/d = 2$, $b = h/2$

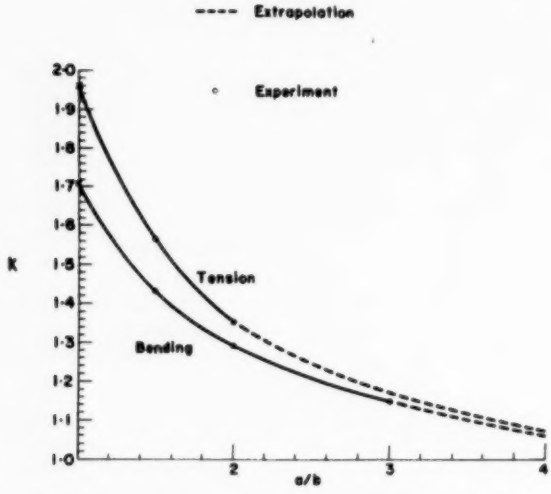

Fig. 7 Comparison of tension and bending, $D/d = 1.5$, $b = h/2$

paring the models and obtaining and processing the data is gratefully acknowledged.

NOTE. An approximation to the factor of stress concentration for elliptical fillets can be obtained from the available data for circular fillets in which $h/r = 1$, where r is the radius of the circular fillet and h is as in Fig. 1. If r is set equal to the maximum radius of curvature of the ellipse, then $r = a^2/b$, and $r/d = a^2/bd$. The factor of stress concentration for a circular fillet with $h/r = 1$ corresponding to $r/d = a^2/bd$ is approximately equal to the factor of stress concentration for the elliptical fillet having the specified values of a, b, and d. Comparison of the experimental values for elliptical fillets with those for circular fillets given in [5, 6] shows that this approximation is quite close for fillets in tension and is about 10 per cent low for fillets in bending.

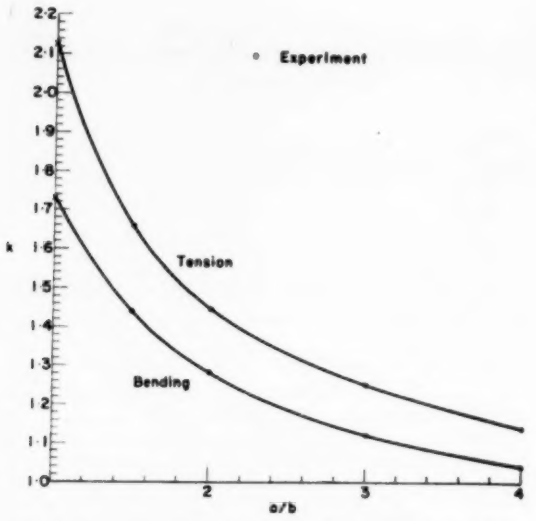

Fig. 8 Comparison of tension and bending, $D/d = 2$, $b = h/4$

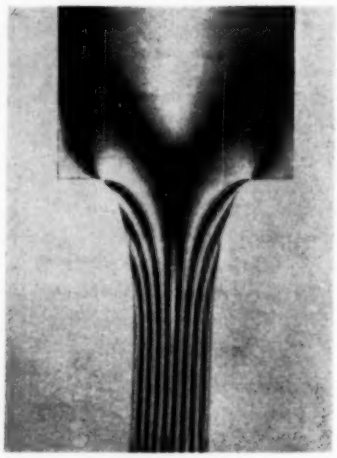

Fig. 9 Typical stress pattern for elliptical fillets in bending

$D = 3.0$ in.	$d = 1.0$ in.	$r = 0.2$ in.
$h = 1.0$ in.	$a = 2.0$ in.	$b = 0.5$ in.
$a/b = 4$	$D/d = 3$	$b = h/2$

Load = 156.41 lb Moment = 117.3 lb-in.
k = 1.01

References

1 R. E. Peterson, "Stress Concentration Design Factors," John Wiley & Sons, Inc., New York, N. Y., 1953.

2 D. C. Berkey, "Reducing Stress Concentrations With Elliptical Fillets," Proceedings, Society of Experimental Stress Analysis, vol. 1, 1944, no. 2.

3 R. Lansard, "Fillets Without Stress Concentration," Proceedings, Society of Experimental Stress Analysis, vol. 13, no. 1, 1955.

4 R. B. Heywood, "Designing by Photoelasticity," Chapman Hall, Ltd., London, England, 1952.

5 M. M. Frocht, "Photoelastic Studies in Stress Concentration," *Mechanical Engineering*, vol. 58, 1936, pp. 485–489. Also, "Factors of Stress Concentration Photoelastically Determined," JOURNAL OF APPLIED MECHANICS, TRANS. ASME, vol. 57, 1935, pp. A-67–A-68.

6 M. M. Frocht, "Strength of Materials," Ronald Press, New York, N. Y., 1951.

Journal of APPLIED MECHANICS

Brief Notes

On the recommendation of the Executive Committee of the ASME Applied Mechanics Division, it was decided to initiate a section devoted to brief notes on technical matters in mechanics. These notes must not be longer than 750 words (about $2^1/_2$ double-spaced typewritten pages, including figures) and will be subject to the usual review procedure prior to publication. After approval such notes will be published as soon as possible, normally in the next issue of the Journal. The notes should be submitted to the Technical Editors of the Journal of Applied Mechanics.

Creep of an Elastic Belt on a Pulley

G. V. TORDION[1]

A NEW, more general, relation between belt tensions of an elastic belt on a pulley as well as the expressions for the creep velocity distribution and creep losses are obtained, using the theory of the ideal compressible fluid flow.

Nomenclature

E = modulus of elasticity of the belt, psi
ρ, ρ_0 = mass density of the belt material, lb sec^2/in.^{4}
q = cross section of the belt, in.^{2}
b = belt width, in.
T, T_1, T_2 = belt tensions at φ, $\varphi = 0$, and $\varphi = \alpha$, respectively, lb
σ, σ_1, σ_2 = belt stresses due to T, T_1, and T_2, psi
σ_c = belt stress due to centrifugal inertia, psi
R = radius of the pulley, in.
V_0 = tangential velocity of the pulley, in/sec
V = belt velocity, in/sec
$\Delta V = V - V_0$ = creep velocity of the belt relative to pulley, in/sec
$c_0 = \sqrt{\dfrac{E}{\rho_0}}$ = longitudinal wave velocity, in/sec
p = pressure between belt and pulley, psi
μ = friction coefficient between belt and pulley
φ = polar co-ordinate angle of an element on the pulley measured with respect to fixed space, rad
α = active contact angle, rad

Let us consider that the belt is an elastic, homogeneous, isotropic one-dimensional body like a string. Moreover, the belt being endless, we can consider that the supply of belt matter through a space-fixed arc element $d\varphi$ is continuous. The total tangential acceleration of mass passing the element will be

$$\frac{dV}{dt} = \frac{\partial V}{\partial t} + V\frac{\partial V}{R\partial\varphi}$$

Since $\partial V/\partial t$ vanishes for the steady motion, V will be a function of φ alone, then

$$\frac{dV}{dt} = \frac{V}{R}\frac{dV}{d\varphi}$$

The forces acting on the mass element are shown in Fig. 1. We can write the equations of motion in tangential and radial directions

$$\rho R d\varphi q \frac{V}{R}\frac{dV}{d\varphi} = dT + \mu p b R d\varphi \tag{1}$$

$$\rho R d\varphi q \frac{V^2}{R} = dT\, d\varphi - pRb d\varphi \tag{2}$$

For a steady one-dimensional and compressible mass flow, the continuity equation will take the form

$$\frac{d(\rho V)}{R d\varphi} = 0$$

or

$$\rho\frac{dV}{d\varphi} + V\frac{d\rho}{d\varphi} = 0 \tag{3}$$

Since the belt material is considered to be elastic, its density will be a linear function of the tension (Hooke's law). We neglect the cross-section change, then

$$\rho = \rho_0\left(1 - \frac{\sigma}{E}\right) \tag{4}$$

Introducing the stress $\sigma = T/q$, rearranging the terms, and eliminating the pressure p between Equation (1) and (2), we get

$$\rho V\frac{dV}{d\varphi} = \frac{d\sigma}{d\varphi} + \mu\sigma - \mu\rho V^2 \tag{5}$$

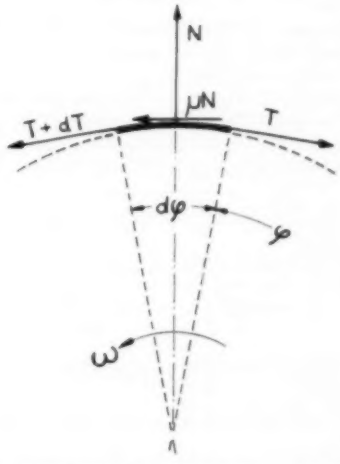

Fig. 1 Belt element on a driving pulley. $n = pRbd\varphi$

[1] Professor of Machine Design, Laval University, Quebec, P. Q., Canada.

Discussion of papers in Brief Notes should be addressed to the Secretary, ASME, 29 West 39th Street, New York, N. Y., and will be accepted until October 10, 1959, for publication at a later date. Discussion received after the closing date will be returned.

NOTE: Statements and opinions advanced in papers are to be understood as individual expressions of their authors and not those of the Society. Manuscript received by Applied Mechanics Division, July 15, 1958; final draft received February 27, 1959.

Since from Equation (4)

$$\frac{d\rho}{d\varphi} = -\frac{\rho_0}{E}\frac{d\sigma}{d\varphi} = -\frac{1}{c_0^2}\frac{d\sigma}{d\varphi} \tag{6}$$

we obtain from Equation (3)

$$\rho\frac{dV}{d\varphi} = \frac{V}{c_0^2}\frac{d\sigma}{d\varphi} \tag{7}$$

This relation introduced in Equation (5) leads to the nonlinear differential equation for V, σ, and ρ:

$$\left[1 - \left(\frac{V}{c_0}\right)^2\right]\frac{d\sigma}{d\varphi} + \mu\sigma = \mu\rho V^2 \tag{8}$$

We take the first approximation, linearizing the equation. The belt speed is $V = V_0 + \Delta V$, where the creep velocity ΔV is small in comparison with the pulley velocity V_0. In the same way the influence of the density change on the inertia forces in the radial direction is of second order, too; therefore $\rho = \rho_0$. With $\rho_0 V_0^2 = \sigma_e$ (stress due to centrifugal inertia) and $V_0/c_0 = \mathbf{M}$ (Mach number) we get

$$\frac{d\sigma}{d\varphi} + \frac{\mu}{1 - \mathbf{M}^2}\sigma = \frac{\mu}{1 - \mathbf{M}^2}\sigma_e \tag{9}$$

The solution for a driving pulley must satisfy the boundary condition: $\varphi = 0, \sigma = \sigma_1 + \sigma_e$; then

$$\sigma = \sigma_e + \sigma_1 \exp\left[-\frac{\mu}{1 - \mathbf{M}^2}\varphi\right] \tag{10}$$

This is the stress distribution along the active contact angle. Since for the end of the active contact angle $\varphi = \alpha$, the stress is $\sigma = \sigma_2 + \sigma_e$, we obtain the main relation between the belt stresses σ_1 and σ_2 ($\sigma_1 > \sigma_2$) on a driving pulley

$$\sigma_1 = \sigma_2 \exp\left[\frac{\mu}{1 - \mathbf{M}^2}\alpha\right] \tag{11}$$

Two particular cases have to be distinguished:

1 For the nonelastic belt the wave velocity c_0 is infinite and therefore the Mach number is zero.

2 For the elastic belt, but on a nonrotating pulley, the speed V_0 is zero and therefore the Mach number is also zero.

Only in these cases the classical relation (Euler, 1765)

$$\sigma_1 = \sigma_2 \exp\left[\mu\alpha\right] \tag{12}$$

is valid. The use of the fluid concept is necessary to show how the pulley speed affects the belt stresses. We can see that the "apparent" friction coefficient $\bar{\mu} = \mu/(1 - \mathbf{M}^2)$ increases with increasing pulley velocity. Since only the first-order theory is presented here, this relation is a good approach for $\mathbf{M} < 1$.

From Equation (7) we can develop the formula for the creep velocity distribution along the active angle of the pulley

$$\frac{\Delta V}{V_0} = -\frac{\sigma_1}{E}\left[1 - \exp\left(-\bar{\mu}\varphi\right)\right] \tag{13}$$

We have for $\varphi = \alpha$ the maximum creep

$$\left(\frac{\Delta V}{V_0}\right)_{\max} = -\frac{\sigma_1 - \sigma_2}{E} \tag{14}$$

This formula is well known and it is usually derived in a different manner.[2, 3]

[2] C. Bach, "Die Maschinen Elemente," ninth edition, Stuttgart, 1903, p. 269.

[3] M. ten Bosch, "Vorlesungen über Maschinenelemente," second edition, Springer, Berlin, 1940, p. 302.

The power loss due to creep of the belt on the driving pulley is given by the integral

$$\int_{\varphi=0}^{\alpha} \bar{\mu}pbRd\varphi\Delta V = -\bar{\mu}qV_0\frac{\sigma_1^2}{E}\int_0^{\alpha}\left[\exp(-\bar{\mu}\varphi) - \exp(-2\bar{\mu}\varphi)\right]d\varphi = -\frac{qV_0}{2E}(\sigma_1 - \sigma_2)^2$$

Since the transmitted power is $q(\sigma_1 - \sigma_2)V_0$, we finally obtain a simple expression for the belt efficiency, valid also for a driven pulley ($\sigma_1 > \sigma_2$)

$$\text{eff.} = 1 - \frac{\sigma_1 - \sigma_2}{2E} \tag{15}$$

A Modification of Rayleigh's Principle for Calculating Beam Frequencies

F. M. LEWIS[1]

The following modification of Rayleigh's principle was designed with a view to obtaining a method of beam-frequency calculation of good accuracy but minimum labor. Application is limited to hinged end, cantilever, and free-free beams. As applied to the calculation of the lowest mode frequency of beams, Rayleigh's principle is stated as follows. Assume a "reasonable" curve of ordinates y for the relative amplitude curve. If the beam vibrates in this curve the potential energy in extreme position is given by

$$\text{PE} = \frac{1}{2}\int\frac{M^2\,dx}{EI} = \frac{1}{2}\int EI\left(\frac{d^2y}{dx^2}\right)^2 dx \tag{1}$$

and the kinetic energy in mean position by

$$\text{KE} = \frac{\omega^2}{2g}\int wy^2\,dx \tag{2}$$

Then equating PE to KE

$$f = \frac{\omega}{2\pi} = \frac{1}{2\pi}\left(\frac{2g\ \text{PE}}{\int wy^2\,dx}\right)^{1/2} \tag{3}$$

In application to irregular beams where the moment of inertia changes from end to end, a purely arbitrary choice of y, even if it satisfies the end conditions, may lead to an unrealistic value of PE and, in consequence, low accuracy for ω.

Good accuracy can be obtained by assuming for y the gravity deflection of the beam. This gives the commonly used formula

$$f = \frac{1}{2\pi}\sqrt{\frac{g\int wy\,dx}{\int wy^2\,dx}} \tag{4}$$

For beams of irregular loading and stiffness distribution, the computation of the gravity deflection y, which involves several integrations or equivalent operations, makes formula (4) less simple in application than it appears.

We avoid these difficulties inherent in (3) and (4) by assuming slightly different reasonable curves in computing PE and KE. Consider the case of the hinged end beam. In (3) let the reasonable curve used in computing PE be that produced by a load

[1] Professor of Marine Engineering, Massachusetts Institute of Technology, Cambridge, Mass.

Manuscript received by ASME Applied Mechanics Division, November 21, 1958.

F acting at the center and of such magnitude that it produces unity deflection there. Let the curve used in computing KE be any other curve of unity deflection at the center and of a "reasonable" shape. The reactions are $F/2$, and the bending moments are $Fx/2$, $Fx_1/2$ for the left and right halves, respectively (see Fig. 1). Equating the internal energy as given by (1) to the external work done by F, there is obtained

$$\frac{1}{2}\left[\int_0^{L/2}\frac{F^2x^2dx}{4EI}+\int_0^{L/2}\frac{F^2x_1^2dx_1}{4EI}\right]=\frac{1}{2}F \tag{5}$$

and since PE $= {}^1/_2F$

$$\text{PE}=\frac{2E}{\int_0^{L/2}\frac{x^2dx}{I}+\int_0^{L/2}\frac{x_1^2dx_1}{I}} \tag{6}$$

The integrations for x and x_1 are for the right and left halves of the beam, respectively, with the origin taken at the ends in both cases. Then from (3)

$$f=\frac{1}{2\pi}\left(\frac{4Eg}{\left[\int_0^{L/2}\frac{x^2dx}{I}+\int_0^{L/2}\frac{x_1^2dx_1}{I}\right]\left[\int wy^2dx\right]}\right)^{1/2} \tag{7}$$

The wy^2 integral is over the length of the beam.

This formula can be modified in various ways.

Let us assume that the I distribution can be approximated by a stepwise distribution in the manner of Fig. 2; let the loads be concentrated; then

$$f=\frac{1}{2\pi}\left(\frac{12Eg}{\left[\sum_0^{L/2}\frac{x_b^3-x_a^3}{I}+\sum_0^{L/2}\frac{x_b'^3-x_a'^3}{I}\right]\Sigma Wy^2}\right) \tag{8}$$

an easy assumption for y is the curve $y = \sin(\pi x/L)$.

The accuracy of these formulas can be assessed by comparison with the known exact solution in simple cases.

For the simple beam with uniform total load W and uniform inertia distribution I

$$\left.\begin{aligned}&\Sigma x_b^3-x_a^3=\Sigma x_b'^3-x_a'^3=\frac{L^3}{8}\\&\Sigma W\left(\sin\frac{\pi x}{L}\right)^2=\frac{W_t}{2}\end{aligned}\right\} \tag{9}$$

W_t = total load

$$f=\frac{1}{2\pi}\sqrt{\frac{96EIg}{W_tL^3}}=\frac{9.796}{2\pi}\sqrt{\frac{EIg}{W_tL^3}} \tag{10}$$

while the exact constant is $\dfrac{\pi^2}{2\pi}=\dfrac{9.869}{2\pi}$.

In Fig. 3 is shown the load and inertia distribution of a turbine shaft and the complete calculation follows. A one-step Stodola calculation for this gives $f = 148$.

Free-Free Beam

For the free-free beam a load F is applied at the center, and loads $F/2$ at the ends, of such magnitude that the relative amplitude of the ends and the center is unity. Then PE is the same as for the hinged end case. For the ΣWy^2 term we assume a y which has unity relative deflection of the center to the ends but is so adjusted that

$$\Sigma Wy=0 \text{ and } \Sigma Wyx_g=0 \tag{11}$$

where x_g is the distance of any load from the center of gravity.

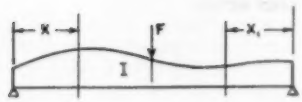

Fig. 1

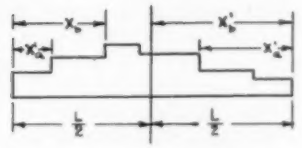

Fig. 2

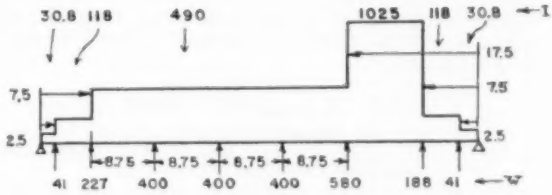

Fig. 3

These equations mean that no external forces or moments act on the system. y is determined as follows. An initial assumption y_a is made. It is convenient to use a sine curve $y_a = \sin(\pi x/L)$ for this with zero amplitude at the free ends. Subtract from this the zero-noded mode or lateral displacement given by

$$y_0=\frac{\Sigma Wy_a}{\Sigma W} \tag{12}$$

and the one-noded mode, or rotation around the center of gravity, given by

$$y_1=\frac{x_g\Sigma Wy_ax_g}{\Sigma Wx_g^2} \tag{13}$$

so that the y to be used in (8) is

$$y=y_a-y_0-y_1 \tag{14}$$

For a uniform free-free beam

$$\frac{x_b^3-x_a^3}{I}=\frac{x_b'^3-x_a'^3}{I}=\frac{L^3}{8I}$$

assume $y_a = \sin(\pi x/L)$, then $y_0 = 2/\pi$, $y_1 = 0$, $y = \sin(\pi x/L) - 2/\pi$ and with W_t = total load (8) yields

$$f=\frac{22.51}{2\pi}\left(\frac{EIg}{W_tL^3}\right)^{1/3}$$

The exact constant is 22.4.

This method is of utility in calculating the two-noded mode of a ship, taking account of the stiffness and load (including fluid inertia) variation along the ship.

Cantilever Beams

For the cantilever beam the PE is computed by assuming a load F at the free end of such magnitude that it produces a unit deflection there. With x measured from the free end, the frequency formula is then

$$f=\frac{1}{2\pi}\left[\frac{Eg}{\left(\int_0^L\frac{x^2dx}{I}\right)\left(\int Wy^2dx\right)}\right]^{1/3} \tag{15}$$

or

$$f = \frac{1}{2\pi}\left[\frac{3Eg}{[\Sigma(x_b^3 - x_a^3)/L]\ \Sigma W y^2}\right]^{1/2} \tag{16}$$

For a uniform cantilever the assumption $y = 1 - \cos(\pi x/2L)$ with the origin at the support, (16) leads to

$$f = \frac{3.635}{2\pi}\sqrt{\frac{Eg}{W_t L^3}}$$

The exact constant is 3.52.

Rayleigh's theorem in its pure form will always give a frequency which is too high. The modified form here may yield a frequency either high or low depending on the choice of y for the load summation. Obviously other modifications of the same nature are possible.

Table 1

Stiffness Summation

	x	x^3	$x_b^3 - x_a^3$	I	$(x_b^3 - x_a^3)/I$
Left	30	27,000			
	7.5	422	26,578	490	54.20
	2.5	15.6	406.4	118	3.44
	0	0	15.6	30.8	1.98
Right	30	27,000			
	17.5	5,360	21,640	490	44.20
	7.5	422	4,938	1025	4.82
	2.5	15.6	406.4	118	3.44
	0	0	15.6	30.8	1.98
					$\Sigma = 114.06$

Load Summation

	x	$180\frac{x}{L}$	$\sin^2\left(\frac{180°\,x}{L}\right)$	W	$W\sin^2\left(\frac{180°\,x}{L}\right)$
Left	2.50	7.5	.0019	41	.08
	7.50	22.5	.0169	227	3.84
	16.25	48.75	.5660	400	224.40
	25.00	75.0	.9310	400	372.40
Right	2.50	7.5	.0019	41	.08
	7.50	22.5	.0169	188	3.18
	17.50	52.5	.6300	580	365.00
	26.25	78.75	.9630	400	385.20
					$\Sigma = 1{,}354.18$

$$= \frac{1}{2\pi}\left(\frac{12 \times 30 \times 10^6 \times 386}{114.06 \times 1354.18}\right)^{1/2} = 151 \text{ V.P.S.}$$

Yield Point Load of an Annular Plate[1]

PHILIP G. HODGE, Jr.[2]

The yield point load is computed for an annular plate, simply supported at its inner and outer edges and subjected to a uniform load. A previously published solution is shown to be incorrect.

AN INCORRECT SOLUTION to the problem of an annular plate subjected to a uniform load was recently given[3] and it is perhaps of some interest to present the correct solution. The loaded plate is shown in Fig. 1; it will be discussed in terms of dimensionless variables defined by

$$m_r = M_r/M_0 \qquad m_\theta = M_\theta/M_0$$
$$r = R/A \qquad b = B/A \qquad p = PA^2/6M_0 \tag{1}$$

where M_0 is the yield bending moment; primes will be used to indicate differentiation with respect to r. The bending moments must satisfy the equilibrium equation

$$(rm_r)' - m_\theta = C - 3pr^2 \tag{2}$$

and the boundary conditions $m_r = 0$ at $r = b$ and $r = 1$. The flow law states that the strain rate vector

$$\mathbf{q} = -(W'', W'/r) \tag{3}$$

must be directed along the outward directed normal to the yield curve. The velocity W must be zero at $r = b$ and $r = 1$.

Fig. 2(*a*) shows the stress profile assumed in the incorrect solution.[3] A stress solution can be found according to this hypothesis which satisfies Equation (1), the boundary conditions on m_r, and the inequalities $0 \leq m_\theta \leq 1$. Therefore this solution is statically admissible and hence furnishes a lower bound on the yield point load. Fig. 2(*d*) shows the associated velocity profile. The vector $\mathbf{q}$ is normal to side BC since $W'' = 0$. However, for $b < r < \xi$, W is an increasing function of r, hence $W' > 0$. It follows from Equation (3) that $\mathbf{q}$ is directed inward to the side BC. Therefore the proposed solution is not kinematically admissible and hence is not the true solution.

A consideration of the entire problem shows that at $r = b$, m_r and W must equal zero and W' must be positive. Thus q_θ is negative and the stress point can only be at the corner F. Similar reasoning shows that the stress point at $r = 1$ must be at C. Finally, the plate may generally be expected to have compressive radial stresses in the top surface so that $m_r > 0$.

Figs. 2(*b*) and (*e*) show a hypothesis which satisfies these requirements. However, although this solution is kinematically admissible and leads to an upper bound on p, it is not statically admissible. This may be easily seen by observing that, if $m_r(\xi) = 1$ and $m_r \leq 1$, then $m_r'(\xi^-) \geq 0$ and $m_r'(\xi^+) \leq 0$. Therefore, if there is a discontinuity in m_r', it must satisfy

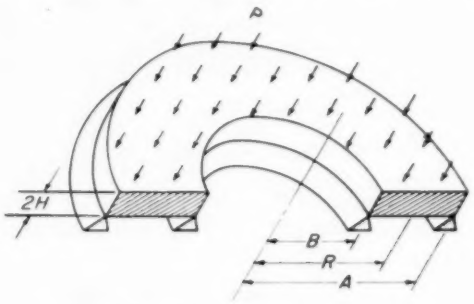

Fig. 1 Annular plate, showing load and dimensions

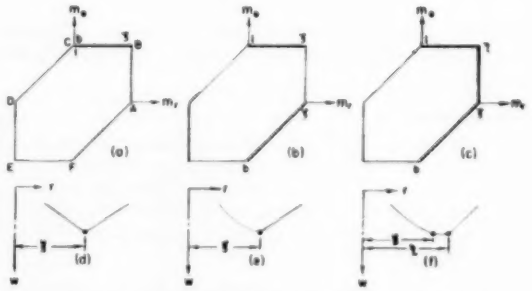

Fig. 2 Assumed stress and velocity profiles. (*a*) incorrect stress profile; (*b*) incorrect stress profile; (*c*) correct stress profile; (*d*) velocity profile for (*a*); (*e*) velocity profile for (*b*); (*f*) velocity profile for (*c*).

[1] This investigation was sponsored by the Office of Naval Research.

[2] Professor of Mechanics, Illinois Institute of Technology, Chicago, Ill. Mem. ASME.

[3] V. S. Chernina, "Approximate Carrying Capacity of an Annular Plate Under a Uniformly Distributed Pressure," *Izvestia Akademii Nauk SSSR*, No. 7, 1958, pp. 33–39.

Manuscript received by the ASME Applied Mechanics Division, February 11, 1959.

$$m_r'] \leq 0 \tag{4}$$

However, it follows from Equation (2) that the discontinuities existing at $r = \xi$ must be related by

$$\xi m_r'] + m_r] - m_\theta] = C] - 3p\xi^2] \tag{5}$$

The pressure is given continuous, and equilibrium demands that m_r and C which is related to the shear force be continuous. Therefore Equation (5) leads to

$$m_r'] = m_\theta]/\xi = 1/\xi > 0$$

in contradiction to Inequality (4). Thus the proposed solution is not statically admissible.

The preceding incorrect hypothesis suggests the hypothesis shown in Figs. 2(*e*) and (*f*). The corresponding equations are easily solved, the results being

$$m_r = \left[1 + \frac{3}{2}p(\xi^2 - b^2)\right]\frac{\log(r/b)}{\log(\xi/b)} - \frac{3}{2}p(r^2 - b^2)$$

$$m_\theta = m_r - 1 \quad W = W_0 \frac{\log(r/b)}{\log(\xi/b)} \quad b \leq r < \xi$$

$$m_r = 1 \quad m_\theta = 3p(r^2 - \xi^2) \quad W = W_0 \quad \xi < r < \eta$$

$$m_r = \left[(1 + \eta + \eta^2)p - \frac{\eta}{1 - \eta}\right]\left[1 - \frac{1}{r}\right] + p\left[\frac{1}{r} - r^2\right]$$

$$m_\theta = 1 \quad W = W_0(1 - r)/(1 - \eta) \quad \eta < r \leq 1 \tag{6}$$

It is readily verified that this solution satisfies the equilibrium equation and flow law throughout; that W is continuous and vanishes at $r = b$ and $r = 1$; that m_r is continuous, vanishes at $r = b$ and $r = 1$, and is equal to 1 at $r = \xi$ and $r = \eta$.

For the same reasons advanced in discussing Inequality (4), m_r' and hence m_θ must be continuous at $r = \xi$ and $r = \eta$. The requirement that $m_\theta(\eta^-) = 1$, together with the requirement that the constant C be the same in each of the three regions, leads to the following three relations:

$$p = (2/3)[\xi^2 \log(\xi^2/b^2) - (\xi^2 - b^2)]^{-1} \tag{7a}$$

$$p = [(1 - \eta)^2(1 + 2\eta)]^{-1} \tag{7b}$$

$$p = (1/3)(\eta^2 - \xi^2)^{-1} \tag{7c}$$

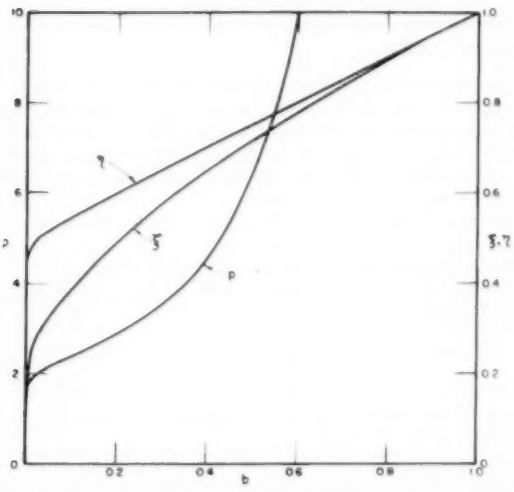

Fig. 3 Plastic regimes and yield point load as functions of inner radius

For a given value of b, Equations (7) define the parameters ξ, η, and the yield point load p. In practice it is more convenient to determine b, ξ, and p in terms of the parameter η. Thus, for a given η, Equation (7*b*) determines p and Equation (7*c*) then defines ξ. A simple numerical or graphical calculation then furnishes the value of b from Equation (7*a*). The regime boundaries ξ and η and the yield point load p are shown as functions of b in Fig. 3.

Similar solutions may be obtained if either or both edges of the plate are clamped. If the inner edge is clamped, the stress profile runs along EFABC. If the outer edge is clamped, the stress profile runs along FABCD. Finally, if both edges are clamped the stress profile runs along EFABCD. The resulting computations become rather involved and are not here reproduced.

Matric Analysis of Statically Indeterminate Structures by the Displacement Method[1]

P. H. DENKE[2] and C. K. WANG[3]

In the displacement method of analysis for statically indeterminate structures, the displacements of the joints of the structure appear as unknowns. Matric formulations of this method have been given by Argyris[4] and others. In these formulations the most important matrix is the spring matrix K. This matrix is usually represented as being easily derivable by inspection from a diagram of the structure. Actually, K can be derived efficiently in this way for simple structures. But in aircraft structures, which are complicated space frameworks composed of shear panels, and bars subjected to combined axial stress, bending, shear and torsion, the derivation by inspection is not an efficient process, especially if the digital computer is to be utilized, because a fundamental principle of good computer programming is that the computer shall do as much of the work as possible.

In this note it is demonstrated, on the basis of virtual work, that the spring matrix can be derived by considering separately the statics of each joint and member of the structure. Elastic properties enter only in the stiffness factors of the individual members. Thus the awkward and difficult process of visualizing member deformations resulting from joint displacements in space frameworks is eliminated by a simple procedure based on statics.

An important feature of the following derivation is the distinction between internal forces and internal reactions. As a result of this distinction, the spring matrix K is shown to be of the form aSa^T, which is a symmetric form when S is symmetric; and therefore the deflection influence matrix $\delta = K^{-1}$ is symmetric. Thus Maxwell's law is demonstrated.

Nomenclature

A jointed structure may be defined as one in which the constituent members are connected at a finite number of joints. The number of degrees of freedom of a joint is the number of displacement components required to completely define the movement of the joint. For instance, a frictionless joint in a space structure has three degrees of freedom; a rigid joint has six.

[1] The work reported in this note was done in the Strength Section of the Douglas Aircraft Company, Inc., Santa Monica, Calif.

[2] Strength Analysis Methods Engineer, Douglas Aircraft Company, Inc., Santa Monica, Calif.

[3] Professor of Architectural Engineering, University of Illinois, Urbana, Ill.

[4] J. H. Argyris, "Energy Theorems and Structural Analysis," *Aircraft Engineering*, 1955, pp. 89–94.

Manuscript received by ASME Applied Mechanics Division, November 15, 1957; final draft received January 5, 1959.

Divide the forces (including moments) exerted on the ends of each member by the joints into a group of internal forces and another of internal reactions. For instance, if the member is under combined axial stress and bending about one principal axis, the three internal forces may be the axial force at one end and the two end moments; the three internal reactions may be the axial force at the other end and the two end shears.

Define a column matrix of unknown joint displacements X. Define also a partitioned column matrix d as a matrix consisting of two submatrices u and ρ, which contain the components of the joint displacements in the directions of the internal forces and reactions, respectively. Define the column matrix of member deformations e, wherein e_j is the displacement of the jth internal force, when displacements of the internal reactions are reduced to zero by rigid body motions of the members. Also define $\bar{u}$ as a column matrix of the displacements of the internal forces resulting from the rigid-body motions of the members to produce displacements $\bar{\rho} + \rho = 0$.

Define P as a column matrix of known external forces. Define q as a partitioned column matrix of f and r, wherein f and r are the internal forces and reactions, respectively. Define the matrix J wherein J_{ij} is the value of the ith external force resulting from a unit value of jth internal force or reaction. Define M as a partitioned matrix of I and m, wherein I is a unit matrix and m is called the subordinate member matrix, m_{ij} being the ith internal reaction resulting from a unit jth internal force.

Define a matrix of member stiffnesses S, wherein S_{ij} is the ith internal force resulting from a unit value of the jth member deformation.

The Spring Matrix

Consider the joints of the structure by themselves, without their connecting members. Assume that the internal forces or reactions are all zero except q_j, which has a unit value. Then the external forces acting upon the joints are given by J_{ij}. Permit the joint displacements X_i to occur. The resulting displacement of the jth internal force or reaction is d_j. Since the joints are rigid bodies and the external forces J_{ij} are in equilibrium with the internal force or reaction $q_j = 1$, the work done must be zero.

$$\therefore \sum_i J_{ij} X_i - 1 \cdot d_j = 0 \qquad j = 1, 2 \ldots .$$

The minus sign appears in the equation because the forces q_j are defined as positive on the members, negative on the joints. In matrix notation,

$$J^T X - d = 0 \tag{1}$$

Now consider the members by themselves, without the joints. Assume that the internal forces are all zero except f_j, which has a unit value. Then the internal reactions acting upon the members are given by m_{ij}. Permit the rigid body displacements of the members $\bar{\rho}_i$ to occur. These $\bar{\rho}_i$ are displacements of the internal reactions. The resulting displacement of the jth internal force is $\bar{u}_j$. The work done is zero.

$$\therefore \sum_i m_{ij} \bar{\rho}_i + 1 \cdot \bar{u}_j = 0$$

In matrix notation,

$$m^T \bar{\rho} + \bar{u} = 0 \tag{2}$$

Now u_j is the displacement of jth internal force, and $\bar{u}_j$ is the displacement of the jth internal force resulting from the displacements $\bar{\rho}_i$ necessary to produce zero displacements of the internal reactions. Therefore the jth *member deformation* is given by

$$e_j = u_j + \bar{u}_j$$

and

$$e = u + \bar{u} \tag{3}$$

Substituting (2) and $\rho + \bar{\rho} = 0$ into (3),

$$e = u + m^T \rho = [I \; m^T] \begin{bmatrix} u \\ \rho \end{bmatrix}$$

But $$M = \begin{bmatrix} I \\ m \end{bmatrix} \text{ and } d = \begin{bmatrix} u \\ \rho \end{bmatrix}$$

$$\therefore e = M^T d$$

$$\therefore e = (J \; M)^T X \tag{4}$$

from (1). Now from the definition of the stiffness matrix S,

$$f_i = \sum_j S_{ij} e_j \qquad i = 1, 2 \ldots .$$

$$\therefore f = S e \tag{5}$$

Also by definition,

$$P = J q \tag{6}$$

and

$$r = m f$$

but

$$q = \begin{Bmatrix} f \\ r \end{Bmatrix} = \begin{Bmatrix} f \\ mf \end{Bmatrix} = \begin{bmatrix} I \\ m \end{bmatrix} f$$

$$\therefore q = M f \tag{7}$$

Eliminating d, e, f, and q from (4), (5), (6), and (7) gives

$$P = (J \; M) \, S \, (J \; M)^T X$$

Define the spring matrix K implicitly by

$$P = K X$$

$$\therefore K = (J \; M) \, S \, (J \; M)^T \tag{8}$$

Internal Damping of Thermal Origin in Thin Wires

P. SRINIVASAN[1]

THE OBJECT of this note is to study the effects of wire diameter, length, and material of the wire on its damping ability. This knowledge is essential in order to understand the performance of wire damping devices for alleviating high vibratory stresses set up in turbine blades by such effects as resonance, rotating stall, and stall flutter. For instance, Di Taranto[2] has recently presented a report on such a device and indicated the need for a study such as undertaken in this note.

The mathematically simplest way to consider damping in the material of the wire is to assume that the damping force is a linear function of the strain rate, that is

$$\text{Damping force} = \xi \frac{\delta e}{\delta t} \tag{1}$$

[1] Assistant Professor of Mechanical Engineering, Indian Institute of Science, Bangalore, India.

[2] R. A. Di Taranto, "A Blade-Vibration-Damping Device—Its Testing and a Preliminary Theory of Its Operation," JOURNAL OF APPLIED MECHANICS, vol. 25, TRANS. ASME, vol. 80, 1958, pp. 21–27.

where ϵ is the tensile strain, and ξ is a constant which is a measure of damping ability.

On the basis of this simple law, Suyehiro[3] obtained an expression for the resisted vibrations of a wire which is a simple extension of Sezawa's equation. In discussing the solution of the equation, Suyehiro has shown that there exists an upper limit to the frequency of transverse vibrations of the wire. This upper limit is a function of the modulus of elasticity of the material E and damping coefficient ξ. In fact,

$$W_S = \frac{2E}{\xi} \tag{2}$$

where W_S is the upper bound for the frequency of transverse vibrations of the wire in radians/sec.

Once the logarithmic decrement δ and fundamental frequency of vibrations W_1 radians/sec are known, it is possible to estimate W_S. Suyehiro[3] has shown

$$W_S = 2\pi \frac{W_1}{\delta} \tag{3}$$

From dynamical considerations it is concluded that, for wires whose transverse dimensions are small compared to its length, the frequency cannot exceed W_S given by equation (3).

It has been shown that δ for practically all solid materials shows no such dependence upon frequency as given by equation (3). But equation (3) is the result of assuming a linear damping law, viz., equation (1). The results of this note are therefore limited to materials which do follow the damping assumed.

Zener[4] from thermodynamic considerations has predicted that damping arising from the thermoelastic source (that is, flow of heat back and forth) is a maximum at a frequency W_Z given by

$$W_Z = \frac{2\pi \times 0.539D}{a^2} \tag{4}$$

where

W_Z = frequency in rad/sec at which damping is a maximum
D = thermal diffusion coefficient
$= \dfrac{\text{thermal conductivity}}{\text{specific heat} \times \text{density}}$
a = radius of the wire

From dynamical considerations the frequency cannot exceed W_S. In view of this, it can be stated

$$W_S \geq W_Z \tag{5}$$

If it is assumed that internal damping in the wire is of purely thermal origin, then W_Z is the frequency at which this damping is a maximum according to Zener. Maximum damping implies minimum value of W_S according to equation (3). In view of this, the equality holds in equation (5); that is,

$$W_S = W_Z \tag{6}$$

Equation (6) states that if internal damping is of purely thermal origin for wires whose transverse dimensions are small compared to their length, the frequency at which maximum damping occurs according to Zener is equal to the maximum frequency in transverse vibrations of the wire according Suyehiro. Substituting for W_S and W_Z from equations (3) and (4), respectively, we have

$$\frac{W_1}{\delta} = \frac{0.539D}{a^2} \tag{7}$$

For a cantilever we have the well-known formula

$$W_1 = 3.52 \sqrt{\frac{EI}{\mu_1 l^4}} \tag{8}$$

where EI = bending stiffness of the section
l = length of the wire
μ_1 = mass per unit length $= W/gl$
W = total weight of the wire
g = acceleration due to gravity

For a wire of circular cross section of radius a and density μ from equation (7) and (8)

$$\delta = \frac{2\pi \times 0.735}{D} \frac{a^3}{l^3} \sqrt{\frac{Eg}{\mu}} \tag{9}$$

Equation (9) gives a relation between the maximum damping (thermal) and parameters of the wire, namely, radius, length, and the material of the wire.

Example: Copper wire. For copper δ (thermal) maximum according to Zener[4] is $\pi \times 0.0015$. Taking

$E = 16 \times 10^6$ psi
$\mu = 0.322$ lb/cu in.
$D = \dfrac{1.124}{(2.54)^2}$ in.^{2}/sec

Substituting the afore-mentioned values in equation (9) we have

$$a^3/l^3 = 0.129 \times 10^{-3} \tag{9a}$$

Equation (9a) gives a relation between the radius of the wire and its length for the material constants assumed above.

Taking the value of $l = 3.1$ in. from Di Taranto,[2] Fig. 4, p. 24, and substituting in equation (9a) the radius of the wire $a \cong 0.0023$ inches.

The wire used by Di Taranto was 0.0025-in. radius.

Acknowledgment

The author's thanks are due to Prof. A. Ramachandran for useful discussion. Thanks are also due to the reviewers for their suggestions.

[3] K. Suyehiro, "On the Upper Limit of Frequency of the Transversal Vibration of Prismatic Bars," Proceedings of the Imperial Academy, Tokyo, vol. 4, 1928, p. 263.

[4] C. Zener, "Internal Friction in Solids—General Theory of Thermoelastic Internal Friction," *Physical Review*, vol. 53, 1938, p. 90.

Manuscript received by ASME Applied Mechanics Division, August 15, 1958; revised draft received February 27, 1959.

On the Lateral Buckling of a Tapered Narrow Rectangular Beam

L. H. N. LEE[1]

The bending strength of a beam with large flexural rigidity in the plane of bending in comparison with its lateral rigidity is frequently governed by the condition of its lateral stability. The lateral buckling of beams with constant cross sections has been investigated since six decades ago. In this note the elastic lateral buckling of a tapered rectangular beam subjected to pure bending in its plane is considered. The tapered beam is under simple lateral restraints at the two ends, as shown in Fig. 1. When two couples, M, of a certain critical value are applied at its ends, the beam may twist and buckle sideways. This critical

[1] Associate Professor of Engineering Science, University of Notre Dame, Notre Dame, Ind.

Manuscript received by ASME Applied Mechanics Division, March 2, 1959.

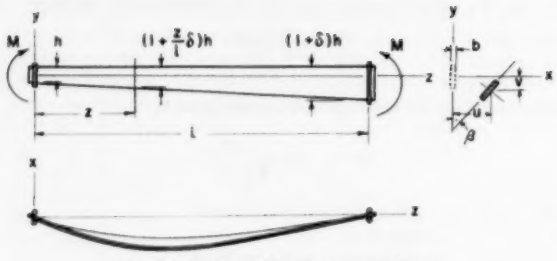

Fig. 1 Lateral buckling of a tapered beam

moment may be determined by the familiar equilibrium method used in stability analysis. According to the concept of the equilibrium method, the critical moment M_{cr} is the smallest value of M which is necessary to keep the beam in equilibrium in a slightly buckled form.

Referring to the co-ordinate system shown in Fig. 1, the deformation of the beam is defined by u and v, the displacements of the centroid of a cross section in the x and y-directions, and by β, the angular rotation of the cross section. Based on the moment-curvature and torque-rotation relationships for a tapered rectangular strip,[2] it can be shown that, for a very small angle β, the following system of differential equations determines the deformation of the beam along the z-direction:

$$\left.\begin{aligned} B\frac{d^2u}{dz^2} &= \beta M \\ B'\frac{d^2v}{dz^2} &= M \\ C\frac{d\beta}{dz} &= -\frac{du}{dz}M \end{aligned}\right\} \tag{1}$$

Equations (1) are similar to the analogous system of equations for a beam of constant cross section[3] except that the principal flexural rigidities B and B' as well as the torsional rigidity C will now vary with z according to the expressions

$$\left.\begin{aligned} B &= B_0\left(1+\frac{z}{l}\delta\right) \\ B' &= B_0'\left(1+\frac{z}{l}\delta\right)^3 \\ C &= C_0\left(1+\frac{z}{l}\delta\right) \end{aligned}\right\} \tag{2}$$

Here B_0, B_0', and C_0 are the flexural and torsional rigidities of the beam at the origin, or

$$B_0 = \frac{hb^3}{12}E;\quad B_0' = \frac{h^3b}{12}E;\quad C_0 = \frac{hb^3}{3}G \tag{3}$$

b and h being the width and depth of the section at the origin, respectively. E is Young's modulus, G is the shear modulus, and $(1+\delta)$ is the ratio of the depths at the two ends of the beam.

Eliminating u from the first and the third of Equations (1), we obtain

$$\frac{d^2\beta}{dz^2} + \frac{\delta}{l\left(1+\frac{\delta}{l}z\right)}\frac{d\beta}{dz} + \frac{M^2}{B_0C_0}\frac{\beta}{\left(1+\frac{\delta}{l}z\right)^2} = 0 \tag{4}$$

Setting $\left(1+\frac{\delta}{l}z\right) = \eta$ and $k^2 = \frac{M^2l^2}{B_0C_0\delta^2}$,

Equation (4) may be reduced to the form

$$\eta^2\frac{d^2\beta}{d\eta^2} + \eta\frac{d\beta}{d\eta} + k^2\beta = 0 \tag{5}$$

This is a homogeneous linear equation, and the method of solving such an equation is well known. In this case, the general solution of Equation (5) is

$$\beta = A_1\sin(k\log_e\eta) + A_2\cos(k\log_e\eta) \tag{6}$$

At the ends of the beam, $z = 0$ and $z = l$, the angle β must be equal to zero. The first condition will be satisfied by making $A_2 = 0$, and the second by letting

$$\sin[k\log_e(1+\delta)] = 0 \tag{7}$$

The smallest root of Equation (7), other than the trivial zero, yields the critical moment

$$M_{cr} = \frac{\delta}{\log_e(1+\delta)}\frac{\pi\sqrt{B_0C_0}}{l} \tag{8}$$

The corresponding buckled shape is given by

$$\beta = A_1\sin\left[\frac{\log_e\left(1+\delta\frac{z}{l}\right)}{\log_e(1+\delta)}\pi\right] \tag{9}$$

where A_1 indicates an arbitrary amplitude of a small magnitude. Fig. 1 shows the mode of buckling of a beam when $\delta = 1$. It can be shown that, when $\delta \to 0$, the buckling mode approaches a sinusoidal form and the critical moment approaches that of a beam of uniform cross section.

[2] L. H. N. Lee, "Non-Uniform Torsion of Tapered I-Beams," *Journal of the Franklin Institute*, vol. 262, 1956, p. 237.

[3] S. Timoshenko, "Theory of Elastic Stability," McGraw-Hill Book Co., Inc., New York, N. Y., 1936, p. 236.

The Stresses in Infinite Wedges Linearly Tapered in Width and Thickness

H. D. CONWAY[1]

The solutions are given for some plane stress problems of an infinite wedge linearly tapered in width and thickness, the corresponding solutions for the constant thickness cases being well known. The loadings chosen for illustrative purposes are: (a) concentrated load at end, (b) concentrated couple at end, and (c) uniform normal pressure on one face.

Introduction

In a previous article,[2] a general solution was given for the plane stress problem in polar co-ordinates with varying thickness $h = f(r)$, it being found that the resulting stress function equation was

$$\left(r^2\frac{\partial^2}{\partial r^2} + [2+\nu]r\frac{\partial}{\partial r} - \nu\frac{\partial^2}{\partial\theta^2}\right)\left(\frac{1}{h}\frac{\partial^2\phi}{\partial r^2}\right) - \left(\nu r^2\frac{\partial^2}{\partial r^2} + [2\nu+1]r\frac{\partial}{\partial r} - \frac{\partial^2}{\partial\theta^2}\right)\left(\frac{1}{hr}\frac{\partial\phi}{\partial r} + \frac{1}{hr^2}\frac{\partial^2\phi}{\partial\theta^2}\right) + 2(1+\nu)\frac{\partial}{\partial r}\left(r\frac{\partial}{\partial\theta}\left[\frac{1}{h}\frac{\partial}{\partial r}\left(\frac{1}{r}\frac{\partial\phi}{\partial\theta}\right)\right]\right) = 0 \tag{1}$$

[1] Julius F. Stone Visiting Professor, Department of Engineering Mechanics, The Ohio State University, Columbus, Ohio.

[2] H. D. Conway, "Analysis of Plane Stress in Polar Co-ordinates and With Varying Thickness," ASME Paper No. 59—APM-1.

Manuscript received by ASME Applied Mechanics Division, February 13, 1959.

the stresses being given by

$$h\sigma_r = \frac{1}{r}\frac{\partial\phi}{\partial r} + \frac{1}{r^2}\frac{\partial^2\phi}{\partial\theta^2}$$

$$h\sigma_\theta = \frac{\partial^2\phi}{\partial r^2}$$

$$h\tau_{r\theta} = -\frac{\partial}{\partial r}\left(\frac{1}{r}\frac{\partial\phi}{\partial\theta}\right) \qquad (2)$$

Equation (1) is easily tractable if $h = h_0 r^m$, where h_0 and m are constants.

The solutions will now be given for three infinite wedge problems of academic and practical interest assuming linear radial taper, that is, for m unity.

Analysis

(a) Force acting on end of wedge, Fig. 1. For this problem, a stress function is considered of the form $\phi = rF(\theta)$ whence by writing $h = h_0 r$ and substituting in Equation (1), $F(\theta)$ is obtained giving

$$\phi = Ar\begin{Bmatrix}\sin\theta\\ \cos\theta\end{Bmatrix};\ Ar\begin{Bmatrix}\sin k\theta\\ \cos k\theta\end{Bmatrix};\ k^2 = 2(1-\nu) \qquad (3)$$

The first two functions produce no stresses and, choosing $\phi = Ar\cos k\theta$ for symmetry, we obtain from Equations (2)

$$\sigma_r = \frac{A(1-k^2)}{h_0 r^2}\cos k\theta, \quad \sigma_\theta = \tau_{r\theta} = 0$$

For vertical equilibrium

$$-P = \int_{-\alpha}^{\alpha} hr\sigma_r\cos\theta\, d\theta$$

the constant A is found in terms of P, and finally

$$\sigma_r = \frac{-(k^2-1)P\cos k\theta}{h_0 r^2[(k-1)\sin(k+1)\alpha + (k+1)\sin(k-1)\alpha]}$$

$$\sigma_\theta = \tau_{r\theta} = 0;\ k^2 = 2(1-\nu) \qquad (4)$$

This solution is indeterminate for $k = 1$, $\nu = 1/2$, and, by the use of l'Hospital's rule, it is found for this value of Poisson's ratio

$$\sigma_r = \frac{-2P\cos\theta}{hr(2\alpha + \sin 2\alpha)}, \qquad \sigma_\theta = \tau_{r\theta} = 0 \qquad (5)$$

This is also the well-known solution for the constant thickness case. The solution for a horizontal load is naturally obtainable from $\phi = Ar\sin k\theta$, $k^2 = 2(1-\nu)$, but will not be given here.

(b) Couple acting on end of wedge, Fig. 2. Consider first a stress function of the form $\phi = A\sin n\theta$, whence by writing $h = h_0 r$ and substituting in Equation (1), it is found that $n^2 = (7 - 2\nu)$. The appropriate stress function for Fig. 2 is then

$$\phi = An(\theta-\alpha) + B\sin n(\theta-\alpha);\ n^2 = (7-2\nu) \qquad (6)$$

From equations (2)

$$h\sigma_r = \frac{-Bn^2}{r^2}\sin n(\theta-\alpha), \qquad h\sigma_\theta = 0,$$

$$h\tau_{r\theta} = \frac{An}{r^2} + \frac{Bn}{r^2}\cos n(\theta-\alpha)$$

Since $\tau_{r\theta}$ is zero at $\theta = 0, 2\alpha$, $A = -B\cos n\alpha$ and

$$h\tau_{r\theta} = \frac{-Bn}{r^2}\left(\cos n\alpha - \cos n\,[\theta-\alpha]\right)$$

For equilibrium

$$M = -\int_0^{2\alpha} h\tau_{r\theta}r^2 d\theta$$

which gives B in terms of the couple M and hence

$$\sigma_r = \frac{-Mn^2\sin n(\theta-2\alpha)}{h_0 r^3(2n\alpha\cos n\alpha - 2\sin n\alpha)}, \qquad \sigma_\theta = 0$$

$$\tau_{r\theta} = \frac{-Mn\,(\cos n\alpha - \cos n[\theta-\alpha])}{h_0 r^3(2n\alpha\cos n\alpha - 2\sin n\alpha)} \qquad (7)$$

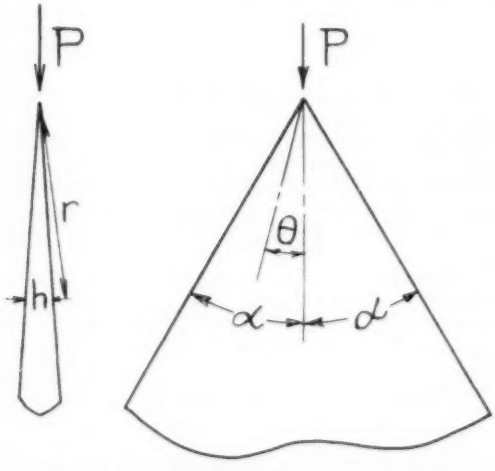

Fig. 1 Infinite wedge with concentrated load at end

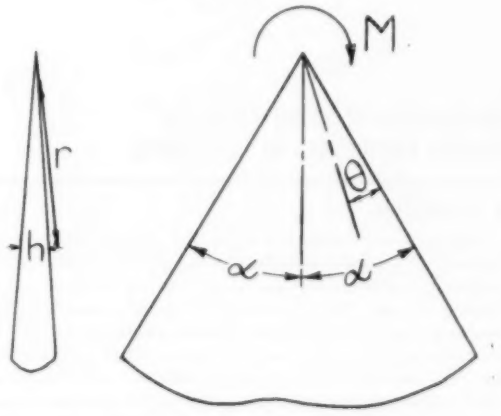

Fig. 2 Infinite wedge with couple at end

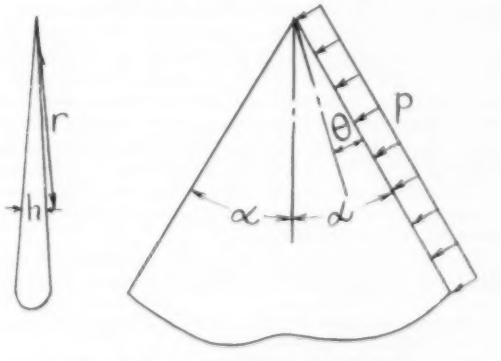

Fig. 3 Infinite wedge with uniformly loaded face

With $n = 2$, this solution would be identical with that for a wedge of constant thickness. However, this would necessitate a fictitious ν of 3/2.

(c) Uniform Pressure on Edge, Fig. 3. The stress function required here is

$$\phi = r^2(A + B \sin n\theta + C \cos n\theta + D\theta); \quad n^2 = (7 - 2\nu) \quad (8)$$

whence

$$h\sigma_r = 3Ar + (3 - n^2)Br \sin n\theta + (3 - n^2)Cr \cos n\theta + 3Dr\theta$$

$$h\sigma_\theta = 6Ar + 6Brn \sin n\theta + 6Crn \cos n\theta + 6Dr\theta$$

$$h\tau_{r\theta} = -2Br \cos n\theta + 2Cr \sin n\theta - 2Dr; \quad h = h_0 r \quad (9)$$

From the boundary conditions and Fig. 3

$$\theta = 0, \qquad h\sigma_\theta = -h_0 pr, \qquad \tau_{r\theta} = 0$$

$$\theta = 2\alpha, \qquad h\sigma_\theta = 0, \qquad \tau_{r\theta} = 0$$

we obtain

$$A = -ph_0(1 - \cos 2n\alpha - 2n\alpha \sin 2n\alpha)/N$$

$$Bn = -D = ph_0 n \sin 2n\alpha/N$$

$$C = -ph_0(1 - \cos 2n\alpha)/N \quad (10)$$

where $N = 6(2 - 2 \cos 2n\alpha - 2n\alpha \sin 2n\alpha)$. The stresses, obtained by substituting Equations (10) in (9), are seen to be independent of r.

Minimization of Spring Torque in Flexible Connections to Instruments

T. VREELAND, Jr.[1]

PRECISION electromechanical measuring instruments of various kinds often require establishing electrical connection to the suspended part of the instrument, with minimum introduction of disturbing torques. Requirements are especially demanding in the case of gyroscopes. Gyroscopes of high-precision type, as used in inertial-guidance systems and in advanced flight-control systems, generally take the form of a gimbal member which contains the rotor and which is supported relative to the case by some form of minimum-friction bearings. Usually, at least three electrical connections are required (for the polyphase rotor drive motor), which take the form of wires or ribbons extending from the case to the gimbal member. Disturbing-torque levels about the gimbal axis or axes must be kept to extremely low values; the total tolerable disturbing torque from all sources whatever is often of the order of one dyne-cm or less. Special attention must be given to the electrical lead-in connections (a) to minimize mechanical hysteresis effects, which result in erratic bias changes, and (b) to minimize spring rate. While spring coercion is a conservative type of force, it nevertheless must be kept very small, otherwise a shift of null of the pickoff which detects gimbal displacement will result in a steady spring bias.

The present note is restricted to the optimization of the electrical lead-in configuration from the point of view of minimizing spring rate. In general, the axis of the gimbal member is inaccessible, so that electrical connections will take the form of curved wires or ribbons, bypassing the axis.

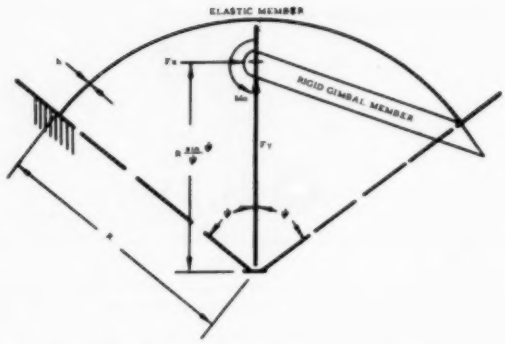

Fig. 1 Application of forces to an elastic member by a gimbal member pivoted at the elastic center

Consider the elastic member with flexural rigidity EI, in the form of a circular arc of radius R, and length $2R\psi$, with one end fixed to a point on the instrument case as shown in Fig. 1. A rigid arm which represents the gimbal member is attached to the free end of the elastic member. Forces F_x and F_y, and a moment M_0, applied to the rigid arm at a point $R(\sin \psi/\psi)$ from the arc center on the arc bisector produce the following displacements of that point:

$$\delta_x = \frac{1}{K_x} F_x \text{ (independent of } F_y \text{ and } M_0),$$

$$\delta_y = \frac{1}{K_y} F_y \text{ (independent of } F_x \text{ and } M_0), \text{ and rotation}$$

$$a = \frac{1}{K_0} M_0 \text{ (independent of } F_x \text{ and } F_y),$$

where

$$\left.\begin{aligned} \frac{1}{K_x} &= \frac{2R^3}{EI}\left(\frac{\psi}{2} + \frac{\sin 2\psi}{4} - \frac{\sin^2 \psi}{\psi}\right), \\ \frac{1}{K_y} &= \frac{2R^3}{EI}\left(\frac{\psi}{2} - \frac{\sin 2\psi}{4}\right), \\ \frac{1}{K_0} &= \frac{2R\psi}{EI}, \end{aligned}\right\} \quad (1)$$

and it is assumed that the values of δ/R, h/R, and a/ψ are all much less than unity.

The point of application of F_x and F_y is called the "elastic center." The torsional stiffness, or spring rate of the elastic member for rotation about any point other than the elastic center, is larger than K_0, as shown below. Minimum spring rate then occurs when the axis of the gimbal member passes through the elastic center.

A simplified method for computing the torsional spring rate for rotation about any point in the plane of the arc is given below. Consider a rotation a, of a rigid gimbal member about point x, y, as shown in Fig. 2. The rotation is produced by F_x, F_y, and M_0 acting at the elastic center.

The rotation produces displacements

$$\delta_x = ay, \qquad \delta_y = -ax, \qquad a = a$$

of the elastic center. These displacements are related to F_x, F_y, and M_0 as follows:

[1] Associate Professor of Mechanical Engineering, California Institute of Technology, Pasadena, Calif.

Manuscript received by ASME Applied Mechanics Division, February 18, 1959.

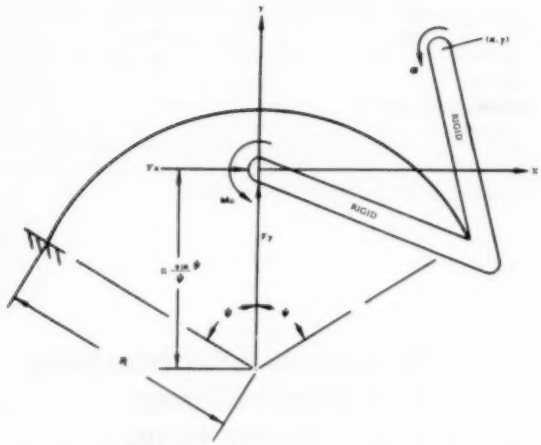

Fig. 2 Application of forces to an elastic member by a gimbal member pivoted at a point other than the elastic center

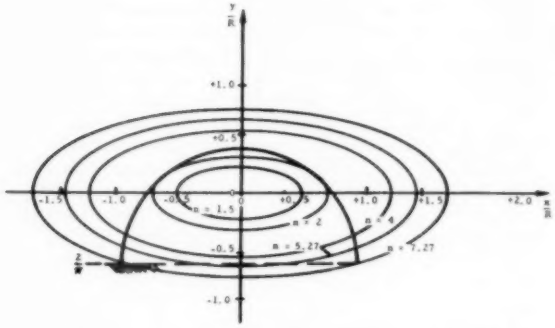

Fig. 3 Trajectories of $n = K_{xy}/K_0$ for several rotation centers, for the special case $\psi = \pi/2$

$$F_x = K_x a y, \qquad F_y = -K_y a x, \quad \text{and} \quad M_0 = K_0 a.$$

The same displacements are produced by applying a statically equivalent set of reactions F_x, F_y, and M_{xy} to the rigid gimbal member at the point of rotation (x, y), where $M_{xy} = M_0 + F_x y - F_y x$, or $M_{xy} = K_0 a + K_x a y^2 + K_y a x^2$. The torsional spring rate about x, y is then M_{xy}/a, or

$$K_{xy} = K_0 + K_x y^2 + K_y x^2. \tag{2}$$

The minimum spring rate occurs for rotation about the elastic center $x = y = 0$. Equation (2) may be used to calculate the torsional spring rate about any point x, y after evaluation of the constants K_0, K_x, and K_y, equation (1) [for a particular member of radius R, length $2R\psi$, and flexural rigidity EI].

Centers of rotation which lie on the ellipse

$$\frac{x^2}{\dfrac{K_0(n-1)}{K_y}} + \frac{y^2}{\dfrac{K_0(n-1)}{K_x}} = 1 \tag{3}$$

have a torsional spring rate $K_{xy} = nK_0$. When $K_x = K_y$ ($\sin \psi = 0$, $\psi = \tan \psi$), the torsional spring rate about any point on a circle of radius $r = [K_0(n-1)/K_x]^{1/2}$ with its center at the elastic center is $K_{xy} = nK_0$.

Values of $n = K_{xy}/K_0$ for several rotation centers are shown in Fig. 3 for the special case wherein

$$\psi = \frac{\pi}{2}, \quad \frac{1}{K_0} = \frac{\pi R}{EI}, \quad \frac{K_x}{K_0} = \frac{\pi}{\left(\dfrac{\pi}{2} - \dfrac{4}{\pi}\right) R^2}, \quad \frac{K_y}{K_0} = \frac{2}{R^2}.$$

Acknowledgment

Acknowledgment is due to Messrs. J. M. Slater and W. A. Ebert of Autonetics Division, North American Aviation, Inc., for suggesting the investigation reported herein and for helpful discussions.

Steady-State Response of Linear Vibration Systems With Viscous Damping

MORTON E. GURTIN[1]

The basic matrix[2] equation for forced vibration is:

$$M\ddot{q} + C\dot{q} + Kq = fe^{j\omega t} \tag{1}$$

Guderley[3] demonstrates that any nth order equation of this form may be transformed into one of the first order by a suitable change of co-ordinates. In the present case, the following form suggested by Foss,[4] as well as by other investigators[5,6,7], is used.

$$B\dot{z} + Dz = f'e^{j\omega t}, \tag{2}$$

where

$$B = \begin{bmatrix} 0 & M \\ M & C \end{bmatrix}, \quad D = \begin{bmatrix} -M & 0 \\ 0 & K \end{bmatrix}, \quad z = \begin{Bmatrix} \dot{q} \\ q \end{Bmatrix}, \quad f' = \begin{Bmatrix} 0 \\ f \end{Bmatrix}, \tag{3}$$

$$j = \sqrt{-1}$$

The homogeneous solution will be of the form

$$z = le^{\alpha t}, \tag{4}$$

and the homogeneous equation then gives

$$\alpha Bl + Dl = 0. \tag{5}$$

If N was the original number of degrees of freedom, then (5) will yield $2N$ eigenvectors and eigenvalues

[1] General Engineering Laboratory, General Electric Company, Schenectady, N. Y.

[2] The following matrix nomenclature will be used: An upper-case letter will denote a matrix, and a lower-case letter a vector; a t superscript will denote the transpose.

[3] K. G. Guderley, "On Nonlinear Eigenvalue Problems of Matrices," *Journal of the Society for Industrial and Applied Mathematics*, vol. 6, December, 1958, pp. 335–353.

[4] K. A. Foss, "Co-Ordinates Which Uncouple the Equations of Motion of Damped Linear Dynamic Systems," JOURNAL OF APPLIED MECHANICS, vol. 25, TRANS. ASME, vol. 80, 1958, pp. 361–364.

[5] F. L. Bauer, "Zur numerischen Behandlung von algebraischen Eigenwertproblemen hoherer Ordnung," *Zeitschrift für Angewandte Mathematik und Mechanik*, vol. 36, 1956, pp. 244–245.

[6] J. Morris, "Linear Simultaneous Equations and Cognate Quadratic Forms," Report No. SME 4039, Royal Aircraft Establishment, Farnsborough, England.

[7] W. J. Duncan and A. R. Collar, "Matrices Applied to the Motions of Damped Systems," *Philosophical Magazine*, series 7, vol. 19, 1935, p. 197.

Manuscript received by ASME Applied Mechanics Division, February 2, 1959.

$$\alpha_r \quad \text{and} \quad l^r = \begin{Bmatrix} \alpha_r \varphi^r \\ \varphi^r \end{Bmatrix} \tag{6}$$

The eigenvalues and vectors will occur as complex conjugate pairs and the modal matrix will be of the form

$$\Theta = [l^1 l^2 \ldots . l^N \bar{l}^1 \bar{l}^2 \ldots . \bar{l}^N]. \tag{7}$$

(The bar over a letter denotes the complex conjugate). Due to orthogonality, $\Theta^t B \Theta$ and $\Theta^t D \Theta$ are diagonal. If each mode is normalized such that

$$\Theta^t B \Theta = I \tag{8}$$

then

$$\Theta^t D \Theta = -[\alpha_r] = - \begin{bmatrix} \alpha_1 & 0 & 0 & \ldots & & & 0 \\ 0 & \alpha_2 & 0 & & & & \\ 0 & 0 & & & & & \\ \vdots & & & & & & \\ & & & \alpha_N & 0 & 0 & \\ & & & 0 & \bar{\alpha}_1 & 0 & \\ & & & 0 & 0 & \bar{\alpha}_2 & \\ & & & & & & 0 \\ & & & & & & 0 \\ 0 & & & & & 0\ 0 & \bar{\alpha}_N \end{bmatrix} \tag{9}$$

The steady-state solution of equation (2) will be of the form

$$z = y e^{j\omega t} \tag{10}$$

and equation (2) becomes

$$j\omega B y + D y = f' \tag{11}$$

If the eigenvectors and eigenvalues are known, the solution to equation (11) can be written immediately[8]

$$y = \begin{Bmatrix} j\omega q_0 \\ q_0 \end{Bmatrix} = \sum_{r=1}^{r=N} \frac{(l^{rt} f') l^r}{j\omega - \alpha_r} + \frac{(\bar{l}^{rt} f') \bar{l}^r}{j\omega - \bar{\alpha}_r} \tag{12}$$

However, since

$$\phi^{rt} f' = \begin{Bmatrix} \alpha_r \varphi^r \\ \varphi^r \end{Bmatrix}^t \begin{Bmatrix} 0 \\ f \end{Bmatrix} = \varphi^{rt} f \tag{13}$$

it follows that

$$q_0 = \sum_{r=1}^{r=N} \frac{(\varphi^{rt} f) \varphi^r (j\omega - \bar{\alpha}_r) + (\bar{\varphi}^{rt} f) \bar{\varphi}^r (jw - \alpha_r)}{-\omega^2 + \alpha_r \bar{\alpha}_r - j\omega(\alpha_r + \bar{\alpha}_r)} \tag{14}$$

To put (14) in more familiar form, the following definition is made:

$$\alpha_r \equiv -\frac{\omega_r}{2Q_r} + j\omega_r \left[1 - \frac{1}{4Q_r^2}\right]^{1/2} \tag{15}$$

Then

$$\alpha_r + \bar{\alpha}_r = \frac{\omega_r}{Q_r}$$

$$\alpha_r \bar{\alpha}_r = \omega_r^2. \tag{16}$$

where equations (15) and (16) are taken from McCalley.[9] With this definition of α_r, equation (14) becomes

$$q_0 = \sum_{r=1}^{r=N} \frac{(\varphi^{rt} f) \varphi^r (j\omega - \bar{\alpha}_r) + (\bar{\varphi}^{rt} f) \bar{\varphi}^r (j\omega - \alpha_r)}{\omega_r^2 - \omega^2 + j \dfrac{\omega \omega_r}{Q_r}} \tag{17}$$

Acknowledgment

The author would like to express his appreciation to Dr. P. R. Paslay of the General Engineering Laboratory for his constructive criticism of the manscript.

[8] F. B. Hildebrand, "Methods of Applied Mathematics," Prentice-Hall, Inc., New York, N. Y., 1956, pp. 44–45.

[9] Discussion of Foss[4] in JOURNAL OF APPLIED MECHANICS, vol. 26, TRANS. ASME, vol. 81, 1959, pp. 306–307.

Concerning the Further Understanding of the Shakedown Theorems Used for Structural Analysis

MELVIN ZAID[1]

IT IS the purpose of this note to clarify certain concepts that are basic to the use of the shakedown theorems associated with an ideally plastic material. Although the following discussion is intended to apply specifically to two-dimensional frame-type structures, the complete understanding of such structures is useful in the extension of theory to more complex problems.

As is well known, a necessary and sufficient condition for shakedown is that a residual stress (and bending moment) distribution must exist such that, when this is added to the elastic stress (and moment) distribution obtained from considering all combinations of external loads, the allowable stress state (and limit moment distribution) must not be exceeded.

The above statement holds for any ideal elastic-plastic structure without the need for explicit consideration of bending moments. However, since it is convenient to consider moments in frame-type structures, the conditions on those quantities are usually included in the shakedown criterion; thus in the frame analysis it is customary to consider separately the over-all moments in the frame as well as the detailed stress distribution at each cross section. It can be shown[2] that these considerations lead to the following two inequalities.

$$-M_{pi} \leq M_{ri} + M_{ei}'' \leq M_{ri} + M_{ei}' \leq M_{pi} \tag{1}$$

$$M_{ei}' - M_{ei}'' \leq 2\frac{M_{pi}}{\alpha} \tag{2}$$

where M_{pi} is the limit moment, M_{ri} is the residual moment, and M_{ei}'' and M_{ei}' are the minimum and maximum elastic moments at the i^{th} section.

In order that the frame structure shake down, it is necessary and sufficient that inequalities (1) and (2) be satisfied. It is important to note that inequality (1) enforces over-all structural restrictions and inequality (2) enforces detailed cross-section stress restrictions for the occurrence of shakedown.

Eliminating M_{ri} from inequality (1), one obtains

$$M_{ei}' - M_{ei}'' \leq 2M_{pi} \tag{3}$$

It is seen that inequality (3) is very much like inequality (2) ex-

[1] Scientific Research Staff, Republic Aviation Corporation, Farmingdale, N. Y.

[2] P. S. Symonds and B. G. Neal, "Recent Progress in the Plastic Methods of Structural Analysis—Part II," *Journal of the Franklin Institute*, vol. 252, 1951, pp 469–492.

Manuscript received by ASME Applied Mechanics Division, January 9, 1959.

cept that it concerns the plastic range of the structural "hinge" without consideration of the internal hinge stresses.

For the purpose of further discussion we will classify the collapse loads in the following manner. The largest external loads which satisfy inequalities (1), (2), and (3) will be respectively called the *structure* shakedown loads (P_1), the *section* cyclic collapse loads (P_{cyc}), and the *structure* cyclic loads (P_{cyc}'). In addition, the *structure* incremental collapse loads (P_{inc}) are defined as the smallest loads under which a collapse mechanism is still possible.

Considering, first, only the effects of moments, the structure shakedown load (P_1) is the smaller of the two structure collapse loads, or

$$P_1 = \min (P_{inc}, P_{cyc}')$$

It is this and only this load which will satisfy inequality (1).

The over-all shakedown load (P_s) is the smallest of all the separate collapse loads, which consider both moment and detailed stress, or

$$P_s = \min (P_1, P_{cyc})$$

Since $\alpha \geq 1$, we see that $P_{cyc} \leq P_{cyc}'$, so that

$$P_s = \min (P_{inc}, P_{cyc}) \tag{4}$$

Equation (4) is the usual definition of shakedown that appears in literature.[2, 3, 4]

It should be noted again that it will be impossible to find a set of residual moments which can be associated with the elastic moments, subject to the incremental collapse load, which will completely satisfy inequality (1), unless inequality (3) is also satisfied. That is, "structure" shakedown [as defined by inequality (1)] not only requires that no mechanism be formed through incremental deformations, but in addition there must be no repeated reversals of one or more hinges.

To illustrate the foregoing discussion, a particularly simple (and almost obvious) example is presented for the case where structure cyclic collapse predominates structure incremental collapse. It is not at all uncommon to find this occurrence in more complex (and less obvious) cases.

Consider a uniform beam, clamped on the left-hand end and simply supported on the other, loaded downward at the center. The range of the central load (P) is given by $-W/n \leq P \leq W$, $n > 1$, and the limit moment is taken to be M_0.

From inequality (3) the section cyclic collapse load can be shown to be

$$\frac{WL}{M_0} = \frac{32}{3(1 + 1/n)\alpha}$$

and the structure cyclic collapse load is

$$\frac{WL}{M_0} = \frac{32}{3(1 + 1/n)}$$

The structure incremental collapse load is $WL/M_0 = 6$, which is also the limit load.

From the foregoing we see, for $1 \leq n < 9/7$, that structure cyclic collapse predominates incremental collapse and must be considered for the complete satisfaction of inequality (1). The reader will find it instructive to assign a set of residual moments to the structure incremental collapse load, for this range of n, and see how inequality (1) is violated.

[3] B. G. Neal, "The Plastic Methods of Structural Analysis," John Wiley & Sons, Inc., New York, N. Y., 1956.

[4] P. G. Hodge, Jr., "Plastic Analysis of Structures," McGraw-Hill Book Co., Inc., New York, N. Y., 1959.

A Series Solution for Ellipsoidal Shells

ROBERT SCHMIDT[1]

A SERIES SOLUTION of Meissner's equations for ellipsoidal shells of revolution subjected to axisymmetrical load is obtained for the case of uniform thickness. The edge moments and forces are presented for a particular shell with clamped edge.

In Cartesian co-ordinates an ellipse can be represented by the equation

$$\frac{x^2}{a^2} + \frac{y^2}{b^2} = 1. \tag{1}$$

The middle surface of the shell is formed by revolution of an arc of the ellipse (1), about the y-axis. The radii of curvature of the middle surface in the meridional plane and in the normal plane perpendicular to meridian are

$$r = ac^2(c^2 + \lambda \sin^2 \varphi)^{-3/2}$$

and

$$R = a(c^2 + \lambda \sin^2 \varphi)^{-1/2}, \tag{2a, b}$$

respectively, where $c = b/a$, $\lambda = 1 - c^2$, and φ is the angle between the axis of revolution and the radius R.

The homogeneous Meissner equations for shells of uniform thickness[2] are

$$\frac{R}{r}\frac{d^2}{d\varphi^2}(RQ) + \left[\frac{d}{d\varphi}\left(\frac{R}{r}\right) + \frac{R}{r}\cot\varphi\right]\frac{d}{d\varphi}(RQ) - \left(\frac{r}{R}\cot^2\varphi - \nu\right)RQ = EhVr, \tag{3a}$$

$$\frac{R}{r}\frac{d^2V}{d\varphi^2} + \left[\frac{d}{d\varphi}\left(\frac{R}{r}\right) + \frac{R}{r}\cot\varphi\right]\frac{dV}{d\varphi} - \left(\frac{r}{R}\cot^2\varphi + \nu\right)V = -\frac{rRQ}{D}, \tag{3a}$$

where

Q = shearing force, per unit length, in the direction of the normal
E = modulus of elasticity
h = thickness
V = rotation of a meridian
ν = Poisson's ratio
$D = Eh^3/12(1 - \nu^2)$

With the variables

$t = \sin^2 \varphi$,
$I = RQ/\sin \varphi$,
$J = Ehc^4RV/\sin \varphi$

Equations (3) assume the following form for an ellipsoidal shell.

$$4t(1 - t)(c^2 + \lambda t)^2\frac{d^2I}{dt^2} + 2(c^2 + \lambda t)[4c^2 + (6\lambda - 5c^2)t - 7\lambda t^2]\frac{dI}{dt} + [c^2(4 - 5c^2 + \nu c^2) + \lambda(3 - 9c^2 + \nu c^2)t - 4\lambda^2 t^2]I = J, \tag{4a}$$

[1] Assistant Professor of Theoretical and Applied Mechanics, University of Illinois, Urbana, Ill.

[2] S. Timoshenko, "Theory of Plates and Shells," McGraw-Hill Book Co., Inc., New York, N. Y., 1940, p. 456.

Manuscript received by ASME Applied Mechanics Division, November 24, 1958.

$$4t(1-t)(c^2+\lambda t)^3\frac{d^2J}{dt^2}+2(c^2+\lambda t)^2[4c^2+(8-13c^2)t$$

$$-9\lambda t^2]\frac{dJ}{dt}+(c^2+\lambda t)^2(8-9c^2-\nu c^2-10\lambda t)J=-\mu I, \quad (4b)$$

where $\mu = Eha^2c^4/D$.

The solution of Equations (4) is assumed in the form of the series

$$I=\sum_{n=0,\,1,\ldots}^{\infty}A_nt^n, \qquad J=\sum_{n=0,\,1,\ldots}^{\infty}B_nt^n. \quad (5a,b)$$

Substitution of these series in Equations (4) yields the following recurrence formulas:

$$4c^4(n+1)(n+2)A_{n+1}+c^2[2(2-3c^2)n(2n+3)+4-$$
$$(5-\nu)c^2]A_n+\lambda[4(3\lambda-2)n^2-1+(3+\nu)c^2]A_{n-1}$$
$$-2\lambda^2n(2n-3)A_{n-2}=B_n, \quad (6a)$$

$$4c^6(n+1)(n+2)B_{n+1}-c^4[4(1-4\lambda)n^2$$
$$+2(3-13\lambda)n-8+(9+\nu)c^2]B_n$$
$$+2\lambda c^2[6(2\lambda-1)n^2-(1-3\lambda)n+(1-\nu)c^2]B_{n-1}$$
$$+\lambda^2[4(4\lambda-3)n^2+2(7-9\lambda)n-c^2(1+\nu)]B_{n-2}$$
$$-2\lambda^3(2n^2-5n+2)B_{n-3}=-\mu A_n, \quad (6b)$$

where $n = 0, 1, 2, 3, \ldots, A_{-n} = B_{-n} = 0$.

The recurrence relationships indicate that there are only two independent constants, A_0 and B_0, in the series. The values of these two constants are determined from the conditions at the edge. The conditions at the crown of the shell, $Q = V = 0$, are automatically satisfied by the choice of the variables I and J. This implies that the shell under consideration may not have an opening at the crown ($\varphi = 0$), i.e., it may have only one edge.

Example. The values of the moments and forces at the clamped edge of an ellipsoidal shell subjected to uniform external pressure p are calculated in this example. It is assumed that

$$\nu = 0.3; \; a = 20h; \; c = 0.8;$$

and

$$\varphi = 30°, \text{ i.e., } t = \sin^2\varphi = 0.25 \text{ at the edge}$$

The membrane theory yields the following formulas for the radial displacement η_m and rotation V_m:

$$\eta_m = -\frac{pR^2\sin\varphi}{Eh}\left(1-\frac{\nu}{2}-\frac{R}{2r}\right), \quad (7)$$

$$V_m=\frac{p}{Eh}\left\{R\cot\varphi\left[\nu-\frac{1}{2}+(1-\nu)\frac{R}{r}-\frac{R^2}{2r^2}\right]\right.$$
$$\left.-\frac{1}{r}\frac{d}{d\varphi}\left[R^2\left(\frac{\nu}{2}-1+\frac{R}{2r}\right)\right]\right\}. \quad (8)$$

The boundary conditions require that the radial displacement η and the rotation V vanish at the clamped edge, i.e.,

$$\eta = \eta_m + \eta_h = 0, \qquad V = V_m + V_h = 0 \quad (9a,b)$$

where

$$\eta_h=\frac{\sin\varphi}{Eh}\left[\nu I\cos\varphi-\frac{R}{r}\frac{d}{d\varphi}(I\sin\varphi)\right], \quad (10)$$

$$V_h = J\sin\varphi/Ehc^4R \quad (11)$$

The values of the coefficients in series (5) are calculated using Equations (6) to (11).

Other relationships necessary for the completion of this problem can be found in the cited reference.[2]

The values of the moments and forces at the edge of the shell are:

Meridional moment	$M_\varphi = -0.0101\ pa^2$
Circumferential moment	$M_\theta = -0.00268\ pa^2$
Meridional tension	$N_\varphi = -0.372\ pa$
Circumferential tension	$N_\theta = +0.239\ pa$
Shearing force	$Q = -0.123\ pa$

Thirteen terms in series (5) are necessary to obtain the indicated accuracy.

The method of analysis described herein is not suitable for ellipsoidal pressure-vessel heads, as the convergence of series (5) becomes unsatisfactory for large values of t.

Axially Symmetric Buckling of Shallow Spherical Shells Under External Pressure[1]

S. R. BODNER.[2] The author has demonstrated a novel approach to the problem of the snap through buckling of spherical caps. The emphasis on the relation between the deformation state prior to buckling and the buckling characteristics is well taken. The change in buckling mode with the geometric parameter ρ suggested by the experimental results appears, by all accounts, to be directly related to changes in the prebuckling deformation state. The writer believes, however, that the change in mode is from an axially symmetrical pattern for low values of ρ ($\rho <$ about 20) to one that is not axially symmetric at higher values of ρ. For the higher range of ρ the prebuckling normal deflection and compressive membrane stresses are maximum away from the center of the spherical cap. Since the membrane stresses are of great importance in the buckling problem, it is likely to expect asymmetric buckling modes to develop. For large ρ the buckle pattern does not extend over the complete shell so that buckles would tend to form in the regions of largest compressive stresses.

It is worth while noting that the experimental results have almost invariably indicated nonaxially symmetric buckling whenever ρ is greater than about 20. In addition to the author's references, the writer is familiar with some, as yet unpublished, experimental work on spherical caps performed at the AVCO Manufacturing Corporation. These were fairly well-controlled tests and the specimens always buckled in an asymmetrical manner. As the author points out, further changes in the mode pattern can be expected to occur as ρ continues to increase. The extreme case of a hemispherical shell is characterized by a complicated buckled shape that is, of course, not axially symmetric.

A similar effect has been shown[3] to occur in the nonlinear problem of the large deflection of circular plates. For sufficiently large deformation, a plate subjected to uniform lateral or edge loading buckles from a symmetric bent or buckled state into an asymmetric pattern due to induced compressive stresses around the plate edge. In the spherical-cap problem, the additional compressive stresses away from the center also arise due to the restraint at the edge. Although the investigation of asymmetric buckling states is a formidable problem, the writer believes that further understanding of the buckling of spherical caps lies in this direction.

ABNER KAPLAN.[4] The author is to be commended for having presented a very intriguing explanation for the apparent scatter in the experimental results for the buckling of shallow spherical shells and for using this explanation to develop an approximate theory. It is a good example of the results which can develop from the interaction between theory and experiment. It is hoped that this will lead eventually to a complete understanding of the buckling behavior of shallow and not so shallow spherical shells.

The author discusses at length the reasons for the differences between his theoretically determined transition points and those determined by the peaks in the experimental results. The writer believes, however, that a more likely reason for the discrepancy lies in the limitation of the theory.

The theoretical transition points are determined from the reversal of curvature at the center for an infinitesimal deflection. However, at a given value of ρ, this curvature can change with increasing finite deflection. Therefore, it should not be unexpected that the buckling-mode transitions will occur at a lower value of ρ than is predicted by the theory.

Author's Closure

The author wishes to thank Professor Bodner and Dr. Kaplan for their pertinent comments.

In the paper, the peaks in the buckling loads are related to the change in the mode of deformation of the shell from one axially symmetric state to another. Professor Bodner conjectures that the peaks are a result of the change in the mode from a symmetric to an unsymmetric state. This may be true and could explain the first transition, or peaking point. However, if the conjecture is correct, it would then be difficult to explain the second transition unless it is assumed that a considerable change in the unsymmetric deflection mode occurs. The results[5] of a numerical solution of a nonlinear formulation for axially symmetric buckling indicate that the *mechanism* of buckling of a real shell may vary with ρ. Shells with $\rho < 20$ (the first mode) appear to buckle according to the "energy criterion." For larger values of ρ the actual buckling may be more closely related to the "classical criterion." However, the theoretical and experimental results are, at this time, too scarce to draw definite conclusions in this respect.

Yanowitch[3] has discussed the possibility of a "second buckling"; that is, an unsymmetric buckling about an initially symmetric buckled or bent shape. This second buckling is related to the existence of a large compressive circumferential membrane stress concentrated in a ring adjacent to the edge of the plate. To obtain this state of stress the boundary conditions must be sufficiently "mild."[3] For example, if the edge of the plate is built-in, then the circumferential membrane stress is everywhere tensile[6] and the possibility of a second buckling is less likely. Calculations[5,7] made for built-in spherical shells show that, although

[1] By E. L. Reiss, published in the December, 1958, issue of the JOURNAL OF APPLIED MECHANICS, vol. 25, TRANS. ASME, vol. 80, 1958, pp. 556–560.

[2] Assistant Professor of Engineering, Brown University, Providence, R. I.

[3] M. Yanowitch, "Non-Linear Buckling of Circular Elastic Plates," *Communications on Pure and Applied Mathematics*, vol. 9, 1956, pp. 661–672.

[4] Member of Technical Staff, Space Technology Laboratories, Inc., Los Angeles, Calf.

[5] H. B. Keller and E. L. Reiss, "Spherical Cap Snapping," to appear.

[6] H. B. Keller and E. L. Reiss, "Iterative Solutions for the Nonlinear Bending of Circular Plates," Communications on Pure and Applied Mathematics, vol. 11, 1958, pp. 273–292.

[7] E. L. Reiss, H. J. Greenberg, and H. B. Keller, "Nonlinear Deflections of Shallow Spherical Shells," *Journal of the Aeronautical Sciences*, vol. 24, 1957, pp. 533–543.

the circumferential membrane stress is everywhere compressive, there is no region of concentration. However, experimental boundary conditions may deviate sufficiently from built-in to permit the development of a compressive ring. Hence, as Professor Bodner suggests, the question of unsymmetrical buckling may be quite complicated and certainly merits further consideration.

Dr. Kaplan's comment concerning the variation of mode of deformation with P as well as $\mathcal{L}$ is substantiated by the results of calculations with the nonlinear formulation of the problem.[7]

Analysis of the Thermoelectric Effects by Methods of Irreversible Thermodynamics[1]

O. K. MAWARDI.[2] The authors have given a very lucid presentation of the derivation of the thermoelectric effects. An alternative interpretation of the Onsager relations, based on some well-known properties of linear operators, may be of general interest. One of the main advantages of this derivation is its compactness.

The starting point of the discussion is Equation (10) of the paper. This equation, which reads

$$\frac{dS'}{dx} = J_u\tau' - J_n(\mu\tau)'$$

in the notation of the paper, may be interpreted as the scalar product of two vectors. The first of them, $\mathbf{J}$, has the components J_u and J_n, and the other, $\mathbf{T}$, has the components τ' and $(-\mu\tau)'$. This leads us to write dS'/dx formally as

$$\frac{dS'}{dx} = \mathbf{JT} \tag{1}$$

Similarly, the Onsager relations, Equations (11) and (12) of the paper, can be imagined to express a linear transformation

$$\mathbf{J} = O(\mathbf{T}) \tag{2}$$

in which O is the transformation operator.

The foregoing is explicitly expressed by

$$J_u = L_{11}\tau' + L_{12}(-\mu\tau)' \tag{3}$$

$$J_n = L_{12}\tau' + L_{22}(-\mu\tau)' \tag{4}$$

or in matrix form

$$\begin{pmatrix} J_u \\ J_n \end{pmatrix} = \mathfrak{L}\begin{pmatrix} \tau' \\ -(\mu\tau)' \end{pmatrix} \tag{5}$$

where

$$\mathfrak{L} = \begin{pmatrix} L_{11} & L_{12} \\ L_{12} & L_{22} \end{pmatrix}$$

is the transformation matrix.

The pair of relations (1) and (5) of this discussion will yield all the results of the paper at once.

In order to show this, we start by rewriting (3) and (4) with $(\mu\tau)'$ expanded, i.e.,

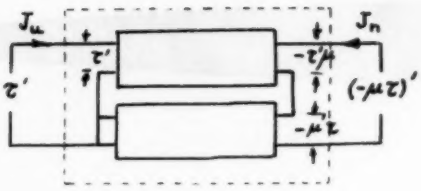

Fig. 1

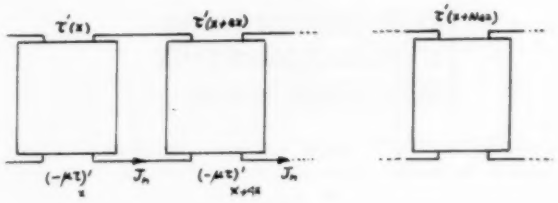

Fig. 2

$$J_u = L_{11}\tau' + L_{12}(-\mu\tau') + L_{12}(-\tau\mu') \tag{6}$$

$$J = L_{12}\tau' + L_{22}(-\mu\tau') + L_{22}(-\tau\mu') \tag{7}$$

Considering (1) as playing the role of a conservation relation, and (2) as describing the dependence of the input and output of some four-pole network of characteristic matrix $\mathfrak{L}$, we can draw, by inspection from (6) and (7), the equivalent network, Fig. 1. From the operation of the "network" of Fig. 1, we deduce the following results:

1 Open-circuit performance of the right-hand side of the network, i.e., $J_n = 0$,

$$J_u)_{J_n=0} = K_1\tau' \tag{8}$$

The coefficient of proportionality, K_1, is a constant with respect to τ'. Its value is found from (6) and (7). This is Fourier's law of heat conduction.

2 Since we always want to include heat-conduction effects in the study, $J_u = 0$ (open circuit) has no meaning. However, $\tau' = 0$ corresponds to the interesting case of the isothermal situation. This is equivalent to short-circuiting the left-hand side of our circuit, which leads to

$$J_n)_{\tau'=0} = K_2\tau\mu' \tag{9}$$

The constant K_2 is independent of μ'. This is, of course, Ohm's law. The short-circuit current for this situation

$$J_u)_{\tau'=0} = L_{12}\tau\mu' \tag{10}$$

which is the heat required to maintain the conductor at constant temperature as a result of the Joule's heat.

To deduce the Thomson effect we must remember that the network of Fig. 1 refers to local properties. In order to arrive at the relations for the large we have to compound in cascade networks similar to that of Fig. 1. The result of this combination is shown in Fig. 2.

If we consider the conductor to be subdivided in N segments each of length Δx, then the variables τ', $(\mu\tau)'$ are functions of $x, 2x, \ldots, N\ x$ successively. Since the charge carriers are conserved $J_n' = 0$. On the other hand, the phonons are not conserved so that $J_u' \neq 0$. This is consistent with our representation since it is apparent from Fig. 2 that imposing the requirement of constant J_n implies a variable J_u (with respect to x). Manipulation of Equations (6) and (7) of this discussion leads us to an expression identical to Equation (40) found by the other approach of the authors.

[1] By G. N. Hatsopoulos and J. H. Keenan, published in the December, 1958, issue of the JOURNAL OF APPLIED MECHANICS, vol. 25, TRANS. ASME, vol. 80, pp. 428–432.

[2] Associate Professor, Massachusetts Institute of Technology, Cambridge, Mass.

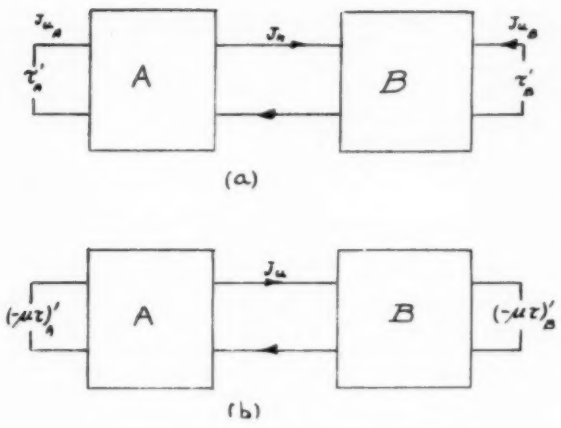

Fig. 3

The Peltier effect and the Seebeck effect are also estimated readily by the approach outlined in this discussion. Here we wish to estimate the behavior of two four-pole networks connected in cascade.

One of these corresponds to material A, the other to material B. We have two possible methods of compounding the networks. In the first arrangement, A and B have J_u identical, Fig. 3(a) of this discussion. This is the compounding necessary to study the Peltier effect. In the other alternative, J_u is identical, Fig. 3(b).

The quantity

$$(J_{uA} - J_{uB})/J_u = \frac{J_{uA}}{J_u} - \frac{J_{uB}}{J_u} = \Pi_{AB}$$

represents the difference in the transfer function for the currents. On the other hand,

$$\frac{d}{dT}(\mu_B - \mu_A) = \frac{d}{dx}(\mu_B - \mu_A)\frac{dx}{dT}$$

$$= -(\mu_A' - \mu_B')\tau^2/\tau' = \epsilon_{AB}$$

represents the difference in the transfer functions for the potentials across the four-pole networks. By referring back to Equations (6) and (7) of the discussion, one finds at once that

$$\Pi_{AB} = \epsilon_{AB}/\tau$$

J. S. THOMSEN.[2] The authors have presented a worthwhile analysis of thermoelectric phenomena from the viewpoint of irreversible thermodynamics and Onsager's principle. It is well to emphasize, as they have done, that this principle may be regarded as an additional axiom of macroscopic thermodynamics without reference to the statistical concepts which led Onsager to first state this law.

There is, however, one point which might merit further discussion and clarification. The term "electrochemical potential" is used; it is stated that this is identical to electrical potential for an isothermal, homogeneous conductor. It might be helpful to give a discussion of the physical significance of this quantity in cases where it is not identical to the electrical potential.

Furthermore, there seem to be differences in the role of this term in the expression for entropy production, Equation (10) in the paper. Denbigh[4] gives a corresponding result which involves only electrical potential; possibly his derivation contains implicit assumptions which are not entirely valid here. De Groot[5] and Sommerfeld[6] obtain expressions in which both electrical and chemical potentials appear, but apparently not in the combination given by the authors; all three, of course, obtain the same Kelvin relations. However, it would seem that the entropy production expression should have some direct physical significance so that only one of the forms can be rigorously correct. A further discussion of the physical meaning of electrochemical potential in the present application should help to clear up this point.

[2] Assistant Professor, Department of Mechanical Engineering, The Johns Hopkins University, Baltimore, Md.

Authors' Closure

Professor Mawardi has given a very interesting discussion on two alternate representations of the coupled flow equations. His first method is to use a shorthand vector representation, which is helpful in regard to compactness of notation. However, it is not clear how this method can be used in analyzing the problem. His second method is to use an electric circuit analog to represent the thermoelectric effect. Such a method can be useful in obtaining results without actually solving the algebraic expressions. Concerning this latter approach, however, there are certain minor modifications that must be made in Professor Mawardi's discussion in order for the analog to be consistent with the actual phenomenon. First, in the circuit of Fig. 1 it is not clear how the voltage-dividing network can differentiate between the components $(-\mu\tau')$ and $(-\mu'\tau)$ of the term $(-\mu\tau)'$. After a discussion with Professor Mawardi, he indicated that a feedback loop from the input τ' should be included for that purpose. In any case, it was agreed that the splitting of the input $(-\mu\tau)'$ is not necessary for the analysis.

The second modification concerns the block diagram of Fig. 2. Since, as pointed out in the text, $J_u \neq 0$, a current source or sink must be incorporated in the network of Fig. 2. This current source or sink would simulate the condition of a transverse heat transfer that takes place in the thermoelectric conductor.

Professor Thomsen, in his discussion of our paper, brought up the very interesting point of differentiating the electrochemical potential from the electrical potential. In the case of a solid electrical conductor, the electrochemical potential difference is identical to the difference in Fermi levels between two points in the conductor. This quantity can be easily measured microscopically in a solid conductor. Therefore splitting the electrochemical potential into electrical potential and chemical potential is phenomenologically meaningless.

[4] K. G. Denbigh, "Thermodynamics of the Steady State," Methuen, London, 1951, p. 51.

[5] S. R. de Groot, "Thermodynamics of Irreversible Processes," North-Holland Publishing Company, Amsterdam, 1952, p. 148.

[6] A. Sommerfeld, "Thermodynamics and Statistical Mechanics," Academic Press, New York, N. Y., 1956, p. 158.

Ductile Fracture Instability in Shear[1]

B. M. WUNDT.[2] This paper constitutes an outstanding contribution to the problem of fracture dynamics. The mechanical engineer whose interest is centered on the macroscopic aspects of fracture will be indebted to the author for his analysis of conditions under which a slowly growing crack will change into a fast-mov-

[1] By F. A. McClintock, published in the December, 1958, issue of the JOURNAL OF APPLIED MECHANICS, vol. 25, TRANS. ASME, vol. 80, 1958, pp. 582–588.

[2] Structural Engineer, Large Steam Turbine-Generator Department, General Electric Company, Schenectady, N. Y.

ing, unstable crack. The model is an infinitely large body with a longitudinal crack exposed to a uniform shear strain τ.

The author describes the behavior of cracks in terms of well-known variables, shearing strain γ, shearing stress τ, yield stress K, modulus of shear G, initial crack length c_0. In addition, he introduces two important parameters, the fracture strain in shear γ_f and material size parameter ρ.

With the help of these parameters he succeeds in defining the extent of the plastic zone ahead of the crack as a function of applied shear stress and introduces a mathematical condition for instability.

The two parameters γ_f and ρ are not well understood as yet. The author assumes that they are essentially constant, but it is not out of the question that either one may be a function of other variables such as state of stress, physical properties, and microstructure. It is hoped that properly executed experiments will succeed in clarifying the foregoing parameters and that the author will extend the theory to behavior of cracks under different states of stress which have hydrostatic tension.

Although the instability criterion proposed by the author seems reasonable, the following question emerges. It is seen from Fig. 4 that, when near the instability point, after a rather slow growth accompanied by stress increases, the crack begins to enlarge at an accelerated rate but at a practically constant stress level. If equations (17) apply at this stage of crack growth, the plastic-zone ratio remains constant because the stress hardly changes. Therefore the plastic zone R ahead of the crack increases steadily in proportion to the currently increasing crack length. Intuitively, it seems that under such conditions the crack tends to be arrested rather than to become unstable and fast propagating. It is more likely that when instability occurs the plastic-zone ratio may decrease with increasing crack length rather than remain constant. The author's comments will be appreciated.

It appears possible to obtain an insight and a rather rough estimate of material size parameter ρ. For this we turn to Neuber's plastically deformed region "building-block" concept (5) of the paper. We assume a thick and wide plate with a centrally located crack $2c$, which is subject to a uniformly distributed tension stress S_∞ at sections away from the crack. The tension stress distribution ahead of the crack under elastic conditions is given by

$$S = K/\sqrt{2r}$$

where K is the stress intensity factor and r is the radial distance from the tip of the crack to the point in question on a line coinciding with the crack extension ([4],[3] Equations (8), (9); [2], Equation (10); [1], Equations (6), (7)).

The average stress across the width of the building block is S_{avg}

$$S_{avg}\rho = \int_0^\rho S dr = \int_0^\rho \frac{K}{\sqrt{2r}}\, dr = K\sqrt{2\rho}$$

([1], Equation (9)), and

$$K = S_{avg}\sqrt{\rho/2}$$

It is further assumed that the "elementary structural unit" ρ, ahead of the notch, cracks open when the average stress S_{avg} reaches some characteristic fracture stress; for instance, the "elusive technical cohesive strength" S_c. Therefore,

$$K = S_c\sqrt{\rho/2} \quad \text{and} \quad \rho = 2K^2/S_c^2$$

If the writer is permitted to make another, rather far-fetched assumption, i.e., that the strain-energy-release concept is applicable to the process of fracturing across ρ, then

$$K^2 = \frac{\mathcal{G}E}{\pi(1-\nu^2)} \quad ([1], \text{Equation (6)})$$

where

$\mathcal{G}$ = strain-energy release rate
E = modulus of elasticity
ν = Poisson's constant

Therefore,

$$\rho = 2\frac{K^2}{S_c^2} = 2\frac{\mathcal{G}E}{\pi(1-\nu^2)S_c^2} = 2\frac{\mathcal{G}_cE}{\pi(1-\nu^2)S_c^2}$$

We have replaced $\mathcal{G}$ with $\mathcal{G}_c$, the critical fracture extension force, fracture toughness.[4] Obviously, the numerical coefficients in the foregoing expression are only roughly approximate and only an order of magnitude for ρ may be obtained in this manner.

However, as a result of this heuristic approach it follows that the elementary structural unit ρ is proportional to fracture toughness $\mathcal{G}_c$. This means that for a given crack length c, the ratio c/ρ decreases with increasing fracture toughness $\mathcal{G}_c$ and the crack initiation as well as crack instability occurs at a higher stress than in case of a smaller ρ.

This deduction seems reasonable and follows from Fig. 4 of the paper.

Continuing this intuitive approach the following relationship is obtained. It can be shown that in case of tension applied to a wide place with a crack $2c$ long, the length of plastic zone along the crack may be represented as

$$R = m\,\mathcal{G}_cE/S_y^2 \quad (\text{See [6]})$$

S_y is yield strength in tension and m is a number, which contains Poisson's ratio and whose magnitude depends on the state of stress at the tip of the crack. m appears to be about 10 times as large for plain stress as for plain strain and its exact value is not yet known. If the uniformly distributed stress at the far end of the plate is designated S_∞ then the relation for crack propagation is

$$S_\infty^2 = \frac{\mathcal{G}_cE}{\pi c(1-\nu^2)} \quad ([4], \text{Equation (5}a\text{)})$$

and

$$\mathcal{G}_cE = \pi(1-\gamma^2)cS_\infty^2$$

Therefore, the plastic zone

$$R = m\frac{\mathcal{G}_cE}{S_y^2} = n\left(\frac{S_\infty}{S_y}\right)^2 c$$

and

$$\frac{R}{c} = n\left(\frac{S_\infty}{S_y}\right)^2$$

However, n is a number not too well defined. This equation for the plastic-zone ratio in tension along the extending crack is very similar to Equation (17a) in the paper, derived for shearing strain.

References

1 G. R. Irwin, J. A. Kies, and H. L. Smith, "Fracture Strengths Relative to Onset and Arrest of Crack Propagation," paper presented at ASTM Meeting, Boston, Mass., June 23–27, 1958.

2 G. R. Irwin, "Analysis of Stresses and Strains Near the End of a Crack Traversing a Plate," JOURNAL OF APPLIED MECHANICS, vol. 24, TRANS. ASME, vol. 79, 1957, pp. 361–364.

3 Discussion of [2] by F. A. McClintock and author's closure, JOURNAL OF APPLIED MECHANICS, vol. 25, TRANS. ASME, vol. 80, 1958, pp. 299–301.

[3] Numbers in brackets designate References at end of this discussion.

[4] Reference [4], p. 1647.

4 D. H. Winne and B. M. Wundt, "Application of the Griffith-Irwin Theory of Crack Propagation to the Bursting Behavior of Disks," TRANS. ASME, vol. 80, 1958, pp. 1643–1658.

5 P. Kuhn, "Effect of Geometric Size on Notch Fatigue," Proceedings Colloquium on Fatigue, Stockholm, Springer-Verlag, Berlin, 1955, pp. 131–140.

6 Letter by F. A. McClintock to B. M. Wundt, dated January 16, 1958.

Author's Closure

The author wishes to thank Mr. Wundt for his intense interest in the paper and his pertinent questions.

In regard to the physical significance of the fracture strain γ_f and the structural size parameter ρ, torsion experiments have been made on circumferentially notched bars by Mackenzie [7] and longitudinally notched bars by Kayan [8]. Both direct observation and deduction from the effect of notch radius on fracture initiation have shown that the fracture strain γ_f is just that in an unnotched specimen, and the structural size parameter ρ is of the order of a few grain diameters. Hult [9] has obtained similar values for ρ in fatigue tests. Theoretical and experimental work on crack propagation in these cases should be carried out, as well as studies of the effect of hydrostatic pressure, as suggested by Mr. Wundt. The problem of obtaining elastic-plastic solutions for plane stress or plane strain is likely to be very difficult, for not only is there one more component of stress and strain, but also the deformation is such as to change the shape of the body even before cracking begins.

The intuitive feeling that an expanding plastic zone, even at a constant stress level, should arrest rather than promote the crack probably comes from an impression that more energy is absorbed the larger the plastic zone. But the incremental nature of the plastic stress-strain relations means that the strain, and hence the energy absorbed in the plastic zone, depend not only on the size of the zone but also on the history of the plastic deformation. Thus the strain in a plastic zone spreading at nearly constant stress due to the growth of a crack may be considerably different from that in a zone produced by increasing the stress on a crack of fixed length. Furthermore, the longer the crack the more deformation can be supplied from its elastic surroundings.

Instability actually arises from the fact that if the stress on the body is applied at distances large compared to the crack depth, then the growth of the crack will produce a negligible decrease in the applied stress, even in the fixed-grip condition. Thus as soon as the stress required to propagate the crack begins to decrease, there is a stress difference available to produce acceleration, and the crack becomes unstable immediately, without the necessity of the stress falling so far that the plastic zone becomes of constant size.

It seems to the writer that rather than using the "strain energy release rate" $\mathcal{G}$ to explain ρ, one should use the structural size constant to explain $\mathcal{G}$, if indeed that concept is still desirable. If in the shear case one defines values of $\mathcal{G}$ for initiation under increasing stress and for instability on cutting under constant stress so that

$$\tau_i = \sqrt{\frac{\mathcal{G}_i G}{c}} \quad \text{and} \quad \tau_c = \sqrt{\frac{\mathcal{G}_c G}{c}}, \tag{1}$$

then for low stress levels the combination of Equation (17*a*) with first Equation (6) and then (21) (neglecting unity where it appears explicitly) yields similar equations:

$$\tau_i = \sqrt{\frac{\rho\gamma_f k^2}{\gamma_y c}} \quad \text{and} \quad \tau_c = \sqrt{\frac{k^2 \exp\left(\sqrt{2\gamma_f/\gamma_y}\right)}{c/\rho}} \tag{2}$$

Comparison of Equations (1) and (2) yields the following expressions for $\mathcal{G}$:

$$\mathcal{G}_i = \rho k \gamma_f \quad \text{and} \quad \mathcal{G}_c = \rho k \gamma_y \exp\left(\sqrt{2\gamma_f/\gamma_y}\right) \tag{3}$$

At higher stress levels Equations (3) would be more complicated. It is not possible to give an explicit expression for the value of $\mathcal{G}$ for the instability of a crack under increasing stress, but the numerical results obtained so far indicate that it would be greater than $\mathcal{G}_c$ by a small factor. It should be pointed out that in this formulation of fracture mechanics, the quantities ρ and γ_f are properties whereas the critical value of the strain energy release rate $\mathcal{G}$ is not; it depends on the history of loading.

The use of a critical radius of the plastic zone to describe the condition for instability is also subject to the disadvantage that it depends on history, but the radius of the plastic zone is more concrete and more useful in determining, for example, whether plane stress or plane strain conditions exist, as pointed out by Irwin (reference [1] of the discussion).

It is interesting to note that the Griffith fracture criterion for brittle materials can be stated in terms of the fracture hypothesis used in this paper, if one equates the structural size to the lattice spacing a, and the fracture strain to the theoretical elastic strain of, say, $1/4$. Elasticity theory shows that, inserting a factor of two to account for nonlinearity, the strain one structural size ahead of a sharp crack is given by

$$\epsilon = \epsilon_f = \frac{2\sigma_\infty}{E}\sqrt{\frac{c}{2a}}$$

Again allowing for nonlinearity, the surface energy can be approximately related to the fracture strain and the modulus of elasticity by

$$\alpha = \epsilon_f E a/4$$

Combination of the above equations yields

$$\sigma_\infty = \sqrt{\alpha E/2c}$$

which is similar to the original Griffith equation and identical to an equation derived by Orowan [10] based on a crack whose minimum radius was of atomic dimension. Thus one form of fracture hypothesis can be used for both brittle and ductile fracture.

References

7 A. C. Mackenzie, "Crack Initiation in Circumferentially Notched Bars in Torsion," MS thesis, M.I.T., September, 1958.

8 I. Kayan, Research in progress at M.I.T.

9 J. A. H. Hult, "Fatigue Crack Propagation in Torsion," *Journal of the Mechanics and Physics of Solids*, vol. 6, 1957, pp. 47–52.

10 E. Orowan, "Fracture and Strength of Solids," Reports on Progress in Physics, vol. 12, 1949, pp. 185–232.

Laminar Flow in a Uniformly Porous Channel[1]

C. W. GORTON.[2] The authors are to be commended for solving an important problem in a complete yet concise manner.

There is one question the writer would like to ask concerning the form of the stream function introduced by Berman. Equation (27) and Fig. 3 of the paper show that the inlet-velocity profile has a different shape depending on the wall Reynolds number. Shouldn't solutions exist for prescribed inlet-velocity profiles?

[1] By F. M. White, Jr., B. F. Barfield, and M. J. Goglia, published in the December, 1958, issue of the JOURNAL OF APPLIED MECHANICS, vol. 25, TRANS. ASME, vol. 80, 1958, pp. 613–617.

[2] Associate Professor, Mechanical Engineering Department, Georgia Institute of Technology, Atlanta, Ga.

In other words, doesn't this paper present a family of solutions compatible with the assumption that $\psi(x, \lambda) = g(x)f(\lambda)$?

J. A. NOHEL.[3] The writer would like to compliment the authors on a most interesting and stimulating problem. Not being an engineer, he will restrict himself solely to mathematical questions.

1 The writer carried out the suggested reduction of the system (2) and he finds the following:

(*a*) The relation (8) indeed holds, but subject to the condition that $f(\lambda)$, $f'(\lambda)$, $f''(\lambda)$ are finite on $0 \leq \lambda \leq 1$.

(*b*) Utilizing (8), (5), and (6) and (7) in the first part of (2), the reviewer obtains not (9) but the relation given later, namely, (16):

$$f^{iv} + R\{f'f'' - ff'''\} = 0$$

However, adding and subtracting $f'f''$ inside the bracket in the foregoing relation, one can immediately obtain relation (9) as a first integral of the cited equation. It also should be remarked that, to obtain either (9) or the foregoing equation, one must assume that

$$\frac{\partial^2 p}{\partial x \partial \lambda} = \frac{\partial^2 p}{\partial \lambda \partial x},$$

which probably follows on physical grounds.

2 Special cases:

(*a*) Case I. $R = 0$

$$f(\lambda) = \frac{3}{2}\lambda - \frac{1}{2}\lambda^3$$

is a solution of (9) with $R = 0$ if and only if $k_0 = -3$.

(*b*) Case II. First of all, it is not at all clear what the case $R = -\infty$ means. The statement "Equation (13) is exactly the same regardless of whether $R = +\infty$ or $-\infty$" is also not clear. It is suggested that this be worked out by letting $1/R = \epsilon$, regarding ϵ small, and considering the cases $\epsilon > 0$ and $\epsilon < 0$. Also, in case II*a* $f(\lambda) = \sin(\pi/2)\lambda$ solves (13) if and only if $k_{-\infty} = \pi^2/4$. Also in case II_t $f(\lambda) = \lambda$ solves (13) if and only if $k_{+\infty} = 1$.

(*c*) However, the "solutions" given in all special cases are solutions of the more general equation on (16).

3 Solution for arbitrary R:

(*a*) Obvious misprint in (19). The first boundary condition should be $\phi(0) = 0$.

(*b*) The solution here should not be called "general solutions," since (18) being nonlinear may have many other forms of solutions.

(*c*) To make the arguments of the paper rigorous, what is needed is an existence, and especially a uniqueness theorem for the original problem (2), (3), (4); this is probably quite difficult. The "proof" of convergence does not seem convincing; the statement above relation (25), referring to "this single term, *in all cases*, . . ." is vague.

4 A mathematical problem. It would seem relevant to consider the following problem: Divide (16) by R and let $1/R = \epsilon$. Solve the physical problem for $\epsilon = 0$ and study in detail the behavior of solutions for $\epsilon \neq 0$ but small. Note that the order of the equation changes from three to four when one passes from the cases $\epsilon = 0$ to the case $\epsilon \neq 0$. This type of problem is called a "singular perturbation problem," and has been studied extensively by Levinson and some of his students.[4]

[3] Professor, School of Mathematics, Georgia Institute of Technology, on leave at Mathematics Research Center, U. S. Army, University of Wisconsin, Madison, Wis.

[4] N. Levinson, "A Boundary-Value Problem for a Singularly Perturbed Differential Equation," *Duke Mathematical Journal*, vol. 25, no. 2, June, 1958, pp. 331–342; references to earlier literature included in this work.

Authors' Closure

The authors wish to thank Professors Gorton and Nohel for their constructive discussion regarding the paper.

Professor Gorton brings up a key point when he inquires into the effect of varying the shape of the inlet axial velocity profile. It is entirely possible that the solutions given in the paper might be unstable in the sense that a given arbitrary inlet profile might not actually develop into the similar profiles given in the paper. The authors have not investigated this problem. Clearly, the solutions given in the paper are "fully developed" flows in the sense that the shape of the velocity profiles is completely specified by the choice of stream function used in the paper. At the same time, the position of the inlet, $x = 0$, is completely arbitrary for these similar solutions.

Professor Nohel's comments are all quite correct and clearly need no further discussion on the authors' part. He is quite justified in being dissatisfied with the proof of convergence, since the acceptance of the proof requires acceptance of a fact which the reader could not possibly establish without considerable further study. The authors felt that space requirements prohibited further detailed discussion of convergence. Mr. White's doctoral dissertation contains more detailed information, along with a discussion which definitely helps to dispel doubt concerning general behavior of the series solution.

Buckling of Struts of Variable Bending Rigidity[1]

I. A. EL-DEMIRDASH.[2] Fig. 1 of this discussion shows three struts of variable cross section as included in DIN 120. The corresponding coefficients:

$$\mu_a = 0.34 + 0.66(I_1/I_0)^{1/2}, \quad \mu_b = 0.20 + 0.80[(I_1/I_0)^2]^{1/2},$$

and

$$\mu_c = 0.61 + 0.39(I_1/I_0)^{1/2}$$

are plotted in Fig. 2. For the sake of comparison, the coefficients

$$\mu_1 = {}^1/_4(1 + \sqrt{\alpha}),^2 \quad \mu_2 = 4[(1 - \sqrt{\alpha})/\log \alpha]^2$$

and

$$\mu_4 = \sqrt{\alpha}$$

as found by the author for $m = 1$, 2, and 4, respectively, are plotted on the same figure.

A study of all six curves shows the following characteristics:

1 For $\alpha > 0.5$, the values μ_1, μ_2, and μ_4 are practically the same. This means that the buckling load will be almost the same whether $m = 1$, 2, or 4.

2 As α approaches 0, the values of μ_2 and μ_4 fall down quickly toward 0. In other words, if the end sections are very small with respect to the central section, the buckling load becomes nearly 0. This result is not practicably acceptable.

3 For a plate-girder section with straight tapered flanges of constant area, the power $m \cong 2$. However, the values of μ_c nearly coincide with μ_b and not with μ_a.

4 On the whole, the values μ_1, μ_2, and μ_4 as found by the author are less than the values μ_a and obviously μ_c of DIN 120.

[1] By M. M. Abbassi, published in the December, 1958, issue of the JOURNAL OF APPLIED MECHANICS, vol. 25, TRANS. ASME, vol. 80, pp. 537–540.

[2] Professor, Faculty of Engineering, Cairo University, Giza, Egypt, U.A.R.

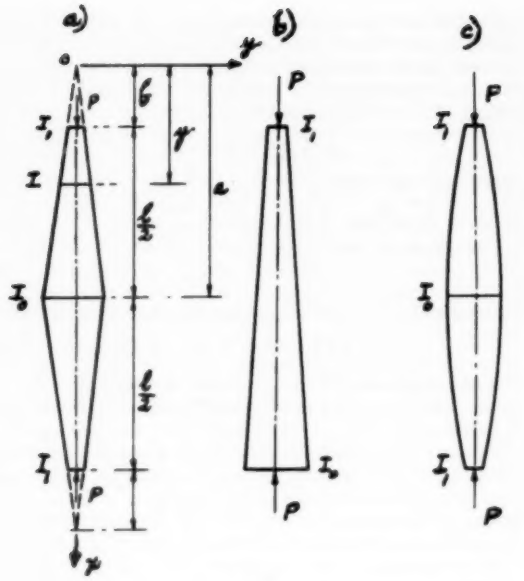

Fig. 1

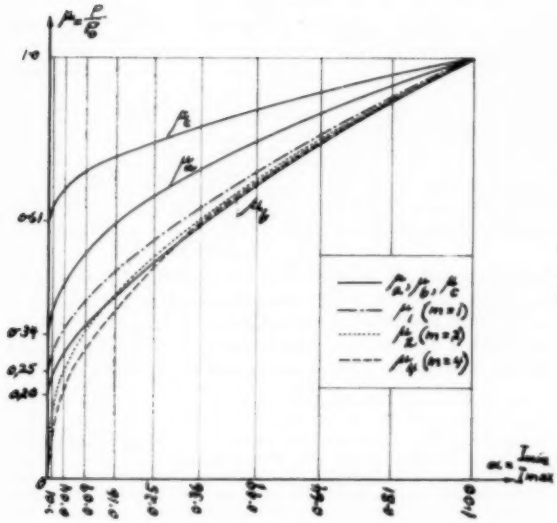

Fig. 2

Consequently, the corresponding critical loads will be smaller than the values calculated according to the specifications.

It follows that the approximation given by the author is more conservative or less economical than that contained in DIN 120. Which of the two assumptions is a better practical approximation is the concern of exact calculations or experimental investigation.

For a uniform strut of constant moment of inertia subject to the action of a linear or a c/x^2 variation of the axial load, the author gives:

$$\mu_a = \frac{9}{4}\left[\frac{1+\alpha}{1+\alpha+\alpha^2}\right]^2$$

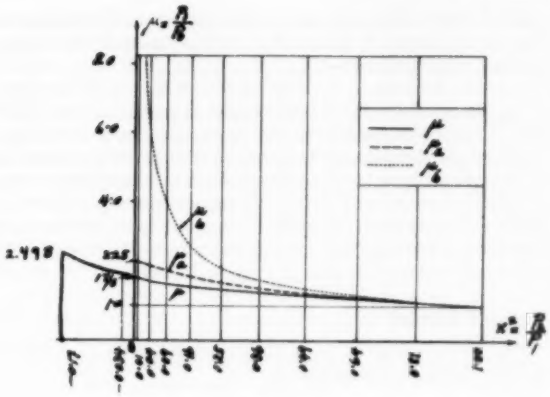

Fig. 3

and

$$\mu_b = \left[\frac{1-\alpha}{\alpha \log \alpha}\right]$$

respectively. These two factors are plotted against α^2 in Fig. 3. The following characteristics are here observed:

1 As α^2 decreases from 1 to 0, the factor μ_a increases steadily from 1 to 2.25. The first condition refers to the case of a constant axial load, while the latter corresponds to a triangular loading.

2 For $\alpha^2 > 0.5$ or $\alpha > 0.7$, the factors μ_a and μ_b are almost identical. However, μ_a is always slightly less than μ_b. On the other hand, for $\alpha^2 < 0.5$ or $\alpha < 0.7$, the factor μ_b increases rapidly and then very rapidly toward ∞. This extreme case has no practical significance.

3 For the special case of a triangular variation, $P_{max} = 2.25\ P_0$. In other words, the strut can carry an average load which is $^1/_8$ bigger than the critical constant load. Or, the strut can carry the maximum load by a reduced length $l_0 = {}^2/_3 l$.

Referring to the case of a vertical bar hinged at the ends and submitted to the action of its own weight g per unit length in addition to the end load P, the critical value of the end load is given by the equation:

$$P_{cr} = \frac{mEI}{l^2} = \frac{m}{\pi^2} P_0$$

The factor m depends on the ratio $n = gl \div P_0$. The corresponding values of m and n are found in Timoshenko's "Theory of Elastic Stability."

Using the same notations as before,

$$\alpha^2 = \frac{m}{\pi^2} \div \left(\frac{m}{\pi^2} + n\right)$$

and

$$\mu = \frac{m}{\pi^2} + n$$

The corresponding curve is shown in Fig. 3. For $\alpha^2 > 0.36$ or $\alpha > 0.6$, this curve almost coincides with the curve of μ_a. However, for smaller values of α^2 the μ-values are smaller than the corresponding μ_a-values. At $m = 0$ or $\alpha^2 = 0$, $\mu = n \cong 1^2/_3$. This is less than the value 2.25 given by the author.

According to Timoshenko, the strut can either carry an average load about $^1/_{16}$ less than the critical constant load for its total length, or the full maximum load by a reduced length $l_0 \cong {}^2/_3 l$, which is more than ${}^2/_3 l$ as found by the author. Here again the

question which of the two assumptions constitutes a better practical approximation is answered by an exact mathematical solution or by a laboratory test.

Last but not least, it must be mentioned that, in all the foregoing, the critical load has been derived as function of the Euler load. This latter depends on the elastic modulus E of the material. It is, therefore, obvious that all these investigations refer to the case of elastic buckling, where the critical stress lies within the elastic limit of the material. It remains the object of future investigation to study buckling beyond this limit for struts of variable bending rigidity, or for uniform struts under the action of a varying axial load.

Author's Closure

The author wishes to thank Dr. El-Demirdash for his criticism and for his valuable suggestions.

The Wedge Under a Concentrated Couple: A Paradox in the Two-Dimensional Theory of Elasticity[1]

W. H. HOPPMANN, II.[2] The initiative of the authors in attacking this problem is to be commended, but it appears to the writer that their attempt to explain a "paradox" by transform theory in analyzing singularities of systems of linear differential equations is somewhat beside the point.

For a continuous range of the apex angle α a regular solution of the linear differential equations of elasticity exists. However, as α approaches a certain value, called by the authors α_*, the stresses and corresponding relative displacements become unbounded throughout the region of the wedge. Consequently, the problem *ipso facto* becomes one in the general theory of elasticity (finite deformation). The phenomenon may appear odd to one accustomed to dealing only with linear problems; however, the logic of the situation is clear-cut.

One must face up to the fact and not seek the answer in transform solution of linear differential equations which obviously do not hold in the neighborhood of α_*. The problem is apparently not one of singularities in linear theory. In any event the writer is of the opinion that analysis in terms of the complete nonlinear theory of elasticity will throw the necessary light on the problem.

G. HORVAY.[3] The authors have presented a fascinating study of the way stress singularities may creep into innocent-looking solutions and play havoc with carelessly stated uniqueness theorems and Saint Venant principles. In particular they call for increased vigilance in the use of the mathematical fiction, "concentrated load." To the writer the paper had added significance. It clarified, at long last, the method of selecting the integration path in inverse Mellin transforms. The comments which are presented in this discussion make their entry into the problem at the far end of the sector, rather than at the vertex; they aim to give an alternate explanation for the appearance of the two critical sector angles $2\omega_e = \pi$ and $2\omega_0 = 1.43\pi$ (e = even, 0 = odd).

Consider the circular sector of radius 1 and central angle 2ω, subject to some boundary-layer distribution (which has no overall force or moment resultant, so that the problem is one of statics). The stress function may be written as[4] [see equation (3) of an earlier paper by the writer and K. L. Hanson[4]]:

$$\Phi = \Phi_1 + \Phi_2 + \Phi_3 \tag{1}$$

where, for $0 < \omega < \pi/2$

$$\Phi_1 = a_0 r^2 + r^{\pi/2\omega}[(a_1 + b_1 r^2)\cos \pi\theta/2\omega + (c_1 + d_1 r^2)\sin \pi\theta/2\omega] + r^{\pi/\omega}[(a_2 + b_2 r^2)\cos \pi\theta/\omega + (c_2 + d_2 r^2)\sin \pi\theta/\omega] \tag{2a}$$

while for $\pi/2 < \omega < \pi$ the a_1, c_1 terms have to be replaced by

$$r^{-\pi/\omega}[B_2 r^2 \cos \pi\theta/\omega + D_2 r^2 \sin \pi\theta/\omega] \tag{2b}$$

The nine coefficients in (2) are determined from the nine conditions which impose individual self-equilibration on the three boundaries, $\theta = \pm\omega$, $r = 1$. Φ_2 and Φ_3 then represent the effects of self-equilibrating loads acting on $\theta = \pm\omega$ and on $r = 1$, respectively (leaving the other boundaries stressless), and thus are solutions of appropriate biharmonic eigenvalue problems. The problem of Φ_3 leads to two infinite sets of characteristic boundary traction pairs, say to τ_k^{I}, σ_{rk}^{I} and to τ_k^{II}, $\sigma_{rk}^{\mathrm{II}}$ ($k = 2, 3, 4, \ldots$). The corresponding stress functions Φ_k have the radial variation[5]

$$H_k(r) = ar^{\xi_k + i\eta_k} + br^{\xi_k - i\eta_k} \tag{3a}$$

or

$$H_k(r) = ar^{\xi_{kI}} + br^{\xi_{kII}} \tag{3b}$$

depending on whether the eigenvalue parameter

$$\zeta_k = \xi_k + i\eta_k \tag{4}$$

which satisfies the equation

$$\sin [2\omega(\zeta - 1)] = \begin{cases} +(\zeta - 1)\sin 2\omega, & k = 2, 4, 6, \ldots \\ -(\zeta - 1)\sin 2\omega, & k = 3, 5, 7, \ldots \end{cases} \tag{5}$$

is complex or real.[6] Equation (5) was studied previously by M. L. Williams,[7] C. Ricci,[8] and—according to Goodier-Hodge[9]—by a host of Russian investigators (Papkovitz, Kitover, Prokopov, and so on). The equation was studied, in a variational approximation, also in the writer's earlier paper,[4,10] and in Fig. 3 of that

[1] By Eli Sternberg and W. T. Koiter, published in the December, 1958, issue of the JOURNAL OF APPLIED MECHANICS, vol. 25, TRANS. ASME, vol. 80, 1958, pp. 575–581.

[2] Professor of Mechanics, Department of Mechanics, Rensselaer Polytechnic Institute, Troy, N. Y.

[3] General Electric Research Laboratory, Metallurgy and Ceramics Research Department, General Electric Company, Schenectady, N. Y. Mem. ASME.

[4] G. Horvay and K. L. Hanson, "The Sector Problem," JOURNAL OF APPLIED MECHANICS, vol. 24, TRANS. ASME, vol. 79, 1957, p. 574, and p. 316, 1958. For the sake of easier cross reference we retain the symbols ω, ζ, ξ, η, of this paper; they appear as α, $\zeta + 1$, $\xi + 1$, η in the authors' paper. A detailed analysis of a sector, on the basis of the steps outlined in the foregoing, is given in the paper, "Thermal Stresses in a Sector Prism," by K. L. Hanson and G. Horvay, Proceedings of the Third National Congress of Applied Mechanics, 1958, p. 347.

[5] Ibid., equation (27).

[6] For the complete sector, $0 \leqslant r \leqslant 1$, use the two roots ζ_k with equal positive real parts when ζ_k is complex, and use of the two larger roots ζ_{kI}, ζ_{kII} when ζ_k is real. Equation (5) has two further roots: $2 - \zeta_k$. When the sector is incomplete, $0 < r_1 \leqslant r \leqslant 1$, the corresponding r powers must also be included in $H_k(r)$.

[7] M. L. Williams, "Stress Singularities Resulting From Various Boundary Conditions in Angular Corners of Plates in Extension," JOURNAL OF APPLIED MECHANICS, vol. 19, TRANS. ASME, vol. 74, 1952, p. 526.

[8] C. Ricci, "Tavola di Radici di Bass Modulo di un Equazio Interessante la Scienza della Construzione," Publication 296, Istituto per le Applicazioni del Calcolo, Roma, 1951.

[9] J. N. Goodier and P. G. Hodge, "Elasticity and Plasticity," John Wiley and Sons, New York, N. Y., 1958.

[10] I. K. Silverman, "Approximate Stress Functions for Triangular Wedges," JOURNAL OF APPLIED MECHANICS, vol. 22, TRANS. ASME, vol. 77, 1955, p. 123, has studied a closely related problem.

paper there were plotted, versus ω, the real and imaginary parts of the roots ζ_2, ζ_3, ζ_4. Clearly, $\xi_3 - 2$ gives the rate of decay of the stress associated with ζ_3. The plots show that when ω exceeds ω_a, the decay constant $\xi_2 - 2$ becomes negative, and when ω exceeds ω_b, also $\xi_3 - 2$ becomes negative.[11] Hence the self-equilibrated boundary tractions, distributed along $r = 1$, but clearing the radii $\theta = \pm\omega$, funnel their effects, for $\omega > \omega_{crit}$, into the vertex of the sector, and create there infinite stresses. Since, by Fig. 3,[4] there exist, for $2\omega < 2\pi$, at most two linearly independent characteristic boundary tractions with negative decay constants, there exist at most two linearly independent singular self-equilibrating stress distributions that may be created at the vertex whose behavior contradicts the conventional formulation of Saint Venant's principle; namely, the even distribution which belongs to ζ_2 and enters the problem when $\omega > \omega_a$, and the odd distribution which belongs to ζ_3 and enters the problem when $\omega > \omega_b$. Their expression is given, in a variational approximation, in equation (24).[4] If overlapping sectors, $2\omega > 2\pi$, are also permitted then, as seen from Fig. 3,[4] further singularly behaving self-equilibrating tractions—associated with ζ_4, ζ_5, and so on—are also possible.

P. M. NAGHDI.[12] This illuminating paper on the title problem concludes that the classical solution of Carothers is valid only in the range[13] $0 < 2\alpha \leq \pi$.

Breakdowns similar to that in Carothers' solution occur also in other two-dimensional problems of the linear theory of elasticity; e.g., in the case of a wedge under uniform normal surface traction on one face only,[14] where again a formal breakdown occurs at $\alpha = \alpha_* \cong 0.715\pi$. The writer would appreciate the authors' comments on the question of the range of the validity of this latter solution.[14]

W. R. OSGOOD.[15] Would the authors elaborate on their footnote 13? Since the classical solution apparently has physical validity only for angles of the wedge in the range $0 < 2\alpha \leq \pi$, the "real" critical angle would appear to be $\alpha^* = \pi/2$. Whereas the components of stress σ_r and $\tau_{r\theta}$ obviously become infinite at $\alpha = \alpha_*$, there is nothing in equations (1) and (2) which indicates that $\alpha = \pi/2$ is a limiting angle.

Something else bothers the writer about the authors' critical angle. By choosing an angle less than α_* but sufficiently near to it, for any value of $r > a$, σ_r may be made as large as one pleases, however small Q is. Does not this in itself deprive the solution of physical meaning? It is not a question of the infinite stresses associated with a concentrated load.

Authors' Closure

The authors agree that their analysis of the wedge under a concentrated couple is beside the point raised by Professor Hoppmann. If the discusser were to be consistent he would have to dismiss *all* solutions which possess infinities in the stress distribution and thus violate the approximative assumptions underlying the linear theory of elasticity. In particular, he would be forced to banish all problems involving concentrated loads from consideration within the linear theory. Professor Hoppmann's misgivings in this particular instance are prompted by the paradoxical behavior of the classical "solution" to the problem at hand, the stresses of which become infinite throughout the entire wedge region (rather than merely at the point of application of the couple) when the opening angle approaches the value $2\alpha_* \doteq 1.43\pi$.

The notion of a concentrated force or couple represents a meaningful and useful idealization of physically realistic loading conditions provided the formulation of the corresponding singular problem is based on a suitable limit process. Such a limit process was adopted by the authors as the defining criterion of validity for the solution to Carothers' problem, the conventional formulation of which was demonstrated to be incomplete. As shown in the paper, the classical results are obtained in the limit as the replacement loading is contracted to the apex, for an *arbitrary* choice of this distributed loading, if and only if the opening angle is confined to the range $0 < 2\alpha \leq \pi$. Consequently, Carothers' solution is valid for opening angles up to and including π but invalid for all opening angles exceeding π; within its range of validity the correct stress distribution is finite except at the apex. (The fact that a transform technique was used as a convenient tool for carrying out the preceding limit process has, of course, no bearing on the conclusions reached.)

In view of this state of affairs, Professor Hoppmann's objection, which rests on the pathological behavior of a demonstrably incorrect solution to a deficiently formulated problem, is hardly tenable. In fact, the proposed escape into nonlinear elasticity theory appears to us to beg the central issue of the paper, which is inherently one that has to be settled within the framework of the linear theory.

Dr. Horvay's observation that the characteristic equation (35)[16] is also encountered in the plane problem of a circular sector, loaded along the curved portion of its boundary, is interesting and reflects a close connection between this particular sector problem and the wedge problem under discussion. The list of publications in which Equation (35) arises can no doubt be further augmented.

Professor Osgood's final comment, to the effect that the behavior of Carothers' solution (2) at *and near* $\alpha = \alpha_*$ provides sufficient grounds for questioning the meaning of the entire solution, is well taken. It is precisely this behavior which prompted our investigation of the range of opening angles (if any) for which formulas (2) are in fact valid. That question is related to the concept of concentrated load inasmuch as the incompleteness of the conventional formulation of concentrated-load problems is responsible for the pseudo character of Carothers' results when $2\alpha > \pi$.

As emphasized by Professor Osgood—and insufficiently emphasized in the paper[17]—the actual critical opening angle is π rather than $2\alpha_*$. There is, of course, no *a priori* reason why "solution" (2) should display a formal breakdown at $2\alpha = \pi$, analogous to its singular behavior at $\alpha = \alpha_*$. In fact, since the conventional derivation of Carothers' results presupposes that the solution is antisymmetric, the breakdown which stems from the symmetric component of the replacement loading is bound to remain hidden in (2). Incidentally, there are intuitive indications[18] that Carothers' results cease to be valid for $2\alpha > \pi$: the shear stress $\tau_{r\theta}$ in (2), which is positive for $0 < 2\alpha \leq \pi$, undergoes a twofold reversal in sign on any arc $r = \text{const}$, $-\alpha \leq \theta \leq \alpha$, when $2\alpha > \pi$.

The authors welcome Professor Osgood's request for an elaboration on the effect of the symmetric component of the replacement loading which, they feel now, should have been discussed more explicitly in the paper. The basic equations needed in this connection were derived previously by Tranter (reference [15] of the paper). In the case of the symmetric component of

[11] In the text of footnote 4, ω_a was correctly stated as 90 deg, but ω_b was roughly referred to as 135 deg.

[12] Professor of Engineering Science, University of California, Berkeley, Calif. Mem. ASME.

[13] See "Note Added in Proof," as well as footnote 13 of paper.

[14] S. Timoshenko and J. N. Goodier, "Theory of Elasticity," second edition, McGraw-Hill Book Company, Inc., New York, N. Y., 1951, pp. 123–125.

[15] Professor of Mechanics, Department of Mechanics, Rensselaer Polytechnic Institute, Troy, N. Y. Mem. ASME.

[16] Numbers in parentheses refer to the equations in our paper.

[17] Cf. the clarifying Note Added in Proof.

[18] The authors are indebted to Professor R. D. Mindlin for this observation.

the normal replacement tractions the boundary conditions (10) are to be replaced with

$$\left.\begin{array}{ll} \sigma_\theta(r, \alpha) = \sigma_\theta(r, -\alpha) = q(r) & (0 \leq r < \infty), \\ q(r) = 0 & (a < r < \infty); \\ \tau_{r\theta}(r, \alpha) = \tau_{r\theta}(r, -\alpha) = 0 & (0 \leq r < \infty). \end{array}\right\} \quad (a)$$

Let the Mellin transform of $r^s q(r)$ be denoted by $\hat{q}(s)$, whence

$$\hat{q}(s) = \int_0^a q(r) r^{s+1} dr. \quad (b)$$

Since the *entire* loading is to be statically equivalent to a couple, its symmetric component must be self-equilibrated, i.e., $\hat{q}(-1) = 0$. The stresses corresponding to the loading (a) are again given by (30), where the transformed stresses now take the form

$$\left.\begin{aligned} \hat{\sigma}_r &= \frac{\hat{q}(s)}{H(s, \alpha)} [(s+2) \sin (s+2)\alpha \cos s\theta \\ &\quad - (s+4) \sin s\alpha \cos (s+2)\theta], \\ \hat{\sigma}_\theta &= \frac{\hat{q}(s)}{H(s, \alpha)} [s \sin s\alpha \cos (s+2)\theta \\ &\quad - (s+2) \sin (s+2)\alpha \cos s\theta], \\ \hat{\tau}_{r\theta} &= \frac{\hat{q}(s)}{H(s, \alpha)} (s+2)[\sin (s+2)\alpha \sin s\theta \\ &\quad - \sin s\alpha \sin (s+2)\theta], \end{aligned}\right\} \quad (c)$$

and the function $H(s, \alpha)$ is defined by

$$H(s, \alpha) = (s+1) \sin 2\alpha + \sin 2(s+1)\alpha. \quad (d)$$

Here, as in the antisymmetric case, the transformed stresses are regular at $s = -1$ and the line of integration $\mathrm{Re}(s) = c$ in (30) must again be chosen in the strip of regularity of the s-plane containing the point $s = -1$. Likewise, the behavior of the solution as $a \to 0$ while r and θ are held fixed is governed by the leading terms in the residue expansions for the stresses (30) when the contour is closed in the half-plane $\mathrm{Re}(s) > -1$. These dominating terms, in turn, stem from the zeros of $H(s, \alpha)$ that have the smallest real part and lie in $\mathrm{Re}(s) > -1$. One easily verifies that $H(s, \alpha)$ has no zeros in the strip $-1 < \mathrm{Re}(s) \leq 0$ if $2\alpha < \pi$. On the other hand, for $2\alpha > \pi$ there exists a real negative zero μ; if $2\alpha = \pi$, the critical zero is $\mu = 0$. Consequently, the leading terms in the residue expansions for the stresses due to the symmetric load component, which are analogous to the dominating terms (44), (47), (50) in the stresses due to the antisymmetric load component, are of the order $\rho^{-2-\mu}$, where $\mu > 0$, $\mu = 0$, $\mu < 0$ according as $2\alpha < \pi$, $2\alpha = \pi$, $2\alpha > \pi$. Hence the leading terms arising from the symmetric load component are dominant over those appropriate to the antisymmetric load component in the range of wedge angles $\pi < 2\alpha < 2\alpha_*$. It follows that Carothers' results (2) are invalid also in this range unless the replacement loading is artificially restricted to be purely antisymmetric.

Professor Naghdi's pertinent question concerning the range of validity of another well-known solution to a wedge problem, i.e., Levy's solution for a wedge under a uniform normal loading applied to one face and extending to infinity, is indeed intimately related to the present analysis. Here again the conventional formulation of the problem fails to characterize its solution uniquely and the classical results break down for the same critical wedge angle $2\alpha_*$.

A physically natural definition of the solution to Levy's problem is obtained by considering, first, the modified problem in which the uniform normal loading on one face extends only over the finite interval $0 < r \leq a$, and by subsequently proceeding to the limit as $a \to \infty$ while (r, θ) remain fixed. The modified loading may again be decomposed into its antisymmetric and symmetric components. The corresponding solutions in integral form are once more given by (30) in conjunction with (26) to (28) and (c), (d), respectively. In the present instance $s = -1$ is a pole of the integrands in (30) since neither $\hat{p}(-1)$ nor $\hat{q}(-1)$ vanish here. The line of integration must now be taken immediately to the left of $s = -1$ and the stresses for $r < a$ may be evaluated by completing the contour in the half-plane $\mathrm{Re}(s) < -1$.

It is readily seen that the zeros of both $G(s, \alpha)$ and $H(s, \alpha)$ are distributed symmetrically with respect to the line $\mathrm{Re}(s) = -1$. Moreover, $\hat{p}(s)$ and $\hat{q}(s)$ now have a simple pole at $s = -2$. Hence the leading terms in the residue expansions for the stresses due to the *antisymmetric* load component, as $a \to \infty$, are at present of order unity for $2\alpha < 2\alpha_*$ and of order ρ^{s_1} for $2\alpha > 2\alpha_*$, where $s_1 < 0$ for $2\alpha > 2\alpha_*$ and is once more given by Fig. 2 of the paper; at the critical opening angle $2\alpha^*$ the pole $s = -2$ is a double pole and the stresses are of order $\log \rho$. The leading terms in the analogous residue expansions due to the *symmetric* load component, as $a \to \infty$, are found to be of order unity when $2\alpha \leq \pi$, and of order ρ^μ when $2\alpha > \pi$, where $\mu < 0$ is the zero of $H(s, \alpha)$ in the strip $-1 < \mathrm{Re}(s) < 0$; it should be noted that for $2\alpha = \pi$ the pole $s = -2$ remains simple in the symmetric loading case.

Combining the foregoing conclusions regarding the antisymmetric and the symmetric load component, one sees that finite stresses result in the limit as $a \to \infty$ only for wedge angles in the range $0 < 2\alpha \leq \pi$; the limit solution in this range coincides with Levy's solution. If $2\alpha > \pi$, the limit as $a \to \infty$ of the solution to the modified problem fails to exist and hence the classical solution is invalid for $2\alpha > \pi$. Although Levy's solution exhibits no formal breakdown at $2\alpha = \pi$, its invalidity for opening angles exceeding π may be anticipated on intuitive grounds: when $2\alpha > \pi$ the tip of the wedge becomes a reentrant corner at which an infinite concentration of stress is to be expected; yet the classical results contain no such singularity at $r = 0$.

A Simple Approach to an Approximate Two-Dimensional Cascade Theory[1]

HANS KRAFT.[2] It is always a welcome sign to see that there still are men working on cascade theory. There are not too many of them in this country. The reasons for this state of affairs are not hard to see:

1 Cascade theory is a very difficult subject.

2 Too many people have already written off or are writing off the turbine as an important prime mover. In the air the rocket is expected to replace the gas turbine, and on land electricity of the future is expected to be generated by fusion power without need for prime movers. However, we will need air transportation and electricity up to the time when this has all come about.

It seems that for at least another generation we, or rather some of us, will have to grapple with the intricacies of this theory.

The author tries to deal with the first objection, which is the difficulty of computing a cascade. More power to anybody who can arrive at a truly simple formula. However, the modern electronic computer is introducing itself so fast in the industry that one may wonder whether too much sincere effort should be expended toward further simplification. Once a servant is available who can do such dirty work, let him do it. This has a great

[1] By M. J. Schilhansl, published in the December, 1958, issue of the JOURNAL OF APPLIED MECHANICS, vol. 25, TRANS. ASME, vol. 80, 1958, pp. 607–612.

[2] Aerodynamics Engineer, Large Steam Turbine-Generator Department, General Electric Company, Schenectady, N. Y.

advantage. The problem can be treated without simplifications. This eliminates the worry as to what extent whatever simplifications have been made are justified. For sharply curved, highly loaded cascade profiles, both the vortex distribution of the profile proper and the influence coefficients of the others can behave in a very peculiar manner. Besides, in this case, it is not permissible to have sources lying outside of the profile.

The primary purpose for most cascade computations must always be kept in mind. It is not intended to find the lift vector and turning moments. What is primarily wanted is a pressure distribution along the profiles which will help to study the character of the boundary layers both on convex and concave-partition flanks. In a cascade, especially the highly loaded turbined blade, it becomes quickly apparent that this pressure distribution must be known fairly accurately. After all, the loss (or drag) is only a small percentage of the lift and it is the loss that is required to be known to enough accuracy to be able to make a meaningful choice between some alternatives.

This brings up the question of the optimum profile for given deflections. Here one does not compute fields for given cascades but tries to compute the shape of a cascade profile for good boundary-layer behavior.

The Large Turbine Department of the writer's company has worked on both approaches. We now have a good method to compute the flow around the given cascade, no matter what shape, and no holds barred as to accuracy. The only limitations are those of two-dimensional, incompressible potential flow. Such a computation takes less than 15 min on a 704 computer. The method will be published at some later date.

We also will show a computation which is in use to obtain favorable profiles.

While these results are very gratifying, they have their limits and still leave very much room for additional effort. It is in this sense that the author's contribution is so much welcomed and the hope is expressed that he will do more of the same.

Author's Closure

I would like to thank Mr. Kraft for his comments; they bring out a point of great significance, namely, the question: Are approximate solutions justified at a time at which so much effort has been put into the development of digital and analog computers?

I still think that approximations are not yet obsolete and never will be, for the following reasons:

First, when talking to undergraduate students about a two-dimensional approach to turbine theory, I had the impression that a mere explanation of the basic concepts of cascade theory, a remark about the computation to be done by a digital computer and a discussion of the numerical results, was not as well understood by the students as a representation of the subject as given in my paper. Thus it might be of some help for the education of the coming engineering generation.

Second, even if the infallibility of a digital computer is admitted, there is no guarantee of infallibility of the programming personnel. In a case in which the results turned out by a computer do not agree with expectation, an approximate method might offer a quick judgment whether or not something went wrong.

Journal of APPLIED MECHANICS

Book Reviews

Mechanical Vibration

Introduction to a Study of Mechanical Vibration. By G. W. Van Santen. The Macmillan Company, New York, 1958. Second Edition. Cloth, 9 × 6 in., xvi and 310 pp., illus. $8.50.

REVIEWED BY R. PLUNKETT[1]

This little volume is very aptly named; it is indeed an introduction to the subject and presented in a very lively manner. The author takes his courage in both hands and covers many important aspects of the subject that are untouched by our standard texts. In addition to the usual coverage of simple lumped and distributed systems (including some very useful tables of frequencies), traveling waves, acoustics, balancing, damping phenomena, fatigue (human and metal), instruments and instrumentation, and physiology of the human ear are at least introduced! The presentation is descriptive rather than analytical and is greatly influenced by the author's obvious preference for the experimental approach. As a result, this is not a textbook, but it should be very valuable for the practicing engineer who wants a quick survey of the whole field and some practical help in industrial problems. It is unfortunate that such a useful book suffers from a great many typographical errors which are aggravated by a poor translation from the Dutch. Most of these errors are trivial, if annoying, but a few are serious. The chapters on instruments are mainly a description of N. V. Philips' products.

All in all, this is a useful book for practicing mechanical engineers which, with a little more care, could have been indispensable.

[1] Consulting Engineer, General Electric Company, Schenectady, N. Y. Mem. ASME.

Mathematics of Physics

Mathematics of Physics and Modern Engineering. By I. S. Sokolnikoff and R. M. Redheffer. McGraw-Hill Book Co., Inc., New York, 1958. Cloth, 9¼ × 6¼ in., ix and 810 pp., illus. $9.50.

REVIEWED BY H. P. GREENSPAN[2]

This text is the successor to the senior author's "Higher Mathematics for Engineers and Physicists." It is intended to provide a sound introduction to applied mathematics and therefore a great number and variety of topics are discussed. The text consists of nine chapters, each of which is virtually independent of the others: 1 Ordinary Differential Equations; 2 Infinite Series; 3 Functions of Several Variables; 4 Algebra and Geometry of Vectors, Matrices; 5 Vector Field Theory; 6 Partial Differential Equations; 7 Complex Variable; 8 Probability; 9 Numerical Analysis. In addition, determinants and

[2] Assistant Professor of Applied Mathematics, Division of Engineering and Applied Physics, Harvard University, Cambridge, Mass.

Laplace transforms are treated in separate appendixes. Emphasis has been placed on balancing the presentation so that the rigorous developments and the applications complement each other. All material is amply illustrated by worked examples, and the numerous problems at the conclusion of each section are relevant, meaningful, and occasionally thought-provoking. It is praiseworthy that attention is given to the formulation of physical problems and not only to their solution, as is so often the case.

The major difficulty in evaluating this work is to decide exactly what constitutes an effective introduction to a subject and the extent to which the material can be used. Unfortunately, when the scope is broadened, the penetration into any single subject must be made somewhat shallow. The subject matter of this text is certainly sufficient for an intensive year's course. It is the authors' contention, however, that the material is sufficient for four or five semester courses and that separate courses can be made from either Chaps. 6 or 7 or the combinations of 4 and 5 or 8 and 9. The individual chapters are too "introductory" to compete with the more complete texts that already exist in each field. For example, the discussion of series solutions of ordinary differential equations is weak, primarily because little mention is made of singular points. Analysis of the hypergeometric differential equation is left as an exercise, and there is no discussion of first-order partial differential equations. The chapter on complex variables contains little on conformal mapping, almost nothing on multivalued functions, branch lines, branch points, Riemann sheets, and analytic continuation. In discussing the Laplace transform no inversion formula is introduced and the reader is told to consult the tables. Similar remarks apply to Chaps. 1 and 6 to 9. Although the individual chapters would have difficulty standing separately, together they constitute an extremely effective and worth-while text. It will be very successfully used in introductory courses which survey several areas of applied mathematics.

Automation

Handbook of Automation, Computation, and Control. Vol. 1—Control Fundamentals. Edited by Eugene M. Grabbe, Simon Ramo, Dean E. Wooldridge. John Wiley & Sons, Inc., New York, 1958. Cloth, $9^1/_4 \times 6^1/_4$ in., xx and 999 pp., illus. $17.

REVIEWED BY JOHN R. WARD[3]

This is the first part of a three-volume handbook which is intended to bring together the principles and techniques lying behind the allied and interwoven fields of control and data processing.

This first volume is in the form of an extensive and essentially theoretical introduction. The first section, "General Mathematics" (214 pp.), ranges clearly and concisely from sets and relations through—among other topics—finite difference, differential and integral equations, to Boolean algebra, probability, and statistics. Following upon this are comparatively short sections on "Numerical Analysis" (90 pp.), "Operations Research" (129 pp.), and "Information Theory" (114 pp.). The volume is concluded by a rather longer section (427 pp.) on the theory of "Feedback Control." In passing, the foreword, by Gordon S. Brown, is a good summary of the status of automation in the contemporary scene.

The second volume is to treat the design and application of computers and data processors; and the third, systems engineering, process control, and component design.

The general editors have succeeded commendably in co-ordinating the contributions of the many specialist authors. Each section is well written and arranged, each gives a clear outline of its particular subject matter in its logical relationship to the other sections.

The treatment is too laconic for the book to be used directly as a text—and, indeed, it is not so intended—but it will certainly be useful for providing advanced graduate students with a perspective of the whole area. Primarily, the book is directed toward practicing engineers—and others—who may wish to either broaden and consolidate their knowledge of the over-all field or to refer to some aspect of automation outside their own area of specialization. To assist in this, each chapter contains a list of the relevant primary source material.

Summarizing, the reviewer can only hope that the succeeding volumes reach the same high standard as the first. Certainly the first volume will be a valuable asset in any library—personal or otherwise—for many years.

[3] Assistant Professor of Engineering, Brown University, Providence, R. I.

Vibrations

Engineering Vibrations, With Applications to Structures and Machinery. By Lydik S. Jacobsen and Robert S. Ayre. McGraw-Hill Book Co., Inc., New York, 1958. xii and 564 pp., illus. $10.

REVIEWED BY F. R. ERSKINE CROSSLEY[4]

Here is an excellent new book on mechanical vibration in theory and practice; it is notable for the new material included and for the new proportions allotted to the various parts of the subject material. More than half the book is devoted to the study of systems having only one degree of freedom, but in this the authors give full rein to the modern interest in transients and nonlinearities. They emphasize strongly the phase-plane diagram, especially for the representation of step form shock excitation of vibration, and they develop well the great intuitive advantages of this method.

This has inevitably curtailed the treatment given to systems of more than one degree of freedom; a reasonable compromise is, however, made by following carefully through the solutions to a number of specific numerical types. Lagrange's equations do not appear here, nor is there any mention of normal co-ordinates or such things.

The aim has been to produce a textbook for the first course in the subject, suitable for senior or early graduate level but also for the practicing engineer. The reader is expected to be familiar with elementary linear differential equations. When treating multi-free systems, matrix notation is introduced, but matrix manipulation is not used. The authors are to be commended on many excellent problems, on an extensive bibliographical list, and on certain omissions, such as the matter of the balancing of rotors, which is relegated to a place among the problems. The book will undoubtedly have a strong effect on the teaching of vibration theory in our colleges.

[4] Associate Professor of Mechanical Engineering, Yale University, New Haven, Conn.

Journal of APPLIED MECHANICS

Information for Authors

• Manuscripts should be submitted in final form to the Technical Editors. Each manuscript must be accompanied by a statement that it has not been published elsewhere nor has it been submitted for publication elsewhere. A paper which would occupy more than five pages of the Journal may be returned to the author for abridgment.

• The author should state his business connection, the title of his position, and his mailing address. A short abstract (50 to 100 words) should be included on the first page immediately preceding the introductory paragraph of the paper.

• Three copies of the manuscript are required. One of these must be a carefully prepared printer's copy, typed in double spacing, on one side of the page only, with wide margins, on $8^1/_2$ by 11-in. opaque white paper. Mimeographed manuscripts, if prepared with exceptional care, can be accepted provided they are completely edited.

• As far as possible, all mathematical expressions should be typewritten. Greek letters and other symbols not available on the typewriter should be carefully inserted in ink. Care should be taken to distinguish between capital and lowercase letters, between zero (0) and the letter (*O*), between the numeral (1) and the letter (*l*), etc. A letter representing a vector cannot be printed with an arrow above or below it. The letter should be underscored with a single wavy line, wherever it appears in the text, to designate boldface type. A list of symbols carefully marked for the use of the editor (thus: κ, Greek l.c. kappa), if it has not been included in the body of the paper, should accompany the manuscript on a separate page.

• Before preparing a manuscript the author should study printed articles in the Journal, with special attention to the form and style of mathematical expressions, tables, footnotes, references, and abstract. Numbers that identify mathematical expressions should be enclosed in parentheses. Numbers that identify references at the end of the paper should be enclosed in brackets. Care should be taken to arrange all tables and mathematical expressions in such a way that they will fit into a single column when set in type. Equations that might extend beyond the width of one column (fractions that should not be broken or long expressions enclosed in parentheses) should be rephrased to go on two or more lines within column width. Fractional powers are preferred to root signs and should always be used in more elaborate formulas. The solidus should be used instead of the horizontal line for fractions wherever possible.

• A normal paper should not exceed five pages in the Journal. It is about 6000 words or twenty to twenty-five double-spaced typewritten pages inclusive of drawings. A Brief Note should not exceed 750 words or about one column in the Journal inclusive of drawings.

• Originals and two copies of figures must accompany the manuscript. Line drawings should not be larger than $8^1/_2 \times 11$ inches and should be planned for reduction to column width. Lettering should be large enough to be clearly legible when the illustration is reduced. The originals of line drawings must be in India ink on white or pale blue tracing paper or tracing cloth. Photographs of equipment or test specimens must be glossy prints and should be used sparingly. Captions for figures should be typed double-spaced and included as the last page of the manuscript. The figure number and author's name should be written in the margin or on the back of each illustration.

• Titles of papers should be brief.

• Authors can obtain copies of the ASME Manual MS-4, "An ASME Paper," from the Technical Editors and are urged to do so before drafting their papers in final form.

• Papers published in the Journal of Applied Mechanics must be presented at a Meeting, either in person or by title. Scheduling of papers is in the hands of the Secretary of the Applied Mechanics Division. Authors should indicate their preference in this respect to the Technical Editors when submitting a paper.

• An author is entitled to 25 preprints free of charge (in the case of two authors, 15 each; three or more authors, 10 each). Larger quantities of preprints or reprints can be ordered from Editorial Department, The American Society of Mechanical Engineers, 29 West 39th Street, New York 18, N. Y. Quotations will be sent on request.

ASME Publications Committee

Please address all communications to:

Technical Editors

Journal of Applied

Mechanics, ASME

Division of Engineering

Brown University

Providence 12, R. I.

1962

FOURTH U. S. NATIONAL CONGRESS OF

Applied Mechanics

PRELIMINARY ANNOUNCEMENT

The Fourth U. S. National Congress of Applied Mechanics will be held on the Berkeley campus of the University of California during June 18–21, 1962. The cooperating societies and other interested organizations are urged not to schedule conflicting meetings on these dates.

Research workers in the theoretical and applied mechanics of solids and fluids are invited to submit papers for consideration by the Editorial Committee. Further announcements concerning the preparation of papers and deadlines for submission will be made as the Congress draws nearer.

The members of the organizing committee on the Berkeley campus are:

Professor W. GOLDSMITH, *Secretary*
Professor E. V. LAITONE, *Treasurer*
Professor R. M. ROSENBERG, *Chairman of the Editorial Committee*
Professor W. W. SOROKA, *General Chairman*

Inquiries regarding the Congress should be addressed to Professor W. Goldsmith, Secretary, Division of Mechanics and Design, University of California, Berkeley 4, California.